USGS
science for a changing world

Baseline and Projected Future Carbon Storage and Greenhouse-Gas Fluxes in Ecosystems of Alaska

Professional Paper 1826

U.S. Department of the Interior
U.S. Geological Survey

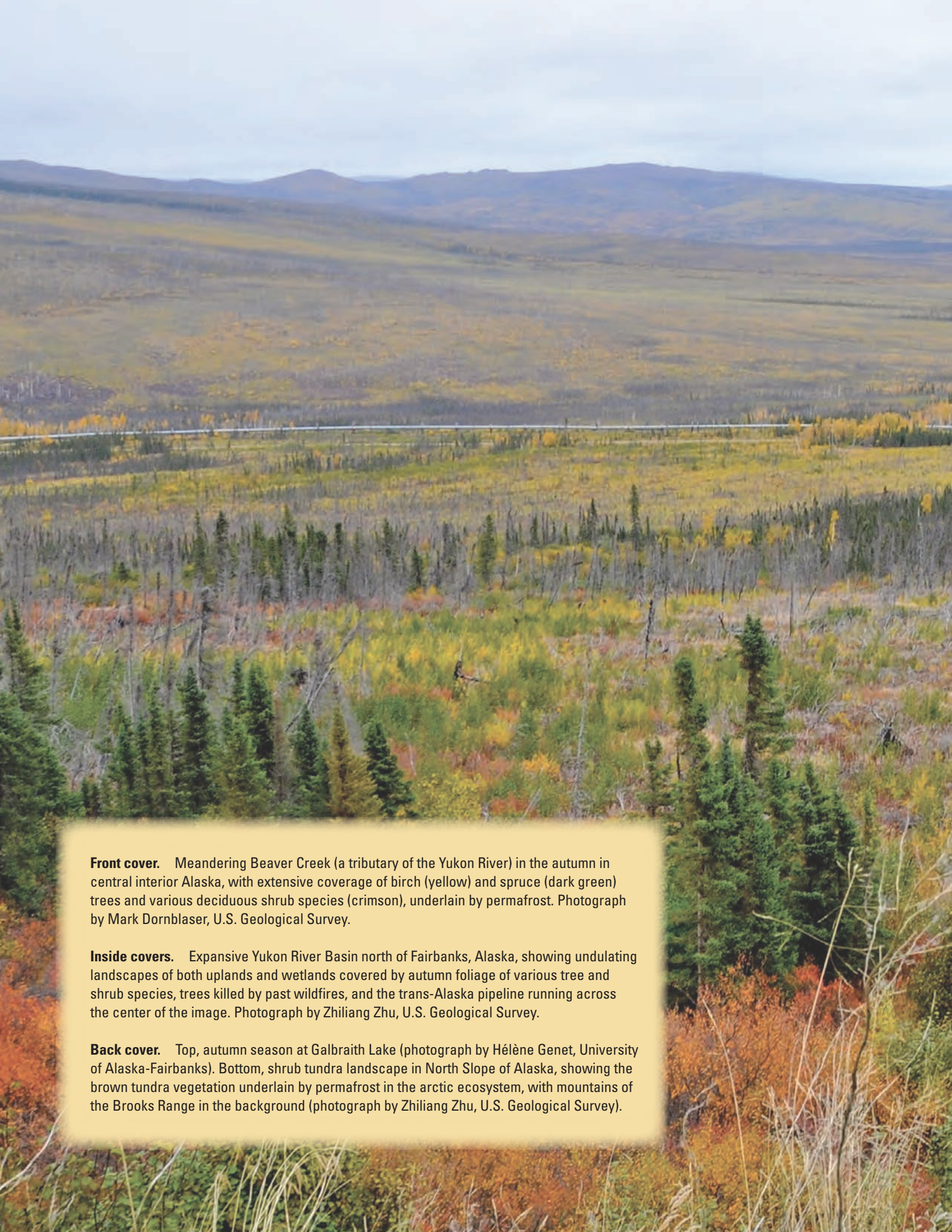

Front cover. Meandering Beaver Creek (a tributary of the Yukon River) in the autumn in central interior Alaska, with extensive coverage of birch (yellow) and spruce (dark green) trees and various deciduous shrub species (crimson), underlain by permafrost. Photograph by Mark Dornblaser, U.S. Geological Survey.

Inside covers. Expansive Yukon River Basin north of Fairbanks, Alaska, showing undulating landscapes of both uplands and wetlands covered by autumn foliage of various tree and shrub species, trees killed by past wildfires, and the trans-Alaska pipeline running across the center of the image. Photograph by Zhiliang Zhu, U.S. Geological Survey.

Back cover. Top, autumn season at Galbraith Lake (photograph by Hélène Genet, University of Alaska-Fairbanks). Bottom, shrub tundra landscape in North Slope of Alaska, showing the brown tundra vegetation underlain by permafrost in the arctic ecosystem, with mountains of the Brooks Range in the background (photograph by Zhiliang Zhu, U.S. Geological Survey).

Baseline and Projected Future Carbon Storage and Greenhouse-Gas Fluxes in Ecosystems of Alaska

Edited by Zhiliang Zhu and A. David McGuire

Professional Paper 1826

U.S. Department of the Interior
U.S. Geological Survey

U.S. Department of the Interior
SALLY JEWELL, Secretary

U.S. Geological Survey
Suzette M. Kimball, Director

U.S. Geological Survey, Reston, Virginia: 2016

For more information on the USGS—the Federal source for science about the Earth, its natural and living resources, natural hazards, and the environment—visit http://www.usgs.gov or call 1–888–ASK–USGS.

For an overview of USGS information products, including maps, imagery, and publications, visit http://store.usgs.gov.

Suggested citation:
Zhu, Zhiliang, and McGuire, A.D., eds., 2016, Baseline and projected future carbon storage and greenhouse-gas fluxes in ecosystems of Alaska: U.S. Geological Survey Professional Paper 1826, 196 p., http://dx.doi.org/10.3133/pp1826.

ISSN 1044-9612 (print)
ISSN 2330-7102 (online)
ISBN 978-1-4113-4038-1

Contents

Conversion Factors

Multiply	By	To obtain
	Length	
centimeter (cm)	0.3937	inch (in.)
millimeter (mm)	0.03937	inch (in.)
meter (m)	3.281	foot (ft)
kilometer (km)	0.6214	mile (mi)
	Area	
hectare (ha)	2.471	acre
square meter (m^2)	10.76	square foot (ft^2)
square centimeter (cm^2)	0.1550	square inch (ft^2)
square kilometer (km^2)	0.3861	square mile (mi^2)
	Volume	
cubic centimeter (cm^3)	0.06102	cubic inch (in^3)
cubic meter (m^3)	35.31	cubic foot (ft^3)
	Flow rate	
cubic meter per second (m^3/s)	35.31	cubic foot per second (ft^3/s)
cubic meter per day (m^3/d)	264.2	gallon per day (gal/d)
cubic meter per day per square kilometer [$(m^3/d)/km^2$]	684.28	gallon per day per square mile [$(gal/d)/mi^2$]
millimeter per year (mm/yr)	0.03937	inch per year (in/yr)
	Mass	
gram (g)	0.03527	ounce, avoirdupois (oz)
kilogram (kg)	2.205	pound avoirdupois (lb)
	Pressure	
atmosphere, standard (atm)	101.3	kilopascal (kPa)
	Hydraulic conductivity	
meter per day (m/d)	3.281	foot per day (ft/d)
	Transmissivity*	
meter squared per day (m^2/d)	10.76	foot squared per day (ft^2/d)
	Application rate	
kilograms per hectare per year [(kg/ha)/yr]	0.8921	pounds per acre per year [(lb/acre)/yr]

*Transmissivity: The standard unit for transmissivity is cubic meter per day per square meter times meter of aquifer thickness [$(m^3/d)/m^2$]m. In this report, the mathematically reduced form, meter squared per day (m^2/d), is used for convenience.

Datum and Supplemental Information

Vertical coordinate information is referenced to the North American Vertical Datum of 1988 (NAVD 88).

Horizontal coordinate information is referenced to the North American Datum of 1983 (NAD 83).

Altitude, as used in this report, refers to distance above the vertical datum.

Temperature in degrees Celsius (°C) may be converted to degrees Fahrenheit (°F) as

$$°F = (1.8 \times °C) + 32.$$

Specific conductance is given in microsiemens per centimeter at 25 degrees Celsius (µS/cm at 25 °C).

Concentrations of chemical constituents in water are given in either milligrams per liter (mg/L) or micrograms per liter (µg/L).

The resolution of pixels in spatial datasets follows the conventions used in the spatial data and modeling communities. The format is "*n*-meter resolution," where *n* is a numerical value for the length. The usage translates into a pixel with a length of *n* on all sides that covers an area of *n* meters × *n* meters.

How Megagrams, Gigagrams, Teragrams, and Petagram Relate to Metric Tons

1 megagram (Mg)	=	1 million grams (10^6 g)	=	1 metric ton (t)
1 gigagram (Gg)	=	1 billion grams (10^9 g)	=	1,000 metric tons
1 teragram (Tg)	=	1 trillion grams (10^{12} g)	=	1 million metric tons (Mt)
1 petagram (Pg)	=	1 quadrillion grams (10^{15} g)	=	1 billion metric tons (Gt)

Abbreviations, Acronyms, and Chemical Symbols

°C	degree Celsius
µatm	microatmosphere
AICC	Alaska Interagency Coordination Center
ALFRESCO	Alaska Frame-Based Ecosystem Code
ALT	active-layer thickness
BCR	Bird Conservation Region
CALM	Circumpolar Active Layer Monitoring
CAVM	Circumpolar Arctic Vegetation Map
CGCM3.1	version 3.1-T47 of the Canadian Centre for Climate Modelling and Analysis' Coupled Global Climate Model
CH_4	methane
cm	centimeter
CMIP3	Coupled Model Intercomparison Project phase 3
CO	carbon monoxide
CO_2	carbon dioxide
CO_2-eq	carbon dioxide equivalent
CO_2-eq/yr	carbon dioxide equivalent per year
CRU	Climatic Research Unit
DIC	dissolved inorganic carbon
DOC	dissolved organic carbon
DOS-TEM	Dynamic Organic Soil version of the Terrestrial Ecosystem Model
ECHAM5	version 5 of the Max Planck Institute's European Centre Hamburg Model
EDNA	Elevation Derivatives for National Applications database
EISA	Energy Independence and Security Act of 2007
EPA	U.S. Environmental Protection Agency
FIA	Forest Inventory and Analysis National Program
FVS	Forest Vegetation Simulator
gC/m^2	gram of carbon per square meter
$gC/m^2/yr$	gram of carbon per square meter per year
GCM	general circulation model
gCO_2-eq/m^2/yr	gram of carbon dioxide equivalent per square meter per year
GHG	greenhouse gas

Abbreviations, Acronyms, and Chemical Symbols—Continued

GIPL 1.3	Geophysical Institute Permafrost Laboratory version 1.3 transient model
GIS	geographic information system
GPP	gross primary productivity
GWP	global warming potential
HPU	hydropedologic unit
HR	heterotrophic respiration
HUC	hydrologic unit code
IPCC	Intergovernmental Panel on Climate Change
kgC/m^2	kilogram of carbon per square meter
km	kilometer
km^2	square kilometer
km^2/yr	square kilometer per year
km^3/yr	cubic kilometer per year
LAI	leaf area index
LANDFIRE	Landscape Fire and Resource Management Planning Tools Project
LCC	Landscape Conservation Cooperative
LOADEST	USGS Load Estimator program
LTER	Long Term Ecological Research
m	meter
m/d	meter per day
MDM-TEM	Methane Dynamics Module of the Terrestrial Ecosystem Model
mg/L	milligram per liter
MgC/yr	megagram of carbon per year
MLR	multiple linear regression
mm	millimeter
mm/yr	millimeter per year
MODIS	Moderate Resolution Imaging Spectroradiometer
NALCMS	North American Land Change Monitoring System
NASA	National Aeronautics and Space Administration
NCSCDv2	Northern Circumpolar Soil Carbon Database version 2
NECB	net ecosystem carbon balance
NEP	net ecosystem production

Abbreviations, Acronyms, and Chemical Symbols—Continued

NHD	National Hydrography Dataset
NLCD	National Land Cover Database
NOAA	National Oceanic and Atmospheric Administration
NPP	net primary productivity
NSP	near-surface permafrost
NWI	National Wetlands Inventory
NWIS	National Water Information System
OLT	organic-layer thickness
PCTR	perhumid coastal temperate rainforest
PDO	Pacific Decadal Oscillation
PgC	petagram of carbon
POC	particulate organic carbon
ppm	part per million
PRISM	Parameter-elevation Relationships on Independent Slopes Model
s.d.	standard deviation
SMU	soil map unit
SNAP	Scenarios Network for Alaska and Arctic Planning
SOC	soil organic carbon
SRES	Special Report on Emissions Scenarios
STATSGO	state soil geographic database
TgC	teragram of carbon
TgC/yr	teragram of carbon per year
$TgCO_2$-eq/yr	teragram of carbon dioxide equivalent per year
TOC	total organic carbon
USDA	U.S. Department of Agriculture
USGS	U.S. Geological Survey

Executive Summary—Baseline and Projected Future Carbon Storage and Greenhouse-Gas Fluxes in Ecosystems of Alaska

By A. David McGuire,[1] Bruce K. Wylie,[2] David V. D'Amore,[3] Xiaoping Zhou,[4] T. Scott Rupp,[5] Hélène Genet,[5] Yujie He,[6] Sarah Stackpoole,[7] and Zhiliang Zhu[8]

Alaska is approximately one-fifth the area of the conterminous United States and spans a broad range in climate from the maritime coastal regions of south-central and southeast Alaska to the boreal forest region in interior Alaska to arctic and maritime tundra regions of northern and western Alaska. The cold temperatures of Alaska have led to the storage of vast quantities of soil and vegetation carbon. Although forest ecosystems of southeast Alaska have been regularly included in national resource or greenhouse-gas inventory programs, other regions of Alaska have not been included in national-level resource or greenhouse-gas inventory programs because of the large size of Alaska, the lack of extensive transportation infrastructure, and the low density of field data to support such programs. Yet, high-latitude ecosystems are potentially more vulnerable to climate change than ecosystems in the temperate zone during the remainder of the 21st century because temperature is projected to increase more in boreal and arctic regions. In particular, these increases in temperature may expose the substantial stores of carbon in the region to loss from more wildfire and permafrost thaw, which could turn the ecosystems of Alaska into a net carbon source. Therefore, the assessment of Alaska ecosystem carbon stocks and fluxes as well as methane fluxes, as reported here, was conducted to better understand the baseline and projected carbon distributions and potential responses to a rapidly changing environment. The results of this assessment will inform national climate and carbon management policies.

Major components of the assessment included carbon and methane fluxes in upland and lowland (wetland) ecosystems, carbon fluxes of inland aquatic ecosystems, synthesis of soil carbon stocks and permafrost distribution, effects of forest management, and effects of climate change and associated shifts in vegetation and wildfire regime over space and time. Methods varied depending on the components, as described in respective chapters of this report. For uplands and wetlands, the boundaries of four Landscape Conservation Cooperatives (LCCs) in Alaska were used to stratify and report the assessment. For inland aquatic ecosystems, the boundaries of six hydrologic regions were used for stratification and reporting. Major findings from the assessment are:

- Estimates of total soil organic carbon (SOC) storage in boreal and arctic regions in Alaska, derived from both field observations and model simulations, ranged from 31 to 72 petagrams of carbon (PgC) from 1950 through 2009. In ecosystems with permafrost, the mean active-layer thickness (ALT; the maximum annual thaw depth) ranged between 76 and 84 centimeters (cm) from surface-derived field data; model simulations indicated that mean ALT was 86 cm.
- A conceptual model of soil susceptibility to climate change indicated that the Arctic LCC and Western Alaska LCC lowland shrub tundra ecotypes are highly susceptible to climate change because of large frozen and unfrozen SOC stocks potentially available for loss by decomposition.

[1]U.S. Geological Survey, Fairbanks, Alaska.

[2]U.S. Geological Survey, Sioux Falls, S. Dak.

[3]U.S. Department of Agriculture Forest Service, Juneau, Alaska.

[4]U.S. Department of Agriculture Forest Service, Portland, Oreg.

[5]University of Alaska-Fairbanks, Fairbanks, Alaska.

[6]Purdue University, West Lafayette, Ind.

[7]U.S. Geological Survey, Denver, Colo.

[8]U.S. Geological Survey, Reston, Va.

- Although there is a high variability in fire regime across interior Alaska, fire frequency, severity, and area burned have increased in recent years, and the trend was projected to continue for the rest of the century across most of the regions and most of the climate scenarios, with the boreal region projected to see the highest increase in fire activities. Correspondingly, in the boreal region late successional vegetation, such as spruce forest, was projected to decline, whereas early- to mid-successional vegetation, such as deciduous forest, was projected to increase. In tundra regions, shrub tundra was generally projected to increase and graminoid tundra to decrease.
- During the historical period of this assessment (1950–2009), upland ecosystems in Alaska were, on average, an overall carbon sink across the State of 5.0 teragrams of carbon per year (TgC/yr). However, the boreal region of the State has been a carbon source, losing 5.1 TgC/yr as the result of increased fire activity in recent decades. The overall carbon sink was projected to increase to 14.7 to 34.6 TgC/yr during the projection period (2010–2099).
- Perhumid coastal rainforest watersheds in southeast Alaska were net carbon sinks of an average 142 grams of carbon per square meter per year ($gC/m^2/yr$) from 2006 through 2009. The non-fire-prone, cool, forested region is expected to remain a stable carbon sink, and potentially increase this sink strength in the future.
- During the historical period (1950–2009), wetland ecosystems in Alaska were, on average, an overall carbon source at 1.3 TgC/yr across the State. Net biogenic methane emissions increased from 27.93 teragrams of carbon dioxide equivalent per year ($TgCO_2$-eq/yr) in the first decade (1950–1959) to 30.93 $TgCO_2$-eq/yr in the last decade (2000–2009). The combined global warming potential (GWP) of both carbon dioxide (CO_2) and methane (CH_4) was 33 $TgCO_2$-eq/yr over the historical period. Wetland ecosystems in Alaska were projected to be a net carbon sink ranging from 3.0 to 6.8 TgC/yr and an increased methane source ranging from 37 to 90 $TgCO_2$-eq/yr by 2099, yielding a GWP of 17 to 64 $TgCO_2$-eq/yr.
- Temperate forests in south-central and southeast coastal Alaska store 1,018 teragrams of carbon (TgC) in live and dead tree biomass. If managed with the current management plan (with forest harvesting) and assuming no climate change, the forest carbon could increase by 1 percent by the end of the century. Forest carbon could increase by 8 percent and 27 percent under the scenarios of climate change with and without management, respectively.
- The total net carbon flux (coastal export plus CO_2 emissions from rivers and lakes minus burial in lake sediments) from inland waters of Alaska was approximately 41.2 TgC/yr (ranging from 30 to 60 TgC/yr in terms of 5th and 95th percentiles). Total carbon yield based on total land surface area was 27 $gC/m^2/yr$ (uncertainty of 20 to 40 $gC/m^2/yr$).
- Putting it all together, we estimate that between 1950 and 2009 the upland and wetland ecosystems of the State sequestered an average of 3.7 TgC/yr, which is almost 2 percent of the net primary productivity (NPP) of the upland and wetland ecosystems. We estimate that inland aquatic ecosystems of Alaska lost 41.2 TgC/yr, or about 17 percent of upland and wetland NPP. We estimate that the greenhouse gas (GHG) forcing potential of upland and wetland ecosystems of Alaska was 17.3 $TgCO_2$-eq/yr during the historical period.
- Carbon sequestration of upland and wetland ecosystems of Alaska in the projection period (2010–2099) would increase substantially to 18.2 to 34.4 TgC/yr, primarily because of an increase in NPP of 12 to 30 percent associated with responses to rising atmospheric CO_2, increased nitrogen cycling, and longer growing seasons. Although carbon emissions to the atmosphere from wildfire were projected to increase substantially for all of the projected climates, the increases in NPP would more than compensate for those losses. Our analysis indicates that upland and wetland ecosystems would be sinks for GHGs for all simulations during the projection period.

Limitations of the Assessment Report

The known limitations of the assessment report include the following: (1) So far as substantial progress was made in this assessment in terms of findings from data, remote sensing, and model simulations for Alaska ecosystems, the availability of field data is severely limited relative to the conterminous United States in all but the coastal forest region (North Pacific LCC). This limitation, and implications to uncertainties in the results, applies to analyses of permafrost and soil carbon in chapter 3, analyses of upland and wetland carbon and CH_4 in chapters 6, 7, and 9, and analysis of aquatic CO_2 in chapter 8. (2) The analysis of future forest carbon projections (chapter 5) in the temperate coastal Alaska region did not include all major management and climate change scenarios. (3) The estimates of terrestrial ecosystem carbon stocks and fluxes were based on a static land-cover distribution. Land-cover changes associated with wildfire disturbances that were reported in chapter 2

were not represented in the model simulations conducted in chapters 6 and 7. Instead, the effects of fire disturbances on carbon and CH_4 were simulated internally by the biogeochemical modeling. (4) Similarly, CH_4 emission was simulated based on one wetland distribution map. Given the high sensitivity of modeled CH_4 emission to the inundation area, the current assessment did not quantify the uncertainty associated with wetland mapping. (5) The assessment included wildfires as the major disturbance regime in assessing its effects on carbon and CH_4 dynamics in boreal and arctic regions of Alaska. However, effects of other major disturbances, such as forest insects in temperate and boreal regions, and thermokarst disturbances associated with ice-rich permafrost thaw in lowland boreal and arctic regions, were not included in the assessment. (6) The process-based models used in this study, although extensively evaluated in this assessment and in previous studies, have substantial conceptual and parameterization uncertainties. (7) The study of inland aquatic ecosystems was not integrated with that of upland and wetland ecosystems in a seamless analysis, which likely would compromise the estimates of heterotrophic respiration because losses of carbon to aquatic ecosystems from upstream ecosystems are not taken into account.

With regard to future assessments, the technical needs for reduction of uncertainties present in this assessment will require enhancements in observation systems, research on landscape dynamics, process-based research, and modeling research. Key enhancements in observation systems include forest inventory measurements in interior Alaska, CO_2 concentration measurements in large lakes, and CH_4 emissions from lakes and wetlands. Key enhancements in landscape dynamics include improved regional datasets on vegetation dynamics, lake dynamics, insect disturbance, and thermokarst disturbance. Key enhancements in process-based research include improved understanding of the transfer of carbon between terrestrial and inland aquatic ecosystems, of CH_4 dynamics of inland aquatic ecosystems, and of controls over insect and thermokarst disturbance. Finally, key enhancements in modeling research include the development of models that can treat terrestrial-aquatic carbon linkages as an integrated system, improved modeling of wetland and lake CO_2 and CH_4 dynamics, and the prognostic modeling of insect and thermokarst disturbance and their impacts on carbon dynamics. Although there are substantial uncertainties in our analyses, the analyses themselves represent state-of-the-art science, and this assessment provides information for priorities in reducing uncertainties that should improve future assessments.

Chapter 1. Introduction

By A. David McGuire,[1] T. Scott Rupp,[2] Tom Kurkowski,[2] and Sarah Stackpoole[3]

1.1. Requirements

This report is the result of an assessment focused on ecosystems of the State of Alaska and conducted by an interagency and interdisciplinary team composed of scientists from the U.S. Geological Survey (USGS), the U.S. Department of Agriculture (USDA) Forest Service, and the University of Alaska-Fairbanks. The reporting of the assessment results partially fulfills requirements set forth by the U.S. Congress through the Energy Independence and Security Act (EISA) of 2007 for a national carbon sequestration and greenhouse-gas (GHG) flux assessment. The national assessment has been completed for the conterminous United States, with results provided in three separate regional reports (Zhu and others 2011; Zhu and Reed, 2012, 2014). The main outcomes of this Alaska assessment include (1) estimates of the amount of carbon stored in ecosystems (such as forests and wetlands), (2) estimates of the capacity of ecosystems to sequester carbon, (3) estimates of the rate of GHG fluxes in and out of the ecosystems, and (4) evaluation of the effects of processes or driving forces that control ecosystem carbon balance and GHG fluxes. Climate change, ecosystem disturbances, wildfire, land use change, and land management represent the major driving forces, but their relative effects on an ecosystem's potential for carbon sequestration vary regionally within Alaska. Information derived from the assessment is intended to inform mitigation and adaptation policies and land management decisions. This assessment also adds to our scientific understanding of the effects of environmental change on high-latitude ecosystem processes.

The relative importance of driving forces that affect carbon storage and other ecosystem services vary regionally within Alaska (Wolken and others, 2011). For example, ongoing warming in arctic and boreal regions of Alaska, which influences ecosystem disturbances such as wildfire, insect outbreaks, and permafrost degradation, has the potential to substantially alter (1) the exchange of carbon dioxide (CO_2) and methane (CH_4) between ecosystems and the atmosphere and (2) the overall ecosystem carbon balance (Kurz and others, 2008; McGuire and others, 2009, 2010; Hayes and others, 2012; Yuan and others, 2012). The maritime region of southern and southeastern Alaska features dense forest cover and active forest management and other land uses such as recreation and urban centers (Wolken and others, 2011). Forest harvesting and changes in forest management policies have had profound effects on age, composition, carbon stock, and productivity of the temperate moist forests and forested wetlands in southeast Alaska (Leighty and others, 2006). Thus, the dynamics of ecosystem carbon balance and CO_2 and CH_4 exchange of arctic, boreal, and maritime regions of Alaska in response to changes in major driving factors are the focus of this assessment. Arctic tundra, alpine tundra, boreal forests, maritime forests, surface waters (rivers and lakes), and arctic, boreal, and maritime wetlands are the main ecosystem types considered in this assessment.

To support the outcomes of the assessment for the entire State of Alaska, the assessors sought to address questions within regions of Alaska. These questions include (1) what are the magnitudes of carbon pools and fluxes of soil, biomass, and surface waters for different regions of Alaska?; (2) how are changes in fire regime, vegetation distribution, permafrost dynamics, and forest management influencing carbon balance in different regions of Alaska?; and (3) how might estimated sources and sinks of CO_2 and CH_4 of arctic, boreal, and maritime ecosystems change in response to projected changes in climate, fire regime, permafrost dynamics, and forest management?

Unlike the rest of the United States, much of Alaska has not traditionally been included in various resource inventories, nor has the State previously been included in any major national carbon and greenhouse inventory reports. The lack of field data as input into assessment methods, the diverse land cover, and the rapid changes in driving factors were a challenge to the assessors and necessitated the use of methods and models (introduced below) that are different from those used for the conterminous United States.

[1]U.S. Geological Survey, Fairbanks, Alaska.

[2]University of Alaska-Fairbanks, Fairbanks, Alaska.

[3]U.S. Geological Survey, Denver, Colo.

1.2. Geography

1.2.1. Reporting Regions for the Inland Waters' Component of the Assessment

The reporting regions for the inland waters' component of this assessment are based on the six main hydrologic units of Alaska: the Arctic Slope (called North Slope in this report), Northwest, Yukon, Southwest, South-Central, and Southeast (Seaber and others, 1987). These regions were chosen as the reporting units because, unlike the Alaska Landscape Conservation Cooperatives used in the terrestrial component of this report as described below, the hydrologic units have boundaries that coincide with natural drainage areas for rivers within the State, as hydrologic data from these units were important for developing estimates on inland water carbon fluxes. Descriptions and a map of the regional hydrologic units are presented in chapter 8.

1.2.2. Reporting Regions for the Terrestrial Component of the Assessment

The five reporting regions for the terrestrial component of this assessment are based on the four large terrestrial Landscape Conservation Cooperatives (LCCs) in Alaska: (1) the Arctic LCC, (2) the Western Alaska LCC, (3) the Northwest Boreal LCC (split into northern and southern reporting regions), and (4) the North Pacific LCC (fig. 1.1). These regions were chosen so that the results of the terrestrial component of the assessment could inform regional consortia of natural resource agencies, which have been organized into these LCCs. The Northwest Boreal LCC was split into two reporting regions because the fire regime is quite different between the northern and southern parts of this LCC, which are separated by the Alaska Range. The boundaries of these LCCs are based on several sources discussed below, including six level II U.S. Environmental Protection Agency (EPA) ecoregions in Alaska (Gallant and others, 1995), which are derived from the ecoregions of Omernik (1987; http://archive.epa.gov/wed/ecoregions/web/html/na_eco.html), listed from north to south: the Alaska Tundra, Brooks Range Tundra, Alaska Boreal Interior, Taiga Cordillera, Boreal Cordillera, and Marine West Coast Forest Ecoregions (fig. 1.2). The following sections provide a brief description of each LCC, list the level III ecoregions, and provide links to additional details for each LCC region. A detailed description of each level III ecoregion, summarizing the climate, physiography, hydrology, and vegetation, can be found in Gallant and others (1995). This geographic characterization provides a foundation for understanding the differences in carbon sequestration and fluxes among LCCs and ecoregions in Alaska.

The LCCs' geographic areas were developed by a team of U.S. Fish and Wildlife Service and U.S. Geological Survey scientists and experts by integrating several data sources

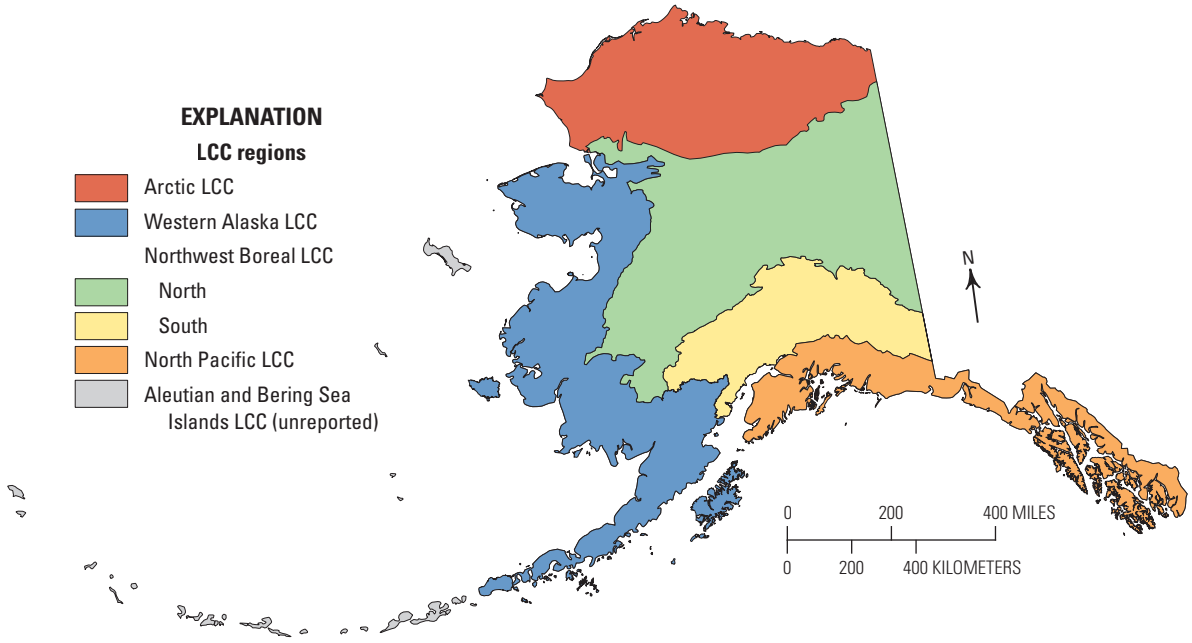

Figure 1.1. Reporting regions considered in this assessment; the regions were based on the boundaries of the Arctic, Western Alaska, Northwest Boreal, and North Pacific Landscape Conservation Cooperatives (LCCs) in Alaska. The land area within the Aleutian and Bering Sea Islands LCC (identified as unreported) was not considered because the models used in this study are poorly suited to represent ecosystem dynamics in this unique region. The Northwest Boreal LCC was divided into northern and southern reporting regions owing to differences in fire regime on either side of the Alaska Range.

(U.S. Fish and Wildlife Service, 2010). First, Bird Conservation Regions (BCRs) were incorporated; they are biologically based units used by long-term partners to facilitate conservation planning and design at landscape scales. To account for aquatic species' needs, the Freshwater Ecoregions of the World, which is the same framework adopted by the National Fish Habitat Action Plan (NFHAP), was incorporated. To account for terrestrial species' needs, Omernik's level II and other existing ecological units were used (U.S. Fish and Wildlife Service, 2010). The resulting geographic framework identified large regions that crossed State and Federal administrative boundaries. In most geographic areas, the boundaries of key partnerships were left intact to preserve existing conservation and science capacities.

1.2.2.1. Arctic Landscape Conservation Cooperative and Associated Ecoregions

The Arctic LCC (www.arcticlcc.org) region includes the Arctic Plains and Mountains Bird Conservation Region (BCR), which spans northern Alaska and Canada. The Arctic LCC encompasses three level III ecoregions: (1) the rugged slopes and valleys of the Brooks Range ecoregion, (2) the rolling hills and plateaus of the Arctic Foothills ecoregion, and (3) the broad, flat Arctic Coastal Plain ecoregion, which is characterized by extensive wetlands and numerous water bodies. The Arctic LCC has arctic climate conditions, with very low mean annual temperatures and very low annual precipitation. It is essentially a treeless region dominated by herbaceous vegetation, although shrub vegetation is found in better drained areas where soil moisture is not limiting. The region is underlain by continuous permafrost. Wildfire is constrained to mesic sites and, although common, represents a minimal amount of the area burned annually statewide.

1.2.2.2. Western Alaska Landscape Conservation Cooperative and Associated Ecoregions

The Western Alaska LCC (https://westernalaskalcc.org/SitePages/Western Alaska LCC.aspx) includes the Western Alaska Bird Conservation Region as well as small portions of the Northwestern Pacific Rainforest and Northwest Interior Forest BCRs. The LCC spans over 1,200 kilometers (km) from north to south and includes a wide diversity of terrain. Landscapes include the permafrost-dominated tundra of the Seward Peninsula, complex delta systems of the Yukon and Kuskokwim Rivers, abundant volcanoes of the Alaska Peninsula, and transitional forests of permafrost-free Kodiak Island. The Western Alaska LCC includes portions of seven level III ecoregions: (1) the Subarctic Coastal Plains, (2) the Seward Peninsula, (3) the Ahklun and Kilbuck Mountains, (4) the Bristol Bay-Nushagak Lowlands, (5) the Alaska Peninsula Mountains, (6) the Interior Forested Lowlands and Uplands, and (7) the Interior Bottomlands ecoregions.

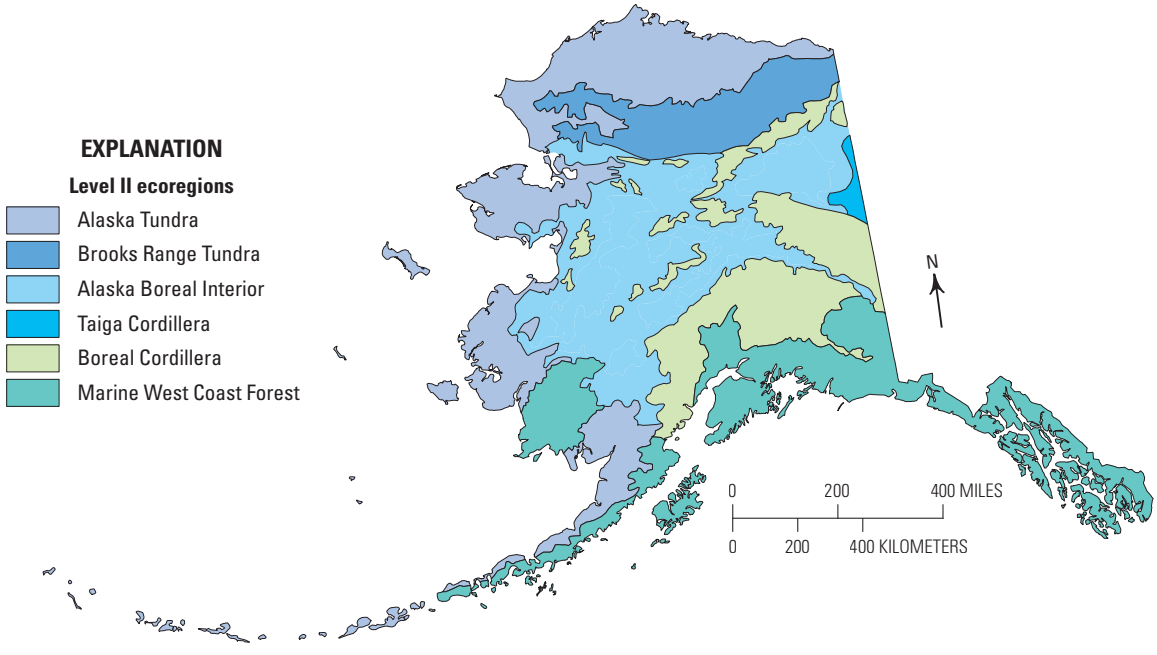

Figure 1.2. The six level II ecoregions for the State of Alaska from Gallant and others (1995).

The climate is transitional between maritime and continental influences, and temperature and precipitation are variable throughout the region. Most of the region is treeless and supports wet to mesic graminoid herbaceous vegetation. Some forest stands are present in valley bottom regions. Permafrost distribution is discontinuous and variable. Wildfires are common in the more mesic portions of the region and range in size from less than 1 to more than 1,000 square kilometers (km^2).

1.2.2.3. Northwest Boreal Landscape Conservation Cooperative and Associated Ecoregions

The Northwest Boreal LCC (http://nwblcc.org/) boundary closely follows that of the Northwestern Interior Forest Bird Conservation Region. The LCC falls within the boreal forest biome and includes south-central and interior Alaska and parts of Canada: most of the Yukon Territory, the northern portion of British Columbia, and a small part of the Northwest Territories. The area includes over 1.3 million km^2 and encompasses large portions of the Yukon, Kuskokwim, Susitna, and Copper River Basins. The Northwest Boreal LCC includes nine level III ecoregions: (1) the Interior Forested Lowlands and Uplands, (2) the Interior Highlands, (3) the Interior Bottomlands, (4) the Yukon Flats, (5) the Ogilvie Mountains, (6) the Cook Inlet, (7) the Alaska Range, (8) the Copper Plateau, and (9) the Wrangell Mountains ecoregions.

The Northwest Boreal LCC domain encompasses not only a very large land area but also significant gradients in climate, hydrology, and disturbance dynamics (particularly with respect to wildfire and insect outbreaks). For this reason, the Northwest Boreal LCC was divided into northern and southern subregions that reflect the substantial differences in climate (continental versus maritime influenced) and disturbance (wildfire versus insects) found on opposite sides of the Alaska Range; the division was based on an existing model's specific subregion calibration related to the "Unified Ecoregions of Alaska" (Nowacki and others, 2003). For assessment reporting purposes throughout the remainder of this report, results are reported for Northwest Boreal LCC North and Northwest Boreal LCC South.

The Northwest Boreal LCC North has a discontinuous permafrost distribution that is highly variable. The region is influenced by a strong continental climate with seasonal temperature extremes and low precipitation. The region is primarily forested. Wildfire is common, and fires range in size from less than 1 to more than 3,000 km^2.

The Northwest Boreal LCC South also has a discontinuous permafrost distribution that is highly variable. The region includes significant high-elevation mountainous terrain. The region is influenced by a maritime climate with variable but relatively high precipitation. The region is primarily forested. Wildfire is common but represents a relatively small proportion of the area burned annually statewide.

1.2.2.4. North Pacific Landscape Conservation Cooperative and Associated Ecoregions in Alaska

The North Pacific LCC (http://northpacificlcc.org/) encompasses the Northwest Pacific Rainforest Bird Conservation Region. The LCC includes the entire range of the Pacific Coastal Temperate Rainforest extending over 3,500 km from Alaska through British Columbia in Canada and into three States in the conterminous United States: Washington, Oregon, and northern California. For this assessment, the focus is on only the portion of the LCC within Alaska. In Alaska, the North Pacific LCC includes three level III ecoregions: (1) the Alaska Peninsula Mountains, (2) the Pacific Coastal Mountains, and (3) the Coastal Western Hemlock-Sitka Spruce Forests ecoregions.

The North Pacific LCC is characterized by complex topography with steep and rugged mountains and significant glaciers and ice fields. Its climate has a maritime influence with moderate temperatures and high but variable annual precipitation ranging from 510 to 3,900 millimeters (mm). Wildfires are rare, usually human caused, and restricted to sizes less than 0.4 km^2. Through 2014, about 452,000 acres of timber have been harvested within the national forest lands of this region (U.S. Department of Agriculture Forest Service, 2014). The region is generally free of permafrost. Forests of western hemlock (*Tsuga heterophylla*) and Sitka spruce (*Picea sitchensis*) along with western redcedar (*Thuja plicata* Donn ex D. Don) and yellow-cedar (*Callitropsis nootkatensis* (D. Don) D.P. Little; naming after Hennon and others, 2016) are widespread.

1.3. A Brief Overview of Previous Studies of Carbon Dynamics in Alaska

The historical carbon dynamics of ecosystems in Alaska have been studied at local, subregional, and regional scales. Methods of analysis included the use of observations and process-based models. This section summarizes recent syntheses of data on historical carbon storage and dynamics by methodology.

There have been several observational syntheses of data on soil carbon storage in Alaska at the statewide level. These include studies focused on understanding controls over carbon storage across the State, as well as studies focused on estimating the magnitude of carbon storage in the State. Johnson and others (2011) conducted a first-order assessment of the spatial distributions of soil carbon in Alaska from a soil carbon database compiled to better understand controls over soil carbon storage across the State. Temperature and landform type were the dominant controls on soil carbon distribution for selected ecoregions. Mean soil carbon pools (to a depth of 1 meter [m]) varied by threefold, sevenfold, and tenfold across ecoregion, landform, and ecosystem types, respectively. Climate interactions with landform type and soil

carbon were greatest in the uplands. For upland soil, there was a sixfold nonlinear increase in soil carbon with a decrease in latitude (that is, with an increasing temperature gradient), where soil carbon was lowest in the intermontane boreal ecoregion compared to the arctic tundra and coastal rainforest regions. Additional factors that appeared to be related to soil carbon distribution within ecoregions included stand age, aspect (direction faced by a slope), and permafrost presence or absence in black spruce (*Picea mariana* (Mill.) Britton, Sterns & Poggenb.) stands. Johnson and others (2011) estimated that soil carbon storage to a depth of 1 m in Alaska soils ranged from 14,000 grams of carbon per square meter (gC/m^2) in intermontane boreal forests to 25,000 gC/m^2 in coastal rainforests to 44,000 gC/m^2 in arctic tundra. Bliss and Maursetter (2010) estimated soil organic carbon in Alaska totaling 48 petagrams of carbon (PgC) and used much of the same information as Johnson and others (2011). Using a geostatistical approach, Mishra and Riley (2012) estimated that Alaska soils stored 77 PgC, of which 61 percent was in the active layer, 27 percent was in permafrost, and 12 percent was in nonpermafrost soils. The differences among these estimates indicate that substantial gaps exist in the soil carbon databases used to develop these estimates (see Johnson and others, 2011).

Analyses of vegetation carbon storage in Alaska have focused primarily on forests. Yarie and Billings (2002) estimated that aboveground carbon storage was approximately 400 teragrams of carbon (TgC) (averaging about 2,400 gC/m^2) in the boreal forests of the State; their work was based on several one-time inventories between 1963 and 1994. Leighty and others (2006) and Barrett (2014) estimated that aboveground carbon storage in trees was between 420 and 530 TgC in the Tongass National Forest of southeast Alaska, with another 120 TgC in belowground roots. Barrett and Christensen (2011) estimated that coastal forests of southeast and south-central Alaska stored approximately 650 TgC in aboveground trees. Statewide, these estimates indicate that aboveground carbon of forests in Alaska was likely greater than 1,000 TgC in 2009.

Some observational syntheses of the exchange of carbon with the atmosphere in Alaska have been based largely on scaling of chamber and eddy covariance measurements of CO_2 and CH_4 exchange. Manual chambers, automatic chambers, and eddy covariance towers use infrared gas analyzers that measure CO_2 concentrations. For CH_4, the field technology is less developed and has relied on gas sample collection in the field, with laboratory estimates of CH_4 concentrations made by using gas chromatographs. Eddy covariance measurement systems have recently been developed that allow continuous direct CH_4 concentration estimates in the field, and these are starting to be more commonly used to measure CH_4 exchange.

In an observational synthesis for arctic tundra of North America, which was dominated by measurements made in Alaska, McGuire and others (2012) suggested that arctic tundra in Alaska was an annual source of CO_2 to the atmosphere between 1990 and 2009 of 10±20 gC/m^2 and that the release of CO_2 in winter more than offset the uptake of CO_2 during the summer. Although the synthesis suggested that arctic tundra in Alaska was a source of CO_2 to the atmosphere, the uncertainties include the possibility that it could have been an annual sink of CO_2 between 1990 and 2009. The synthesis also suggested that arctic tundra in Alaska was an annual source of CH_4 to the atmosphere of 5.4±3.5 grams of carbon in methane per square meter ($gC\text{-}CH_4/m^2$) between 1990 and 2009.

In a recent synthesis of eddy covariance studies in Alaska, Ueyama and others (2013) evaluated factors influencing CO_2 exchange in eight Arctic tundra and five boreal ecosystems in the State and found that all of the boreal and seven of the eight Arctic tundra ecosystems acted as CO_2 sinks during the growing season. The analysis revealed that there was a high sensitivity of the sink strength in tundra ecosystems to growing season length, whereas time since fire disturbance played a major role in the sink strength of boreal ecosystems. Thus, the analysis suggested that tundra ecosystems might increase sink strength during the growing season in response to warming, but that an increasing fire frequency would likely decrease sink strength in boreal ecosystems of Alaska.

Some syntheses of the exchange of carbon with the atmosphere within Alaska have been based on the analysis of forest inventory data. The repeated inventory of forests in Alaska has largely been focused on Tongass National Forest in southeast Alaska and Chugach National Forest in south-central Alaska, although some one-time inventories have been conducted in other parts of Alaska. The most recent analyses by the Forest Inventory and Analysis (FIA) program of the USDA Forest Service indicates that forest carbon stocks in southeast and south-central Alaska increased by approximately 6±3 teragrams of carbon per year (TgC/yr) between 1990 and 2013 (U.S. Department of Agriculture Forest Service, 2015). On the basis of the analysis of one-time inventories conducted between 1963 and 1987 outside of maritime coastal Alaska, Yarie and Billings (2002) estimated that boreal forests in Alaska were an annual sink for 9.65 TgC in the last few decades of the last century.

Previous research regarding carbon fluxes of rivers in Alaska has focused on the main stem Yukon River and its tributaries, large rivers that drain the North Slope, and small streams in the southeast. Yukon River total carbon exports have been estimated to be 7.8 TgC/yr, with 70 percent of the total carbon flux as dissolved inorganic carbon (Striegl and others, 2007). For the North Slope, estimates of organic carbon export from the Sagavanirktok, Kuparuk, and Colville Rivers were approximately 0.3 TgC/yr. The Yukon River Basin has an area of 831,000 square kilometers (km^2), and the three North Slope rivers sum to a total drainage area of 80,000 km^2, producing yields of 9.4 grams of carbon per square meter per year ($gC/m^2/yr$) and 2.5 $gC/m^2/yr$, respectively. Rates of stream organic carbon exports for the southeastern regions of Alaska, mainly draining the coastal temperate rain forest, have been estimated as being between 10.5 and 30 $gC/m^2/yr$ (D'Amore and others, 2015).

Riverine CO_2 fluxes to the atmosphere have also been documented in the Yukon River Basin at 7.7 TgC/yr, or 9.2 $gC/m^2/yr$. These emission rates are roughly equivalent to total lateral carbon transport. Estimates of CO_2 emissions for rivers in the Kuparuk River Basin ranged between 0.02 $gC/m^2/yr$ for the time period of 2001 to 2013 (Cory and others, 2014) and 1.7 $gC/m^2/yr$ for 1994 to 1996 (Hobbie and Kling, 2014). Lake CO_2 fluxes in the North Slope region of Alaska have been documented as being between 0.4 and 1.1 $gC/m^2/yr$ (Cory and others, 2014; Hobbie and Kling, 2014). Many studies of glacial lakes, with objectives that included documenting long-term climate change (Anderson and others, 2001; Yu and others, 2008) and its effects on wildlife population dynamics (Barto, 2004; Rogers and others, 2013), are based on sediment analyses that provide lake carbon burial rates. From these studies and many others, estimates for carbon burial in glacial lakes throughout the State range between 0.62 and 30 $gC/m^2/yr$ (for example, Anderson and others, 2001; Yu and others, 2008; Rogers and others, 2013). Carbon burial estimates for thermokarst lakes in the interior and North Slope regions of Alaska are between 2 and 23 $gC/m^2/yr$ (Lynch and others, 2002; Mann and others, 2002).

Comparisons among Terrestrial Biosphere Models (TBMs) indicate that the models do not agree about whether the North Slope of Alaska is a source or a sink for atmospheric CO_2. An analysis of model output from numerous TBMs indicates that net ecosystem exchange of CO_2 with the atmosphere is -10 ± 190 $gC/m^2/yr$ (the minus sign indicates a sink; Fisher and others, 2014). It is important to note that most of the TBMs in the model comparison represent tundra on the North Slope of Alaska as equivalent to temperate grassland, which is not physiologically representative of the wetland, graminoid, and shrub tundra that occurs on the North Slope. The analysis of TBM output results in inflated estimates of uncertainty about carbon dynamics in Alaska because these TBMs generally do not include processes such as permafrost dynamics and wildfire that are relevant to the region.

An analysis of tundra carbon dynamics in the Arctic Ocean Drainage Basin suggested that arctic tundra has been a weakening sink for atmospheric CO_2 in recent decades because of the effects of climate in enhancing decomposition even though vegetation carbon of tundra was estimated to be increasing (McGuire and others, 2010; Hayes and others, 2011, 2014). An analysis by Euskirchen and others (2009) suggested that vegetation carbon in tundra of the North Slope of Alaska will continue to increase in the 21st century because of longer growing seasons and increased soil nitrogen availability leading to more leaf area, but that soil carbon losses will greatly outpace the gains in vegetation carbon.

An analysis of boreal forest carbon dynamics in the Arctic Ocean Drainage Basin, which is dominated by boreal forest, suggested that boreal forest was transitioning from being a sink to being a source because of the combination of both enhanced decomposition associated with permafrost thaw and an increase in wildfires throughout the region (McGuire and others, 2010; Hayes and others, 2011, 2014). A process-based model analysis of boreal forest carbon dynamics in the Yukon River Basin in Alaska and Canada is consistent with the panboreal analysis, as it indicated that soil carbon stocks would have increased by 158 TgC between 1960 and 2006 if the basin had not undergone warming and changes in fire regime (Yuan and others, 2012). Together, these analyses of the results of process-based models suggest that there is a complex interplay between the effects of climate and wildfire on vegetation and soil carbon dynamics, and that both climate and wildfire can influence these dynamics through effects on permafrost.

Similar to the analysis of CO_2 exchange, comparisons among TBMs indicate that the models do not agree about whether the North Slope of Alaska is a source or a sink for atmospheric CH_4. An analysis of model output from several CH_4 models indicated that emissions were estimated to be 2.52 ± 4.02 grams of methane per square meter per year ($gCH_4/m^2/yr$) in the early 2000s (Fisher and others, 2014). Another analysis indicated that estimated emissions of CH_4 between 1980 and 1996 were 4.01 $gCH_4/m^2/yr$ in tundra of the North Slope of Alaska, 2.00 $gCH_4/m^2/yr$ in interior Alaska, and 0.99 $gCH_4/m^2/yr$ in southern Alaska (Zhuang and others, 2007). Zhuang and others (2007) estimated that combined emissions for Alaska between 1980 and 1996 were approximately 3 teragrams of methane per year ($TgCH_4/yr$), which is somewhat higher than the estimate of 2.1 teragrams of methane ($TgCH_4$) for Alaska from May to September 2012 that was based on data from an aircraft sampling campaign (Chang and others, 2014). The analysis by Zhuang and others (2007) further estimated that climate change would cause CH_4 emissions to increase by 58 percent in northern Alaska, 77 percent in interior Alaska, and 153 percent in southern Alaska by the end of the 21st century. Sensitivity analysis in the study indicated that soil temperature and depth to water table were the two most important drivers influencing changes in emissions. This regional analysis suggests that the response of methane emissions depends on interactions between changes in projected temperature and soil hydrology.

In summary, analyses to date have indicated substantial variability in estimates of carbon pools and carbon fluxes in Alaska. Estimates of soil carbon storage varied from 48 to 77 PgC. Estimates of total vegetation carbon at the statewide scale have not been formally assessed; however, estimates of vegetation carbon storage conducted for forests at the regional scale indicated that aboveground carbon is likely greater than 1,000 TgC at the statewide scale. Analyses of carbon fluxes in tundra and boreal forests in Alaska indicate substantial uncertainty as these ecosystems have been estimated to be both sources and sinks for atmospheric CO_2 in different studies. There is general agreement that maritime forests of Alaska are a sink for atmospheric CO_2 of less than 10 TgC/yr. Although analyses indicate that there are substantive fluxes of carbon from inland waters in some hydrologic basins of Alaska, these fluxes have not yet been estimated for all inland waters in Alaska. Finally, analyses of CH_4 emissions for Alaska are quite variable and indicate substantial uncertainty.

1.4. Overall Methodology

The methodology developed for this assessment was designed to produce a scientific synthesis of carbon dynamics in the State that would be useful both to stakeholders in Alaska and to State, national, and international decision makers. This goal required the organization of input data for the State and technical components to make use of these data (fig. 1.3). The technical components include (1) the organization of input data for models and data syntheses; (2) modeling of processes in biogeography, fire regime, permafrost, and hydrologic dynamics; (3) syntheses of carbon dynamics via biogeochemical modeling for upland and wetland ecosystems, empirical syntheses of carbon cycling for ecosystems in south-central and southeast coastal Alaska, and syntheses of carbon fluxes for surface waters of Alaska; and (4) analysis, synthesis, report development, data distribution, and communication of results to stakeholders. The assessment is prepared for a historical period (1950–2009) and a future projection period (2010–2099).

Input data were organized for soil carbon; soil texture; permafrost distribution; active-layer thickness; vegetation carbon; historical forest harvest; future forest management; land-cover distribution; fire disturbance; wetland and surface-water distribution; historical and future climate; upland and wetland biogeochemistry; and the transport, emission, and burial of aquatic carbon. The historical and future climate and fire disturbance datasets are described in chapter 2; data syntheses for soil carbon, permafrost, and soil texture are described in chapter 3; biogeochemical cycling, vegetation biomass, historical forest harvest, and future forest management scenarios for forests in south-central and southeast Alaska are described in chapters 4 and 5; upland extent and biogeochemistry are described in chapter 6; wetland extent and biogeochemistry are described in chapter 7; and the transport, emission, and burial of aquatic carbon are described in chapter 8.

The assessment uses the Alaska Frame-Based Ecosystem Code (ALFRESCO; Rupp and others, 2000, 2002) to simulate changes in fire regime and vegetation distribution from 2010 through 2099. ALFRESCO was calibrated on the basis of historical data about fire occurrence for Alaska from 1950 through 2009 (see chapter 2 for more details). The contemporary spatial distribution of permafrost was estimated by two different empirical approaches (see chapter 3). The empirical estimates were then used to validate permafrost simulation for the historical period (1950–2009) by the Dynamic Organic Soil version of the Terrestrial Ecosystem Model (DOS-TEM; Yi, Manies, and others, 2009; Yi, McGuire, and others, 2009; Yi and others, 2010; Yuan and others, 2012; Genet and others, 2013).

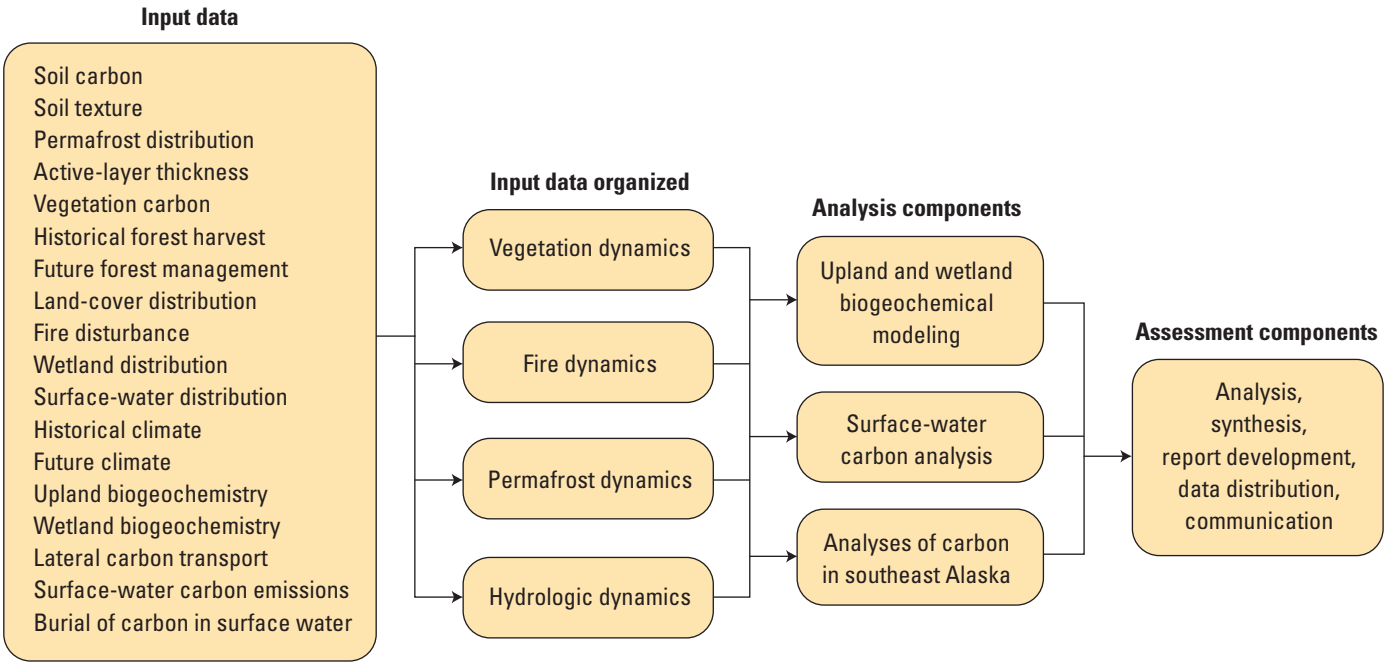

Figure 1.3. The general methodology used in the assessment of carbon storage and fluxes in Alaska. Input data were organized to provide information used to assess historical and future changes in vegetation, fire, permafrost, and hydrologic dynamics. The data on these changes were then used to assess carbon dynamics of inland aquatic ecosystems for the historical period (1950–2009) and carbon dynamics of upland and wetland ecosystems for the historical period and the future projection period (2010–2099). The results of these carbon assessments have been synthesized and are summarized in this report. The data from this assessment are being made available for distribution.

The DOS-TEM model used input data on soil texture, land cover, historical climate, historical fire, historical forest harvest, and model projections of future climate, fire disturbance, and forest management to estimate changes in ecosystem pools and fluxes for the two time periods for upland and wetland ecosystems. In addition, these upland and wetland estimates were also separately evaluated as described in chapters 6 and 7. The Methane Dynamics Module of the Terrestrial Ecosystem Model (MDM-TEM; Zhuang and others, 2004, 2007) was used to estimate methane consumption in upland ecosystems (chapter 6) and both methane consumption and emissions in wetland ecosystems (chapter 7). An empirical model was used to estimate contemporary net ecosystem carbon balance of forest ecosystems in southeast Alaska (chapter 4). A Forest Vegetation Simulator (FVS) model was also used, together with FIA forest inventory data, for estimating contemporary and future forest carbon balance in relation to management actions in south-central and southeast coastal Alaska (chapter 5).

A statewide map of lake area (U.S. Geological Survey, 2012); modeled discharge, velocity and width values for streams (Kost and others, 2002); carbon concentration in surface waters; and carbon burial rates in lakes were assimilated into empirical models to estimate regional and statewide estimates of carbon transport, emission, and burial in aquatic ecosystems of Alaska (chapter 8).

1.5. Land-Cover Maps Used in the Assessment

To make comparisons between various aspects of this assessment, a common land-cover classification was required; this section describes the development of the common land-cover classification used for the assessment from existing land-cover maps. Other datasets used in the assessment are described in various chapters, as indicated above. The definition of land-cover types in the common land-cover classification we developed for this assessment was primarily driven by the needs of ALFRESCO and DOS-TEM, which required highly aggregated land-cover types. Remote-sensing datasets defining land cover for Alaska and western Canada were used to develop more aggregated baseline vegetation input data as the spatial foundation for the assessment. These input datasets represented highly modified output originating from the North American Land Change Monitoring System 2005 (NALCMS 2005) dataset (North American Land Change Monitoring System, 2010; for arctic and subarctic ecosystem types) and the National Land Cover Database (NLCD) 2001 (Homer and others, 2007; for coastal maritime ecosystem types). The NALCMS 2005 data were originally at a 250-m resolution and the NLCD at a 30-m resolution. The modified input data from both datasets were resampled to a consistent 1-km resolution to reduce the volume of data and meet modeling requirements.

Several adjustments were made to the thematic classes to facilitate this assessment and to correspond with the capabilities of the methods used. To define land-cover types for the Arctic, Western Alaska, and Northwest Boreal LCCs, the NALCMS 2005 classes were adjusted to represent the general land-cover types of black spruce (*Picea mariana* (Mill.) Britton, Sterns & Poggenb.) forest, white spruce (*Picea glauca* (Moench) Voss) forest, deciduous forest, shrub tundra, graminoid tundra, wetland tundra (including wet-sedge and tussock tundra), and heath tundra. Partitioning of coniferous forest into late successional spruce forest types was based on topographic position. Tundra land-cover types were partitioned primarily on the basis of ecoregion distribution and growing season temperature thresholds; the Circumpolar Arctic Vegetation Map (CAVM Team, 2003) was used to define the tree line. Heath tundra includes xeric ecosystems dominated by lichen crust and moss and was defined as high-elevation barren land not covered by snow or ice, as well as land included in the barren lichen-moss classes from the NALCMS 2005 classification. For this assessment, the NALCMS 2005 classes did not adequately represent the land-cover types of the maritime zone in the North Pacific LCC region of Alaska and in the vicinity of Kodiak Island. Therefore, NLCD 2001 classes were adjusted to represent land-cover types specific to the maritime zone: maritime upland forest, maritime wetland forest, maritime alder shrubland, and maritime fen. The correlation between the general NLCD classification and the maritime land-cover types was determined through spatial comparison with local vegetation maps.

1.6. Organization of the Report

This report has an executive summary followed by nine chapters, which are briefly described below. Each chapter has its own references cited list.

Chapter 1 (Introduction) describes the requirements of this assessment, the geography of Alaska, the previous understanding of carbon dynamics in Alaska, the overall methodology of the assessment, the strategy for the land-cover maps used in the assessment, and the organization of the report.

Chapter 2 (Climate Simulations, Land Cover, and Wildfire in Alaska) describes historical observations of climate and wildfire, the downscaling and development of climate data, and results from the application of ALFRESCO to simulate changes in vegetation distribution and wildfire from 2010 through 2099.

Chapter 3 (Soil Carbon and Permafrost Estimates and Susceptibility to Climate Change in Alaska) reports on syntheses of data about soil carbon, permafrost (distribution and active-layer thickness), and soil texture for Alaska. A key feature of this chapter is the comparison of DOS-TEM outputs with these data syntheses.

Chapter 4 (Watershed Carbon Budgets in the Southeastern Alaskan Coastal Forest Region) reports results from an empirical model based on a synthesis of carbon cycling data from southeast Alaska.

Chapter 5 (Forest Inventory-Based Analysis and Projections of Forest Carbon Stocks and Changes in Alaska Coastal Forests) reports results of outputs from the USDA Forest Service Forest Vegetation Simulator (FVS) for contemporary conditions and for future forest management scenarios.

Chapter 6 (Terrestrial Carbon Modeling: Baseline and Projections in Upland Ecosystems of Alaska) reports on simulated changes in carbon pools and fluxes for the historical (1950–2009) and future projection (2010–2099) periods for upland terrestrial ecosystems of Alaska.

Chapter 7 (Terrestrial Carbon Modeling: Baseline and Projections in Lowland Ecosystems of Alaska) reports on the simulated changes in carbon pools and fluxes for the historical (1950–2009) and future projection (2010–2099) periods for wetland terrestrial ecosystems of Alaska.

Chapter 8 (Carbon Transport, Emission, and Burial from Inland Aquatic Ecosystems in Alaska) reports on contemporary estimates of the transport of carbon to coastal ecosystems, emissions of carbon from inland aquatic ecosystems to the atmosphere, and carbon burial in inland aquatic ecosystems based on syntheses of data for Alaska.

Chapter 9 (Alaska Carbon Balance) reports on the integrated carbon balance of the entire State of Alaska for the historical (1950–2009) and future projection (2010–2099) periods based on a synthesis of estimates from the other chapters in this report. The carbon balance estimates at the regional scale can be found in chapters 6, 7, and 8. This chapter is intended as a summary for use by those interested in the role that the State of Alaska plays in national and international carbon budgets.

1.7. Acknowledgments

For use of the North American Land Change Monitoring System 2005 (NALCMS 2005) dataset, we would like to acknowledge Natural Resources Canada, Instituto Nacional de Estadística y Geografía, the U.S. Geological Survey, and the Commission for Environmental Cooperation.

1.8. References Cited

Anderson, Lesleigh, Abbott, M.B., and Finney, B.P., 2001, Holocene climate inferred from oxygen isotope ratios in lake sediments, central Brooks Range, Alaska: Quaternary Research, v. 55, no. 3, p. 313–321, http://dx.doi.org/10.1006/qres.2001.2219.

Barrett, T.M., 2014, Storage and flux of carbon in live trees, snags, and logs in the Chugach and Tongass National Forests: U.S. Department of Agriculture, Forest Service, Pacific Northwest Research Station, General Technical Report PNW–GTR–889, 44 p. [Also available at http://www.fs.fed.us/pnw/pubs/pnw_gtr889.pdf.]

Barrett, T.M., and Christensen, G.A., tech. eds., 2011, Forests of southeast and south-central Alaska, 2004–2008; Five-year forest inventory and analysis report: U.S. Department of Agriculture, Forest Service, Pacific Northwest Research Station, General Technical Report PNW–GTR–835, 156 p. [Also available at http://www.fs.fed.us/pnw/pubs/pnw_gtr835.pdf.]

Barto, David, 2004, Assessing the production of sockeye salmon (*Oncorhynchus nerka*) at Chilkat Lake, southeast Alaska, using current trophic conditions and the paleolimnologic sediment record: Fairbanks, Alaska, University of Alaska, M.S. thesis, 111 p.

Bliss, N.B., and Maursetter, John, 2010, Soil organic carbon stocks in Alaska estimated with spatial and pedon data: Soil Science Society of America Journal, v. 74, no. 2, p. 565–579, http://dx.doi.org/10.2136/sssaj2008.0404.

CAVM [Circumpolar Arctic Vegetation Map] Team, 2003, Circumpolar Arctic vegetation map: U.S. Fish and Wildlife Service Conservation of Arctic Flora and Fauna (CAFF) Map No. 1, scale 1:7,500,000, http://www.geobotany.uaf.edu/cavm/.

Chang, R.Y.-W., Miller, C.E., Dinardo, S.J., Karion, Anna, Sweeney, Colm, Daube, B.C., Henderson, J.M., Mountain, M.E., Eluszkiewicz, Janusz, Miller, J.B., Bruhwiler, L.M.P., and Wofsy, S.C., 2014, Methane emissions from Alaska in 2012 from CARVE airborne observations: National Academy of Science Proceedings, v. 111, no. 47, p. 16694–16699, http://dx.doi.org/10.1073/pnas.1412953111.

Cory, R.M., Ward, C.P., Crump, B.C., and Kling, G.W., 2014, Sunlight controls water column processing of carbon in arctic fresh waters: Science, v. 345, no. 6199, p. 925–928, http://dx.doi.org/10.1126/science.1253119.

D'Amore, D.V., Edwards, R.T., Herendeen, P.A., Hood, Eran, and Fellman, J.B., 2015, Dissolved organic carbon fluxes from hydropedologic units in Alaskan coastal temperate rainforest watersheds: Soil Science Society of America Journal, v. 79, no. 2, p. 378–388, http://dx.doi.org/10.2136/sssaj2014.09.0380.

Euskirchen, E.S., McGuire, A.D., Chapin, F.S., III, Yi, S., and Thompson, C.C., 2009, Changes in vegetation in northern Alaska under scenarios of climate change 2003–2100; Implications for climate feedbacks: Ecological Applications, v. 19, no. 4, p. 1022–1043, http://dx.doi.org/10.1890/08-0806.1.

Fisher, J.B., Sikka, M., Oechel, W.C., Huntzinger, D.N., Melton, J.R., Koven, C.D., Ahlström, A., Arain, M.A., Baker, I., Chen, J.M., Ciais, P., Davidson, C., Dietze, M., El-Masri, B., Hayes, D., Huntingford, C., Jain, A.K., Levy, P.E., Lomas, M.R., Poulter, B., Price, D., Sahoo, A.K., Schaefer, K., Tian, H., Tomelleri, E., Verbeeck, H., Viovy, N., Wania, R., Zeng, N., and Miller, C.E., 2014, Carbon cycle uncertainty in the Alaskan Arctic: Biogeosciences, v. 11, p. 4271–4288, http://dx.doi.org/10.5194/bg-11-4271-2014.

Gallant, A.L., Binnian, E.F. Omernik, J.M., and Shasby, M.B., 1995, Ecoregions of Alaska: U.S. Geological Survey Professional Paper 1567, 73 p., 1 pl., scale 1:5,000,00. [Also available at http://pubs.er.usgs.gov/publication/pp1567.]

Genet, H., McGuire, A.D., Barrett, K., Breen, A., Euskirchen, E.S., Johnstone, J.F., Kasischke, E.S., Melvin, A.M., Bennett, A., Mack, M.C., Rupp, T.S., Schuur, E.A.G., Turetsky, M.R., and Yuan, F., 2013, Modeling the effects of fire severity and climate warming on active layer thickness and soil carbon storage of black spruce forests across the landscape in interior Alaska: Environmental Research Letters, v. 8, no. 4, letter 045016, 13 p., http://dx.doi.org/10.1088/1748-9326/8/4/045016.

Hayes, D.J., Kicklighter, D.W., McGuire, A.D., Chen, Min, Zhuang, Qianlai, Yuan, Fengming, Melillo, J.M., and Wullschleger, S.D., 2014, The impacts of recent permafrost thaw on land-atmosphere greenhouse gas exchange: Environmental Research Letters, v. 9, no. 4, letter 045005, 12 p., http://dx.doi.org/10.1088/1748-9326/9/4/045005.

Hayes, D.J., McGuire, A.D., Kicklighter, D.W., Gurney, K.R., Burnside, T.J., and Melillo, J.M., 2011, Is the northern high latitude land-based CO_2 sink weakening?: Global Biogeochemical Cycles, v. 25, no. 3, article GB3018, 14 p., http://dx.doi.org/10.1029/2010GB003813.

Hayes, D.J., Turner, D.P., Stinson, Graham, McGuire, A.D., Wei, Yaxing, West, T.O., Heath, L.S., de Jong, Bernardus, McConkey, B.G., Birdsey, R.A., Kurz, W.A., Jacobson, A.R., Huntzinger, D.N., Pan, Yude, Post, W.M., and Cook, R.B., 2012, Reconciling estimates of the contemporary North American carbon balance among terrestrial biosphere models, atmospheric inversions and a new approach for estimating net ecosystem exchange from inventory-based data: Global Change Biology, v. 18, no. 4, p. 1282–1299, http://dx.doi.org/10.1111/j.1365-2486.2011.02627.x.

Hennon, P.E., McKenzie, C.M., D'Amore, D.V., Wittwer, D.T., Mulvey, R.L., Lamb, M.S., Biles, F.E., and Cronn, R.C., 2016, General information on yellow-cedar, *in* A climate adaptation strategy for conservation and management of yellow-cedar in Alaska: U.S. Department of Agriculture, Forest Service, Pacific Northwest Research Station, General Technical Report PNW–GTR–917, p. 11–13. [Also available at http://www.fs.fed.us/pnw/pubs/pnw_gtr917.pdf.]

Hobbie, J.E., and Kling, G.W., eds., 2014, Alaska's changing Arctic; Ecological consequences for tundra, streams, and lakes: New York, Oxford University Press, 321 p.

Homer, Collin, Dewitz, Jon, Fry, Joyce, Coan, Michael, Hossain, Nazmul, Larson, Charles, Herold, Nate, McKerrow, Alexa, VanDriel, J.N., and Wickham, James, 2007, Completion of the 2001 National Land Cover Database for the conterminous United States: Photogrammetric Engineering and Remote Sensing, v. 73, no. 4, p. 337–341. [Also available at http://www.asprs.org/a/publications/pers/2007journal/april/highlight.pdf.]

Johnson, K.D., Harden, Jennifer, McGuire, A.D., Bliss, N.B., Bockheim, J.G., Clark, Mark, Nettleton-Hollingsworth, Teresa, Jorgenson, M.T, Kane, E.S., Mack, Michelle, O'Donnell, Jonathan, Ping, C.-L., Schuur, E.A.G., Turetsky, M.R., and Valentine, D.W., 2011, Soil carbon distribution in Alaska in relation to soil-forming factors: Geoderma, v. 167–168, p. 71–84, http://dx.doi.org/10.1016/j.geoderma.2011.10.006.

Kost, J.R., Verdin, K.L., Worstell, B.B., and Kelly, G.G., 2002, Methods and tools for the development of hydrologically conditioned elevation data and derivatives for national applications, *in* 2nd Annual Conference on Watershed Modeling, Las Vegas, Nev., 2002: 12 p., accessed February 24, 2015, at http://edna.usgs.gov/Edna/pubs/KostEDNA.pdf.

Kurz, W.A., Dymond, C.C., Stinson, G., Rampley, G.J., Neilson, E.T., Carroll, A.L., Ebata, T., and Safranyik, L., 2008, Mountain pine beetle and forest carbon feedback to climate change: Nature, v. 452, no. 7190, p. 987–990, http://dx.doi.org/10.1038/nature06777.

Leighty, W.W., Hamburg, S.P., and Caouette, John, 2006, Effects of management on carbon sequestration in forest biomass in southeast Alaska: Ecosystems, v. 9, no. 7, p. 1051–1065, http://dx.doi.org/10.1007/s10021-005-0028-3.

Lynch, J.A., Clark, J.S., Bigelow, N.H., Edwards, M.E., and Finney, B.P., 2002, Geographic and temporal variations in fire history in boreal ecosystems of Alaska: Journal of Geophysical Research; Atmospheres, v. 107, no. D1, p. FFR 8–1 to FFR 8–17, http://dx.doi.org/10.1029/2001JD000332.

Mann, D.H., Heiser, P.A., and Finney, B.P., 2002, Holocene history of the Great Kobuk Sand Dunes, northwestern Alaska: Quaternary Science Reviews, v. 21, nos. 4–6, p. 709–731, http://dx.doi.org/10.1016/S0277-3791(01)00120-2.

McGuire, A.D., Anderson, L.G., Christensen, T.R., Dallimore, Scott, Guo, Laodong, Hayes, D.J., Heimann, Martin, Lorenson, T.D., Macdonald, R.W., and Roulet, Nigel, 2009, Sensitivity of the carbon cycle in the Arctic to climate change: Ecological Monographs, v. 79, no. 4, p. 523–555, http://dx.doi.org/10.1890/08-2025.1.

McGuire, A.D., Christensen, T.R., Hayes, D., Heroult, A., Euskirchen, E., Kimball, J.S., Koven, C., Lefleur, P., Miller, P.A., Peylin, P., Oechel, W., Williams, M., and Yi, Y., 2012, An assessment of the carbon balance of Arctic tundra; Comparisons among observations, process models, and atmospheric inversions: Biogeosciences, v. 9, p. 3185–3204, http://dx.doi.org/10.5194/bg-9-3185-2012.

McGuire, A.D., Hayes, D.J., Kicklighter, D.W., Manizza, M., Zhuang, Q., Chen, M., Follows, M.J., Gurney, K.R., McClelland, J.W., Melillo, J.M., Peterson, B.J., and Prinn, R.G., 2010, An analysis of the carbon balance of the Arctic Basin from 1997 to 2006: Tellus; Series B, Chemical and Physical Meteorology, v. 62B, no. 5, p. 455–474, http://dx.doi.org/10.1111/j.1600-0889.2010.00497.x.

Mishra, U., and Riley, W.J., 2012, Alaskan soil carbon stocks; spatial variability and dependence on environmental factors: Biogeosciences, v. 9, no. 9, p. 3637–3645, http://dx.doi.org/10.5194/bg-9-3637-2012.

North American Land Change Monitoring System, 2010, 2005 North American land cover at 250 m spatial resolution (edition 1.0): Natural Resources Canada/Canadian Center for Remote Sensing (NRCan/CCRS), United States Geological Survey (USGS); Insituto Nacional de Estadística y Geografía (INEGI), Comisión Nacional para el Conocimiento y Uso de la Biodiversidad (CONABIO), and Comisión Nacional Forestal (CONAFOR), accessed October 30, 2011, at http://www.cec.org/tools-and-resources/map-files/land-cover-2005.

Nowacki, Gregory, Spencer, Page, Fleming, Michael, Brock, Terry, and Jorgenson, Torre, 2003, Unified ecoregions of Alaska; 2001: U.S. Geological Survey Open-File Report 02–297, 1 map. [Also available at http://agdc.usgs.gov/data/usgs/erosafo/ecoreg/index.html.]

Omernik, J.M., 1987, Ecoregions of the conterminous United States: Annals of the Association of American Geographers, v. 77, no. 1, p. 118–125, map supplement, scale 1:7,500,000, http://dx.doi.org/10.1111/j.1467-8306.1987.tb00149.x.

Rogers, L.A., Schindler, D.E., Lisi, P.J., Holtgrieve, G.W., Leavitt, P.R., Bunting, Lynda, Finney, B.P., Selbie, D.T., Chen, Guangjie, and Gregory-Eaves, Irene, 2013, Centennial-scale fluctuations and regional complexity characterize Pacific salmon population dynamics over the past five centuries: National Academy of Sciences Proceedings, v. 110, no. 5, p. 1750–1755, http://dx.doi.org/10.1073/pnas.1212858110.

Rupp, T.S., Starfield, A.M., and Chapin, F.S., III, 2000, A frame-based spatially explicit model of subarctic vegetation response to climatic change; Comparison with a point model: Landscape Ecology, v. 15, no. 4, p. 383–400, http://dx.doi.org/10.1023/A:1008168418778.

Rupp, T.S., Starfield, A.M., Chapin, F.S., III, and Duffy, P., 2002, Modeling the impact of black spruce on the fire regime of Alaskan boreal forest: Climatic Change, v. 55, nos. 1–2, p. 213–233, http://dx.doi.org/10.1023/A:1020247405652.

Seaber, P.R., Kapinos, F.P., and Knapp, G.L., 1987, Hydrologic units maps: U.S. Geological Survey Water-Supply Paper 2294, 63 p., 1 pl., scale 1:7,500,000. [Also available at http://pubs.usgs.gov/wsp/wsp2294/.]

Striegl, R.G., Dornblaser, M.M., Aiken, G.R., Wickland, K.P., and Raymond, P.A., 2007, Carbon export and cycling by the Yukon, Tanana, and Porcupine Rivers, Alaska, 2001–2005: Water Resources Research, v. 43, no. 2, article W02411, http://dx.doi.org/10.1029/2006WR005201.

Ueyama, Masahito, Iwata, Hiroki, Harazono, Yoshinobu, Euskirchen, E.S., Oechel, W.C., and Zona, Donatella, 2013, Growing season and spatial variations of carbon fluxes of Arctic and boreal ecosystems in Alaska (USA): Ecological Applications, v. 23, no. 8, p. 1798–1816, http://dx.doi.org/10.1890/11-0875.1.

U.S. Department of Agriculture Forest Service, 2014, Tongass young growth management strategy 2014: U.S. Department of Agriculture Forest Service, Tongass National Forest, 39 p.

U.S. Department of Agriculture Forest Service, 2015, Baseline estimates of carbon stocks in forests and harvested wood products for National Forest System Units; Alaska region: U.S. Department of Agriculture Forest Service, whitepaper, 34 p., http://www.fs.fed.us/climatechange/documents/AlaskaRegionCarbonAssessment.pdf.

U.S. Fish and Wildlife Service, 2010, Developing the National Geographic Framework: U.S. Fish and Wildlife Service, LCC Information Bulletin, no. 2, 18 p., http://lccnetwork.org/sites/default/files/Resources/LCC_Bulletin_2.pdf.

U.S. Geological Survey, 2012, National Hydrography Dataset: U.S. Geological Survey dataset, accessed March 19, 2015, at http://nhd.usgs.gov.

Wolken, J.M., Hollingsworth, T.N., Rupp, T.S., Chapin, F.S., III, Trainor, S.F., Barrett, T.M., Sullivan, P.F., McGuire, A.D., Euskirchen, E.S., Hennon, P.E., Beever, E.A., Conn, J.S., Crone, L.K., D'Amore, D.V., Fresco, Nancy, Hanley, T.A., Kielland, Knut, Kruse, J.J., Patterson, Trista, Schuur, E.A.G., Verbyla, D.L., and Yarie, John, 2011, Evidence and implications of recent and projected climate change in Alaska's forest ecosystems: Ecosphere, v. 2, no. 11, article 124, 35 p., http://dx.doi.org/10.1890/ES11-00288.1.

Yarie, John, and Billings, Sharon, 2002, Carbon balance of the taiga forest within Alaska; Present and future: Canadian Journal of Forest Research, v. 32, no. 5, p. 757–767, http://dx.doi.org/10.1139/x01-075.

Yi, Shuhua, Manies, Kristen, Harden, Jennifer, and McGuire, A.D., 2009, Characteristics of organic soil in black spruce forests; Implications for the application of land surface and ecosystem models in cold regions: Geophysical Research Letters, v. 36, no. 5, letter L05501, 5 p., http://dx.doi.org/10.1029/2008GL037014.

Yi, Shuhua, McGuire, A.D., Harden, Jennifer, Kasischke, Eric, Manies, Kristen, Hinzman, Larry, Liljedahl, Anna, Randerson, Jim, Liu, Heping, Romanovsky, Vladimir, Marchenko, Sergei, and Kim, Yongwon, 2009, Interactions between soil thermal and hydrological dynamics in the response of Alaska ecosystems to fire disturbance: Journal of Geophysical Research; Biogeosciences, v. 114, no. G2, article G02015, 20 p., http://dx.doi.org/10.1029/2008JG000841.

Yi, Shuhua, McGuire, A.D., Kasischke, Eric, Harden, Jennifer, Manies, Kristen, Mack, Michelle, and Turetsky, Merritt, 2010, A dynamic organic soil biogeochemical model for simulating the effects of wildfire on soil environmental conditions and carbon dynamics of black spruce forests: Journal of Geophysical Research; Biogeosciences, v. 115, no. G4, article G04015, 15 p., http://dx.doi.org/10.1029/2010JG001302.

Yu, Zicheng, Walker, K.N., Evenson, E.B., and Hajdas, Irka, 2008, Lateglacial and early Holocene climate oscillations in the Matanuska Valley, south-central Alaska: Quaternary Science Reviews, v. 27, nos. 1–2, p. 148–161, http://dx.doi.org/10.1016/j.quascirev.2007.02.020.

Yuan, F.-M, Yi, S.-H., McGuire, A.D., Johnson, K.D., Liang, J., Harden, J.W., Kasischke, E.S., and Kurz, W.A., 2012, Assessment of historical boreal forest C dynamics in the Yukon River Basin; Relative roles of warming and fire regime change: Ecological Applications, v. 22, no. 8, p. 2091–2109, http://dx.doi.org/10.1890/11-1957.1.

Zhu, Zhiliang, ed., Bouchard, Michelle, Butman, David, Hawbaker, Todd, Li, Zhengpeng, Liu, Jinxun, Liu, Shuguang, McDonald, Cory, Reker, Ryan, Sayler, Kristi, Sleeter, Benjamin, Sohl, Terry, Stackpoole, Sarah, Wein, Anne, and Zhu, Zhiliang, 2011, Baseline and projected future carbon storage and greenhouse-gas fluxes in the Great Plains region of the United States: U.S. Geological Survey Professional Paper 1787, 28 p. [Also available at http://pubs.usgs.gov/pp/1787/.]

Zhu, Zhiliang, and Reed, B.C., eds., 2012, Baseline and projected future carbon storage and greenhouse-gas fluxes in ecosystems of the Western United States: U.S. Geological Survey Professional Paper 1797, 192 p. [Also available at http://pubs.usgs.gov/pp/1797/.]

Zhu, Zhiliang, and Reed, B.C., eds., 2014, Baseline and projected future carbon storage and greenhouse-gas fluxes in ecosystems of the Eastern United States: U.S. Geological Survey Professional Paper 1804, 204 p. [Also available at http://dx.doi.org/10.3133/pp1804.]

Zhuang, Q., Melillo, J.M., Kicklighter, D.W., Prinn, R.G., McGuire, A.D., Steudler, P.A., Felzer, B.S., and Hu, S., 2004, Methane fluxes between terrestrial ecosystems and the atmosphere at northern high latitudes during the past century; A retrospective analysis with a process-based biogeochemistry model: Global Biogeochemical Cycles, v. 18, no. 3, article GB3010, 23 p., http://dx.doi.org/10.1029/2004GB002239.

Zhuang, Q., Melillo, J.M., McGuire, A.D., Kicklighter, D.W., Prinn, R.G., Steudler, P.A., Felzer, B.S., and Hu, S., 2007, Net emissions of CH_4 and CO_2 in Alaska; Implications for the region's greenhouse gas budget: Ecological Applications, v. 17, no. 1, p. 203–212, http://dx.doi.org/10.1890/1051-0761(2007)017[0203:NEOCAC]2.0.CO;2.

Chapter 2. Climate Simulations, Land Cover, and Wildfire

By T. Scott Rupp,[1] Paul Duffy,[2] Matthew Leonawicz,[1] Michael Lindgren,[1] Amy Breen,[1] Tom Kurkowski,[1] Angelica Floyd,[1] Alec Bennett,[1] and Lena Krutikov[1]

2.1. Highlights

- Climate models suggest a projected annual and seasonal increase in mean temperature throughout Alaska during the next 85 years. Warming has been projected to be greatest in the winter and spring and most pronounced in the northern and western regions of the State.
- Winter temperatures are projected to increase by as much as 8 degrees Celsius (°C) in the Arctic and Western Alaska Landscape Conservation Cooperatives (LCCs) by the end of this century.
- Wildfires burned an annual average of 3,791 square kilometers (km^2) between 1950 and 2009 in Alaska. The inter-annual variability in the area that was burned was high—from as few as 10 km^2 burned in 1961, 1964, and 1965 to as much as 27,071 km^2 burned in 2004.
- Wildfire frequency and extent are projected to increase across most of the six future climate simulations used in this assessment and across the five LCC regions, with the Northwest Boreal LCC North projected to see the largest increase in fire activity.
- The areas of late successional boreal forest land cover are projected to decrease under almost all climate simulations, ranging from approximately 8 to 44 percent; a concomitant increase in early successional deciduous forest land cover is also projected.
- Under most of the future climate simulations used in this assessment, the area of graminoid tundra land cover is projected to decrease whereas the area of shrub tundra land cover is projected to increase.

2.2. Introduction

As indicated in chapter 1, the ongoing warming trend of northern high-latitude regions, which influences vegetation distribution, ecosystem disturbances, and their interactions, has the potential to substantially alter the overall ecosystem carbon balance. Development of baseline and projected land-cover and wildfire data as well as the driving climate projections provide several of the primary spatial data foundations for this assessment. The simulations of future land-cover change and wildfire activity feed into other components of the assessment—primarily the simulation of carbon storage and greenhouse-gas (GHG) fluxes (see chapters 6 and 7).

Global temperature increases during the 20th century (Solomon and others, 2007) were amplified at high latitudes (Chapman and Walsh, 1993; Serreze and others, 2000; Overland and others, 2004; Serreze and Francis, 2006). In Alaska, warming since the 1950s appears to be unprecedented in at least the past 400 years (Overpeck and others, 1997; Barber and others, 2004; Kaufman and others, 2009). Mean annual air temperature in the boreal region of interior Alaska has increased by 1.3 degrees Celsius (°C) during the past 50 years, with the greatest warming occurring in winter (Hartmann and Wendler, 2005; Shulski and Wendler, 2007). Air temperature is projected to increase by an additional 3 to 7 °C by the end of this century (Walsh and others, 2008).

Across Alaska, significant shifts in vegetation composition and production have been observed, including yellow-cedar (*Callitropsis nootkatensis* (D. Don) D.P. Little) decline throughout the coastal temperate forest region (Hennon and others, 2006), decreased spruce growth in boreal Alaska (Barber and others, 2000; McGuire and others, 2010; Beck and others, 2011), woody vegetation encroachment into wetlands (Berg and others, 2009), and positive productivity throughout tundra regions with concurrent negative productivity throughout forested regions (for example, Goetz and

[1]University of Alaska-Fairbanks, Fairbanks, Alaska.

[2]Neptune and Company, Inc., Fort Collins, Colo.

others, 2005; Verbyla, 2008; Beck and others, 2011). Recent changes in major disturbance regimes in Alaska are linked to changes in climate. Wildfire, the dominant driver of ecosystem change in much of Alaska, is strongly linked to climate, where the average June temperature explains 78 percent of the inter-annual variability in total area burned (Duffy and others, 2005). In the past decade, the average annual area burned has doubled compared with any decade of the previous 50 years (Kasischke and others, 2010).

This chapter describes the methodology and results for the foundational modeling work required for this assessment. The following sections describe the major input datasets used for the entire assessment process, including climate, land cover, and wildfire; a description of the transient biogeographic model Alaska Frame-Based Ecosystem Code (ALFRESCO) and the methodology used for the simulation and analysis of climate-vegetation-wildfire dynamics follows. The result sections first present the historical period (1950–2009), followed by the projection period (2010–2099). Both the historical and projected periods sections contain specific subsections covering climate, vegetation, and wildfire trends.

2.2.1. Climate

Alaska's large climate gradient is influenced by latitude, elevation, and proximity to water bodies, including the influence of sea ice. This is reflected in the distribution of maritime, transitional, and continental climates across the State.

The most recent U.S. National Climate Assessment—Alaska Technical Regional Report (Markon and others, 2012), which included a comprehensive synthesis of the literature on Alaska's climate records, indicated that average annual statewide temperatures have increased significantly—on the order of 2 °C over the past 50 years (Stafford and others, 2000; Shulski and Wendler, 2007). The warming is not uniform across the State and is not consistent across seasons. The greatest observed temperature increases have occurred over winter and spring—at two to three times the level of warming found in summer and fall. Regionally, the interior continental portions of the State have experienced the most warming, with some areas experiencing an increase of more than 4 °C, whereas coastal and maritime areas have experienced change on the order of 0.5 to 1 °C (Shulski and Wendler, 2007).

A significant portion of the observed warming in Alaska occurred as a sudden, step-like change in the mid-1970s coinciding with a major shift in the Pacific Decadal Oscillation (PDO) (Markon and others, 2012). The PDO index captures this shift as a transition from predominantly negative to predominantly positive values around 1976–77 (Mantua and others, 1997). The temperature increase in Alaska, however, mirrors trends across the arctic and subarctic (Hinzman and others, 2005; Solomon and others, 2007), suggesting that large-scale atmospheric circulation patterns (such as PDO) may have amplified or accelerated an underlying long-term warming trend.

These climate dynamics further highlighted the need to identify the most accurate general circulation models (GCMs) to develop realistic and consistent climate simulations to be used in this assessment. Walsh and others (2008) evaluated the Coupled Model Intercomparison Project phase 3 (CMIP3; Meehl and others, 2007) models to identify the best performing GCMs for the Alaska region. The core statistic of the study was a root-mean-square-error (RMSE) evaluation of the differences between mean model output for each grid point and calendar month, and data from the European Centre for Medium-Range Weather Forecasts (ECMWF) Reanalysis, ERA–40. ERA–40 is one of the most consistent and accurate gridded representations of these variables available. From this analysis, the best performing CMIP3 models were identified for further consideration.

The climate data described here were aligned with the Intergovernmental Panel on Climate Change's Special Report on Emissions Scenarios (IPCC-SRES; Nakićenović and Swart, 2000). This assessment used three emissions scenarios (A2, A1B, and B1, from high to low projected carbon dioxide emissions; table 2.1) to force the GCMs and capture the uncertainties within and across the models. Two of the best performing CMIP3 models were used in this assessment—version 3.1-T47 of the Canadian Centre for Climate Modelling and Analysis' Coupled Global Climate Model (CGCM3.1; McFarlane and others, 1992; Flato, 2005) and version 5 of the Max Planck Institute's European Centre Hamburg Model (ECHAM5; Roeckner and others, 2003, 2004). The selected GCMs represented a range of projected climate change and were those to which the fire regime simulations were considered sensitive.

2.2.2. Land Cover

Land cover in Alaska includes substantial expanses of forest (both boreal and maritime) and tundra (including shrub-dominated and heath). There are six level II ecoregions covered by this assessment (see chapter 1). These six ecoregions correspond approximately to four primary Landscape Conservation Cooperatives (LCCs) in Alaska, which were used to summarize regional ecosystem characteristics.

Unlike the rest of the United States, Alaska does not have a consistent high-spatial-resolution remote sensing product that provides regular land-cover classification statewide, nor does it have consistent and widespread vegetation monitoring networks across the State. To simulate biological processes, including plant growth dynamics, tree line dynamics, vegetation composition and distribution, wildfire, and biogeochemistry across the landscape, this assessment used the North American Land Change Monitoring System (NALCMS) 2005 dataset (North American Land Change Monitoring System, 2010; for arctic and subarctic ecosystem types) and the National Land Cover Database (NLCD) 2001 (Homer and others, 2007; for coastal temperate forest ecosystem types). See chapter 1 for descriptions of the input land-cover data.

Table 2.1. Assumptions about the primary driving forces affecting land-use and land-cover change.

[These assumptions were used to downscale the B1, A1B, and A2 and scenarios, in order of low to high projected CO_2 emissions, of the Intergovernmental Panel for Climate Change's Special Report on Emissions Scenarios (Nakićenović and Swart, 2000). Population and per capita income projections are from Strengers and others (2004)]

Driving forces	A1B	A2	B1
Population growth (global and United States)	Medium; globally, 8.7 billion by 2050, then declining; in the United States, 385 million by 2050	High; globally, 15.1 billion by 2100; in the United States, 417 million by 2050	Medium; globally, 8.7 billion by 2050, then declining; in the United States, 385 million by 2050
Economic growth	Very high; U.S. per capita income $72,531 by 2050	Medium; U.S. per capita income $47,766 by 2050	High; U.S. per capita income $59,880 by 2050
Regional or global innovation	Global	Regional	Global
Technological innovation	Rapid	Slow	Rapid
Energy sector	Balanced use	Adaptation to local resources	Smooth transition to renewable
Environmental protection	Active management	Local and regional focus	Protection of biodiversity

2.2.3. Wildfire

Climate warming is also thought to be responsible for recent changes in fire regime in North American high-latitude regions (Gillett and others, 2004). In recent decades, annual area burned has increased in Alaska (Kasischke and Turetsky, 2006; Kasischke and others, 2010) and Canada (Gillett and others, 2004) and is hypothesized to have increased in Eurasia (Hayes and others, 2011; Kharuk and others, 2013). Several studies indicate that this increase would be maintained at least during the first half of the 21st century (Balshi and others, 2009; Mann and others, 2012). Greater burned area as well as possible changes in fire severity have substantial implications for permafrost, as increased severity leads to greater consumption of the organic layer that may increase active-layer thickness (Dyrness and Norum, 1983; Yoshikawa and others, 2002; Burn and others, 2009; Genet and others, 2013) and may potentially cause thermokarst disturbance in ice-rich soils (Jorgenson and others, 2001; Myers-Smith and others, 2008). Carbon cycling, albedo, and stand structure in the boreal forest are strongly influenced by the frequency and severity of wildfires (Randerson and others, 2006; Euskirchen and others, 2009; Johnstone and others, 2010; Turetsky and others, 2011), and burning is an important disturbance mechanism by which stored carbon is released to the atmosphere (Kasischke and others, 2000, 2005; Amiro and others, 2001).

A synthesis of contemporary fire trends in Alaska by Kasischke and others (2010) suggests a mixture of climatic and human controls on fire patterns. Between 2000 and 2009, an annual average of 7,670 square kilometers (km^2) was burned, 50 percent more area burned than in any previous decade since the 1940s. Over the past 60 years, there was a decrease in the number of lightning-ignited fires, an increase in extreme lightning-ignited fire events, an increase in human-ignited fires, and a decrease in the number of extreme human-ignited fire events. The fraction of area burned from human-ignited fires fell from 26 percent for the 1950s and 1960s to 5 percent for the 1990s and 2000s as a consequence of the change in fire policy that gave the highest suppression priorities to fire events that occurred near human settlements. The amount of area burned during late-season fires has also increased over the past two decades. Deeper burning of surface organic layers in black spruce (*Picea mariana* (Mill.) Britton, Sterns & Poggenb.) forests occurred during late-growing-season fires and on more well-drained sites, with consequences for forest regeneration. These trends all point to the importance of accounting for the potential changes in the Alaska fire regime with respect to a credible assessment of carbon storage and fluxes.

2.2.4. Other Drivers of Land-Cover Change

As discussed in the preceding sections, land-cover changes in Alaska are driven primarily by climate-induced environmental variability and disturbance (primarily wildfire-associated forest mortality and succession). There are, however, other drivers of land-cover change acting upon specific portions of the Alaskan landscape. For example, insects are affecting forests in the southern portions of the Alaskan boreal forest. In recent decades, warmer temperatures contributed to spruce beetle outbreaks, in part owing to a reduction of the beetle life cycle from 2 years to 1 year (Werner and others, 2006). This reduction in life cycle of an endemic species allowed populations to exceed critical thresholds that ultimately led to mortality across all forest age classes. This has led to white spruce (*Picea glauca* (Moench) Voss) mortality throughout the region of 12,000 km^2 between 1990 and 2000 (Werner and others, 2006). In addition, earlier snowmelt and persistent early spring freezing have had important implications for Alaska cedar decline in the coastal temperate forest region of Alaska, where over 2,000 km^2 of pristine forests have died in the past 100 years (Hennon and others, 2006). The loss of thermal cover and associated

dehardening of the species in late winter has resulted in fine-root damage in early spring.

Agricultural lands in Alaska occupy a small portion of the total land area of the State. Although roughly 90,000 km^2 have been identified as having current agricultural potential, only 0.1 percent is currently being cropped (U.S. Department of Agriculture, National Agricultural Statistics Service, 2014). Likewise, human settlements contribute a minor fraction of the Alaskan land cover. State population is approximately 736,000, which equates to approximately 2 persons per square kilometer. Although these other land-cover-change drivers impart little influence on the overall carbon assessment of Alaska, these drivers could play a larger role in altering the future carbon budget—especially with respect to forest insect- and disease-related mortality.

2.3. Input Data and Methods

2.3.1. Input Data Sources

The PRISM (Parameter-elevation Relationships on Independent Slopes Model; http://www.prism.oregonstate.edu) by Daly and others (2008) was used to provide gridded climate normals (monthly temperature and precipitation) for 1961–1990 at a 2-kilometer (km) spatial resolution. These data were resampled to 1 km and used as the baseline climatology for the climate downscaling procedure.

We used the CRU TS v. 3.10.01 high-resolution (0.5 degree [°]×0.5°) gridded data (Harris and others, 2014) from the Climatic Research Unit (CRU; http://www.cru.uea.ac.uk) at the University of East Anglia to provide historical climate data for the period 1950–2009. These data were downscaled and served as driving climate data input for the retrospective model simulations including model spin-up, which used the downscaled CRU data starting in 1900.

Analysis and synthesis of historical fire activity data (1950–2009) were based on estimates from fire management records maintained by the Alaska Interagency Coordination Center (M. Henderson, Alaska Interagency Coordination Center, unpub. data, June 1, 2010). This database includes digitized fire perimeters, which were used to generate summary statistics across the assessment domain as well as the five LCC regions and for both annual and decadal time periods. The tables and figures presented in the historical fire activity subsection summarize these results.

2.3.2. Methods and Analysis

The baseline period for this assessment was defined as the period from 1950 through 2009. This historical period is bounded by the beginning of reliable wildfire observations and statistics (1950) and the end of contemporary downscaled historical climate observations (2009). The projection period was defined as the period from 2010 through 2099. The results in this chapter, both historical and projected, were summarized across the full assessment domain as well as for the five LCC regions described in chapter 1.

Historical (CRU TS v. 3.10.01) and projected (CMIP3) output variables of surface temperature and precipitation were downscaled via the delta method (Hay and others, 2000; Hayhoe, 2010) using PRISM 1961–1990 2-km-resolution climate normals as baseline climate (Daly and others, 2008). The delta method was implemented by calculating climate anomalies applied as differences for temperature or quotients for precipitation between monthly future CMIP3 data and calculated CRU climate normals for 1961–1990 (see http://www.snap.uaf.edu for data and details). These coarse-resolution anomalies were then interpolated to PRISM spatial resolution via a spline technique and then added to (temperature) or multiplied by (precipitation) the PRISM climate normals. The downscaled climate data were then interpolated to a 1-km resolution for modeling purposes. Our modeling used the two GCMs of the best performing subset models for Alaska (Walsh and others, 2008), which bound the climate scenarios from most warming (ECHAM5) to least warming (CGCM3.1). Each model was downscaled for the three emissions scenarios (A1B, A2, B1; table 2.1).

Historical (CRU) and projected (CMIP3) output variables of surface downwelling shortwave radiation (RSDS; expressed as megajoules per square meter per day) and vapor pressure (VP; expressed as hectopascals) were calculated and downscaled for use by the biogeochemical Terrestrial Ecosystem Model (TEM). The historical data constitute the result of the delta-method downscaling procedure using the monthly time series (CRU TS v. 3.10.01; 1950–2009, 0.5° spatial resolution) and global climatology (CRU CL v. 2.0; 1961–1990, 10-minute spatial resolution) data. The projected data constitute the same CMIP3 models used for temperature and precipitation. The data were bias corrected and downscaled to 1-km resolution.

For the surface downwelling shortwave radiation data, the baseline climatology for the top of the atmosphere solar radiation data (referred to as *girr*) was calculated using an equation from Allen and others (1998) at a monthly timestep, which is used to represent the historical period RSDS data at 1-km spatial scale. The downscaled cloud cover time series was then used to calculate the surface solar radiation (referred to as *nirr*) from *girr* and downscaled cloud cover using the following equation:

$$nirr = monthly\_girr \times (0.251 + (0.509(1.0 - cloud\_cover/100))) \quad (2.1)$$

The CRU TS v. 3.10.01 data are distributed as vapor pressure and were converted to relative humidity using the conversion equation from the World Meteorological Organization's Commission for Instruments and Methods of Observation (CIMO) guide (2008) using the following equations:

$$saturated\_vapor\_pressure = 6.112 \times \exp((22.46 \times temperature)/(272.62 + temperature)) \quad (2.2)$$

$$relative\_humidity = (vapor\_pressure / saturated\_vapor\_pressure) \times 100 \quad (2.3)$$

Proportional anomalies were then generated using the newly converted CRU TS v. 3.10.01 historical VP data where the climatological period used was 1961–1990. These CRU TS v. 3.10.01 proportional anomalies were then interpolated using a spline interpolation to a 10-minute resolution grid for downscaling with the CRU CL v. 2.0 relative humidity data. The final step was to convert the downscaled relative humidity data to vapor pressure using the below conversion equation:

$$saturated\_vapor\_pressure = 6.112 \times \exp((17.62 \times temperature)/(243.12 + temperature)) \quad (2.4)$$

$$vapor\_pressure = (relative\_humidity \times saturated\_vapor\_pressure)/100 \quad (2.5)$$

Additional methodological details for all the downscaled climate variables can be found in the individual metadata files at the Scenarios Network for Alaska and Arctic Planning (SNAP) data download Web site (https://www.snap.uaf.edu/tools/data-downloads).

We used the biogeographic simulation model ALFRESCO (Rupp and others, 2000, 2002, 2007; Johnstone and others, 2011; Mann and others, 2012; Gustine and others, 2014; Amy Breen, University of Alaska-Fairbanks, written commun., January 15, 2015) to simulate changes in vegetation dynamics and fire regime for the projection period (2010–2099) in response to the climate simulations used in this assessment. ALFRESCO is a spatially explicit, stochastic landscape succession model for arctic, subarctic, and boreal vegetation types that operates in the Alaska and Northwest Canada region at a 1-km resolution and an annual timestep. The model represents seven general vegetation types (shrub tundra, graminoid tundra, wetland tundra, white spruce forest, black spruce forest, early successional deciduous forest, and coastal temperate forest) in Alaska. Currently, the coastal temperate forest and the wetland tundra vegetation types are represented as static vegetation states.

The fire module of ALFRESCO uses a cellular automata approach with separate subroutines for cell ignition and spread to simulate annual fire season activity. Both ignition and fire spread (that is, flammability) are a function of growing-season climate (Duffy and others, 2005), vegetation type, and time since last fire. The ignition of any given cell is stochastic in nature and determined by comparing a randomly generated number against the flammability coefficient of that cell. The flammability coefficient allows for changes in flammability that take place through succession (that is, fuel build up).

Following a wildfire in ALFRESCO, general successional trajectories for forested systems are as follows: burned spruce forest (white or black) transitions into early successional deciduous forest, and burned deciduous forest self-replaces. Vegetation transition times differed probabilistically between climax black and white spruce trajectories (Rupp and others, 2002). Transitional times were modeled probabilistically to represent early successional (that is, recolonization) deciduous forest following wildfires in spruce and deciduous forest and to determine the amount of time, in the absence of fire, until the climax spruce stage dominates the site again. Self-replacement of deciduous forest can occur when repeated burning and (or) climate conditions preclude transition to climax spruce. ALFRESCO incorporates the effects of fire severity on transition times using measurements of the area of the wildfire (that is, fire size), complex topography, and vegetation type on flat landscapes (Duffy and others, 2007; Johnstone and others, 2011).

Transitions in tundra are driven by succession or colonization and infilling. These processes are influenced by climate and fire history, which affect seedling establishment and growth conditions and proximity to seed source (Breen and others, written communication). For the transition from tundra to forest at the tree line, seed dispersal occurs within a 1-km neighborhood. White spruce colonization and infilling are possible in both graminoid and shrub tundra with transition rates to spruce forest mediated by climate effects and basal area growth. Vegetation succession from graminoid to shrub tundra is modeled probabilistically, with a greater likelihood of transition to shrub tundra post-fire. In the case of wildfire activity, shrub tundra transitions to graminoid tundra and graminoid tundra self-replaces. Wetland tundra in the model does not currently burn and is represented as a static vegetation type.

The relationship between climate and fire was calibrated by comparing model output (such as, fire regime, stand age structure) to the corresponding historical data (Mann and others, 2012). Simulated vegetation and fire dynamics were analyzed and synthesized across the full ensemble of simulations (number of replicates [n]=200) and for all six climate simulations (combinations of the three emissions scenarios and the two GCMs) used in this assessment. Vegetation transitions, defined as at least one shift in vegetation type during the projection period (2010–2099), were calculated as a percent of total area for each of the five LCC regions. Tables and figures presented in the projected land-cover and wildfire subsections include synthesis of these results.

2.4. Results and Discussion

2.4.1. Baseline Land Cover

Our baseline land-cover classes for the assessment domain, based on the NALCMS remote sensing product from 2005, consisted of forest (51 percent), tundra (28 percent), and nonvegetated (21 percent) (table 2.2). Forest land cover was dominated by early successional deciduous forest (30 percent), followed by white spruce forest (9 percent), black spruce forest (6 percent), and coastal temperate forest (6 percent). Tundra land cover was dominated by shrub tundra (17 percent), followed by graminoid tundra (10 percent) and wetland tundra (1 percent). The nonvegetated regions were composed of rock, ice, snow, water, and coastlines and represent land-cover classes not modeled.

Table 2.2. Land-cover types used in this assessment for the Alaska Frame-Based Ecosystem Code (ALFRESCO) model simulations, percent of area, and the source of the input data.

[Percent of area calculated in 2005. Land-cover types ordered from late to early successional forest to tundra to other cover types. NALCMS 2005, North American Land Change Monitoring System 2005 dataset; NLCD 2001, 2001 National Land Cover Database]

Land-cover type	Area (percent)	Source
Black spruce forest	6	NALCMS 2005
White spruce forest	9	NALCMS 2005
Deciduous forest	30	NALCMS 2005
Shrub tundra	17	NALCMS 2005
Graminoid tundra	10	NALCMS 2005
Wetland tundra	1	NALCMS 2005
Heath tundra	0	NALCMS 2005
Coastal temperate forest	6	NLCD 2001
Nonvegetated	21	NALCMS 2005

The Arctic LCC is dominated by tundra land-cover types with a relatively even distribution between shrub and graminoid tundra, 108,226 square km^2 and 119,027 km^2, respectively (table 2.3). There were minor components of deciduous forest (15,460 km^2) and wetland tundra (10,621 km^2) and very small components of black and white spruce forests.

The Western Alaska LCC has a relatively even distribution of tundra land-cover types and deciduous forest (table 2.3). Deciduous forest (130,904 km^2) is the dominant land-cover type. The LCC also has minor components of white and black spruce forests (9,424 km^2 and 5,873 km^2, respectively). Of the tundra land-cover types, shrub tundra dominates (119,517 km^2) with a minor component of graminoid tundra (12,379 km^2) and a very small component of wetland tundra. There is also a minor component of coastal temperate forest (9,268 km^2) within the LCC and along the border with the far northwestern portion of the North Pacific LCC.

The Northwest Boreal LCC North and South are both dominated by boreal forest land-cover types (table 2.3). In the Northwest Boreal LCC South, early successional deciduous forest dominates (66,673 km^2), followed by white spruce (18,706 km^2) and then black spruce (11,812 km^2). In the Northwest Boreal LCC North, there is a similar distribution of forest land-cover types; however, the areal extent is significantly greater than the Northwest Boreal LCC South. In the Northwest Boreal LCC North, early successional deciduous forest dominates (238,414 km^2), followed by white spruce (101,688 km^2) and then black spruce (77,183 km^2). Both LCC regions also have minor components of tundra land-cover types; however, neither region contains wetland tundra. The

Table 2.3. Land-cover types used in this assessment summarized by area for the five Landscape Conservation Cooperative (LCC) regions.

[Data may not add to totals shown because of independent rounding. km^2, square kilometer]

LCC region	Area in 2005 (km^2)									
	Black spruce forest	White spruce forest	Deciduous forest	Shrub tundra	Graminoid tundra	Wetland tundra	Heath tundra	Coastal temperate forest	Non-vegetated	Total
Arctic LCC	248	648	15,460	108,226	119,027	10,621	0	0	54,363	**308,593**
Western Alaska LCC	5,873	9,424	130,904	119,517	12,379	515	0	9,268	90,341	**378,221**
Northwest Boreal LCC North	77,183	101,688	238,414	11,942	16,961	0	9	0	10,387	**456,584**
Northwest Boreal LCC South	11,812	18,706	66,673	12,961	3,238	0	0	2,542	70,371	**186,303**
North Pacific LCC	636	392	603	8	2	0	0	75,999	85,721	**163,361**

Northwest Boreal LCC South contains a minor component of coastal temperate forest along the southern boundary and along the border with the North Pacific LCC.

The North Pacific LCC is dominated by coastal temperate forest (75,999 km^2) as well as nonvegetated areas, mostly snow and ice (table 2.3). There are very small components of boreal forest land-cover types in the extreme northern portion of the LCC bordering the Northwest Boreal LCC South.

2.4.2. Baseline Wildfire

From fire management records, the number of wildfires between 1950 and 2009 across the full simulation domain of this assessment ranged from as high as 176 fires in 2005 to less than or equal to 1 in 1952, 1961, 1964, and 1965 (table 2.4). The minimum number of fires is difficult to estimate owing to detection issues associated with the remoteness and size of Alaska. These issues were likely more pronounced in the earlier period of the historical data. Consequently, the estimate of the minimum number of fires is highly uncertain. Similar issues exist with the estimation of area burned in years with little activity. Annual area burned averaged 3,791 km^2—that is, 0.25 percent of the total area of the Alaska simulation domain, which has a total area of 1.49 million km^2. The maximum annual area burned was 27,071 km^2 (that is, 1.3 percent of the total area), which occurred in 2004. There were three years (1961, 1964, and 1965) where less than 10 km^2 were recorded as being burned. As reported by Kasischke and others (2002), the wildfire perimeter records for the 1960s were rated fair and included many missing data records. Historical data for each of the LCC regions is subsequently discussed in order of decreasing fire activity as measured by annual area burned.

The Northwest Boreal LCC North had most (approximately 85 percent of the statewide total) of the fire activity among the five LCC regions of the assessment (table 2.4, fig. 2.1). The number of wildfires between 1950 and 2009 ranged from a high of 137 in 2005 to 0 in both 1961 and 1964. The annual area burned averaged 3,262 km^2. The inter-annual variability in area burned was high, and area burned ranged from 0 km^2 in both 1961 and 1964 to 26,684 km^2 in 2004. The range of annual area burned was between 0 and 5.8 percent of the Northwest Boreal LCC North, which has a total area of 456,584 km^2.

The Western Alaska LCC had the second most (approximately 10 percent) fire activity among the five LCC regions of the assessment (table 2.4, fig. 2.1). In the Western Alaska LCC, the number of wildfires between 1950 and 2009 averaged 6 per year—with a high of 37 in 1972 and 13 years recording no fires. Annual area burned averaged 394 km^2, or 0.1 percent of the Western Alaska LCC, which has a total area of 378,221 km^2. The range of annual area burned was between 0 and 2.2 percent of the Western Alaska LCC.

In the Arctic LCC, the number of wildfires between 1950 and 2009 averaged 2 per year—with a high of 13 in 2005 and 31 years recording no fires (table 2.4, fig. 2.1). Annual area

Table 2.4. Baseline (1950–2009) wildfire statistics for each Landscape Conservation Cooperative (LCC) region and the full assessment domain (Alaska).

[Data from fire management records maintained by the Alaska Interagency Coordination Center. km^2, square kilometer]

Metric	Number of wildfires per year	Annual area burned (km^2)
Arctic LCC		
Mean	2.1	60.49
Standard deviation	3.2	178.16
Minimum	0	0
Median	0	0
Maximum	13	1,106.82
Year of maximum	2005	2007
Western Alaska LCC		
Mean	5.82	393.81
Standard deviation	7.68	1,258.46
Minimum	0	0
Median	3.5	33.42
Maximum	37	8,313.5
Year of maximum	1972	1957
Northwest Boreal LCC North		
Mean	31.8	3,262.26
Standard deviation	33.07	5,178.67
Minimum	0	0
Median	20	1,296.82
Maximum	137	26,683.54
Year of maximum	2005	2004
Northwest Boreal LCC South		
Mean	2.15	54.49
Standard deviation	2.7	112.52
Minimum	0	0
Median	1	4.28
Maximum	15	615.4
Year of maximum	2009	2009
North Pacific LCC		
Mean	0.6	2.21
Standard deviation	0.92	6.93
Minimum	0	0
Median	0	0
Maximum	4	36.31
Year of maximum	1991	1991
Alaska		
Mean	41.3	3,791.5
Standard deviation	41.92	5,709.97
Minimum	0	0
Median	27	1,596.77
Maximum	176	27,071.72
Year of maximum	2005	2004

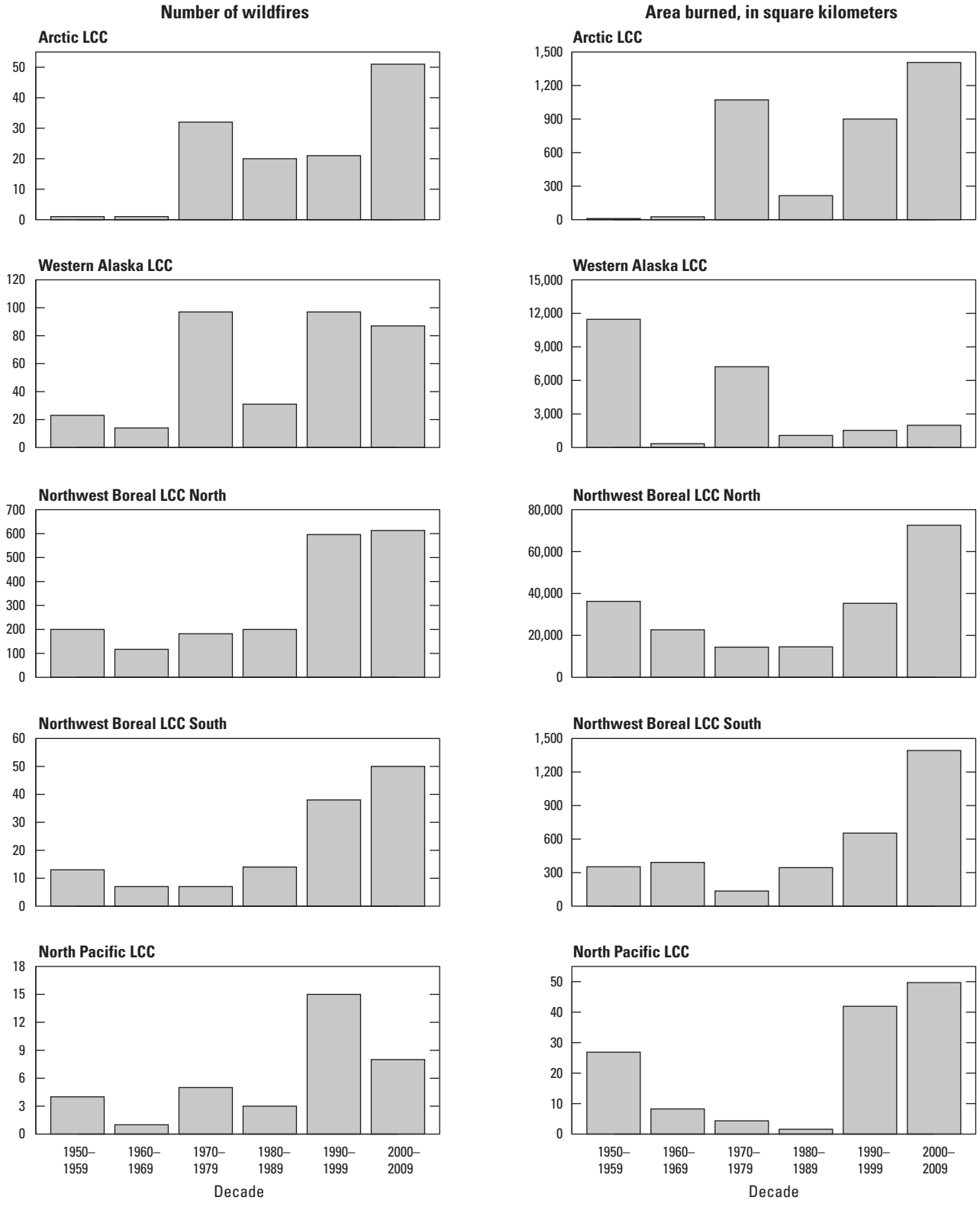

Figure 2.1. A decadal summary of number of wildfires and area burned for each Landscape Conservation Cooperative (LCC) region for the historical period (1950–2009).

burned averaged 60 km², or 0.01 percent of the Arctic LCC, which has a total area of 308,593 km². The range of annual area burned was between 0 and 0.35 percent of the Arctic LCC.

In the Northwest Boreal LCC South, the number of wildfires between 1950 and 2009 averaged 2 per year—with a high of 15 in 2009 and 15 years recording no fires (table 2.4, fig. 2.1). Annual area burned averaged 54 km², or 0.03 percent of the Northwest Boreal LCC South, which has a total area of 186,303 km². The range of annual area burned was between 0 and 0.33 percent of the Northwest Boreal LCC South.

Of the five assessment regions, the North Pacific LCC had the least amount of fire activity reflecting the LCC's wet and cool climate (table 2.4, fig. 2.1). The number of wildfires between 1950 and 2009 averaged 1 per year—with a high of 4 in 1991 and 37 years recording no fires. Annual area burned averaged 2 km² and ranged from 0 to 36 km². The range of annual area burned was between 0 and 0.02 percent of the North Pacific LCC, which has a total area of 163,361 km².

2.4.3. Climate Simulations

Visualizations of seasonal baseline (1950–2009) climate patterns for mean monthly temperature in degrees Celsius (°C) and total monthly precipitation in millimeters (mm), based on the downscaled CRU data (http://www.snap.uaf.edu), are presented in figure 2.2. The downscaled CRU historical period data exhibited strong variability across seasons and also indicated high spatial variability.

Figure 2.3 and table 2.5 present projected changes in mean monthly temperature (°C) and total precipitation (mm) by season, calculated using the difference in mean values from the last two decades of the historical period (1980–2009) to those of the projection period (2070–2099). Warming trends are projected by both GCMs and across all three emissions scenarios. Warming would be greatest in the northern and western regions of Alaska. There was greater projected variability among the scenarios than between GCMs. The A2 scenario projected the greatest warming and the B1 scenario the least warming. The ECHAM5 climate simulations project warmer temperatures than the CGCM3.1 simulations. Projected warming is not uniform seasonally and both GCMs project substantially greater warming during the winter (December, January, February) and fall (September, October, November). Growing season (defined here as April through September) is a particularly important annual time period as plant production and wildfire activity are constrained within these months. Growing season temperatures are projected to increase in all six climate simulations (fig. 2.4) across the full assessment period (1950–2099).

Precipitation increases are also projected by both GCMs and across all three emissions scenarios (table 2.5). Across the full assessment domain, differences between GCMs were

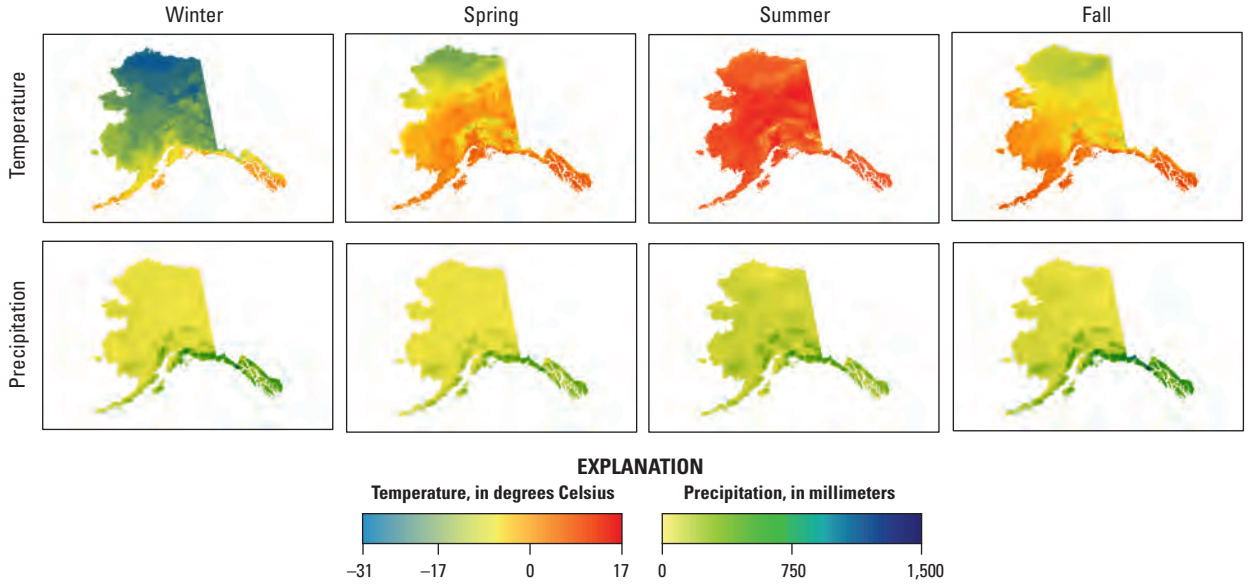

Figure 2.2. Baseline (1950–2009) seasonal mean monthly temperature and total precipitation by season using downscaled Climate Research Unit data (http://www.snap.uaf.edu). Winter included December, January, and February; spring included March, April, and May; summer included June, July, and August; and fall included September, October, and November.

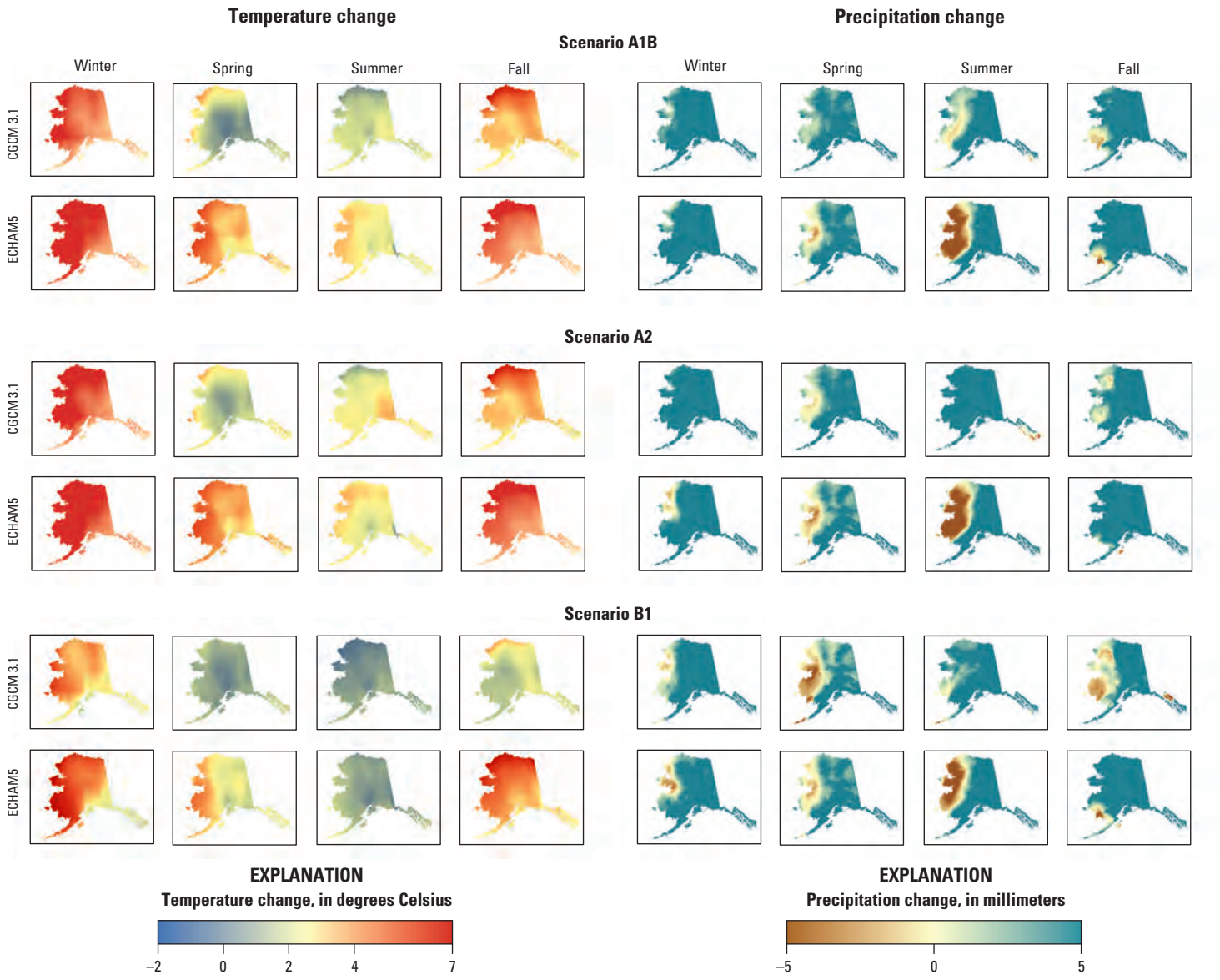

Figure 2.3. Projected changes in mean monthly temperature and total precipitation by season, calculated using the difference in mean values between 1980–2009 and 2070–2099 using downscaled data for version 3.1-T47 of the Canadian Centre for Climate Modelling and Analysis' Coupled Global Climate Model (CGCM3.1) and version 5 of the Max Planck Institute's European Centre Hamburg Model (ECHAM5) general circulation models and for the three scenarios A1B, A2, and B1 from the Intergovernmental Panel on Climate Change's Special Report on Emissions Scenarios (http://www.snap.uaf.edu). Winter included December, January, and February; spring included March, April, and May; summer included June, July, and August; and fall included September, October, and November.

Table 2.5. Summary statistics of projected changes in mean monthly temperature and total precipitation by season, calculated using the difference in mean values from 1980–2009 and 2070–2099 for each Landscape Conservation Cooperative (LCC) region and the full assessment domain (Alaska).

[Values represent the integration of all 1-kilometer pixels within the full assessment domain and individual subregions using downscaled data for the version 3.1-T47 of the Canadian Centre for Climate Modelling and Analysis' Coupled Global Climate Model (CGCM3.1) and version 5 of the Max Planck Institute's European Centre Hamburg Model (ECHAM5) general circulation models and for the three scenarios, B1, A1B, and A2, in order of low to high projected CO_2 emissions, from the Intergovernmental Panel on Climate Change's Special Report on Emissions Scenarios used in the assessment (http://www.snap.uaf.edu). Winter includes December, January, and February; spring includes March, April, and May; summer includes June, July, and August; and fall includes September, October, and November]

Season	Monthly temperature (degree Celsius)						Total precipitation (millimeter)					
	CGCM3.1			ECHAM5			CGCM3.1			ECHAM5		
	A1B	A2	B1	A1B	A2	B1	A1B	A2	B1	A1B	A2	B1
Arctic LCC												
Winter	6.36	8.09	3.55	8.03	8.19	4.93	8.42	9.55	6.81	9.94	7.08	5.25
Spring	2.55	2.46	1.26	3.78	3.96	2.53	5.30	4.82	2.45	4.33	3.72	3.99
Summer	1.25	1.79	0.23	2.76	2.94	1.08	6.75	14.73	8.04	3.73	3.10	4.03
Fall	4.92	5.77	2.58	7.21	7.51	5.56	9.59	7.39	5.96	18.39	20.08	16.53
Western Alaska LCC												
Winter	6.24	7.52	3.76	8.23	8.37	5.79	12.06	15.47	6.50	19.67	14.53	9.09
Spring	1.87	2.13	1.19	4.21	4.34	3.51	9.68	8.71	2.45	6.34	4.91	5.36
Summer	1.97	2.47	0.87	3.00	2.72	1.51	4.89	12.39	5.32	0.21	1.11	1.91
Fall	3.20	3.83	1.61	5.38	5.65	4.20	5.51	11.89	1.66	5.80	10.67	6.43
Northwest Boreal LCC North												
Winter	5.28	6.26	3.40	6.95	7.28	4.31	10.38	10.75	7.61	11.62	7.94	5.97
Spring	1.08	1.45	0.82	3.38	3.60	2.47	5.17	5.54	2.44	4.08	3.14	3.63
Summer	1.88	2.51	0.74	2.50	2.50	0.93	7.69	14.84	7.53	8.19	6.28	8.53
Fall	3.43	4.13	1.77	5.12	5.58	4.07	9.11	10.84	5.67	14.65	18.08	14.84
Northwest Boreal LCC South												
Winter	4.67	5.38	2.90	5.56	6.05	3.24	32.39	31.99	23.01	41.83	33.07	21.17
Spring	0.60	1.37	0.70	2.78	3.06	2.07	17.92	20.22	13.85	17.32	15.45	17.24
Summer	1.99	2.79	0.93	2.21	2.06	0.72	20.94	25.35	16.08	19.50	22.23	20.33
Fall	3.25	3.93	1.85	4.17	4.59	3.26	22.20	33.97	12.52	29.26	35.55	27.46
North Pacific LCC												
Winter	3.71	4.29	2.42	3.87	4.48	2.05	95.77	92.63	64.82	99.84	106.87	53.70
Spring	1.26	2.17	1.32	2.85	3.05	2.02	43.99	73.92	56.37	58.04	57.77	49.64
Summer	2.05	2.91	1.17	2.28	2.30	1.13	17.10	13.14	13.87	24.40	36.90	25.60
Fall	3.08	3.80	1.99	3.77	3.97	2.94	51.48	91.26	31.82	45.93	76.57	49.87
Alaska												
Winter	5.50	6.64	3.36	7.00	7.30	4.44	22.06	22.89	15.06	26.29	22.88	13.49
Spring	1.54	1.90	1.04	3.54	3.74	2.65	11.98	15.15	9.49	11.98	10.94	10.64
Summer	1.80	2.43	0.73	2.62	2.57	1.10	9.44	15.35	8.82	8.37	9.52	9.20
Fall	3.62	4.33	1.93	5.36	5.70	4.19	14.37	21.68	8.31	18.30	24.92	18.31

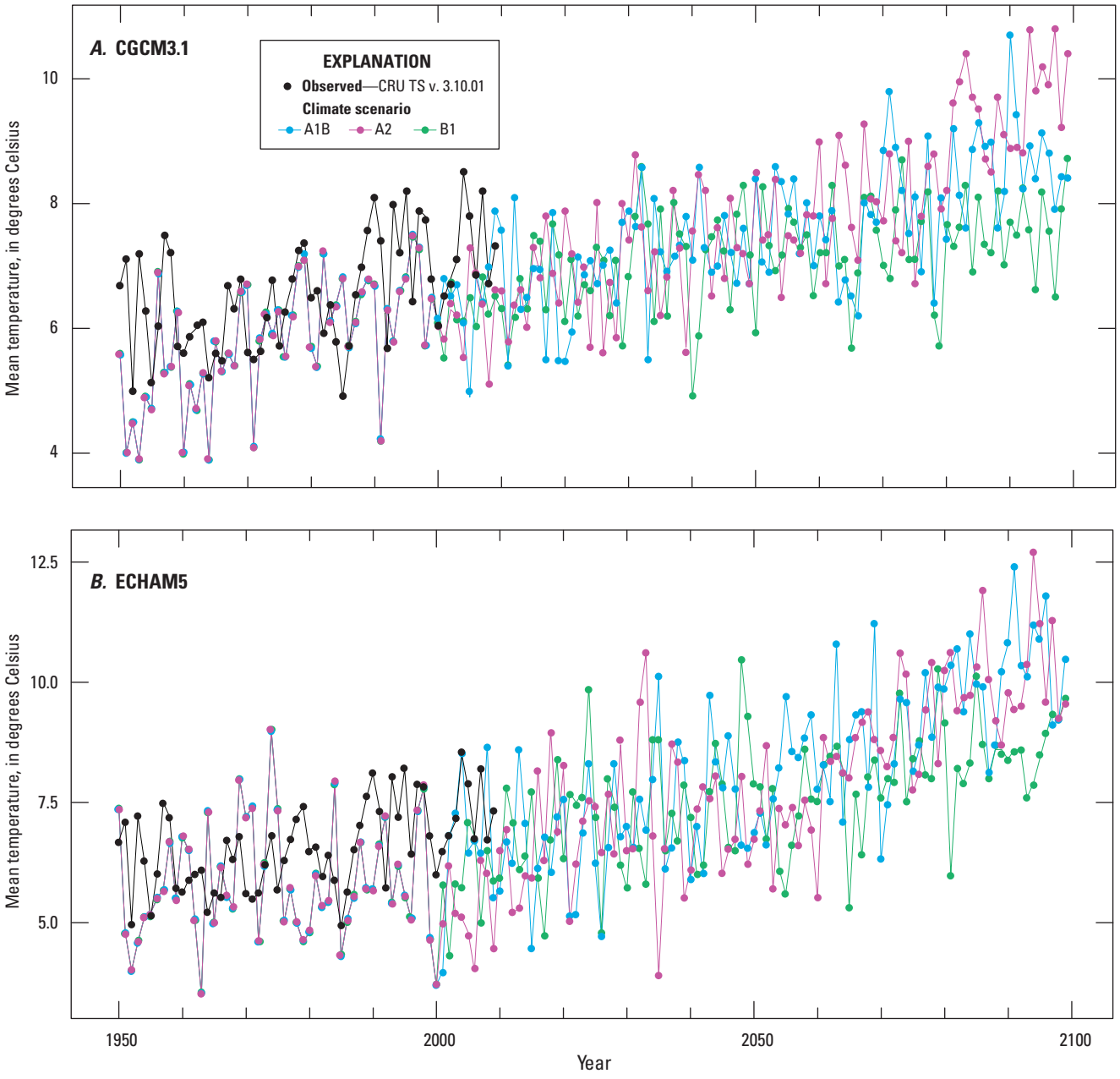

Figure 2.4. Projected growing season (April–September) mean temperature across the full assessment period (1950–2099). *A*, climate simulations by version 3.1-T47 of the Canadian Centre for Climate Modelling and Analysis' Coupled Global Climate Model (CGCM3.1) and *B*, climate simulations by version 5 of the Max Planck Institute's European Centre Hamburg Model (ECHAM5). Historical observations are from the Climate Research Unit time series CRU TS v. 3.10.01. Climate scenarios A1B, A2, and B1 from the Intergovernmental Panel on Climate Change's Special Report on Emissions Scenarios.

smaller than the differences among scenarios. Portions of western Alaska are projected to increase the least and some areas would likely experience some seasonal decreases in spring and summer (fig. 2.3). Regional trends varied considerably among climate simulations, with the CGCM3.1 model projecting slightly larger increases for the A1B scenario than for the A2 scenario. In contrast, the ECHAM5 model projected slightly larger increases for the A2 scenario than for the A1B scenario. Of the simulations, that for scenario B1 with ECHAM5 produced the largest seasonal increases in precipitation in spring (March, April, May) and summer (June, July, August).

2.4.4. Projected Land Cover

The projected changes in land cover varied substantially across the assessment domain, but varied little across GCM climate scenarios (table 2.6). Differences between the GCMs were minimal except for the Arctic LCC. Change was defined as the percentage of the domain that changed land-cover type at least once over the projection period (2010–2099). Total projected land-cover change across the full domain ranged from a low of 56.5 percent in the B1 scenario of the CGCM3.1 model to a high of 61.2 percent in the A1B scenario of the ECHAM5 model. The greatest amount of change occurred within the Northwest Boreal LCC North (approximately 97.5 percent in both models) and the least amount of change, not including the primarily static North Pacific LCC, was simulated in the Arctic LCC (ranging from 30 to 46 percent for the CGCM3.1 and ECHAM5 models, respectively) (fig. 2.5).

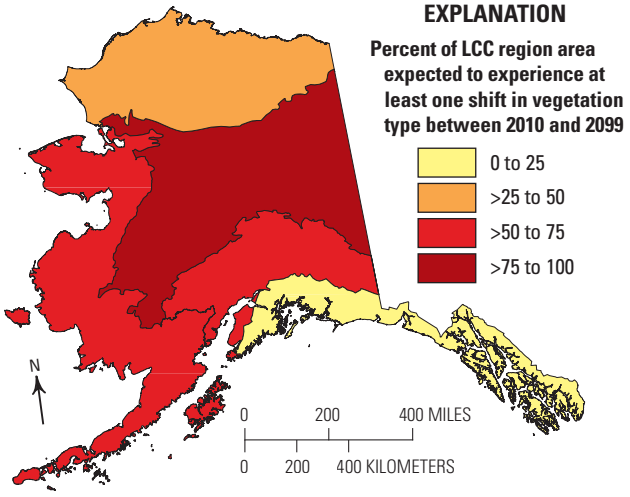

Figure 2.5. Projected land-cover change footprint visualized by Landscape Conservation Cooperative (LCC) region. This visualization is for the version 3.1-T47 of the Canadian Centre for Climate Modelling and Analysis' Coupled Global Climate Model (CGCM3.1) general circulation model, but the version 5 of the Max Planck Institute European Centre Hamburg Model (ECHAM5) model produces the same results for the binned categories depicted, and the results are also consistent across climate change scenarios A1B, A2, and B1 from the Intergovernmental Panel on Climate Change's Special Report on Emissions Scenarios. Finer differences between the two general circulation models and the three climate change scenarios are presented in table 2.6. Change was defined as the portion of the domain that changed cover type at least once over the projection period (2010–2099).

Table 2.6. Projected land-cover-change footprint for the Landscape Conservation Cooperative (LCC) regions and the full assessment domain (Alaska).

[Change was defined as the percentage of the domain that changed land-cover type at least once over the projection period (2010–2099). This assessment used downscaled data for two general circulation models, version 3.1-T47 of the Canadian Centre for Climate Modelling and Analysis' Coupled Global Climate Model (CGCM3.1) and version 5 of the Max Planck Institute's European Centre Hamburg Model (ECHAM5), and three scenarios, B1, A1B, and A2, in order of low to high projected CO_2 emissions, from the Intergovernmental Panel on Climate Change's Special Report on Emissions Scenarios. km^2, square kilometer]

LCC region	Area (km^2)	Land-cover change (percent)					
		CGCM3.1			ECHAM5		
		A1B	A2	B1	A1B	A2	B1
Arctic LCC	308,593	33.5	38.8	30.8	46.2	43.7	41.8
Western Alaska LCC	378,221	55.7	56.1	52.9	58.0	57.6	56.5
Northwest Boreal LCC North	456,584	97.5	97.5	97.4	97.5	97.5	97.5
Northwest Boreal LCC South	186,303	55.3	56.0	54.9	56.2	56.0	55.4
North Pacific LCC	163,361	0.9	0.9	0.9	0.9	0.9	0.9
Alaska	**1,493,062**	**57.8**	**59.1**	**56.5**	**61.2**	**60.5**	**59.8**

Projected land-cover changes across the full assessment domain between 2009 and 2099 occurred within both the forest and tundra types (table 2.7, fig. 2.6). No changes were projected in land cover for coastal temperate forest, heath tundra, or wetland tundra owing to the static nature in which the vegetation succession model treats these land-cover types. Model results for the full assessment domain indicated projected decreases in late successional white and black spruce forests and concomitant increase in early successional deciduous forest across GCMs and climate scenarios with the magnitudes of change being greatest for the ECHAM5 simulations. The exception was the simulation under scenario B1 with CGCM3.1, which projected a small increase in black spruce forest (1.9 percent) and a moderate increase in white spruce forest (12.1 percent). Forest land-cover changes were greatest under the A2 scenario with the CGCM3.1 model, but were greatest under the A1B scenario with the ECHAM5 model. The CGCM3.1 simulations projected a consistent decreases in both graminoid and shrub tundra, whereas the ECHAM5 simulations projected moderate decreases in graminoid tundra (20–26 percent) but increases in shrub tundra (4–8 percent).

Consistent decreases in white and black spruce forests and concomitant increases in deciduous forest were projected for all regions and scenarios under the ECHAM5 simulations (table 2.7). Projected decreases were greatest under the A1B scenario and smallest under the B1 scenario. For the CGCM3.1 simulations, the model results varied among regions and scenarios. The magnitude of change was greatest under the A2 scenario except for the Western Alaska LCC. Within the boreal-forest-dominated Northwest Boreal LCC North and South, the B1 scenario projected small increases in spruce forests whereas the A2 scenario projected moderate decreases. The A1B scenario produced opposite trends with small increases in spruce forests projected for the Northwest Boreal LCC South and small decreases projected for the Northwest Boreal LCC North.

Although the Arctic and Western Alaska LCCs are both dominated by tundra, projected changes in tundra land cover exhibited opposite trends consistently across GCMs and scenarios. For the Arctic LCC, decreases in graminoid tundra and increases in shrub tundra were projected, with a greater magnitude of change under the ECHAM5 simulations. For the Western Alaska LCC, in contrast, increases in graminoid tundra and decreases in shrub tundra were projected, with a greater magnitude of change under the CGCM3.1 simulations.

In the Arctic LCC, white spruce forest was projected to increase (18.2–66.3 percent) whereas black spruce forest was projected to decrease (8.4–36.1 percent) under the CGCM3.1 simulations with the magnitude of change greatest under the B1 scenario for white spruce and under the A2 scenario for black spruce (table 2.7). In contrast, both white and black spruce forests were projected to decrease (24.9–63.6 percent) under the ECHAM5 simulations with the magnitude of the decreases greatest under the A2 scenario and smallest under the B1 scenario. For all simulations, graminoid tundra was projected to decrease (8.4–23.6 percent), whereas shrub tundra was projected to increase (2.1–21.3 percent). Projected changes in tundra land cover were slightly greater under the A1B scenario than the A2 scenario and the least amount of change was projected under the B1 scenario.

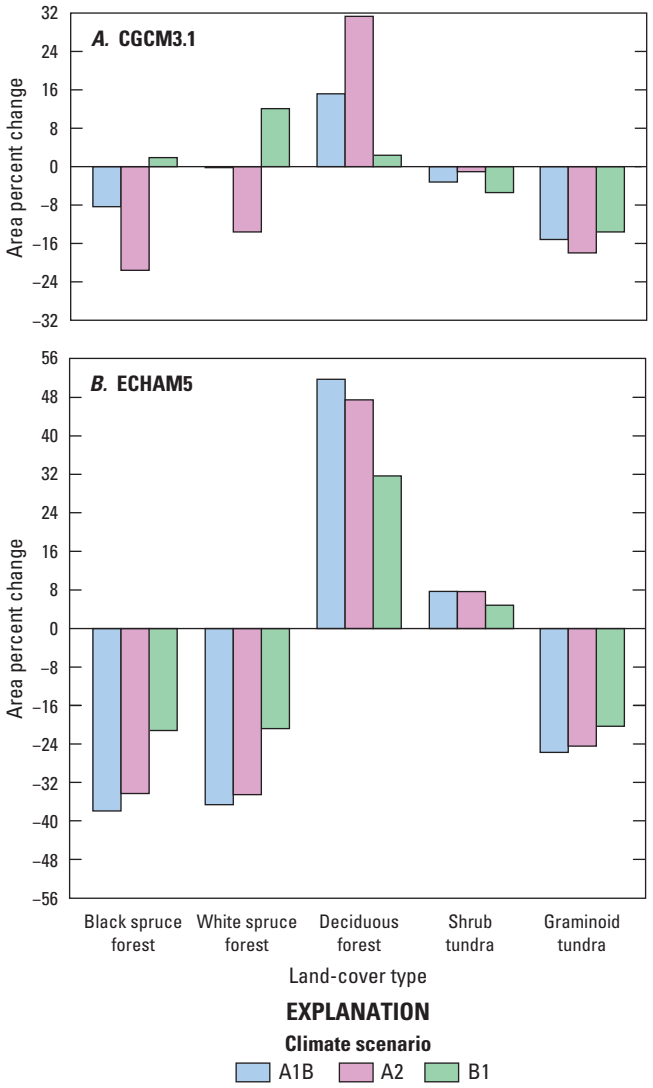

Figure 2.6. Projected land-cover change between 2009 and 2099 across the full assessment domain under the three emissions scenarios A1B, A2, and B1 of the Intergovernmental Panel on Climate Change's Special Report on Emissions Scenarios. *A*, changes projected by version 3.1-T47 of the Canadian Centre for Climate Modelling and Analysis' Coupled Global Climate Model (CGCM3.1) climate simulations and *B*, changes projected by version 5 of the Max Planck Institute's European Centre Hamburg Model (ECHAM5) climate simulations.

In the Western Alaska LCC, white and black spruce forests were projected to decrease (12.0–45.6 percent) under all simulations, except for the CGCM3.1 simulation under the B1 scenario, which resulted in a 6.4-percent projected increase in white spruce forest (table 2.7). Graminoid tundra was projected to increase (0.4–9.2 percent) across all simulations. In contrast, shrub tundra was projected to decrease (3.6–11.3 percent) across all simulations.

Table 2.7. Projected change in land-cover type between the end of the historical period (2009) and the end of the projection period (2099) for each Landscape Conservation Cooperative (LCC) region and the full assessment domain (Alaska).

[Heath tundra, wetland tundra, and coastal temperate forest are not presented due to the static nature of these cover types in the Alaska Frame-Based Ecosystem Code (ALFRESCO) model. This assessment used downscaled data for two general circulation models, version 3.1-T47 of the Canadian Centre for Climate Modelling and Analysis' Coupled Global Climate Model (CGCM3.1) and version 5 of the Max Planck Institute's European Centre Hamburg Model (ECHAM5), and three scenarios, B1, A1B, and A2, in order of low to high projected CO_2 emissions, from the Intergovernmental Panel on Climate Change's Special Report on Emissions Scenarios. NA, not applicable]

Land-cover type	Change in land-cover type (percent)					
	CGCM3.1			ECHAM5		
	A1B	A2	B1	A1B	A2	B1
Arctic LCC						
Black spruce forest	–19.7	–36.1	–8.4	–63.0	–63.6	–54.7
White spruce forest	49.8	18.2	66.3	–36.8	–46.1	–24.9
Deciduous forest	232.5	396.8	129.1	620.4	598.3	527.0
Shrub tundra	4.2	8.9	2.1	21.3	20.6	13.8
Graminoid tundra	–10.2	–14.4	–8.4	–23.6	–22.1	–16.4
Western Alaska LCC						
Black spruce forest	–24.9	–29.4	–12.0	–45.6	–43.1	–33.6
White spruce forest	–11.6	–16.1	6.4	–40.5	–40.3	–30.6
Deciduous forest	63.1	73.7	34.0	106.0	102.6	81.4
Shrub tundra	–9.5	–9.8	–11.3	–4.4	–3.6	–3.6
Graminoid tundra	8.2	9.2	6.6	3.9	3.7	0.4
Northwest Boreal LCC North						
Black spruce forest	–8.0	–25.9	3.0	–43.9	–34.1	–13.6
White spruce forest	–7.9	–24.3	3.7	–41.9	–33.8	–12.2
Deciduous forest	24.5	69.2	–5.1	113.0	91.4	34.8
Shrub tundra	1.8	1.5	1.0	4.5	5.0	4.7
Graminoid tundra	–49.7	–46.3	–46.1	–45.6	–44.3	–44.0
Northwest Boreal LCC South						
Black spruce forest	1.3	–15.2	9.6	–30.2	–27.4	–14.9
White spruce forest	4.4	–10.9	13.9	–32.6	–30.5	–18.7
Deciduous forest	3.0	15.4	–3.9	29.1	27.5	17.4
Shrub tundra	–17.5	–13.6	–25.1	3.9	1.9	3.2
Graminoid tundra	–72.6	–69.9	–71.4	–67.9	–66.5	–67.9
North Pacific LCC						
Black spruce forest	–6.4	–9.5	–1.9	–20.0	–13.4	–4.3
White spruce forest	–7.2	–10.0	–1.6	–19.4	–14.9	–3.6
Deciduous forest	90.0	127.3	20.9	248.2	174.5	53.2
Shrub tundra	0.0	0.0	0.0	0.0	0.0	0.0
Graminoid tundra	NA	NA	NA	NA	NA	NA
Alaska						
Black spruce forest	–8.3	–21.6	1.9	–37.8	–34.2	–21.1
White spruce forest	–0.2	–13.6	12.1	–36.5	–34.4	–20.7
Deciduous forest	15.2	31.3	2.4	51.6	47.4	31.6
Shrub tundra	–3.2	–1.0	–5.4	7.7	7.7	4.8
Graminoid tundra	–15.2	–18.0	–13.6	–25.7	–24.4	–20.2

In the Northwest Boreal LCC North, white and black spruce forests were projected to decrease substantially (7.9–43.9 percent) under all simulations, except for the simulations under the B1 scenario, which resulted in minimal increases of approximately 3 percent (table 2.7). Graminoid tundra was also projected to decrease (44.0–49.7 percent) under all simulations. In contrast, shrub tundra was projected to increase (1.0–5.0 percent) under all simulations.

In the Northwest Boreal LCC South, small to moderate changes (that varied from decreases to increases) were projected in white and black spruce forests across the scenarios with CGCM3.1 (table 2.7). In contrast, decreases in white and black spruce forests were projected for all scenarios with ECHAM5. Graminoid and shrub tundra were projected to decrease (13.6–72.6 percent) under the CGCM3.1 simulations. However, under the ECHAM5 simulations graminoid tundra was projected to decrease (66.5–67.9 percent), whereas shrub tundra was projected to increase minimally (1.9–3.9 percent).

Because ALFRESCO does not model changes in temperate forest types, projected land-cover changes were minimal in the North Pacific LCC where this land-cover type is dominant. For the small amount of spruce forest land-cover types found within this LCC, both white and black spruce forests were projected to decrease (1.6–20.0 percent) under all simulations.

Distributional trends across the full assessment domain revealed projected decreases in area of spruce forest land cover across all simulations (fig. 2.7). These decreases were greatest for the ECHAM5 simulations. An associated increase in early successional deciduous forest was projected under all simulations. Graminoid tundra was also projected to decrease in area across all simulations. In contrast, the area of shrub tundra was projected to be relatively stable under the CGCM3.1 simulations, whereas a small increase was projected under the ECHAM5 simulations.

Distributional trends among the LCC regions varied substantially (figs. 2.8 through 2.12). In the Arctic LCC, all simulations projected decreases in graminoid tundra and increases in shrub tundra (fig. 2.8). Under the CGCM3.1 simulations, a small increase in white spruce forest was projected.

The Western Alaska LCC exhibited similar results to its tundra-dominated Arctic LCC counterpart for forest land-cover types, but opposite trends for the tundra land-cover types (fig. 2.9). In contrast to the Arctic LCC, the Western Alaska LCC simulations projected variable but decreasing shrub tundra trends across all simulations. Under the CGCM3.1 simulations, graminoid tundra was projected to increase slightly whereas under the ECHAM5 simulations, an increase at the beginning of the century was projected, followed by a decline ending in areal extents similar to beginning levels.

The simulations for the Northwest Boreal LCC North projected moderate to large changes in forest distribution (fig. 2.10). For the CGCM3.1 simulations, white and black spruce forest extent was projected to vary from moderate decreases under the A2 scenario to small increases under the B1 scenario. In contrast, the ECHAM5 simulations projected large decreases in white and black spruce forest extent across all scenarios, with concomitant increases in early successional deciduous forest. Graminoid tundra was projected to decrease in all simulations. Projected changes in shrub tundra extent were opposite for the GCMs, with projected decreases under CGCM3.1 but increases under ECHAM5.

The projections for the Northwest Boreal LCC South mirrored the trends exhibited in the Northwest Boreal LCC North, except that under the CGCM3.1 simulations shrub tundra was projected to increase across all scenarios—in contrast to the CGCM3.1 simulations for the Northwest Boreal LCC North (fig. 2.11). In all simulations, the projected areal extent of change was substantially smaller than for the Northwest Boreal LCC North.

The simulations for the North Pacific LCC projected only minor changes owing to the static nature of the major ecosystem type (coastal temperate forest) in ALFRESCO. Along the extreme northern portions of this LCC, minor decreases in spruce forests were projected with concomitant increases in deciduous forest (fig. 2.12). These trends were consistent across all simulations.

2.4.5. Projected Wildfire

2.4.5.1. Retrospective Simulations

Calibration simulations were performed to tune the modeled relationship between climate and fire. Calibrations iteratively adjusted the quantitative linkage between climate and fire by comparing model output (such as, fire numbers and extent, stand age structure) to the corresponding historical data. Several metrics were used to calibrate the performance of ALFRESCO simulations (Rupp and others, 2000, 2002, 2006, 2007). These metrics included (1) the frequency-area distribution of the fire sizes, (2) the inter-annual variability from 1950 through 2009, and (3) the mean area burned from 1950 through 2009. Calibration results are not presented here but followed the methods outlined in Mann and others (2012). Once a sufficient correspondence between the historical data and the simulation output was obtained across multiple metrics, the calibration optimization was halted.

ALFRESCO simulations of the historical period of record provided reasonable depictions of the fire regime in Alaska. Specifically, the frequency-area distribution, inter-annual variability in area burned, and spatial distribution of fires were consistent with those from the observed record. To account for stochastic components of the fire regime (such as, ignitions, duration of vegetation dominance through succession, and so forth), multiple replicates (n=200) of fire activity and subsequent succession were simulated. Projected model results were then assembled and distributional properties across replicates were analyzed. The model performed relatively well in simulating historical wildfire activity driven by historical climate data (table 2.8). The simulated number of wildfires averaged 60 per year, ranging from 48 to 78.

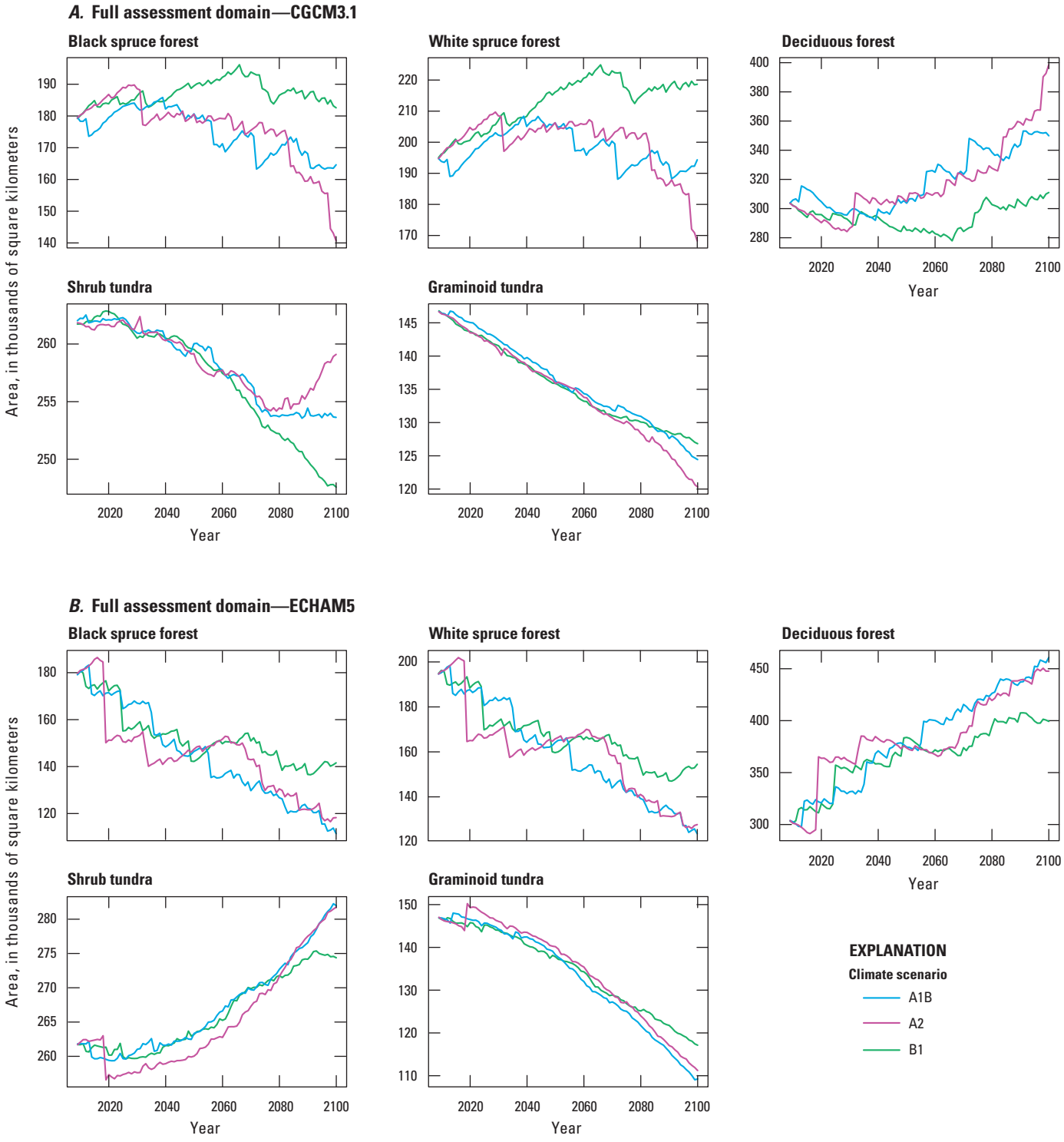

Figure 2.7. Projected change in land-cover type from 2009 through 2099 across the full assessment domain. *A*, changes projected by version 3.1-T47 of the Canadian Centre for Climate Modelling and Analysis' Coupled Global Climate Model (CGCM3.1) climate simulations and *B*, changes projected by version 5 of the Max Planck Institute's European Centre Hamburg Model (ECHAM5) climate simulations under the three emissions scenarios A1B, A2, and B1 of the Intergovernmental Panel on Climate Change's Special Report on Emissions Scenarios. Heath tundra, wetland tundra, and coastal temperate forest land-cover types are not presented owing to the static nature of these land-cover types in the Alaska Frame-Based Ecosystem Code (ALFRESCO) model.

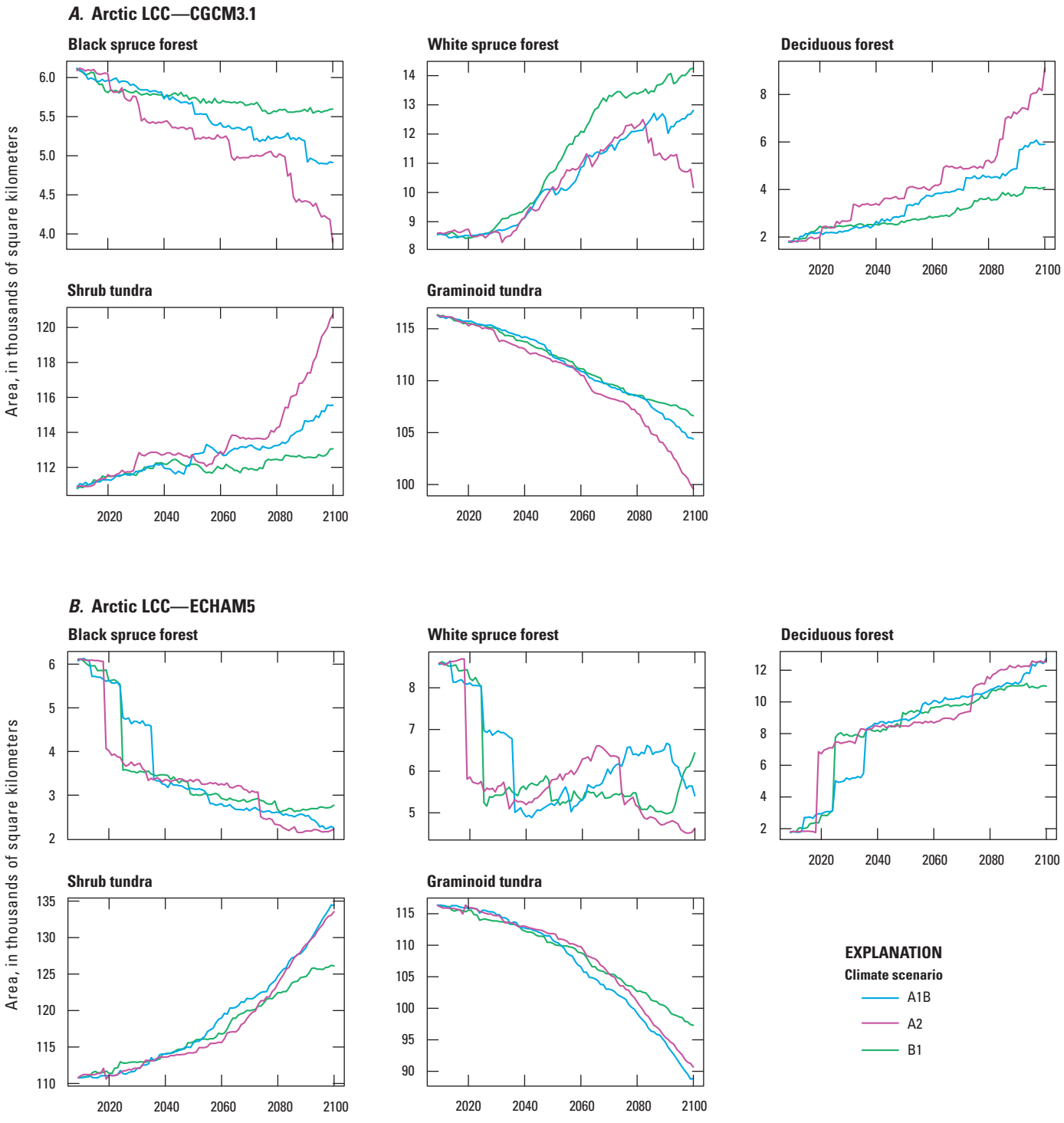

Figure 2.8. Projected change in land-cover type from 2009 through 2099 across the Arctic Landscape Conservation Cooperative (LCC). Details regarding the simulations of land-cover change shown can be found in figure 2.7.

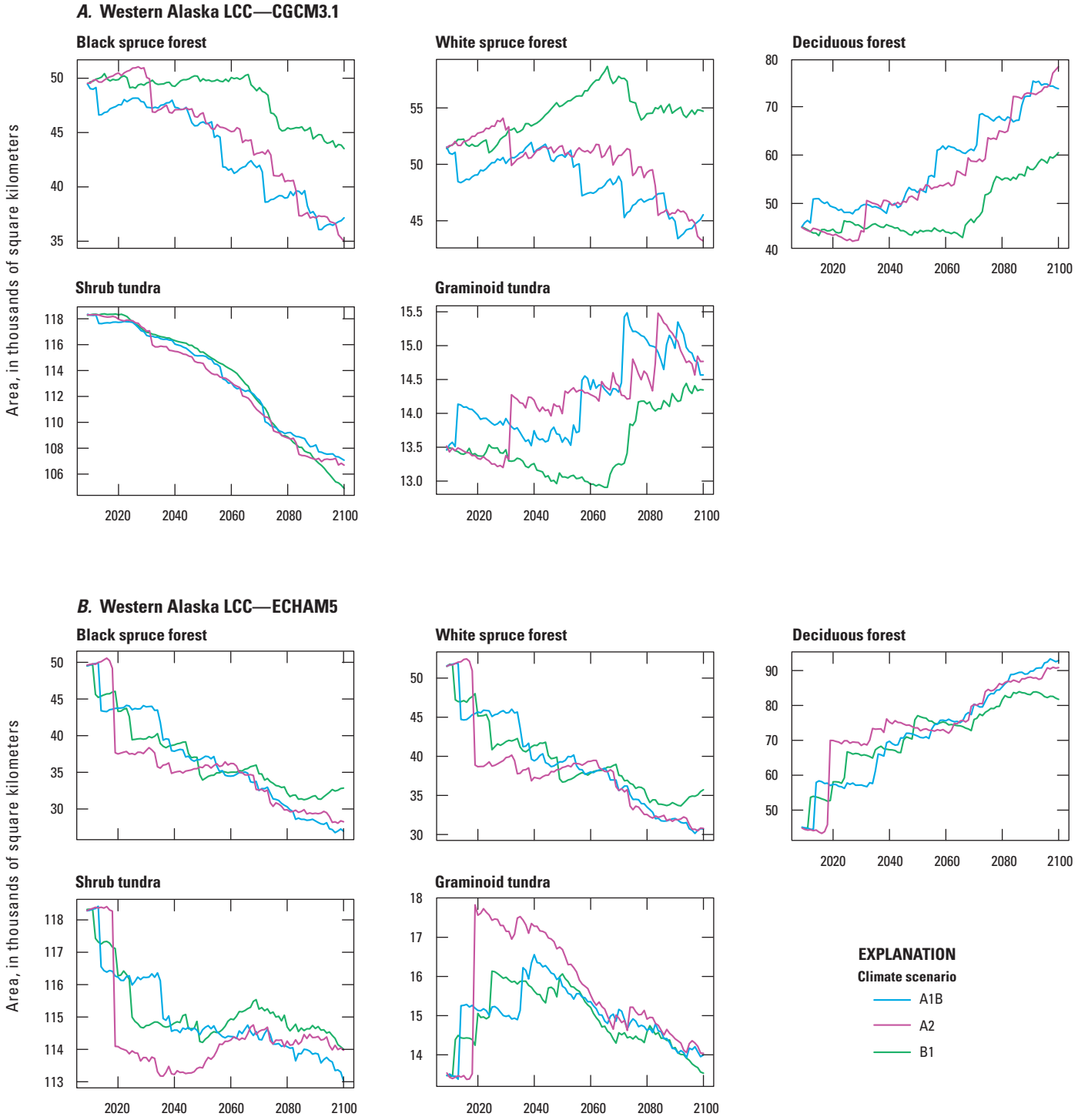

Figure 2.9. Projected change in land-cover type from 2009 through 2099 across the Western Alaska Landscape Conservation Cooperative (LCC). Details regarding the simulations of land-cover change shown can be found in figure 2.7.

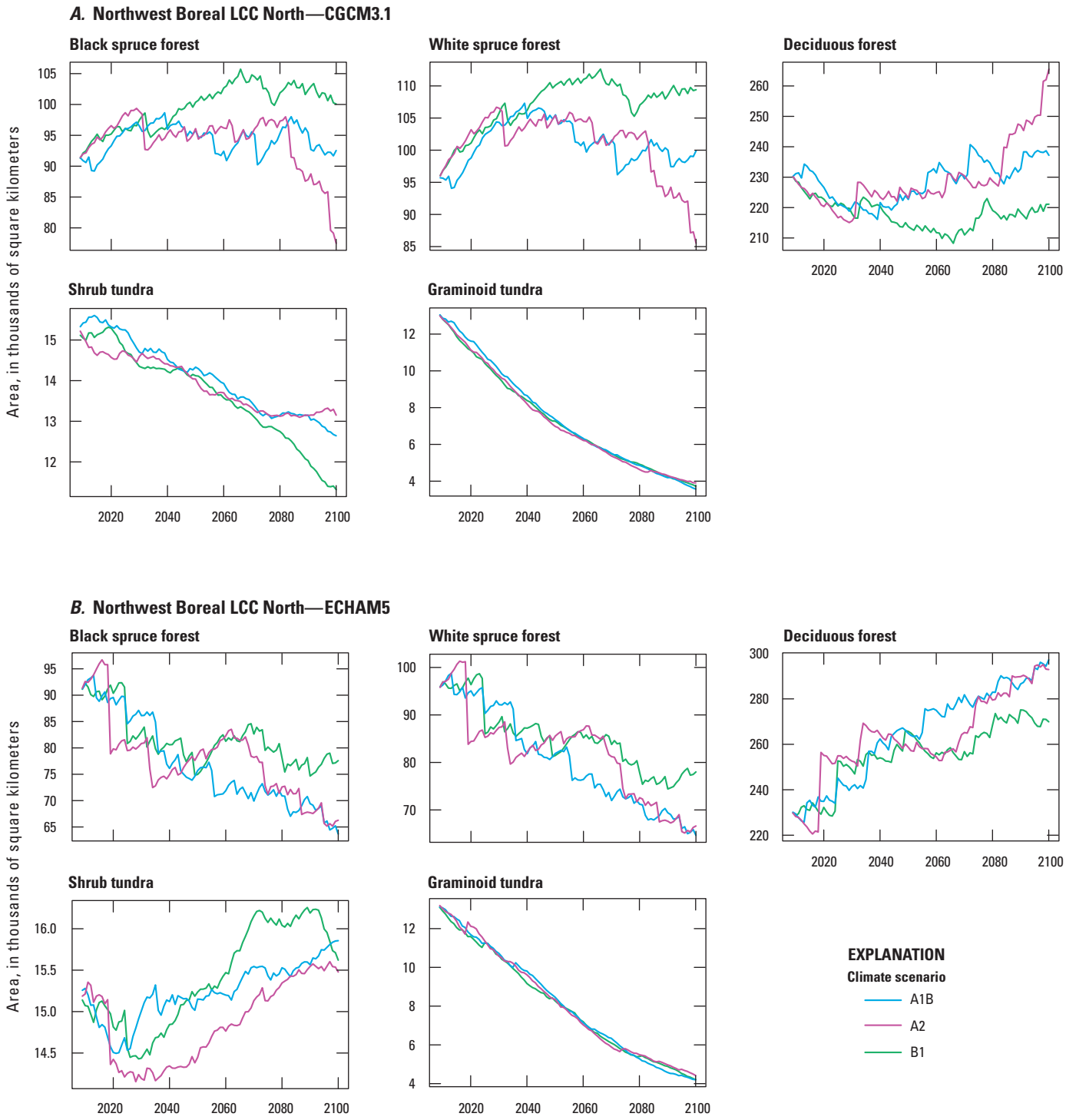

Figure 2.10. Projected change in land-cover type from 2009 through 2099 across the Northwest Boreal Landscape Conservation Cooperative (LCC) North. Details regarding the simulations of land-cover change shown can be found in figure 2.7.

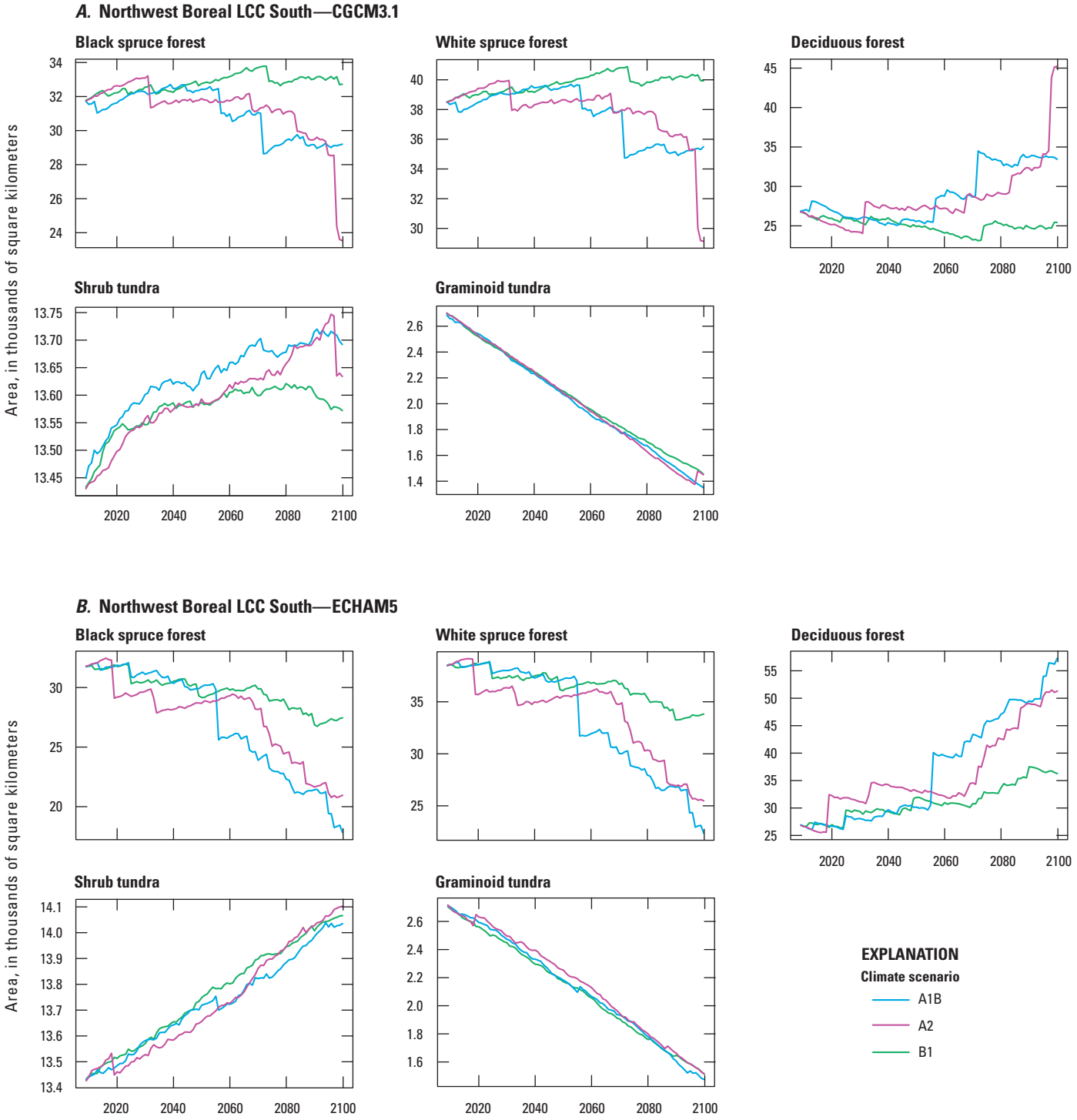

Figure 2.11. Projected change in land-cover type from 2009 through 2099 across the Northwest Boreal Landscape Conservation Cooperative (LCC) South. Details regarding the simulations of land-cover change shown can be found in figure 2.7.

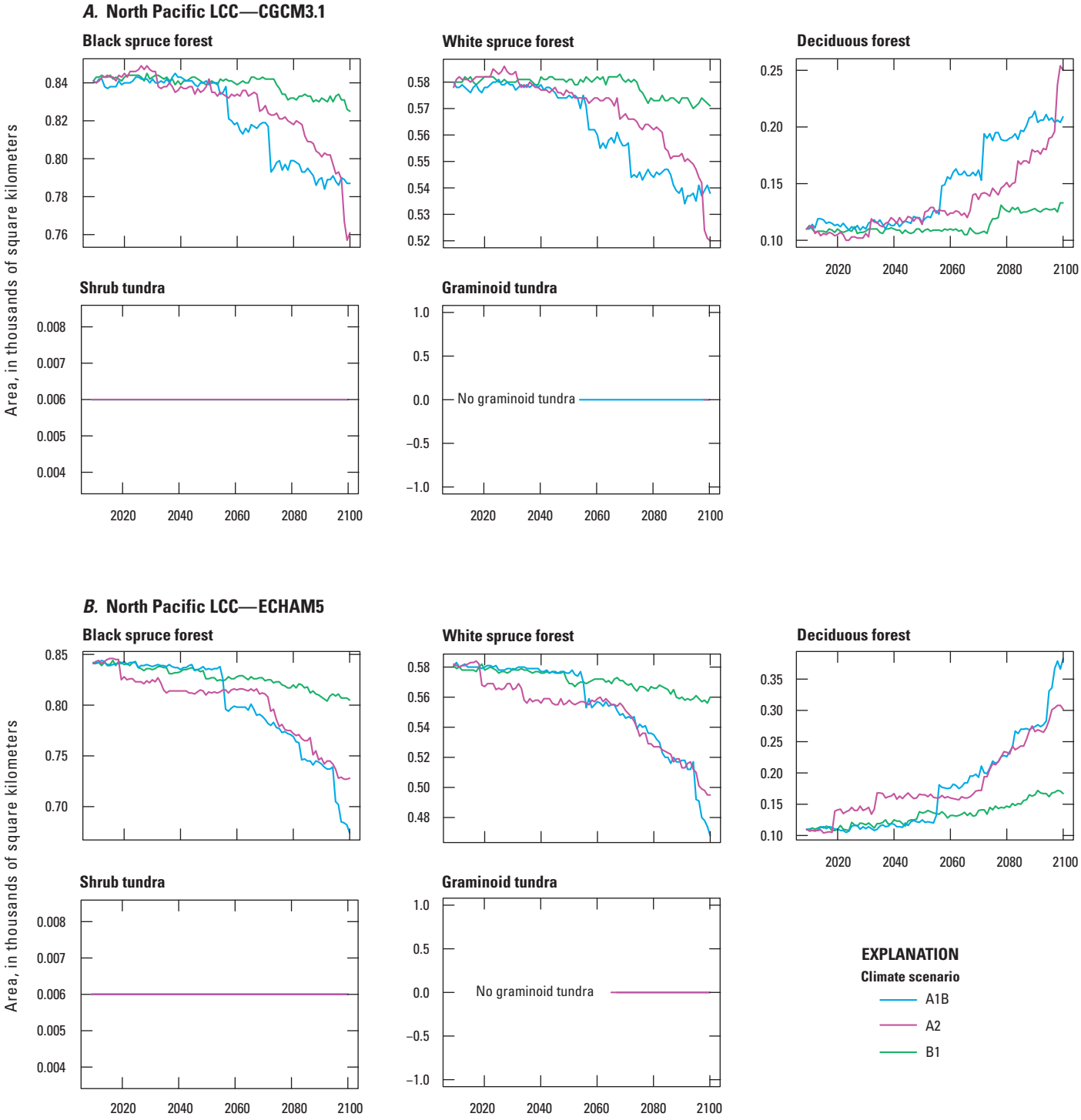

Figure 2.12. Projected change in land-cover type from 2009 through 2099 across the North Pacific Landscape Conservation Cooperative (LCC). Details regarding the simulations of land-cover change shown can be found in figure 2.7.

Table 2.8. Observed and simulated fire data from Alaska Frame-Based Ecosystem Code (ALFRESCO) model for each Landscape Conservation Cooperative (LCC) region and the full assessment domain (Alaska) during the baseline period (1950–2009).

[Summary statistics are based on 200 model replicates. km^2, square kilometer; —, not applicable]

Metric	Observed		Simulated	
	Number of wildfires per year	Annual area burned (km^2)	Number of wildfires per year	Annual area burned (km^2)
Arctic LCC				
Mean	2.1	60.49	0.9	86
Standard deviation	3.2	178.16	0.3	210
Minimum	0	0	0	2
Median	0	0	1	10
Maximum	13	1,106.82	2	1,130
Year of maximum	2005	2007	—	—
Western Alaska LCC				
Mean	5.82	393.81	8	762
Standard deviation	7.68	1,258.46	2	1,168
Minimum	0	0	5	23
Median	3.5	33.42	8	255
Maximum	37	8,313.50	12	6,411
Year of maximum	1972	1957	—	—
Northwest Boreal LCC North				
Mean	31.8	3,262.26	44	2,802
Standard deviation	33.07	5,178.67	5	3,089
Minimum	0	0	35	335
Median	20	1,296.82	43	1,612
Maximum	137	26,683.54	57	13,983
Year of maximum	2005	2004	—	—
Northwest Boreal LCC South				
Mean	2.15	54.49	10	331
Standard deviation	2.7	112.52	2	441
Minimum	0	0	6	31
Median	1	4.28	9	187
Maximum	15	615.4	14	2,059
Year of maximum	2009	2009	—	—
North Pacific LCC				
Mean	0.6	2.21	0.1	4
Standard deviation	0.92	6.93	0.2	2
Minimum	0	0	0	1
Median	0	0	0	3
Maximum	4	36.31	1	11
Year of maximum	1991	1991	—	—
Alaska				
Mean	41.3	3,791.50	60	3,789
Standard deviation	41.92	5,709.97	7	4,343
Minimum	0	0	48	433
Median	27	1,596.77	59	2,028
Maximum	176	27,071.72	78	18,391
Year of maximum	2005	2004	—	—

The average number of simulated fires is slightly higher than the historical average; however, the estimate of the average for the historical data is likely biased low owing to under-reporting in the first decade of the observational record. Historical annual area burned averaged 3,791 km^2 (table 2.4)—that is, 0.25 percent of the total area of the Alaska simulation domain, which has a total area of 1.49 million km^2. Simulation results for that same period had an average annual area burned of 3,789 km^2. The inter-annual variability of the simulated fire activity was smaller than that of the historical data. This is largely due to deficiencies in the model's ability to depict inter-annual variability in the ignitions because of a lack of reliable historical data regarding ignitions.

2.4.5.2. Future Simulations

The simulation results of fire activity for the last decade of the projection period (2090–2099) were compared with simulated results from the most recent full decade (2000–2009), referred to as the historical reference period. Results are summarized using percentiles from the distribution of output (such as, number of wildfires, area burned) across 200 model replicates for each simulation. Greater differences were found between simulated output from GCMs across all emissions scenarios than among emissions scenarios within a given GCM. Across the full domain of this assessment and across all simulations, the median (across 200 model replicates) projected number of wildfires for 2090–2099 ranged from 51 to 88 (table 2.9, fig. 2.13). The projected annual area

Table 2.9. Summary of fire activity for the full assessment domain simulated for the last decades of the historical period (2000–2009) and the projection period (2090–2099).

[The 50th (median) and 95th percentiles were computed across 200 model replicates for each future climate simulation. The six simulations were combinations of the two general circulation models, version 3.1-T47 of the Canadian Centre for Climate Modelling and Analysis' Coupled Global Climate Model (CGCM 3.1; McFarlane and others, 1992; Flato, 2005) and version 5 of the Max Planck Institute's European Centre Hamburg Model (ECHAM5; Roeckner and others, 2003, 2004), and three climate change scenarios, B1, A1B, and A2, in order of low to high projected CO_2 emissions, of the Intergovernmental Panel on Climate Change's Special Report on Emissions Scenarios (Nakićenović and Swart, 2000). km^2, square kilometer]

Climate scenario	Metric (percentile)	Historical period		Projection period		Change in number of wildfires (percent)	Change in area burned (percent)
		Number of wildfires	Area burned (km^2)	Number of wildfires	Area burned (km^2)		
CGCM3.1							
A1B	Median	60	3,398	60	2,887	0.8	–15.0
A1B	95th	84	17,971	84	19,259	0.9	7.2
A2	Median	59	3,155	62	5,324	4.2	68.8
A2	95th	84	17,880	88	32,569	5.2	82.2
B1	Median	59	3,089	66	3,636	12.7	17.7
B1	95th	84	17,667	88	16,038	4.8	–9.2
ECHAM5							
A1B	Median	59	3,135	55	4,904	–6.8	56.4
A1B	95th	85	18,079	83	25,677	–2.5	42.0
A2	Median	59	3,060	51	3,412	–13.6	11.5
A2	95th	84	17,579	79	23,435	–5.9	33.3
B1	Median	59	3,159	53	2,576	–10.2	–18.5
B1	95th	85	17,428	75	11,429	–11.4	–34.4

burned across 200 model replicates averaged 12,591 km^2, or 0.85 percent of the assessment domain, which has a total area of 1.49 million km^2. The median (across 200 model replicates) annual area burned ranged from 2,477 km^2 (0.16 percent of total area) to 33,039 km^2 (2.2 percent of total area).

Under the CGCM3.1 simulations, the 50th (median) and 95th percentiles for the number of wildfires were projected to increase across all scenarios (table 2.9, fig. 2.13*A*). The increases for both percentiles were least pronounced and somewhat negligible under the A1B scenario. Projections of future area burned varied in magnitude and direction of change (relative to present) across scenarios. The 50th percentile of area burned for the B1 and A2 scenarios was projected to increase by 17.7 percent and 68.8 percent, respectively. In contrast, the 50th percentile of area burned for the A1B scenario was projected to decrease by 15 percent. The 95th percentile of area burned was projected to increase for the A1B and A2 scenarios by 7.2 percent and 82.2 percent, respectively. In contrast, the 95th percentile of area burned for the B1 scenario was projected to decrease by 9.2 percent.

Under the ECHAM5 simulations, the 50th and 95th percentiles for the number of wildfires were projected to decrease across all scenarios (table 2.9, fig. 2.13*B*), with the greatest projected decrease under the A2 scenario and the smallest projected decrease under the B1 scenario. The area burned was projected to increase for the A1B and A2 scenarios; in contrast, the area burned was projected to decrease for the B1 scenario. The greatest change from present was projected under the A1B scenario, with 56-percent and 42-percent increases for the 50th and 95th percentiles of area burned, respectively.

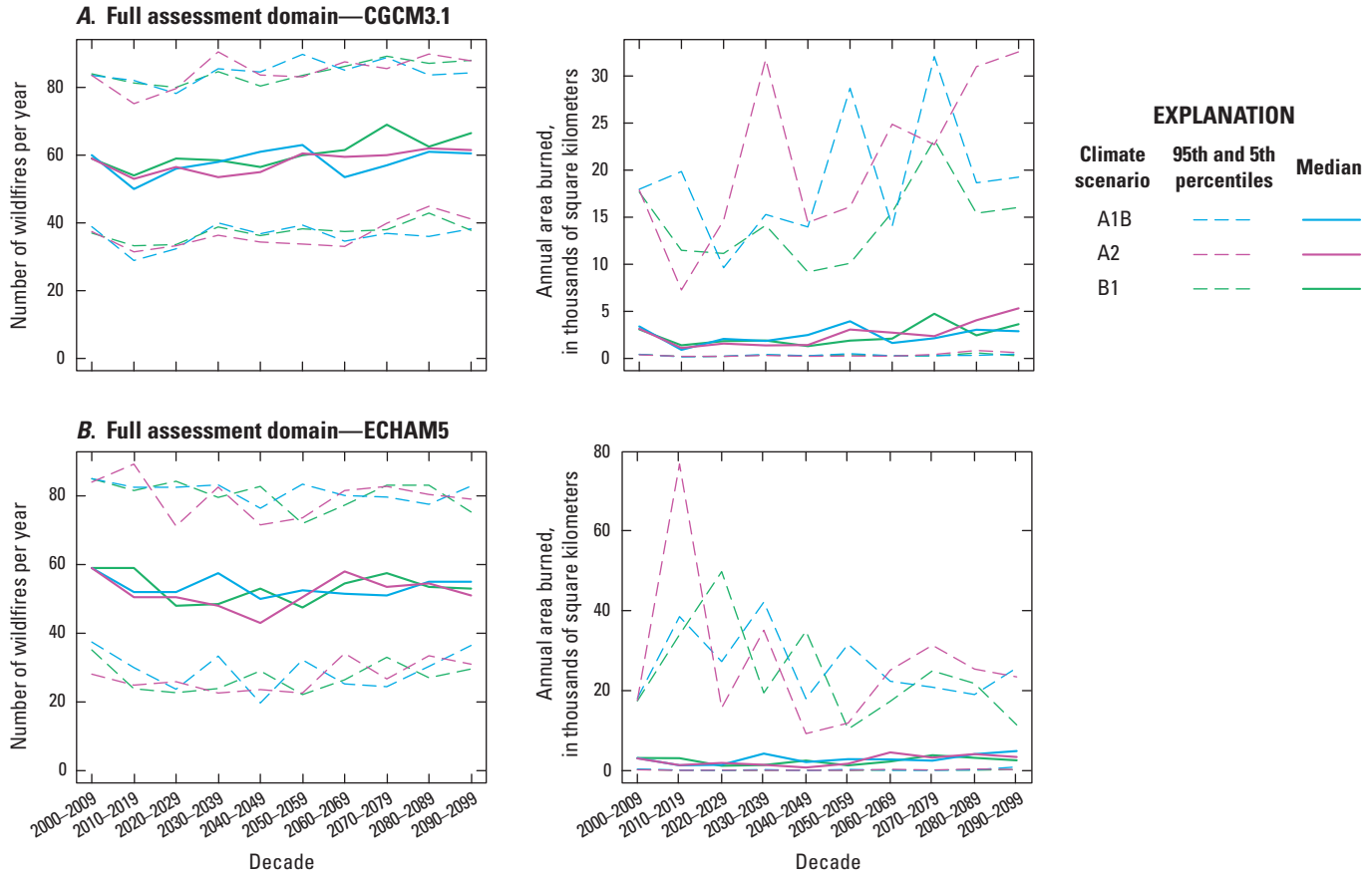

Figure 2.13. Simulated fire activity showing decadal summaries of annual projected number of wildfires and area burned for each decade from 2000 through 2099 across the full assessment domain for the *A*, version 3.1-T47 of the Canadian Centre for Climate Modelling and Analysis' Coupled Global Climate Model (CGCM3.1) simulation and *B*, version 5 of the Max Planck Institute's European Centre Hamburg Model (ECHAM5) simulation. The 50th (median), 5th, and 95th percentiles were computed across 200 simulations for climate change scenarios A1B, A2, and B1 of the Intergovernmental Panel on Climate Change's Special Report on Emissions Scenarios.

The Northwest Boreal LCC North had the most (approximately 85 percent of the statewide total) historical fire activity among the five LCC regions of the assessment and was also projected to have the most future fire activity. Under the CGCM3.1 simulations, the 50th and 95th percentiles for the number of wildfires were projected to increase for all scenarios (table 2.10, fig. 2.14*A*). The projected magnitude and direction of change in area burned varied across scenarios. The 50th percentile was projected to increase (0.9–47.6 percent) for all scenarios. In contrast, the 95th percentile was projected to decrease under the A1B and B1 scenarios and increase under the A2 scenario. Under the ECHAM5 simulations, the 50th and 95th percentiles for the number of wildfires were projected to decrease across all scenarios (table 2.10, fig. 2.14*B*). General increases in the distribution of area burned were projected under the A1B and A2 scenarios, whereas decreases were projected under the B1 scenario. The simulation under the A1B scenario projected the largest change, with 44-percent and 17-percent increases projected for the 50th and 95th percentiles of area burned, respectively.

Table 2.10. Summary of fire activity for the Northwest Boreal Landscape Conservation Cooperative North simulated for the last decades of the historical period (2000–2009) and the projection period (2090–2099).

[The 50th (median) and 95th percentiles were computed across 200 model replicates for each future climate simulation. Details regarding the models and scenarios shown can be found in table 2.9. km², square kilometer]

Climate scenario	Metric (percentile)	Historical period		Projection period		Change in number of wildfires (percent)	Change in area burned (percent)
		Number of wildfires	Area burned (km²)	Number of wildfires	Area burned (km²)		
CGCM3.1							
A1B	Median	42	2,274	45	2,295	5.9	0.9
A1B	95th	62	10,342	64	10,199	3.5	–1.4
A2	Median	42	2,194	44	3,239	7.2	47.6
A2	95th	63	10,459	66	16,626	5.3	59.0
B1	Median	42	2,216	48	2,622	15.5	18.3
B1	95th	62	10,511	67	7,855	7.3	–25.3
ECHAM5							
A1B	Median	42	2,200	40	3,174	–3.6	44.3
A1B	95th	63	10,426	62	12,217	–0.6	17.2
A2	Median	42	2,186	37	2,176	–10.8	–0.5
A2	95th	63	10,422	61	12,642	–3.1	21.3
B1	Median	42	2,230	38	1,798	–7.2	–19.4
B1	95th	63	10,264	57	8,090	–9.2	–21.2

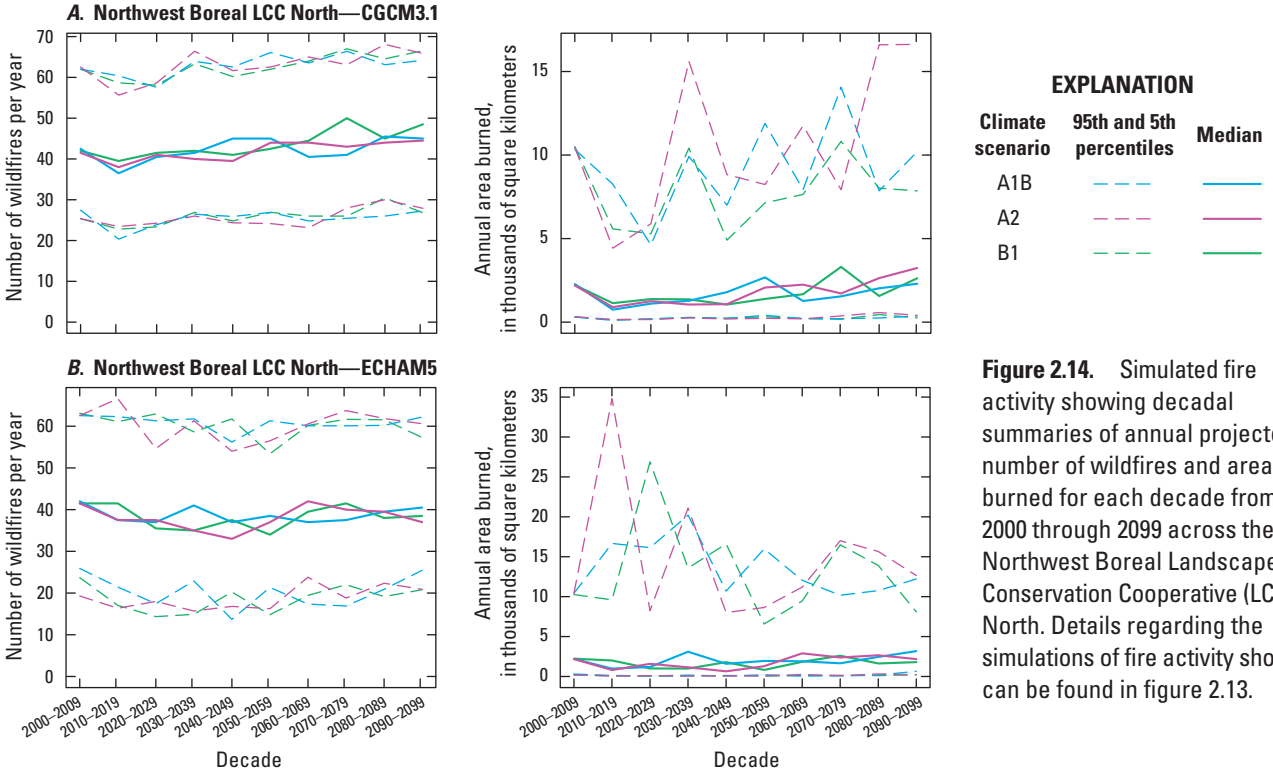

Figure 2.14. Simulated fire activity showing decadal summaries of annual projected number of wildfires and area burned for each decade from 2000 through 2099 across the Northwest Boreal Landscape Conservation Cooperative (LCC) North. Details regarding the simulations of fire activity shown can be found in figure 2.13.

The Western Alaska LCC had the second most historical fire activity among the five LCC regions and was also projected to have the second most future fire activity. Under the CGCM3.1 simulations, projected median changes in number of wildfires varied in magnitude and direction. Under the B1 and A2 scenarios, moderate increases were projected in the 50th percentile, whereas the greatest change among the scenarios was projected under the A1B scenario, with a decrease of 22.2 percent (table 2.11, fig. 2.15*A*). The distribution in area burned was projected to increase for all scenarios, except for the 50th percentile under the A1B scenario, which was projected to decrease. Under the B1 and A2 scenarios, large increases (139 percent and 180 percent, respectively) were projected in the 50th percentile. Under the ECHAM5 simulations, the 50th and 95th percentiles for the number of wildfires were projected to decrease across all scenarios (table 2.11, fig. 2.15*B*). The distribution of area burned was projected to increase under the A1B and A2 scenarios, whereas the 95th percentile under the B1 scenario was projected to decrease. The 50th percentile was projected to increase under each of the scenarios with the largest increases under the A2 and A1B scenarios (146 percent and 302 percent, respectively).

Table 2.11. Summary of fire activity for the Western Alaska Landscape Conservation Cooperative simulated for the last decades of the historical period (2000–2009) and the projection period (2090–2099).

[The 50th (median) and 95th percentiles were computed across 200 model replicates for each future climate simulation. Details regarding the models and scenarios shown can be found in table 2.9. km², square kilometer]

Climate scenario	Metric (percentile)	Historical period		Projection period		Change in number of wildfires (percent)	Change in area burned (percent)
		Number of wildfires	Area burned (km²)	Number of wildfires	Area burned (km²)		
CGCM3.1							
A1B	Median	9	714	7	344	–22.2	–51.8
A1B	95th	17	7,735	16	9,185	–7.9	18.8
A2	Median	8	332	8	929	6.2	179.8
A2	95th	17	7,315	16	10,729	–6.0	46.7
B1	Median	8	336	8	802	6.2	138.7
B1	95th	17	7,533	17	8,400	–2.6	11.5
ECHAM5							
A1B	Median	8	330	7	1,329	–17.6	302.7
A1B	95th	17	7,529	15	9,979	–14.4	32.5
A2	Median	8	334	7	824	–17.6	146.7
A2	95th	17	7,407	15	10,651	–12.1	43.8
B1	Median	8	332	6	360	–23.5	8.4
B1	95th	17	7,251	14	5,842	–18.1	–19.4

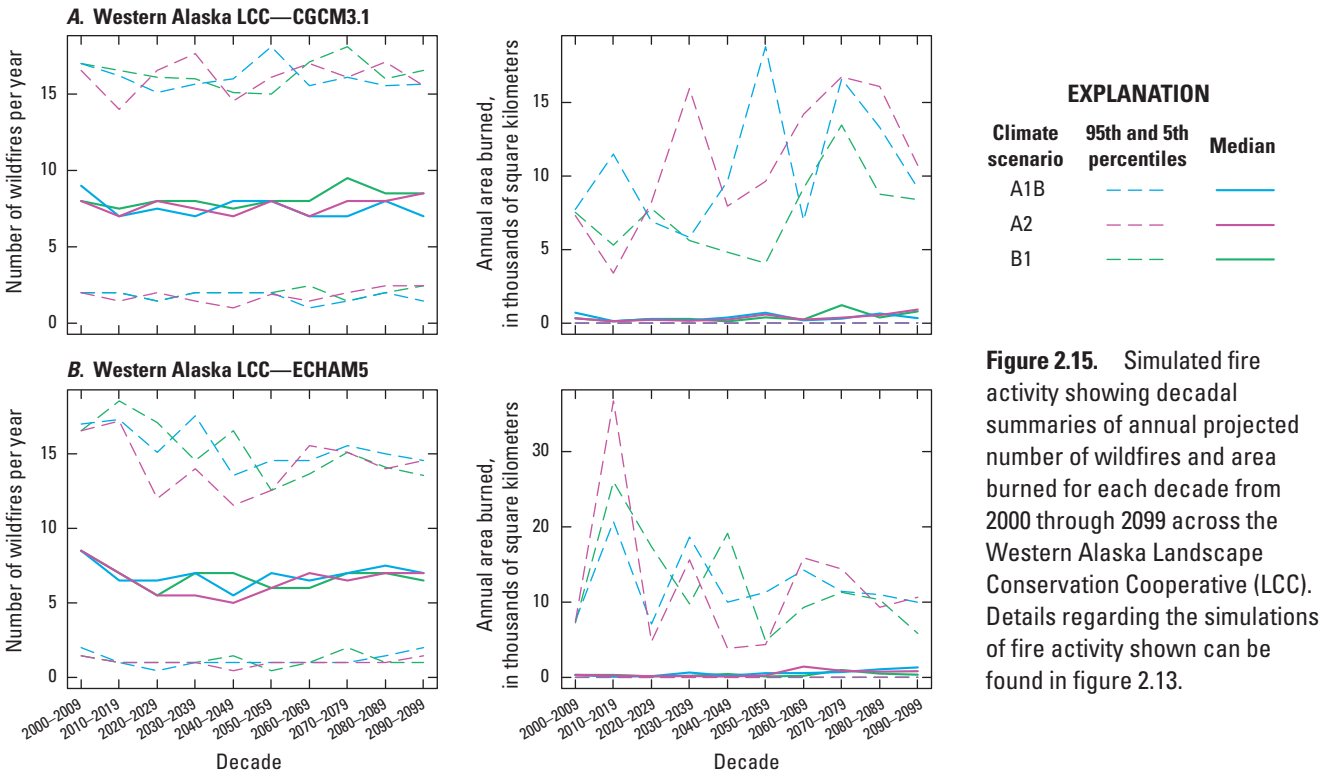

Figure 2.15. Simulated fire activity showing decadal summaries of annual projected number of wildfires and area burned for each decade from 2000 through 2099 across the Western Alaska Landscape Conservation Cooperative (LCC). Details regarding the simulations of fire activity shown can be found in figure 2.13.

In the Arctic LCC, no change was projected in the 50th percentile of the number of wildfires across all scenarios with CGCM3.1 (table 2.12, fig. 2.16*A*). The 95th percentile under the A1B and A2 scenarios was projected to increase. The projected change in area burned varied in magnitude and direction across scenarios. The 50th percentile was projected to increase under scenarios B1 and A2, whereas no change was projected under scenario A1B. The largest change was projected under the A2 scenario with an increase of 1,300 percent. The 95th percentile was projected to decrease under the B1 and A1B scenarios; however, the 95th percentile under the A2 scenario was projected to increase. Under the ECHAM5 simulations, the 50th percentile for the number of wildfires was not projected to change across all scenarios (table 2.12, fig. 2.16*B*). The 95th percentile under the B1 and A2 scenarios was projected to decrease, whereas that under the A1B scenario was projected to increase. The 50th percentile of the distribution of area burned was projected to increase across all of the scenarios, with the greatest (2,050-percent) increase projected under the A1B scenario. The 95th percentile was projected to decrease under the B1 and A2 scenarios, whereas an increase in the 95th percentile was projected under the A1B scenario.

Table 2.12. Summary of fire activity for the Arctic Landscape Conservation Cooperative simulated for the last decades of the historical period (2000–2009) and the projection period (2090–2099).

[The 50th (median) and 95th percentiles were computed across 200 model replicates for each future climate simulation. Details regarding the models and scenarios shown can be found in table 2.9. km², square kilometer]

Climate scenario	Metric (percentile)	Historical period		Projection period		Change in number of wildfires (percent)	Change in area burned (percent)
		Number of wildfires	Area burned (km²)	Number of wildfires	Area burned (km²)		
CGCM3.1							
A1B	Median	1	22	1	22	0	0
A1B	95th	3	5,553	4	4,128	18.3	–25.7
A2	Median	1	10	1	140	0	1,300
A2	95th	3	5,919	4	8,362	33.3	41.3
B1	Median	1	10	1	16	0	60
B1	95th	3	6,230	3	3,323	0	–46.7
ECHAM5							
A1B	Median	1	10	1	215	0	2,050
A1B	95th	3	6,058	4	7,525	18.3	24.2
A2	Median	1	10	1	56	0	460
A2	95th	3	6,042	3	5,473	–15	–9.4
B1	Median	1	10	1	40	0	300
B1	95th	4	6,232	3	1,421	–28.2	–77.2

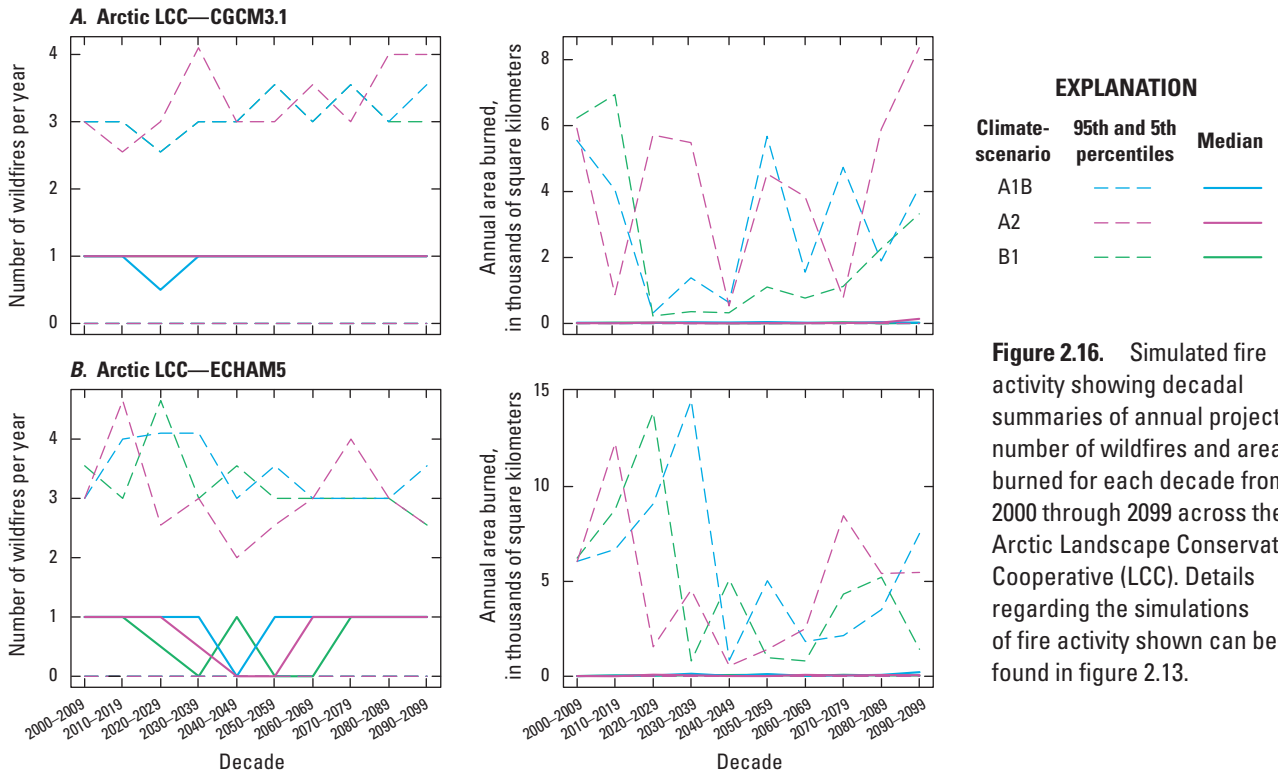

Figure 2.16. Simulated fire activity showing decadal summaries of annual projected number of wildfires and area burned for each decade from 2000 through 2099 across the Arctic Landscape Conservation Cooperative (LCC). Details regarding the simulations of fire activity shown can be found in figure 2.13.

In the Northwest Boreal LCC South, increases in the 50th and 95th percentiles for the number of wildfires were projected under the B1 and A2 scenarios with CGCM3.1, whereas decreases were projected under the A1B scenario (table 2.13, fig. 2.17*A*). The projected change in area burned varied in magnitude and direction across scenarios. The 50th percentile was projected to increase under the B1 and A2 scenarios. A decrease in the 95th percentile was projected under the B1 scenario, whereas an increase was projected under the A2 scenario. The magnitude of change was largest under the A2 scenario with the 50th percentile projected to increase by 107 percent and the 95th percentile projected to increase by 432 percent. Under the ECHAM5 simulations, the 50th and 95th percentiles for the number of wildfires were projected to decrease across all scenarios (table 2.13, fig. 2.17*B*). The 50th and 95th percentiles of the distribution of area burned were projected to increase under the A1B and A2 scenarios, whereas decreases were projected under the B1 scenario. The largest increase in the 50th percentile (51 percent) was projected under the A1B scenario, and the largest increase in the 95th percentile (110 percent) was projected under the A2 scenario.

Table 2.13. Summary of fire activity for the Northwest Boreal Landscape Conservation Cooperative South simulated for the last decades of the historical period (2000–2009) and the projection period (2090–2099).

[The 50th (median) and 95th percentiles were computed across 200 model replicates for each future climate simulation. Details regarding the models and scenarios shown can be found in table 2.9. km², square kilometer]

Climate scenario	Metric (percentile)	Historical period		Projection period		Change in number of wildfires (percent)	Change in area burned (percent)
		Number of wildfires	Area burned (km²)	Number of wildfires	Area burned (km²)		
CGCM3.1							
A1B	Median	10	264	10	167	–5	–36.7
A1B	95th	20	2,337	18	1,355	–7.9	–42.0
A2	Median	10	208	10	430	10.5	106.7
A2	95th	20	2,355	22	12,523	10.2	431.8
B1	Median	10	204	11	258	15.8	26.5
B1	95th	20	2,328	20	2,064	2.3	–11.3
ECHAM5							
A1B	Median	10	203	9	308	–5.3	51.7
A1B	95th	20	2,362	19	8,689	–2.3	267.9
A2	Median	10	200	8	203	–15.8	1.5
A2	95th	20	2,289	18	4,810	–10.2	110.1
B1	Median	10	212	8	143	–10.5	–32.5
B1	95th	20	2,283	17	1,298	–15.3	–43.1

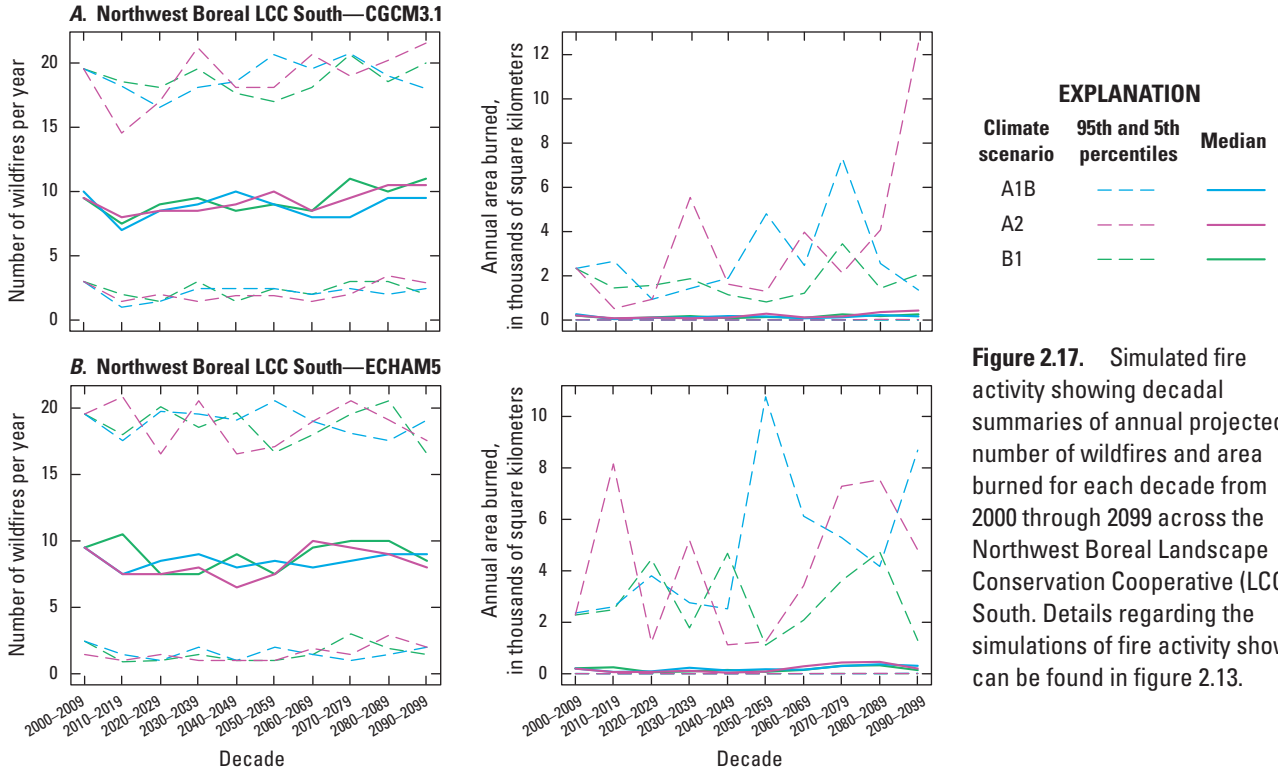

Figure 2.17. Simulated fire activity showing decadal summaries of annual projected number of wildfires and area burned for each decade from 2000 through 2099 across the Northwest Boreal Landscape Conservation Cooperative (LCC) South. Details regarding the simulations of fire activity shown can be found in figure 2.13.

Of the five assessment regions, the North Pacific LCC had the least amount of fire activity reflecting the LCC's wet and cool climate. Future simulations showed little indication of any meaningful future fire activity in this region (table 2.14, fig. 2.18*A*, *B*).

Table 2.14. Summary of fire activity for the North Pacific Landscape Conservation Cooperative simulated for the last decades of the historical period (2000–2009) and the projection period (2090–2099).

[The 50th (median) and 95th percentiles were computed across 200 model replicates for each future climate simulation. Details regarding the models and scenarios shown can be found in table 2.9. km², square kilometer; —, not applicable]

Climate scenario	Metric (percentile)	Historical period		Projection period		Change in number of wildfires (percent)	Change in area burned (percent)
		Number of wildfires	Area burned (km²)	Number of wildfires	Area burned (km²)		
CGCM3.1							
A1B	Median	0	2	0	2	—	—
A1B	95th	2	27	2	28	–22.5	3.7
A2	Median	0	2	0	5	—	—
A2	95th	2	25	3	160	64.52	540
B1	Median	0	2	0	2	—	—
B1	95th	2	25	2	25	0	0
ECHAM5							
A1B	Median	0	2	0	6	—	—
A1B	95th	2	25	3	274	93.55	996
A2	Median	0	2	0	4	—	—
A2	95th	2	24	3	121	64.52	404.17
B1	Median	0	2	0	2	—	—
B1	95th	2	23	2	44	29.03	91.3

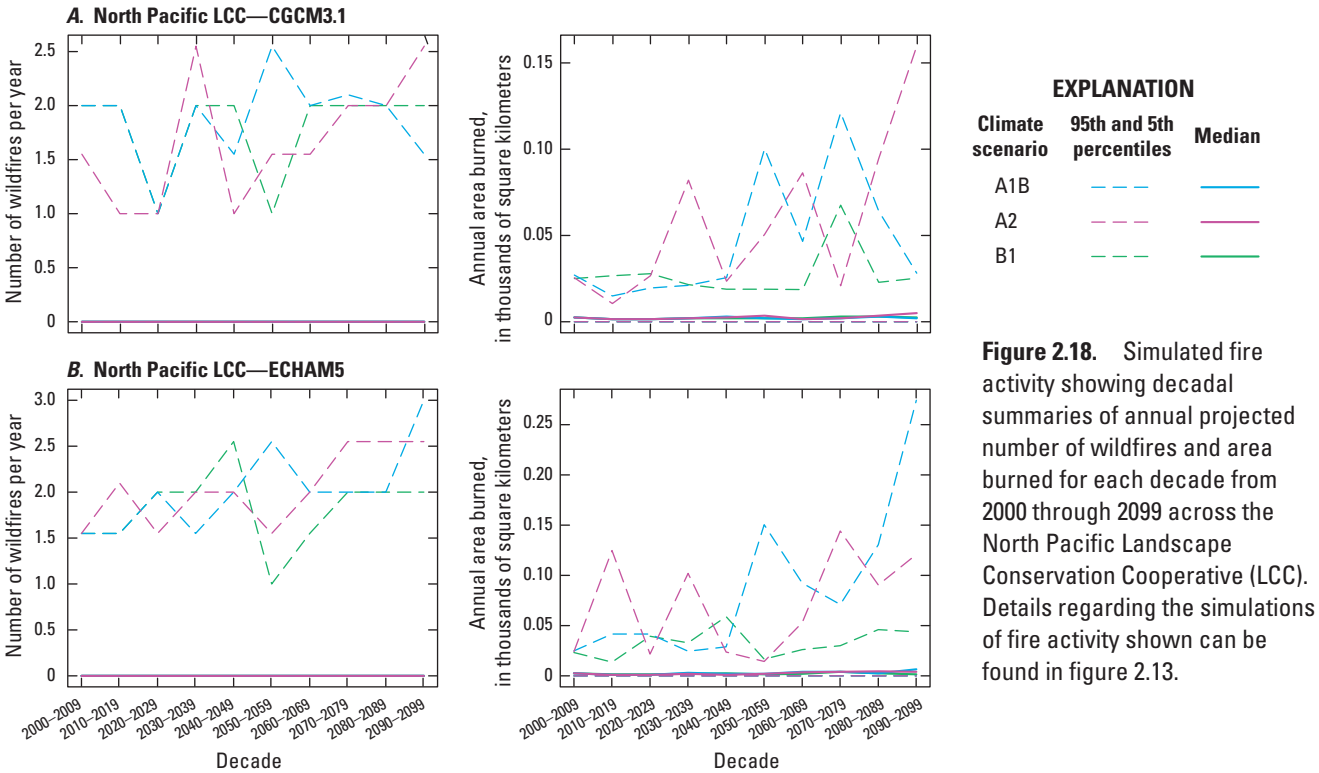

Figure 2.18. Simulated fire activity showing decadal summaries of annual projected number of wildfires and area burned for each decade from 2000 through 2099 across the North Pacific Landscape Conservation Cooperative (LCC). Details regarding the simulations of fire activity shown can be found in figure 2.13.

2.4.6. Discussion and Conclusions

Climate effects, both direct and indirect, are projected to influence the vegetation-disturbance dynamics of Alaska through the 21st century. Most of the vegetation change simulated by ALFRESCO would result from the indirect effects of climate as mediated by the fire regime. On the basis of the characterization of fire-climate relationships from the past six decades, fire regimes are forecast to change for most of the simulations considered. The Northwest Boreal LCC North would exhibit the greatest amount of change in simulated fire activity relative to historical observations. One of the dominant results following from this projected change in fire regimes is a projected decrease in the area occupied by late successional spruce forests. This decrease would be consistent across all the climate simulations for Alaska as a whole and in most of the five LCC regions.

One of the defining characteristics of the fire regime in Alaska is significant variability across both space and time. The simulated fire activity from both GCMs produced large inter-annual variability in the fire activity in a manner consistent with the historical fire data in Alaska. A steady increase in both the number of wildfires and median area burned after 2050 was projected for CGCM3.1 simulations under all scenarios. The variability of the distribution of simulated area burned also was projected to increase, as depicted by the increase in the 95th percentiles across the second half of the 21st century. In contrast, under the ECHAM5 simulations across all scenarios a small decrease in the number of wildfires and an increase in the median area burned after 2050 were projected as well as a decrease in the variability of the distribution of simulated area burned, shown in the 95th percentile.

The differences between the CGCM3.1 and ECHAM5 simulation output for the period 2010–2030 is driven largely by changes in the climate forcing of the fire activity. This is a consequence of the fact that the initial spatial distribution of differentially flammable vegetation is relatively consistent among simulations since it is determined by the patterns of historical fire. As the changes in future climate affect the landscape configuration of vegetation types through fire-initiated secondary succession, there are potential feedbacks to the fire regime. This is likely the reason that there are differences in the trends of the number of wildfires between the GCMs. That is, differences in the spatial configuration of differentially flammable vegetation types emerge uniquely for the GCMs as a function of the climate forcing effects on the fire regime. Ultimately, the configuration of the landscape dictates how the fire activity emerges for the climate signal in each year.

Simulated land-cover types in tundra-dominated portions of the assessment domain exhibited moderate levels of change. Graminoid tundra was projected to decrease under most of the future climate simulations, whereas shrub tundra was projected to increase. The magnitude and direction of change would vary considerably across the LCC regions, though consistently within each region. That is, in the Arctic LCC, graminoid tundra was projected to decrease and shrub tundra was projected to increase across the simulations, whereas opposite trends were projected for the Western Alaska LCC. These patterns reflect positive influences of a warming climate, in the case of shrub tundra increases in the Arctic LCC, as well as the indirect effects through wildfire activity, in the case of shrub tundra decreases in the Western Alaska LCC.

2.4.6.1. Uncertainty

The use of models to simulate future fire activity provides a means to assemble the state of the science and assess the likely responses to future scenarios. Generally speaking, models are developed with the intent to characterize the functional relationships between ecological responses and environmental drivers. One metric of model performance is to meaningfully explain the observed variability in an ecological response at varying resolutions of space and time. Best performing models are able to parsimoniously explain variability in a manner that is robust to the multiple sources of uncertainty that are constrained through assumptions.

The projections presented here were generated through the development of several layers of modeling, each with its own corresponding uncertainty. The process starts with data. One can consider data to be an observation of some underlying true latent process. In most settings, observed data are considered to be truth. That is, the difference between the observed value and the true state of the underlying latent process is zero. This is the implementation of the time-honored uncertainty reduction technique of assumption making. In some cases this is appropriate, in others it may make more sense to employ a hierarchical modeling approach to separate the uncertainty associated with the input data from that of the process model (Calder and others, 2003; Cressie and Wikle, 2011). When constructing simulation models, whether statistical, process-based, or otherwise, there is uncertainty associated with the functional form of the model. Finally, there is uncertainty associated with the parameters that are estimated in the modeling process.

In the work presented here, we explicitly considered uncertainty in the simulations of future fire activity that is associated with the GCMs and emissions scenarios. This was done by running simulations for different combinations of GCMs and scenarios. Bounding results were presented in the sense that the ECHAM5 model generally corresponds to the most active future fire regime and the CGCM3.1 model to the least. In using this approach, we conditioned on the functional relationship depicted in the ALFRESCO model and assumed this was the best model through the application of calibration to the historical data. That is, uncertainty in the depiction of the functional linkage between future climate and fire was constrained. One potential source of uncertainty associated with the results is the potential for the functional linkage between climate and fire to change in the future.

The historical data were also assumed, for the sake of these analyses, to be unbiased representations of the true underlying latent process of fire across the boreal forest. This assumption was used when quantifying the linkage between climate and area burned based on the historical data. There is good reason to think this is not the case in Alaska and, understandably, the reliability of the historical fire data is more questionable for the earlier part of the record (Kasischke and others, 2002, 2006). To some extent, issues related to the uncertainty associated with the data are potentially reduced owing to the increased detectability associated with large fire events. That is, it is more likely to miss a smaller fire in the record than a larger one. Since over half of the area burned in Alaska comes from approximately the largest 2.5 percent of the fires (Kasischke and Turetsky, 2006), these issues associated with uncertainty in the data are likely negligible relative to the uncertainty associated with the actual unfolding of the future climate scenario.

When considering the full assessment domain, the uncertainty associated with the projected results was greater between GCMs than it was between the emissions scenarios for a given GCM, which tend to be generally consistent. This assertion holds less credence when considering the LCC regions. To some extent this may be driven by the simple fact that there was greater variability among replicates for the consideration of smaller landscape areas.

2.4.6.2. Sensitivity

When considering the greatest potential for change in the future scenarios, it is of interest to examine not only the measure of central tendency for the future scenarios but also higher statistical moments as well. Across the entire State, there were divergent results among GCMs with respect to the change in number of wildfires. The 50th and 95th percentiles of the wildfire distributions were projected to increase for all scenarios in the CGCM3.1 model, whereas the corresponding simulated data were projected to decrease in the ECHAM5 model. Projected ignitions were placed in a spatially random manner so an increase would correspond to increases in the temperature and (or) prevalence of flammable vegetation across the landscape. The increase in number of wildfires suggests the potential for a subsequent increase in the heterogeneity of the landscape as a consequence. Across the entire State, the simulation output projected an increase in the area burned with more burning associated with the CGCM3.1 model. Interestingly, along with the increase in area burned was an opposite response in the change through time between the 95th percentiles of the CGCM3.1 and the ECHAM5 models. The CGCM3.1 model projected an increase in number of wildfires and an increase in the variability of area burned, whereas the ECHAM5 model projected a relatively stable number of wildfires and a steady decrease in the variability of area burned through time. In this context, the CGCM3.1 model projects a much more variable future with respect to landscape-scale disturbance.

When considering the LCC regions, several stand out as being most sensitive in terms of future changes in the fire regime. The North Pacific LCC had the lowest historical fire activity so any future increase would be a relatively large shift, although the absolute amount of fire activity may be negligible in the context of statewide area burned. The variability of the number of wildfires and the variability associated with the distribution of the simulated area burned were projected to increase consistently over the projection period in the North Pacific LCC. In this sense, the simulated results are consistent among all simulations, projecting that there would be a relatively large increase in fire activity. This is an example of a region where there appears to be potential for a threshold to be crossed (that is, for greater influence of fire activity) in the next century.

The simulation results also indicate that the Northwest Boreal LCC South may experience increased wildfires and area burned in the future. The ECHAM5 model projected a relatively constant number of wildfires but an increase in the variability of the area burned under the A2 and A1B scenarios. The CGCM3.1 model projected an increase in number of wildfires, but only under the A2 scenario was a corresponding increase in the variability of the area burned projected.

The simulation results for the Western Alaska LCC were relatively divergent between the two GCMs. For the CGCM3.1 model, the number of wildfires forecast was relatively constant; however, a forecast increase in the variability of area burned was consistent across the scenarios considered. Conversely, for the ECHAM5 model, the number of wildfires was projected to decrease with a corresponding decrease in the variability associated with the distribution of area burned. Thus, the sensitivity of the Western Alaska LCC to changes in future climate over the 21st century is dependent on the model used to simulate the future climate, with the CGCM3.1 model being more sensitive and the ECHAM5 model relatively stable and therefore less sensitive to climate change.

2.5. References Cited

Amiro, B.D., Todd, J.B., Wotton, B.M., Logan, K.A., Flannigan, M.D., Stocks, B.J., Mason, J.A., Martell, D.L., and Hirsch, K.G., 2001, Direct carbon emissions from Canadian forest fires, 1959–1999: Canadian Journal of Forest Research, v. 31, no. 3, p. 512–525, http://dx.doi.org/10.1139/x00-197.

Balshi, M.S., McGuire, A.D., Duffy, Paul, Flannigan, Mike, Walsh, John, and Melillo, Jerry, 2009, Assessing the response of area burned to changing climate in western boreal North America using a Multivariate Adaptive Regression Splines (MARS) approach: Global Change Biology, v. 15, no. 3, p. 578–600, http://dx.doi.org/10.1111/j.1365-2486.2008.01679.x.

Barber, V.A., Juday, G.P., and Finney, B.P., 2000, Reduced growth of Alaskan white spruce in the twentieth century from temperature-induced drought stress: Nature, v. 405, no. 6787, p. 668–673, http://dx.doi.org/10.1038/35015049.

Barber, V.A., Juday, G.P., Finney, B.P., and Wilmking, Martin, 2004, Reconstruction of summer temperatures in interior Alaska from tree-ring proxies; Evidence for changing synoptic climate regimes: Climatic Change, v. 63, nos. 1–2, p. 91–120, http://dx.doi.org/10.1023/B:CLIM.0000018501.98266.55.

Beck, P.S.A., Juday, G.P., Alix, Claire, Barber, V.A., Winslow, S.E., Sousa, E.E., Heiser, Patricia, Herriges, J.D., and Goetz, S.J., 2011, Changes in forest productivity across Alaska consistent with biome shift: Ecology Letters, v. 14, no. 4, p. 373–379, http://dx.doi.org/10.1111/j.1461-0248.2011.01598.x.

Berg, E.E., Hillman, K.M., Dial, Roman, and DeRuwe, Allana, 2009, Recent woody invasion of wetlands on the Kenai Peninsula Lowlands, south-central Alaska; A major regime shift after 18,000 years of wet *Sphagnum*-sedge peat recruitment: Canadian Journal of Forest Research, v. 39, no. 11, p. 2033–2046, http://dx.doi.org/10.1139/X09-121.

Burn, C.R., Mackay, J.R., and Kokelj, S.V., 2009, The thermal regime of permafrost and its susceptibility to degradation in upland terrain near Inuvik, N.W.T.: Permafrost and Periglacial Processes, v. 20, no. 2, p. 221–227, http://dx.doi.org/10.1002/ppp.649.

Calder, Catherine, Lavine, Michael, Müller, Peter, and Clark, J.S., 2003, Incorporating multiple sources of stochasticity into dynamic population models: Ecology, v. 84, no. 6, p. 1395–1402, http://dx.doi.org/10.1890/0012-9658(2003)084[1395:IMSOSI]2.0.CO;2.

Chapman, W.L., and Walsh, J.E., 1993, Recent variations of sea ice and air temperature in high latitudes: Bulletin of the American Meteorological Society, v. 74, no. 1, p. 33–47, http://dx.doi.org/10.1175/1520-0477(1993)074<0033:RVOSIA>2.0.CO;2.

Cressie, Noel, and Wikle, C.K., 2011, Statistics for spatio-temporal data: Hoboken, N.J., John Wiley & Sons, Inc., 588 p.

Daly, Christopher, Halbleib, Michael, Smith, J.I., Gibson, W.P., Doggett, M.K., Taylor, G.H., Curtis, Jan, and Pasteris, P.P., 2008, Physiographically sensitive mapping of climatological temperature and precipitation across the conterminous United States: International Journal of Climatology, v. 28, no. 15, p. 2031–2064, http://dx.doi.org/10.1002/joc.1688.

Duffy, P.A., Epting, Justin, Graham, J.M., Rupp, T.S., and McGuire, A.D., 2007, Analysis of Alaskan burn severity patterns using remotely sensed data: International Journal of Wildland Fire, v. 16, no. 3, p. 277–284, http://dx.doi.org/10.1071/WF06034.

Duffy, P.A., Walsh, J.E., Graham, J.M., Mann, D.H., and Rupp, T.S., 2005, Impacts of large-scale atmospheric-ocean variability on Alaskan fire season severity: Ecological Applications, v. 15, no. 4, p. 1317–1330, http://dx.doi.org/10.1890/04-0739.

Dyrness, C.T., and Norum, R.A., 1983, The effects of experimental fires on black spruce forest floors in interior Alaska: Canadian Journal of Forest Research, v. 13, no. 5, p. 879–893, http://dx.doi.org/10.1139/x83-118.

Euskirchen, E.S., McGuire, A.D., Rupp, T.S., Chapin, F.S., III, and Walsh, J.E., 2009, Projected changes in atmospheric heating due to changes in fire disturbance and the snow season in the western Arctic, 2003–2100: Journal of Geophysical Research; Biogeosciences, v. 114, no. G4, article G04022, 15 p., http://dx.doi.org/10.1029/2009JG001095.

Flato, G.M., 2005, The third generation Coupled Global Climate Model (CGCM3) [and included links to the description of the AGCM3 atmospheric model]: Canadian Centre for Climate Modelling and Analysis, accessed September 1, 2014, at http://ec.gc.ca/ccmac-cccma/default.asp?lang=En&n=1299529F-1.

Genet, H., McGuire, A.D., Barrett, K., Breen, A., Euskirchen, E.S., Johnstone, J.F., Kasischke, E.S., Melvin, A.M., Bennett, A., Mack, M.C., Rupp, T.S., Schuur, E.A.G., Turetsky, M.R., and Yuan, F., 2013, Modeling the effects of fire severity and climate warming on active layer thickness and soil carbon storage of black spruce forests across the landscape in interior Alaska: Environmental Research Letters, v. 8, no. 4, letter 045016, 13 p., http://dx.doi.org/10.1088/1748-9326/8/4/045016.

Gillett, N.P., Weaver, A.J., Zwiers, F.W., and Flannigan, M.D., 2004, Detecting the effect of climate change on Canadian forest fires: Geophysical Research Letters, v. 31, no. 18, letter L18211, 4 p., http://dx.doi.org/10.1029/2004GL020876.

Goetz, S.J., Bunn, A.G., Fiske, G.J., and Houghton, R.A., 2005, Satellite-observed photosynthetic trends across boreal North America associated with climate and fire disturbance: National Academy of Sciences Proceedings, v. 102, no. 38, p. 13521–13525, http://dx.doi.org/10.1073/pnas.0506179102.

Gustine, D.D., Brinkman, T.J., Lindgren, M.A., Schmidt, J.I., Rupp, T.S., and Adams, L.G., 2014, Climate-driven effects of fire on winter habitat for caribou in the Alaskan-Yukon Arctic: PLOS ONE, v. 9, no. 7, article e100588, 11 p., http://dx.doi.org/10.1371/journal.pone.0100588.

Harris, I., Jones, P.D., Osborn, T.J., and Lister, D.H., 2014, Updated high-resolution grids of monthly climatic observations—the CRU TS3.10 dataset: International Journal of Climatology, v. 34, no. 3, p. 623–642, http://dx.doi.org/10.1002/joc.3711.

Hartmann, Brian, and Wendler, Gerd, 2005, The significance of the 1976 Pacific climate shift in the climatology of Alaska: Journal of Climate, v. 18, no. 22, p. 4824–4839, http://dx.doi.org/10.1175/JCLI3532.1.

Hay, L.E., Wilby, R.L., and Leavesley, G.H., 2000, A comparison of delta change and downscaled GCM scenarios for three mountainous basins in the United States: Journal of the American Water Resources Association, v. 36, no. 2, p. 387–397, http://dx.doi.org/10.1111/j.1752-1688.2000.tb04276.x.

Hayes, D.J., McGuire, A.D., Kicklighter, D.W., Gurney, K.R., Burnside, T.J., and Melillo, J.M., 2011, Is the northern high-latitude land-based CO_2 sink weakening?: Global Biogeochemical Cycles, v. 25, no. 3, article GB3018, 14 p., http://dx.doi.org/10.1029/2010GB003813.

Hayhoe, K.A., 2010, A standardized framework for evaluating the skill of regional climate downscaling techniques: Urbana-Champaign, Ill., University of Illinois, Ph.D. dissertation, 153 p. [Also available at http://hdl.handle.net/2142/16044.]

Hennon, P., D'Amore, D., Wittwer, D., Johnson, A., Schaberg, P., Hawley, G., Beier, C., Sink, S., and Juday, G., 2006, Climate warming, reduced snow, and freezing injury could explain the demise of yellow-cedar in southeast Alaska, USA: World Resource Review, v. 18, no. 2, p. 427–450. [Also available at http://www.fs.usda.gov/Internet/FSE_DOCUMENTS/fsbdev2_038021.pdf.]

Hinzman L.D., Bettez, N.D., Bolton, W.R., Chapin, F.S., Dyurgerov, M.B., Fastie, C.L., Griffith, Brad, Hollister, R.D., Hope, Allen, Huntington, H.P., Jensen, A.M., Jia, G.J., Jorgenson, Torre, Kane, D.L., Klein, D.R., Kofinas, Gary, Lynch, A.H., Lloyd, A.H., McGuire, A.D., Nelson, F.E., Oechel, W.C., Osterkamp, T.E., Racine, C.H., Romanovsky, V.E., Stone, R.S., Stow, D.A., Sturm, Matthew, Tweedie, C.E., Vourlitis, G.L., Walker, M.D., Walker, D.A., Webber, P.J., Welker, J.M., Winker, K.S., and Yoshikawa, Kenji, 2005, Evidence and implications of recent climate change in northern Alaska and other arctic regions: Climatic Change, v. 72, no. 3, p. 251–298, http://dx.doi.org/10.1007/s10584-005-5352-2.

Johnstone, J.F., Chapin, F.S., III, Hollingsworth, T.N., Mack, M.C., Romanovsky, Vladimir, and Turetsky, Merritt, 2010, Fire, climate change, and forest resilience in interior Alaska: Canadian Journal of Forest Research, v. 40, no. 7, p. 1302–1312, http://dx.doi.org/10.1139/X10-061.

Johnstone, J.F., Rupp, T.S., Olson, Mark, and Verbyla, David, 2011, Modeling impacts of fire severity on successional trajectories and future fire behavior in Alaskan boreal forests: Landscape Ecology, v. 26, no. 4, p. 487–500, http://dx.doi.org/10.1007/s10980-011-9574-6.

Jorgenson, M.T., Racine, C.H., Walters, J.C., and Osterkamp, T.E., 2001, Permafrost degradation and ecological changes associated with a warming climate in central Alaska: Climatic Change, v. 48, no. 4, p. 551–579, http://dx.doi.org/10.1023/A:1005667424292.

Kasischke, E.S., Hyer, E.J., Novelli, P.C., Bruhwiler, L.P., French, N.H.F., Sukhinin, A.I., Hewson, J.H., and Stocks, B.J., 2005, Influences of boreal fire emissions on Northern Hemisphere atmospheric carbon and carbon monoxide: Global Biogeochemical Cycles, v. 19, no. 1, article GB1012, 16 p., http://dx.doi.org/10.1029/2004GB002300.

Kasischke, E.S., O'Neill, K.P., French, N.H.F., and Bourgeau-Chavez, L.L., 2000, Controls on patterns of biomass burning in Alaskan boreal forests, chap. 10 *of* Kasischke, E.S., and Stocks, B.J., eds., Fire, climate change, and carbon cycling in the boreal forest: New York, Springer-Verlag, Ecological Studies, v. 138, p. 173–196.

Kasischke, E.S., Rupp, T.S., and Verbyla, D.L., 2006, Fire trends in the Alaskan boreal forest, chap. 17 *of* Chapin, F.S., III, Oswood, M.W., Van Cleve, Keith, Viereck, L.A., and Verbyla, D.L., eds., Alaska's changing boreal forest: New York, Oxford University Press, p. 285–301.

Kasischke, E.S., and Turetsky, M.R., 2006, Recent changes in the fire regime across the North American boreal region—Spatial and temporal patterns of burning across Canada and Alaska: Geophysical Research Letters, v. 33, no. 9, letter L09703, 5 p., http://dx.doi.org/10.1029/2006GL025677.

Kasischke, E.S., Verbyla, D.L., Rupp, T.S., McGuire, A.D., Murphy, K.A., Jandt, Randi, Barnes, J.L., Hoy, E.E., Duffy, P.A., Calef, Monika, and Turetsky, M.R., 2010, Alaska's changing fire regime—Implications for the vulnerability of its boreal forests: Canadian Journal of Forest Research, v. 40, no. 7, p. 1313–1324, http://dx.doi.org/10.1139/X10-098.

Kasischke, E.S., Williams, David, and Barry, Donald, 2002, Analysis of the patterns of large fires in the boreal forest region of Alaska: International Journal of Wildland Fire, v. 11, no. 2, p. 131–144, http://dx.doi.org/10.1071/WF02023.

Kaufman, D.S., Schneider, D.P., McKay, N.P., Ammann, C.M., Bradley, R.S., Briffa, K.R., Miller, G.H., Otto-Bliesner, B.L., Overpeck, J.T., Vinther, B.M., and Arctic Lakes 2k Project Members, 2009, Recent warming reverses long-term Arctic cooling: Science, v. 325, no. 5945, p. 1236–1239, http://dx.doi.org/10.1126/science.1173983.

Kharuk, V.I., Dvinskaya, M.L., and Ranson, K.J., 2013, Fire return intervals within the northern boundary of the larch forest in central Siberia: International Journal of Wildland Fire, v. 22, no. 2, p. 207–211, http://dx.doi.org/10.1071/WF11181.

Mann, D.H., Rupp, T.S., Olson, M.A., and Duffy, P.A., 2012, Is Alaska's boreal forest now crossing a major ecological threshold?: Arctic, Antarctic, and Alpine Research, v. 44, no. 3, p. 319–331, http://dx.doi.org/10.1657/1938-4246-44.3.319.

Mantua, N.J., Hare, S.R., Zhang, Yuan, Wallace, J.M., and Francis, R.C., 1997, A Pacific interdecadal climate oscillation with impacts on salmon production: Bulletin of the American Meteorological Society, v. 78, no. 6, p. 1069–1079, http://dx.doi.org/10.1175/1520-0477(1997)078<1069:APICOW>2.0.CO;2.

Markon, C.J., Trainor, S.F., and Chapin, F.S., III, eds., 2012, The United States National Climate Assessment—Alaska Technical Regional Report: U.S. Geological Survey Circular 1379, 148 p. [Also available at http://pubs.usgs.gov/circ/1379/.]

McFarlane, N.A., Boer, G.J., Blanchet, J.-P., and Lazare, M., 1992, The Canadian Climate Centre second-generation general circulation model and its equilibrium climate: Journal of Climate, v. 5, no. 10, p. 1013–1044, http://dx.doi.org/10.1175/1520-0442(1992)005<1013:TCCCSG>2.0.CO;2.

McGuire, A.D., Ruess, R.W., Lloyd, A., Yarie, J., Clein, J.S., and Juday, G.P., 2010, Vulnerability of white spruce tree growth in interior Alaska in response to climate variability; Dendrochronological, demographic, and experimental perspectives: Canadian Journal of Forest Research, v. 40, no. 7, p. 1197–1209, http://dx.doi.org/10.1139/X09-206.

Meehl, G.A., Covey, Curt, Taylor, K.E., Delworth, Thomas, Stouffer, R.J., Latif, Mojib, McAvaney, Bryant, and Mitchell, J.F.B., 2007, The WCRP CMIP3 multimodel dataset—A new era in climate change research: Bulletin of the American Meteorological Society, v. 88, no. 9, p. 1383–1394, http://dx.doi.org/10.1175/BAMS-88-9-1383.

Myers-Smith, I.H., Harden, J.W., Wilmking, M., Fuller, C.C., McGuire, A.D., and Chapin, F.S., III, 2008, Wetland succession in a permafrost collapse; Interactions between fire and thermokarst: Biogeosciences, v. 5, no. 5, p. 1273–1286, http://dx.doi.org/10.5194/bg-5-1273-2008.

Nakićenović, Nebojša, and Swart, Robert, eds., 2000, Special report on emissions scenarios—A special report of Working Group III of the Intergovernmental Panel on Climate Change: Cambridge, United Kingdom, Cambridge University Press, 599 p. [Also available at http://www.ipcc.ch/ipccreports/sres/emission/index.php?idp=0.]

North American Land Change Monitoring System, 2010, 2005 North American land cover at 250 m spatial resolution (edition 1.0): Natural Resources Canada/Canadian Center for Remote Sensing (NRCan/CCRS), United States Geological Survey (USGS); Insituto Nacional de Estadística y Geografía (INEGI), Comisión Nacional para el Conocimiento y Uso de la Biodiversidad (CONABIO), and Comisión Nacional Forestal (CONAFOR), accessed October 30, 2011, at http://www.cec.org/tools-and-resources/map-files/land-cover-2005.

Overland, J.E., Spillane, M.C., Percival, D.B., Wang, Muyin, and Mofjeld, H.O., 2004, Seasonal and regional variation of pan-Arctic surface air temperature over the instrumental record: Journal of Climate, v. 17, no. 17, p. 3263–3282, http://dx.doi.org/10.1175/1520-0442(2004)017<3263:SARVOP>2.0.CO;2.

Overpeck, J., Hughen, K., Hardy, D., Bradley, R., Case, R., Douglas, M., Finney, B., Gajewski, K., Jacoby, G., Jennings, A., Lamoureux, S., Lasca, A., MacDonald, G., Moore, J., Retelle, M., Smith, S., Wolfe, A., and Zielinski, G., 1997, Arctic environmental change of the last four centuries: Science, v. 278, no. 5341, p. 1251–1256, http://dx.doi.org/10.1126/science.278.5341.1251.

Randerson, J.T., Liu, H., Flanner, M.G., Chambers, S.D., Jin, Y., Hess, P.G., Pfister, G., Mack, M.C., Treseder, K.K., Welp, L.R., Chapin, F.S., Harden, J.W., Goulden, M.L., Lyons, E., Neff, J.C., Schurr, E.A.G., and Zender, C.S., 2006, The impact of boreal forest fire on climate warming: Science, v. 314, no. 5802, p. 1130–1132, http://dx.doi.org/10.1126/science.1132075.

Roeckner, E., Bäuml, G., Bonaventura, L., Brokopf, R., Esch, M., Giorgetta, M., Hagemann, S., Kirchner, I., Kornblueh, L., Manzini, E., Rhodin, A., Schlese, U., Schulzweida, U., and Tompkins, A., 2003, The atmospheric general circulation model ECHAM5, part I—Model description: Max-Planck-Institut für Meteorologie Report, no. 349, 127 p. [Also available at https://www.mpimet.mpg.de/fileadmin/publikationen/Reports/max_scirep_349.pdf.]

Roeckner, E., Brokopf, R., Esch, M., Giorgetta, M., Hagemann, S., Kornblueh, L., Manzini, E., Schlese, U., and Schulzweida, U., 2004, The atmospheric general circulation model ECHAM5, part II—Sensitivity of simulated climate to horizontal and vertical resolution: Max-Planck-Institut für Meteorologie Report, no. 354, 56 p. [Also available at http://pubman.mpdl.mpg.de/pubman/item/escidoc:995221:8/component/escidoc:995220/MPI_Report354.pdf.]

Rupp, T.S., Chen, Xi, Olson, Mark, and McGuire, A.D., 2007, Sensitivity of simulated boreal fire dynamics to uncertainties in climate drivers: Earth Interactions, v. 11, no. 3, p. 1–21, http://dx.doi.org/10.1175/EI189.1.

Rupp, T.S., Olson, Mark, Adams, L.G., Dale, B.W., Joly, Kyle, Henkleman, Jonathan, Collins, W.B., and Starfield, A.M., 2006, Simulating the influences of various fire regimes on caribou winter habitat: Ecological Applications, v. 16, no. 5, p. 1730–1743, http://dx.doi.org/10.1890/1051-0761(2006)016[1730:STIOVF]2.0.CO;2.

Rupp, T.S., Starfield, A.M., and Chapin, F.S., III, 2000, A frame-based spatially explicit model of subarctic vegetation response to climatic change; Comparison with a point model: Landscape Ecology, v. 15, no. 4, p. 383–400, http://dx.doi.org/10.1023/A:1008168418778.

Rupp, T.S., Starfield, A.M., Chapin, F.S., III, and Duffy, P., 2002, Modeling the impact of black spruce on the fire regime of Alaskan boreal forest: Climatic Change, v. 55, nos. 1–2, p. 213–233, http://dx.doi.org/10.1023/A:1020247405652.

Serreze, M.C., and Francis, J.A., 2006, The Arctic amplification debate: Climatic Change, v. 76, nos. 3–4, p. 241–264, http://dx.doi.org/10.1007/s10584-005-9017-y.

Serreze, M.C., Walsh, J.E., Chapin, F.S., III, Osterkamp, T., Dyurgerov, M., Romanovsky, V., Oechel, W.C., Morison, J., Zhang, T., and Barry, R.G., 2000, Observational evidence of recent change in the northern high-latitude environment: Climatic Change, v. 46, nos. 1–2, p. 159–207, http://dx.doi.org/10.1023/A:1005504031923.

Shulski, Martha, and Wendler, Gerd, 2007, The climate of Alaska: Fairbanks, Alaska, University of Alaska Press, 216 p.

Solomon, Susan, Qin, Dahe, Manning, Martin, Chen, Zhenlin, Marquis, Melinda, Averyt, Kristen, Tignor, M.M.B., and Miller, H.L., Jr., eds., 2007, Climate change 2007—The physical science basis, Contribution of Working Group I to the Fourth Assessment Report of the Intergovernmental Panel on Climate Change: Cambridge, United Kingdom, Cambridge University Press, 996 p. [Also available at https://www.ipcc.ch/publications_and_data/publications_ipcc_fourth_assessment_report_wg1_report_the_physical_science_basis.htm.]

Stafford, J.M., Wendler, G., and Curtis, J., 2000, Temperature and precipitation of Alaska; 50 year trend analysis: Theoretical and Applied Climatology, v. 67, nos. 1–2, p. 33–44, http://dx.doi.org/10.1007/s007040070014.

Strengers, Bart, Leemans, Rik, Eickhout, Bas, de Vries, Bert, and Bouwman, Lex, 2004, The land-use projections and resulting emissions in the IPCC SRES scenarios as simulated by the IMAGE 2.2 model: GeoJournal, v. 61, no. 4, p. 381–393, http://dx.doi.org/10.1007/s10708-004-5054-8.

Turetsky, M.R., Kane, E.S., Harden, J.W., Ottmar, R.D., Manies, K.L., Hoy, Elizabeth, and Kasischke, E.S., 2011, Recent acceleration of biomass burning and carbon losses in Alaskan forests and peatlands: Nature Geoscience, v. 4, no. 1, p. 27–31, http://dx.doi.org/10.1038/ngeo1027.

U.S. Department of Agriculture, National Agricultural Statistics Service, 2014, 2012 census of agriculture; United States summary and State data: U.S. Department of Agriculture, Geographic Area Series, v. 1, pt. 51, 586 p.

Verbyla, David, 2008, The greening and browning of Alaska based on 1982–2003 satellite data: Global Ecology and Biogeography, v. 17, no. 4, p. 547–555, http://dx.doi.org/10.1111/j.1466-8238.2008.00396.x.

Walsh, J.E., Chapman, W.L., Romanovsky, Vladimir, Christensen, J.H., and Stendel, Martin, 2008, Global climate model performance over Alaska and Greenland: Journal of Climate, v. 21, no. 23, p. 6156–6174, http://dx.doi.org/10.1175/2008JCLI2163.1.

Werner, R.A., Holsten, E.H., Matsuoka, S.M., and Burnside, R.E., 2006, Spruce beetles and forest ecosystems in south-central Alaska; A review of 30 years of research: Forest Ecology and Management, v. 227, no. 3, p. 195–206, http://dx.doi.org/10.1016/j.foreco.2006.02.050.

World Meteorological Organization, 2008, Guide to meteorological instruments and methods of observation (7th ed.): Commission for Instruments and Methods of Observation, World Meteorological Organization, no. 8, accessed December 15, 2014, at https://www.wmo.int/pages/prog/www/IMOP/CIMO-Guide.html.

Yoshikawa, Kenji, Bolton, W.R., Romanovsky, V.E., Fukuda, Masami, and Hinzman, L.D., 2002, Impacts of wildfire on the permafrost in the boreal forests of interior Alaska: Journal of Geophysical Research; Atmospheres, v. 107, no. D1, p. FFR 4–1 to FFR 4–14, http://dx.doi.org/10.1029/2001JD000438.

Chapter 3. Soil Carbon and Permafrost Estimates and Susceptibility to Climate Change in Alaska

By Bruce K. Wylie,[1] Neal J. Pastick,[2] Kristopher D. Johnson,[3] Norman Bliss,[4] and Hélène Genet[5]

3.1. Highlights

- Several soil carbon and permafrost data products in Alaska, either produced for this assessment or available from the literature, were evaluated to synthesize observation-based estimates of distributions of soil organic carbon (SOC), permafrost, and other variables. The synthesis was also compared to simulated estimates by an ecosystem carbon dynamic model called DOS-TEM (Dynamic Organic Soil version of the Terrestrial Ecosystem Model).
- The total SOC storage in boreal and arctic regions in Alaska ranged from 31 to 72 petagrams of carbon (PgC) among different mapped products, and SOC simulated by DOS-TEM was well within this range at 46 PgC (with a standard deviation [s.d.] of 22 PgC).
- Near-surface (within 1 meter [m]) permafrost (NSP) was estimated to underlie 36 to 67 percent of Alaska among different map products used in the evaluation, and NSP simulated by DOS-TEM was within this range at 44 percent. Furthermore, DOS-TEM simulations of NSP fell within the range of map product estimates for 87 percent of ecotypes, and outlier ecotypes constitute approximately 16 percent of Alaska.
- Average active-layer thickness (ALT) ranged from 76 to 84 centimeters (cm) from surface among different mapped products, and ALT simulated by DOS-TEM was slightly outside of this range at 86 ± 8 cm, but within the range of map product uncertainty. The ALT derived from the state soil geographic database (STATSGO) was generally higher than other estimates, possibly owing to how ALT is described in soil pedon datasets and measured in the field.
- Organic soils were estimated to underlie 8 to 30 percent of Alaska among different map products, and organic soil simulations by DOS-TEM were within this range at 18 percent.
- A simple conceptual model of soil susceptibility to climate change indicated that Arctic Landscape Conservation Cooperative (LCC) lowland shrub tundra and Western Alaska LCC lowland shrub tundra ecotypes are highly susceptible to climate change because of large and potentially liable frozen and unfrozen SOC stocks.
- Intermediate susceptible ecotypes were Arctic LCC upland shrub and graminoid tundra with susceptibility being driven by potential changes to continuous NSP extent and the lack of thick insulating layers of organic soils.

[1]U.S. Geological Survey, Sioux Falls, S. Dak.

[2]Stinger Ghaffarian Technologies, Inc., Sioux Falls, S. Dak., and University of Minnesota, St. Paul, Minn.

[3]U.S. Department of Agriculture Forest Service, Newtown Square, Pa.

[4]ASRC Federal InuTeq, Sioux Falls, S. Dak.

[5]University of Alaska-Fairbanks, Fairbanks, Alaska.

3.2. Conceptual Discussion of Roles and State of the Knowledge About Soil Carbon and Permafrost in Boreal and Arctic Ecosystems

There are large accumulations of soil organic carbon in arctic and boreal forest ecosystems. Hugelius and others (2014) indicated that the northern permafrost regions of the world contain approximately 1,300 petagrams of organic carbon (PgC), of which 800 PgC (61 percent) occurs in perennially frozen soils and deposits. For comparison, the amount of carbon as carbon dioxide (CO_2) currently in the atmosphere is approximately 800 PgC, of which 240 PgC represents the net accumulation in the atmosphere from fossil-fuel and land-use emissions between 1750 and 2011 (Stocker and others, 2013). Thus, the carbon in permafrost-affected ground is nearly double the carbon in the atmosphere. The thaw and decay of permafrost and permafrost carbon will be irreversible with the onset of warming trend of the 2014 and 2100 timeframes, and the release of this carbon (the permafrost carbon feedback) is not currently accounted for in the climate models used by the Intergovernmental Panel on Climate Change (IPCC) Fifth Assessment Report (Stocker and others, 2013). Accounting for this additional carbon will require larger reductions in fossil-fuel emissions to reach a target atmospheric CO_2 concentration and therefore a target limit on global temperature increase (Schaefer and others, 2011).

To estimate the quantity of soil organic carbon in Alaska, Johnson and others (2011) compiled data for many soil profile measurements and evaluated the distributions of soil carbon by climate regions, landforms, ecoregions, and ecosystem types. Bliss and Maursetter (2010) estimated a total of 48 PgC of soil organic carbon for Alaska and Mishra and Riley (2012) estimated 77 PgC, with these estimates influenced by assumptions and data availability for deeper soils (for example, between 1 and 3 meters [m]). Although these soil carbon inventory studies largely used the same soil carbon measurements, with slight variations and additions between assessments, each study made use of different upscaling approaches.

The status of the permafrost system can be measured using deep boreholes with accurate measurements of the change of temperature with depth through the Global Terrestrial Network for Permafrost (GTN–P; Clow, 2014). The thickness of the active layer (that is, maximum annual thaw depth) is another measure for the status of the permafrost system. With warmer temperatures, the thickness of the active layer is expected to increase. Although point-based measurements are useful for understanding local permafrost dynamics, these measurements are typically sparse and there is an increasing need to monitor and map permafrost properties at larger scales (National Research Council, 2014). As part of an international network of Circumpolar Active Layer Monitoring (CALM) sites, Hinkel and Nelson (2003) concluded that in Alaska, active-layer thickness is correlated with inter-annual variability in summer temperature and that local variations in active-layer thickness and near-surface soil moisture are influenced by vegetation, substrate properties, snow cover dynamics, and terrain. More recently, empirical models have also been used to relate permafrost and soil characteristics to environmental factors for regional-scale mapping. For instance, remotely sensed or derived datasets have been combined with digital elevation models and field data to map permafrost properties over large areas of Alaska (Pastick and others, 2013; Pastick, Jorgenson, and others, 2014).

Time-series analyses of aerial photos and remote sensing imagery are also useful for understanding the rate and extent of change associated with permafrost degradation. Using aerial photo analyses, Jorgenson and others (2001) found that in the Tanana Flats in central Alaska, permafrost degradation has been widespread and rapid, causing large shifts in ecosystems from birch forests to fens and bogs. With warming, areas that are ice-rich experience a collapse of the surface topography (thermokarst) on the order of 1 to 1.5 m. In arctic Alaska, Jorgenson and others (2006) found that recent degradation has mainly affected massive wedges of ice that previously had been stable for thousands of years. Thermokarst potentially can affect 10 to 30 percent of arctic lowland landscapes and severely alter tundra ecosystems even with modest climate warming (Jorgenson and others, 2006). Additionally, approximately 40 percent of subarctic Alaska may also be susceptible to permafrost degradation and thermokarst (Jorgenson and others, 2008).

A variety of methods are used to understand the potential rate of carbon release with warming, including chronosequences (Johnston and others, 2014), flux studies on wetland gradients (McConnell and others, 2013), incubation of soil samples (Wickland and Neff, 2008; Mu and others, 2014; Treat and others, 2014), and manipulations that artificially warm the soil (Natali and others, 2011, 2012). The insulating effect of moss may depend on the water content (O'Donnell and others, 2009). Microtopography and slope may influence groundwater and surface water flow and thus the formation of taliks, thermokarst ponds, and pond drainage (Yoshikawa and Hinzman, 2003; Osterkamp and others, 2009; Wellman and others, 2013).

Schaefer and others (2014) synthesized results from 14 studies projecting the magnitude of the permafrost carbon feedback across the pan-Arctic to the year 2100, and found an ensemble average of 120±85 PgC and a median of 100 PgC. There is considerable uncertainty from the variety of methods and assumptions, but this amount of carbon would be equivalent to 5.7 percent of projected anthropogenic emissions through 2100 (IPCC scenario RCP 8.5; Riahi and others, 2011), and would increase global temperatures by 0.29±0.21 degrees Celsius (°C), or 7.8±5.7 percent. Projections indicate that 60 percent of the permafrost emissions will occur after 2100, so releases of greenhouse gases from thawing permafrost will continue for centuries. Schuur and others (2015) suggest a similar median magnitude for the permafrost carbon feedback with evidence for a gradual and

prolonged release of greenhouse-gas emissions in a warming climate, and present a research strategy for reducing the uncertainties. Schaefer and others (2011) suggest that the Arctic as a whole may change from a carbon sink to a carbon source after the mid-2020s.

Structural and functional changes in boreal forest ecosystems associated with warming (for example, reduced growth of dominant tree species, plant disease and insect outbreaks, warming and thawing of permafrost, and increased wildfire extent) that are unprecedented in the past 6,000 years are expected over the next few decades (Chapin and others, 2010; Euskirchen and others, 2010). A shift from coniferous to deciduous vegetation in Alaska began about 1990 (Mann and others, 2012), and there has also been a documented increase in the frequency, intensity, and extent of fire disturbance associated with warming and drying trends (Kasischke and others, 2010).

Fire directly releases carbon from ecosystems, and resulting changes in heat absorption and organic-layer thickness influence the degradation and (or) reformation of permafrost. Large fires have become more frequent in recent years in interior Alaska, with 17 percent of the land area burning in a decade (Barrett and others, 2011). Barrett and others (2011) estimated that 39 percent (approximately 4,000 square kilometers [km^2]) of all burned black spruce (*Picea mariana* (Mill.) Britton, Sterns & Poggenb.) stands in 2004 had less than 10 centimeters (cm) of residual organic layer, which may lead to a post-fire loss of permafrost and high-quality seedbeds better suited for the establishment of deciduous species. With a severe fire, the trees and moss will be killed, leaving a blackened soil surface that absorbs sunlight directly onto the soil, transferring heat into the soil and thawing permafrost (Genet and others, 2013). Harden and others (2006) found that for every centimeter of soil organic-layer thickness, the temperature at 5-cm depth was about 0.5 °C cooler in summer months. Turetsky and others (2011) indicate that some black spruce stands have become a net source of carbon to the atmosphere, and Chambers and Chapin (2002) show there can be an initial reduction of minimum albedo following fire from 0.09 to 0.06, followed by a rapid increase to 0.135 as the vegetation increased. Increases in fire disturbance will augment the amount of carbon released to the atmosphere and thus contribute to climate warming, and shifts in species composition also have the potential to influence the regional climate by changing surface albedo and rates of evapotranspiration and conductance (Amiro and others, 2006).

From the conceptual description above, it is shown that to properly represent the spatial and temporal variability of soil carbon stocks in high-latitude ecosystems, process-based ecosystem models need to (1) correctly initialize soil carbon stocks and permafrost distribution as a function of drainage conditions, soil properties (for example, texture, organic-layer thickness), and vegetation composition and (2) represent the effects of climate and disturbance regimes on permafrost dynamics and the consequences on soil carbon stocks over time. One way to evaluate how well process-based ecosystem models simulate regional ecological processes and estimate the spatial and temporal variability of soil properties is by comparing modeled outputs to a set of data products developed using other methods and observations, as is described below.

3.3. Objectives of the Study and General Methods

As part of this assessment, one objective of this chapter is a synthesis of available current and new data products of permafrost distribution and soil carbon in Alaska. Several new soil property products were created as part of this study to help improve and refine soil property estimates, to increase the number of product versions beyond the existing spatial products, and to better quantify and assess landscape-scale map uncertainties. The new soil property products incorporated new field data, higher resolution inputs layers, and (or) different mapping algorithms relative to previous studies. Statistical-empirical techniques were used in the development of new products to quantify near-surface soil properties throughout Alaska. The convergence of multiple products derived from observations, both in terms of spatial patterns and quantification of uncertainties, was the basis for a confidence measure used for the evaluation of a process-based model (that is, DOS-TEM). Multiproduct comparisons reduce the consequences of both false-positive and false-negative results that may occur when only one reference product is used.

The second objective of this chapter is to evaluate how well processes related to the spatial distribution of soil properties were represented in the biogeochemical process-based model used in this assessment by observing the differences between the model and the mapped products. The Dynamic Organic Soil version of the Terrestrial Ecosystem Model (DOS-TEM) is a large-scale ecosystem model designed to study interactions among carbon and nitrogen cycling, vegetation composition, and the effects of climate change and disturbances on soil physical properties, including permafrost and active-layer dynamics. Over the last two decades, DOS-TEM has been developed to simulate biogeochemical cycles and vegetation dynamics in high latitudes, including development of an environmental module to reproduce the thermal and hydrological regimes of the organic and mineral layers in permafrost soils (Zhuang and others, 2003; Yi and others, 2009). The DOS-TEM model is a widely used model for high-latitude boreal and arctic systems and one of the primary models used in this Alaska assessment for current and future fluxes and stock of carbon. The synthesis provided in the present chapter was designed to provide a baseline to evaluate how DOS-TEM reproduced the spatial variability of historical soil carbon and permafrost distribution in Alaska compared to other empirical and process-based models. DOS-TEM used a soil texture data source independent of datasets (see chapter 6) discussed in this chapter because

of an issue with timing. The state soil geographic database (STATSGO) soil texture maps were not available at the time DOS-TEM simulations began. Chapters 6 and 7 present how DOS-TEM represents the temporal variability of soil carbon stocks and permafrost.

The final objective of this chapter was to develop a simple conceptual model and map of soil relative susceptibility to climate change based on expert knowledge, new soil and ecotype maps, and the literature. Here we define relative susceptibility as the degree to which particular "ecotypes" (that is, combinations of ecoregion [Landscape Conservation Cooperative, LCC region], upland or lowland, and land-cover type) and soils are open, liable, or sensitive to climate stimuli (Smit and others, 1999). The results of this analysis will be informative for land use and land management decision making and provide actionable science information for sustainable resource management practices.

3.4. Methods and Analysis of Soil Products

Statistical and geospatial methods were used to produce and examine spatially explicit estimates of near-surface soil properties (that is, soil organic carbon, SOC; permafrost distribution; active-layer thickness, ALT; and organic-layer thickness, OLT) throughout Alaska, although parameters related to permafrost and soil carbon were not assessed in the North Pacific LCC because (1) permafrost occurrence in this region is typically rare, (2) a portion of the spatial datasets did not cover this region, and (3) carbon simulation results were not available at the time of these analyses and were being done separately for this report (see chapter 4). The newly generated products were then compared with other existing assessments. Accuracy assessments were conducted for a portion of these map products, but accuracies can't be directly compared because of model and mapping differences. Because the various products were generated at different resolutions and with different mapping methods, comparisons were conducted at the ecotype level. DOS-TEM outputs were compared to the means, ranges, and uncertainties of the other spatial products within ecotype units. Masked areas or areas with no data were excluded from ALT and OLT comparisons. Ecotypes are broad strata that can have significant soil carbon and permafrost variability related to adjacency to water, soil texture, and effect of fire. Uncertainty was characterized in three ways: (1) as the mean absolute difference (MAD) from the ecotype mean, (2) as the data range of the spatial product means for each ecotype, and (3) as the difference between product ecotype means and respective DOS-TEM ecotype means. We employ convergence of evidence in our analysis approach, but acknowledge that the true value can potentially be one of the outliers. The ecotype product means (excluding DOS-TEM) were used to develop six ecologically based sensitivity criteria. A simple susceptibility index was developed related to an inter-criteria score (sum of 0 [false] or 1 [true] across the six criteria) and the potential area affected, as is further described in section 3.4.4. Environmental factors controlling the distribution of near-surface soil properties and distributions are also briefly highlighted and discussed.

It is also important to note that all empirically derived products rely heavily on the same soil pedon dataset (with varying additions of other field data and albeit different extrapolation methods) but these observations are not a systematic or random sample of Alaska's ecotypes. Thus, some ecotypes are poorly represented whereas others are fairly well represented, which creates a source of uncertainty between ecotypes that is difficult to quantify (Johnson and others, 2011). For example, the Western Alaska LCC has the lowest representation of soil carbon observations, having a sample density of 2, 8, and 15 times lower than the Northwest Boreal LCC North, Arctic LCC, and Northwest Boreal LCC South, respectively. Thus, soil carbon estimates of the Western Alaska LCC should qualitatively be considered the most uncertain compared to other regions.

3.4.1. Soil Organic Carbon

For the analysis of multiple products conducted for this assessment, the available SOC products included two new SOC maps and several existing maps (table 3.1).

The JOHNSON SOC product (fig. 3.1*A*) developed by Johnson and others (2011) and modified for the present report was created using 724 soil pedon observations. Soil pedon data sources included data from the U.S. Geological Survey (USGS) and the National Resources Conservation Service (NRCS) and a variety of data available from the Bonanza Creek Long Term Ecological Research (LTER) Web site. The SOC was estimated for the surface organic layer (OL), the mineral soil to a 1-m depth below the OL (MIN1m), and the total organic plus mineral soils (OL+MIN1m). These three soil carbon pools are directly comparable to DOS-TEM outputs. Additionally, the OL and MIN1m pools were partitioned into frozen and unfrozen components based on horizon designation (that is, the presence or absence of the "f" suffix). Frozen and unfrozen soil carbon were used to analyze the vulnerability of SOC loss from thawing permafrost and associated decomposition. Cryoturbated organic horizons were included as mineral soil. The means of the components (and their totals) were scaled up to land-cover types using the methods described in Hugelius and others (2012). A total of 33 land-cover types were derived for the soil carbon analysis from a landform map (Johnson and others, 2011), National Land Cover Database (NLCD) vegetation cover (Homer and others, 2004), and additional information on white spruce (*Picea glauca* (Moench) Voss) distribution from LANDFIRE (2008). These carbon statistics were crosswalked to the ecotypes in this study using similar land-cover types with large areas in each ecotype.

The STATSGO SOC data layer was developed from the 1:500,000-scale state soil geographic database (STATSGO) for Alaska (Soil Survey Staff, 2012), using expert knowledge

Table 3.1. Summary of spatial products and process-based model evaluated for soil organic carbon (SOC) in this assessment.

[STATSGO, state soil geographic database; NCSCDv2, Northern Circumpolar Soil Carbon Database version 2; CAVM, Circumpolar Arctic Vegetation Map; DOS-TEM, Dynamic Organic Soil version of the Terrestrial Ecosystem Model; OL, surface organic layer; MIN1m, mineral soil to 1-meter depth below the bottom of the surface organic layer; OL+MIN1m, the sum of OL and MIN1m]

Product name	Extent	Resolution	Method	Depth	Reference
JOHNSON	Alaska	1 kilometer	Means extrapolated to raster	OL, MIN1m, OL+MIN1m	Johnson and others (2011) and this report
STATSGO	Alaska	1 kilometer	Means extrapolated to polygons	OL, MIN1m, OL+MIN1m	This report
MISHRA	Alaska	60 meter	Geostatistical	"whole profile"	Mishra and Riley (2012)
NCSCDv2	Boreal and arctic Alaska	0.012°	Means extrapolated to polygons	0 to 152 centimeters	Hugelius and others (2013)
CAVM	Arctic Alaska	1 kilometer	Means extrapolated to polygons	OL, 0 to 1 meter	Ping and others (2008)
DOS-TEM	Alaska	1 kilometer	Process-based model	OL, MIN1m, OL+MIN1m	This report

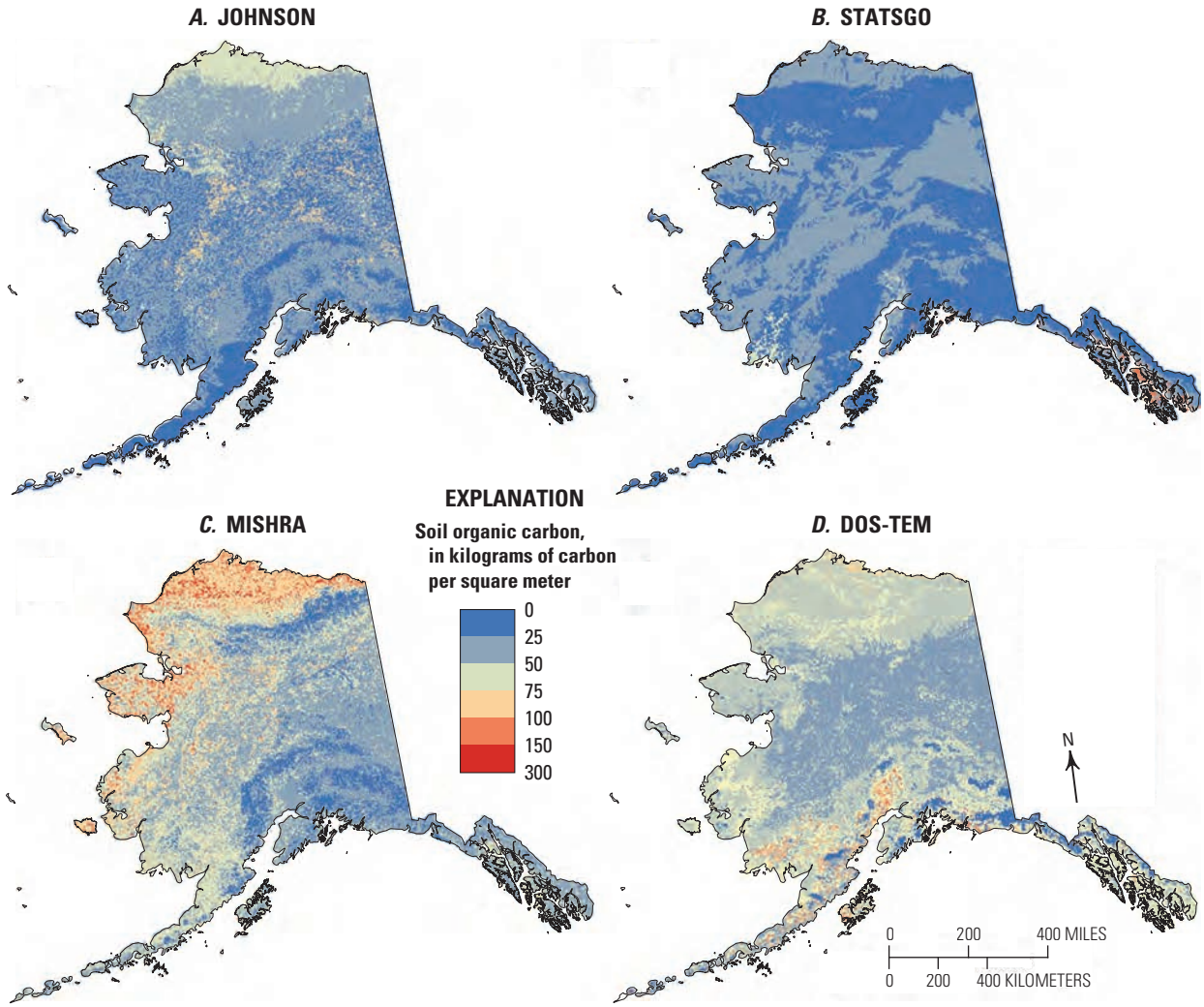

Figure 3.1. Total profile soil organic carbon (SOC) for those products used in the assessment that covered all of Alaska. *A*, SOC from Johnson and others (2011). *B*, SOC derived from the state soil geographic database (STATSGO). *C*, SOC from Mishra and Riley (2012). *D*, SOC simulated by the Dynamic Organic Soil version of the Terrestrial Ecosystem Model (DOS-TEM).

to extrapolate NRCS soil pedon observations and rasterized to 1-kilometer (km) resolution. The SOC was computed for each horizon from the representative organic matter attribute (om_r) by converting organic matter to organic carbon with a 0.58 factor and accounting for rock fragments. A map unit average soil carbon in kilograms of carbon per square meter (kgC/m^2) was computed for each analysis depth zone (for example, OL or OL+MIN1m) by accumulating across horizons and components with the mass of soil and the component percentage (comppct_r) as weighting factors with methods following Bliss and others (2014) (fig. 3.1*B*).

Several other existing products were available for comparisons of SOC density or SOC totals. The MISHRA SOC product (fig. 3.1*C*) represents "whole profile from the surface to the C horizon" SOC predicted from topographic, land-cover type, geologic, and climate data and 472 soil profiles for all of Alaska at a 60-m resolution (Mishra and Riley, 2012). In contrast to the other products of this study, it is the only one to use a geostatistical approach (geographically weighted regression). The Northern Circumpolar Soil Carbon Database version 2 (NCSCDv2) SOC product assigns mean SOC values to a compilation of soil polygon maps for the whole circumpolar arctic but does not include southeastern Alaska (Hugelius and others, 2013). The data are reported by meter depth (that is, 0–100 cm, 100–200 cm, and 200–300 cm) but for comparability to the other products of this study the first two depths were converted to represent SOC to usually the 152-cm depth, or the C horizon. The CAVM SOC product is similar to other SOC products mentioned in this study in that mean SOC values were assigned to land-cover types for upscaling (Ping and others, 2008). However, land-cover types were determined from a separate map, the Circumpolar Arctic Vegetation Map (CAVM), and only cover the Arctic LCC and the Aleutian and Bering Sea Islands LCC ecoregions.

The DOS-TEM SOC product (fig. 3.1*D*) provides estimates of SOC in the organic layer and the mineral soil (down to 1 m below the OL) separately. DOS-TEM simulates the dynamic changes of the SOC pools as a result of the incorporation of the litterfall to the soil, the carbon loss from decomposition by microbes, and combustion during wildfire. Therefore, soil carbon pools in DOS-TEM depend mainly on climate history, drainage conditions, vegetation productivity, and the fire regime (frequency and intensity). DOS-TEM estimates of SOC are provided at a 1-km resolution for the entire State. Readers are referred to Yi and others (2010) for a description of the processes that drive soil carbon dynamics in DOS-TEM. The DOS-TEM output at spin-up (models are run repetitively to get equilibrium conditions) were selected for the comparisons shown in this section.

3.4.2. Permafrost and Active-Layer Thickness

For the multiple product analysis of this report, the available permafrost products included three new permafrost maps and one existing map (table 3.2).

The "LANDCARBON" (products produced in this assessment) permafrost and associated ALT map products were developed using machine learning algorithms (that is, regression and classification trees) that spatially and statistically extended late-season field observations (sample size [n] ~17,000), collected from 1990 to 2013, for the mapping of near-surface permafrost (NSP, within the upper 1 m of the soil column) throughout Alaska (Pastick and others, 2015). This approach made use of remotely sensed, climatic, and biophysical geospatial data to produce moderate-resolution (30-m pixel) maps of the presence or absence of NSP, probability of NSP, and ALT (seasonal maximum depth of the permafrost) (figs. 3.2*A*, 3.3, and 3.4*A*). Readers are referred to Pastick and others (2015) for a detailed discussion of those data and methods used to derive and assess the map products. Climate variables (that is, mean annual air temperature, length of growing season, annual and winter precipitation) were identified to be the most important environmental factors controlling landscape-level distributions of permafrost. Whereas climate was identified to have first-order controls on landscape NSP distributions, permafrost-climate-ecological interactions are scale dependent. Remotely sensed or mapped data were also an influential predictor in the model and suggested that certain surface features (that is, vegetation, topography) are also good indicators of NSP properties. Accuracy assessments consisted of independent test datasets and f-fold cross-validations (Martin and others, 2011). Cross-validation and independent test accuracies indicated that the NSP map had an overall accuracy of 85 percent (95-percent confidence interval [CI]: 84.7, 85.8). Independent tests showed that the ALT map had a mean average error (MAE), mean bias error (MBE), relative mean average error (rMAE), relative mean bias error (rMBE), and Pearson's correlation coefficient of 15 cm, 0 cm, 27 percent, 0 percent, and 0.61, respectively.

The STATSGO permafrost estimates of the presence or absence of NSP were computed by evaluating the texture designation for the horizon at 100-cm depth. If the horizon was designated as "frozen" ("PF" in the texture code), then the component was flagged as having NSP. If the sum of the component percentages flagged in this way was at least 50 percent, then the map unit was coded as having NSP "present" and if it was less than 50 percent, then permafrost was considered "absent" (fig. 3.2*B*). The ALT for a component was the depth of the soil at the top of a permanently frozen soil horizon. If permafrost was not present in the component or the permafrost was deeper than 100 cm, then the ALT for the component was set to 101 cm for comparability of methods with other datasets being evaluated in this study. A weighted average of ALT was computed with the component percentage as the weighting factor and assigned to the map units, as shown in figure 3.4*B*.

The GIPL 1.3 permafrost products were made using the University of Alaska-Fairbanks, Geophysical Institute Permafrost Laboratory (GIPL; 2011) version 1.3 transient model. The GIPL 1.3 spatial transient model simulates

Table 3.2. Summary of spatial products and process-based model evaluated for permafrost in this assessment.

[LANDCARBON, data product developed for this assessment; STATSGO, state soil geographic database; GIPL 1.3, Geophysical Institute Permafrost Laboratory version 1.3 transient model; DOS-TEM, Dynamic Organic Soil version of the Terrestrial Ecosystem Model]

Product name	Extent	Resolution	Method	Near-surface permafrost depth threshold	Time period	Reference
LANDCARBON	Alaska	30 meter	Machine learning	1 meter	1990–2013	Pastick and others (2015) and this report
STATSGO	Alaska	1 kilometer	Means extrapolated to polygons	1 meter	Not specified (expert judgment in 2012)	This report
GIPL 1.3	Alaska	2 kilometer	Process-based model	1 meter	2000–2009	Marchenko and others (2008)
DOS-TEM	Alaska (excluding the North Pacific Landscape Conservation Cooperative)	1 kilometer	Process-based model	1 meter	1950–1960	This report

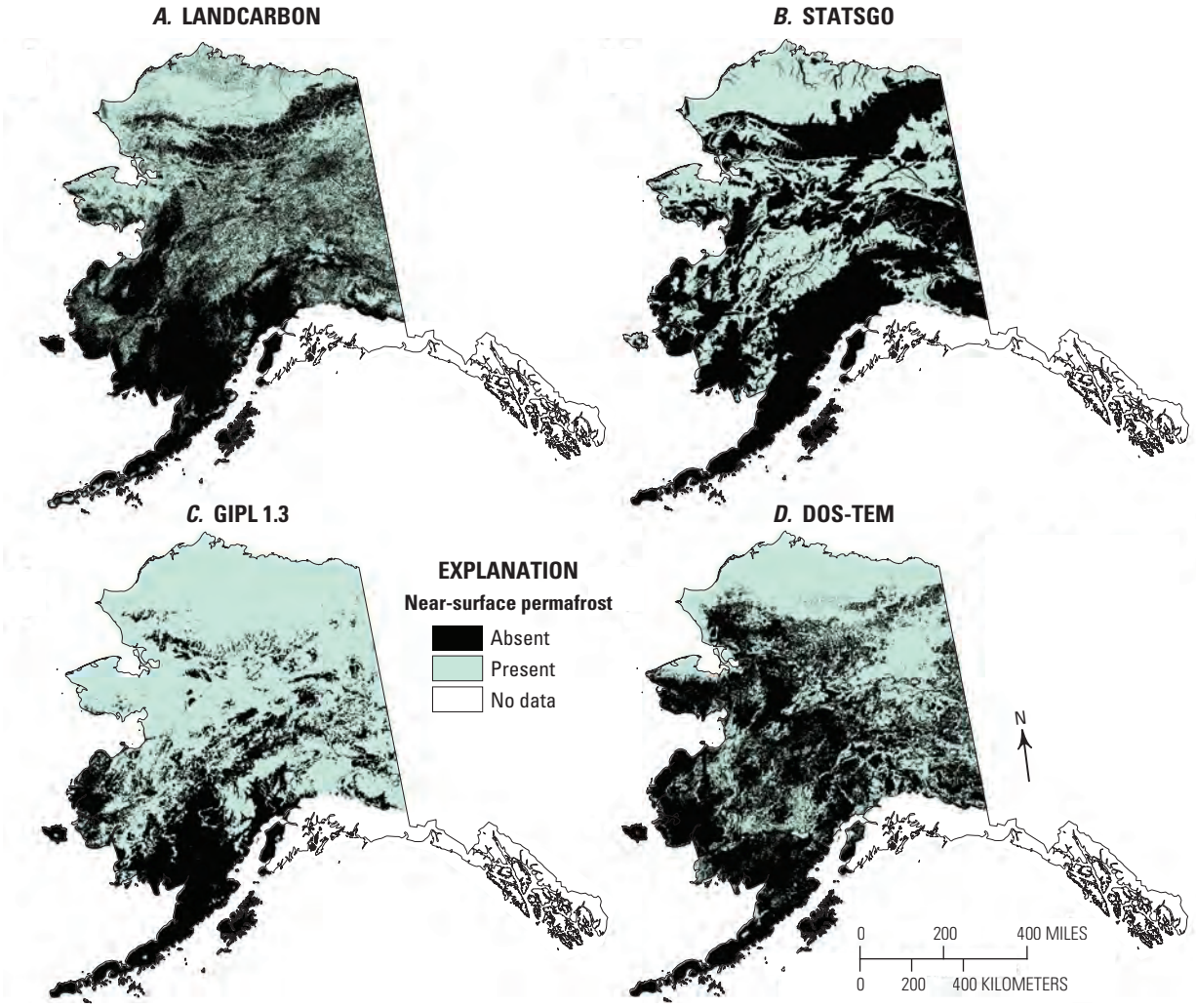

Figure 3.2. Estimated presence or absence of near-surface (within 1 meter) permafrost for Alaska. *A*, Permafrost from LANDCARBON (Pastick and others, 2015). *B*, Permafrost derived from the state soil geographic database (STATSGO). *C*, Permafrost simulated by the Geophysical Institute Permafrost Laboratory version 1.3 transient model (GIPL 1.3). *D*, Permafrost simulated by the Dynamic Organic Soil version of the Terrestrial Ecosystem Model (DOS-TEM). Map estimates are not reported for the North Pacific LCC.

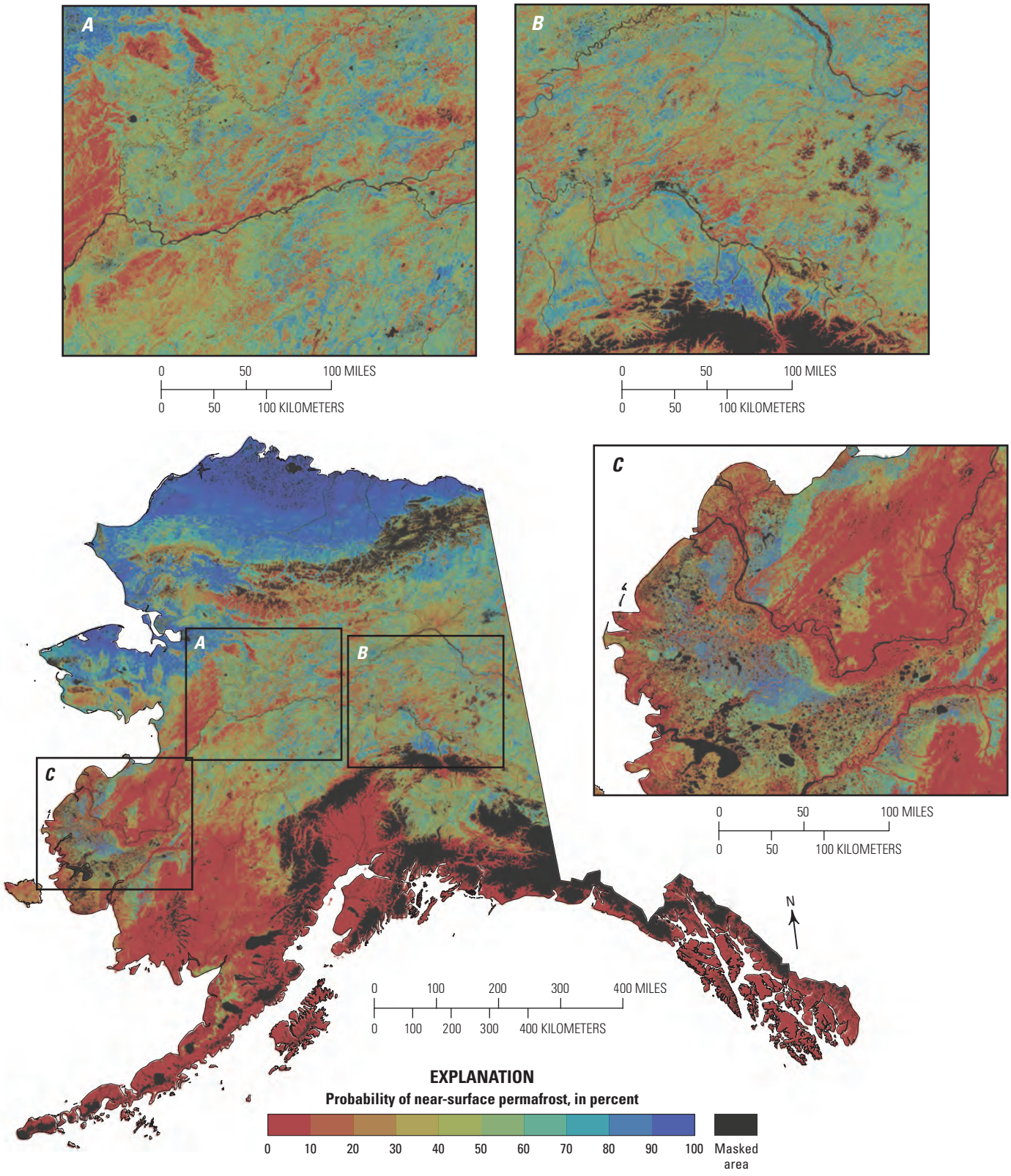

Figure 3.3. Probabilistic estimation of near-surface (within 1 meter) permafrost occurrence for the State of Alaska at 30-meter spatial resolution derived from LANDCARBON. Estimates were made using machine learning algorithms, field observations, remotely sensed or mapped imagery, and climatic data (Pastick and others, 2015).

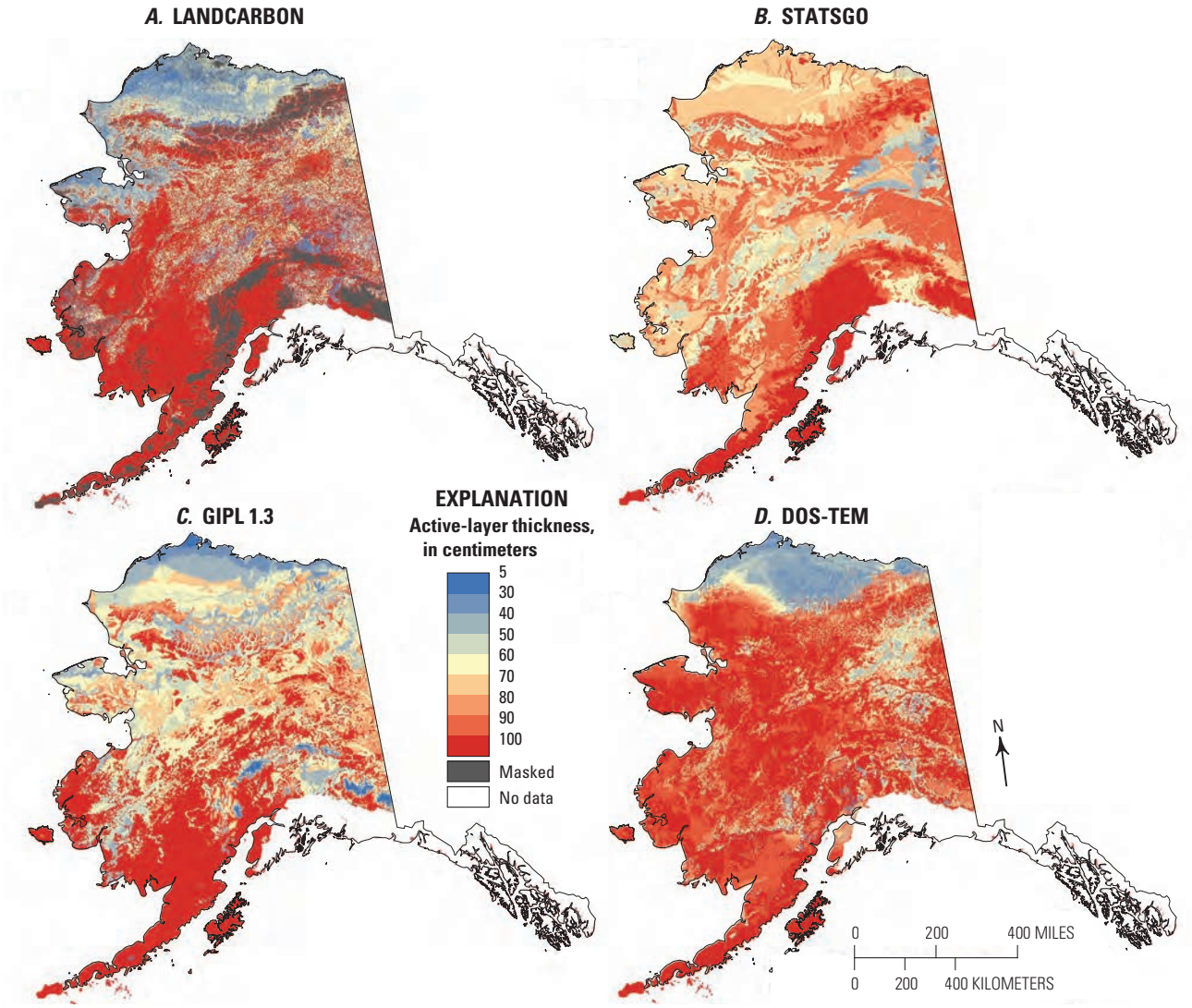

Figure 3.4. Active-layer thickness (ALT) estimates for Alaska. *A*, ALT derived from LANDCARBON (Pastick and others, 2015). *B*, ALT derived from the state soil geographic database (STATSGO). *C*, ALT simulated by the Geophysical Institute Permafrost Laboratory version 1.3 transient model (GIPL 1.3). *D*, ALT simulated by the Dynamic Organic Soil version of the Terrestrial Ecosystem Model (DOS-TEM). Map estimates are not reported for the North Pacific LCC. Areas where ALT was estimated to be greater than 1 meter were given a consistent value (dark red) because of differences in investigation depths and for direct comparison. ALT greater than 1 meter is dependent on site, soil, climate, and fire history.

depth of seasonal freezing and thaw by numerically solving one-dimensional nonlinear heat equations with phase change (Marchenko and others, 2008). Note that the spatial resolution (2-km pixels) of the GIPL 1.3 product is different than products developed in this study. Furthermore, predictions of seasonal frost or thaw depths greater than 1 m made by GIPL 1.3, for the years 2000 to 2009, were recoded to 101 cm for direct comparison with estimates of NSP and ALT produced for this study (figs. 3.2*C*, 3.4*C*).

The DOS-TEM permafrost products were produced from the historical simulations for Alaska at a 1-km resolution. In this process-based model, NSP and ALT were assessed based on soil temperature and soil moisture simulations over a 5-m-deep soil column. NSP is considered present when soil temperature at 1 m from the surface remained frozen for two consecutive years. Soil temperature and soil moisture in DOS-TEM are driven by climate, soil texture, and drainage conditions. The insulating properties of the snow cover, moss, and organic layers are also reproduced in the model. Soil moisture is also affected by water uptake from vegetation and runoff. NSP and ALT distributions were estimated by averaging annual estimates from 1950 to 1960, which is temporally inconsistent from other products but the only TEM outputs available for comparison at the time of analyses (figs. 3.2*D*, 3.4*D*).

3.4.3. Organic-Layer Thickness

For the multiple product analysis of this report, the available organic soil products included three new maps and one existing map (table 3.3).

The LANDCARBON OLT products were developed for this assessment using decision tree classifications to spatially extend field observations of soil organic-layer thickness (OLT; excluding buried O horizons) throughout Alaska. This approach made use of approximately 3,500 field observations and topographical, climatic, and remotely sensed geospatial data to map the presence or absence of organic soils (that is, OLT ≥ 40 cm = organic soil present; OLT < 40 cm = organic soil absent) (fig. 3.5*A*). The 40-cm depth interval was chosen because it coincides with Soil Taxonomy (Soil Survey Staff, 1999) nomenclature for organic soils (that is, Histosol or Histel) that are commonly associated with peatlands. Field observations were primarily collected by the National Resource Conservation Service, ABR, Inc., and the USGS (Pastick, Rigge, and others, 2014). Topography (that is, slope, soil-wetness proxies), length of growing season, and remotely sensed or mapped data (that is, land cover, vegetation indices) were identified to be the most important factors in estimating organic soil distributions in Alaska. Cross-validation accuracy assessments indicated that the map of the presence or absence of organic soil had an overall accuracy of 71 percent (95-percent CI: 69.5, 73.2). Readers are referred to Pastick, Rigge, and others (2014) for a thorough discussion on digital mapping of organic soils in Alaska.

The STATSGO OLT product was developed by evaluating the textural component of the horizons from the surface to 152-cm depth. For the STATSGO OLT, each horizon is labeled as organic or not organic, and the thickness of organic horizons is summed to create a component-level variable. This is weighted by the component percentage to give an average OLT at the map unit level. If an organic layer is not present, the thickness will be recorded as zero, and this will be included in the weighted average. The thicknesses of the organic layers in the 0- to 152-cm-depth zone were summed for each component, and a weighted average (with component percentage as the weight) was computed. If the average was more than 40 cm, then the map unit was labeled as "OLT ≥ 40 cm" in figure 3.5*B*.

The NCSCDv2 OLT product assigns soil type frequencies to a compilation of soil polygon maps for the whole circumpolar region, but does not include a large portion of southeastern Alaska (Hugelius and others, 2013). Although available at approximately 1-km resolution, the polygon representation of soils is considerably coarser than that represented by other products in this study. The data used for comparison are frequency of Histel occurrence estimates, which are comparable to organic soil products developed for this study.

The DOS-TEM OLT product (fig. 3.5*C*) provides estimates of OLT as a function of SOC content in the organic layer. The dynamic organic soil module of DOS-TEM simulates post-fire re-accumulation of the organic layer as dead organic soil horizons accumulate above the mineral horizons with post-fire vegetation succession. DOS-TEM estimates of organic soils are provided at a 1-km resolution for the entire State, excluding the North Pacific LCC, and represent averaged model estimates from 1950 to 1960.

3.4.4. Soil Susceptibility to Climate Change

The permafrost, soil carbon, and organic soils summaries presented in this study can yield useful information about the potential effects of climate change, particularly when multiple ecotype attributes are combined. For this purpose, ecotype means and measures of uncertainty from the multiple sources of relative frequency of NSP, relative frequency of organic soils, and mean ALT were combined in a database with ecotype estimates of frozen carbon and total organic carbon in the depth range of 0 to 1 m. This synthesis effort was constrained to the soil parameters presented in this chapter to focus on relative susceptibility. Important susceptibility

Table 3.3. Summary of spatial products and process-based model evaluated for soil organic-layer thickness in this assessment.

[LANDCARBON, data product developed for this assessment; STATSGO, state soil geographic database; NCSCDv2, Northern Circumpolar Soil Carbon Database version 2; DOS-TEM, Dynamic Organic Soil version of the Terrestrial Ecosystem Model; —, not applicable]

Product name	Extent	Resolution	Method	Number of observations	Reference
LANDCARBON	Alaska	30 meter	Machine learning	~3,500	This report
STATSGO	Alaska	1 kilometer	Means extrapolated to polygons	—	This report
NCSCDv2	Boreal and arctic Alaska	Polygons	Means extrapolated to polygons	—	Hugelius and others (2013)
DOS-TEM	Alaska (excluding the North Pacific Landscape Conservation Cooperative)	1 kilometer	Process-based model	—	This report

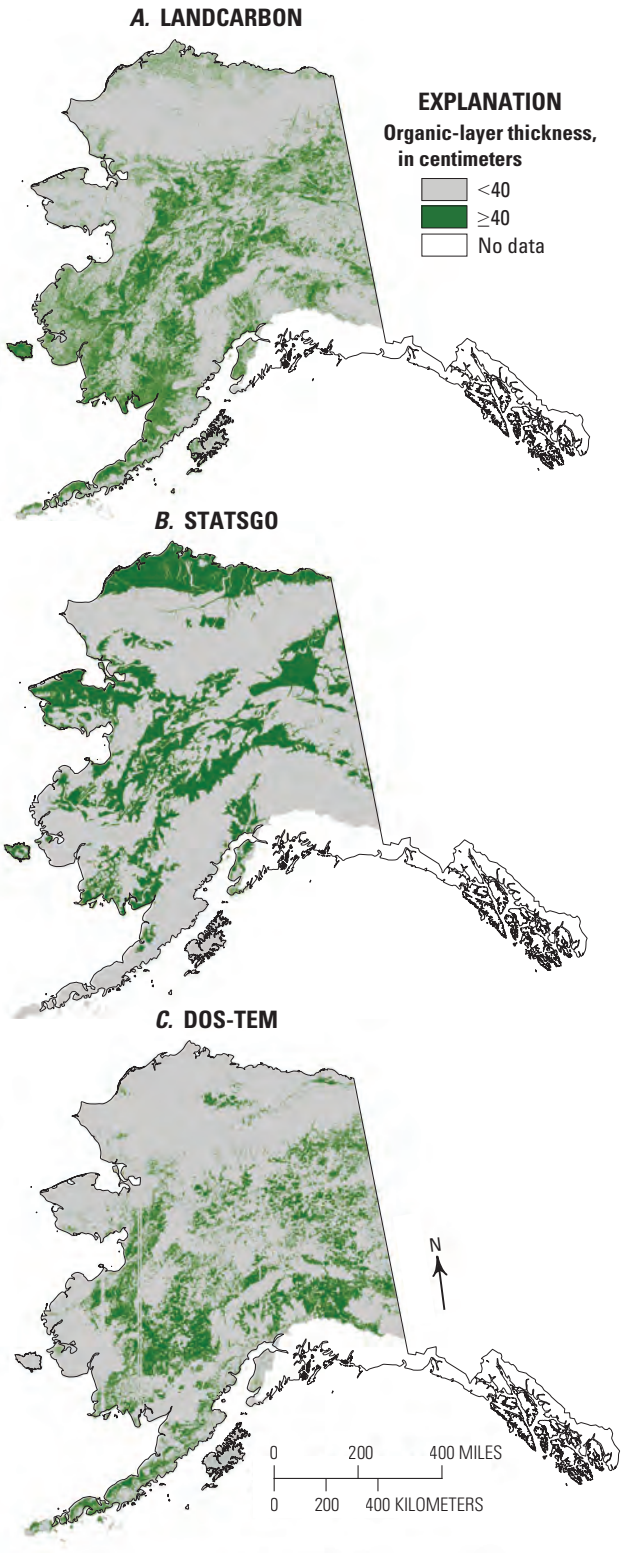

Figure 3.5. Organic-layer thickness (OLT) estimates for Alaska. *A*, OLT derived from LANDCARBON (Pastick and others, 2015). *B*, OLT derived from the state soil geographic database (STATSGO). *C*, OLT simulated by the Dynamic Organic Soil version of the Terrestrial Ecosystem Model (DOS-TEM). DOS-TEM model estimates are not reported for the North Pacific LCC.

drivers, such as fire return interval and temperature, were not included and are included in other chapters. Six ecologically driven criteria were constructed with each criterion having its separate binary response (0=false and 1=true). Generally, the first condition in these criteria sought to capture one-third of the ecotypes and subsequent condition constraints with other variables sought to identify the top two to six ecotypes. The six criteria consisted of:

1. Thicker soil organic layers provide protecting insulation for NSP (Johnson and others, 2013). To identify areas which may be prone to permafrost degradation, we selected ecotypes with a higher chance of having thin organic soils (relative frequency of organic soils less than 20 percent) and with permafrost close to the surface (relative frequency of NSP greater than 50 percent).

2. Criterion 2 is a subset of criterion 1. In the sensitive areas where criterion 1 is focused (NSP and thin organic soils), high uncertainty and wide variations in ecotype ALT would affect current and future hydrology and greenhouse-gas emissions significantly. Given the significance of future permafrost degradation related to greenhouse gases (Schaefer and others, 2011) and changing permafrost's potential effects on hydrologic flows (Walvoord and others, 2012), ecotypes with high uncertainties of ALT could experience greater-than-expected permafrost degradation and increased ecosystem respiration. We refined criterion 1 to NSP with thin organic soils, with an additional requirement of a relatively high uncertainty of ALT (inter-product ecotype ALT MAD greater than 6 cm).

3. Moderate to high OLTs could be particularly susceptible to wildfire (Kasischke and Johnstone, 2005). The fire susceptibility criterion was defined here as an organic soil relative frequency greater than 20 percent and not to include land-cover types with low flammability (deciduous forests and wetlands).

4. Thermokarst land surfaces often occur in regions with near-surface, ice-rich permafrost and moderate to thick soil organic layers. This criterion consisted of ecotypes with relative frequency of organic soils greater than 20 percent, with the relative frequency of NSP greater than 50 percent, and with ALT less than 76 cm.

5. Areas with high carbon stocks in the organic layer and in the mineral layers in the top 1 to 1.5 m represent potential hot spots for massive carbon loss owing to warming, fires, and accelerated soil respiration and greenhouse-gas emissions (Schuur and others, 2008). This criterion was simply ecotypes with inter-product total profile soil carbon ecotype means greater than 40 kgC/m^2.

6. Criterion 6 is a subset of criterion 5. Permafrost can contain significant organic carbon. If this permafrost carbon is close to the soil surface, it may be susceptible to thaw and be available for decomposition (Schuur and others, 2008). As permafrost thaws, the active layer thickens. This criterion consisted of ecotypes where the frozen carbon was greater than 10 kgC/m^2 and the total carbon in the top 1 to 1.5 m of soil was more than 40 kgC/m^2.

These six diverse criteria were focused on known or expected dynamics of permafrost, carbon, and the organic layer in boreal and arctic systems. To summarize overall factors, a susceptibility score, or ranking, was computed by summing all of the binary criteria variables and using area as a tie-breaker.

3.5. Results and Discussion

3.5.1. Comparison of Soil Organic Carbon Estimates

Generally, SOC densities of the three soil product properties (total profile, surface organic layer, and 1-m mineral layer; fig. 3.6) had the largest range of estimated values as well as high uncertainty in the Arctic LCC. Additional field data collection in these regions could reduce uncertainty in these important arctic systems. STATSGO SOC estimates appeared to be consistently low and MISHRA estimates tended to be consistently high in nearly all the ecotypes, but particularly so in the Arctic LCC. DOS-TEM estimates generally agreed with mean organic carbon estimates for each ecotype, falling within the range of estimates for 78 percent of the major ecotypes. However, in some forests of the Northwest Boreal LCC North, DOS-TEM SOC estimates were either near or below the lower data range of the SOC ecotype ranges. DOS-TEM estimates were only substantially above the range of other SOC estimates in the Northwest Boreal LCC South upland heath tundra.

The SOC density of the surface organic layer had high magnitudes and narrow data ranges (less uncertainty) in the deciduous forest, black spruce forest, and white spruce forest in the Northwest Boreal LCC North lowlands. DOS-TEM estimates of surface organic-layer carbon were substantially lower in these ecotypes and also in the Western Alaska LCC lowland shrub tundra. Thirty percent of all the ecotypes had DOS-TEM estimates within the soil organic-layer prediction range. The mean surface organic-layer carbon among all ecosystem types accounted for about 30 percent of the mean total soil carbon.

Only two spatial estimates (STATSGO and JOHNSON) of carbon in the mineral soil layer down to a depth of 1 m below the surface organic layer were available for comparison with estimates from DOS-TEM. The highest values for both spatial estimates occurred in the Arctic LCC. Disagreement between the two estimates and DOS-TEM estimates indicated possible overestimation by DOS-TEM in the Northwest Boreal LCC South upland heath tundra and the Western Alaska LCC.

In terms of total soil carbon storage (in PgC) by LCC region, DOS-TEM SOC estimates were close to the mean and within the range of four products in the Arctic and Western Alaska LCCs (table 3.4). However, DOS-TEM estimates were 40 percent lower than the mean of all the products in the Northwest Boreal LCC North and 94 percent higher than the mean in the Northwest Boreal LCC South. These general differences were true even when compared to the JOHNSON SOC product with exactly comparable SOC by depth. Despite these differences in distribution of SOC pools by LCC region, when all the LCC regions were summed, DOS-TEM estimates were only 2 percent higher than the mean.

Table 3.4. Comparisons of soil organic carbon storage for each of the Landscape Conservation Cooperative (LCC) regions in Alaska (except the North Pacific LCC) estimated using spatial products and DOS-TEM outputs.

[PgC, petagram of carbon; STATSGO, state soil geographic database; NCSCDv2, Northern Circumpolar Soil Carbon Database version 2; CAVM, Circumpolar Arctic Vegetation Map; DOS-TEM, Dynamic Organic Soil version of the Terrestrial Ecosystem Model; OL, surface organic layer; MIN1m, mineral soil to 1-meter depth below the bottom of the surface organic layer; OL+MIN1m, the sum of OL and MIN1m; —, not applicable]

Product name	Depth	Soil organic carbon (PgC)				
		Arctic LCC	Western Alaska LCC	Northwest Boreal LCC North	Northwest Boreal LCC South	Total or mean
JOHNSON	OL+MIN1m	13.6	11.3	14.4	4.4	43.7
STATSGO	OL+MIN1m	6.2	9.8	12.5	2.7	31.2
MISHRA	"whole profile"	20.7	22.8	22.6	6.1	72.1
NCSCDv2	0–152 centimeters	11.6	8.6	10.9	2.1	33.2
Mean	—	**13.0**	**13.1**	**15.1**	**3.8**	**45.2**
DOS-TEM	OL+MIN1m	12.4	17.3	9.0	7.4	46.1
MAD[1]	—	**0.6**	**4.2**	**6.1**	**3.6**	**0.9**
% Diff[2]	—	**4.8**	**31.8**	**40.4**	**93.5**	**2.1**

[1]Mean Absolute Difference (MAD) = |DOS-TEM – Mean|

[2]% Diff = (MAD / Mean) × 100

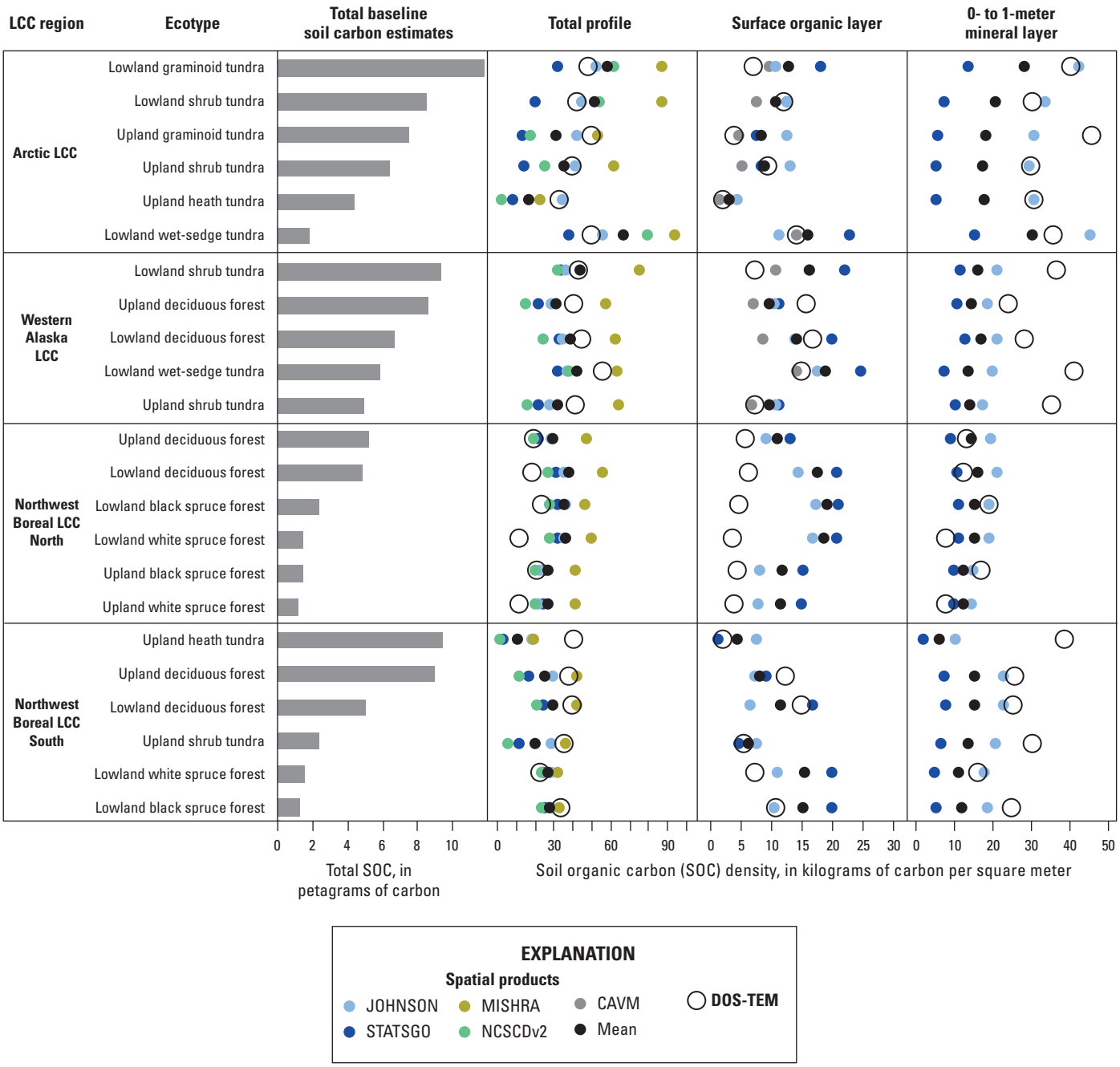

Figure 3.6. Soil organic carbon (SOC) characterization for the largest (in terms of SOC, in petagrams of carbon, PgC) five or six ecotype classes in each Landscape Conservation Cooperative (LCC) region. Total baseline SOC estimates simulated by the Dynamic Organic Soil version of the Terrestrial Ecosystem Model (DOS-TEM). Total profile SOC density is the sum of the surface organic layer and the 0- to 1-meter mineral layer for all estimates. "Mean" refers to the mean of all spatial products: JOHNSON, SOC from Johnson and others (2011); STATSGO, SOC from the state soil geographic database; MISHRA, SOC from Mishra and Riley (2012); NCSCDv2, SOC from the Northern Circumpolar Soil Carbon Database version 2; and CAVM, SOC from the Circumpolar Arctic Vegetation Map. Estimates are not reported for the North Pacific LCC.

The lower estimate of SOC in the organic layer provided by DOS-TEM compared with the other models in the Northwest Boreal LCC North may be attributed to the effect of fire simulated in the model. The version of DOS-TEM used for the present assessment has been designed to reproduce the effect of fire on nitrogen and carbon cycles in the soil and vegetation and on the soil environment, including the re-accumulation of the organic layer after a fire (Yi and others, 2009, 2010). Furthermore, a fire severity model has also been implemented in order to reproduce the spatial and temporal variability of fire severity on the organic layer (Genet and others, 2013). During the model spin-up, the fire regime was simulated by a constant fire return interval computed from the historical fire records for Alaska. Because the fire return interval is shortest in the Northwest Boreal LCC North, more organic layer is burned and less SOC accumulates.

The higher SOC in the mineral layers observed in DOS-TEM compared with the JOHNSON SOC and STATSGO SOC estimates in the Western Alaska LCC might be related to the underestimation of the effect of the warmer climate on soil decomposition processes in this region. However, given that there are only two products available for comparison and the low sample density in the Western Alaska LCC, there is less confidence that the mineral SOC product is a reliable reference.

3.5.2. Comparison of Permafrost Estimates

NSP estimates (fig. 3.2) were summarized as relative frequency in percent by LCC region and DOS-TEM land-cover type in tables 3.5 and 3.6. According to empirically or numerically derived NSP products, NSP was estimated to underlie a large portion of Alaska with a wide range of estimates (36 to 67 percent). The mean NSP frequency of DOS-TEM outputs (44 percent) falls within this range. On average, NSP distributions followed north-to-south temperature gradients as expected, with the largest NSP frequencies in the Arctic LCC (73 percent), followed by the Northwest Boreal LCC North (55 percent), and Western Alaska LCC and Northwest Boreal LCC South (30 percent each). DOS-TEM outputs were consistently within the range of other model outputs and were (on average) within 3 percent of the mean of other products (table 3.5).

A mean estimate (excluding DOS-TEM) of NSP frequencies varied nearly seventyfold between DOS-TEM land-cover types (table 3.6). Graminoid tundra had the highest mean product frequency of being underlain by NSP (73 percent), followed by shrub tundra (60 percent), black spruce forest (53 percent), white spruce forest (52 percent), deciduous forest (40 percent), wet-sedge tundra (34 percent), nonvegetated areas (31 percent), heath tundra (29 percent), and maritime classes (1 percent). Vegetation succession can serve as a positive feedback to permafrost systems, where increasing components of soil organics and moisture can provide insulation to permafrost, consistent with higher NSP frequencies in white and black spruce forests (late successional stages) compared with deciduous forests (early successional stages). Furthermore, DOS-TEM outputs were significantly correlated (p-value <0.05) with mean product NSP frequencies when stratified by LCC region (coefficient of determination, $R^2=0.86$; n=5) or land-cover type ($R^2=0.69$; n=9). Empirically derived NSP maps (that is, STATSGO and LANDCARBON) were significantly correlated when comparing NSP estimates stratified by LCC region ($R^2=0.82$; n=5) and DOS-TEM land-cover type ($R^2=0.63$; n=9). DOS-TEM outputs best correlated with the GIPL 1.3 map when examining mean NSP estimates stratified by LCC region ($R^2=0.98$; n=5) and DOS-TEM land-cover type ($R^2=0.72$; n=9). Large differences between model outputs are most evident for areas estimated to have little to no vegetation. Mean product NSP frequencies indicate that lowland areas are more frequently underlain by NSP than uplands in Alaska (57 percent versus 36 percent), consistent with trends in DOS-TEM outputs (49 percent versus 41 percent). Large differences between mean NSP frequencies in uplands suggest that estimates of NSP distributions are relatively more uncertain for upland than lowland ecosystems, coinciding with large differences in NSP estimates for areas with little to no vegetation. A portion of these differences can be attributed to how models handled glaciated areas.

Finer scale comparisons were also made where NSP estimates were stratified by ecotype in each LCC region (excluding the North Pacific LCC; fig. 3.7). Empirically derived NSP maps were in global accordance with one another and with DOS-TEM outputs when mean frequency estimates are stratified by ecotype. For instance, the empirically derived NSP maps (that is, STATSGO and LANDCARBON) were significantly (p-value <0.05) correlated when estimates were stratified by ecotype in each LCC region ($R^2=0.83$; n=23). Additionally, DOS-TEM outputs were significantly correlated ($R^2=0.67$; n=23) with mean product NSP frequencies stratified by ecotype. Furthermore, in 87 percent of the major ecotype classes the DOS-TEM output is within the range of other products, whereas three of the DOS-TEM outputs were outside the range. The three low DOS-TEM outputs were within upland and lowland shrub tundra in the Western Alaska LCC and lowland deciduous forests in the Northwest Boreal LCC North. These significant differences could have a large effect on future model simulations because these ecotypes account for a substantial portion of Western Alaska LCC (33 percent) and Northwest Boreal LCC North (25 percent). The lower DOS-TEM estimate of NSP distribution compared with the other models in interior Alaska (Northwest Boreal LCC North) might be related to the lower estimate of OLT related to the effect of fire activity and high fire return interval in the region (see section 2.4.2.). With a thinner organic layer, the soil is less insulated from large variability of air temperature, especially high summer temperature. As a consequence, the annual mean of soil temperature increases, thawing permafrost and increasing ALT.

Table 3.5. Comparisons of the frequency of near-surface (within 1 meter) permafrost, mean active-layer thickness, and frequency of organic soils for Landscape Conservation Cooperative (LCC) regions in Alaska (except the North Pacific LCC) estimated using spatial products and DOS-TEM outputs.

[Organic soils are defined here as those soils with a surface organic epipedon that is greater than or equal to 40 centimeters. LANDCARBON, data product developed for this assessment; STATSGO, state soil geographic database; GIPL 1.3, Geophysical Institute Permafrost Laboratory version 1.3 transient model; DOS-TEM, Dynamic Organic Soil version of the Terrestrial Ecosystem Model; NCSCDv2, Northern Circumpolar Soil Carbon Database version 2]

Product name	Landscape Conservation Cooperative region				
	Arctic LCC	Western Alaska LCC	Northwest Boreal LCC North	Northwest Boreal LCC South	Mean
Frequency of near-surface permafrost (percent)					
LANDCARBON	66	21	44	22	38
STATSGO	56	28	49	11	36
GIPL 1.3	97	41	72	57	67
Mean	**73**	**30**	**55**	**30**	**47**
DOS-TEM	73	22	45	38	44
MAD[1]	**0**	**8**	**10**	**8**	**3**
% Diff[2]	**0**	**26**	**19**	**25**	**5**
Mean active-layer thickness (centimeter)					
LANDCARBON	59.51	88.94	81.14	91.43	80.26
STATSGO	79.71	85.08	76.68	95.60	84.27
GIPL 1.3	60.88	85.55	78.49	78.34	75.81
Mean	**66.70**	**86.52**	**78.77**	**88.45**	**80.11**
DOS-TEM	72.80	95.86	88.63	87.46	86.19
MAD[1]	**6.10**	**9.34**	**9.86**	**0.99**	**6.08**
% Diff[2]	**9.14**	**10.79**	**12.51**	**1.12**	**7.58**
Frequency of organic soils (percent)					
LANDCARBON	6	31	35	19	24
STATSGO	27	25	37	9	30
NCSCDv2	4	13	7	2	8
Mean	**12**	**23**	**26**	**10**	**21**
DOS-TEM	3	24	26	38	18
MAD[1]	**10**	**1**	**1**	**29**	**3**
% Diff[2]	**77**	**4**	**2**	**298**	**15**

[1]Mean Absolute Difference (MAD) = |DOS-TEM – Mean|

[2]% Diff = (MAD / Mean) × 100

Table 3.6. Comparisons of the frequency of near-surface (within 1 meter) permafrost, mean active-layer thickness, and frequency of organic soils by DOS-TEM land-cover type estimated using spatial products and DOS-TEM outputs.

[Areas estimated to have active-layer thicknesses greater than 1 meter were given a value of 101 centimeters for direct comparison and to account for differences in investigation depths. Organic soils are defined here as those soils with a surface organic epipedon that is greater than or equal to 40 centimeters. LANDCARBON, data product developed for this assessment; STATSGO, state soil geographic database; GIPL 1.3, Geophysical Institute Permafrost Laboratory version 1.3 transient model; DOS-TEM, Dynamic Organic Soil version of the Terrestrial Ecosystem Model; NCSCDv2, Northern Circumpolar Soil Carbon Database version 2]

Product name	Land-cover type							
	Black spruce forest	White spruce forest	Deciduous forest	Shrub tundra	Graminoid tundra	Wet-sedge tundra	Heath tundra	Non-vegetated
Frequency of near-surface permafrost (percent)								
LANDCARBON	40	38	30	54	70	27	7	44
STATSGO	52	48	35	55	57	27	1	8
GIPL 1.3	66	70	55	71	93	49	77	40
Mean	**53**	**52**	**40**	**60**	**73**	**34**	**29**	**31**
DOS-TEM	49	52	36	47	62	59	40	20
MAD[1]	**4**	**0**	**4**	**13**	**11**	**24**	**11**	**11**
% Diff[2]	**7**	**1**	**9**	**22**	**15**	**71**	**39**	**35**
Mean active-layer thickness (centimeter)								
LANDCARBON	84.1	85.0	88.6	67.1	60.3	44.3	101.0	92.0
STATSGO	76.5	78.2	83.5	79.3	78.9	81.5	97.9	96.1
GIPL 1.3	80.2	77.9	83.3	72.5	59.7	39.6	101.0	85.8
Mean	**80.3**	**80.3**	**85.1**	**72.9**	**66.3**	**55.1**	**100.0**	**91.3**
DOS-TEM	87.9	85.9	90.4	84.2	76.0	74.9	90.9	91.2
MAD[1]	**7.7**	**5.6**	**5.2**	**11.3**	**9.7**	**19.8**	**9.0**	**0.1**
% Diff[2]	**9.5**	**6.9**	**6.2**	**15.5**	**14.7**	**35.9**	**9.0**	**0.1**
Frequency of organic soils (percent)								
LANDCARBON	34	32	36	16	10	48	1	7
STATSGO	40	36	27	22	38	39	1	17
NCSCDv2	8	8	5	6	6	28	0	8
Mean	**27**	**25**	**23**	**15**	**18**	**38**	**1**	**11**
DOS-TEM	25	22	43	7	1	4	0	8
MAD[1]	**2**	**3**	**21**	**7**	**17**	**35**	**0**	**2**
% Diff[2]	**8**	**13**	**91**	**49**	**95**	**90**	**62**	**21**

[1]Mean Absolute Difference (MAD) = |DOS-TEM − Mean|

[2]% Diff = (MAD / Mean) × 100

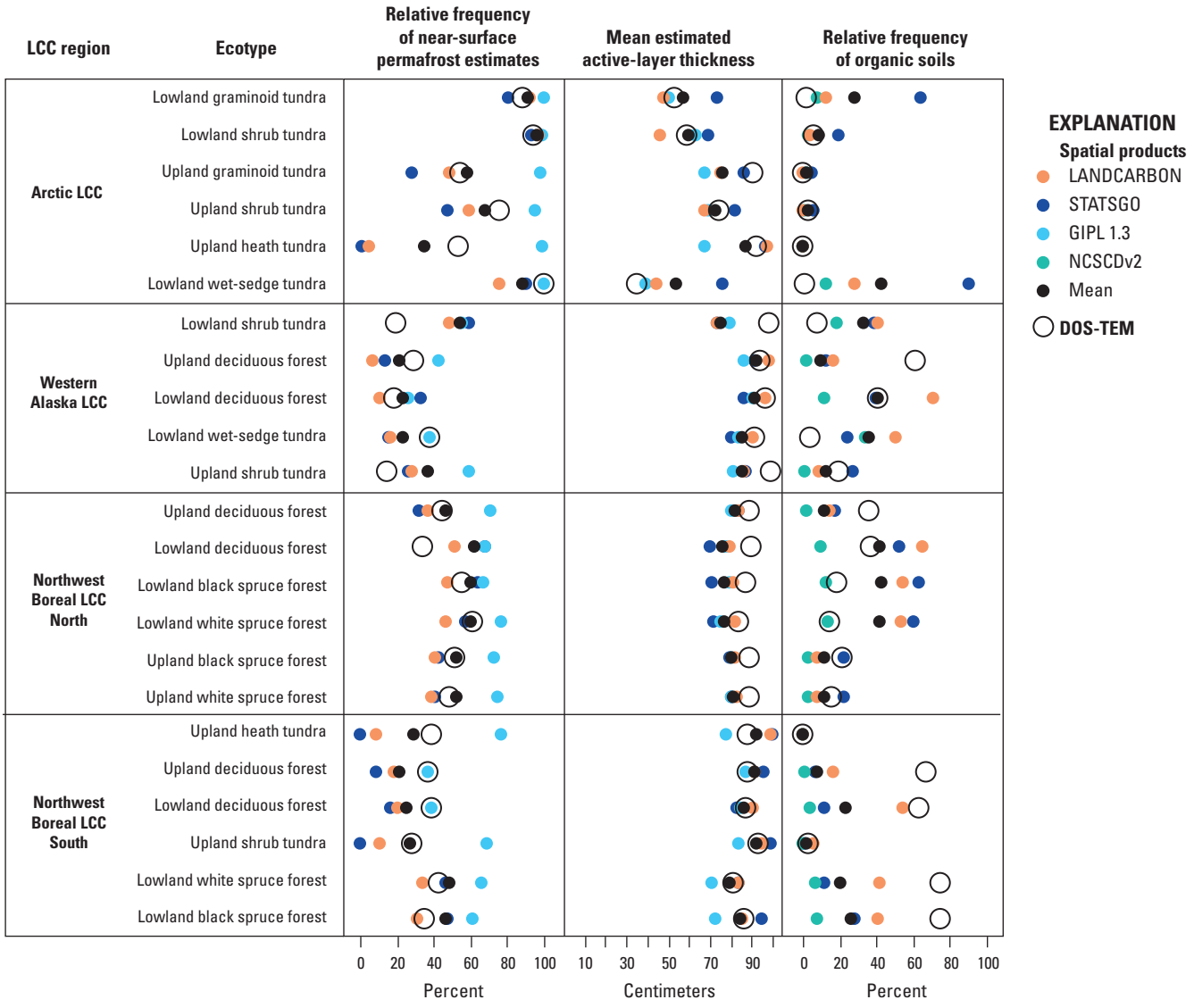

Figure 3.7. Permafrost and organic soil characterization for the largest (in terms of soil organic carbon, in petagrams of carbon) five or six ecotype classes in each Landscape Conservation Cooperative (LCC) region. Areas estimated to have active-layer thicknesses greater than 1 meter were given a value of 101 centimeters for direct comparison and to account for differences in investigation depths. Organic soils are defined here as those soils with a surface organic epipedon that is greater than or equal to 40 centimeters. "Mean" refers to the mean of all relevant estimates except the Dynamic Organic Soil version of the Terrestrial Ecosystem Model (DOS-TEM): LANDCARBON, permafrost and organic soil data from Pastick and others (2015); STATSGO, permafrost and organic soil data from the state soil geographic database; GIPL 1.3, permafrost data from the Geophysical Institute Permafrost Laboratory version 1.3 transient model; and NCSCDv2, organic soil data from the Northern Circumpolar Soil Carbon Database version 2.

Spatial predictions of ALT (fig. 3.4) were also summarized by LCC region and DOS-TEM land-cover type in tables 3.5 and 3.6. Areas where the ALT was estimated to be greater than 1 m were given a consistent value (101 cm) because of differences in investigation depths and for a direct comparison of ALT products. Empirically or numerically derived ALT estimates had a mean ALT of 80 cm in Alaska (excluding the North Pacific LCC), with a range of 76 to 84 cm between estimates (table 3.5). The mean ALT estimate of the DOS-TEM output (86 cm) was slightly outside the range of other products, but within the range of uncertainty between other products (that is, MAD from product averages was 6 cm). The mean product ALT was thinnest in the Arctic LCC (67 cm), followed by the Northwest Boreal LCC North (79 cm), Western Alaska LCC (87 cm), and Northwest Boreal LCC South (88 cm). The mean ALT estimates of the DOS-TEM model were generally higher than other estimates. Furthermore, there was no significant correlation between DOS-TEM and mean product ALT estimates when stratified by LCC region. It is important to note, however, that there were significant correlations between mean ALT estimates of DOS-TEM, GIPL 1.3, and LANDCARBON when stratified by LCC region ($R^2 > 0.75$; n = 5). The lack of correlation between the mean product and DOS-TEM estimates was due to higher estimates of ALT in the STATSGO product for the Arctic LCC, which drives up the mean of other products. Higher Arctic LCC ALT estimates in the STATSGO product may stem from the fact that a frozen soil horizon was recorded in the database only if ice lenses were visible, not using a temperature criterion as in the definition of permafrost. Furthermore, there was no temporal constraint on those observations used during the creation of the STATSGO-derived ALT map.

Mean product ALT estimates varied approximately twofold between DOS-TEM land-cover types with no significant correlation to mean product NSP frequency estimates (table 3.6). Wet-sedge tundra had the lowest mean product ALT (55 cm), followed by graminoid tundra (66 cm), shrub tundra (73 cm), black and white spruce forests (80 cm each), deciduous forest (85 cm), nonvegetated areas (91 cm), heath tundra (100 cm), and maritime vegetation (>100 cm). DOS-TEM ALT outputs were significantly correlated with the mean ALT of other products when stratified by land-cover type ($R^2 = 0.87$; n = 9), despite 67 percent of the DOS-TEM outputs falling outside of the range of other ALT products. The largest differences between DOS-TEM output and the mean of other product ALT outputs were for tundra vegetation (that is, shrub, graminoid, wet-sedge, and heath tundra), which accounts for approximately 32 percent of Alaska, and where there is the largest range in other ALT estimates.

ALT estimates were also stratified and averaged by ecotype in each LCC region (excluding the North Pacific LCC; fig. 3.7). Empirically or numerically derived ALT maps were generally in global accordance with one another and with DOS-TEM outputs. For instance, the ALT maps produced by Pastick and others (2015) (LANDCARBON) and Marchenko and others (2008) (GIPL 1.3) were significantly correlated when ALT estimates are averaged by ecotype ($R^2 = 0.67$; n = 23). The DOS-TEM and GIPL 1.3 products had the highest correlation ($R^2 = 0.78$; n = 23) when comparing mean ALT estimates of each major ecotype, but DOS-TEM outputs were also significantly correlated ($R^2 = 0.73$; n = 23) with estimates made by Pastick and others (2015) (LANDCARBON). DOS-TEM outputs were significantly correlated with the mean ALT of other outputs ($R^2 = 0.73$; n = 23). Furthermore, in 48 percent of the ecotype classes, the DOS-TEM output was within the range of other products, whereas 12 of the DOS-TEM outputs were outside the range. It is important to note, however, that DOS-TEM ALT outputs were generally close to the intra-product means. For example, the rMAE or MAE of DOS-TEM outputs compared to the mean of all products was 8 percent or 7 cm, respectively. More than three-fourths of the high DOS-TEM outputs were for the Northwest Boreal LCC North and Western Alaska LCC, where permafrost is particularly vulnerable to climate warming (Shur and Jorgenson, 2007) and the ranges in mean ALT estimates are lowest. A spatially exhaustive comparison of continuous estimations of ALT could not be made because of differences in investigation depths.

3.5.3. Comparison of Soil Organic-Layer Estimates

Organic soil estimates were summarized by LCC region and DOS-TEM land-cover type in tables 3.5 and 3.6. According to observation-based OLT products, organic soils were estimated to underlie a fairly small portion of Alaska (excluding the North Pacific LCC) with a narrow range (8 to 30 percent) in frequency of occurrence. The mean organic soil frequency from DOS-TEM outputs (18 percent) falls within this range. On average, organic soils most frequently occurred in Northwest Boreal LCC North (26 percent), followed by the Western Alaska LCC (23 percent), the Arctic LCC (12 percent), and the Northwest Boreal LCC South (10 percent). At the LCC region level, DOS-TEM outputs were within the range of other products 60 percent of the time, with the largest difference occurring in the Northwest Boreal LCC South (table 3.5).

Wet-sedge tundra was estimated to be most frequently underlain by organic soils (38 percent; table 3.6), followed by black spruce forest (27 percent), white spruce forest (25 percent), deciduous forest (23 percent), graminoid tundra (18 percent), shrub tundra (15 percent), nonvegetated areas (11 percent), and heath tundra (1 percent). For a comparison, organic soil frequencies, as estimated in the LANDCARBON OLT product, varied considerably when stratified by NLCD class (wetlands and moss equal 97 to 100 percent; deciduous forest and dwarf shrub equal 0 to 8 percent) (Homer and others, 2007) but this land-cover dataset was also used for model development. DOS-TEM outputs were not significantly (p-value >0.18) correlated with the individual organic soil

products or the mean of those products when estimates were averaged by land-cover type. However, 63 percent of DOS-TEM outputs were within the range of other product estimates, with only three outputs outside of the range of other products. Moreover, two of the three outlier DOS-TEM outputs were only slightly outside the range of other products, with the largest difference occurring in areas mapped as wet-sedge tundra, which represents a small fraction (4 percent) of the land cover of Alaska. Empirical model estimates (that is, STATSGO, LANDCARBON) were significantly correlated (R^2=0.53; n=9) when stratified by land-cover type.

Empirically derived organic soil maps are in global accordance with one another, when mean frequency estimates are stratified by ecotype in each LCC region, but less so in correspondence with DOS-TEM outputs (fig. 3.7). In 57 percent of the ecotype classes, the DOS-TEM output is within the range of other products, whereas 10 of the DOS-TEM outputs were outside the range. Moreover, DOS-TEM outputs were not significantly correlated (p-value=0.63; n=23) with the mean of other estimates when stratified by ecotype in each LCC region. Mean product organic soil frequencies indicate that lowlands are more frequently underlain by organic soils than uplands in Alaska (32 percent versus 8 percent), a pattern not seen in DOS-TEM outputs (19 percent versus 22 percent). The Western Alaska LCC and Northwest Boreal LCC South had the largest differences in organic soil estimates. Large differences in the range of model outputs suggest that the simulation of thick soil organic layers is difficult, partially owing to a large and complex set of biophysical factors (for example, soil moisture, disturbances) influencing organic soil distributions, and that DOS-TEM outputs of organic soils are currently highly uncertain.

3.5.4. Soil Susceptibility to Climate Change

The conceptual model of ecotype and soil susceptibility to climate change resulted in susceptibility scores ranging from a high of 4 to a low of 0. The map produced from this model can be seen in figure 3.8.

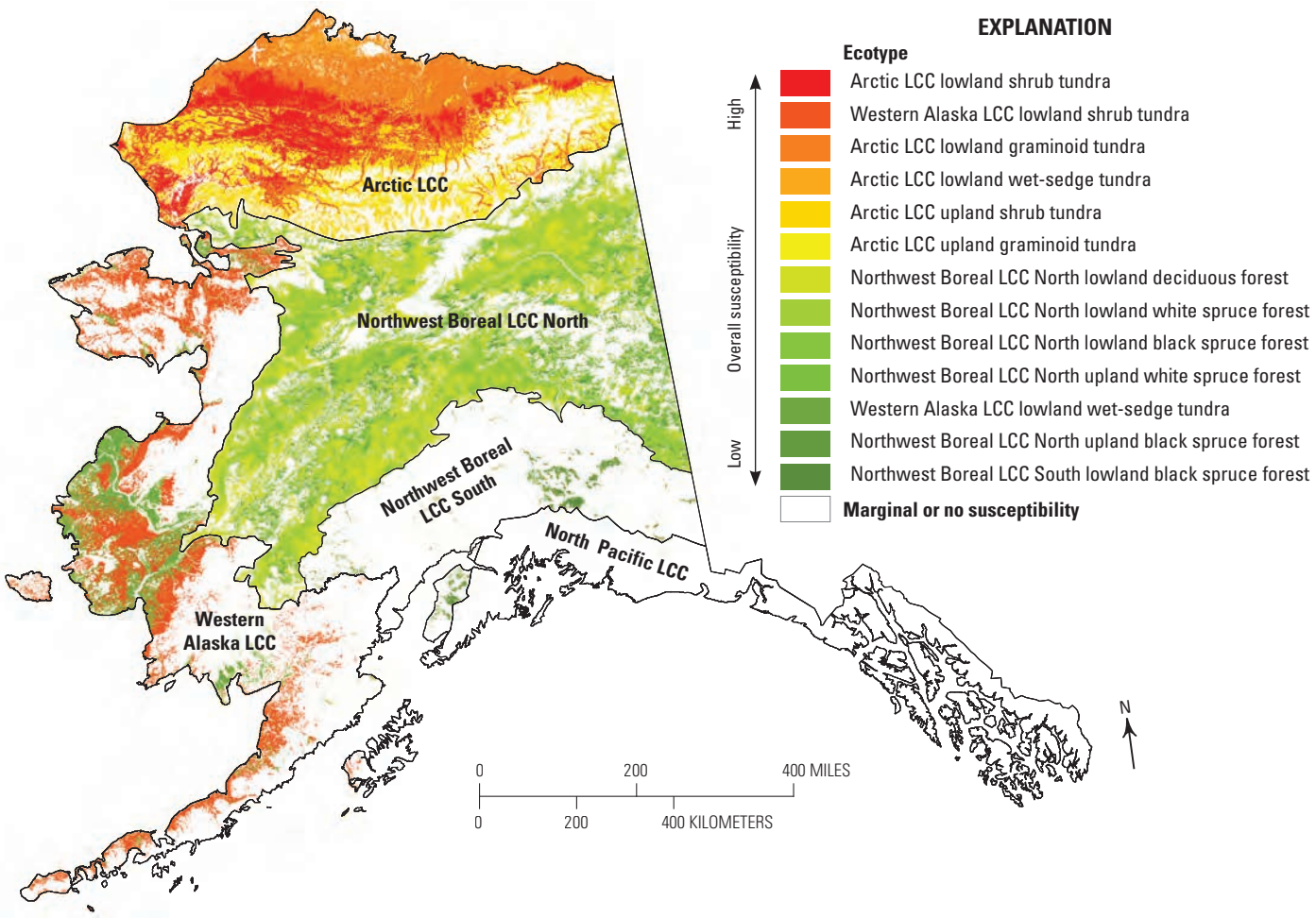

Figure 3.8. Overall soil susceptibility of major ecotypes in Alaska. Susceptibility was higher in ecotypes with greater respiration to the atmosphere, burning, and near-surface (within 1 meter) permafrost thaw.

The tundra ecotypes, Arctic LCC lowland graminoid, shrub, and wet-sedge tundra and Western Alaska LCC lowland shrub tundra, had the highest susceptibility scores. These four ecotypes had the highest total profile organic carbon product mean values, ranging from 44.5 to 66.9 kgC/m^2, and generally high frozen organic carbon and NSP (in three out of the four ecotypes). Arctic LCC upland shrub and graminoid tundra ecotypes had intermediate susceptibility scores, which were driven by susceptibility of NSP and high uncertainty. The persistence of the Arctic LCC within these top susceptibility scores is compounded by also having the highest carbon stocks and high uncertainty of SOC densities (fig. 3.6). The Arctic LCC graminoid and shrub tundra ecotypes had the highest ecotype frequencies of NSP. Western Alaska LCC lowland shrub tundra makes up 33 percent of the Western Alaska LCC and has the second highest susceptibility score. DOS-TEM outputs in this ecotype tended to underestimate organic-layer carbon, NSP, and organic soil relative frequencies and to overestimate ALT in this system with known permafrost vulnerabilities (Shur and Jorgenson, 2007). Extended ground surveys linked with mapping efforts in these susceptible ecotypes could reduce uncertainty and provide more accurate baseline datasets for assessing future changes and effects.

Ecotypes with low susceptibility scores (Northwest Boreal LCC North lowland black spruce, deciduous, and white spruce forests; Northwest Boreal LCC North upland black and white spruce forests; Northwest Boreal LCC South lowland black spruce forest; and Western Alaska LCC lowland wet-sedge tundra) further underscore the susceptibility of the Western Alaska LCC and Northwest Boreal LCC systems over the other remaining Alaska ecotypes, which had the lowest susceptibility scores. Low susceptibility scores of some Northwest Boreal LCC North ecotypes might have been higher if fire return interval or temperature were included in selected criteria. Given expected increases in fire severity and frequency (Barrett and others, 2011), this LCC region is important for understanding and forecasting future ecosystem responses. Organic-layer carbon estimates in Northwest Boreal LCC North lowland forest ecotypes had high magnitudes (fig. 3.6). DOS-TEM outputs for the Northwest Boreal LCC North tended to underestimate total profile carbon, soil organic-layer carbon, and mineral soil carbon (fig. 3.6) and to overestimate ALT (fig. 3.7).

Ecotypes with the lowest susceptibility scores were Arctic LCC upland heath tundra; Northwest Boreal LCC North upland deciduous forest; Northwest Boreal LCC South lowland deciduous and white spruce forests; Northwest Boreal LCC South upland deciduous forest and heath and shrub tundra; Western Alaska LCC lowland deciduous forest; and Western Alaska LCC upland deciduous forest and shrub tundra. Remarkably the separation of northern and southern components of the Northwest Boreal LCC was captured in susceptibility scores based solely on soil properties with no fire probability or climate inputs.

Despite the discrepancies between DOS-TEM outputs and those of other products highlighted above, in general DOS-TEM did a reasonable job capturing the spatial variations of important high-latitude soil attributes. The DOS-TEM total profile carbon, soil organic-layer carbon, ALT, and organic soil relative frequency were within the other product data range for 78 percent, 30 percent, 48 percent, and 57 percent of the ecotypes, respectively.

3.6. Conclusions

Soil carbon, permafrost, and organic soils are important components of high-latitude ecosystems. This chapter provides fundamental information as to the current state of knowledge of the distribution of these soil properties. This information will be of use for future field campaigns aimed at quantifying the resilience and vulnerability of high-latitude ecosystems to changes in climate and environment.

The synoptic comparison of estimates from multiple soil products with those of a process-based model (DOS-TEM) was useful to (1) identify areas of high soil attribute uncertainty, (2) identify areas of disagreement with the DOS-TEM estimates and mapped current conditions, (3) provide inter-product mean values which may be useful as baseline data for assessing and understanding future changes, and (4) identify areas of potential susceptibility to changing climates through inter-soil attribute combinations. These uncertainties could help prioritize field collections and studies on ecotypes with high uncertainties and high soil carbon stocks (particularly, the Arctic LCC). Discrepancies between DOS-TEM and other product estimates in Northwest Boreal LCC North SOC and ALT and upland versus lowland OLT will be useful for informing the uncertainty of future ecosystem responses to a changing climate made by DOS-TEM. The high soil susceptibility scores for the Arctic and Western Alaska LCCs may reinforce DOS-TEM future change projections.

This soil product spatial synthesis was constrained to the soil parameters presented in this chapter and was done at a relatively coarse resolution, at ecotype or coarser levels (LCC region or land-cover type). These coarser evaluation units helped to mitigate possible geolocation errors and to not penalize coarser polygon approaches. However, significant variations of permafrost and soil carbon related to adjacency to water and soil texture changes certainly occur within the broad ecotypes used in this study.

Refined and higher resolution products for Alaska can potentially be used to better insure that the current status of Alaska systems are captured in process-based models. This would improve confidence of future predictions made by these models.

3.7. References Cited

Amiro, B.D., Orchansky, A.L., Barr, A.G., Black, T.A., Chambers, S.D., Chapin, F.S., III, Goulden, M.L., Litvak, M., Liu, H.P., McCaughey, J.H., McMillan, A., and Randerson, J.T., 2006, The effect of post-fire stand age on the boreal forest energy balance: Agricultural and Forest Meteorology, v. 140, nos. 1–4, p. 45–50, http://dx.doi.org/10.1016/j.agrformet.2006.02.014.

Barrett, K., McGuire, A.D., Hoy, E.E., and Kasischke, E.S., 2011, Potential shifts in dominant forest cover in interior Alaska driven by variations in fire severity: Ecological Applications, v. 21, no. 7, p. 2380–2396, http://dx.doi.org/10.1890/10-0896.1.

Bliss, N.B., and Maursetter, John, 2010, Soil organic carbon stocks in Alaska estimated with spatial and pedon data: Soil Science Society of America Journal, v. 74, no. 2, p. 565–579, http://dx.doi.org/10.2136/sssaj2008.0404.

Bliss, N.B., Waltman, S.W., West, L.T., Neale, Anne, and Mehaffey, Megan, 2014, Distribution of soil organic carbon in the conterminous United States, *in* Hartemink, A.E., and McSweeney, Kevin, eds., Soil carbon: Cham, Switzerland, Springer International Publishing, p. 85–93, http://dx.doi.org/10.1007/978-3-319-04084-4_9.

Chambers, S.D., and Chapin, F.S., III, 2002, Fire effects on surface-atmosphere energy exchange in Alaskan black spruce ecosystems; Implications for feedbacks to regional climate: Journal of Geophysical Research; Atmospheres, v. 107, no. D1, p. FFR 1–1 to FFR 1–17, http://dx.doi.org/10.1029/2001jd000530.

Chapin, F.S., III, McGuire, A.D., Ruess, R.W., Hollingsworth, T.N., Mack, M.C., Johnstone, J.F., Kasischke, E.S., Euskirchen, E.S., Jones, J.B., Jorgenson, M.T., Kielland, K., Kofinas, G.P., Turetsky, M.R., Yarie, J., Lloyd, A.H., and Taylor, D.L., 2010, Resilience of Alaska's boreal forest to climatic change: Canadian Journal of Forest Research, v. 40, no. 7, p. 1360–1370, http://dx.doi.org/10.1139/X10-074.

Clow, G.D., 2014, Temperature data acquired from the DOI/GTN–P Deep Borehole Array on the Arctic Slope of Alaska, 1973–2013: Earth System Science Data, v. 6, no. 1, p. 201–218, http://dx.doi.org/10.5194/essd-6-201-2014.

Euskirchen, E.S., McGuire, A.D., Chapin, F.S., III, and Rupp, T.S., 2010, The changing effects of Alaska's boreal forests on the climate system: Canadian Journal of Forest Research, v. 40, no. 7, p. 1336–1346, http://dx.doi.org/10.1139/X09-209.

Genet, H., McGuire, A.D., Barrett, K., Breen, A., Euskirchen, E.S., Johnstone, J.F., Kasischke, E.S., Melvin, A.M., Bennett, A., Mack, M.C., Rupp, T.S., Schuur, E.A.G., Turetsky, M.R., and Yuan, F., 2013, Modeling the effects of fire severity and climate warming on active layer thickness and soil carbon storage of black spruce forests across the landscape in interior Alaska: Environmental Research Letters, v. 8, no. 4, letter 045016, 13 p., http://dx.doi.org/10.1088/1748-9326/8/4/045016.

Harden, J.W., Manies, K.L., Turetsky, M.R., and Neff, J.C., 2006, Effects of wildfire and permafrost on soil organic matter and soil climate in interior Alaska: Global Change Biology, v. 12, no. 12, p. 2391–2403, http://dx.doi.org/10.1111/j.1365-2486.2006.01255.x.

Hinkel, K.M., and Nelson, F.E., 2003, Spatial and temporal patterns of active layer thickness at Circumpolar Active Layer Monitoring (CALM) sites in northern Alaska, 1995–2000: Journal of Geophysical Research; Atmospheres, v. 108, no. D2, p. ALT 9–1 to ALT 9–13, http://dx.doi.org/10.1029/2001jd000927.

Homer, Collin, Dewitz, Jon, Fry, Joyce, Coan, Michael, Hossain, Nazmul, Larson, Charles, Herold, Nate, McKerrow, Alexa, VanDriel, J.N., and Wickham, James, 2007, Completion of the 2001 National Land Cover Database for the conterminous United States: Photogrammetric Engineering and Remote Sensing, v. 73, no. 4, p. 337–341. [Also available at http://www.asprs.org/a/publications/pers/2007journal/april/highlight.pdf.]

Homer, Collin, Huang, Chengquan, Yang, Limin, Wylie, Bruce, and Coan, Michael, 2004, Development of a 2001 National Land-Cover Database for the United States: Photogrammetric Engineering and Remote Sensing, v. 70, no. 7, p. 829–840, http://dx.doi.org/10.14358/PERS.70.7.829.

Hugelius, G., Strauss, J., Zubrzycki, S., Harden, J.W., Schuur, E.A.G., Ping, C.-L., Schirrmeister, L., Grosse, G., Michaelson, G.J., Koven, C.D., O'Donnell, J.A., Elberling, B., Mishra, U., Camill, P., Yu, Z., Palmtag, J., and Kuhry, P., 2014, Estimated stocks of circumpolar permafrost carbon with quantified uncertainty ranges and identified data gaps: Biogeosciences, v. 11, no. 23, p. 6573–6593, http://dx.doi.org/10.5194/bg-11-6573-2014.

Hugelius, G., Tarnocai, C., Broll, G., Canadell, J.G., Kuhry, P., and Swanson, D.K., 2013, The Northern Circumpolar Soil Carbon Database; Spatially distributed datasets of soil coverage and soil carbon storage in the northern permafrost regions: Earth System Science Data, v. 5, no. 1, p. 3–13, http://dx.doi.org/10.5194/essd-5-3-2013.

Hugelius, Gustaf, Routh, Joyanto, Kuhry, Peter, and Crill, Patrick, 2012, Mapping the degree of decomposition and thaw remobilization potential of soil organic matter in discontinuous permafrost terrain: Journal of Geophysical Research; Biogeosciences, v. 117, no. G2, article G02030, 14 p., http://dx.doi.org/10.1029/2011JG001873.

Johnson, K.D., Harden, Jennifer, McGuire, A.D., Bliss, N.B., Bockheim, J.G., Clark, Mark, Nettleton-Hollingsworth, Teresa, Jorgenson, M.T., Kane, E.S., Mack, Michelle, O'Donnell, Jonathan, Ping, C.-L., Schuur, E.A.G., Turetsky, M.R., and Valentine, D.W., 2011, Soil carbon distribution in Alaska in relation to soil-forming factors: Geoderma, v. 167–168, p. 71–84, http://dx.doi.org/10.1016/j.geoderma.2011.10.006.

Johnson, K.D., Harden, J.W., McGuire, A.D., Clark, Mark, Yuan, Fengming, and Finley, A.O., 2013, Permafrost and organic layer interactions over a climate gradient in a discontinuous permafrost zone: Environmental Research Letters, v. 8, no. 3, letter 035028, 12 p., http://dx.doi.org/10.1088/1748-9326/8/3/035028.

Johnston, C.E., Ewing, S.A., Harden, J.W., Varner, R.K., Wickland, K.P., Koch, J.C., Fuller, C.C., Manies, Kristen, and Jorgenson, M.T., 2014, Effect of permafrost thaw on CO_2 and CH_4 exchange in a western Alaska peatland chronosequence: Environmental Research Letters, v. 9, no. 8, letter 085004, 12 p., http://dx.doi.org/10.1088/1748-9326/9/8/085004.

Jorgenson, M.T., Racine, C.H., Walters, J.C., and Osterkamp, T.E., 2001, Permafrost degradation and ecological changes associated with a warming climate in central Alaska: Climatic Change, v. 48, no. 4, p. 551–579, http://dx.doi.org/10.1023/A:1005667424292.

Jorgenson, M.T., Shur, Y.L., and Osterkamp, T.E., 2008, Thermokarst in Alaska, *in* Kane, D.L., and Hinkel, K.M., eds., Proceedings of the Ninth International Conference on Permafrost, Fairbanks, Alaska, June 29 to July 3, 2008: Institute of Northern Engineering, University of Alaska-Fairbanks, p. 869–876.

Jorgenson, M.T., Shur, Y.L., and Pullman, E.R., 2006, Abrupt increase in permafrost degradation in Arctic Alaska: Geophysical Research Letters, v. 33, no. 2, letter L02503, 4 p., http://dx.doi.org/10.1029/2005gl024960.

Kasischke, E.S., and Johnstone, J.F., 2005, Variation in post-fire organic layer thickness in a black spruce forest complex in interior Alaska and its effect on soil temperature and moisture: Canadian Journal of Forest Research, v. 35, no. 9, p. 2164–2177, http://dx.doi.org/10.1139/X05-159.

Kasischke, E.S., Verbyla, D.L., Rupp, T.S., McGuire, A.D., Murphy, K.A., Jandt, Randi, Barnes, J.L., Hoy, E.E., Duffy, P.A., Calef, Monika, and Turetsky, M.R., 2010, Alaska's changing fire regime—Implications for the vulnerability of its boreal forests: Canadian Journal of Forest Research, v. 40, no. 7, p. 1313–1324, http://dx.doi.org/10.1139/X10-098.

LANDFIRE, 2008, Existing vegetation type layer (ver. 1.1.0): LANDFIRE spatial data, accessed December 15, 2014, at http://landfire.cr.usgs.gov/viewer/.

Mann, D.H., Rupp, T.S., Olson, M.A., and Duffy, P.A., 2012, Is Alaska's boreal forest now crossing a major ecological threshold?: Arctic, Antarctic, and Alpine Research, v. 44, no. 3, p. 319–331, http://dx.doi.org/10.1657/1938-4246-44.3.319.

Marchenko, Sergei, Romanovsky, Vladimir, and Tipenko, Gennady, 2008, Numerical modeling of spatial permafrost dynamics in Alaska, *in* Kane, D.L., and Hinkel, K.M., eds., International Conference on Permafrost, 9th, Fairbanks, Alaska, June 29–July 3, 2008, Proceedings: Fairbanks, Alaska, Institute of Northern Engineering, University of Alaska, Fairbanks, p. 190–204.

Martin, M.P., Wattenbach, M., Smith, P., Meersmans, J., Jolivet, C., Boulonne, L., and Arrouays, D., 2011, Spatial distribution of soil organic carbon stocks in France: Biogeosciences, v. 8, no. 5, p. 1053–1065, http://dx.doi.org/10.5194/bg-8-1053-2011.

McConnell, N.A., Turetsky, M.R., McGuire, A.D., Kane, E.S., Waldrop, M.P., and Harden, J.W., 2013, Controls on ecosystem and root respiration across a permafrost and wetland gradient in interior Alaska: Environmental Research Letters, v. 8, no. 4, letter 045029, 11 p., http://dx.doi.org/10.1088/1748-9326/8/4/045029.

Mishra, U., and Riley, W.J., 2012, Alaskan soil carbon stocks; Spatial variability and dependence on environmental factors: Biogeosciences, v. 9, no. 9, p. 3637–3645, http://dx.doi.org/10.5194/bg-9-3637-2012.

Mu, Cuicui, Zhang, Tingjun, Schuster, P.F., Schaefer, Kevin, Wickland, K.P., Repert, D.A., Liu, Lin, Schaefer, Tim, and Cheng, Guodong, 2014, Carbon and geochemical properties of cryosols on the North Slope of Alaska: Cold Regions Science and Technology, v. 100, p. 59–67, http://dx.doi.org/10.1016/j.coldregions.2014.01.001.

Natali, S.M., Schuur, E.A.G., and Rubin, R.L., 2012, Increased plant productivity in Alaskan tundra as a result of experimental warming of soil and permafrost: Journal of Ecology, v. 100, no. 2, p. 488–498, http://dx.doi.org/10.1111/j.1365-2745.2011.01925.x.

Natali, S.M., Schuur, E.A.G., Trucco, Christian, Hicks Pries, C.E., Crummer, K.G., and Baron Lopez, A.F., 2011, Effects of experimental warming of air, soil and permafrost on carbon balance in Alaskan tundra: Global Change Biology, v. 17, no. 3, p. 1394–1407, http://dx.doi.org/10.1111/j.1365-2486.2010.02303.x.

National Research Council, 2014, Opportunities to use remote sensing in understanding permafrost and related ecological characteristics; Report of a workshop: Washington, D.C., The National Academies Press, 52 p.

O'Donnell, J.A., Romanovsky, V.E., Harden, J.W., and McGuire, A.D., 2009, The effect of moisture content on the thermal conductivity of moss and organic soil horizons from black spruce ecosystems in interior Alaska: Soil Science, v. 174, no. 12, p. 646–651, http://dx.doi.org/10.1097/SS.0b013e3181c4a7f8.

Osterkamp, T.E., Jorgenson, M.T., Schuur, E.A.G., Shur, Y.L., Kanevskiy, M.Z., Vogel, J.G., and Tumskoy, V.E., 2009, Physical and ecological changes associated with warming permafrost and thermokarst in interior Alaska: Permafrost and Periglacial Processes, v. 20, no. 3, p. 235–256, http://dx.doi.org/10.1002/ppp.656.

Pastick, N.J., Jorgenson, M.T., Wylie, B.K., Minsley, B.J., Ji, Lei, Walvoord, M.A., Smith, B.D., Abraham, J.D., and Rose, J.R., 2013, Extending airborne electromagnetic surveys for regional active layer and permafrost mapping with remote sensing and ancillary data, Yukon Flats ecoregion, central Alaska: Permafrost and Periglacial Processes, v. 24, no. 3, p. 184–199, http://dx.doi.org/10.1002/ppp.1775.

Pastick, N.J., Jorgenson, M.T., Wylie, B.K., Nield, S.J., Johnson, K.D., and Finley, A.O., 2015, Distribution of near-surface permafrost in Alaska; Estimates of present and future conditions: Remote Sensing of Environment, v. 168, p. 301–315, http://dx.doi.org/10.1016/j.rse.2015.07.019.

Pastick, N.J., Jorgenson, M.T., Wylie, B.K., Rose, J.R., Rigge, Matthew, and Walvoord, M.A., 2014, Spatial variability and landscape controls of near-surface permafrost within the Alaskan Yukon River Basin: Journal of Geophysical Research; Biogeosciences, v. 119, no. 6, p. 1244–1265, http://dx.doi.org/10.1002/2013JG002594.

Pastick, N.J., Rigge, Matthew, Wylie, B.K., Jorgenson, M.T., Rose, J.R., Johnson, K.D., and Ji, Lei, 2014, Distribution and landscape controls of organic layer thickness and carbon within the Alaskan Yukon River Basin: Geoderma, v. 230–231, p. 79–94, http://dx.doi.org/10.1016/j.geoderma.2014.04.008.

Ping, C.-L., Michaelson, G.J., Jorgenson, M.T., Kimble, J.M., Epstein, Howard, Romanovsky, V.E., and Walker, D.A., 2008, High stocks of soil organic carbon in the North American Arctic region: Nature Geoscience, v. 1, no. 9, p. 615–619, http://dx.doi.org/10.1038/ngeo284.

Riahi, Keywan, Rao, Shilpa, Krey, Volker, Cho, Cheolhung, Chirkov, Vadim, Fischer, Guenther, Kindermann, Georg, Nakicenovic, Nebojsa, and Rafaj, Peter, 2011, RCP 8.5—A scenario of comparatively high greenhouse gas emissions: Climatic Change, v. 109, nos. 1–2, p. 33–57, http://dx.doi.org/10.1007/s10584-011-0149-y.

Schaefer, Kevin, Lantuit, Hugues, Romanovsky, V.E., Schuur, E.A.G., and Witt, Ronald, 2014, The impact of the permafrost carbon feedback on global climate: Environmental Research Letters, v. 9, no. 8, letter 085003, 9 p., http://dx.doi.org/10.1088/1748-9326/9/8/085003.

Schaefer, Kevin, Zhang, Tingjun, Bruhwiler, Lori, and Barrett, A.P., 2011, Amount and timing of permafrost carbon release in response to climate warming: Tellus; Series B, Chemical and Physical Meteorology, v. 63B, no. 2, p. 165–180, http://dx.doi.org/10.1111/j.1600-0889.2011.00527.x.

Schuur, E.A.G., Bockheim, James, Canadell, J.G., Euskirchen, Eugenie, Field, C.B., Goryachkin, S.V., Hagemann, Stefan, Kuhry, Peter, Lafleur, P.M., Lee, Hanna, Mazhitova, Galina, Nelson, F.E., Rinke, Annette, Romanovsky, V.E., Shiklomanov, Nikolay, Tarnocai, Charles, Venevsky, Sergey, Vogel, J.G., and Zimov, S.A., 2008, Vulnerability of permafrost carbon to climate change—Implications for the global carbon cycle: BioScience, v. 58, no. 8, p. 701–714, http://dx.doi.org/10.1641/B580807.

Schuur, E.A.G., McGuire, A.D., Schädel, C., Grosse, G., Harden, J.W., Hayes, D.J., Hugelius, G., Koven, C.D., Kuhry, P., Lawrence, D.M., Natali, S.M., Olefeldt, D., Romanovsky, V.E., Schaefer, K., Turetsky, M.R., Treat, C.C., and Vonk, J.E., 2015, Climate change and the permafrost carbon feedback: Nature, v. 520, no. 7546, p. 171–179, http://dx.doi.org/10.1038/nature14338.

Shur, Y.L., and Jorgenson, M.T., 2007, Patterns of permafrost formation and degradation in relation to climate and ecosystems: Permafrost and Periglacial Processes, v. 18, no. 1, p. 7–19, http://dx.doi.org/10.1002/ppp.582.

Smit, B., Burton, I., Klein, R.J.T., and Street, R., 1999, The science of adaptation; A framework for assessment: Mitigation and Adaptation Strategies for Global Change, v. 4, nos. 3–4, p. 199–213, http://dx.doi.org/10.1023/A:1009652531101.

Soil Survey Staff, 1999, Soil taxonomy; A basic system of soil classification for making and interpreting soil surveys (2d ed.): U.S. Department of Agriculture, Natural Resources Conservation Service, Agriculture Handbook, no. 436, 871 p., http://www.nrcs.usda.gov/Internet/FSE_DOCUMENTS/nrcs142p2_051232.pdf.

Soil Survey Staff, 2012, General soil map of Alaska—STATSGO data: U.S. Department of Agriculture, Natural Resources Conservation Service, accessed [date], at http://websoilsurvey.nrcs.usda.gov/.

Stocker, T.F., Qin, Dahe, Plattner, G.-K., Tignor, M.M.B., Allen, S.K., Boschung, Judith, Nauels, Alexander, Xia, Yu, Bex, Vincent, and Midgley, P.M., eds., 2013, Climate change 2013—The physical science basis, Contribution of Working Group I to the Fifth Assessment Report of the Intergovernmental Panel on Climate Change: Cambridge, United Kingdom, Cambridge University Press, 1535 p. [Also available at http://www.ipcc.ch/report/ar5/wg1/.]

Treat, C.C., Wollheim, W.M., Varner, R.K., Grandy, A.S., Talbot, J., and Frolking, S., 2014, Temperature and peat type control CO_2 and CH_4 production in Alaskan permafrost peats: Global Change Biology, v. 20, no. 8, p. 2674–2686, http://dx.doi.org/10.1111/gcb.12572.

Turetsky, M.R., Kane, E.S., Harden, J.W., Ottmar, R.D., Manies, K.L., Hoy, Elizabeth, and Kasischke, E.S., 2011, Recent acceleration of biomass burning and carbon losses in Alaskan forests and peatlands: Nature Geoscience, v. 4, no. 1, p. 27–31, http://dx.doi.org/10.1038/ngeo1027.

University of Alaska-Fairbanks, Geophysical Institute Permafrost Lab [GIPL], 2011, Simulated active layer thickness: Fairbanks, Alaska, Arctic Landscape Conservation Cooperative, http://arcticlcc.org/products/spatial-data/show/simulated-active-layer-thickness.

Walvoord, M.A., Voss, C.I., and Wellman, T.P., 2012, Influence of permafrost distribution on groundwater flow in the context of climate-driven permafrost thaw—Example from Yukon Flats Basin, Alaska, United States: Water Resources Research, v. 48, no. 7, article W07524, 17 p., http://dx.doi.org/10.1029/2011WR011595.

Wellman, T.P., Voss, C.I., and Walvoord, M.A., 2013, Impacts of climate, lake size, and supra- and sub-permafrost groundwater flow on lake-talik evolution, Yukon Flats, Alaska (USA): Hydrogeology Journal, v. 21, no. 1, p. 281–298, http://dx.doi.org/10.1007/s10040-012-0941-4.

Wickland, K.P., and Neff, J.C., 2008, Decomposition of soil organic matter from boreal black spruce forest; Environmental and chemical controls: Biogeochemistry, v. 87, no. 1, p. 29–47, http://dx.doi.org/10.1007/s10533-007-9166-3.

Yi, Shuhua, McGuire, A.D., Harden, Jennifer, Kasischke, Eric, Manies, Kristen, Hinzman, Larry, Liljedahl, Anna, Randerson, Jim, Liu, Heping, Romanovsky, Vladimir, Marchenko, Sergei, and Kim, Yongwon, 2009, Interactions between soil thermal and hydrological dynamics in the response of Alaska ecosystems to fire disturbance: Journal of Geophysical Research; Biogeosciences, v. 114, no. G2, article G02015, 20 p., http://dx.doi.org/10.1029/2008JG000841.

Yi, Shuhua, McGuire, A.D., Kasischke, Eric, Harden, Jennifer, Manies, Kristen, Mack, Michelle, and Turetsky, Merritt, 2010, A dynamic organic soil biogeochemical model for simulating the effects of wildfire on soil environmental conditions and carbon dynamics of black spruce forests: Journal of Geophysical Research; Biogeosciences, v. 115, no. G4, article G04015, 15 p., http://dx.doi.org/10.1029/2010JG001302.

Yoshikawa, Kenji, and Hinzman, L.D., 2003, Shrinking thermokarst ponds and groundwater dynamics in discontinuous permafrost near Council, Alaska: Permafrost and Periglacial Processes, v. 14, no. 2, p. 151–160, http://dx.doi.org/10.1002/ppp.451.

Zhuang, Q., McGuire, A.D., Melillo, J.M., Clein, J.S., Dargaville, R.J., Kicklighter, D.W., Myneni, R.B., Dong, J., Romanovsky, V.E., Harden, J., and Hobbie, J.E., 2003, Carbon cycling in extratropical terrestrial ecosystems of the Northern Hemisphere during the 20th century—A modeling analysis of the influences of soil thermal dynamics: Tellus; Series B, Chemical and Physical Meteorology, v. 55B, no. 3, p. 751–776, http://dx.doi.org/10.1034/j.1600-0889.2003.00060.x.

Chapter 4. Watershed Carbon Budgets in the Southeastern Alaskan Coastal Forest Region

By David V. D'Amore,[1] Frances E. Biles,[1] S. Mark Nay,[2] and T. Scott Rupp[3]

4.1. Highlights

- The perhumid coastal temperate rainforest (PCTR) of the North Pacific coast has some of the densest terrestrial carbon stocks in the world. Net carbon balance in this region has a distinct lateral loss vector through both dissolved organic and inorganic carbon.
- Estimates of net ecosystem carbon balance averaged 142 grams of carbon per square meter per year ($gC/m^2/yr$) and ranged from 117 to 177 $gC/m^2/yr$ among three watersheds in the region, illustrating the net terrestrial carbon gain in coastal forests. These estimates are consistent with carbon gains associated with mature temperate forests worldwide and illustrate the potential for carbon sequestration across a range of landscape types in the PCTR.

4.2. Introduction

Forests worldwide provide a substantial carbon sink of approximately 1.1 ± 0.8 petagrams of carbon per year (PgC/yr) (Pan and others, 2011). The northeast Pacific coastal margin has extensive and densely forested stands across the coastal temperate rainforest biome. The perhumid subregion (PCTR) of this biome includes the coastal forests of southeast Alaska (fig. 4.1). In addition to the extensive forests in the PCTR, sparsely forested and nonforested peatlands with deep (~3–5 meter [m]) organic soils are abundant. The spatial heterogeneity of ecosystems across the PCTR and the variability in the carbon pools associated with these ecosystems creates complex conditions for estimating carbon balance. To develop carbon balance models across the diverse PCTR region, spatially explicit estimates of carbon flux are needed for scaling plot measurements across the varying terrain and ecosystem types (Schimel, 1995).

The PCTR of southeast Alaska has functioned as a carbon sink during the postglacial Holocene as this region is cold and wet and does not have a fire regime. There is little urban development in the region, and the primary sources of disturbance are small-scale wind disturbances leading to gap-phase-type forest structures, and forest harvest, which has been limited to a relatively small portion of the landscape. Mean carbon densities in the region exceed 30 kilograms of carbon per square meter (kgC/m^2) (Heath and others, 2011). About 66 percent of this carbon is belowground, where carbon densities in wetlands are as high as 50 to 90 kgC/m^2 (Leighty and others, 2006). Carbon stocks in the soils and forests of the Tongass National Forest have been estimated to contain 2.8 ± 0.5 petagrams of carbon (PgC) (Leighty and others, 2006). The consideration of the exchange of carbon in both the dense belowground stock and the aboveground biomass pool is essential to accurately estimate carbon balance. In addition, the belowground stock in the PCTR is unfrozen, and the aboveground stock is not subject to fire, making the stability of carbon stocks in the PCTR an important feature of carbon accounting for North America.

Our approach in this chapter is to compare the common carbon balance model used to calculate net ecosystem production (NEP) with the calculation of net ecosystem carbon balance (NECB; Chapin and others, 2006). In areas where major disturbances (such as fire and forest harvest) are absent, as in much of the Alaska PCTR, it has been argued that NEP can be used interchangeably with NECB (Turner and others, 2011). Unlike NECB, however, the NEP model does not account for lateral exports of dissolved carbon in the carbon balance. Dissolved carbon, both in organic and inorganic forms, constitutes a major export vector from both forested and nonforested systems in the PCTR (D'Amore and others, 2015). Using ground-based measurements, we can construct estimates of NECB to compare with NEP estimates to illustrate the importance of accounting for dissolved carbon fluxes in carbon balance models for the Alaska PCTR.

[1]U.S. Department of Agriculture Forest Service, Juneau, Alaska.

[2]U.S. Department of Agriculture Forest Service, Corvallis, Oreg.

[3]University of Alaska-Fairbanks, Fairbanks, Alaska.

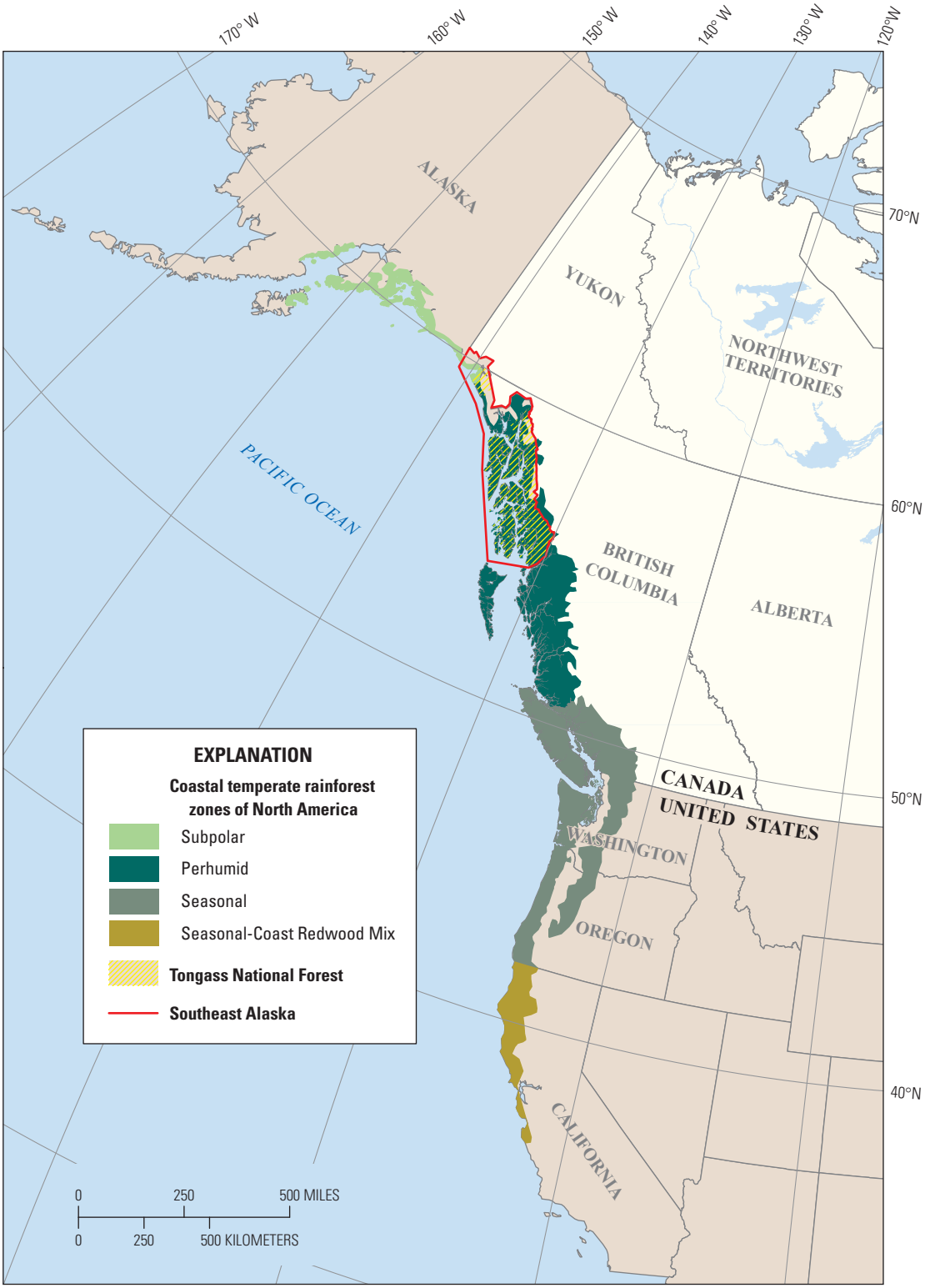

Figure 4.1. North American Pacific coastal temperate rainforest extent. The "panhandle" or southeast Alaska region is noted along with the Tongass National Forest. Adapted from Wolf and others (1995).

The varying distribution of abundant water across the Alaska PCTR creates a mosaic of ecosystem types ranging from well-drained, densely forested uplands to forested wetlands and nonforested peatlands (Neiland, 1971). To measure carbon flows and evaluate terrestrial-aquatic linkages associated with these three ecosystem types, we created a sampling scheme based on a hydropedologic framework (D'Amore and others, 2012). Measurements taken across this framework can then be generalized across the overall landscape. The field measurements can also be used to calibrate carbon budget estimates based on remote sensing or process-based models. The carbon cycle science research program in the Alaska PCTR developed by the U.S. Department of Agriculture Forest Service Pacific Northwest Research Station (PNW) has established a series of plots distributed across component landscape units in three watersheds to estimate major carbon fluxes (fig. 4.2). Data collected from these plots along with remotely sensed estimates of net primary productivity (NPP) were used to determine the NECB for the three PCTR watersheds.

This assessment is primarily a landscape analysis for use in national and regional reporting and evaluations. The process-based Dynamic Organic Soil version of the Terrestrial Ecosystem Model (DOS-TEM) was the main tool used for deriving carbon stock and flux in all regions of Alaska for the assessment. Measurements from the PNW plots were used to calibrate DOS-TEM for the coastal forests region (chapters 6 and 7). In this chapter, we present an alternate approach to estimating carbon stock and flux for coastal forests using the plot-based measurements combined with values of NPP from remote sensing.

4.3. Input Data and Methods

4.3.1. Site Descriptions

The research was conducted within three watersheds in the Alaska PCTR. The watersheds are located in Juneau, Alaska, with mean annual precipitation of 1,580 millimeters (mm) and mean annual average temperatures ranging from 2 to 9 degrees Celsius (°C). We chose watersheds in three different ecological subsections that represent three distinct landscapes characterized by different lithology and dominant forms of landscape evolution (Nowacki and others, 2001; fig. 4.2). Peterson Creek watershed is a wetland-dominated watershed (53 percent of watershed area) in the Stephens Passage Glaciomarine Terraces ecological subsection that is composed primarily of slowly permeable glaciomarine sediments (Miller, 1973) along with bedrock outcrops that occur on moderate to low slopes. Disturbance in the Peterson Creek watershed is limited to hiking trails in addition to a small area (~4 kilometers [km]) with roads and light rural-residential development near the watershed outlet. In contrast, the McGinnis Creek watershed is composed primarily of recently deglaciated areas within the Boundary Ranges Icefields ecological subsection and has low wetland coverage (less than 5 percent of watershed area). Hiking trails are the only type of anthropogenic disturbance present in the McGinnis Creek watershed. Fish Creek watershed consists of intrusive volcanic and sedimentary rocks in the Stephens Passage Volcanics ecological subsection and has a mix of physiographic features that include alpine, productive temperate rainforest, and wetlands. The Fish Creek watershed contains hiking trails, a road, and a small (~0.01 square kilometer [km^2]) rock pit, but these features cover only a minor portion of the watershed. In addition, a ski area occupies part of the upper Fish Creek watershed, but this area is not included in the final carbon budget estimates owing to the lack of soil map data for the upper watershed (see section 4.3.8).

Within each of the three watersheds we identified three sub-catchments representing discrete hydropedologic units that characterize key ecosystem processes occurring within the vegetated portion of the PCTR landscape: maritime fen, maritime wetland forest, and maritime upland forest (D'Amore and others, 2012; fig. 4.2). A hydropedologic unit (HPU) is "a grouping of variations in soil morphology that directly relate influence of water table regime, flow paths, and soil saturation to soil development" (Gannon and others, 2014). The forms of the HPUs influence soil function including biogeochemistry, runoff production, and vegetation diversity and structure, which all, in turn, affect carbon cycling.

Each HPU type (maritime fen, maritime wetland forest, and maritime upland forest) represents an experimental unit, replicated in each watershed for a total of nine sites in the experimental design (fig. 4.2). Freshwater discharge, dissolved carbon, and soil respiration measurements were collected at the nine sub-catchments at various times from 2006 through 2009.

4.3.2. Soil Respiration Rates

Soil respiration measurements were taken every 2 to 4 weeks during the spring, summer, and fall over a 4-year (yr) period from 2006 through 2009. Measurements were taken on collars constructed of 21-centimeter (cm)-inside-diameter PVC pipe that were permanently installed at the ground surface. The soil respiration collars were deployed in three seven-collar clusters arranged in a 2-m spacing pattern within each HPU for a total of 21 collars per HPU per watershed. Each HPU sampled had a total of 63 collars. Respiration data were collected within 1 to 2 days over the entire study area, for a total of 189 possible measurements at each temporal sampling. All soil respiration measurements were accompanied by a soil temperature measurement (at 10-cm depth) at each collar. Soil respiration measurements were achieved using a dynamic-closed chamber procedure without drawdown

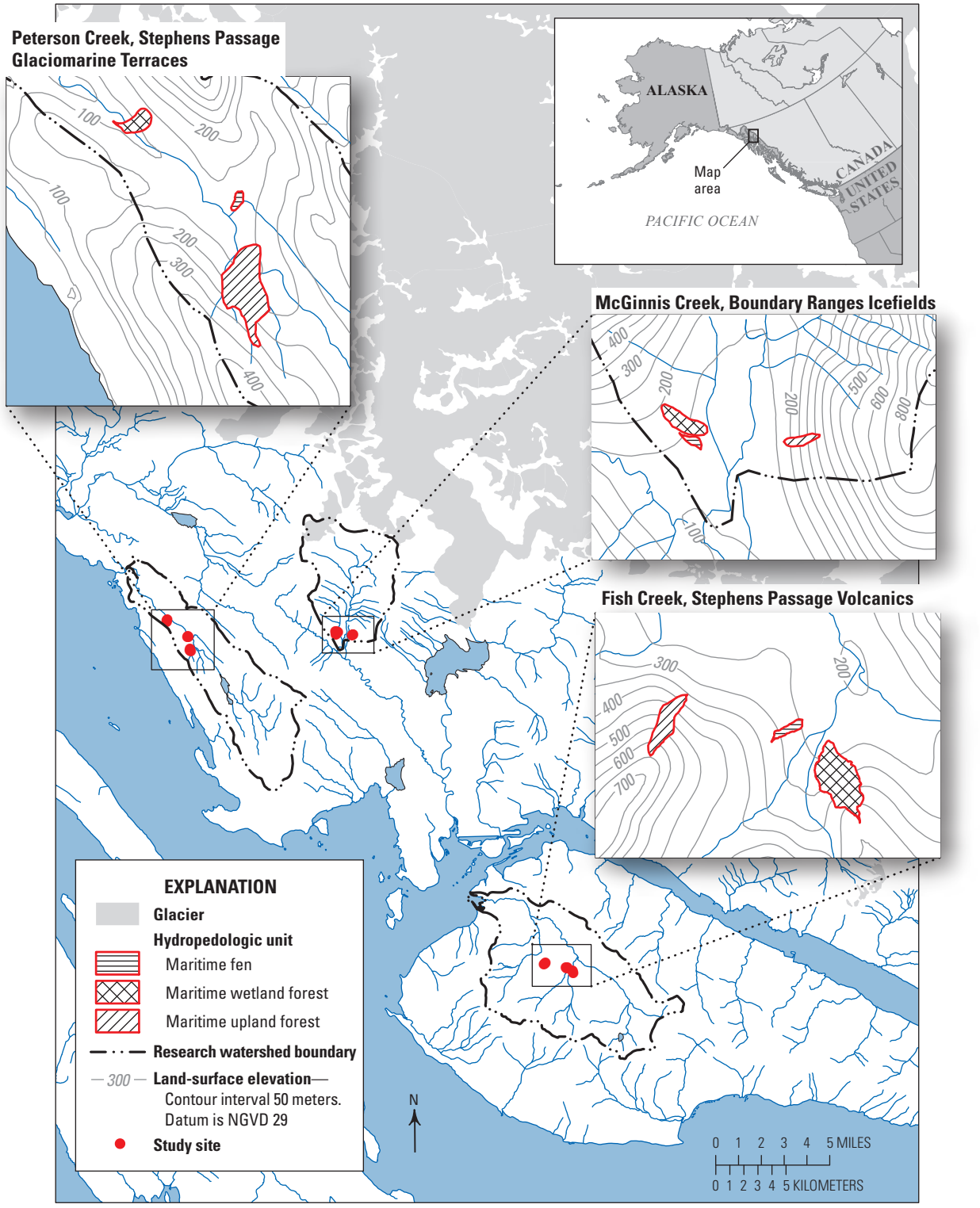

Contours generated from the USGS 2-arc-second National Elevation Dataset, 2008, from seamless.usgs.gov (replaced by The National Map)
Watershed boundaries modified from USDA-NRCS, USGS, and EPA 12-Digit Watershed Boundary Data, 2012
Water features from USDA Forest Service, Tongass National Forest, 2012
Glaciers from Randolph Glacier Inventory, version 5.0

Figure 4.2. Locations of the study sites for three component hydropedologic units (maritime fen, maritime wetland forest, and maritime upland forest) within three watersheds (Peterson Creek, McGinnis Creek, and Fish Creek) on different ecological subsections (Stephens Passage Glaciomarine Terraces, Boundary Ranges Icefields, and Stephens Passage Volcanics) near Juneau, Alaska.

(Nay and others, 1994). The collars were designed to receive a portable closed-chamber field respirometer that used a LiCor 820 infrared gas analyzer (LiCor Inc., Lincoln, Nebr.). We measured soil respiration on coarse woody debris in contact with the soil. Decomposition of aboveground (or aerial) coarse woody debris (that is, snags and elevated logs) was not accounted for, but we make the assumption that this component is small owing to the age of the forest system (Janisch and others, 2005).

Annual fluxes were estimated by combining temperature-dependent models with soil temperature measurements (D'Amore, 2011). Soil respiration measurements were not made during winter; however, owing to the low soil temperatures and snow cover during that period, we believe that the total unaccounted for carbon dioxide (CO_2) flux is small based on our observations of CO_2 flux and soil temperature. We partitioned autotrophic and heterotrophic respiration differently between the maritime wetland forest and maritime upland forest HPUs. Wetland units were estimated to have 40-percent heterotrophic contribution based on peatland measurements in boreal Alaska (McConnell and others, 2013). The maritime upland forests were estimated to have 60-percent contribution from heterotrophic respiration based on measurements in forested systems in British Columbia (Lalonde and Prescott, 2007). The contribution of root respiration to total soil respiration across both maritime wetland forest and maritime fen, and maritime upland forest systems was similar to a 50-percent partitioning based on the overall mean reported in a review of the contribution of root respiration to soil respiration (Hanson and others, 2000). Local measurements indicate that values for root respiration range from 40 to 70 percent (David D'Amore, U.S. Department of Agriculture Forest Service, unpub. data, September 30, 2014).

4.3.3. Dissolved Organic Carbon Export

Stream water dissolved organic carbon (DOC) flux was calculated from continuous discharge measurements combined with intermittent stream water samples of DOC concentration (D'Amore and others, 2015). Concentration-discharge relationships and estimation of DOC flux were calculated using the U.S. Geological Survey Load Estimator program, LOADEST (Runkel and others, 2004). Estimates of annual flux were calculated by interpolation from the concentration-discharge relationship to account for days when stream water DOC concentrations were not measured.

4.3.4. Estimate of Particulate Organic Carbon

Particulate organic carbon (POC) was not measured in the study. We estimated POC for each HPU from our measured DOC values based on the proportion of POC:DOC from similar regions (Hope and others, 1994).

4.3.5. Estimate of Dissolved Inorganic Carbon

Dissolved inorganic carbon (DIC) estimates were derived from stream water concentrations measured in outlet streams from each HPU. DIC fluxes were derived from the relationship between stream water DIC concentration and flux in similar systems (Worrall and others, 2005). A relationship between annual stream water DIC concentration and annual DIC flux was constructed from published values of bicarbonate (HCO_3^-) and partial pressure of CO_2 (pCO_2) in stream water (Worrall and others, 2005). The total annual export of DIC was estimated based on measured stream water HCO_3^- and pCO_2 values from the HPU streams.

4.3.6. Estimate of Net Primary Productivity

Net primary productivity (NPP) estimates at a 1-km resolution were obtained from the Moderate Resolution Imaging Spectroradiometer (MODIS) satellite MOD17 project (Zhao and others, 2005; ftp://ftp.ntsg.umt.edu/pub/MODIS/NTSG_Products/MOD17/GeoTIFF/MOD17A3/GeoTIFF_30arcsec/). Refer to the MOD17 User's Guide (Heinsch and others, 2003) for a detailed description of the MOD17 algorithm. Raster datasets of total annual NPP were downloaded for 2006 through 2009, overlapping the time period of our field sampling. Using ArcGIS software (Esri, 2012), we created a single output raster containing the average annual total NPP for the 2006–2009 period across the three study watersheds using the following general formula:

$$\text{Integer}(\text{Mean}(\text{2006 Total NPP, 2007 Total NPP, 2008 Total NPP, 2009 Total NPP}) + 0.5) \quad (4.1)$$

Average annual NPP data were missing for 2.5 percent (2.91 km^2) of the McGinnis Creek watershed (fig. 4.3, white pixels). These areas are composed of a mix of bare rock, snow, alpine vegetation, alder-covered slopes, and high-elevation forest. NPP values for these "no data" cells were estimated by taking the average NPP of surrounding pixels having similar land cover.

We concluded that these remote sensing values were a reasonable estimation of the average total NPP based on comparisons with similar coniferous forests in the Pacific Northwest. However, the estimated NPP values for maritime fen were extremely high compared to published values for similar fen ecosystem NPP estimates based on ground surveys (Asada and Warner, 2005; Wania and others, 2009). We attributed this to the inclusion of forested areas mixed within the maritime fens in the 1-km MODIS pixels. In order to avoid a greatly biased estimate of maritime fen productivity, we used a fixed input value of 177 grams of carbon per square meter per year ($gC/m^2/yr$) calculated from the average reported NPP for peatlands in two studies (Asada and Warner, 2005; Wania and others, 2009).

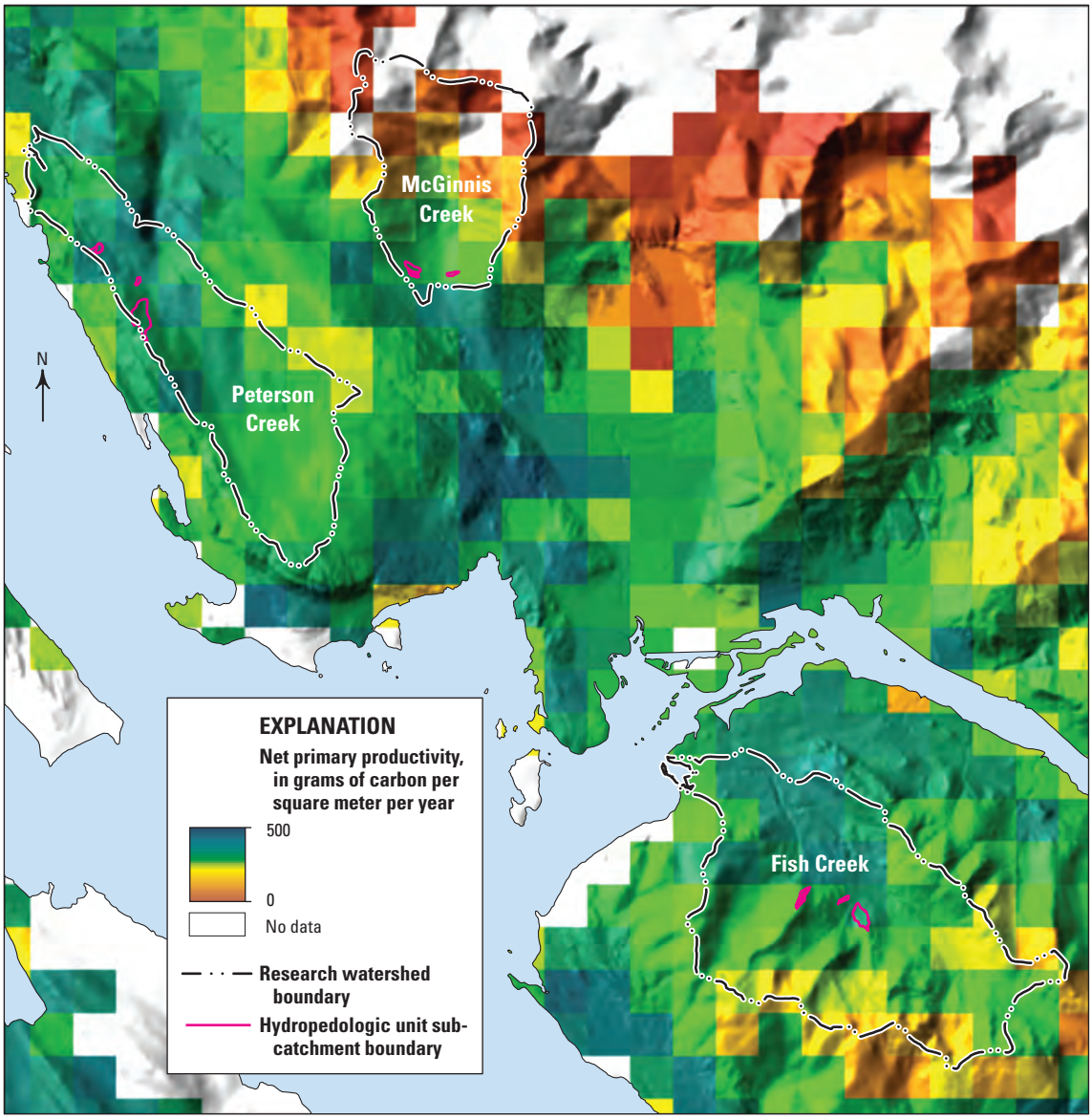

Figure 4.3. Distribution of 2006–2009 average total net primary productivity across the three research watersheds and hydropedologic sub-catchments in southeast Alaska. Net primary productivity data from the Moderate Resolution Imaging Spectroradiometer (MODIS) satellite MOD17 project (Zhao and others, 2005). See figure 4.2 for location.

4.3.7. Carbon Budget Model

We used both the NEP (equation 4.2) and NECB (equation 4.3) accounting methods to determine the carbon flux from HPU sub-catchments and the larger watersheds. The NECB method includes the exchange of CO_2 from the atmosphere to the terrestrial ecosystem, losses owing to lateral transfers of dissolved carbon, and losses from major ecosystem disturbances such as fire and forest harvest. NEP and NECB are similar in that heterotrophic respiration is subtracted from NPP estimates in both cases; however, NECB accounts for the additional loss of carbon (exports) from the ecosystem. In this study, the only additional export of carbon in the watersheds was the lateral export of DOC, POC, and DIC as there was no forest harvest removal or other large disturbances occurring in the study area.

$$NEP = NPP - HR \quad (4.2)$$

$$NECB = NEP - DOC - POC - DIC \quad (4.3)$$

where

NEP is net ecosystem productivity,
NECB is net ecosystem carbon balance,
NPP is net primary productivity,
HR is heterotrophic soil respiration,
DOC is dissolved organic carbon,
POC is particulate organic carbon, and
DIC is dissolved inorganic carbon.

Fluxes of methane (CH_4), carbon monoxide (CO), and volatile organic compounds (VOCs) are also considered in the calculation of the NECB (Chapin and others, 2006); however, we did not have adequate site-specific measurements to include these additional components into the overall NECB budget. In the Alaska PCTR, annual fluxes of CH_4, CO_2, and VOCs and their overall effect on NECB are assumed to be small (chapter 7; Zhuang and others, 2007; U.S. Environmental Protection Agency, 2014). So although we are likely over-estimating the NECB by excluding CH_4, CO_2, and VOC fluxes from the budget, we do not believe that omitting these three elements will appreciably change our results or conclusions.

4.3.8. Alaska Assessment Vegetation Components

NECB and NEP were calculated for each watershed using two methods of spatial assignment for carbon flux. The first approach defined HPUs according to mapped soil drainage classes (DCs). The soil DC was created as a weighted average of the soil map unit (SMU) component DCs in the Tongass National Forest soil geographic information system (GIS) dataset (U.S. Department of Agriculture Forest Service, unpub. data, 2014). The soil DC categories and associated values are as follows: very poorly drained (1), poorly drained (2), somewhat poorly drained (3), moderately well drained (4), and well drained (5). The DCs were divided into three bins that corresponded to the drainage characteristics of the HPUs:

Drainage Class (DC)	Hydropedologic Unit (HPU)
$0 < DC < 1.5$	Maritime fen
$1.5 \leq DC < 3.5$	Maritime wetland forest
≥ 3.5	Maritime upland forest

SMUs classified as alpine soils, which existed in both the Fish Creek and McGinnis Creek watersheds, did not follow the assignment rules in the above table. Alpine SMUs had average DC values ranging from 2.63 to 4.45, which would have placed alpine areas into the wetland or upland forest HPUs, leading to inflated estimates of alpine productivity. Instead, alpine SMUs were assigned to the lower productivity maritime fen HPU. NECB and NEP flux densities were then calculated for each HPU in the three experimental watersheds using remotely sensed inputs (NPP) and field measurement outputs (DIC, DOC, HR, POC). Next, annual NECB and NEP fluxes were computed by extrapolating the HPU flux density estimates across each HPU's total area (fig. 4.4).

The second approach used the vegetation map developed for this assessment to delineate HPUs (fig. 4.5). This vegetation map is a 1-km-resolution map derived from several input variables as described in chapters 1 and 2. Maritime fen, maritime wetland forest, and maritime upland forest already exist as vegetation classes in the vegetation map; therefore, these classes were used to represent the HPUs. The subsequent calculation of NECB and NEP flux density and total flux followed the same method as above for soil DCs. We excluded the portion of the Fish Creek watershed where SMU mapping was absent from the vegetation map carbon balance calculations.

The two approaches for defining HPUs (SMU DCs versus vegetation map classes) enabled us to compare NECB results from the more finely resolved HPU map derived from the SMU DCs with the NECB results based on aggregating HPUs by the more generalized vegetation map. SMU data were not available for nearly half of the Fish Creek watershed (fig. 4.4). Therefore, in order to compare carbon balance estimates between the SMU-DC-based and vegetation-map-based HPUs, we limited the area over which the carbon balance was calculated in the Fish Creek watershed to only the portion where SMUs were present. In the McGinnis Creek watershed, the vegetation map identified a large portion of the area as rock and ice, which decreased the area of the watershed that contained any carbon. This altered the comparison of the total carbon in the watershed calculated from the vegetation map HPU versus the SMU-DC HPU.

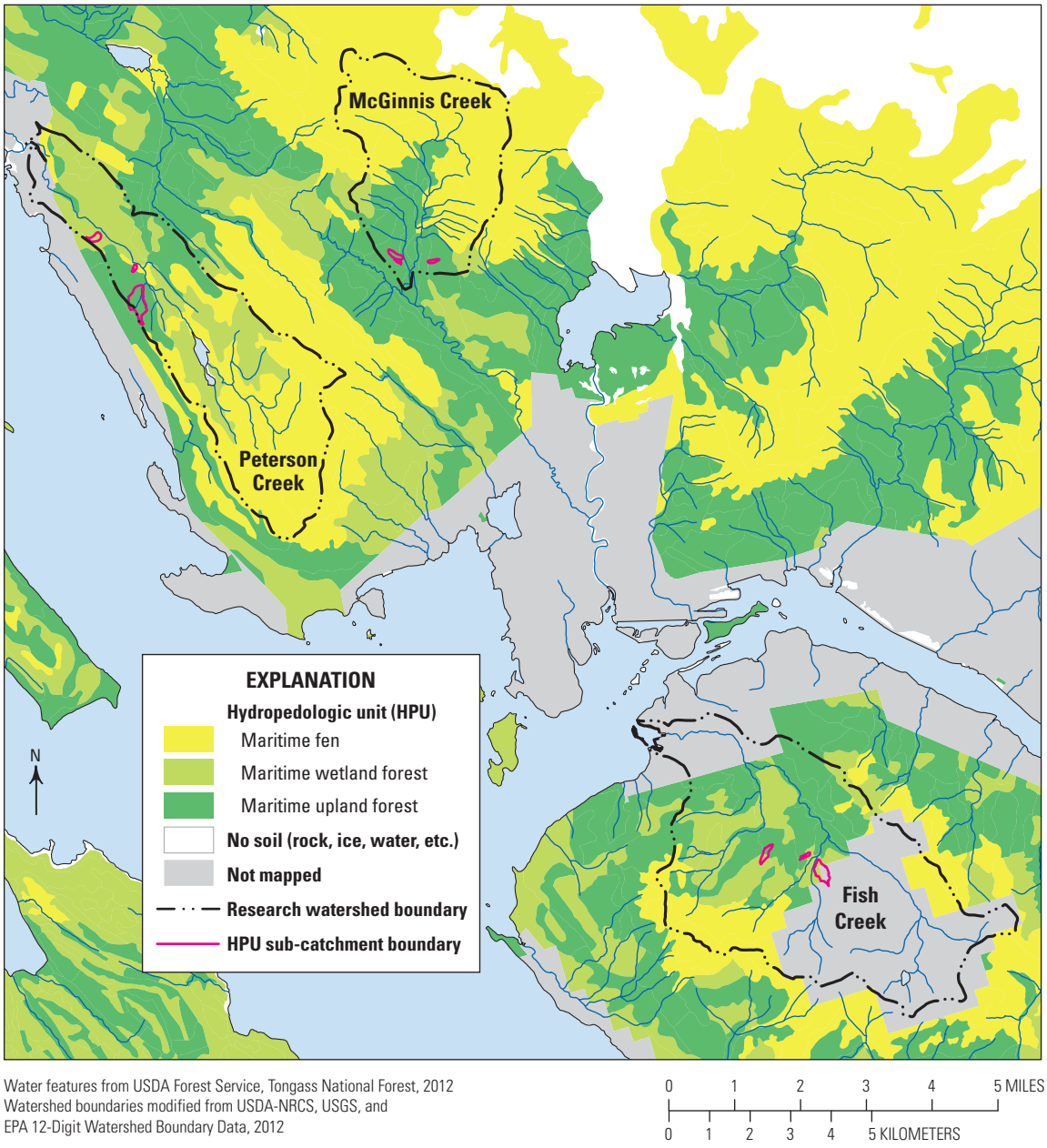

Figure 4.4. Distribution of hydropedologic units derived from soil map unit drainage classes. See figure 4.2 for location.

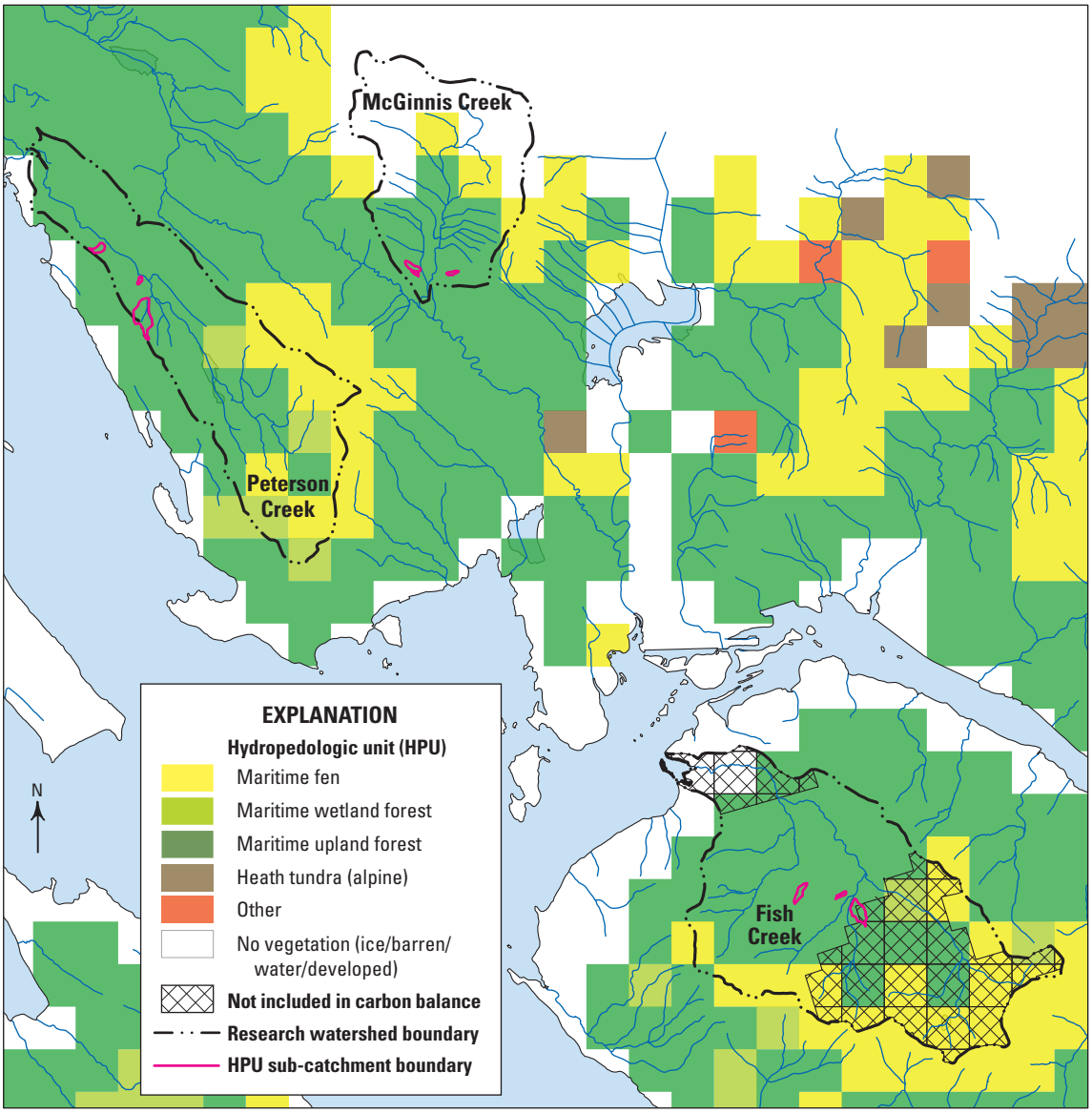

Figure 4.5. Distribution of hydropedologic units derived from the vegetation map developed for this assessment. See figure 4.2 for location.

4.3.9. Geographic Information System Analysis

We used ArcGIS to combine the average annual total NPP raster for 2006–2009 with the SMU, vegetation map, and watershed boundary datasets. Before the datasets were combined, the NPP raster was projected to Alaska Albers (North American Datum of 1983) using nearest neighbor resampling and snapped to the vegetation map raster. The Alaska Albers projection was used for all GIS data. Both the NPP and vegetation map rasters were converted to vector polygon datasets and combined with the SMU and watershed boundary polygons. The combined dataset was exported to a spreadsheet for the carbon balance accounting.

4.4. Results

4.4.1. Watershed Net Ecosystem Carbon Budgets

Each of the watersheds had a net gain in carbon stock calculated from both the NEP and NECB carbon balance models (table 4.1). The calculation method had a notable effect on the amount calculated for each watershed overall. The NEP values were 18 percent, 32 percent, and 51 percent higher than the NECB values in the Peterson Creek, McGinnis Creek, and Fish Creek watersheds, respectively. The lowest unit-area carbon accretion values were in the youngest landscape of the postglacial McGinnis Creek watershed. The highest values were calculated in Peterson Creek, whereas Fish Creek values were intermediate between the other two watersheds.

Net carbon balance tended to increase with stand age, until it appeared to reach a plateau at 200 years (fig. 4.6). Owing to the limited number of data points used in the assessment, it was not possible to make definitive statements regarding these trends, but the overall carbon balance was consistent with the expected phases of stand development in southeast Alaskan coniferous forests. The increase was greatest during the period of stem exclusion (~100–200 yr). The plateau in net balance occurred in the range of understory re-initiation (~200–400 yr). There was an outlier in the trend from the Fish Creek maritime upland forest where the net carbon balance calculated as NECB was much lower than the general trend in the rest of the data. The discrepancy in this value was due to the high rate of DIC loss in this HPU. The remaining carbon loss values were similar to the other HPUs.

4.4.2. Comparison of Carbon Budgets from Drainage Class Versus Vegetation Map Hydropedologic Units

All watersheds had a net gain in carbon calculated by either the finer resolution DC HPUs or the less highly resolved vegetation-map-based HPUs. The area-weighted average NECB calculated for the three watersheds using the DC HPUs was 148 gC/m^2/yr, with an NEP of 194 gC/m^2/yr (table 4.1), very similar to the average vegetation map NECB of 142 gC/m^2/yr, with a NEP of 193 gC/m^2/yr (table 4.2). The watershed totals for NEP and NECB were also of roughly similar magnitude in both models. Therefore, the details regarding the implications of the magnitude of the carbon balance and patterns among landscape units and watersheds are discussed relative to values in table 4.1.

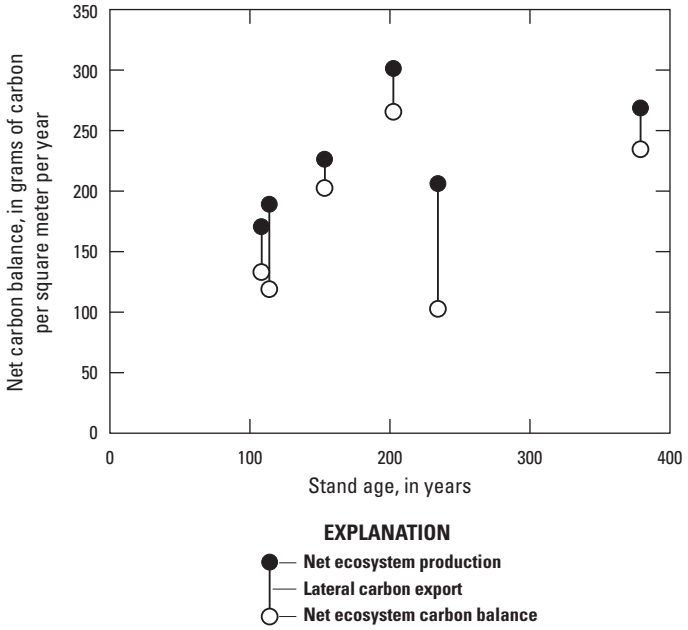

Figure 4.6. Average stand age compared to net carbon balance as both net ecosystem production (NEP) and net ecosystem carbon balance (NECB). The difference in these two values is the amount of lateral carbon export added to the NEP to calculate NECB.

4.4.3. Relationship of Carbon Budget Estimates to Measures of Net Primary Productivity and Net Ecosystem Production in Other Systems

Examining the relationship of NPP with NEP and NECB provides a means for evaluating our carbon budget estimates (Pregitzer and Euskirchen, 2004). The modeled ratios of NPP:NEP and NPP:NECB were consistent with the regression model for these measures in ecosystems worldwide (fig. 4.7). In addition, the model estimates ranged along the mean ratio of NPP to NEP and NECB along a similar slope as the world biome model. The shift in the relationship of NPP to NEP and NECB was evident in each comparison among the models. The reduction in NEP using NECB was consistent across the watershed partitioning.

A major influence on the relationships illustrated in figure 4.7 was the value for NPP calculated for each SMU-DC HPU and vegetation map HPU. The NPP estimates varied among the HPUs coincident with the range of ecosystem types located within the watershed (tables 4.1, 4.2). In table 4.1, the highest mean NPP was in the Fish Creek watershed with 305 gC/m^2/yr, closely followed by the Peterson Creek watershed with

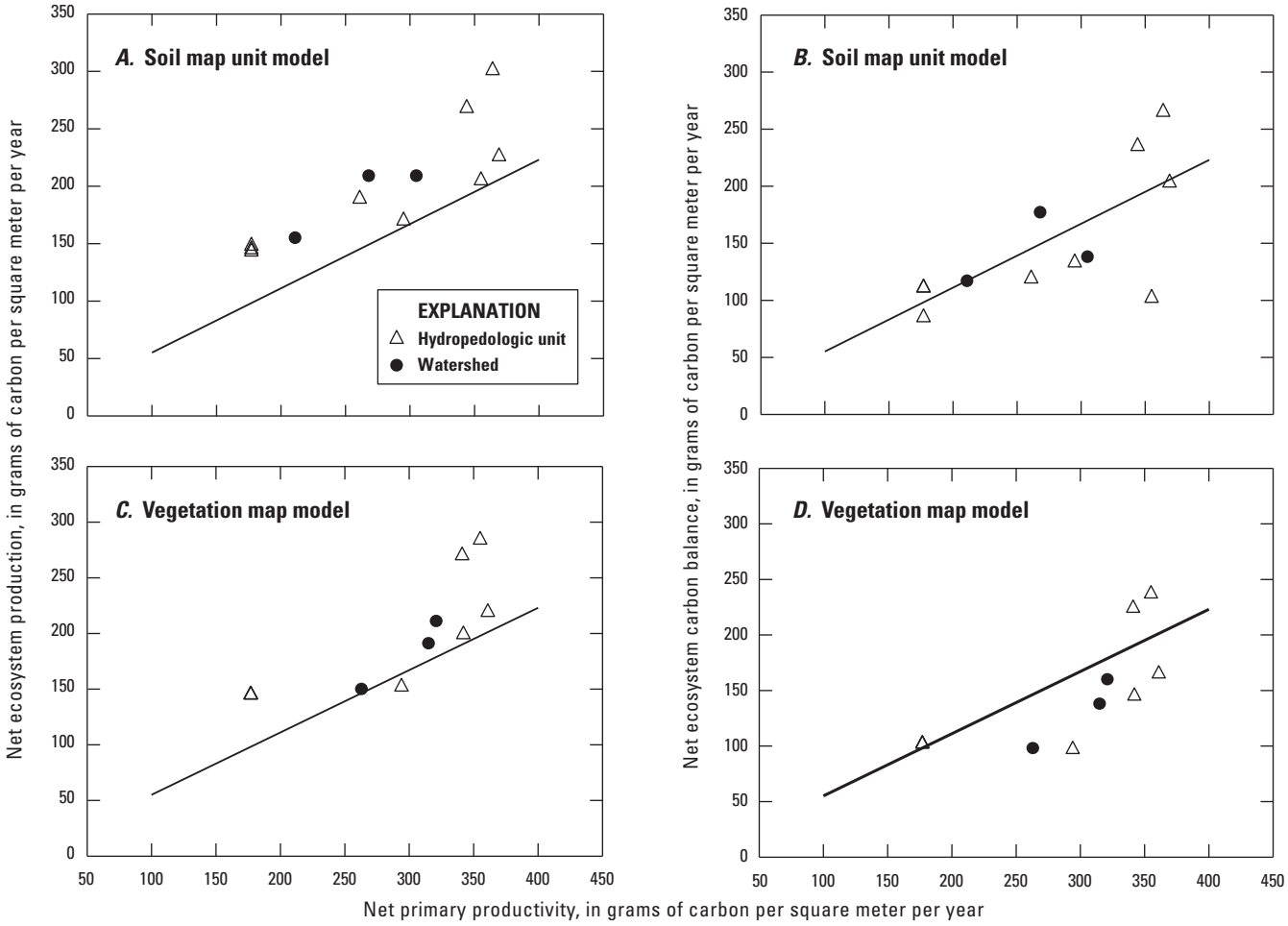

Figure 4.7. Comparison of ratios of net primary productivity (NPP) to both net ecosystem production (NEP) and net ecosystem carbon balance (NECB) calculated in each hydropedologic unit and watershed in both the finer scale SMU drainage class model and the coarser vegetation map model. The regression line is derived from values for worldwide forests (Pregitzer and Euskirchen, 2004) and used as a comparison to the values calculated in the present study. The graphs are for *A*, soil map unit drainage class NPP:NEP; *B*, soil map unit drainage class NPP:NECB; *C*, vegetation map NPP:NEP; and *D*, vegetation map NPP:NECB.

268 gC/m^2/yr. These estimates were influenced primarily by the amount of mature forest in the watersheds. The Peterson Creek watershed is completely located on uplifted marine sediment, which has promoted the development of wetland (maritime fen and maritime wetland forest) plant communities. The lowest mean watershed NPP was in the McGinnis Creek watershed with 211 gC/m^2/yr. This value was likely due to extensive areas with early successional alpine vegetation, bare rock, and ice. The mean values for all watersheds were below 400 gC/m^2/yr, which is at the low range of values for similar forests of the Pacific Northwest where NPP values are often greater than 500 gC/m^2/yr (Hudiburg and others, 2009).

4.4.4. Soil Carbon Export Pathways

Heterotrophic respiration was the largest export pathway among the various export components of the NECB (equation 4.3) and accounted for 57 percent, 60 percent, and 65 percent of the carbon export in the Fish Creek, McGinnis Creek, and Peterson Creek watersheds, respectively. Estimated heterotrophic respiration rates were 56 gC/m^2/yr, 59 gC/m^2/yr, and 96 gC/m^2/yr in the McGinnis Creek, Peterson Creek, and Fish Creek watersheds, respectively (table 4.1).

The export of DOC from the Peterson Creek, McGinnis Creek, and Fish Creek watersheds was 19 gC/m^2/yr, 20 gC/m^2/yr,

Table 4.1. Carbon balance, inputs, and outputs in three watersheds in the Alaskan coastal forest region modeled from hydropedologic units defined by soil map unit drainage classes.

[Flux: NPP, net primary productivity from remote sensing (MODIS); Rs, soil respiration; HR, heterotrophic respiration based on proportional estimate of autotrophic to heterotrophic respiration; DOC, stream water dissolved organic carbon; DIC, stream water dissolved inorganic carbon; POC, estimated particulate organic carbon; NEP, calculated net ecosystem production from NPP and HR; NECB, calculated net ecosystem carbon balance from NPP, HR, DOC, DIC, and POC. Units: yr, year; km^2, square kilometer; $gC/m^2/yr$; gram of carbon per square meter per year; MgC/yr, megagram of carbon per year; n.d., no data]

Watershed (ecological subsection)	Hydropedologic unit	Stand age (yr)	Area (km^2)	Flux density ($gC/m^2/yr$)								Annual flux (MgC/yr)	
				NPP	Rs	HR	DOC	DIC	POC	NEP	NECB	NEP	NECB
Peterson Creek (Stephens Passage Glaciomarine Terraces)	Maritime fen	n.d.	12.24	177	85	34	20	7	5	143	111	1,751	1,361
	Maritime wetland forest	203	8.17	364	159	63	21	10	5	301	265	2,458	2,167
	Maritime upland forest	154	3.33	369	238	143	9	12	2	226	203	753	675
	Watershed	**n.d.**	**23.74**	**268**	**132**	**59**	**19**	**8**	**5**	**209**	**177**	**4,962**	**4,203**
McGinnis Creek (Boundary Ranges Icefields)	Maritime fen	n.d.	11.81	177	72	29	24	7	6	148	111	1,751	1,309
	Maritime wetland forest	114	.60	261	181	72	50	7	13	189	119	113	71
	Maritime upland forest	109	4.49	295	208	125	6	29	2	170	133	763	599
	Watershed	**n.d.**	**16.90**	**211**	**112**	**56**	**20**	**13**	**5**	**155**	**117**	**2,627**	**1,979**
Fish Creek (Stephens Passage Volcanics)	Maritime fen	n.d.	4.91	177	79	32	30	23	8	145	85	714	419
	Maritime wetland forest	379	5.72	344	189	75	19	9	5	268	235	1,536	1,343
	Maritime upland forest	234	8.24	355	249	150	17	82	4	205	102	1,692	842
	Watershed	**n.d.**	**18.87**	**305**	**187**	**96**	**21**	**45**	**5**	**209**	**138**	**3,942**	**2,604**
Study area		**n.d.**	**59.51**	**264**	**144**	**70**	**20**	**21**	**5**	**194**	**148**	**11,531**	**8,786**

Table 4.2. Carbon balance, inputs, and outputs in three watersheds in the Alaskan coastal forest region modeled from hydropedologic units defined by vegetation map classes.

[Flux: NPP, net primary productivity from remote sensing (MODIS); Rs, soil respiration; HR, heterotrophic respiration based on proportional estimate of autotrophic to heterotrophic respiration; DOC, stream water dissolved organic carbon; DIC, stream water dissolved inorganic carbon; POC, estimated particulate organic carbon; NEP, calculated net ecosystem production from NPP and HR; NECB, calculated net ecosystem carbon balance from NPP, HR, DOC, DIC, and POC. Units: yr, year; km^2, square kilometer; $gC/m^2/yr$, gram of carbon per square meter per year; MgC/yr, megagram of carbon per year; n.d., no data]

Watershed (ecological subsection)	Hydropedologic unit	Stand age (yr)	Area (km^2)	Flux density ($gC/m^2/yr$)								Annual flux (MgC/yr)	
				NPP	Rs	HR	DOC	DIC	POC	NEP	NECB	NEP	NECB
Peterson Creek (Stephens Passage Glaciomarine Terraces)	Maritime fen	n.d.	5.01	177	79	32	25	12	6	145	102	729	513
	Maritime wetland forest	203	3.25	341	179	72	30	9	8	270	224	878	728
	Maritime upland forest	154	16.42	361	237	142	11	41	3	219	165	3,600	2,705
	Watershed	**n.d.**	**24.68**	**321**	**197**	**110**	**16**	**31**	**4**	**211**	**160**	**5,206**	**3,945**
McGinnis Creek (Boundary Ranges Icefields)	Maritime fen	n.d.	2.36	177	79	32	25	12	6	145	102	344	241
	Maritime wetland forest	n.d.	0	NA	NA	NA	NA	NA	NA	NA	NA	NA	NA
	Maritime upland forest	109	6.58	294	237	142	11	41	3	152	97	998	639
	Watershed	**n.d.**	**8.94**	**263**	**195**	**113**	**14**	**34**	**4**	**150**	**98**	**1,341**	**880**
Fish Creek (Stephens Passage Volcanics)	Maritime fen	n.d.	3.00	177	79	32	25	12	6	145	102	436	306
	Maritime wetland forest	379	.02	355	179	72	30	9	8	284	237	6	5
	Maritime upland forest	234	15.85	342	237	142	11	41	3	199	145	3,159	2,296
	Watershed	**n.d.**	**18.87**	**315**	**212**	**125**	**13**	**37**	**3**	**191**	**138**	**3,601**	**2,607**
Study area		**n.d.**	**52.49**	**309**	**202**	**116**	**15**	**33**	**4**	**193**	**142**	**10,148**	**7,433**

and 21 gC/m^2/yr (table 4.1). The DOC estimates were much more closely aligned than heterotrophic respiration export among the watersheds. The export of DOC accounted for 12 percent, 20 percent, and 21 percent of the total carbon export from the Fish Creek, Peterson Creek, and McGinnis Creek watersheds, respectively.

The export of DIC from the Peterson Creek, McGinnis Creek, and Fish Creek watersheds was 8 gC/m^2/yr, 13 gC/m^2/yr, and 45 gC/m^2/yr (table 4.1). This disparity was driven by high values in the maritime upland forest at Fish Creek. The high calculation of DIC flux from the maritime upland forest had considerable leverage on the total carbon balance for the Fish Creek watershed.

The export of POC from each of the watersheds was 5 gC/m^2/yr (table 4.1). These values vary with the amount of DOC owing to the construction of the model for the prediction of POC driven by DOC. These estimates of POC export accounted for about 4 percent of the total carbon export in the McGinnis Creek, Fish Creek, and Peterson Creek watersheds. The export of POC was the smallest of all the soluble carbon components.

4.5. Discussion

4.5.1. Watershed Carbon Budgets

The visual evidence of abundant woody debris and deep organic soils was consistent with the hypothesis that the PCTR forest and maritime fen ecosystems have been a net sink for carbon during the Holocene. The actual size of the sink was uncertain given the variability in NPP and exported amounts. The modeled carbon budgets indicate that all three study watersheds were net sinks during the period of observation (2006–2009), which agrees with the finding that the North American continent was a sink for carbon during the 2000–2010 decade (King and others, 2015). Our results are also consistent with other studies that have estimated northern high-latitude forests as carbon sinks (Houghton, 2003). For example, mature forest stands (80–200 yr) in the Pacific Northwest had estimated carbon sinks of 286 gC/m^2/yr, whereas older forests (>200 yr) had rates of 165 gC/m^2/yr (Turner and others, 2000). Given that these estimates did not account for lateral carbon losses in the budget, the calculated carbon values using our modeling approach seem to be reasonable carbon budget approximations for the observed watersheds.

In addition to the net carbon balance estimates, the calculated ratio of NPP to NECB in the PCTR was very similar to the average ratio compared to other forested ecosystems (fig. 4.7). The overall watershed estimates and the components (hydropedologic units) within the watershed matrix are in good agreement with the trend. In particular, the maritime fen and maritime wetland forest communities are well represented among the units and contribute considerably to the carbon balance among the watersheds. The relationship illustrated by the model fit in figure 4.7 indicates that the trajectory of NECB is positive, or a net sink for carbon, in the PCTR ecosystem.

Average annual temperature decreased (–0.056 °C per decade; National Oceanic and Atmospheric Administration, National Centers for Environmental Information, 2015) and precipitation increased over the 1981–2010 normal period for Juneau, and average annual temperatures during the 2006–2009 study period were –0.445 to –1.06 °C cooler than the 1981–2010 average (5.56 °C; National Oceanic and Atmospheric Administration, National Centers for Environmental Information, 2015); however, the Alaska PCTR is predicted to warm by 4 to 6 °C by the end of the century and precipitation is predicted to increase (Melillo and others, 2014). Changes in temperature and precipitation lead to variability in the carbon balance by influencing a host of interconnected processes, such as respiration, photosynthesis, and the occurrence of natural disturbance events (Reichstein and others, 2013). For example, average annual soil respiration increased with average annual temperature (National Oceanic and Atmospheric Administration, National Centers for Environmental Information, 2015) at our three study watersheds, suggesting that warmer temperatures in the Alaska PCTR may lead to increases in HR, the largest soil carbon export pathway. Increased HR with increased temperature has been reported in other studies, but the resulting effect on NPP and NECB also depended on other factors, such as the amount and timing of precipitation and presence or absence of disturbance (Arnone and others, 2008; Hirata and others, 2014). Previous carbon balance modeling in Alaska has focused on the arctic and northern interior regions. Models including the Alaska PCTR are difficult to validate because of the lack of data (chapter 7). How climate variability will influence the carbon balance in the Alaska PCTR is highly uncertain. There is a clear need for more field experiments to fill the existing data gap in Alaska's highly productive coastal forests.

4.5.2. Landscape Variability and Carbon Balance

The watersheds in the study have varying geologic and geomorphic histories that influence the carbon balance through both the uptake of atmospheric carbon and the loss of carbon via the multiple export pathways. The variability in the low and high net balance estimates can be explained by the relative postglacial development of the watersheds. The hydropedologic units used in the landscape partitioning reflect the dominant underlying influence on carbon cycling in the watersheds.

The watersheds provide surrogates for many PCTR watershed types, including early seral/postglacial, windthrow-derived forests, and mature or late seral forest communities. The estimates in the two older watersheds reflect the underlying geomorphic history but are also driven by stand age and vegetation type. Peterson Creek has evidence of a large, regional windthrow event, which has been associated with stands originating in the decade beginning around 1880 (Harris, 1989; Nowacki and Kramer, 1998). The average stand age in Peterson Creek is consistent with this period of disturbance in the maritime upland forest. The maritime wetland forest is somewhat older, but still in the mature stand

development phase. The average age of the Fish Creek stands is older, and the aspect of the watershed protects it from the prevailing storm winds from the southeast and southwest.

4.5.3. Potential Application of the Vegetation Map for Regional Carbon Modeling

Our approach using two types of landscape stratification reveals the potential for variability when estimating a carbon balance over smaller areas (such as, subwatershed-scale). It is reasonable to expect discrepancies in carbon balance estimates between the two stratification methods owing to the different resolution and origin of the input data (SMU polygons versus the 1-km vegetation map pixels). However, the consistency across larger areas in the final study results indicates that the alternative scaling approach models are comparable. The consistent array of the carbon balance estimates among varying landscape units and watersheds along with similar regression relationships for NPP:NEP and NPP:NECB (fig. 4.7) illustrate that these carbon balance estimates can be reliably extrapolated to the broader region.

4.5.4. Evaluation of Regional Net Primary Productivity Estimates

The NPP estimate from MOD17 has several challenges that make accurate estimates problematic in the coastal temperate rainforest. One of the more significant obstacles to accurate measurements is the common occurrence of cloud cover, which contaminates some of the satellite source data used for deriving NPP. Cloud-contaminated input data are estimated in the MOD17 product by linear interpolation between the previous and next cloud-free periods (Heinsch and others, 2003). In the three experimental watersheds, the percentage of days during the growing season that NPP values were estimated because of cloud cover ranged from 63 to 93 percent (average 76 percent). The coarse resolution of the MOD17 input climate and vegetation datasets and the biophysical assumptions used in the MOD17 algorithm also contribute to uncertainties in the NPP values (Heinsch and others, 2006).

Studies evaluating the accuracy and utility of MODIS NPP estimates at various scales are limited owing to a lack of empirical validation data and the difficulty of comparing plot-level measurements to a 1-km MODIS grid cell (Turner and others, 2006), and no such assessments have been made for the Alaska coastal forest region. MODIS appears to capture the general variability in the magnitude of NPP in comparison to local data, but has also been shown to overestimate NPP at low-productivity sites and underestimate NPP at high-productivity sites in North America (Turner and others, 2006) and to overestimate NPP in some forests in the northeastern United States (Tang and others, 2010). Nevertheless, at the regional scale MODIS NPP can be useful for broad estimates, and regional estimates can also be improved by incorporating ancillary datasets (Heinsch and others, 2006; Pan and others, 2006). Despite the limitations inherent in the MOD17 product, our estimates of NECB, even at the watershed scale, compared favorably with other reported values in the literature. This general agreement with other findings provides us some assurance that the MODIS data will be useful for providing NPP values for NECB accounting across the expanse of the PCTR. Future work on NEP estimates in the region should include other potential sources of data for NPP, such as other remote sensing products or plot-based estimates.

4.5.5. Net Ecosystem Carbon Balance as a Land Management Tool for the Perhumid Coastal Temperate Rainforest

The carbon-dense region of the PCTR has become a focus for carbon cycling research owing to the large accumulations of carbon in old-growth forests and the potential for accumulating carbon in young-growth forests. Mature forests can continue to sequester carbon (Harmon and others, 1990), and Luyssaert and others (2008) have proposed that old forests retain their sink strength longer than previously thought. Carbon sequestration in this region may provide a long-term reservoir and continuing sink in Alaska and is therefore a key piece of the carbon budget for Alaska and North America. Clearly it is important to use the NECB model for PCTR watersheds, as it illustrates the importance of accounting for lateral carbon losses. It is notable that heterotrophic respiration accounted for only 57 to 65 percent of the carbon export from the watersheds. This is in contrast to most temperate ecosystems where heterotrophic respiration typically accounts for 70 to 90 percent of the carbon export. More accurate regional carbon balance models will need to consider the lateral loss of carbon. Forest inventory measurements do not account for soil carbon or the overall balance in forested ecosystems. This may lead to disparate estimates and conclusions regarding the total carbon balance.

4.6. Conclusions

Watershed NECB estimates for the period of observation (2006–2009) indicate that the Alaska PCTR is a net carbon sink and that carbon is accreting at rates consistent with values for mature (100–300 yr) conifer forests in the Pacific Northwest. Stratifying the landscape into hydropedologic units for the purpose of estimating carbon balance inputs and outputs representative of the dominant landscape processes in a region provides a means to estimate watershed carbon balance and address terrestrial ecosystem heterogeneity. The approach of extrapolating the hydropedologic unit estimates across larger areas can provide preliminary estimates of ecosystem carbon balance, and continued field measurements can improve the accuracy of the predictions within each unit and across varying site conditions.

4.7. References Cited

Arnone, J.A., III, Verburg, P.S.J., Johnson, D.W., Larsen, J.D., Jasoni, R.L., Lucchesi, A.J., Batts, C.M., von Nagy, Christopher, Coulombe, W.G., Schorran, D.E., Buck, P.E., Braswell, B.H., Coleman, J.S., Sherry, R.A., Wallace, L.L., Luo, Yiqi, and Schimel, D.S., 2008, Prolonged suppression of ecosystem carbon dioxide uptake after an anomalously warm year: Nature, v. 455, no. 7211, p. 383–386, http://dx.doi.org/10.1038/nature07296.

Asada, Taro, and Warner, B.G., 2005, Surface peat mass and carbon balance in a hypermaritime peatland: Soil Science Society of America Journal, v. 69, no. 2, p. 549–562, http://dx.doi.org/10.2136/sssaj2005.0549.

Chapin, F.S., III, Woodwell, G.M., Randerson, J.T., Rastetter, E.B., Lovett, G.M., Baldocchi, D.D., Clark, D.A., Harmon, M.E., Schimel, D.S., Valentini, R., Wirth, C., Aber, J.D., Cole, J.J., Goulden, M.L., Harden, J.W., Heimann, M., Howarth, R.W., Matson, P.A., McGuire, A.D., Melillo, J.M., Mooney, H.A., Neff, J.C., Houghton, R.A., Pace, M.L., Ryan, M.G., Running, S.W., Sala, O.E., Schlesinger, W.H., and Schulze, E.-D., 2006, Reconciling carbon-cycle concepts, terminology, and methods: Ecosystems, v. 9, no. 7, p. 1041–1050, http://dx.doi.org/10.1007/s10021-005-0105-7.

D'Amore, D.V., 2011, Hydrologic controls on carbon cycling in Alaskan coastal temperate rainforest soils: Fairbanks, Alaska, University of Alaska-Fairbanks, Ph.D. dissertation, 150 p.

D'Amore, D.V., Edwards, R.T., Herendeen, P.A., Hood, Eran, and Fellman, J.B., 2015, Dissolved organic carbon fluxes from hydropedologic units in Alaskan coastal temperate rainforest watersheds: Soil Science Society of America Journal, v. 79, no. 2, p. 378–388, http://dx.doi.org/10.2136/sssaj2014.09.0380.

D'Amore, D.V., Fellman, J.B., Edwards, R.T., Hood, Eran, and Ping, C.-L., 2012, Hydropedology of the North American coastal temperate rainforest, *in* Lin, Henry, ed., Hydropedology; Synergystic integration of soil science and hydrology: Waltham, Mass., Academic Press, p. 351–380.

Esri, 2012, ArcGIS [software] for desktop, (ver. 10.1): Redlands, Calif., Esri, http://www.esri.com/software/arcgis/arcgis-for-desktop.

Gannon, J.P., Bailey, S.W., and McGuire, K.J., 2014, Organizing groundwater regimes and response thresholds by soils; A framework for understanding runoff generation in a headwater catchment: Water Resources Research, v. 50, no. 11, p. 8403–8419, http://dx.doi.org/10.1002/2014WR015498.

Hanson, P.J., Edwards, N.T., Garten, C.T., and Andrews, J.A., 2000, Separating root and soil microbial contributions to soil respiration; A review of methods and observations: Biogeochemistry, v. 48, no. 1, p. 115–146, http://dx.doi.org/10.1023/A:1006244819642.

Harmon, M.E., Ferrell, W.K., and Franklin, J.F., 1990, Effects on carbon storage of conversion of old-growth to young forests: Science, v. 247, no. 4943, p. 699–702, http://dx.doi.org/10.1126/science.247.4943.699.

Harris, A.S., 1989, Wind in the forests of southeast Alaska and guides for reducing damage: U.S. Department of Agriculture, Forest Service, Pacific Northwest Research Station, General Technical Report PNW–GTR–244, 63 p.

Heath, L.S., Smith, J.E., Woodall, C.W., Azuma, D.L., and Waddell, K.L., 2011, Carbon stocks on forestland of the United States, with emphasis on USDA Forest Service ownership: Ecosphere, v. 2, no. 1, article 6, 21 p., http://dx.doi.org/10.1890/ES10-00126.1.

Heinsch, F.A., Reeves, Matt, Votava, Petr, Kang, Sinkyu, Milesi, Cristina, Zhao, Maosheng, Glassy, Joseph, Jolly, W.M., Loehman, Rachel, Bowker, C.F., Kimball, J.S., Nemani, R.R., and Running, S.W., 2003, User's guide, GPP and NPP (MOD17A2/A3) products, NASA MODIS land algorithm (ver. 2.0): Missoula, Mont., University of Montana, Numerical Terradynamic Simulation Group, accessed June 8, 2012, at http://www.ntsg.umt.edu/sites/ntsg.umt.edu/files/modis/MOD17 UsersGuide.pdf.

Heinsch, F.A., Zhao, Maosheng, Running, S.W., Kimball, J.S., Nemani, R.R., Davis, K.J., Bolstad, P.V., Cook, B.D., Desai, A.R., Ricciuto, D.M., Law, B.E., Oechel, W.C., Kwon, Hyojung, Luo, Hongyan, Wofsy, S.C., Dunn, A.L., Munger, J.W., Baldocchi, D.D., Xu, Liukang, Hollinger, D.Y., Richardson, A.D., Stoy, P.C., Siqueira, M.B.S., Monson, R.K., Burns, S.P., and Flanagan, L.B., 2006, Evaluation of remote sensing based terrestrial productivity from MODIS using tower eddy flux network observations: IEEE Transactions on Geoscience and Remote Sensing, v. 44, no. 7, p. 1908–1925, http://dx.doi.org/10.1109/TGRS.2005.853936.

Hirata, R., Takagi, K., Ito, A., Hirano, T., and Saigusa, N., 2014, The impact of climate variation and disturbances on the carbon balance of forests in Hokkaido, Japan: Biogeosciences, v. 11, no. 18, p. 5139–5154, http://dx.doi.org/10.5194/bg-11-5139-2014.

Hope, D., Billett, M.F., and Cresser, M.S., 1994, A review of the export of carbon in river water; Fluxes and processes: Environmental Pollution, v. 84, no. 3, p. 301–324, http://dx.doi.org/10.1016/0269-7491(94)90142-2.

Houghton, R.A., 2003, Why are estimates of the terrestrial carbon balance so different?: Global Change Biology, v. 9, no. 4, p. 500–509, http://dx.doi.org/10.1046/j.1365-2486.2003.00620.x.

Hudiburg, Tara, Law, Beverly, Turner, D.P., Campbell, John, Donato, Dan, and Duane, Maureen, 2009, Carbon dynamics of Oregon and Northern California forests and potential land-based carbon storage: Ecological Applications, v. 19, no. 1, p. 163–180, http://dx.doi.org/10.1890/07-2006.1.

Janisch, J.E., Harmon, M.E., Chen Hua, Fasth, Becky, and Sexton, Jay, 2005, Decomposition of coarse woody debris originating by clearcutting of an old-growth forest: Ecoscience, v. 12, no. 2, p. 151–160, http://dx.doi.org/10.2980/i1195-6860-12-2-151.1.

King, A.W., Andres, R.J., Davis, K.J., Hafer, M., Hayes, D.J., Huntzinger, D.N., de Jong, B., Kurz, W.A., McGuire, A.D., Vargas, R., Wei, Y., West, T.O., and Woodall, C.W., 2015, North America's net terrestrial CO_2 exchange with the atmosphere 1990–2009: Biogeosciences, v. 12, no. 2, p. 399–414, http://dx.doi.org/10.5194/bg-12-399-2015.

Lalonde, R.G., and Prescott, C.E., 2007, Partitioning heterotrophic and rhizospheric soil respiration in a mature Douglas-fir (*Pseudotsuga menziesii)* forest: Canadian Journal of Forest Research, v. 37, no. 8, p. 1287–1297, http://dx.doi.org/10.1139/X07-019.

Leighty, W.W., Hamburg, S.P., and Caouette, John, 2006, Effects of management on carbon sequestration in forest biomass in southeast Alaska: Ecosystems, v. 9, no. 7, p. 1051–1065, http://dx.doi.org/10.1007/s10021-005-0028-3.

Luyssaert, Sebastiaan, Schulze, E.-D., Börner, Annett, Knohl, Alexander, Hessenmöller, Dominik, Law, B.E., Ciais, Philippe, and Grace, John, 2008, Old-growth forests as global carbon sinks: Nature, v. 455, no. 7210, p. 213–215, http://dx.doi.org/10.1038/nature07276.

McConnell, N.A., Turetsky, M.R., McGuire, A.D., Kane, E.S., Waldrop, M.P., and Harden, J.W., 2013, Controls on ecosystem and root respiration across a permafrost and wetland gradient in interior Alaska: Environmental Research Letters, v. 8, no. 4, letter 045029, 11 p., http://dx.doi.org/10.1088/1748-9326/8/4/045029.

Melillo, J.M., Richmond, T.C., and Yohe, G.W., eds., 2014, Climate change impacts in the United States; The third National Climate Assessment: U.S. Global Change Research Program, 841 p., http://dx.doi.org/10.7930/J0Z31WJ2.

Miller, R.D., 1973, Gastineau Channel Formation, a composite glaciomarine deposit near Juneau, Alaska: U.S. Geological Survey Bulletin 1394–C, 20 p. [Also available at https://pubs.er.usgs.gov/publication/b1394C.]

National Oceanic and Atmospheric Administration, National Centers for Environmental Information, 2015, Climate at a glance—Time series [average annual temperature, 1981– 2010, for Juneau, Alaska]: National Oceanic and Atmospheric Administration, National Centers for Environmental Information, accessed October 8, 2015, at http://www.ncdc.noaa.gov/cag.

Nay, S.M., Mattson, K.G., and Bormann, B.T., 1994, Biases of chamber methods for measuring soil CO_2 efflux demonstrated with a laboratory apparatus: Ecology, v. 75, no. 8, p. 2460–2463, http://dx.doi.org/10.2307/1940900.

Neiland, B.J., 1971, The forest-bog complex in southeast Alaska: Vegetatio, v. 22, no. 1–3, p. 1–64, http://dx.doi.org/10.1007/BF01955719.

Nowacki, G., Krosse, P., Fisher, G., Brew D., Brock, T., Shephard, M., Pawuk, W., Baichtal, J., and Kissinger, E., 2001, Ecological subsections of southeast Alaska and neighboring areas of Canada: U.S. Department of Agriculture, Forest Service, Alaska Region, Technical Publication R10–TP–75.

Nowacki, G.J., and Kramer, M.G., 1998, The effects of wind disturbance on temperate rain forest structure and dynamics of southeast Alaska: U.S. Department of Agriculture, Forest Service, Pacific Northwest Research Station, General Technical Report PNW–GTR–421, 25 p.

Pan, Yude, Birdsey, R.A., Fang, Jingyun, Houghton, Richard, Kauppi, P.E., Kurz, W.A., Phillips, O.L., Shvidenko, Anatoly, Lewis, S.L., Canadell, J.G., Ciais, Philippe, Jackson, R.B., Pacala, S.W., McGuire, A.D., Piao, Shilong, Rautiainen, Aopo, Sitch, Stephen, and Hayes, Daniel, 2011, A large and persistent carbon sink in the world's forests: Science, v. 333, no. 6045, p. 988–993, http://dx.doi.org/10.1126/science.1201609.

Pan, Yude, Birdsey, Richard, Hom, John, McCullough, Kevin, and Clark, Kenneth, 2006, Improved estimates of net primary productivity from MODIS satellite data at regional and local scales: Ecological Applications, v. 16, no. 1, p. 125–132, http://dx.doi.org/10.1890/05-0247.

Pregitzer, K.S., and Euskirchen, E.S., 2004, Carbon cycling and storage in world forests; Biome patterns related to forest age: Global Change Biology, v. 10, no. 12, p. 2052–2077, http://dx.doi.org/10.1111/j.1365-2486.2004.00866.x.

Reichstein, Markus, Bahn, Michael, Ciais, Philippe, Frank, Dorothea, Mahecha, M.D., Seneviratne, S.I., Zscheischler, Jakob, Beer, Christian, Buchmann, Nina, Frank, D.C., Papale, Dario, Rammig, Anja, Smith, Pete, Thonicke, Kirsten, van der Velde, Marijn, Vicca, Sara, Walz, Ariane, and Wattenbach, Martin, 2013, Climate extremes and the carbon cycle: Nature, v. 500, no. 7462, p. 287–295, http://dx.doi.org/10.1038/nature12350.

Runkel, R.L., Crawford, C.G., and Cohn, T.A., 2004, Load estimator (LOADEST); A FORTRAN program for estimating constituent loads in streams and rivers: U.S. Geological Survey Techniques and Methods Book 4, Chapter A5, 69 p.

Schimel, D.S., 1995, Terrestrial ecosystems and the carbon cycle: Global Change Biology, v. 1, no. 1, p. 77–91, http://dx.doi.org/10.1111/j.1365-2486.1995.tb00008.x.

Tang, Guoping, Beckage, Brian, Smith, Benjamin, and Miller, P.A., 2010, Estimating potential forest NPP, biomass and their climatic sensitivity in New England using a dynamic ecosystem model: Ecosphere, v. 1, no. 6, article 18, 20 p., http://dx.doi.org/10.1890/ES10-00087.1.

Turner, D.P., Cohen, W.B., and Kennedy, R.E., 2000, Alternative spatial resolutions and estimation of carbon flux over a managed landscape in western Oregon: Landscape Ecology, v. 15, no. 5, p. 441–452, http://dx.doi.org/10.1023/A:1008116300063.

Turner, D.P., Ritts, W.D., Cohen, W.B., Gower, S.T., Running, S.W., Zhao, Maosheng, Costa, M.H., Kirschbaum, A.A., Ham, J.M., Saleska, S.R., and Ahl, D.E., 2006, Evaluation of MODIS NPP and GPP products across multiple biomes: Remote Sensing of Environment, v. 102, nos. 3–4, p. 282–292, http://dx.doi.org/10.1016/j.rse.2006.02.017.

Turner, D.P., Ritts, W.D., Yang, Zhiqiang, Kennedy, R.E., Cohen, W.B., Duane, M.V., Thornton, P.E., and Law, B.E., 2011, Decadal trends in net ecosystem production and net ecosystem carbon balance for a regional socioecological system: Forest Ecology and Management, v. 262, no. 7, p. 1318–1325, http://dx.doi.org/10.1016/j.foreco.2011.06.034.

U.S. Environmental Protection Agency, 2014, Profile of the 2011 National Air Emissions Inventory (ver. 1.0): U.S. Environmental Protection Agency, Office of Air Quality Planning & Standards, Emissions Inventory & Analysis Group, accessed October 13, 2015, at http://www.epa.gov/sites/production/files/2015-08/documents/lite_finalversion_ver10.pdf.

Wania, R., Ross, I., and Prentice, I.C., 2009, Integrating peatlands and permafrost into a dynamic global vegetation model; 2. Evaluation and sensitivity of vegetation and carbon cycle processes: Global Biogeochemical Cycles, v. 23, no. 3, article GB3015, 15 p., http://dx.doi.org/10.1029/2008GB003413.

Wolf, E.C., Mitchell, A.P., and Schoonmaker, P.K., 1995, The rain forests of home—An atlas of people and place: Portland, Oregon, Ecotrust, Pacific GIS, and Conservation International, 24 p.

Worrall, Fred, Swank, W.T., and Burt, Tim, 2005, Fluxes of inorganic carbon from two forested catchments in the Appalachian Mountains: Hydrological Processes, v. 19, no. 15, p. 3021–3035, http://dx.doi.org/10.1002/hyp.5814.

Zhao, Maosheng, Heinsch, F.A., Nemani, R.R., and Running, S.W., 2005, Improvements of the MODIS terrestrial gross and net primary production global data set: Remote Sensing of Environment, v. 95, no. 2, p. 164–176, http://dx.doi.org/10.1016/j.rse.2004.12.011.

Zhuang, Q., Melillo, J.M., McGuire, A.D., Kicklighter, D.W., Prinn, R.G., Steudler, P.A., Felzer, B.S., and Hu, S., 2007, Net emissions of CH_4 and CO_2 in Alaska; Implications for the region's greenhouse gas budget: Ecological Applications, v. 17, no. 1, p. 203–212, http://dx.doi.org/10.1890/1051-0761(2007)017[0203:NEOCAC]2.0.CO;2.

Chapter 5. Forest Inventory-Based Analysis and Projections of Forest Carbon Stocks and Changes in Alaskan Coastal Forests

By Xiaoping Zhou[1], Svetlana A. Schroder[2], A. David McGuire[3], and Zhiliang Zhu[4]

5.1. Highlights

- Baseline (average of 2004–2013) estimates derived from U.S. Department of Agriculture Forest Service forest inventory show that forests in south-central and southeast coastal Alaska contain 1,018 teragrams of carbon (TgC) in both live and dead tree biomass. Over 80 percent of the forest carbon in coastal Alaska is in the Chugach and Tongass National Forests.
- Projected to 2099 using a forest simulation model, forest carbon stock would increase by 1 percent, 8 percent, and 27 percent under the scenarios of current forest management (including harvesting) with current climate, climate change with forest management, and climate change without forest management, respectively. To conduct the simulations of climate change, the A1B scenario from the Intergovernmental Panel on Climate Change's Special Report on Emissions Scenarios was used to drive the version 3.1-T47 of the Canadian Centre for Climate Modelling and Analysis' Coupled Global Climate Model general circulation model.
- Managed with present forest harvest and present climate, the forest carbon would increase by 10 TgC by the end of the century compared with the baseline (2004–2013). Forest carbon stock would increase by 86 TgC under the climate change with harvesting scenario and by 276 TgC under the climate change without harvesting scenario.

5.2. Introduction

Alaska represents over 15 percent of the total U.S. land area and over 15 percent of U.S. forest land (Oswalt and others, 2014). Coastal Alaska includes two inventory regions by the U.S. Forest Service: southeast Alaska, and south-central Alaska and Kodiak Island (fig. 5.1, Barrett and Christensen, 2011). The two regions are part of the North Pacific Landscape Conservation Cooperative (LCC), except for Kodiak Island, which is in the Western Alaska LCC. Coastal Alaska contains two main forest types: boreal forest and temperate maritime forest. In this region of Alaska, approximately 88 percent of the forest land is publicly owned. The substantial amounts of forest land in reserved status and of old-growth forests make coastal Alaska forests different from those in the other coastal regions. The forests in coastal Alaska store about 1,018 teragrams of carbon (TgC). Smith and others (2013) estimated the average total live tree carbon (aboveground and belowground) to be approximately 12.5 kilograms of carbon per square meter (kgC/m^2) in coastal Alaska compared with an average of 6.9 kgC/m^2 for all U.S. forest land. In addition, they estimated the average carbon stored in dead trees (standing dead and down dead wood) to be 2.8 kgC/m^2 in coastal Alaska compared with 1.1 kgC/m^2 on all U.S. forest land.

The analysis presented in this chapter supports the ecosystem carbon assessment (Zhu and others, 2010) in Alaska, as required by the Energy Independence and Security Act of 2007 (EISA). It uses detailed field-plot data measured by the U.S. Department of Agriculture (USDA) Forest Service

[1]U.S. Department of Agriculture Forest Service, Portland, Oreg.

[2]University of Washington, Seattle, Wash.

[3]U.S. Geological Survey, Fairbanks, Alaska.

[4]U.S. Geological Survey, Reston, Va.

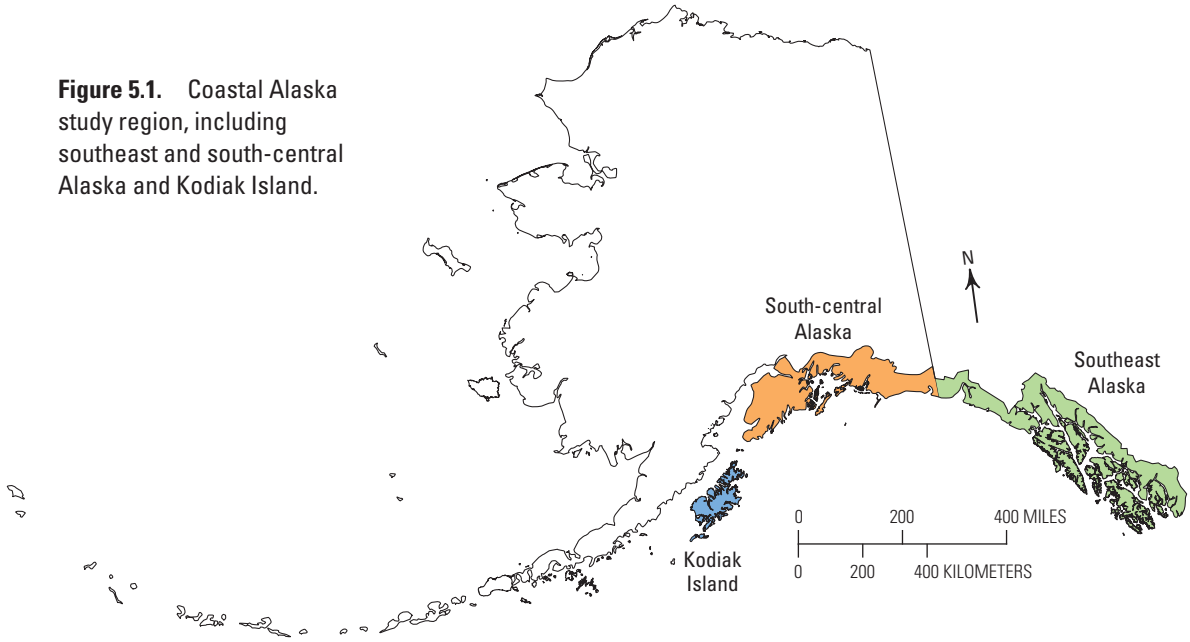

Figure 5.1. Coastal Alaska study region, including southeast and south-central Alaska and Kodiak Island.

as baseline to project the future forest ecosystem carbon under different management activities and climate change assumptions. Such a study will assess the forest carbon from different angles for this heavily forested region. The major objectives of this study are to estimate how much carbon is stored in the coastal forests of Alaska by forest carbon pools except the soil organic carbon, and to assess the responses of carbon storage in this region to potential management activities and climate change.

5.3. Data and Methods

There are over 62,000 square kilometers (km^2) of forest land in coastal Alaska, of which about 89 percent is publicly owned. The USDA Forest Service, Forest Inventory and Analysis (FIA) Program provides information needed to assess the condition of America's forests. FIA collects tree-level field data and provides the public forest inventory data in a standard accessible format for those interested in further analysis. The inventories were conducted on a periodic basis before 1999. With the passage of the 1998 Farm Bill, FIA was required to collect data annually on plots within each State (O'Connell and others, 2014). The USDA Forest Service regional research stations are responsible for measuring the plots and publishing summary reports for each of the States. Note that FIA plots are measured on a moving panel system and it takes about 5 years to measure all the plots in the eastern States and 10 years in the western States.

FIA ground plots are designed to cover a 1-acre (0.00405-km^2) sample area. The recent annual inventories use a national standard, fixed-radius plot layout for sample tree selection and measurement (O'Connell and others, 2014). The variables reported in the FIA database are very detailed, including plot variables, condition variables, and tree-level variables. The plot variables provide information relevant to the entire 1-acre field plot, such as plot location; the condition variables provide information on landscape attributes that define the condition, such as the reserved status, owner group, forest type, and others; and the tree-level variables provide information for each tree 1 inch (2.54 centimeters) in diameter and larger found on the plot, including tree species, diameter at breast height, and height (Barrett and Christensen, 2011). The Pacific Northwest Research Station (PNW) is responsible for collecting and compiling the forest inventory of Alaska, California, Oregon, and Washington. The first full 10-year cycle of annual inventory for coastal Alaska, which was completed by PNW–FIA in 2013 (2004–2013), was used in this study for analyzing current forest conditions and as a baseline for making future projections.

A total of 2,163 plots were used in this study (table 5.1). The current carbon pools were analyzed using tree-level data from the Alaska coastal forest inventory database (Barrett and Christensen, 2011) and were reported by land ownership, forest type, and stand age group.

The USDA Forest Service Forest Vegetation Simulator (FVS) is a widely used modeling tool for predicting forest stand dynamics in U.S. forests (Dixon, 2002). It has been used to summarize current stand conditions, predict future stand conditions under various management alternatives, and update inventory statistics. Basic modules for growth, mortality, regeneration, and volume are built into each variant of the FVS, whereas other linkable extensions are available for modeling specific changes, such as fire and fuels, insects and

Table 5.1. Number of plots and trees by inventory year as measured by the U.S. Department of Agriculture Forest Service Forest Inventory and Analysis Program in the study region.

Inventory year	Number of plots	Number of trees
2004	214	7,055
2005	270	9,754
2006	214	7,795
2007	217	7,234
2008	211	8,126
2009	203	7,295
2010	224	8,385
2011	202	6,984
2012	207	7,340
2013	201	6,989
Total	**2,163**	**76,957**

diseases, and climate-induced effects. In this study, tree-level FIA data were used as inputs into the FVS to produce vegetation projections and corresponding carbon volumes. Because the forest inventory data were collected in different years, the plots collected before 2012 were grown to that point using the FVS model. The FVS simulates vegetation in cycle-by-cycle lists, where a cycle is a period of time for which increments of tree characteristics are predicted.

FVS variants account for the local peculiarities of vegetation and fuel types in different forests throughout the United States. For this study, we used the current Alaska variant of the FVS (Keyser, 2008), which includes models designed specifically for the southeast Alaska coastal forest types found in the study region.

The height and diameter growth rates were adjusted using a previously published validation procedure (Robinson and others, 2005; Leites and others, 2009). To accomplish this, we compiled the FIA data and ran a simulation. The results of the simulation run were compared with the forest inventory data, and we adjusted the growth rates to minimize model-data discrepancies. The comparison showed that the FVS overestimated diameter and height growth, which is consistent with the results reported by Peterson and others (2014). The subsequent growth-rate adjustment reduced the bias in diameter growth to 4.7 percent and height growth to 3 percent.

The carbon modeling simulation was run using the FVS Alaska variant with two modifications. First, we did not use the built-in regeneration model. Instead, we simulated natural regeneration based on the basal area in each plot by species. Using this algorithm, we were able to include regrowth more evenly compared with adding it every 50 years as the built-in regeneration model simulates. Second, we adjusted mortality in the model by using data on historical mortality rates (Haynes, 2003) and updating decay classes to match the classes for different species in Alaska (Keyser, 2008). Decomposition rates were not modified from those in the Alaska variant of the FVS.

For each of the scenarios we ran 25 simulations for each ecological region to assess uncertainty. We ran the model in a stochastic mode and seeded a random number into each simulation run by using the "RANNSEED" keyword in the FVS. This procedure was conducted to achieve random effects via distribution of the errors associated with prediction of the logarithm of basal area increments (Dixon, 2002). In the Alaska variant of the FVS, the inclusion of random effects alters the equations for calculating diameter and crown ratio and thus provides a basis for quantifying uncertainty. There is a random component in the estimate of the height growth as well (Keyser, 2008). For each simulation the output tables (that is, the carbon pools and tree lists) were summarized in 5-year intervals and exported to a separate database for further analysis. The data were then processed and analyzed to describe future projections for different scenarios.

5.4. Management and Climate Scenarios

Three scenarios were developed and analyzed in this assessment: (1) current management with no climate change, (2) climate change with management, and (3) climate change with no management. These scenarios are described below.

The major forest activity associated with management in the study region is forest harvest. Currently, the forest plans for both the Tongass (2008 forest plan) and Chugach (2002 forest plan) National Forests are being revised and amended (visit http://www.fs.usda.gov/tongass/ and http://www.fs.usda.gov/chugach/ for more information and updates). The planned amendment for the Tongass National Forest would make changes to young-growth management, as well as changes to make renewable energy development more permissive. However, no concrete projections of future harvesting rates have yet been made. Therefore, for this study, the most recent 5-year average of harvest volume available was applied to the whole projection for the management scenario (Alexander, 2012; Zhou, 2013) (fig. 5.2). The management scenario also assumed that the harvest would only take place on timberlands (that is, non-reserved, accessible areas with productivity of at least 1.4 cubic meters per hectare per year where merchantable volume is at least 175 cubic meters per hectare). The model also assumes harvesting would not take place on slopes greater than 35 percent owing to the logistical challenges and higher costs associated with working in these areas. Wildfire was evaluated for the coastal region based on the fire incident data from the Alaska Interagency Coordination Center (AICC), but was not modeled because of its low occurrence rate. The effects of insects and disease were modeled using the average mortality rate from the FIA historical database.

For the climate change simulations used in this study, we chose to use one of the climate scenarios from the Intergovernmental Panel on Climate Change's (IPCC's) Special Report on Emissions Scenarios (Nakićenović and Swart, 2000). Version 3.1-T47 of the Canadian Centre for Climate Modelling and Analysis' Coupled Global Climate Model (CGCM3.1; Flato, 2005) general circulation model data for IPCC scenario A1B was coupled with the FVS to simulate climate change effects on forest carbon. It is important to note that the climate extension (Climate-FVS) is not readily available for the Alaska variant, but we were able to obtain a custom version of this extension from the USDA Forest Service's Forest Management Service Center (Crookston, 2014). The FVS simulations were performed using the climate data and species viability scores for that climate; species viability scores were used to adjust the growth of different species in each plot given changed climate conditions. The species viability scores used in this study were calculated by West Virginia University's Forest Resources Management, School of Natural Resources.

The FVS output allows tracking of changes in various carbon pools. It was used to calculate total carbon storage for the study area by weighting each plot with the area it represents in the FIA sample using the statistical analysis software (SAS Institute Inc., 2008).

Forest carbon pools analyzed in this study include live tree biomass (aboveground and belowground), understory vegetation, dead wood (standing dead and down dead wood), forest floor (litter carbon), and soil organic carbon (SOC). The definition of each pool is listed in table 5.2 (Smith and others, 2013; O'Connell and others, 2014). The SOC pool, which is available from FIA data, was not included in projected results because the FVS does not simulate the SOC in the carbon module.

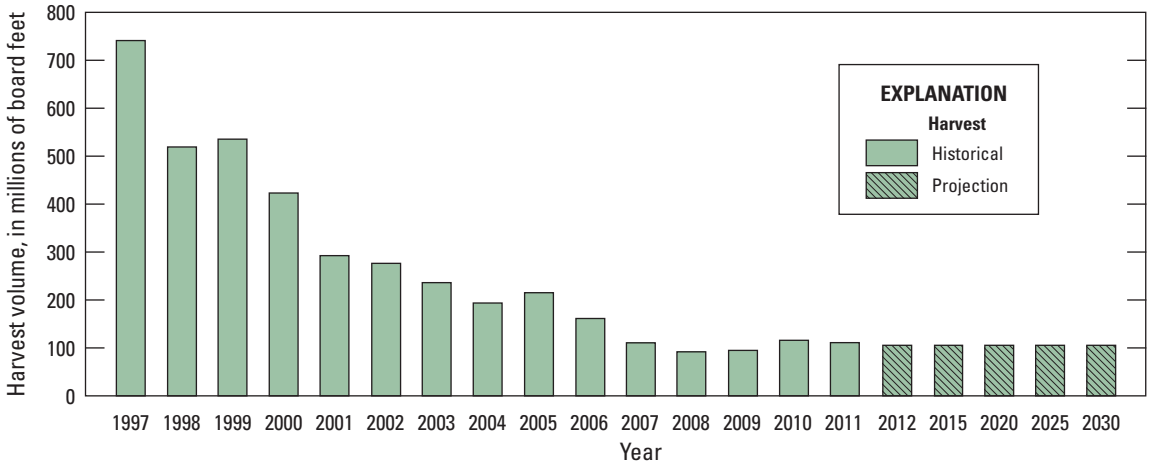

Figure 5.2. Coastal Alaska historical annual harvest and projected harvest.

Table 5.2. Forest carbon pools analyzed in this study.

[cm, centimeter; m, meter]

Carbon pool category	Definition
Aboveground and belowground live tree	Aboveground and belowground portions of the live trees with diameters greater than 2.54 cm at 1.37 m above the forest floor.
Standing dead wood	Standing dead trees, including coarse roots.
Down dead wood	Woody material greater than 7.6 cm in diameter on the ground and stumps and their roots greater than 7.6 cm in diameter.
Understory vegetation	Aboveground and belowground portions of seedlings and woody shrubs.
Forest floor or litter	Organic material on the floor of the forest, including fine woody debris, humus, and fine roots in the organic forest floor layer above mineral soil.
Soil organic carbon	Fine organic material below the soil surface to a depth of 1 m (does not include roots).

5.5. Results and Discussion

5.5.1. Current Status of Forest Carbon Pools

The baseline forest carbon was derived from the USDA Forest Service EVALIDator program (Miles, 2015). The total forest carbon without soil organic carbon (SOC) in coastal Alaska was estimated to be 1,018 TgC (2004–2013), of which about 557 TgC was live biomass carbon (aboveground and belowground), 175 TgC was dead wood carbon (standing dead and down dead wood), and 275 TgC was forest floor carbon. The estimates of forest carbon without SOC are reported below by land ownership, forest type, and stand age class.

5.5.1.1. Current Forest Carbon Pools by Land Ownership Group

The two largest land owners, the Chugach and Tongass National Forests, represent 71 percent of the forest land and contain 80 percent of the forest carbon in coastal Alaska (fig. 5.3). The Tongass National Forest, which is the largest national forest in the country, has 64 percent of the total coastal forest land and over 74 percent of the total Alaska coastal forest carbon. Nearly 18 percent of the forest land in coastal Alaska is in other public ownership (other Federal or State and local government), and over 11 percent of forest land is in private ownership.

5.5.1.2. Current Forest Carbon Stock by Forest Type

The major forest types in coastal Alaska are western hemlock (*Tsuga heterophylla* (Raf.) Sarg.), mountain hemlock (*Tsuga mertensiana* (Bong.) Carrière), Sitka spruce (*Picea sitchensis* (Bong.) Carrière), yellow-cedar (*Callitropsis nootkatensis* (D. Don) D.P. Little), and western red cedar (*Thuja plicata* Donn ex D. Don). These five forest types account for over 90 percent of the coastal forest carbon, of which over 38 percent is stored in the western hemlock forest type (table 5.3).

5.5.1.3. Current Forest Carbon Pools by Stand Age Class

Over 44 percent of coastal Alaska forest land is more than 200 years old, and 58 percent of forest carbon is stored in this age class. The age class of 200 to 300 years old occupies approximately 20,000 km^2 of forest land and stores the greatest proportion of the forest carbon (fig. 5.4).

5.5.2. Projected Changes in Forest Carbon (Not Including Soil Organic Carbon)

The analysis of the FVS simulations conducted for the scenario of current management without considering climate change (fig. 5.5) indicated that forest carbon (live tree, dead wood, forest floor, and understory carbon) in coastal Alaska would decrease by 3.9 teragrams of carbon per year (TgC/yr) until the 2050s and then would increase by 1.8 TgC/yr throughout the remainder of the century. The carbon in live

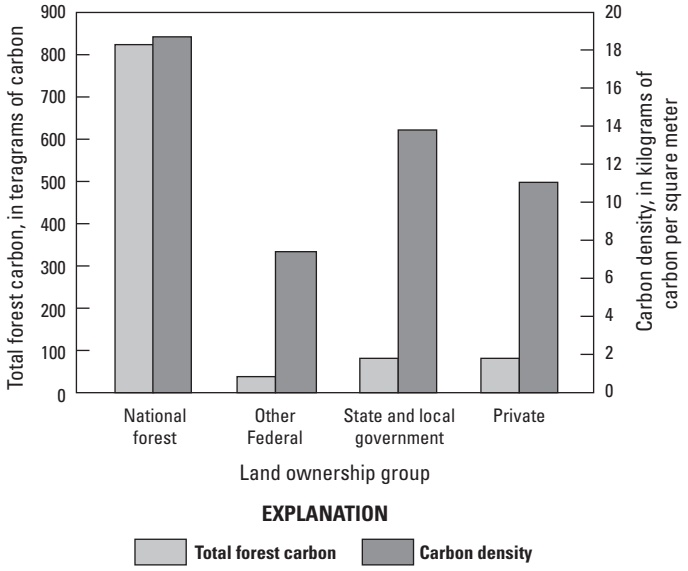

Figure 5.3. Coastal Alaska current forest carbon stock and carbon density by land ownership group (not including soil organic carbon). Data source: USDA Forest Service Forest Inventory and Analysis Program.

Table 5.3. Coastal Alaska current forest carbon distribution by forest type (not including soil organic carbon).

[Data source: USDA Forest Service Forest Inventory and Analysis Program. kgC/m^2, kilogram of carbon per square meter]

Carbon	Forest type						
	Western hemlock	Mountain hemlock	Sitka spruce	Yellow-cedar	Western red cedar	Other softwood	Other hardwood
Distribution (percent)	37.8	17.9	16.2	13.2	8.6	4.5	2.8
Density (kgC/m^2)	23.63	13.97	20.34	14.32	20.92	5.91	6.36

trees (aboveground and belowground) would decrease by 1.2 TgC/yr until the early 2040s and then would increase by 2.6 TgC/yr through 2099. Although the projected harvesting rate was set to the same level for every 5-year cycle, the model does not distribute it evenly, and the intensity of the harvest of live trees at the beginning would contribute to the decrease of live tree carbon. In general, the live trees are the major carbon pool for the region. Carbon in the forest floor would decrease from 2010 to 2050 at the rate of 0.8 TgC/yr before stabilizing until 2070 after which it slightly increases through 2099. Whereas the total forest carbon (not including SOC) would increase by 1 percent, live tree carbon was projected to increase by almost 27 percent by the end of this century under this scenario.

The analysis of the FVS simulations conducted for the scenario of climate change with management (fig. 5.6) indicated that forest carbon stock would increase by 8.5 percent in total forest carbon with a 38-percent increase in live tree carbon storage by the end of the century. The timing of the trajectory was similar to the first scenario. Total forest carbon stock would decrease until the mid-2040s at 3.6 TgC/yr followed by an increase throughout the remainder of the century of 2.5 TgC/yr. Similarly, the live tree carbon would decrease by 0.4 TgC/yr until the early 2040s and then increase by 3.2 TgC/yr. Changes in understory carbon, which is only about 0.5 percent of the total forest carbon, is not influential in the calculation. Carbon in the forest floor would decrease until 2060 at 0.6 TgC/yr then slightly increase or remain constant.

Finally, the analysis of the FVS simulations conducted for the scenario of climate change with no management (fig. 5.7) indicated that forest carbon would decrease by 2.7 TgC/yr for the first decade and then increase by 3.2 TgC/yr throughout the remainder of the century. The live tree carbon was projected to slowly increase through the whole projection period at the rate of 4.0 TgC/yr. The carbon stored in forest floor was relatively stable. At the end of century, the total forest carbon would increase by nearly 27 percent and the live tree carbon by about 68 percent.

Because the management scenarios assume a relatively low rate of harvesting, the estimated amount of carbon

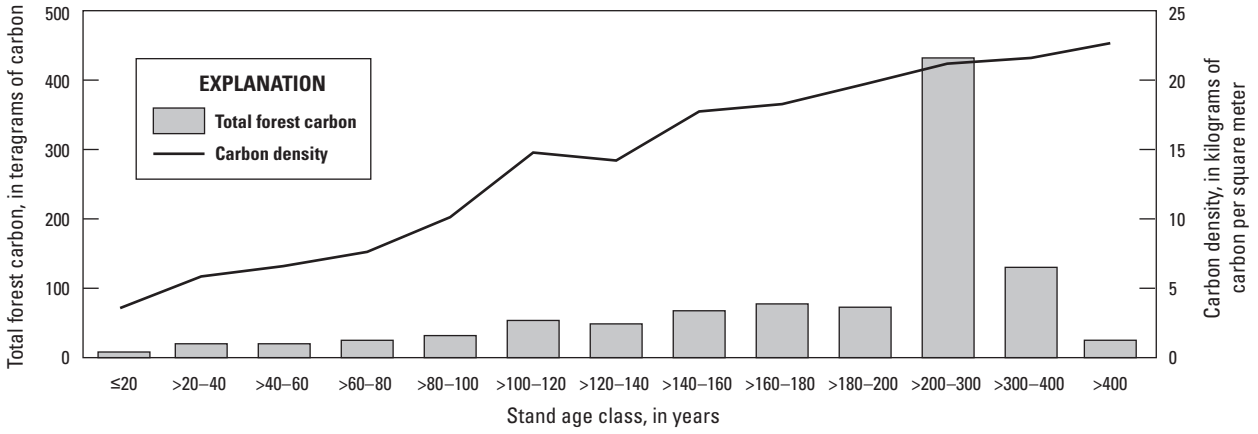

Figure 5.4. Coastal Alaska baseline (2003–2014) forest carbon and carbon density by stand age class (not including soil organic carbon). Data source: USDA Forest Service Forest Inventory and Analysis Program.

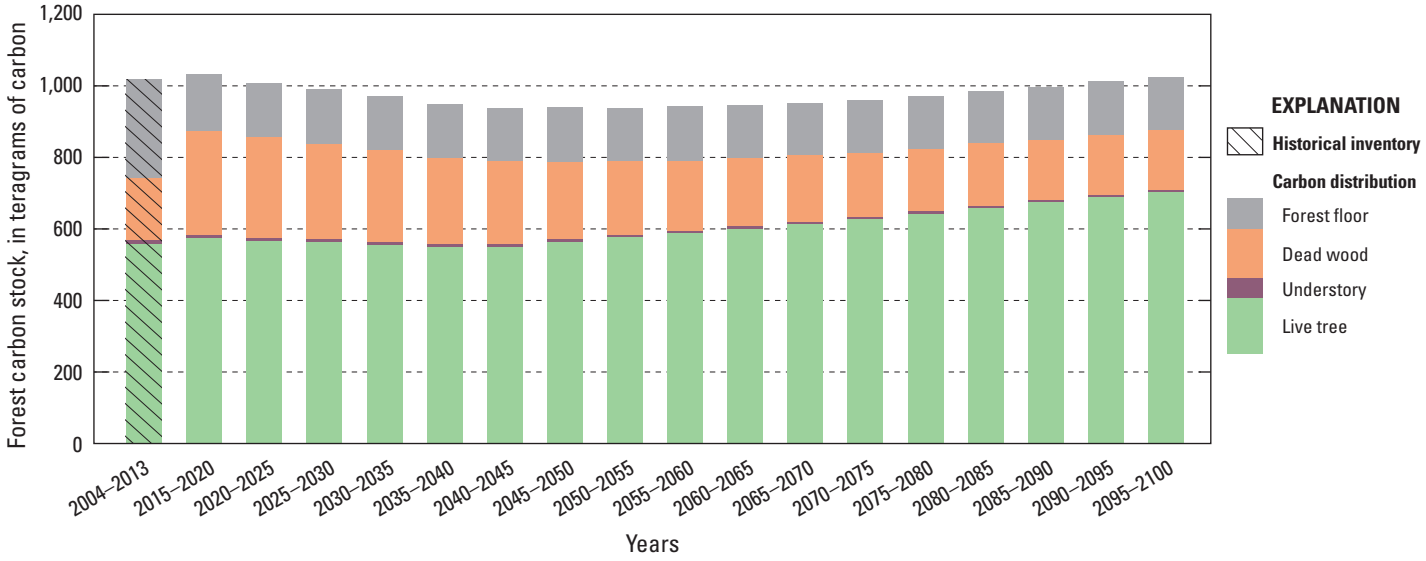

Figure 5.5. Results of projected forest carbon stock (not including soil organic carbon) in coastal Alaska under the scenario of forest management with no climate change. Data source: USDA Forest Service Forest Inventory and Analysis Program.

removed ranged from 0.1 to 0.3 TgC/yr under the climate change scenario and from 0.1 to 0.2 TgC/yr at the present climate in coastal Alaska.

All the scenarios described above showed a significant decrease in the dead wood carbon pool for the first 50- to 60-year period. Such a decrease, especially at the beginning of the projection period, can be explained by the harvest and the relatively fast decomposition in the region. The tree mortality rate derived from the historical database could also be lower compared to the current rate observed in coastal Alaska. Because actual decomposition rates for coastal Alaska are not currently available, we instead used rates derived for the Pacific Northwest region, thus our models may have overestimated this parameter.

Although 25 simulations were run to assess uncertainty for each scenario, little variability was shown in each of the above described scenarios.

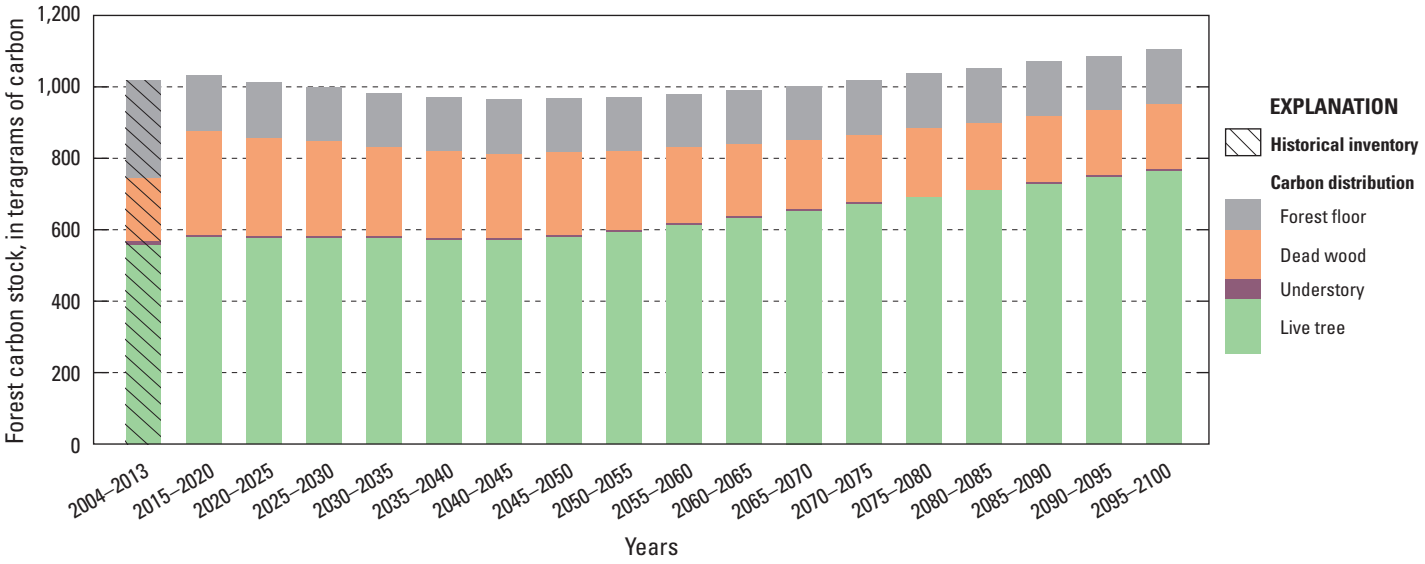

Figure 5.6. Results of projected forest carbon stock (not including soil organic carbon) in coastal Alaska under the scenario of climate change with forest management. Data source: USDA Forest Service Forest Inventory and Analysis Program. To conduct the simulations of climate change, the A1B scenario from the Intergovernmental Panel on Climate Change's Special Report on Emissions Scenarios (Nakićenović and Swart, 2000) was used to drive the version 3.1-T47 of the Canadian Centre for Climate Modelling and Analysis' Coupled Global Climate Model (CGCM3.1; Flato, 2005) general circulation model.

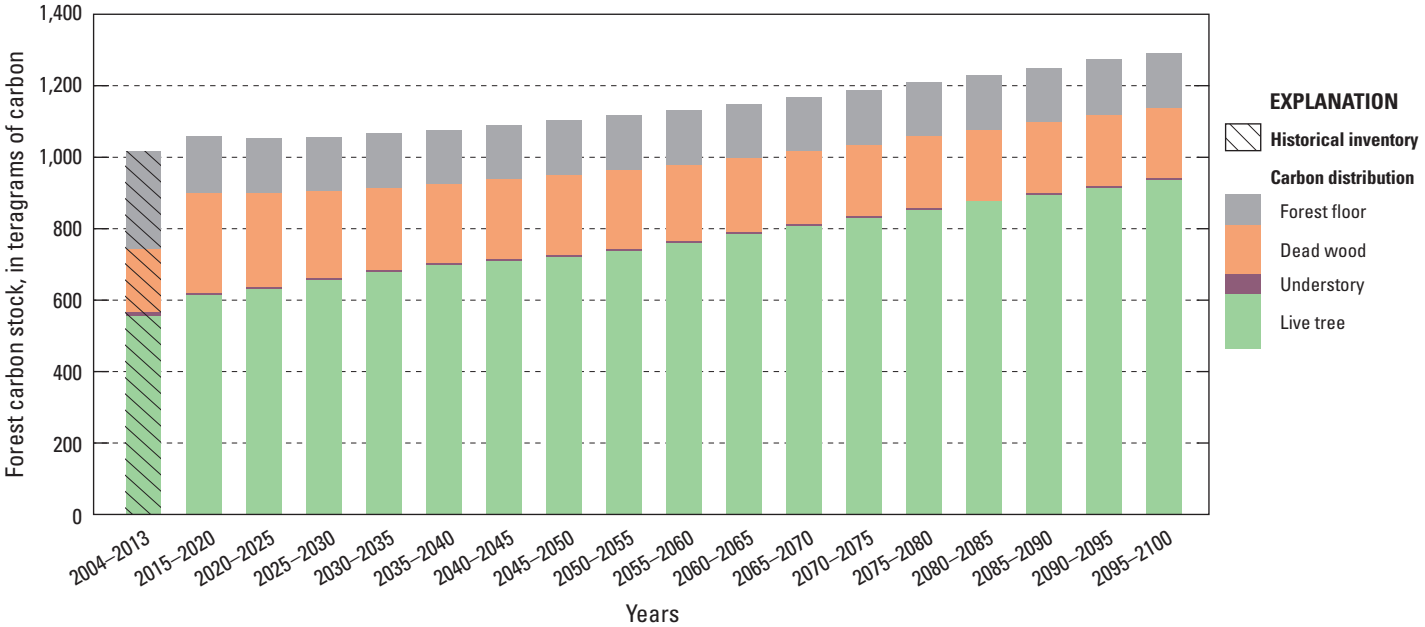

Figure 5.7. Results of projected forest carbon stock (not including soil organic carbon) in coastal Alaska under the scenario of climate change with no forest management. Data source: USDA Forest Service Forest Inventory and Analysis Program. Details regarding the simulations of climate change can be found in figure 5.6.

5.6. Conclusions

Overall, the results show that the balance of forest carbon in the study region in Alaska is sensitive to management actions and climate change. Managed with present forest harvest and present climate, the forest carbon would increase by 10 TgC by the end of the century compared to the baseline (2004–2013). Forest carbon stock would increase by 86 TgC under the climate change with management and by 276 TgC under the climate change with no management (fig. 5.8).

The results suggest relative effects of forest management and climate change on forests of the Alaska coastal region. Forest management by itself would have a negative effect on the balance of forest carbon, whereas the climate change simulation under scenario A1B with CGCM3.1 would lead to increased carbon stock. Since the majority of the forest lands are publicly owned in coastal Alaska, forest policies of State and Federal agencies focused on conservation and carbon sequestration could substantially increase carbon storage in the region by the end of the century. It is important to note that there are several uncertainties in this study. First, the FVS is designed as a growth and yield model—the carbon tool in the current FVS calculates major forest carbon estimates but may not include all ecosystem processes in reporting carbon emission and sequestration, such as soil organic carbon and management-related emissions. Second, the scenario for forest harvest that we used is just one of many possible scenarios. It essentially represents a "business as usual" scenario. Future forest harvest could be substantially affected by amendments to the forest plan for the Tongass National Forest as well as the global market for wood products. Third, there is substantial uncertainty about future projections on climate change, which may affect the species viability and the growth rate for coastal Alaska.

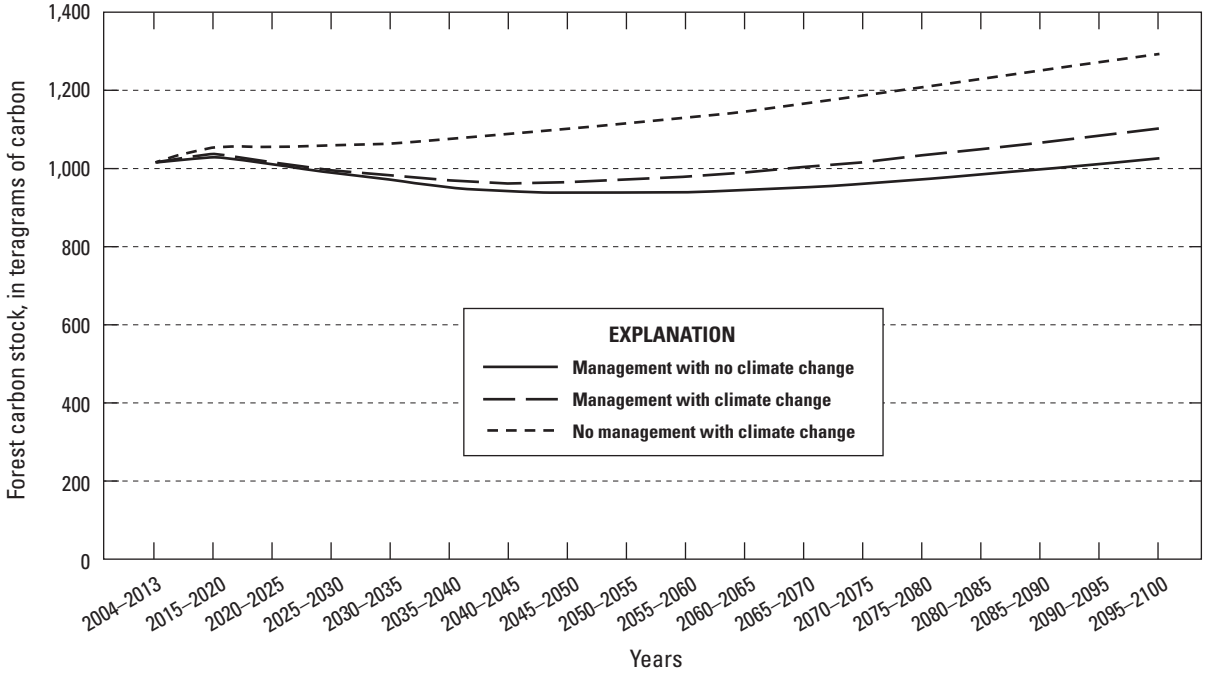

Figure 5.8. Projected coastal Alaska forest carbon stock (not including soil organic carbon) under three scenarios: management with no climate change, climate change with management, and climate change with no management. Data source: USDA Forest Service Forest Inventory and Analysis Program. To conduct the simulations of climate change, the A1B scenario from the Intergovernmental Panel on Climate Change's Special Report on Emissions Scenarios (Nakićenović and Swart, 2000) was used to drive the version 3.1-T47 of the Canadian Centre for Climate Modelling and Analysis' Coupled Global Climate Model (CGCM3.1; Flato, 2005) general circulation model.

5.7. References Cited

Alexander, S.J., 2012, Timber supply and demand, Alaska National Interest Lands Conservation Act, Section 706(a) report to Congress: U.S. Department of Agriculture, Forest Service, Alaska Region, Report Number 27.

Barrett, T.M., and Christensen, G.A., tech. eds., 2011, Forests of southeast and south-central Alaska, 2004–2008; Five-year forest inventory and analysis report: U.S. Department of Agriculture, Forest Service, Pacific Northwest Research Station, General Technical Report PNW–GTR–835, 156 p. [Also available at http://www.fs.fed.us/pnw/pubs/pnw_gtr835.pdf.]

Crookston, N.L., 2014, Climate-FVS Version 2; Content, users guide, applications, and behavior: U.S. Department of Agriculture, Forest Service, Rocky Mountain Research Station, General Technical Report RMRS–GTR–319, 38 p. [Also available at http://www.fs.fed.us/fmsc/ftp/fvs/docs/climateFVS/ClimateFVS_UsersGuide.pdf.]

Dixon, G.E., 2002, Essential FVS—A user's guide to the Forest Vegetation Simulator (revised November 2015): U.S. Department of Agriculture, Forest Service, Forest Management Service Center, 226 p. [Also available at http://www.fs.fed.us/fmsc/ftp/fvs/docs/gtr/EssentialFVS.pdf.]

Flato, G.M., 2005, The third generation coupled global climate model (CGCM3) (and included links to the description of the AGCM3 atmospheric model): Canadian Centre for Climate Modelling and Analysis, available at http://ec.gc.ca/ccmac-cccma/default.asp?lang=En&n=1299529F-1.

Haynes, R.W., tech. coord., 2003, An analysis of the timber situation in the United States; 1952 to 2050: U.S. Department of Agriculture, Forest Service, Pacific Northwest Research Station, General Technical Report PNW–GTR–560, 254 p. [Also available at http://www.fs.fed.us/pnw/pubs/gtr560/.]

Keyser, C.E., comp., 2008, Southeast Alaska and coastal British Columbia (AK) variant overview—Forest Vegetation Simulator (revised September 3, 2014): U.S. Department of Agriculture, Forest Service, Forest Management Service Center, 38 p. [Also available at http://www.fs.fed.us/fmsc/ftp/fvs/docs/overviews/FVSak_Overview.pdf.]

Leites, L.P., Robinson, A.P., and Crookston, N.L., 2009, Accuracy and equivalence testing of crown ratio models and assessment of their impact on diameter growth and basal area increment predictions of two variants of the Forest Vegetation Simulator: Canadian Journal of Forest Research, v. 39, no. 3, p. 655–665, http://dx.doi.org/10.1139/X08-205.

Miles, P.D., 2015, Forest Inventory EVALIDator web application (ver. 1.6.0.01): U.S. Department of Agriculture, Forest Service, Northern Research Station, accessed April 7, 2015, at http://apps.fs.fed.us/Evalidator/evalidator.jsp.

Nakićenović, Nebojša, and Swart, Rob, eds., 2000, Special report on emissions scenarios—A special report of Working Group III of the Intergovernmental Panel on Climate Change: Cambridge, United Kingdom, Cambridge University Press, 599 p., http://www.ipcc.ch/ipccreports/sres/emission/index.php?idp=0.

O'Connell, B.M., LaPoint, E.B., Turner, J.A., Ridley, Ted, Pugh, S.A., Wilson, A.M., Waddell, K.L., and Conkling, B.L., 2014, The Forest Inventory and Analysis database; Database description and user guide version 6.0 for phase 2: U.S. Department of Agriculture Forest Service, 624 p. [Also available at http://www.fia.fs.fed.us/library/database-documentation/historic/ver6/FIADB_user%20guide_6-0_p2_5-6-2014.pdf.]

Oswalt, S.N., Smith, W.B., Miles, P.D., and Pugh, S.A., 2014, Forest resources of the United States, 2012; A technical document supporting the Forest Service 2015 update of the RPA Assessment: U.S. Department of Agriculture, Forest Service, Washington Office, General Technical Report GTR–WO–91, 218 p. [Also available at http://www.srs.fs.usda.gov/pubs/47322.]

Peterson, R.L., Liang, Jingjing, and Barrett, T.M., 2014, Modeling population dynamics and woody biomass in Alaska coastal forest: Forest Science, v. 60, no. 2, p. 391–401, http://dx.doi.org/10.5849/forsci.12-540.

Robinson, A.P., Duursma, R.A., and Marshall, J.D., 2005, A regression-based equivalence test for model validation; Shifting the burden of proof: Tree Physiology, v. 25, no. 7, p. 903–913, http://dx.doi.org/10.1093/treephys/25.7.903.

SAS Institute Inc., 2008, Introduction, chap. 2 *of* SAS/STAT® 9.2 user's guide: Cary, N.C., SAS Institute Inc., p. 19–26.

Smith, J.E., Heath, L.S., and Hoover, C.M., 2013, Carbon factors and models for forest carbon estimates for the 2005–2011 National Greenhouse Gas Inventories of the United States: Forest Ecology and Management, v. 307, p. 7–19, http://dx.doi.org/10.1016/j.foreco.2013.06.061.

Zhou, Xiaoping, 2013, Production, prices, employment, and trade in Northwest forest industries, all quarters 2012: U.S. Department of Agriculture, Forest Service, Pacific Northwest Research Station, Resource Bulletin PNW–RB–265, 163 p. [Also available at http://www.fs.fed.us/pnw/pubs/pnw_rb265.pdf.]

Zhu, Zhiliang, ed., Bergamaschi, Brian, Bernknopf, Richard, Clow, David, Dye, Dennis, Faulkner, Stephen, Forney, William, Gleason, Robert, Hawbaker, Todd, Liu, Jinxun, Liu, Shuguang, Prisley, Stephen, Reed, Bradley, Reeves, Matthew, Rollins, Matthew, Sleeter, Benjamin, Sohl, Terry, Stackpoole, Sarah, Stehman, Stephen, Striegl, Robert, Wein, Anne, and Zhu, Zhiliang, 2010, A method for assessing carbon stocks, carbon sequestration, and greenhouse-gas fluxes in ecosystems of the United States under present conditions and future scenarios: U.S. Geological Survey Scientific Investigations Report 2010–5233, 190 p. [Also available at http://pubs.usgs.gov/sir/2010/5233/.] [Supersedes U.S. Geological Survey Open-File Report 2010–1144.]

Chapter 6. Terrestrial Carbon Modeling: Baseline and Projections in Upland Ecosystems

By Hélène Genet,[1] Yujie He,[2] A. David McGuire,[3] Qianlai Zhuang,[2] Yujin Zhang,[1], Frances E. Biles,[4] David V. D'Amore,[4] Xiaoping Zhou,[5] and Kristopher D. Johnson[6]

6.1. Highlights

- Ecosystem carbon balance of the Alaska assessment domain (as outlined in chapter 1) was examined using a process-based model framework for two time periods: a historical period (1950–2009), for which historical climate and disturbance observations were used, and a projection period (2010–2099), for which projected climate and disturbance data were used.
- During the historical period, upland ecosystems in Alaska were a net carbon sink of an average of 5.01 teragrams of carbon per year (TgC/yr). All Landscape Conservation Cooperative (LCC) regions in Alaska were net carbon sinks, except for the Northwest Boreal LCC North. This carbon sink was mostly due to an increase in vegetation productivity associated with recent warming.
- For the Northwest Boreal LCC North, the carbon source averaged –5.12 TgC/yr and was associated with large carbon losses from wildfire, specifically during large fire years in 1957, 1969, 1977, 1990–1991, 2004, and 2005.
- Carbon loss from forest harvest exports in the North Pacific LCC represented 1.6 percent of the statewide gross carbon losses between 1950 and 2009.
- During the projection period (2010–2099), all LCC regions of Alaska were projected to be carbon sinks, storing between 14.72 and 30.15 TgC/yr statewide.
- Methane consumption in upland ecosystems was projected to be low relative to gross primary productivity (GPP), representing on average 0.0011 percent of the projected GPP by 2099.
- Disturbances, mainly wildfires, would be a strong determinant of the future spatial and temporal variability of carbon dynamics, particularly in the Northwest Boreal LCC North.

6.2. Introduction

Arctic and boreal permafrost soils hold about 1,700 petagrams of organic carbon (Zimov and others, 2006; Schuur and others, 2008; Tarnocai and others, 2009), more than twice the carbon in atmospheric carbon dioxide (CO_2). Thus, changes in the carbon balance of permafrost ecosystems in response to climate warming could profoundly alter the composition of the atmosphere to affect the climate system (Schaefer and others, 2011; Schuur and others, 2013). As permafrost warms, organic matter that has been frozen for hundreds to thousands of years is exposed to microbial decomposition, mineralization, and release to the atmosphere as CO_2 and methane (CH_4) greenhouse gases that may offset carbon gain from potential increases in vegetation productivity in response to climate warming.

[1]University of Alaska-Fairbanks, Fairbanks, Alaska.

[2]Purdue University, West Lafayette, Ind.

[3]U.S. Geological Survey, Fairbanks, Alaska.

[4]U.S. Department of Agriculture Forest Service, Juneau, Alaska.

[5]U.S. Department of Agriculture Forest Service, Portland, Oreg.

[6]U.S. Department of Agriculture Forest Service, Newtown Square, Pa.

Boreal and arctic regions are thought to have been a strong carbon sink during the 20th century (McGuire and others, 2009; Pan and others, 2011). More recent analyses that included consideration of the last decade of intensive fire activity throughout the boreal zone and CH_4 emissions in the region indicate that the carbon sink is weakening and that the region is acting as a net source of greenhouse gases when the global warming potential of CH_4 is considered (McGuire and others, 2010; Hayes and others, 2011). A recent analysis of historical carbon exchange in arctic tundra (1990–2006), using observations, regional and global applications of process-based models, and atmospheric inversion models, suggests that large uncertainties existed that could not be distinguished from neutral balance (McGuire and others, 2012). One of the sources of this uncertainty is related to the weak ability of process-based models to represent the temporal variability of carbon dynamics across the landscape (Fisher and others, 2014). In Alaska, the spatial and temporal variability of carbon dynamics depend primarily on drainage conditions and disturbance regimes (Schuur and others, 2009; Tarnocai and others, 2009; Grosse and others, 2011). Indeed, uplands and wetlands are dominated by different soil carbon processes; vegetation productivity; and nature, frequency, and severity of disturbance regimes.

In this report, we review the main drivers of carbon dynamics separately for uplands (this chapter) and wetlands (chapter 7). Uplands in Alaska are characterized by moderately to well drained ecosystems composed of forest and alpine ecosystems in the boreal and maritime regions and the tundra ecosystem in the arctic region. Because of good drainage conditions, soil biogeochemical dynamics in uplands are dominated by aerobic processes (Schuur and others, 2009). Carbon and nutrient turnover is faster and the vegetation is generally more productive in uplands than in wetlands. In past syntheses of regional carbon dynamics, the role of aerated soils as a sink for atmospheric CH_4 has been neglected. However, it has been documented that CH_4 consumption exceeds CH_4 production in moist tundra soils of Alaska (Whalen and Reeburgh, 1990). Therefore, for a comprehensive assessment of carbon dynamics in northern high latitudes, it is important to consider CH_4 uptake in uplands. Wildfire and forest harvest are two important disturbance regimes in uplands in Alaska. Whereas wildfire occurs mostly in boreal forest and to a lesser extent in arctic tundra (Mack and others, 2011; Turetsky and others, 2011), forest harvest is concentrated in southern coastal Alaska. Annual area burned has increased in Alaska (Kasischke and Turetsky 2006; Kasischke and others, 2010) and Canada (Gillett and others, 2004) during the second half of the 20th century. In Alaska, the decade beginning in 2000 experienced the highest burned area (76,700 square kilometers per year [km^2/yr]) during the modern record period (baseline at 39,970 km^2/yr from 1920 to 2009). In Canada, average burned area increased continuously from the 1940s (81,650 km^2/yr) through the 1990s (317,070 km^2/yr) before sharply decreasing in the 2000s (165,430 km^2/yr). Several studies indicate that this increase is predicted to be maintained at least during the first half of the 21st century (Balshi and others, 2009; Mann and others, 2012; chapter 2). In addition to an increase in carbon emissions from burning, greater fire frequency and severity have substantial implications for permafrost, as increased severity leads to greater consumption of the insulating organic layer, which may accelerate permafrost thaw and associated deep carbon decomposition (Dyrness and Norum, 1983; Yoshikawa and others, 2002; Burn and others, 2009). Finally, commercial harvesting of maritime upland forest (that is, western hemlock [*Tsuga heterophylla* (Raf.) Sarg.] and Sitka spruce [*Picea sitchensis* (Bong.) Carrière]) in southeast and south-central Alaska has been developing since the late 19th century (Rakestraw, 1981; chapter 5). Although harvesting reduces aboveground carbon stocks by exporting wood out of the ecosystem, it might promote vegetation productivity by increasing areas of secondary growth (Cole and others, 2010).

In this chapter, we assess historical and projected carbon dynamics of upland ecosystems in Alaska by using a modeling framework that combines process-based biogeochemical and biogeographic-disturbance models at a spatial resolution of 1 kilometer (km). We evaluated the long-term consequences of a projected warming and disturbance regime on the regional carbon balance in uplands in Alaska from 2009 to 2099 using six climate simulations from two general circulation models (GCMs) for three atmospheric CO_2 emissions scenarios.

6.3. Material and Methods

6.3.1. Model Framework

Changes in soil and vegetation carbon stocks and fluxes in response to climate change and disturbances were analyzed using a modeling framework that combines a wildfire disturbance model, the Alaska Frame-Based Ecosystem Code (ALFRESCO; Rupp and others, 2000, 2002, 2007; Johnstone and others, 2011; Mann and others, 2012; Gustine and others, 2014; Amy Breen, University of Alaska-Fairbanks, written commun., 2015), and two process-based ecosystem models that simulate (1) carbon and nitrogen pools and CO_2 dynamics using the Dynamic Organic Soil version of the Terrestrial Ecosystem Model (DOS-TEM; Raich and others, 1991; McGuire and others, 1992) and (2) CH_4 dynamics using the Methane Dynamics Module of the Terrestrial Ecosystem Model (MDM-TEM; Zhuang and others, 2004). These three models have been coupled in an asynchronous way, in which the time series of fire occurrence simulated by ALFRESCO is used to drive DOS-TEM, which simulates the effects of wildfire, warming, and forest harvest on carbon pools and aerobic carbon processes. Monthly net primary productivity (NPP) and leaf area index (LAI) simulated by DOS-TEM are used to drive MDM-TEM, which simulates anaerobic (methanogenesis) and aerobic (methane oxidation) carbon processes (fig. 6.1). Description of the ALFRESCO model is provided in chapter 2, section 2.3.2. As MDM-TEM

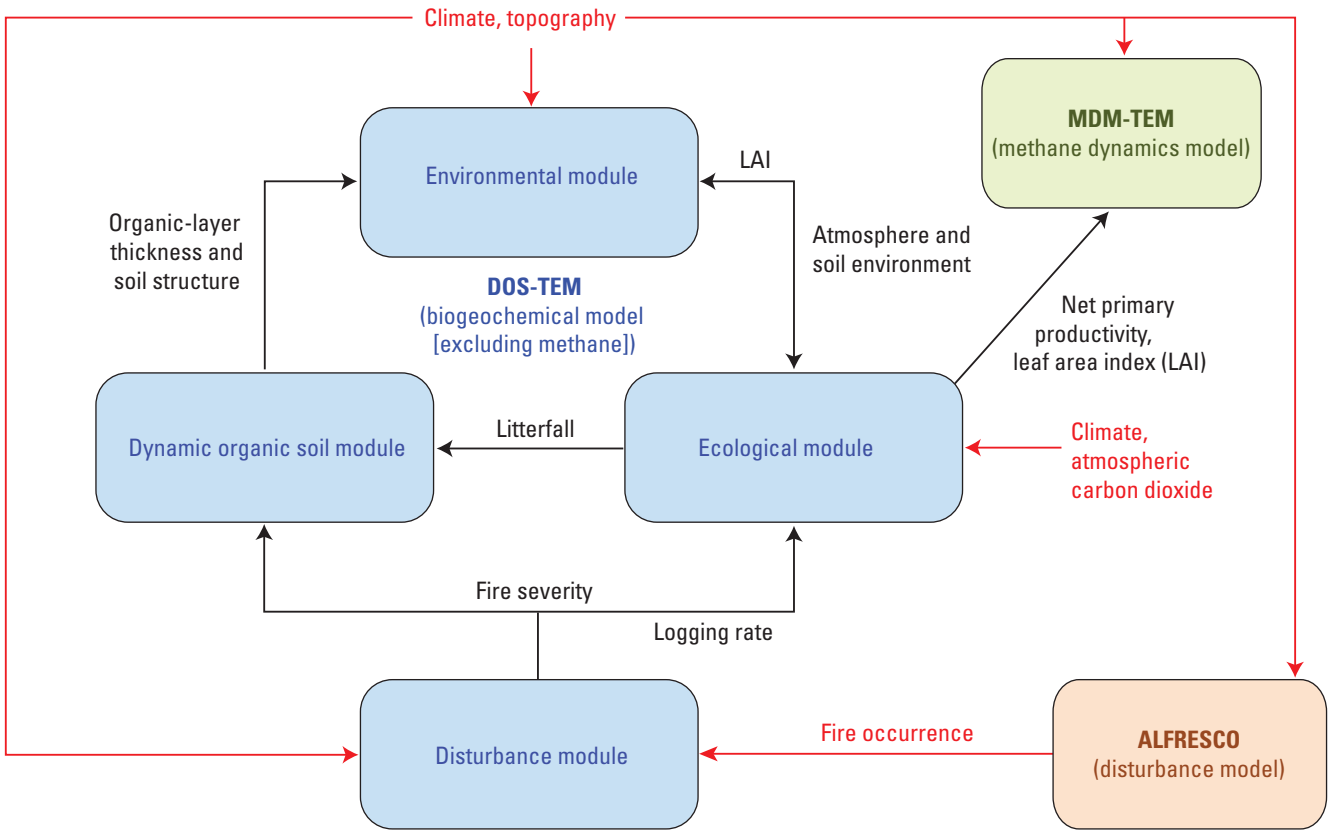

Figure 6.1. Modeling framework for this assessment. Red text and arrows represent input drivers. Black text and arrows represent flows of information within and among models. Blue boxes represent the four modules composing the Dynamic Organic Soil version of the Terrestrial Ecosystem Model (DOS-TEM). The orange box represents the disturbance model Alaska Frame-Based Ecosystem Code (ALFRESCO) and the green box represents the methane dynamics model Methane Dynamics Module of the Terrestrial Ecosystem Model (MDM-TEM).

simulations are of particular importance for simulating wetland carbon dynamics, the MDM-TEM model is described in chapter 7, section 7.3.1. Here we focus on descriptions of DOS-TEM for upland carbon modeling.

6.3.2. Dynamic Organic Soil Version of the Terrestrial Ecosystem Model (DOS-TEM) Description

DOS-TEM belongs to the Terrestrial Ecosystem Model (TEM) family of process-based ecosystem models that has been designed to simulate carbon and nitrogen pools in vegetation and soil, and carbon and nitrogen fluxes among vegetation, soil, and the atmosphere (Raich and others, 1991; McGuire and others, 1992). DOS-TEM is composed of four modules: an environmental module, an ecological module, a disturbance module, and a dynamic organic soil module.

The environmental module computes dynamics of biophysical processes in the soil and the atmosphere, driven by climate and soil texture input data, leaf area index from the ecological module, and soil structure from the dynamic organic soil module. Soil temperature and moisture conditions are calculated for multiple layers within various soil horizons, including moss, fibric and humic organic layers, and mineral horizons. A stable snow/soil thermal model integrated into the environmental module uses the Two-Directional Stefan Algorithm (TDSA; Woo and others, 2004). The TDSA can satisfactorily simulate the positions of the freeze-thaw front and active-layer thickness in a land surface model when proper surface forcing is provided (Yi and others, 2006). The environmental module provides information regarding the atmospheric and soil environment to the ecological module and the disturbance module.

The ecological module simulates carbon and nitrogen dynamics among the atmosphere, the vegetation, and the soil. Carbon and nitrogen dynamics are driven by climate input data, information on soil and atmospheric environment from the environmental module, information on soil structure provided by the dynamic organic soil module, and information on timing and severity of wildfire or forest harvest occurrences provided by the disturbance module.

The dynamic organic soil module calculates the thickness of the fibric and humic organic layers after soil carbon pools are altered by ecological processes (litterfall, decomposition, and burial) and fire disturbance. The estimation of organic

horizon thickness is computed from soil carbon content using relationships that link soil organic carbon content and soil organic thickness (Yi, McGuire, and others, 2009). These relationships have been developed for fibric, humic, and mineral horizons for every vegetation type, based on data from the soil carbon network database for Alaska (Johnson and others, 2011). Once the thickness of each organic soil horizon is estimated, the dynamic organic soil module calculates the number of layers in each organic horizon and the thickness of each layer to maintain stability and efficiency of soil temperature and moisture calculations along the soil column, as a function of the soil characteristics of each layer.

Finally, the disturbance module simulates how forest harvest and wildfire affect carbon and nitrogen pools of the vegetation and the soil. For wildfire, the module computes combustion emissions to the atmosphere, the fate of uncombusted carbon and nitrogen pools, and the flux of nitrogen from the atmosphere to the soil via biological nitrogen fixation in the years following a fire. The amount of soil carbon combusted during a wildfire is determined using input data on topography, drainage, and vegetation, as well as soil (moisture and temperature) and atmospheric (evapotranspiration) data from the environmental module (Genet and others, 2013).

Previous regional applications of DOS-TEM in northern high latitudes have investigated how biogeochemical dynamics of terrestrial ecosystems in these regions are affected at seasonal to century scales by processes like soil thermal activities (Zhuang and others, 2001, 2002, 2003), snow cover (Euskirchen and others, 2006, 2007), and fire (Balshi and others, 2007; Yuan and others, 2012). DOS-TEM has been developed primarily to represent the effects of disturbances, wildfire especially, on carbon stocks in vegetation and soil organic horizons and on the soil environment in permafrost regions (Yi, Manies, and others, 2009; Yi, McGuire, and others, 2009; Yi and others, 2010). Recent model developments have focused on the spatial and temporal heterogeneity of fire severity and carbon loss associated with the influence of drainage conditions, vegetation composition, topography, and weather conditions across the landscape (Genet and others, 2013). In this study, we developed an additional capability for DOS-TEM to consider the effects of forest harvest disturbance on carbon balance, which is described below.

6.3.3. Dynamic Organic Soil Version of the Terrestrial Ecosystem Model (DOS-TEM) Development—Modeling the Effect of Forest Harvest on Carbon Dynamics

For this assessment, we further developed the disturbance module of DOS-TEM to represent the effects of forest harvest on carbon and nitrogen dynamics. The harvesting of timber in southern coastal Alaska took place primarily between the mid-1950s and mid-1990s (fig. 6.2) when two pulp mills opened in Sitka and Ketchikan to process large volumes of low-grade timber, mainly from the Tongass National Forest where the U.S. Department of Agriculture (USDA) Forest Service began offering 50-year timber sale contracts (Colt and others, 2007). After 1990, the USDA Forest Service reduced the volume of timber offered for sale annually, and in 1997, the agency imposed harvest constraints that resulted in large increases in the cost of harvesting timber on national forest lands and a decrease of the annual volume harvested.

Forest harvest by clear-cutting was widespread in southeastern Alaska since the early 1950s (Alaback, 1982; Cole and others, 2010). We developed a harvesting module with an assumption that 95 percent of the aboveground vegetation biomass would be harvested (Deal and others, 2002). Among the residual biomass, 4 percent was considered dead and 1 percent alive to allow post-harvest recruitment. As a consequence, 99 percent of the belowground vegetation biomass (root biomass) was considered dead and transferred to the soil organic matter pool. Exported out of the ecosystem, the carbon in timber will mainly be stored in permanent constructions or furniture.

6.3.4. Model Parameterization and Validation

6.3.4.1. Dynamic Organic Soil Version of the Terrestrial Ecosystem Model (DOS-TEM)

Rate-limiting parameters of the model were calibrated for 11 main land-cover types in Alaska—4 types of tundra (graminoid, shrub, heath, and wet-sedge tundra), 3 types of boreal forest (black spruce [*Picea mariana* (Mill.) Britton, Sterns & Poggenb.], white spruce [*Picea glauca* (Moench) Voss], and deciduous forest), and 4 types of maritime communities (upland forest, wetland forest, fen, and alder shrubland). (See chapter 2, section 2.4.1 for further description of these land-cover types.) In boreal regions, similar vegetation composition can occur in very different drainage conditions leading to high variability in carbon and nitrogen turnover (Schuur and others, 2009; Wickland and others, 2010) and vulnerability to disturbance (Turetsky and others, 2011); therefore, the three types of boreal forest were calibrated separately for uplands and for wetlands. In this chapter, we focus on the calibration of upland ecosystems: graminoid tundra, shrub tundra, heath tundra, boreal upland black spruce forest, boreal upland white spruce forest, boreal upland deciduous forest, and maritime upland forest. (See chapter 7, section 7.3.2.3 for calibration of wetlands and lowland boreal forests.)

We calibrated the rate-limiting parameters of DOS-TEM using target values of carbon and nitrogen pools and fluxes representative of mature ecosystems. These parameters were "tuned" until the model reached target values of the main carbon and nitrogen pools and fluxes (Clein and others, 2002). The calibration of these parameters is an effective means of dealing with temporal scaling issues in ecosystem models (Rastetter and others, 1992). For boreal forest communities, an existing set of target values for vegetation and soil carbon and nitrogen pools and fluxes was assembled using

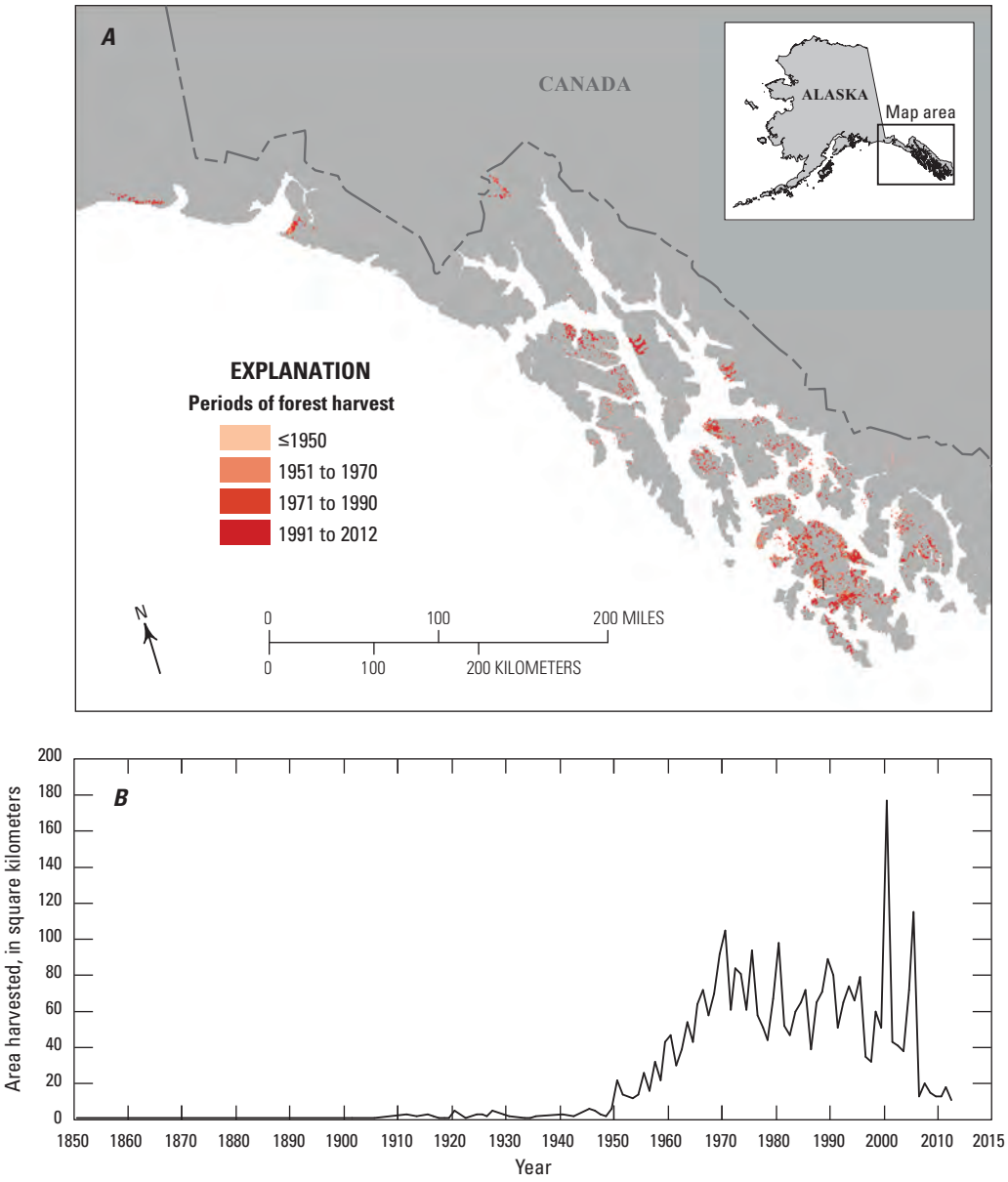

Figure 6.2. Forest harvest history in southeast and south-central Alaska: *A*, spatial distribution of harvests from 1850 through 2012 and *B*, time series of annual area harvested from 1850 through 2012.

data collected in the Bonanza Creek Long Term Ecological Research (LTER) program (Yuan and others, 2012). For the tundra communities, we used data collected at the Toolik Field Station (Shaver and Chapin, 1991; Van Wijk and others, 2003; Sullivan and others, 2007; Euskirchen and others, 2012; Gough and others, 2012; Sistla and others, 2013). Finally, for the maritime upland forest, we used data summarized in chapter 4, collected from a long-term carbon flux study in the North American Carbon Program (D'Amore and others, 2012). The target values for maritime alder shrubland were assessed from Binkley (1982). Target values of vegetation biomass, soil carbon pools, net primary productivity, and gross primary productivity for each upland land-cover type are described in table 6.1.

6.3.4.2. Methane Dynamics Module of the Terrestrial Ecosystem Model (MDM-TEM)

The upland simulation of MDM-TEM was parameterized using CH_4 measurements and key soil and climate factors made at three upland field sites—boreal forest at Bonanza Creek (B-F), tundra at the North Slope of Alaska (Tundra-NS), and moist tundra on Unalaska Island (Tundra-UI) (table 6.2). Because daily time series of CH_4 consumption were not available, we parameterized the MDM-TEM for upland ecosystems such that the difference between the simulated and observed maximum daily CH_4 consumption rate is minimized at these sites. Specifically, we altered the parameters of the methane module until the simulation CH_4 consumption

Table 6.1. Target values for carbon pool and flux variables used to calibrate the Dynamic Organic Soil version of the Terrestrial Ecosystem Model (DOS-TEM) for major upland land-cover types in Alaska.

[$gC/m^2/yr$, gram of carbon per square meter per year; gC/m^2, gram of carbon per square meter]

Upland land-cover type	Net primary productivity ($gC/m^2/yr$)	Gross primary productivity ($gC/m^2/yr$)	Carbon pool (gC/m^2)			
			Vegetation	Soil fibric	Soil humic	Soil mineral[1]
Boreal upland black spruce forest	186	372	6,405	1,199	4,432	19,821
Boreal upland white spruce forest	305	610	9,000	1,156	4,254	11,005
Boreal upland deciduous forest	510	1,020	8,546	996	3,597	11,005
Shrub tundra	136	272	1,808	2,340	5,853	37,022
Graminoid tundra	112	224	561	3,079	7,703	43,403
Heath tundra	23	46	249	1,065	1,071	32,640
Maritime upland forest	375	750	809	825	2,912	23,232
Maritime alder shrubland	300	600	24,290	2,557	4,136	15,564

[1]Soil mineral carbon pools are estimated from the bottom of the organic layer down to 1 meter into the mineral soil.

Table 6.2. Description of sites used in the model parameterization and validation process.

[n.d., no data]

Site name	Location	Elevation (meters)	Land cover	Observed data
Boreal forest at Bonanza Creek (B-F)	148°15' W. 64°41' N.	133	Black spruce (*Picea mariana*), feather moss (*Hylocomium splendens*)	Methane fluxes from late May through September 1990
Tundra at North Slope of Alaska (Tundra-NS)	149°36' W. 68°38' N.	760	Sedge (Carex spp.), moss tussock tundra dominated by *Eriophorum vaginatum*	Static chamber measured methane uptake
Moist tundra on Unalaska Island (Tundra-UI)	167°00' W. 53°00' N.	n.d.	Wet tundra dominated by sedges (Carex spp.)	Static chamber measured methane uptake
Tundra at Fairbanks, Alaska (Tundra-F; validation site)	147°51' W. 64°52' N.	158.5	Tussock tundra dominated by *Eriophorum vaginatum*	Three sites of methane emissions observed using chamber techniques from 1987 to 1990

by soil reached the maximum consumption rates of 31.6 milligrams of carbon dioxide equivalent per square meter per day ($mgCO_2$-eq/m^2/d), 39.9 $mgCO_2$-eq/m^2/d, and 56.5 $mgCO_2$-eq/m^2/d at the B-F, Tundra-NS, and Tundra-UI sites, respectively (Zhuang and others, 2004).

6.3.4.3. Model Validation and Verification

We validated the model by testing the ability of the model to extrapolate carbon dynamics across space and time. We compared model simulations with observations collected outside the spatial and temporal range of the data used for model parameterization and calibration. When independent observations were not available, we tested the ability of the model to reproduce the same data used for parameterization and calibration.

DOS-TEM parameterization has been validated using soil and vegetation biomass data derived from field observations independent of the data used for model parameterization. The National Soil Carbon Network database for Alaska was used to validate DOS-TEM estimates of soil carbon stocks (Johnson and others, 2011). In order to compare similar estimates from the model and observations, only deep profiles were selected from the database—that is, profiles with a description of the entire organic layer and the 90- to 110-centimeter (cm)-thick mineral layer below the organic layer.

Estimates of vegetation carbon stocks for tundra land-cover types were compared with observations recorded in the data catalog of the Arctic LTER at Toolik Field Station (http://toolik.alaska.edu; Shaver and Chapin, 1986). For boreal forest land-cover types, vegetation carbon stocks simulated by

DOS-TEM were compared with estimates from forest inventories conducted by the Cooperative Alaska Forest Inventory (Malone and others, 2009). The forest inventory only provided estimates of aboveground biomass. Aboveground biomass was converted to total biomass by using a ratio of aboveground versus total biomass of 0.8 in forest (Ruess and others, 1996) and 0.6 in tundra land-cover types (Gough and Hobbie, 2003). Carbon content of the biomass was estimated at 50 percent.

Finally, for the land-cover types of southern coastal Alaska (that is, the North Pacific Landscape Conservation Cooperative (LCC) maritime upland and wetland forests and maritime fen), model validation was not possible as no additional independent data were available in this region. For these land-cover types, we compared the model simulations with observed data on the same sites that were used for model parameterization. (See chapter 4, section 4.3.1 for site descriptions).

For MDM-TEM, the model was validated at a tundra site (Tundra-F) at Fairbanks, Alaska, which was not used during the parameterization process (table 6.2). The simulated daily CH_4 fluxes were compared to the observations. The Tundra-NS parameterization was used for the Tundra-F site simulations.

6.3.5. Model Application and Analysis

6.3.5.1. Forcing Data

The distribution of uplands in Alaska was assessed from topographic information. Uplands in Alaska are estimated to cover 1,237,775 square kilometers (km^2), which represents about 84 percent of the total Alaska lands (see chapter 7, section 7.4.1). Simulations were conducted across Alaska at a 1-km resolution from 1950 through 2099. DOS-TEM is driven by monthly mean air temperature, total precipitation, net incoming shortwave radiation, and vapor pressure. To evaluate the effects of historical and projected climate warming, a series of six climate simulations was conducted. The simulations combined (1) historical climate variability from 1901 through 2009 using Climatic Research Unit (CRU TS v. 3.10.01; Harris and others, 2014) data and (2) climate variability from 2010 through 2099 projected by version 3.1-T47 of the Coupled Global Climate Model (CGCM3.1, www.cccma.ec.gc.ca/data/cgcm3/; McFarlane and others, 1992; Flato, 2005) developed by the Canadian Centre for Climate Modelling and Analysis and version 5 of the European Centre Hamburg Model (ECHAM5, www.mpimet.mpg.de/en/wissenschaft/modelle/echam/; Roeckner and others 2003, 2004) developed by the Max Planck Institute. The climate projections were aligned with the Intergovernmental Panel on Climate Change's Special Report on Emissions Scenarios (IPCC-SRES; Nakićenović and Swart, 2000). The assessment used three low-, mid- and high-range CO_2 emissions scenarios (B1, A1B, and A2; see further details in chapter 2, section 2.2.1.). The climate data were bias corrected and downscaled using the delta method (Hay and others, 2000; Hayhoe, 2010) by the Scenarios Network for Alaska and Arctic Planning (SNAP, www.snap.uaf.edu/) from 0.5-degree original resolution data to 1-km resolution. The fire occurrence dataset combined (1) historical records from 1950 through 2009 obtained from the Alaska Interagency Coordination Center (AICC) large fire scar database (http://fire.ak.blm.gov/; see Kasischke and others, 2002) and (2) projected scenarios from ALFRESCO (see chapter 2, section 2.4.5.). These scenarios represent the changes in fire frequency in response to climate change and changes in vegetation composition over time. Topographic information used to compute fire severity was computed from the National Elevation Dataset of the U.S. Geological Survey at 60-meter (m) resolution (NED, http://ned.usgs.gov/). The topographic descriptors included slope, aspect, and log-transformed flow accumulation. Finally, soil texture information originated from the Global Gridded Surfaces of Selected Soil Characteristics dataset (Global Soil Data Task Group, 2000).

Historical records of area harvested from 1950 through 2009 in southeast and south-central Alaska were compiled combining geographic information system (GIS) data from four different sources: (1) The USDA Forest Service, Tongass National Forest; (2) The Nature Conservancy's past harvest repository; (3) three layers obtained from the State of Alaska—one covering Cape Yakataga to Icy Bay harvests, one for southeast Alaska, and one for Haines State Forest harvests; and (4) screen digitizing from high-resolution orthophotos of some harvests not included in the previously listed sources. In addition, the first three sources were edited using high-resolution orthophotos to improve some of the boundary delineations. Second-growth stands owing to forest harvest account for about 3.8 percent of southeast Alaska. We were unable to obtain reliable forest harvest data for areas west of Cape Yakataga and Icy Bay (that is, west of approximately long 142.55° W.). We used the harvest layer for two purposes: (1) to determine where forest harvest has taken place and (2) to identify second-growth areas on the landscape.

6.3.5.2. Analysis of Changes in Carbon Stocks and Climate-Related Uncertainty

Vegetation carbon stock estimates were derived from the sum of the aboveground and belowground living biomass. Soil carbon stocks were composed of carbon stored in the dead woody debris fallen to the ground, moss and litter, organic layers, and mineral layers. Historical changes in soil and vegetation carbon stocks were evaluated by quantifying annual differences of decadal averages between the first decade (1950–1959) and the last decade (2000–2009) of the historical period. Projected changes in soil and vegetation carbon stocks were evaluated by quantifying annual differences of decadal averages between the last decade of the historical period (2000–2009) and the last decade of the projection period (2090–2099).

The net ecosystem carbon balance (NECB) is the difference between total carbon inputs and total carbon outputs to the ecosystem (Chapin and others, 2006). NECB is the sum of all carbon fluxes coming in and out of the ecosystems, through gaseous and nongaseous, dissolved and nondissolved exchanges with the atmosphere and the hydrologic network. This chapter and chapter 7 report the carbon exchange between the terrestrial ecosystem and the atmosphere. Chapter 8 will consider carbon exchanges in inland aquatic ecosystems (gaseous and nongaseous). In terrestrial ecosystems, NECB is the result of net primary productivity (NPP) and net biogenic methane flux ($BioCH_4$) minus heterotrophic respiration (HR), fire emissions (Fire), and forest harvest exports (Harvest).

$$NECB = NPP + BioCH_4 - HR - Fire - Harvest \quad (6.1)$$

NPP results from carbon assimilation from vegetation photosynthesis minus the respiration of the primary producers (autotrophic respiration). In uplands, the activity of soil methanotrophs offset the activity of methanogens. For this reason, $BioCH_4$ is a positive flux in uplands. HR results from the decomposition of unfrozen soil organic carbon. Fire emissions encompass CO_2, CH_4, and carbon monoxide (CO) emissions. Forest harvest quantifies the amount of vegetation carbon that is exported out of the terrestrial ecosystem in the form of timber. For the analysis of the inter-annual variations in sections 6.4.1.2 and 6.4.2.1, carbon fluxes were expressed in grams of carbon per square meter per year ($gC/m^2/yr$). For the regional assessments in sections 6.4.1.4 and 6.4.2.3, carbon fluxes were summed across the regions and expressed in teragrams of carbon per year (TgC/yr). Positive NECB indicates a gain of carbon to the ecosystem from the atmosphere, and negative NECB indicates a loss of carbon from the ecosystem to the atmosphere.

The uncertainty of carbon dynamics projected through the 21st century associated with climate forcing was estimated spatially by computing the range of change in NECB among the six climate simulations. For every 1-km grid cell and every climate scenario, the annual change in NECB was computed as the difference in the mean decadal NECB centered on 2095 and 2005 divided by the length of this period:

$$\Delta NECB = \frac{(NECB_{[2090-2099]} - NECB_{[2000-2009]})}{90} \quad (6.2)$$

The uncertainty was computed as the difference between the maximum and minimum ΔNECB among the six climate simulations.

Global warming potential (GWP) across time and the landscape was estimated taking into consideration that CH_4 has 25 times the GWP of CO_2 over a 100-year timeframe (Forster and others, 2007). GWP values were reported in CO_2 equivalent after first converting C-CH_4 fluxes to CH_4 equivalent by multiplying the fluxes by 16/12, the ratio of the molecular weight of CH_4 to the weight of carbon in CH_4, and then converting CH_4 equivalent fluxes to CO_2 equivalent by multiplying by 25. All C-CO_2 fluxes were converted to CO_2 equivalent by multiplying them by 44/12, the ratio of the molecular weight of CO_2 to the weight of carbon in CO_2. CH_4 production from fire emissions ($Fire_{(CH4)}$) was considered in addition to soil CH_4 uptake and emissions by applying emission factors among CO_2, CH_4, and CO on DOS-TEM simulations of fire emissions (French and others, 2002). The carbon in CO was considered CO_2 because it converts to CO_2 in the atmosphere within a year (Weinstock, 1969).

$$GWP = -44/12 \times (NPP - HR - Harvest - Fire_{(CO2+CO)}) + 25 \times 16/12 \times (Fire_{(CH4)} - BioCH_4) \quad (6.3)$$

Positive GWP indicates net CO_2 loss from the ecosystem to the atmosphere, and negative GWP indicates net CO_2 gain to the ecosystem from the atmosphere.

Analysis of the time series was conducted using linear regression and the Fisher test for test of significance on the time series. For the analysis of the inter-annual variations in sections 6.4.1.2 and 6.4.2.1, carbon fluxes were expressed in $gC/m^2/yr$ with associated standard deviation (s.d.). For the regional assessments in sections 6.4.1.4 and 6.4.2.3, carbon fluxes were summed across the regions and expressed in TgC/yr. The assumptions of normality and homoscedasticity were verified by examining residual plots. The relative effects of temperature, precipitation, total area burned, and atmospheric CO_2 concentration on the carbon fluxes were tested using multiple regression analysis. The effects were considered significant when the p-value is lower than 0.05.

6.4. Results and Discussion

6.4.1. Historical Assessment of Carbon Dynamics (1950–2009)

6.4.1.1. Model Validation and Verification

For the historical period of the simulations (1950–2009), soil and vegetation carbon stocks were validated when possible by comparing modeled and observed estimates at sites independent from the sites used for model parameterization. When independent data (that is, data collected outside of the sites used for model parameterization) were not available, a verification of modeled versus observed stocks was conducted on the same sites used for model parameterization.

Globally, no significant differences were observed between modeled and observed contemporary vegetation carbon stocks (table 6.3; p-value, $p=0.340$) and soil carbon stocks (table 6.4; $p=0.085$). In general, DOS-TEM simulations successfully reproduced differences between land-cover types. Arctic or alpine tundra and shrubland presented the lowest vegetation carbon stocks (table 6.3). Boreal land-cover types had intermediate vegetation carbon stocks and maritime upland forest presented the largest vegetation carbon stocks, with 19.3 kilograms of carbon per square meter (kgC/m^2) observed.

In contrast, arctic and alpine tundra and shrublands presented larger soil carbon stocks than boreal forests and maritime upland forest (table 6.4).

Table 6.3. Comparison of observed and modeled vegetation carbon stocks for the main upland land-cover types in Alaska.

[kgC/m^2, kilogram of carbon per square meter; NA, not applicable]

Land-cover type	Number of sites used for model testing	Vegetation carbon stocks (kgC/m^2)			
		Mean		Standard deviation	
		Observed	Modeled	Observed	Modeled
Black spruce forest	45	2.47	1.99	0.85	0.38
White spruce forest	20	4.40	4.29	0.74	0.32
Deciduous forest	24	6.85	6.56	0.46	0.85
Shrub tundra	4	1.81	2.26	0.12	0.50
Tussock tundra	3	0.56	0.44	0.26	0.21
Wet-sedge tundra	2	0.46	0.83	0.17	0.32
Heath tundra[1]	1	0.25	0.32	NA	NA
Maritime upland forest[1]	3	19.26	22.10	3.79	4.56
Maritime alder shrubland[1]	1	0.81	0.96	NA	NA

[1]Comparisons between observed and modeled vegetation carbon stocks have been conducted for parameterization (that is, verification).

Table 6.4. Comparison of observed and modeled soil carbon stocks for the main upland land-cover types in Alaska.

[kgC/m^2, kilogram of carbon per square meter; NA, not applicable]

Land-cover type	Number of sites used for model testing	Soil carbon stocks (kgC/m^2)			
		Mean		Standard deviation	
		Observed	Modeled	Observed	Modeled
Black spruce forest	40	29.85	46.84	11.15	55.64
White spruce forest	32	23.05	25.18	9.61	54.08
Deciduous forest	65	23.87	22.10	12.96	29.83
Shrub tundra	66	36.73	44.14	19.11	77.93
Tussock tundra	11	62.53	65.44	20.83	49.59
Wet-sedge tundra	23	42.01	50.73	30.49	31.46
Heath tundra	5	34.78	32.71	20.41	38.38
Maritime upland forest[1]	1	15.05	23.89	NA	NA
Maritime alder shrubland[1]	1	26.97	23.55	NA	NA

[1]Comparisons between observed and modeled soil carbon stocks have been conducted for parameterization (that is, verification).

6.4.1.2. Times Series for Upland Alaska

From 1950 to 2000, the long-term trend of vegetation carbon stocks in uplands increased slightly owing to an increase in NPP (fig. 6.3*A*). The increase of NPP (0.185 $gC/m^2/yr$, s.d. 0.254 $gC/m^2/yr$ computed for the entire study area) across the entire historical period was significant (fig. 6.3*C*; Fisher value, F=17.15; p<0.001). However, large fire years in 1957, 1969, 1977, 1990 and 1991 (fig. 6.3*D*) caused sudden decreases of vegetation carbon stocks (by 37 grams of carbon per square meter [gC/m^2], 28 gC/m^2, 3 gC/m^2, and 22 gC/m^2, respectively) that slowed carbon accumulation over the period. The intense fire years of 2004 and 2005 caused the largest loss of vegetation carbon stocks of the historical period—by 80 gC/m^2 over the two consecutive years—shifting the vegetation net change over the historical period from a net carbon gain by 2000 to a net carbon loss by 2009. For the entire historical period, 2.09 $gC/m^2/yr$ of vegetation carbon stocks was exported out of the ecosystem by forest harvest activities (fig. 6.3*D*). By 2009, the vegetation across upland Alaska lost 35.9 gC/m^2 from 1950.

Soil carbon stocks in upland Alaska remained relatively stable from 1950 to the late 1970s (fig. 6.3*B*). The large fire years 1957, 1969, and 1977 induced a loss of soil carbon stocks of 35 gC/m^2, 21 gC/m^2, and 17 gC/m^2, respectively. From the early 1980s through 2009, soil carbon stocks increased mostly because of increases in litterfall associated with increases in NPP and the increase in dead woody debris produced during wildfire, which more than offset the increase of carbon loss from heterotrophic respiration (fig. 6.3*E*) and carbon emissions from wildfire (fig. 6.3*D*). CH_4 uptake by the methanotrophs in upland Alaska is quite low (fig. 6.3*F*), ranging from 3.43 to 6.35 milligrams of carbon dioxide equivalent per square meter per year. The MDM-TEM simulation estimates Alaskan uplands to be a net sink of CH_4. Overall, soils across upland Alaska accumulated carbon throughout the historical period, increasing by 159 gC/m^2 from 1950 through 2009.

The mean NECB throughout the historical period was estimated at 1.66 $gC/m^2/yr$ (s.d. 3.82 $gC/m^2/yr$ computed amongst all five LCC regions; fig. 6.3*G*). Carbon gain to the ecosystem was mainly composed of net primary productivity, CH_4 uptake being negligible. Carbon loss from the ecosystem was composed of heterotrophic respiration (93.6 percent), wildfire emissions (4.7 percent), and forest harvest exports (1.6 percent). Despite the larger CH_4 emissions from fire compared to CH_4 uptake by methanotrophs, upland Alaska was on average a carbon sink through the historical period of –13.3 grams of carbon dioxide equivalent per square meter per year (gCO_2-$eq/m^2/yr$) (s.d. 33.8 gCO_2-$eq/m^2/yr$ computed amongst all five LCC regions; fig. 6.3*H*).

6.4.1.3. Environmental Drivers of the Temporal Variability of Net Ecosystem Carbon Balance in Upland Alaska

During the historical period, NPP was influenced primarily by mean annual temperature (table 6.5). Heterotrophic respiration increased during dry and warm years and large fire years. The positive relationship between heterotrophic respiration and large fire years might be related to (1) permafrost thaw in burned soils and (2) large inputs of carbon to the soil from the dead belowground vegetation biomass. Not surprisingly, fire emissions were driven

Table 6.5. Results of multiple linear regressions testing the main drivers of carbon dioxide and methane fluxes in upland ecosystems among the total annual precipitation, mean annual temperature, annual area burned, and mean annual atmospheric carbon dioxide (CO_2) concentration for the entire study area during the historical period (1950–2009).

[F, Fisher value; P, probability value. Trend: +, positive; –, negative; n.s., trend not significant. Units: mm, milllimeter; °C, degree Celsius; km^2, square kilometer; ppm, part per million]

Driver of carbon dioxide and methane fluxes	Net primary productivity			Heterotrophic respiration			Fire emissions			Methane uptake			Net ecosystem carbon balance		
	F	P	Trend	F	P	Trend	F	P	Trend	F	P	Trend	F	P	Trend
Total annual precipitation (mm)	3.37	0.07	n.s.	8.74	<0.01	–	0.02	0.89	n.s.	0.01	0.93	n.s.	0.94	0.34	n.s.
Mean annual temperature (°C)	14.29	0.00	+	5.78	0.02	+	1.18	0.28	n.s.	31.96	<0.01	+	0.33	0.57	n.s.
Annual area burned (km^2)	3.04	0.09	n.s.	10.29	<0.01	+	252.4	<0.01	+	19.59	<0.01	+	154.85	<0.01	–
Mean annual atmospheric CO_2 concentration (ppm)	1.83	0.07	n.s.	3.72	0.06	n.s.	1.29	0.26	n.s.	0.26	0.61	n.s.	7.43	0.01	+

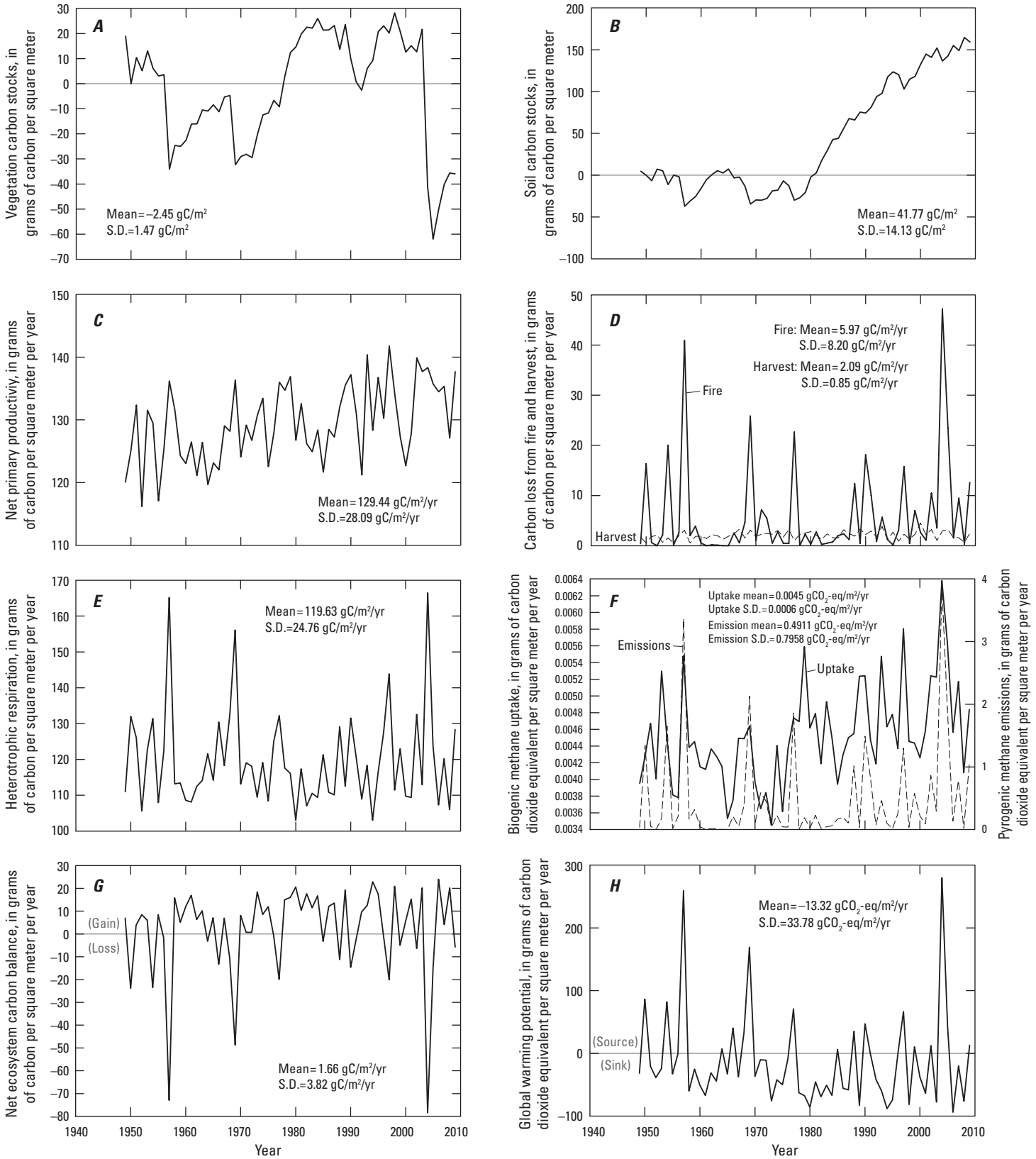

Figure 6.3. Time series of relative changes in carbon stocks and fluxes through the historical period (1950–2009). *A*, vegetation carbon stocks. *B*, soil carbon stocks. *C*, net primary productivity carbon flux. *D*, carbon loss from fire emissions and forest harvest exports. *E*, soil heterotrophic respiration. *F*, biogenic methane uptake and pyrogenic methane emissions. *G*, net ecosystem carbon balance. *H*, global warming potential. Mean and standard deviations for the entire study area are indicated in each panel.

primarily by large fire years. CH_4 uptake was positively correlated to air temperature and large fire years, perhaps because of the influence of fire on soil temperature. Finally, the primary drivers of the temporal variability of NECB were the fire activity and the atmospheric CO_2 concentration. The lack of effect of mean annual temperature on NECB was related to the fact that temperature had a positive effect on NPP and CH_4 uptake, which was offset by its positive effect on heterotrophic respiration.

6.4.1.4. Spatial Distribution of Net Ecosystem Carbon Balance Across Upland Alaska

The largest upland vegetation carbon stocks for the historical period are located in the Northwest Boreal LCC North and North Pacific LCC, whereas the largest soil carbon stocks are located in the Arctic and Western Alaska LCCs (table 6.6). Vegetation carbon storage decreased during the historical period in the regions that represent the largest vegetation carbon stocks: the Northwest Boreal LCC North and North Pacific LCC. The decrease of vegetation carbon stocks in the Northwest Boreal LCC North is related to carbon loss from fire. Carbon exports associated with forest harvest disturbance induced a decrease of vegetation carbon stocks in the North Pacific LCC (tables 6.6 and 6.7; chapter 5, section 5.5). The largest NPP and HR values were found in the two largest ecoregions (Northwest Boreal LCC North and Western Alaska LCC). The Northwest Boreal LCC North and Western Alaska LCC were the two major contributors to the regional total upland CH_4 uptake, together contributing more than 70 percent of the total regional uptake, followed by the Northwest Boreal LCC South and Arctic LCC, which each contributed around 10 percent of the total. Whereas loss of vegetation carbon stocks in the North Pacific LCC was offset

Table 6.6. Average vegetation and soil carbon stocks from the last decade (2000–2009) of the historical period and mean annual change in vegetation and soil carbon stocks between the first (1950–1959) and the last (2000–2009) decades of the historical period in each Landscape Conservation Cooperative region.

[Data may not add to totals shown because of independent rounding. TgC, teragram of carbon; km², square kilometer]

Landscape Conservation Cooperative (LCC) region	Upland total area (km²)	Upland cover (percent)	Vegetation carbon stocks (TgC)		Soil carbon stocks (TgC)	
			Average	Mean annual change	Average	Mean annual change
Arctic LCC	261,481	86	344	0.77	10,864	2.41
Western Alaska LCC	327,327	88	1,054	0.66	17,790	3.13
Northwest Boreal LCC North	335,491	73	1,272	–1.75	6,686	–3.37
Northwest Boreal LCC South	163,388	88	505	0.15	6,975	0.41
North Pacific LCC	150,087	97	1,119	–0.10	4,799	2.69
Total	**1,237,774**	**84**	**4,293**	**–0.26**	**47,113**	**5.27**

Table 6.7. Average vegetation and soil carbon fluxes in upland ecosystems per Landscape Conservation Cooperative region from 2000 through 2009.

[Data may not add to totals or compute to net ecosystem carbon balance shown because of independent rounding. CO, carbon monoxide; CO_2, carbon dioxide; TgC/yr, teragram of carbon per year; $TgCO_2$-eq/yr, teragram of carbon dioxide equivalent per year; NA, not applicable]

Landscape Conservation Cooperative (LCC) region	Fire emissions ($CO+CO_2$) (TgC/yr)	Pyrogenic methane emissions ($TgCO_2$-eq/yr)	Net primary productivity (TgC/yr)	Harvesting (TgC/yr)	Methane uptake ($TgCO_2$-eq/yr)	Heterotrophic respiration (TgC/yr)	Net ecosystem carbon balance (TgC/yr)	Global warming potential ($TgCO_2$-eq/yr)
Arctic LCC	2.47	0.26	32.14	NA	7.58×10^{-4}	26.48	3.18	–11.44
Western Alaska LCC	1.34	0.13	60.29	NA	1.74×10^{-3}	55.15	3.79	–13.78
Northwest Boreal LCC North	22.23	2.00	71.57	NA	2.89×10^{-3}	54.40	–5.12	20.57
Northwest Boreal LCC South	2.75	0.29	22.70	NA	7.61×10^{-4}	19.38	0.57	–1.82
North Pacific LCC	0.14	0.01	25.27	2.91	9.31×10^{-5}	19.62	2.59	–9.49
Total	**28.94**	**2.69**	**211.97**	**2.91**	$\mathbf{6.25\times10^{-3}}$	**175.03**	**5.01 (gain)**	**–15.96 (sink)**

by the increase in soil carbon stocks, resulting in a positive NECB (table 6.7), carbon loss from wildfire caused negative NECB in the Northwest Boreal LCC North, the largest ecoregion of Alaska. Statewide for the historical period, upland ecosystems were a carbon sink, gaining on average 5 TgC/yr. The Arctic and the North Pacific LCCs and southern portions of the Western Alaska LCC were hotspots of high carbon gain (blue shades in fig. 6.4*A*). Areas that lost carbon in Northwest Boreal LCC North mainly correspond to large historical fire scars (fig. 6.4*B*).

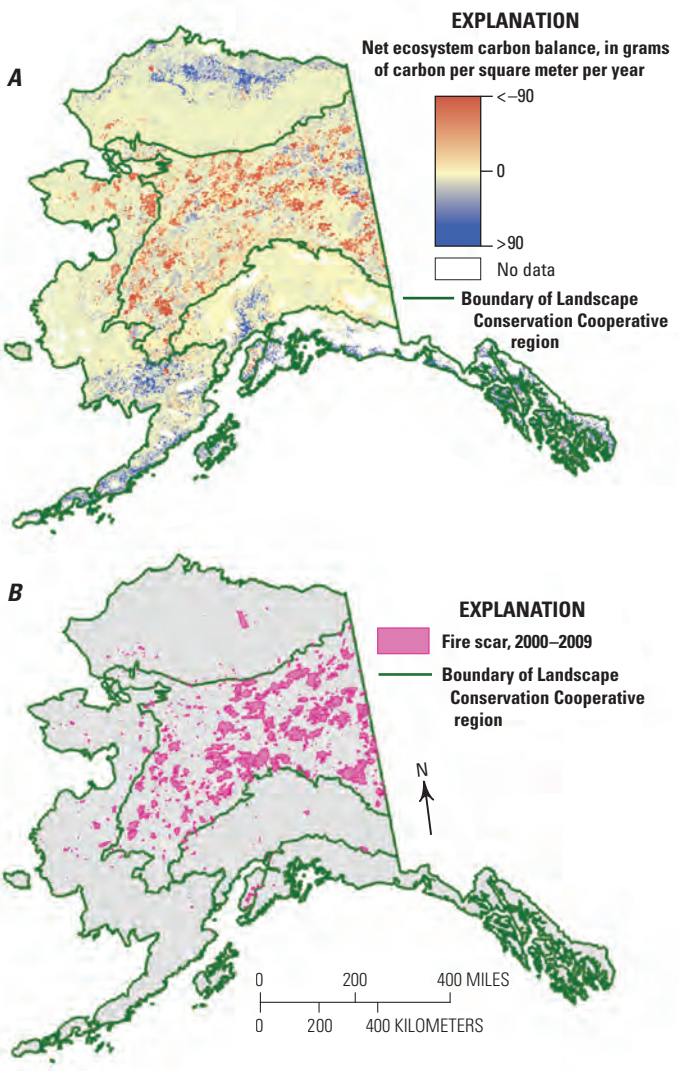

Figure 6.4. Spatial distribution of *A*, annual carbon loss and gain across upland Alaska during the historical period (1950–2009) and *B*, historical fire scars from 2000 through 2009 among the five Landscape Conservation Cooperative regions. See figure 7.2 for the distribution of uplands and wetlands in Alaska.

6.4.2. Assessment of Future Potential Carbon Dynamics (2010–2099)

6.4.2.1. Times Series for Upland Alaska

The carbon accumulation rate in vegetation was projected to increase over the 21st century for all climate simulations. The carbon accumulation rate was higher for the ECHAM5 simulations than for the CGCM3.1 simulations and higher for the highest CO_2 emissions scenarios (A2, followed by A1B and B1) (fig. 6.5*A*). From 2010 through 2099, the mean annual increase of vegetation carbon stocks would range from 310 gC/m^2/yr (under scenario B1 with CGCM3.1) to 579 gC/m^2/yr (under scenario A2 with ECHAM5). Carbon accumulation in the soil was quantitatively more important for the CGCM3.1 simulations than for the ECHAM5 simulations and higher for the higher CO_2 emissions scenarios (fig. 6.5*B*). From 2010 through 2099, the mean annual increase in soil carbon stocks would range from 296 gC/m^2/yr (under scenario A2 with ECHAM5) to 1,041 gC/m^2/yr (under scenario A2 with CGCM3.1). For all climate simulations, NPP and CH_4 uptake were projected to increase over the 21st century (figs. 6.5*C*, 6.5*F*), whereas heterotrophic respiration would not (fig. 6.5*E*). The projected increase in CH_4 uptake in the upland ecosystems is likely attributed to increasing microbial substrate availability as a result of increased vegetation productivity (van den Pol-van Dasselarr and others, 1998). Projected warming may also contribute to the enhanced metabolic activity of methanotroph microbes (Yonemura and others, 2000). The difference in magnitude of CH_4 uptake among emissions scenarios is generally greater than that between the GCMs. The A2 scenario has the highest projected increase in uptake, whereas the projected CH_4 uptake under scenario B1 does not differ significantly from the historical period, owing to the scenario's low anthropogenic CO_2 emissions. CH_4 emissions from wildfire would offset CH_4 uptake by methanotrophs in all climate scenarios (figs. 6.5*F*, 6.5*G*). The mean fire emissions for scenarios B1, A1B, and A2 were projected to be 9.7 gC/m^2/yr, 6.7 gC/m^2/yr, and 15.6 gC/m^2/yr for CGCM3.1 compared with 15.5 gC/m^2/yr, 17.0 gC/m^2/yr, and 18.2 gC/m^2/yr, respectively, for ECHAM5 simulations. CH_4 emissions represented 0.25 percent of the total projected carbon emissions from wildfire. The larger fire emissions associated with the ECHAM5 climate simulations compared with the CGCM3.1 simulations (fig. 6.5*D*) were mostly responsible for lower soil carbon accumulation with the ECHAM5 climate simulations compared with the CGCM3.1 simulations (fig. 6.5*B*).

The projected larger carbon accumulation in the ecosystem for the highest CO_2 emissions scenario was mostly related to the projected increase in ecosystem productivity in response to the fertilization effect of rising atmospheric CO_2

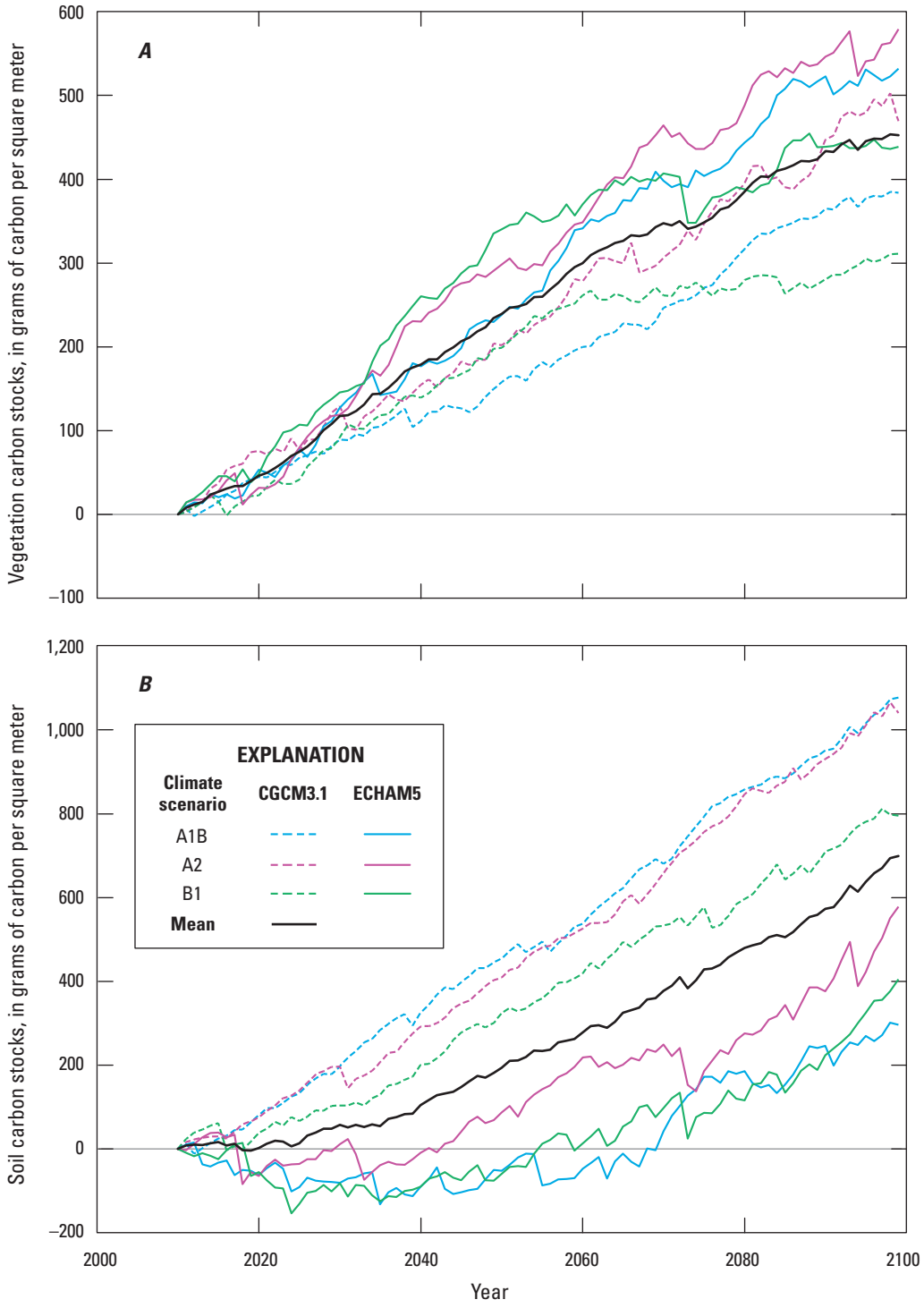

Figure 6.5 (pages 118–122). Time series of relative changes in carbon stocks and fluxes for the projection period (2010–2099) for the six climate simulations: *A*, vegetation carbon stocks; *B*, soil carbon stocks; *C*, net primary productivity; *D*, carbon loss from fire emissions; *E*, soil heterotrophic respiration; *F*, biogenic methane uptake; *G*, pyrogenic methane emissions; *H*, net ecosystem carbon balance; and *I*, global warming potential. Thick black lines represent annual averages amongst all six simulations. The six climate simulations are combinations of two general circulation models, version 3.1-T47 of the Coupled Global Climate Model (CGCM3.1) developed by the Canadian Centre for Climate Modelling and Analysis and version 5 of the European Centre Hamburg Model (ECHAM5) developed by the Max Planck Institute, and three climate scenarios of the Intergovernmental Panel on Climate Change's Special Report on Emissions Scenarios (Nakićenović and Swart, 2000), B1, A1B, and A2, in order of low to high projected CO_2 emissions.

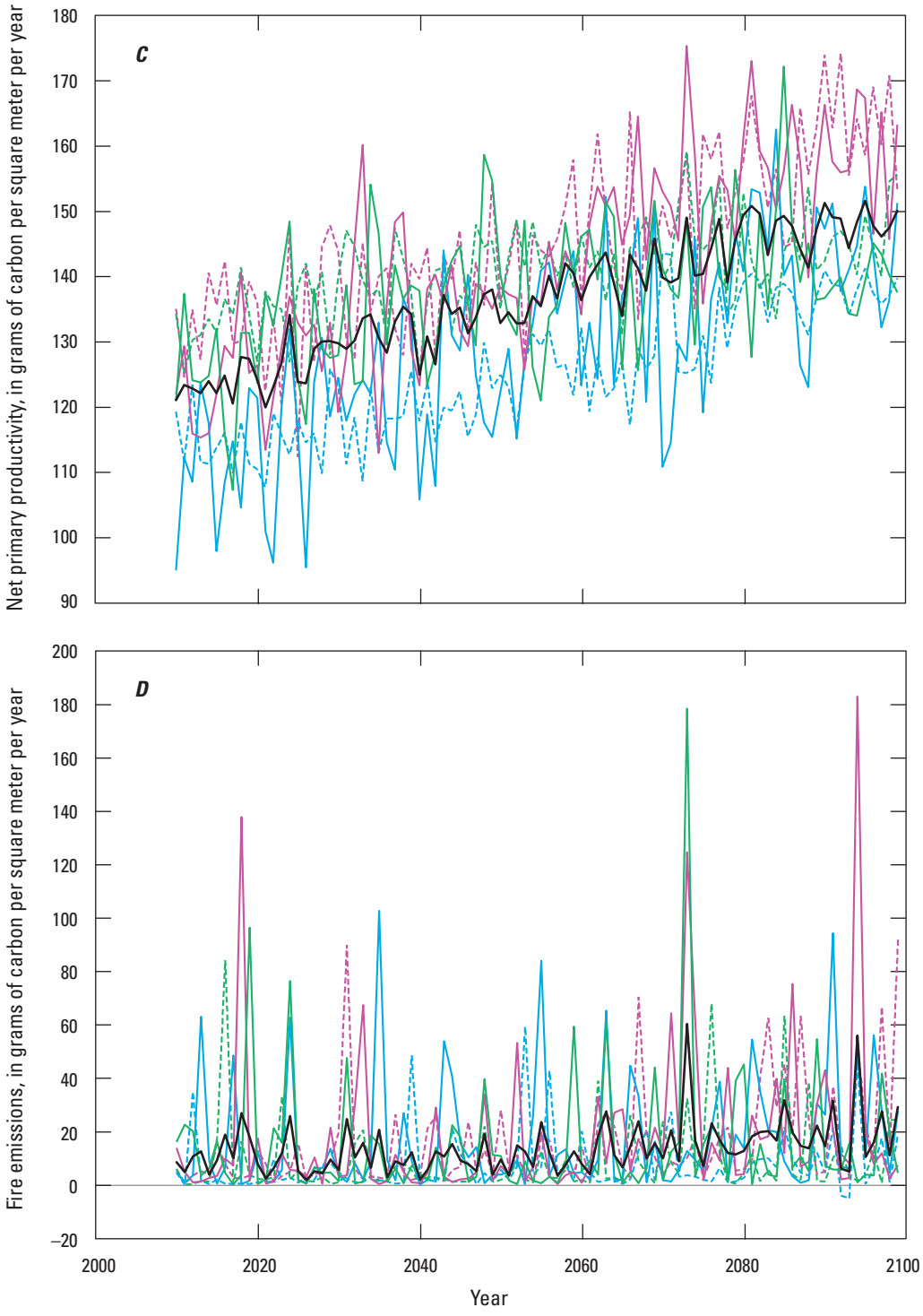

Figure 6.5.—Continued

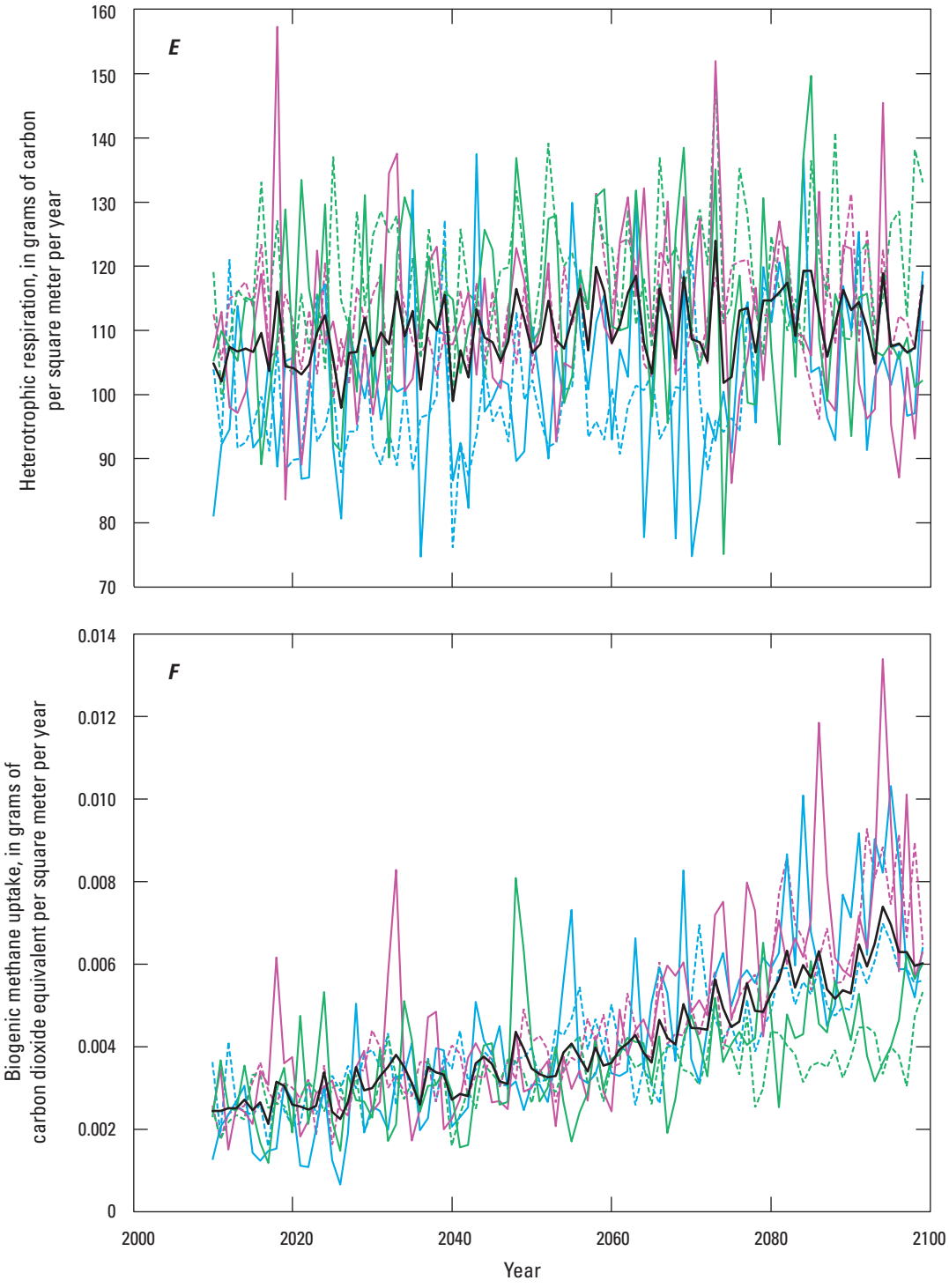

Figure 6.5.—Continued

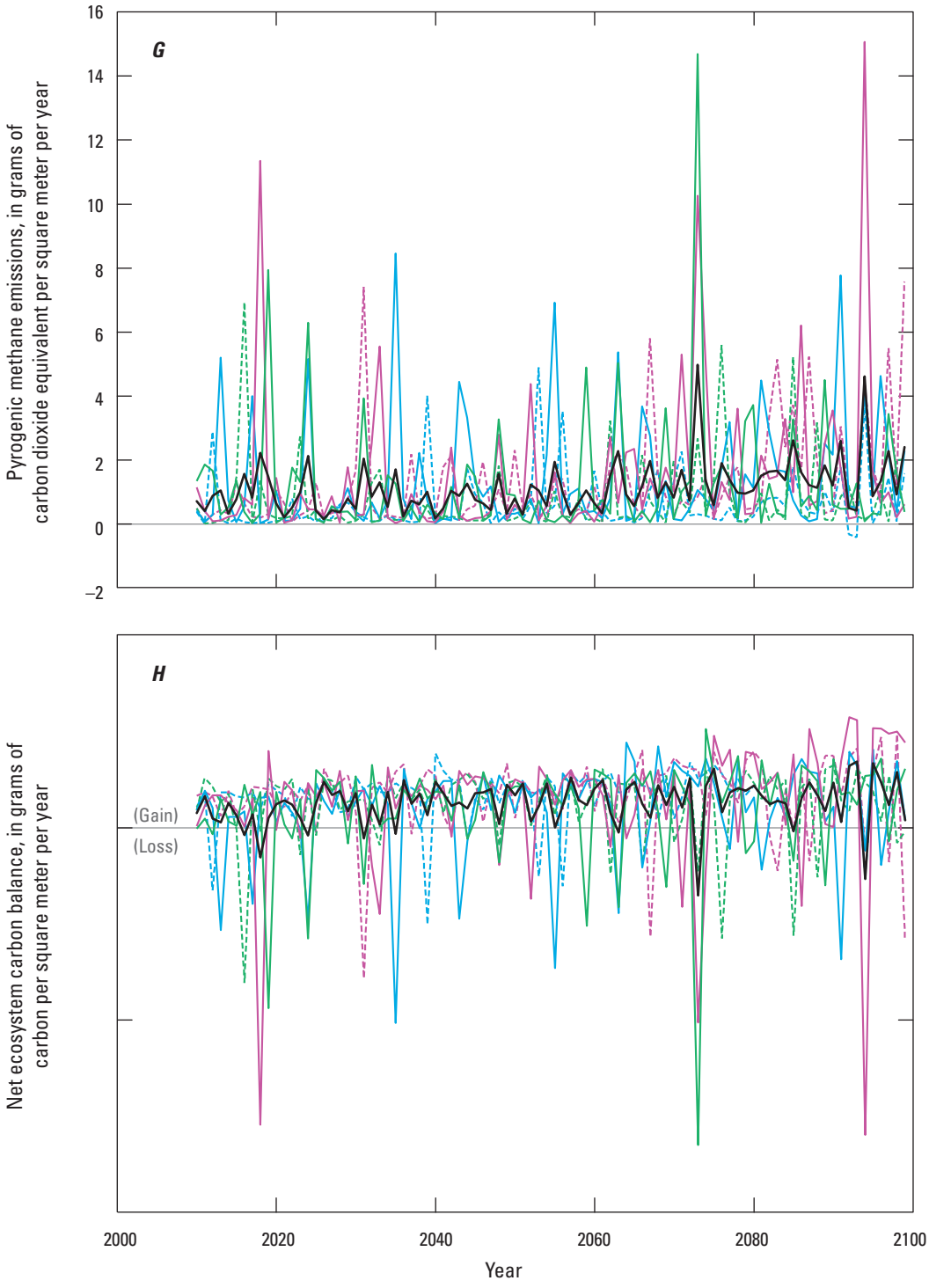

Figure 6.5.—Continued

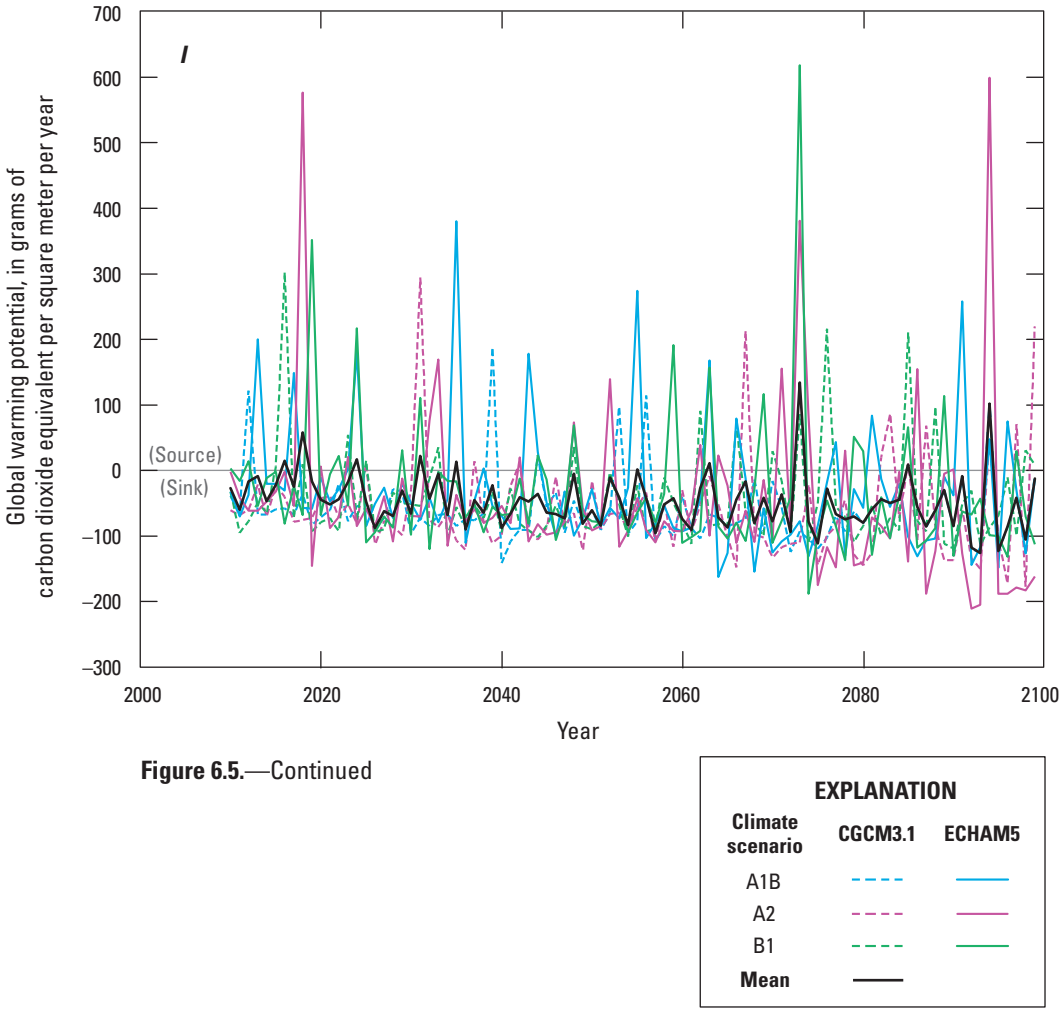

Figure 6.5.—Continued

concentration. NECB would increase during the 21st century for all scenarios (fig. 6.5*H*). However, this increase was only marginally significant because of the large inter-annual variability associated with large fire years (fig. 6.5*D*). On average, annual carbon gain in upland ecosystems in Alaska between 2010 and 2099 was projected to be 12.4 $gC/m^2/yr$, 17.1 $gC/m^2/yr$, and 17.0 $gC/m^2/yr$ for scenarios B1, A1B, and A2, respectively, with CGCM3.1 and 9.4 $gC/m^2/yr$, 9.3 $gC/m^2/yr$, and 12.9 $gC/m^2/yr$ for scenarios B1, A1B, and A2, respectively, with ECHAM5. Despite the large projected CH_4 emissions from wildfires, uplands in Alaska would be a CO_2 sink of –44.82 $gCO_2\text{-eq}/m^2/yr$, –61.12 $gCO_2\text{-eq}/m^2/yr$, and –62.2 $gCO_2\text{-eq}/m^2/yr$ for scenarios B1, A1B, and A2, respectively, with CGCM3.1 and –33.22 $gCO_2\text{-eq}/m^2/yr$, –32.82 $gCO_2\text{-eq}/m^2/yr$, and –45.8 $gCO_2\text{-eq}/m^2/yr$ for scenarios B1, A1B, and A2, respectively, with ECHAM5 for the same period.

6.4.2.2. Environmental Drivers of the Temporal Variability of Net Ecosystem Carbon Balance in Upland Alaska

Mean annual temperature was projected to positively control NPP and CH_4 uptake (table 6.8). Compared with similar analysis on the historical period, the present analysis across climate and CO_2 simulations projected a positive effect of atmospheric CO_2 concentration on NPP and CH_4 uptake, and as a result, NECB. Finally, annual area burned would influence heterotrophic respiration, fire emissions, and CH_4 uptake. As for the historical period, the positive effect of annual area burned on heterotrophic respiration and CH_4 uptake might be related to the effect of wildfire on soil temperature. The positive effect of area burned on heterotrophic respiration and fire emissions would cause a negative relationship between area burned and NECB.

Table 6.8. Results of multiple linear regressions testing the main drivers of carbon dioxide and methane fluxes in upland ecosystems among the total annual precipitation, mean annual temperature, annual area burned, and mean annual atmospheric carbon dioxide (CO_2) concentration for the entire study area during the projection period (2010–2099).

[F, Fisher value; P, probability value. Trend: +, positive; –, negative; n.s., trend not significant. Units: mm, milllimeter; °C, degree Celsius; km^2, square kilometer; ppm, part per million]

Driver of carbon dioxide and methane fluxes	Net primary productivity			Heterotrophic respiration			Fire emissions			Methane uptake			Net ecosystem carbon balance		
	F	P	Trend	F	P	Trend	F	P	Trend	F	P	Trend	F	P	Trend
Total annual precipitation (mm)	0.02	0.88	n.s.	1.69	0.19	n.s.	0.09	0.76	n.s.	3.89	0.05	n.s.	0.56	0.34	n.s.
Mean annual temperature (°C)	24.7	<0.01	+	2.61	0.11	n.s.	1.68	0.19	n.s.	89.4	<0.01	+	1.98	0.57	n.s.
Annual area burned (km^2)	1.68	0.19	n.s.	96.6	<0.01	+	1,144	<0.01	+	78.2	<0.01	+	997	<0.01	–
Mean annual atmospheric CO_2 concentration (ppm)	20.63	<0.01	+	0.72	0.39	n.s.	0.62	0.43	n.s.	85.2	<0.01	+	12.6	<0.01	+

6.4.2.3. Spatial Distribution of Net Ecosystem Carbon Balance Across Upland Alaska

Vegetation carbon stocks in uplands were projected to increase through the 21st century for the six climate simulations and all LCC regions of Alaska, except for the Northwest Boreal LCC South for the A1B and B1 scenarios with CGCM3.1. Statewide projected annual change in vegetation carbon stocks would range from 5.1 to 10.5 TgC/yr. As for the historical period, the largest vegetation carbon accumulation was projected for the North Pacific LCC and the Northwest Boreal LCC North (table 6.9). Soil carbon stocks would increase between 2000–2009 and 2090–2099 for all climate scenarios and LCC regions, except for ECHAM5 simulations in the Western Alaska LCC. In this region, precipitation was projected to increase the least, and some areas would likely experience some seasonal decreases in spring and summer (chapter 2, fig. 2.3). Drought stresses associated with these scenarios might decrease vegetation productivity in the Western Alaska LCC and also increase heterotrophic respiration and fire occurrence by decreasing soil moisture (table 6.10). Statewide, projected annual change in soil carbon stocks between 2000–2009 and 2090–2099 would range from 6.5 to 23.0 TgC/yr.

As a result, by the late 2090s, NECB would be positive for all LCC regions and climate simulations, ranging from 0.1 to 9.84 TgC/yr (table 6.10). Compared with the historical period, NECB would increase for each climate simulation, except for the ECHAM5 simulations in the Western Alaska LCC. Across Alaska, the increase in NPP associated with increasing air temperature would offset the carbon loss from increased wildfire and heterotrophic respiration.

The increase of NECB during the 21st century was higher for the model representing the lowest warming trend (CGCM3.1) compared with the model with the highest warming trend (ECHAM5). The negative relationship between change in NECB and warming was related to the effect of warming on wildfire regime that would offset the increase of vegetation productivity (table 6.11).

The spatial variability of the change in NECB over the 21st century was projected to be largest in the Northwest Boreal LCC North. As for the magnitude of NECB, this might be related to the active fire regime in the region (fig. 6.6*A*). The variability of the projected change in NECB among the six climate simulations was the highest in the Western Alaska LCC (fig. 6.6*B*). The largest uncertainty in this region might not only be related to the uncertainty related to climate and disturbance forcings (uncertainty illustrated in chapter 2, section 2.4.6.1), but also to (1) the weakness of the parameterization and (or) (2) the lack of representation of processes that are at play specifically in this region. The lack of observations in the Western Alaska LCC compared with the other ecoregions greatly limits our current understanding of the drivers of carbon dynamics in the region (fig. 6.6*C*).

Table 6.9. Average vegetation and soil carbon stocks for the last decade (2090–2099) of the projection period and mean annual change in vegetation and soil carbon stocks between the last decades of the historical period (2000–2009) and the projection period (2090–2099) per Landscape Conservation Cooperative region for each of the six climate simulations.

[The six climate simulations are combinations of two general circulation models, version 3.1-T47 of the Coupled Global Climate Model (CGCM3.1) developed by the Canadian Centre for Climate Modelling and Analysis and version 5 of the European Centre Hamburg Model (ECHAM5) developed by the Max Planck Institute, and three climate scenarios of the Intergovernmental Panel on Climate Change's Special Report on Emissions Scenarios (Nakićenović and Swart, 2000), B1, A1B, and A2, in order of low to high projected CO_2 emissions. Data may not add to totals shown because of independent rounding. TgC, teragram of carbon]

Climate scenario	Landscape Conservation Cooperative (LCC) region	Vegetation carbon stocks (TgC)		Soil carbon stocks (TgC)	
		Average	Mean annual change	Average	Mean annual change
		CGCM3.1			
A1B	Arctic LCC	430	0.94	11,424	6.1
	Western Alaska LCC	1,219	1.61	20,591	8.2
	Northwest Boreal LCC North	1,496	2.50	6,942	2.7
	Northwest Boreal LCC South	494	–0.16	7,942	2.0
	North Pacific LCC	1,340	2.30	9,902	3.9
	Total	**4,979**	**7.19**	**56,801**	**23.0**
A2	Arctic LCC	432	0.98	11,227	4.0
	Western Alaska LCC	1,238	2.04	18,176	4.3
	Northwest Boreal LCC North	1,500	2.53	7,197	5.7
	Northwest Boreal LCC South	520	0.17	7,186	2.3
	North Pacific LCC	1,370	2.79	4,979	2.0
	Total	**5,060**	**8.52**	**48,765**	**18.4**
B1	Arctic LCC	410	0.82	10,929	6.9
	Western Alaska LCC	1,137	0.88	19,236	4.6
	Northwest Boreal LCC North	1,423	1.69	6,796	1.7
	Northwest Boreal LCC South	497	–0.09	7,229	1.8
	North Pacific LCC	1,284	1.81	5,115	3.6
	Total	**4,751**	**5.11**	**49,305**	**18.6**
		ECHAM5			
A1B	Arctic LCC	473	1.41	11,106	3.0
	Western Alaska LCC	1,313	2.63	19411	–2.5
	Northwest Boreal LCC North	1,585	3.50	7,023	3.8
	Northwest Boreal LCC South	518	0.11	7,857	1.4
	North Pacific LCC	1,391	2.85	9,628	0.8
	Total	**5,281**	**10.50**	**55,024**	**6.5**
A2	Arctic LCC	473	1.45	11,190	3.8
	Western Alaska LCC	1,293	2.60	18,201	–0.6
	Northwest Boreal LCC North	1,600	3.65	7,079	4.3
	Northwest Boreal LCC South	526	0.24	6,974	1.0
	North Pacific LCC	1,343	2.47	4,856	0.8
	Total	**5,235**	**10.41**	**48,301**	**9.2**
B1	Arctic LCC	426	0.88	11,165	3.5
	Western Alaska LCC	1,226	1.87	17,815	–1.7
	Northwest Boreal LCC North	1,564	3.25	6,942	2.6
	Northwest Boreal LCC South	506	0.00	7,131	0.8
	North Pacific LCC	1,301	2.00	4,931	1.6
	Total	**5,024**	**8.01**	**47,984**	**6.7**

Table 6.10. Average annual vegetation and soil carbon fluxes for the last decade of the projection period (2090–2099) and mean annual change in net ecosystem carbon balance between the last decades of the historical period (2000–2009) and the projection period (2090–2099) per Landscape Conservation Cooperative region for each of the six climate simulations.

[The six climate simulations are combinations of two general circulation models, version 3.1-T47 of the Coupled Global Climate Model (CGCM3.1) developed by the Canadian Centre for Climate Modelling and Analysis and version 5 of the European Centre Hamburg Model (ECHAM5) developed by the Max Planck Institute, and three climate scenarios of the Intergovernmental Panel on Climate Change's Special Report on Emissions Scenarios (Nakićenović and Swart, 2000), B1, A1B, and A2, in order of low to high projected CO_2 emissions. Data may not add to totals or compute to net ecosystem carbon balance shown because of independent rounding. TgC/yr, teragram of carbon per year; $TgCO_2$-eq/yr, teragram of carbon dioxide equivalent per year]

Climate scenario	Landscape Conservation Cooperative (LCC) region	Net primary productivity (TgC/yr)	Hetero-trophic respiration (TgC/yr)	Fire emissions ($CO+CO_2$) (TgC/yr)	Pyrogenic methane emissions ($TgCO_2$-eq/yr)	Methane uptake ($TgCO_2$-eq/yr)	Net ecosystem carbon balance (TgC/yr)	Global warming potential ($TgCO_2$-eq/yr)	Mean annual change in net ecosystem carbon balance (TgC/yr)
				CGCM3.1					
A1B	Arctic LCC	40.7	33.6	0.1	0.01	-7.32×10^{-4}	7.02	–25.8	0.044
	Western Alaska LCC	74.0	53.7	10.5	1.06	-2.19×10^{-3}	9.84	–35.1	0.061
	Northwest Boreal LCC North	78.0	64.1	8.8	0.81	-3.99×10^{-4}	5.17	–18.2	0.115
	Northwest Boreal LCC South	24.0	20.0	2.2	0.21	-5.32×10^{-4}	1.88	–6.7	0.013
	North Pacific LCC	32.9	26.6	0.0	0.00	-1.50×10^{-4}	6.24	–22.9	0.041
	Total	**249.7**	**198.0**	**21.5**	**2.09**	**-3.99×10^{-3}**	**30.15**	**–108.7**	**0.274**
A2	Arctic LCC	45.7	21.9	18.7	1.93	-9.31×10^{-4}	5.02	–16.7	0.020
	Western Alaska LCC	78.1	23.9	47.8	4.89	-3.23×10^{-3}	6.34	–18.9	0.028
	Northwest Boreal LCC North	76.8	55.9	12.7	1.21	-5.32×10^{-3}	8.21	–29.0	0.148
	Northwest Boreal LCC South	25.4	15.3	7.5	0.76	-1.30×10^{-3}	2.51	–8.5	0.022
	North Pacific LCC	36.3	25.4	6.0	0.64	-1.80×10^{-4}	4.80	–17.0	0.025
	Total	**262.3**	**142.4**	**92.7**	**9.44**	**-1.10×10^{-2}**	**26.87**	**–90.1**	**0.243**
B1	Arctic LCC	41.0	33.3	0.1	0.01	-5.65×10^{-4}	7.69	–28.2	0.057
	Western Alaska LCC	69.9	52.4	12.0	1.19	-2.23×10^{-3}	5.48	–19.0	0.020
	Northwest Boreal LCC North	73.5	62.0	8.2	0.76	-3.23×10^{-3}	3.39	–11.8	0.096
	Northwest Boreal LCC South	23.0	16.0	5.3	0.54	-7.98×10^{-4}	1.74	–5.9	0.013
	North Pacific LCC	29.8	24.3	0.0	0.00	-7.65×10^{-5}	5.46	–20.0	0.031
	Total	**237.2**	**187.9**	**25.5**	**2.49**	**-6.98×10^{-3}**	**23.75**	**–84.9**	**0.216**
				ECHAM5					
A1B	Arctic LCC	51.3	24.1	22.7	2.33	-1.13×10^{-3}	4.42	–14.1	0.013
	Western Alaska LCC	83.3	26.3	56.8	5.82	-3.16×10^{-3}	0.10	4.9	−0.050
	Northwest Boreal LCC North	79.6	59.8	12.5	1.18	-5.65×10^{-3}	7.29	–25.7	0.138
	Northwest Boreal LCC South	25.9	15.0	9.4	0.94	-1.33×10^{-3}	1.55	–4.8	0.010
	North Pacific LCC	38.1	24.6	9.8	1.04	-2.09×10^{-4}	3.68	–12.6	0.013
	Total	**278.3**	**149.7**	**111.2**	**11.34**	**-1.16×10^{-2}**	**17.04**	**–52.4**	**0.124**
A2	Arctic LCC	51.2	23.9	22	2.27	-1.13×10^{-3}	5.21	–17.1	0.023
	Western Alaska LCC	84.1	35.3	46.6	4.78	-5.32×10^{-3}	1.97	–3.0	−0.022
	Northwest Boreal LCC North	81.2	61.4	11.9	1.11	-6.32×10^{-3}	7.91	–28.0	0.144
	Northwest Boreal LCC South	26.2	14.5	10.4	1.05	-1.83×10^{-3}	1.25	–3.6	0.008
	North Pacific LCC	33.8	26.2	4.3	0.45	-2.69×10^{-4}	3.24	–11.5	0.006
	Total	**276.5**	**161.3**	**95.3**	**9.66**	**-1.50×10^{-2}**	**19.57**	**–63.1**	**0.159**
B1	Arctic LCC	42.4	30.5	7.6	0.78	-7.65×10^{-4}	4.33	–15.2	0.012
	Western Alaska LCC	70.0	53.5	16.2	1.66	-2.63×10^{-3}	0.21	0.7	−0.041
	Northwest Boreal LCC North	74.1	63.5	4.8	0.45	-3.66×10^{-3}	5.81	–20.9	0.121
	Northwest Boreal LCC South	22.9	18.5	3.6	0.36	-8.31×10^{-4}	0.77	–2.5	0.002
	North Pacific LCC	31.5	24.1	3.8	0.40	-7.98×10^{-5}	3.60	–12.9	0.011
	Total	**240.9**	**190.1**	**36.0**	**3.66**	**-7.98×10^{-3}**	**14.72**	**–50.7**	**0.105**

Table 6.11. Change in decadal averages of mean annual net ecosystem carbon balance between the last decades of the historical period (2000–2009) and projection period (2090–2099) compared with corresponding changes in mean annual temperature, total annual precipitation, mean annual atmospheric carbon dioxide, (CO_2) concentration, and total area burned for each of the six climate change simulations.

[The six climate simulations are combinations of two general circulation models, version 3.1-T47 of the Coupled Global Climate Model (CGCM3.1) developed by the Canadian Centre for Climate Modelling and Analysis and version 5 of the European Centre Hamburg Model (ECHAM5) developed by the Max Planck Institute, and three climate scenarios of the Intergovernmental Panel on Climate Change's Special Report on Emissions Scenarios (Nakićenović and Swart, 2000), B1, A1B, and A2, in order of low to high projected CO_2 emissions. $gC/m^2/yr$, gram of carbon per square meter per year; °C/yr, degree Celsius per year; mm/yr, millimeter per year; ppm/yr, part per million per year; km^2, square kilometer]

Climate scenario	Change in mean annual net ecosystem carbon balance ($gC/m^2/yr$)	Change in mean annual temperature (°C/yr)	Change in total annual precipitation (mm/yr)	Change in mean annual atmospheric CO_2 concentration (ppm/yr)	Change in total area burned (km^2)
CGCM3.1					
A1B	30.17	0.031	1.27	3.72	386,165
A2	25.23	0.046	2.19	4.92	448,945
B1	21.71	0.018	0.83	1.88	353,393
ECHAM5					
A1B	14.16	0.059	1.89	3.72	623,016
A2	17.01	0.061	1.62	4.92	607,247
B1	11.56	0.038	1.09	1.88	504,987

6.5. Conclusion: Carbon Dynamics in Upland Alaska

We have examined carbon dynamics in upland ecosystems of Alaska for the two time periods using a modeling framework coupling biogeographic-disturbance and biogeochemical models. Through the historical period 1950–2009, we used historical climate and disturbance records to simulate annual carbon dynamics through upland Alaska. The assessment was conducted at a 1-km spatial resolution, which is unprecedented for Alaska and allows for integrating the effect of medium-scale diversity in vegetation composition and physiography on regional carbon dynamics. We also projected the potential changes in carbon dynamics through 2099 using a set of climate simulations that best represent the range of warming scenarios for the region. This set of climate simulations allowed us to quantify the uncertainty of future carbon balance in upland Alaska associated with the variability of climate projections.

During the historical period, upland ecosystems in Alaska were gaining 5 TgC/yr of carbon to the ecosystem (NECB); all LCC regions were net carbon sinks, except for the Northwest Boreal LCC North where large carbon losses from wildfire (specifically during large fire years in 1956, 1969, 1977, and in the 1990s and 2000s) in addition to carbon loss from heterotrophic respiration offset carbon gain from net primary productivity. Pyrogenic CH_4 emissions during the historical period were not enough to offset the carbon gain at the State level. Global warming potentials were therefore negative in Alaskan upland ecosystems, with a net carbon sink of –16 $TgCO_2$-eq/yr on average. The historical carbon simulations were validated by comparing modeled vegetation and soil carbon stocks in arctic and boreal ecosystems with independent field observations. Proper validation was not possible for the maritime forests because of the lack of independent, site-specific observations available in the region. Although climate and disturbance history are quite well constrained by field observations at the regional level, uncertainty remains on land-cover distribution and dynamics

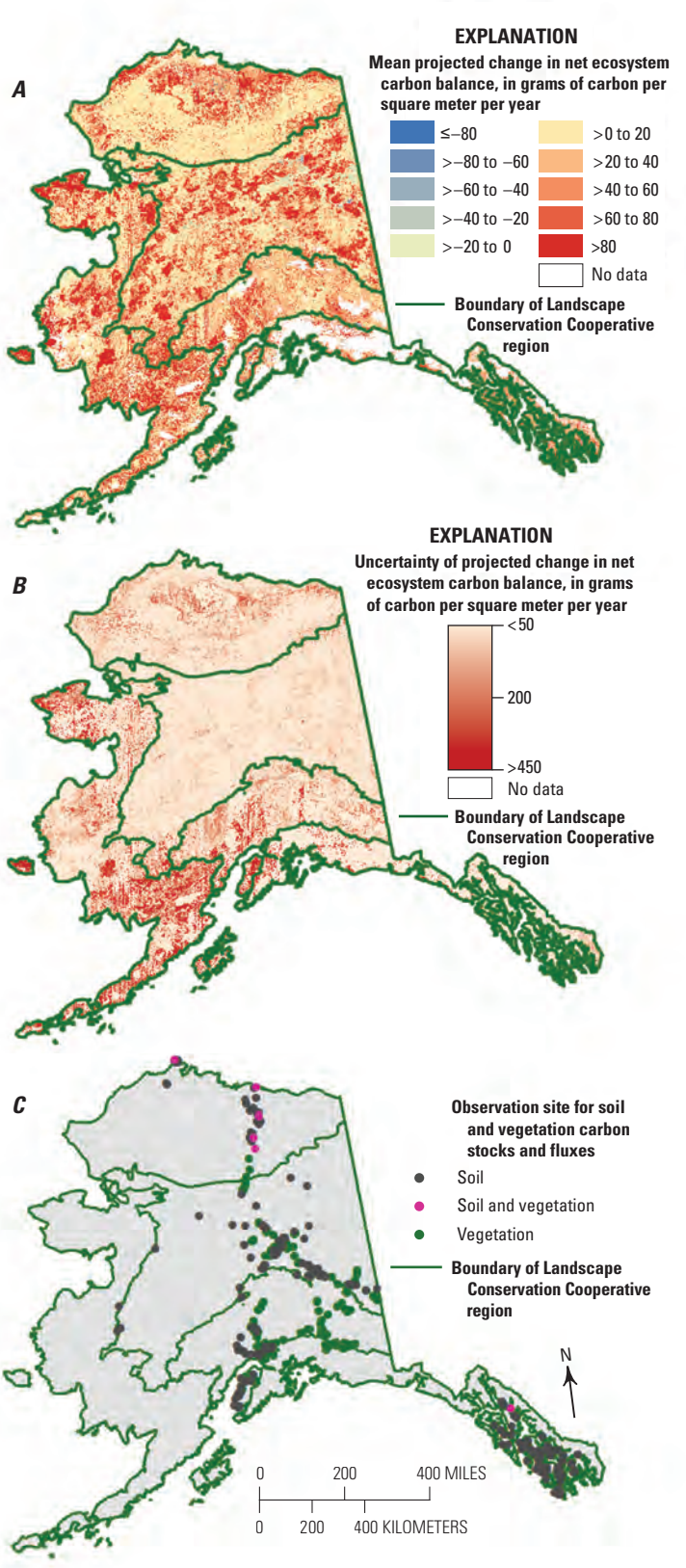

Figure 6.6. Spatial distribution of *A*, average mean change in net ecosystem carbon balance for all climate simulations between the last decades of the historical period (2000–2009) and the projection period (2090–2099) and *B*, corresponding uncertainty. *C*, Distribution of existing observation sites for soil and vegetation carbon stocks and fluxes.

in response to warming in the region. In the present assessment, vegetation was considered static through time. Future assessments may explore how the current vegetation distribution and the effect of fire and permafrost thaw on land cover will affect regional land carbon dynamics. Similarly, soil texture has a large effect on soil hydrologic fluxes that affect soil carbon and permafrost dynamics (see chapter 3), and large uncertainty remains on the spatial distribution of soil texture in Alaska (Liu and others, 2013).

During the projection period (2010–2099), all LCC regions of Alaska were projected to be carbon sinks. On average, upland ecosystems would store 22.0 TgC/yr, associated with the negative global warming potential of –75.0 $TgCO_2$-eq/yr (carbon sink) despite the projected increase in pyrogenic CH_4 emissions. The uncertainty of projected NECB associated with climate forcing would range from 14.7 to 30.2 TgC/yr statewide. Compared with the historical period, carbon storage in upland ecosystems was projected to increase between 0.105 and 0.274 TgC/yr by the end of the century. As shown in chapter 2, projected disturbance regimes associated with future climate changes are highly variable. The current assessment is based on a single disturbance scenario for each climate simulation that reproduces the best historical fire records. However, future assessments may explore the additional uncertainty of future carbon dynamics associated with multiple disturbance regimes.

6.6. References Cited

Alaback, P.B., 1982, Dynamics of understory biomass in Sitka spruce-western hemlock forests of southeast Alaska: Ecology, v. 63, no. 6, p. 1932–1948, http://dx.doi.org/10.2307/1940131.

Balshi, M.S., McGuire, A.D., Duffy, P., Flannigan, M., Kicklighter, D.W., and Melillo, J., 2009, Vulnerability of carbon storage in North American boreal forests to wildfires during the 21st century: Global Change Biology, v. 15, no. 6, p. 1491–1510, http://dx.doi.org/10.1111/j.1365-2486.2009.01877.x.

Balshi, M.S., McGuire, A.D., Zhuang, Q., Melillo, J., Kicklighter, D.W., Kasischke, E., Wirth, C., Flannigan, M., Harden, J., Clein, J.S., Burnside, T.J., McAllister, J., Kurz, W.A., Apps, M., and Shvidenko, A., 2007, The role of historical fire disturbance in the carbon dynamics of the pan-boreal region; A process-based analysis: Journal of Geophysical Research, v. 112, no. G2, article G02029, 18 p., http://dx.doi.org/10.1029/2006JG000380.

Binkley, Dan, 1982, Nitrogen fixation and net primary production in a young Sitka alder stand: Canadian Journal of Botany, v. 60, no. 3, p. 281–284, http://dx.doi.org/10.1139/b82-036.

Burn, C.R., Mackay, J.R., and Kokelj, S.V., 2009, The thermal regime of permafrost and its susceptibility to degradation in upland terrain near Inuvik, N.W.T.: Permafrost and Periglacial Processes, v. 20, no. 2, p. 221–227, http://dx.doi.org/10.1002/ppp.649.

Chapin, F.S., III, Woodwell, G.M., Randerson, J.T., Rastetter, E.B., Lovett, G.M., Baldocchi, D.D., Clark, D.A., Harmon, M.E., Schimel, D.S., Valentini, R., Wirth, C., Aber, J.D., Cole, J.J., Goulden, M.L., Harden, J.W., Heimann, M., Howarth, R.W., Matson, P.A., McGuire, A.D., Melillo, J.M., Mooney, H.A., Neff, J.C., Houghton, R.A., Pace, M.L., Ryan, M.G., Running, S.W., Sala, O.E., Schlesinger, W.H., and Schulze, E.-D., 2006, Reconciling carbon-cycle concepts, terminology, and methods: Ecosystems, v. 9, no. 7, p. 1041–1050, http://dx.doi.org/10.1007/s10021-005-0105-7.

Clein, J.S., McGuire, A.D., Zhang, X., Kicklighter, D.W., Melillo, J.M., Wofsy, S.C., Jarvis, P.G., and Massheder, J.M., 2002, Historical and projected carbon balance of mature black spruce ecosystems across North America; The role of carbon-nitrogen interactions: Plant and Soil, v. 242, no. 1, p. 15–32, http://dx.doi.org/10.1023/a:1019673420225.

Cole, E.C., Hanley, T.A., and Newton, Michael, 2010, Influence of precommercial thinning on understory vegetation of young-growth Sitka spruce forests in southeastern Alaska: Canadian Journal of Forest Research, v. 40, no. 4, p. 619–628, http://dx.doi.org/10.1139/X10-009.

Colt, Steve, Dugan, Darcy, and Fay, Ginny, 2007, The regional economy of southeast Alaska, final report, prepared for Alaska Conservation Foundation: Anchorage, Alaska, University of Alaska-Anchorage, Institute of Social and Economic Research, 134 p. [Also available at http://www.iser.uaa.alaska.edu/Publications/Southeast-EconomyOverviewfinal4.pdf.]

D'Amore, D.V., Fellman, J.B., Edwards, R.T., Hood, Eran, and Ping, C.-L., 2012, Hydropedology of the North American coastal temperate rainforest, *in* Lin, Henry, ed., Hydropedology; Synergystic integration of soil science and hydrology: Waltham, Mass., Academic Press, p. 351–380.

Deal, R.L., and Tappeiner, J.C., 2002, The effects of partial cutting on stand structure and growth of western hemlock–Sitka spruce stands in southeast Alaska: Forest Ecology and Management, v. 159, no. 3, p. 173–186, http://dx.doi.org/10.1016/S0378-1127(00)00727-1.

Dyrness, C.T., and Norum, R.A., 1983, The effects of experimental fires on black spruce forest floors in interior Alaska: Canadian Journal of Forest Research, v. 13, no. 5, p. 879–893, http://dx.doi.org/10.1139/x83-118.

Euskirchen, E.S., Bret-Harte, M.S., Scott, G.J., Edgar, C., Shaver, G.R., 2012, Seasonal patterns of carbon dioxide and water fluxes in three representative tundra ecosystems in northern Alaska: Ecosphere, v. 3, no. 1, article 4, 19 p., http://dx.doi.org/10.1890/ES11-00202.1.

Euskirchen, E.S., McGuire, A.D., and Chapin, F.S., III, 2007, Energy feedbacks of northern high-latitude ecosystems to the climate system due to reduced snow cover during 20th century warming: Global Change Biology, v. 13, no. 11, p. 2425–2438, http://dx.doi.org/10.1111/j.1365-2486.2007.01450.x.

Euskirchen, E.S., McGuire, A.D., Kicklighter, D.W., Zhuang, Q., Clein, J.S., Dargaville, R.J., Dye, D.G., Kimball, J.S., McDonald, K.C., Melillo, J.M., Romanovsky, V.E., and Smith, N.V., 2006, Importance of recent shifts in soil thermal dynamics on growing season length, productivity, and carbon sequestration in terrestrial high-latitude ecosystems: Global Change Biology, v. 12, no. 4, p. 731–750, http://dx.doi.org/10.1111/j.1365-2486.2006.01113.x.

Fisher, J.B., Sikka, M., Oechel, W.C., Huntzinger, D.N., Melton, J.R., Koven, C.D., Ahlström, A., Arain, M.A., Baker, I., Chen, J.M., Ciais, P., Davidson, C., Dietze, M., El-Masri, B., Hayes, D., Huntingford, C., Jain, A.K., Levy, P.E., Lomas, M.R., Poulter, B., Price, D., Sahoo, A.K., Schaefer, K., Tian, H., Tomelleri, E., Verbeeck, H., Viovy, N., Wania, R., Zeng, N., and Miller, C.E., 2014, Carbon cycle uncertainty in the Alaskan Arctic: Biogeosciences, v. 11, p. 4271–4288, http://dx.doi.org/10.5194/bg-11-4271-2014.

Flato, G.M., 2005, The third generation coupled global climate model (CGCM3) (and included links to the description of the AGCM3 atmospheric model): Canadian Centre for Climate Modelling and Analysis, available at http://ec.gc.ca/ccmac-cccma/default.asp?lang=En&n=1299529F-1.

French, N.H.F., Kasischke, E.S., and Williams, D.G., 2002, Variability in the emission of carbon-based trace gases from wildfire in the Alaskan boreal forest: Journal of Geophysical Research; Atmospheres, v. 107, no. D1, p. FFR 7–1 to FFR 7–11, http://dx.doi.org/10.1029/2001JD000480.

Genet, H., McGuire, A.D., Barrett, K., Breen, A., Euskirchen, E.S., Johnstone, J.F., Kasischke, E.S., Melvin, A.M., Bennett, A., Mack, M.C., Rupp, T.S., Schuur, E.A.G., Turetsky, M.R., and Yuan, F., 2013, Modeling the effects of fire severity and climate warming on active layer thickness and soil carbon storage of black spruce forests across the landscape in interior Alaska: Environmental Research Letters, v. 8, no. 4, letter 045016, 13 p., http://dx.doi.org/10.1088/1748-9326/8/4/045016.

Gillett, N.P., Weaver, A.J., Zwiers, F.W., and Flannigan, M.D., 2004, Detecting the effect of climate change on Canadian forest fires: Geophysical Research Letters, v. 31, no. 18, letter L18211, 4 p., http://dx.doi.org/10.1029/2004GL020876.

Global Soil Data Task Group, 2000, Global Gridded Surfaces of Selected Soil Characteristics (IGBP–DIS [International Geosphere-Biosphere Programme–Data and Information System]) dataset: Oak Ridge, Tenn., Oak Ridge National Laboratory Distributed Active Archive Center, http://dx.doi.org/10.3334/ORNLDAAC/569.

Gough, Laura, and Hobbie, S.E., 2003, Responses of moist non-acidic arctic tundra to altered environment; Productivity, biomass, and species richness: Oikos, v. 103, no. 1, p. 204–216, http://dx.doi.org/10.1034/j.1600-0706.2003.12363.x.

Gough, Laura, Moore, J.C., Shaver, G.R., Simpson, R.T., and Johnson, D.R., 2012, Above- and belowground responses of arctic tundra ecosystems to altered soil nutrients and mammalian herbivory: Ecology, v. 93, no. 7, p. 1683–1694, http://dx.doi.org/10.1890/11-1631.1.

Grosse, Guido, Harden, Jennifer, Turetsky, Merritt, McGuire, A.D., Camill, Philip, Tarnocai, Charles, Frolking, Steve, Schuur, E.A.G., Jorgenson, Torre, Marchenko, Sergei, Romanovsky, Vladimir, Wickland, K.P., French, Nancy, Waldrop, Mark, Bourgeau-Chavez, Laura, and Streigl, R.G., 2011, Vulnerability of high latitude soil carbon in North America to disturbance: Journal of Geophysical Research; Biogeosciences, v. 116, no. G4, article G00K06, 23 p., http://dx.doi.org/10.1029/2010JG001507.

Gustine, D.D., Brinkman, T.J., Lindgren, M.A., Schmidt, J.I., Rupp, T.S., and Adams, L.G., 2014, Climate-driven effects of fire on winter habitat for caribou in the Alaskan-Yukon Arctic: PLOS ONE, v. 9, no. 7, article e100588, 11 p., http://dx.doi.org/10.1371/journal.pone.0100588.

Harris, I., Jones, P.D., Osborn, T.J., and Lister, D.H., 2014, Updated high-resolution grids of monthly climatic observations—the CRU TS3.10 dataset: International Journal of Climatology, v. 34, no. 3, p. 623–642, http://dx.doi.org/10.1002/joc.3711.

Hay, L.E., Wilby, R.L., and Leavesley, G.H., 2000, A comparison of delta change and downscaled GCM scenarios for three mountainous basins in the United States: Journal of the American Water Resources Association, v. 36, no. 2, p. 387–397, http://dx.doi.org/10.1111/j.1752-1688.2000.tb04276.x.

Hayes, D.J., McGuire, A.D., Kicklighter, D.W., Gurney, K.R., Burnside, T.J., and Melillo, J.M., 2011, Is the northern high-latitude land-based CO_2 sink weakening?: Global Biogeochemical Cycles, v. 25, no. 3, article GB3018, 14 p., http://dx.doi.org/10.1029/2010gb003813.

Hayhoe, K.A., 2010, A standardized framework for evaluating the skill of regional climate downscaling techniques: Urbana-Champaign, Ill., University of Illinois, Ph.D. dissertation, 153 p. [Also available at http://hdl.handle.net/2142/16044.]

Johnson, K.D., Harden, Jennifer, McGuire, A.D., Bliss, N.B., Bockheim, J.G., Clark, Mark, Nettleton-Hollingsworth, Teresa, Jorgenson, M.T., Kane, E.S., Mack, Michelle, O'Donnell, Jonathan, Ping, C.-L., Schuur, E.A.G., Turetsky, M.R., and Valentine, D.W., 2011, Soil carbon distribution in Alaska in relation to soil-forming factors Geoderma, v. 167–168, p. 71–84, http://dx.doi.org/10.1016/j.geoderma.2011.10.006.

Johnstone, J.F., Rupp, T.S., Olson, Mark, and Verbyla, David, 2011, Modeling impacts of fire severity on successional trajectories and future fire behavior in Alaskan boreal forests: Landscape Ecology, v. 26, no. 4, p. 487–500, http://dx.doi.org/10.1007/s10980-011-9574-6.

Kasischke, E.S., and Turetsky, M.R., 2006, Recent changes in the fire regime across the North American boreal region—Spatial and temporal patterns of burning across Canada and Alaska: Geophysical Research Letters, v. 33, no. 9, letter L09703, 5 p., http://dx.doi.org/10.1029/2006GL025677.

Kasischke, E.S., Verbyla, D.L., Rupp, T.S., McGuire, A.D., Murphy, K.A., Jandt, Randi, Barnes, J.L., Hoy, E.E., Duffy, P.A., Calef, Monika, and Turetsky, M.R., 2010, Alaska's changing fire regime—Implications for the vulnerability of its boreal forests: Canadian Journal of Forest Research, v. 40, no. 7, p. 1313–1324, http://dx.doi.org/10.1139/X10-098.

Kasischke, E.S., Williams, David, and Barry, Donald, 2002, Analysis of the patterns of large fires in the boreal forest region of Alaska: International Journal of Wildland Fire, v. 11, no. 2, p. 131–144, http://dx.doi.org/10.1071/WF02023.

Liu, S., Wei, Y., Post, W.M., Cook, R.B., Schaefer, K., and Thornton, M.M., 2013, The Unified North American Soil Map and its implication on the soil organic carbon stock in North America: Biogeosciences, v. 10, no. 5, p. 2915–2930, http://dx.doi.org/10.5194/bg-10-2915-2013.

Mack, M.C., Bret-Harte, M.S., Hollingsworth, T.N., Jandt, R.R., Schuur, E.A.G., Shaver, G.R., and Verbyla, D.L., 2011, Carbon loss from an unprecedented Arctic tundra wildfire: Nature, v. 475, no. 7357, p. 489–492, http://dx.doi.org/10.1038/nature10283.

Malone, Thomas, Liang, Jingjing, and Packee, E.C., 2009, Cooperative Alaska Forest Inventory: U.S. Department of Agriculture, Forest Service, Pacific Northwest Research Station, General Technical Report PNW–GTR–785, 42 p. [Also available at http://www.fs.fed.us/pnw/pubs/pnw_gtr785.pdf.]

Mann, D.H., Rupp, T.S., Olson, M.A., and Duffy, P.A., 2012, Is Alaska's boreal forest now crossing a major ecological threshold?: Arctic, Antarctic, and Alpine Research, v. 44, no. 3, p. 319–331, http://dx.doi.org/10.1657/1938-4246-44.3.319.

McFarlane, N.A., Boer, G.J., Blanchet, J.-P., and Lazare, M., 1992, The Canadian Climate Centre second-generation general circulation model and its equilibrium climate: Journal of Climate, v. 5, no. 10, p. 1013–1044, http://dx.doi.org/10.1175/1520-0442(1992)005<1013:TCCCSG>2.0.CO;2.

McGuire, A.D., Anderson, L.G., Christensen, T.R., Dallimore, Scott, Guo, Laodong, Hayes, D.J., Heimann, Martin, Lorenson, T.D., Macdonald, R.W., and Roulet, Nigel, 2009, Sensitivity of the carbon cycle in the Arctic to climate change: Ecological Monographs, v. 79, no. 4, p. 523–555, http://dx.doi.org/10.1890/08-2025.1.

McGuire, A.D., Christensen, T.R., Hayes, D., Heroult, A., Euskirchen, E., Kimball, J.S., Koven, C., Lafleur, P., Miller, P.A., Oechel, W., Peylin, P., Williams, M., and Yi, Y., 2012, An assessment of the carbon balance of Arctic tundra; Comparisons among observations, process models, and atmospheric inversions: Biogeosciences, v. 9, p. 3185–3204, http://dx.doi.org/10.5194/bg-9-3185-2012.

McGuire, A.D., Hayes, D.J., Kicklighter, D.W., Manizza, M., Zhuang, Q., Chen, M., Follows, M.J., Gurney, K.R., McClelland, J.W., Melillo, J.M., Peterson, B.J., and Prinn, R.G., 2010, An analysis of the carbon balance of the Arctic Basin from 1997 to 2006: Tellus; Series B, Chemical and Physical Meteorology, v. 62B, no. 5, p. 455–474, http://dx.doi.org/10.1111/j.1600-0889.2010.00497.x.

McGuire, A.D., Melillo, J.M., Joyce, L.A., Kicklighter, D.W., Grace, A.L., Moore, B., III, and Vorosmarty, C.J., 1992, Interactions between carbon and nitrogen dynamics in estimating net primary productivity for potential vegetation in North America: Global Biogeochemical Cycles, v. 6, no. 2, p. 101–124, http://dx.doi.org/10.1029/92GB00219.

Nakićenović, Nebojša, and Swart, Robert, eds., 2000, Special report on emissions scenarios—A special report of Working Group III of the Intergovernmental Panel on Climate Change: Cambridge, United Kingdom, Cambridge University Press, 599 p., accessed [date], at http://www.ipcc.ch/ipccreports/sres/emission/index.php?idp=0.

Pan, Yude, Birdsey, R.A., Fang, Jingyun, Houghton, Richard, Kauppi, P.E., Kurz, W.A., Phillips, O.L., Shvidenko, Anatoly, Lewis, S.L., Canadell, J.G., Ciais, Philippe, Jackson, R.B., Pacala, S.W., McGuire, A.D., Piao, Shilong, Rautiainen, Aapo, Sitch, Stephen, and Hayes, Daniel, 2011, A large and persistent carbon sink in the world's forests: Science, v. 333, no. 6045, p. 988–993, http://dx.doi.org/10.1126/science.1201609.

Raich, J.W., Rastetter, E.B., Melillo, J.M., Kicklighter, D.W., Steudler, P.A., Peterson, B.J., Grace, A.L., Moore, B., III, and Vörösmarty, C.J., 1991, Potential net primary productivity in South America; Application of a global model: Ecological Applications, v. 1, no. 4, p. 399–429, http://dx.doi.org/10.2307/1941899.

Rakestraw, L.W., 1981, A history of the United States Forest Service in Alaska: Anchorage, Alaska, U.S. Department of Agriculture Forest Service, 137 p.

Rastetter, E.B., King, A.W., Cosby, B.J., Hornberger, G.M., O'Neill, R.V., and Hobbie, J.E., 1992, Aggregating fine-scale ecological knowledge to model coarser-scale attributes of ecosystems: Ecological Applications, v. 2, no. 1, p. 55–70, http://dx.doi.org/10.2307/1941889.

Roeckner, E., Bäuml, G., Bonaventura, L., Brokopf, R., Esch, M., Giorgetta, M., Hagemann, S., Kirchner, I., Kornblueh, L., Manzini, E., Rhodin, A., Schlese, U., Schulzweida, U., and Tompkins, A., 2003, The atmospheric general circulation model ECHAM5, part I—Model description: Max-Planck-Institut für Meteorologie Report, no. 349, 127 p. [Also available at https://www.mpimet.mpg.de/fileadmin/publikationen/Reports/max_scirep_349.pdf.]

Roeckner, E., Brokopf, R., Esch, M., Giorgetta, M., Hagemann, S., Kornblueh, L., Manzini, E., Schlese, U., and Schulzweida, U., 2004, The atmospheric general circulation model ECHAM5, part II—Sensitivity of simulated climate to horizontal and vertical resolution: Max-Planck-Institut für Meteorologie Report No. 354, 56 p. [Also available at http://pubman.mpdl.mpg.de/pubman/item/escidoc:995221:8/component/escidoc:995220/MPI_Report354.pdf.]

Ruess, R.W., Van Cleve, K., Yarie, J., Viereck, L.A., 1996, Contributions of fine root production and turnover to the carbon and nitrogen cycling in taiga forests of the Alaskan interior: Canadian Journal of Forest Research, v. 26, no. 8, p. 1326–1336, http://dx.doi.org/10.1139/x26-148.

Rupp, T.S., Chen, Xi, Olson, Mark, and McGuire, A.D., 2007, Sensitivity of simulated boreal fire dynamics to uncertainties in climate drivers: Earth Interactions, v. 11, no. 3, p. 1–21, http://dx.doi.org/10.1175/EI189.1.

Rupp, T.S., Starfield, A.M., and Chapin, F.S., III, 2000, A frame-based spatially explicit model of subarctic vegetation response to climatic change; Comparison with a point model: Landscape Ecology, v. 15, no. 4, p. 383–400, http://dx.doi.org/10.1023/A:1008168418778.

Rupp, T.S., Starfield, A.M., Chapin, F.S., III, and Duffy, P., 2002, Modeling the impact of black spruce on the fire regime of Alaskan boreal forest: Climatic Change, v. 55, no. 1–2, p. 213–233, http://dx.doi.org/10.1023/A:1020247405652.

Schaefer, Kevin, Zhang, Tingjin, Bruhwiler, Lori, and Barrett, A.P., 2011, Amount and timing of permafrost carbon release in response to climate warming: Tellus; Series B, Chemical and Physical Meteorology, v. 63B, no. 2, p. 165–180, http://dx.doi.org/10.1111/j.1600-0889.2011.00527.x.

Schuur, E.A.G., Abbott, B.W., Bowden, W.B., Brovkin, V., Camill, P., Canadell, J.G., Chanton, J.P., Chapin, F.S., III, Christensen, T.R., Ciais, P., Crosby, B.T., Czimczik, C.I., Grosse, G., Harden, J., Hayes, D.J., Hugelius, G., Jastrow, J.D., Jones, J.B., Kleinen, T., Koven, C.D., Krinner, G., Kuhry, P., Lawrence, D.M., McGuire, A.D., Natali, S.M., O'Donnell, J.A., Ping, C.L., Riley, W.J., Rinke, A., Romanovsky, V.E., Sannel, A.B.K., Schädel, C., Schaefer, K., Sky, J., Subin, Z.M., Tarnocai, C., Turetsky, M.R., Waldrop, M.P., Walter Anthony, K.M., Wickland, K.P., Wilson, C.J., and Zimov, S.A., 2013, Expert assessment of vulnerability of permafrost carbon to climate change: Climatic Change, v. 119, no. 2, p. 359–374, http://dx.doi.org/10.1007/s10584-013-0730-7.

Schuur, E.A.G., Bockheim, James, Canadell, J.G., Euskirchen, Eugenie, Field, C.B., Goryachkin, S.V., Hagemann, Stefan, Kuhry, Peter, Lafleur, P.M., Lee, Hanna, Mazhitova, Galina, Nelson, F.E., Rinke, Annette, Romanovsky, V.E., Shiklomanov, Nikolay, Tarnocai, Charles, Venevsky, Sergey, Vogel, J.G., and Zimov, S.A., 2008, Vulnerability of permafrost carbon to climate change; Implications for the global carbon cycle: BioScience, v. 58, no. 8, p. 701–714, http://dx.doi.org/10.1641/B580807.

Schuur, E.A.G., Vogel, J.G., Crummer, K.G., Lee, Hanna, Sickman, J.O., and Osterkamp, T.E., 2009, The effect of permafrost thaw on old carbon release and net carbon exchange from tundra: Nature, v. 459, no. 7246, p. 556–559, http://dx.doi.org/10.1038/nature08031.

Shaver, G.R., and Chapin, F.S., III, 1986, Effect of fertilizer on production and biomass of tussock tundra, Alaska, U.S.A.: Arctic and Alpine Research, v. 18, no. 3, p. 261–268. [Also available at http://dx.doi.org/10.2307/1550883.]

Shaver, G.R., and Chapin, F.S., III, 1991, Production; Biomass relationships and element cycling in contrasting arctic vegetation types: Ecological Monographs, v. 61, no. 1, p. 1–31, http://dx.doi.org/10.2307/1942997.

Sistla, S.A., Moore, J.C., Simpson, R.T., Gough, Laura, Shaver, G.R., and Schimel, J.P., 2013, Long-term warming restructures Arctic tundra without changing net soil carbon storage: Nature, v. 497, no. 7451, p. 615–618, http://dx.doi.org/10.1038/nature12129.

Sullivan, P.F., Sommerkorn, Martin, Rueth, H.M., Nadelhoffer, K.J., Shaver, G.R., and Welker, J.M., 2007, Climate and species affect fine root production with long-term fertilization in acidic tussock tundra near Toolik Lake, Alaska: Oecologia, v. 153, no. 3, p. 643–652, http://dx.doi.org/10.1007/s00442-007-0753-8.

Tarnocai, C., Canadell, J.G., Schuur, E.A.G., Kuhry, P., Mazhitova, G., and Zimov, S., 2009, Soil organic carbon pools in the northern circumpolar permafrost region: Global Biogeochemical Cycles, v. 23, no. 2, article GB2023, 11 p., http://dx.doi.org/10.1029/2008GB003327.

Turetsky, M.R., Kane, E.S., Harden, J.W., Ottmar, R.D., Manies, K.L., Hoy, Elizabeth, and Kasischke, E.S., 2011, Recent acceleration of biomass burning and carbon losses in Alaskan forests and peatlands: Nature Geoscience, v. 4, no. 1, p. 27–31, http://dx.doi.org/10.1038/ngeo1027.

van den Pol-van Dasselaar, A., van Beusichem, M.L., and Oenema, O., 1998, Effects of soil moisture content and temperature on methane uptake by grasslands on sandy soils: Plant and Soil, v. 204, no. 2, p. 213–22, http://dx.doi.org/10.1023/A:1004371309361.

Van Wijk, M.T., Williams, M., Gough, L., Hobbie, S.E., and Shaver, G.R., 2003, Luxury consumption of soil nutrients; A possible competitive strategy in above-ground and below-ground biomass allocation and root morphology for slow-growing arctic vegetation?: Journal of Ecology, v. 91, no. 4, p. 664–676, http://dx.doi.org/10.1046/j.1365-2745.2003.00788.x.

Weinstock, Bernard, 1969, Carbon monoxide—Residence time in the atmosphere: Science, v. 166, no. 3902, p. 224–225, http://dx.doi.org/10.1126/science.166.3902.224.

Whalen, S.C., and Reeburgh, W.S., 1990, Consumption of atmospheric methane by tundra soils: Nature, v. 346, no. 6280, p. 160–162, http://dx.doi.org/10.1038/346160a0.

Wickland, K.P., Neff, J.C., and Harden, J.W., 2010, The role of soil drainage class in carbon dioxide exchange and decomposition in boreal black spruce (*Picea mariana*) forest stands: Canadian Journal of Forest Research, v. 40, no. 11, p. 2123–2134, http://dx.doi.org/10.1139/X10-163.

Woo, M.-K., Arain, M.A., Mollinga, M., and, Yi, S., 2004, A two-directional freeze and thaw algorithm for hydrologic and land surface modelling: Geophysical Research Letters, v. 31, no. 12, letter L12501, 4 p., http://dx.doi.org/10.1029/2004GL019475.

Yi, Shuhua, Arain, M.A., and Woo, M.-K., 2006, Modifications of a land surface scheme for improved simulation of ground freeze-thaw in northern environments: Geophysical Research Letters, v. 33, no. 13, letter L13501, 5 p., http://dx.doi.org/10.1029/2006GL026340.

Yi, Shuhua, Manies, Kristen, Harden, Jennifer, and McGuire, A.D., 2009, Characteristics of organic soil in black spruce forests; Implications for the application of land surface and ecosystem models in cold regions: Geophysical Research Letters, v. 36, no. 5, letter L05501, 5 p., http://dx.doi.org/10.1029/2008GL037014.

Yi, Shuhua, McGuire, A.D., Harden, Jennifer, Kasischke, Eric, Manies, Kristen, Hinzman, Larry, Liljedahl, Anna, Randerson, Jim, Liu, Heping, Romanovsky, Vladimir, Marchenko, Sergei, and Kim, Yongwon, 2009, Interactions between soil thermal and hydrological dynamics in the response of Alaska ecosystems to fire disturbance: Journal of Geophysical Research; Biogeosciences, v. 114, no. G2, article G02015, 20 p., http://dx.doi.org/10.1029/2008JG000841.

Yi, Shuhua, McGuire, A.D., Kasischke, Eric, Harden, Jennifer, Manies, Kristen, Mack, Michelle, and Turetsky, Merritt, 2010, A dynamic organic soil biogeochemical model for simulating the effects of wildfire on soil environmental conditions and carbon dynamics of black spruce forests: Journal of Geophysical Research; Biogeosciences, v. 115, no. G4, article G04015, 15 p., http://dx.doi.org/10.1029/2010JG001302.

Yonemura, S., Kawashima, S., Tsuruta, H., 2000, Carbon monoxide, hydrogen, and methane uptake by soils in a temperate arable field and a forest: Journal of Geophysical Research; Atmospheres, v. 105, no. D11, p. 14347–14362.

Yoshikawa, Kenji, Bolton, W.R., Romanovsky, V.E., Fukuda, Masami, and Hinzman, L.D., 2002, Impacts of wildfire on the permafrost in the boreal forests of interior Alaska: Journal of Geophysical Research; Atmospheres, v. 107, no. D1, p. FFR 4–1 to FFR 4–14, http://dx.doi.org/10.1029/2001JD000438.

Yuan, F.-M., Yi, S.-H., McGuire, A.D., Johnson, K.D., Liang, J., Harden, J.W., Kasischke, E.S., and Kurz, W.A., 2012, Assessment of boreal forest historical C dynamics in the Yukon River Basin; Relative roles of warming and fire regime change: Ecological Applications, v. 22, no. 8, p. 2091–2109, http://dx.doi.org/10.1890/11-1957.1.

Zhuang, Q., McGuire, A.D., Melillo, J.M., Clein, J.S., Dargaville, R.J., Kicklighter, D.W., Myneni, R.B., Dong, J., Romanovsky, V.E., Harden, J., and Hobbie, J.E., 2003, Carbon cycling in extratropical terrestrial ecosystems of the Northern Hemisphere during the 20th century; A modeling analysis of the influences of soil thermal dynamics: Tellus; Series B, Chemical and Physical Meteorology, v. 55B, no. 3, p. 751–776, http://dx.doi.org/10.1034/j.1600-0889.2003.00060.x.

Zhuang, Q., McGuire, A.D., O'Neill, K.P., Harden, J.W., Romanovsky, V.E., and Yarie, J., 2002, Modeling soil thermal and carbon dynamics of a fire chronosequence in interior Alaska: Journal of Geophysical Research; Atmospheres, v. 107, no. D1, p. FFR 3–1 to FFR 3–26, http://dx.doi.org/10.1029/2001JD001244.

Zhuang, Q., Melillo, J.M., Kicklighter, D.W., Prinn, R.G., McGuire, A.D., Steudler, P.A., Felzer, B.S., and Hu, S., 2004, Methane fluxes between terrestrial ecosystems and the atmosphere at northern high latitudes during the past century; A retrospective analysis with a process-based biogeochemistry model: Global Biogeochemical Cycles, v. 18, no. 3, article GB3010, 23 p., http://dx.doi.org/10.1029/2004gb002239.

Zhuang, Q., Romanovsky, V.E., and McGuire, A.D., 2001, Incorporation of a permafrost model into a large-scale ecosystem model; Evaluation of temporal and spatial scaling issues in simulating soil thermal dynamics: Journal of Geophysical Research; Atmospheres, v. 106, no. D24, p. 33649–33670, http://dx.doi.org/10.1029/2001jd900151.

Zimov, S.A., Schuur, E.A.G., and Chapin, F.S., III, 2006, Permafrost and the global carbon budget: Science, v. 312, no. 5780, p. 1612–1613, http://dx.doi.org/10.1126/science.1128908.

Chapter 7. Terrestrial Carbon Modeling: Baseline and Projections in Lowland Ecosystems of Alaska

By Yujie He,[1] Hélène Genet,[2] A. David McGuire,[3] Qianlai Zhuang,[1] Bruce K. Wylie,[4] and Yujin Zhang[2]

7.1. Highlights

- The total area of wetland in Alaska was estimated at 177,069 square kilometers (km^2), which represents nearly 12 percent of the total land surface area (including uplands and inland waters) of the State.
- During the historical period (1950–2009), wetland ecosystems in Alaska lost carbon at a rate of 1.3 teragrams of carbon per year (TgC/yr). The loss was the result of the net carbon source in the Northwest Boreal Landscape Conservation Cooperative (LCC) North, which overrode gains in all other LCC regions in Alaska to yield a net carbon loss statewide.
- Historical biogenic and pyrogenic methane (CH_4) emissions from Alaska wetland ecosystems were estimated to average about 27.93 teragrams of carbon dioxide equivalent per year ($TgCO_2$-eq/yr) and 0.466 $TgCO_2$-eq/yr during the 1950s, respectively. Biogenic and pyrogenic CH_4 emissions significantly increased from 1950 through 2009 by 0.977 grams of carbon dioxide equivalent per square meter per year (gCO_2-eq/m^2/yr) and 0.037 gCO_2-eq/m^2/yr, respectively. The global warming potential (GWP) of wetlands over the historical period indicates a significant source of greenhouse gas forcing of 33 $TgCO_2$-eq/yr.
- By the end of the 21st century, wetland ecosystems of all LCC regions of Alaska were projected to gain carbon, storing between 3.0 and 5.3 TgC/yr statewide by the 2090s, depending on the climate change simulations used in the assessment.
- Future mean annual CH_4 emissions are estimated to range from 37 to 90 $TgCO_2$-eq/yr by 2090–2099, depending on the climate change simulations used in the assessment, representing an increase of 15 to 182 percent compared with those of 2000–2009. The large warming potential of CH_4 emissions would be enough to offset the cooling effect of carbon gain statewide. The average annual GWP of wetlands over the projection period indicates a potential significant source of greenhouse gas forcing of 17 to 64 $TgCO_2$-eq/yr, despite the net carbon storage to wetland ecosystems.
- Biogenic CH_4 emissions during the historical and future periods were found to be positively correlated with the atmospheric carbon dioxide (CO_2) concentrations; future CH_4 emissions were also projected to be significantly influenced by mean annual temperature.

7.2. Introduction

Wetlands accumulate peat owing to positive net ecosystem carbon balance, where net primary productivity and associated litterfall exceeds soil carbon loss from decomposition and methane production (Frolking and Roulet, 2007). Methane (CH_4) is currently the second most important anthropogenic greenhouse gas, for which wetlands are the single largest natural source. CH_4 emissions from high-latitude wetlands are an important component of the global climate system (Fisher and others, 2014). There is major concern about potential feedbacks between the climate system and CH_4 emissions from wetlands, as climate, atmospheric carbon dioxide (CO_2) concentrations, and deposition of sulfate and nitrogen are all known to affect CH_4 emissions positively or negatively (Forster and others, 2007). There is compelling evidence that CH_4 emissions from wetlands have been strongly responsive to climate

[1]Purdue University, West Lafayette, Ind.

[2]University of Alaska-Fairbanks, Fairbanks, Alaska.

[3]U.S. Geological Survey, Fairbanks, Alaska.

[4]U.S. Geological Survey, Sioux Falls, S. Dak.

in the past (He and others, 2014) and will likely continue to be responsive to anthropogenically driven climate change in the future. The high sensitivity of CH_4 emissions to soil temperature and moisture conditions and its subsequent effect on the climate system is an important issue to assess in northern high latitudes, because this region contains nearly half of the world's wetlands (Lehner and Döll, 2004) and because high latitudes have been and are forecast to continue experiencing more rapid warming than elsewhere (Stocker and others, 2013). Another concern is the potential release of previously frozen, labile soil carbon from thawing permafrost in the form of CO_2 and (or) CH_4 through mineralization owing to climate warming over the next century (Schuur and others, 2008; Koven and others, 2011; Schaefer and others, 2011).

In addition to high vulnerability for carbon loss from CH_4 production, wetlands, especially in boreal regions, are susceptible to carbon loss from wildfires. Wetlands generally burn less frequently than uplands because poorly drained conditions are responsible for low flammability, which minimizes fire activity in wetlands compared with better drained uplands. However, extended periods of dry weather along with increased occurrence of late-season burning (Kasischke and Turetsky, 2006) and changes in drainage conditions have the potential to trigger deep organic soil burning in wetlands (Turetsky and others, 2011), making these ecosystems potentially more vulnerable to fire and carbon loss. Wetland distribution also has local effects on wildlife habitat and subsistence resources (Grand and others, 1997). For instance, wetlands are refuges to a number of waterbird species that migrate from across the world to breed in the wetlands of Alaska (Martin and others, 2009). Wetlands are also an important habitat for moose, which represent an important source of food for local populations (Martin and others, 2009). Because of their importance in local and regional carbon dynamics and biodiversity, accurate distribution of wetlands across Alaska is of great importance. However, mapping wetlands in Alaska using remote sensing is challenging, and specific wetland classes, such as bogs, are particularly difficult to discriminate because woody overstory vegetation can block understory wetland vegetation and surface water. To assess carbon dynamics in the wetlands of Alaska, we developed a wetland distribution map that separated bogs and fens using the Alaska National Wetlands Inventory as a reference dataset.

In this chapter, we present a modeling synthesis of changes in carbon stocks and CH_4 emissions and other carbon fluxes among the soil, the vegetation, and the atmosphere over the historical period (1950–2009) and projection period (2010–2099) for Alaska. The modeling framework we used in this assessment couples a wildfire disturbance model with two process-based ecosystem models to estimate current and projected carbon stocks and CO_2 and CH_4 fluxes for wetlands in Alaska. Projections were made for two climate models that simulated future climates for each of three different CO_2 emissions scenarios to estimate uncertainties in future climate forcing. We used the wetland distribution map to quantify CH_4 emissions over the historical and future time period in Alaska.

7.3. Methods

7.3.1. Methane Dynamics Module of the Terrestrial Ecosystem Model (MDM-TEM) Description

Changes in soil and vegetation carbon stocks and CO_2 fluxes in response to climate change and disturbances were simulated using a modeling framework that couples the output of a wildfire disturbance model, the Alaska Frame-Based Ecosystem Code (ALFRESCO; Rupp and others, 2000, 2002, 2007; see chapter 2), to a process-based ecosystem model that simulates carbon and nitrogen pools and CO_2 dynamics, the Dynamic Organic Soil version of the Terrestrial Ecosystem Model (DOS-TEM; Yi, Manies, and others, 2009; Yi, McGuire, and others, 2009; Yi and others, 2010; Genet and others, 2013; see chapter 6). Changes in biogenic CH_4 fluxes were simulated by coupling the output of DOS-TEM with the Methane Dynamics Module (MDM) of the Terrestrial Ecosystem Model (MDM-TEM; Zhuang and others, 2004). The ALFRESCO and DOS-TEM aspects of the model framework used in this assessment are described in chapters 2 and 6. Here we will provide a detailed description of MDM-TEM. MDM-TEM simulates biogenic CH_4 dynamics at daily timesteps for the Terrestrial Ecosystem Model (TEM) and explicitly considers the process of CH_4 production (methanogenesis) as well as CH_4 oxidation (methanotrophy) and the transport of the gas from the soil to the atmosphere (Zhuang and others, 2004). The MDM has been coupled to several existing TEM modules, including the core carbon and nitrogen dynamics module (Zhuang and others, 2003), the soil thermal module that incorporates permafrost dynamics (Zhuang and others, 2001), and a hydrological module that simulates water movements across an atmosphere-vegetation-soil continuum (Zhuang and others, 2002, 2004). Specifically, the soil component of the hydrological module considers moisture dynamics explicitly in moss, organic soil, and mineral soil layers (Zhuang and others, 2002, 2004), and is designed to consider fluctuations in water table depth.

In the MDM-TEM, the fluxes of CH_4 between soils and the atmosphere depend on the relative rates of CH_4 production and oxidation within the soil profile and the transport of CH_4 across the surface of soils. The soil in the model is separated into an upper unsaturated zone and a lower saturated zone according to the water table depth. The net emissions (or uptake) of CH_4 between the soil and the atmosphere are the balance between CH_4 production and oxidation. If the rate of production is larger than the rate of oxidation within the soil profile, CH_4 will be emitted to the atmosphere through diffusion. In wetland ecosystems, two other pathways in addition to diffusion are important for CH_4 transport to the atmosphere. One is plant-aided transport, where CH_4 can move through aerenchyma tissues (that is, "hollow tubes") that run from the roots through the stems to the leaves of some plants. Another is ebullition, where a high concentration of CH_4 causes the formation of CH_4 bubbles that can move through the overlying water or soils and escape into the atmosphere.

CH_4 production is modeled as an anaerobic process that occurs in the saturated zone of the soil profile and is influenced by (1) substrate availability, which is a function of net primary productivity of the overlying vegetation from DOS-TEM wetland/lowland simulations (see more detail below); (2) soil temperature, which uses a Q_{10} function (Q_{10} denotes the change in biogeochemical process rate per 10 °C change in temperature) with a reference temperature and Q_{10} coefficients that vary across ecosystems; (3) soil pH, where the optimum is set to 7.5; and (4) the availability of electron acceptors related to the effects of redox potential. CH_4 oxidation is modeled as an aerobic process that occurs in the unsaturated zone of the soil profile and is influenced by (1) soil temperature and redox potential, (2) substrate availability via a Michaelis-Menten function, and (3) soil moisture, which diminishes oxidation above the optimum soil moisture for oxidation.

7.3.2. Model Parameterization and Validation

7.3.2.1. Wetland Classification

Wetlands are ecosystems that are waterlogged seasonally or year-round. Wetland ecosystems are characterized by poor drainage conditions and a thick organic layer (see table 7.1). Wetlands in tundra regions of the Arctic and Western Alaska Landscape Conservation Cooperatives (LCCs) are composed primarily of graminoid tundra and wet-sedge tundra. In the Arctic LCC, tundra wetland regions consisted of 84.7 percent graminoid tundra and 15.3 percent wet-sedge tundra. In the Western Alaska LCC, tundra wetland regions consisted of 27.6 percent graminoid tundra and 72.4 percent wet-sedge tundra. In the Northwest Boreal LCC, wetlands consisted of 97 percent lowland permafrost plateau forest (46 percent evergreen forest and 51 percent deciduous forest) and 3 percent treeless ecosystems (that is, bogs and fens). Bogs and fens are especially important to assessing CH_4 dynamics owing to their high emissions. Because treeless wetlands were not extensive in the region, we used the parameterization for graminoid tundra for the simulation of these land-cover types. In the North Pacific LCC, wetlands consisted of 86 percent maritime fen and 14 percent maritime wetland forest (dominated by Sitka spruce [*Picea sitchensis* (Bong.) Carrière] and black cottonwood [*Populus trichocarpa* Torr. & A. Gray ex Hook.]).

7.3.2.2. Methane Dynamics Module of the Terrestrial Ecosystem Model (MDM-TEM)

MDM-TEM is parameterized for three different types of wetland (table 7.2) based on specific vegetation and hydrological characteristics. Therefore, the seven wetland land-cover types for the vegetation map were identified with three MDM-TEM parameterizations. Specifically, (1) lowland black spruce (*Picea mariana* (Mill.) Britton, Sterns & Poggenb.), white spruce (*Picea glauca* (Moench) Voss), and deciduous forests and maritime wetland forest were identified with the boreal forest wetland category from MDM-TEM; (2) graminoid tundra was identified with the alpine tundra wetland category from MDM-TEM; and (3) wet-sedge tundra and maritime fen were identified with the moist tundra wetland category from MDM-TEM. The MDM-TEM was parameterized using CH_4 measurements and soil and climate factors from three wetland field sites in arctic tundra and Canadian wetland (first three sites in table 7.2). The MDM-TEM was parameterized by minimizing the differences between observed fluxes and simulated fluxes at the Toolik-D, Toolik-W (Arctic LCC, Alaska), and SSA-FEN (Saskatchewan, Canada) field sites. For each site, the model was initialized by a set of parameter values determined by a literature review. Each individual parameter was bounded by the ranges of values from the literature review and then

Table 7.1. Target values for carbon pool and flux variables used to calibrate the Dynamic Organic Soil version of the Terrestrial Ecosystem Model (DOS-TEM) for major wetland land-cover types in Alaska.

[Soil mineral carbon pools are estimated from the bottom of the organic layer down to 1 meter into the mineral soil. $gC/m^2/yr$, gram of carbon per square meter per year; gC/m^2, gram of carbon per square meter; —, not applicable]

Wetland land-cover type	Net primary productivity ($gC/m^2/yr$)	Carbon pool (gC/m^2)			
		Vegetation	Soil fibric	Soil humic	Soil mineral
Boreal lowland black spruce forest	103	2,105	2,432	10,757	19,821
Boreal lowland white spruce forest	259	4,180	1,875	8,311	11,005
Boreal lowland deciduous forest	299	6,673	1,243	5,523	11,005
Graminoid	112	561	3,079	7,703	43,403
Wet-sedge tundra	54	458	3,358	8,401	44,252
Maritime forested wetland	893	16,344	1,666	28,666	10,380
Maritime fen	113	960	2,666	59,115	—

Table 7.2. Description of sites used in the model parameterization and validation process.

[MDM-TEM, Methane Dynamics Module of the Terrestrial Ecosystem Model; BOREAS, Boreal Ecosystem-Atmosphere Study]

Site name	Location	Elevation (meters)	Land cover	Wetland type in MDM-TEM	Observed data
Tundra at Toolik Field Station (Toolik-D)	149°36' W. 68°38' N.	760	Tussock tundra	Alpine tundra wetland	Soil temperatures at depths of 10, 20, and 50 centimeters, methane fluxes from 1992 and 1993
Tundra at Toolik Field Station (Toolik-W)	149°36' W. 68°38' N.	760	Wet tussock tundra	Moist tundra wetland	Soil temperatures at depths of 3, 5, 7, 9, and 11 centimeters, methane fluxes from 1994 and 1995
Fen at southern study area of BOREAS (SSA-FEN)	105°57' W. 53°57' N.	524.7	Complex fen with buckbean, sedges, birch, and willow	Boreal forest wetland	Soil temperatures at depths of 10 and 20 centimeters, daily evapotranspiration and eddy covariance measurements of methane fluxes for May to October of 1994 and 1995
Fen at northern study area of BOREAS (NSA-FEN; validation site)	98°25' W. 55°55' N.	218	Fen complex including sedge, moss, moat, and shrubs	Boreal forest wetland	Soil temperatures at depths of 5, 10, 20, 50, and 100 centimeters; water-table depth (1994) and chamber measurements of methane fluxes of May through September 1994 and June through October 1996

adjusted so that the root mean square error (RMSE) between the daily simulated and observed CH_4 fluxes was minimized. This procedure was conducted sequentially for all parameters until the minimized RMSE for the Toolik-D, Toolik-W, and SSA-FEN sites were 665 milligrams of carbon dioxide equivalent per square meter per day ($mgCO_2$-eq/m^2/d), 1,729 $mgCO_2$-eq/m^2/d, and 1,396 $mgCO_2$-eq/m^2/d, respectively.

7.3.2.3. Dynamic Organic Soil Version of the Terrestrial Ecosystem Model (DOS-TEM)

Wetland land-cover types considered in DOS-TEM include wet-sedge and graminoid tundra; black spruce, white spruce, and deciduous lowland boreal forests; and maritime wetland forest and maritime fen. We calibrated the rate-limiting parameters of DOS-TEM using target values of carbon and nitrogen pools and fluxes representative of mature ecosystems. These parameters are "tuned" until the model reaches target values of the main carbon and nitrogen pools and fluxes (Clein and others, 2002). The calibration of these parameters is an effective way of dealing with temporal scaling issues in ecosystem models (Rastetter and others, 1992). For boreal forest communities, an existing set of target values for vegetation and soil carbon and nitrogen pools and fluxes were assembled using data collected in the Bonanza Creek Long Term Ecological Research (LTER) program (Yuan and others, 2012). For tundra communities, we used data collected at the Toolik Field Station (Shaver and Chapin, 1991; Van Wijk and others, 2003; Sullivan and others, 2007; Euskirchen and others, 2012; Gough and others, 2012; Sistla and others, 2013). For the maritime and boreal-lowland-forest communities, we used data summarized in chapter 4, collected within three watersheds located near Juneau, Alaska, with mean annual precipitation of 1,580 millimeters (mm) and mean monthly average temperatures ranging from 2 to 9 degrees Celsius (°C) (see chapter 4, section 4.3.1 for details). Target values of vegetation biomass, soil carbon pools, and net primary productivity for each wetland land-cover type are described in table 7.1.

7.3.2.4. Model Validation

Model validation consists of testing the ability of a model to extrapolate carbon dynamics across space and time. It consists of comparing model simulations with observations collected at sites and times independent of the data used for model parameterization and calibration. When independent observations are not available, model verification consists of testing the ability of the model to reproduce the data used for calibration.

For MDM-TEM, the wetland parameterization was validated at the NSA-FEN site in Canada using the parameterization from SSA-FEN site (table 7.2). A geometric mean regression between the simulated monthly mean and observed net emissions was significant ($p < 0.01$; $n = 10$ months; where p denotes p-value, n denotes number of observations) with coefficient of determination, $R^2 = 0.90$; slope $= 24.3 \pm 2.3$ grams of carbon dioxide equivalent per square meter per month (gCO_2-eq/m^2/mo); and intercept $= 11.6 \pm 7.7$ gCO_2-eq/m^2/mo.

DOS-TEM parameterization has been validated using soil and vegetation biomass data derived from field observations

independent of the data used for model parameterization. The National Soil Carbon Network database for Alaska was used to validate DOS-TEM estimates of soil carbon stocks (Johnson and others, 2011). In order to compare similar estimates from model and observation, only deep profiles were selected from the database—that is, profiles with a description of the entire organic layer and the 90- to 110-centimeter (cm)-thick mineral layer beneath the organic layer.

Estimates of vegetation carbon stocks for tundra wetlands were compared with observations recorded in the data catalog of the Arctic LTER at Toolik Field Station (http://toolik.alaska.edu; Shaver and Chapin, 1986). For the boreal forest wetlands, vegetation carbon stocks simulated by DOS-TEM were compared with estimates from forest inventories conducted by the Cooperative Alaska Forest Inventory (Malone and others, 2009). The forest inventory only provided estimates of aboveground biomass. Aboveground biomass was converted to total biomass by using a ratio of aboveground versus total biomass of 0.8 in forest and 0.6 in tundra ecosystems. Carbon content of the biomass was estimated at 50 percent.

Finally, for maritime fen and maritime wetland forests, model validation was not possible as no additional independent data were available in this region. For these wetland ecosystems, we compared the model simulations with observed data at the same sites that were used for model parameterization. (See chapter 4, section 4.3.1 for site descriptions).

7.4. Model Application and Analysis

Spatially explicit data for climate, land cover, and soil texture were used to drive DOS-TEM and MDM-TEM. In addition, MDM-TEM used DOS-TEM estimates of monthly net primary productivity (NPP) and leaf area index (LAI) to simulate CH_4 dynamics. Because MDM-TEM runs at a daily timestep, the monthly forcing data were interpolated to daily timesteps within MDM-TEM (Zhuang and others, 2004). Chapter 6, section 6.3.4.2 provides descriptions of these data sources. To evaluate the effects of historical and projected climate warming, we conducted a series of six climate simulations combining (1) historical climate variability from 1901 through 2009 using Climatic Research Unit (CRU TS v. 3.10.01; Harris and others, 2014; www.cru.uea.ac.uk/) data and (2) climate variability from 2010 through 2099 projected by two general circulation models (GCMs): version 3.1-T47 of the Coupled Global Climate Model (CGCM3.1, www.cccma.ec.gc.ca/data/cgcm3/; McFarlane and others, 1992; Flato, 2005) developed by the Canadian Centre for Climate Modelling and Analysis and version 5 of the European Centre Hamburg Model (ECHAM5, www.mpimet.mpg.de/en/wissenschaft/modelle/echam/; Roeckner and others, 2003, 2004) developed by the Max Planck Institute. The climate projections were aligned with the Intergovernmental Panel on Climate Change's Special Report on Emissions Scenarios (IPCC-SRES; Nakićenović and Swart, 2000). The assessment used three low-, mid- and high-range CO_2 emissions scenarios (B1, A1B, and A2; see further details in chapter 2, section 2.2.1.). A new wetland distribution map of Alaska was developed for this study (see section 7.4.1 below) based on the National Wetlands Inventory (fig. 7.1) and used for both DOS-TEM and MDM-TEM to represent wetland ecosystem distribution (fig. 7.2). The heterogeneity and small clumped nature of wetlands was not possible to reproduce at a 1-kilometer (km) resolution. Therefore, the original wetland map was developed at a 30-meter (m) resolution, and percent cover of wetland was computed for each 1-km pixel.

7.4.1. Development of an Alaska Wetland Distribution Map

In this effort, we developed a new wetland distribution map that separated bogs and fens (fig. 7.2). The Alaska National Wetlands Inventory (NWI; http://www.fws.gov/wetlands/Data/State-Downloads.html) was used as a reference dataset (fig. 7.1), which helped with the development of a representative mapping model to estimate bog and fen distribution. Model development was conducted using a machine-learning, data-driven, nonparametric classification approach driven by Web-enabled Landsat Data spectral and derived indices and ancillary spatially explicit data (table 7.3). Bogs are generally flooded seasonally during spring melt. From the comparison of the NWI classification with field observations collected in the boreal and arctic regions of Alaska, we assumed bogs were identified as saturated scrub shrub in the NWI database because of the presence of dwarf shrubs and mosses. The NWI palustrine codes SS4B (scrub-shrub, needle-leaved, saturated), SS1E (scrub-shrub, broad-leaved, seasonally flooded/saturated), and SS7B (scrub-shrub, deciduous, saturated) were therefore used to define bogs. Fens are generally flooded throughout the growing season. We therefore assumed they were identified as persistent emergent wetlands—that is, the NWI palustrine codes EM1F (emergent, broad-leaved, semipermanently flooded) and EM1E (emergent, broad-leaved, seasonally flooded/saturated).

The wetland distribution map was developed based on a random selection of 18,024 pixels. A database for these pixels was built based on spatial inputs and NWI classes. Attributes from each of the potential input layers (table 7.3) were extracted for each pixel. Out of this set of pixels, 1,030 pixels were randomly selected and withheld for testing purposes. As an additional model sensitivity test, a twentyfold cross-validation was conducted on the model development dataset.

Winnowing was used to select a subset of relevant input spatial variables (Kivinen and others, 1997). A tenfold boosted regression tree (Sutton, 2005), which used the subset of winnowed variables, was developed (table 7.4). Overall accuracies were 75 percent for the independent test and

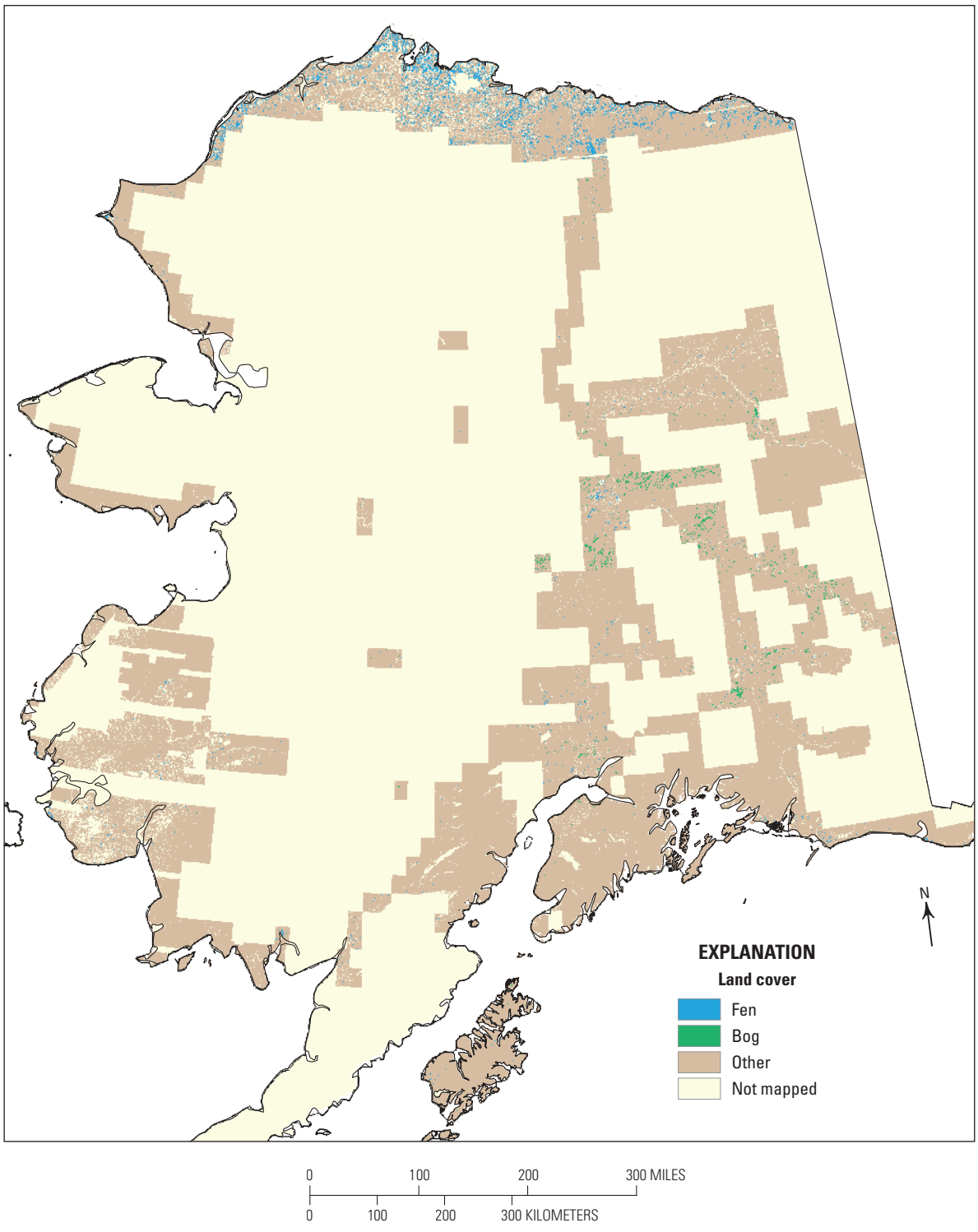

Figure 7.1. National Wetland Inventory data distribution and bog and fen distributions used for the development of an Alaska-wide mapping algorithm.

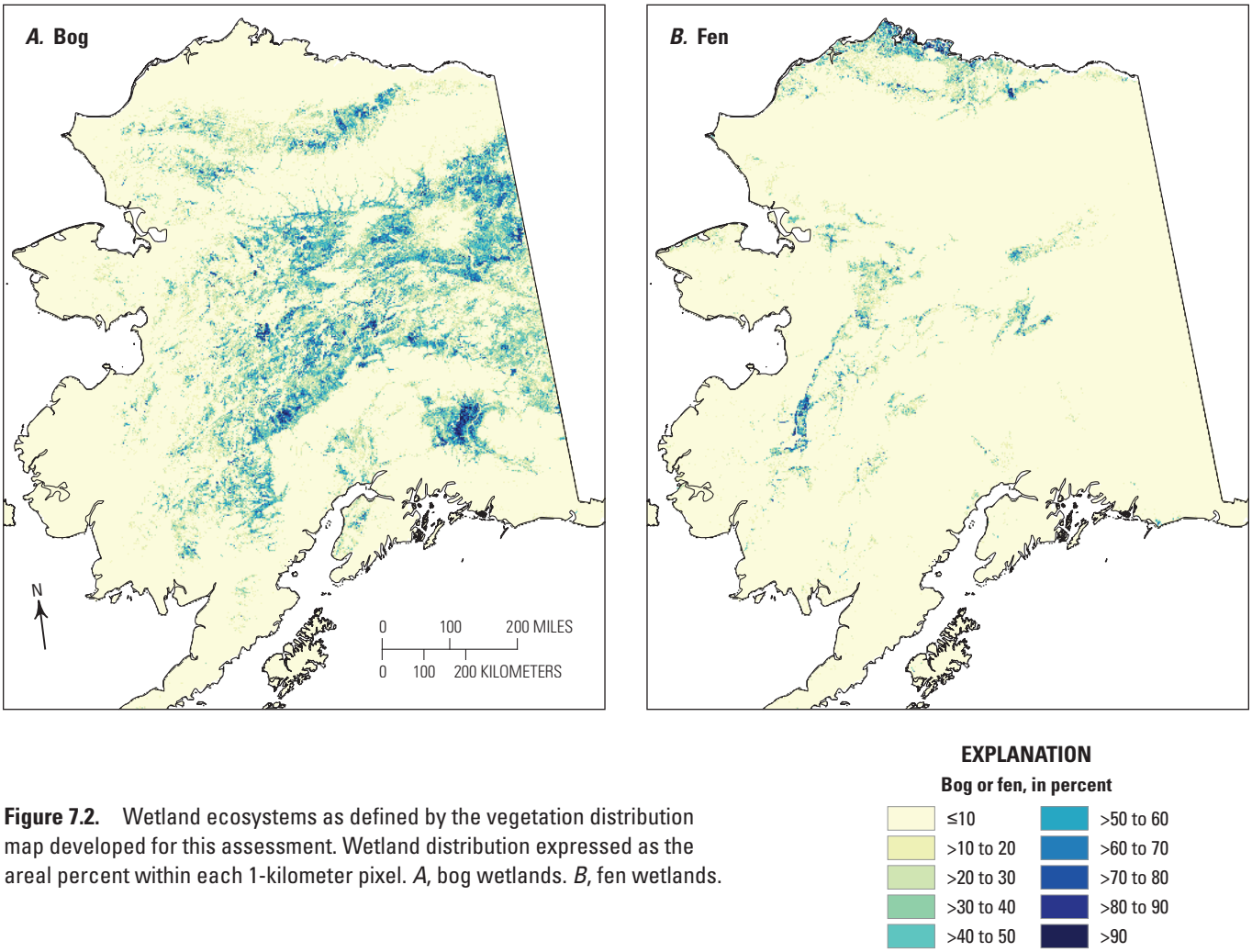

Figure 7.2. Wetland ecosystems as defined by the vegetation distribution map developed for this assessment. Wetland distribution expressed as the areal percent within each 1-kilometer pixel. *A*, bog wetlands. *B*, fen wetlands.

67 percent for the cross-validation (table 7.5). Fens tended to be classed more reliably than bogs, likely because woody overstory vegetation masked bog characteristics. Nonparametric techniques are sensitive to class frequency distributions so the number of pixels per class (bog, fen, other) is representative of the population being mapped.

The original 30-m maps of probable bog and fen distribution were converted to two maps of percent bog and percent fen at a 1-km resolution to match the resolution of the simulations (fig. 7.2).

7.4.2. Scaling Simulation Results for the Alternative Map of Wetland Distribution

Simulations of wetland distribution were conducted for the wetland ecosystems throughout Alaska at 1-km resolution. The estimates for a particular 1-km grid cell were then area-weighted by the wetland fraction for that 1-km grid cell provided by the wetland distribution map. The area-weighted estimates were then aggregated to the scale of LCC regions or to the scale of Alaska for purposes of analysis and reporting.

Table 7.3. Potential spatial input variables and those winnowed and subsequently mapped using a regression tree model.

[X, variable part of winnowed subset; —, variable not part of winnowed subset; ?, unknown; NA, not applicable]

Potential spatial input variables	Winnowed subset of variables	Variable usage by regression tree model (percent)	Reference
Web-enabled Landsat Data band 1	X	32	Roy and others (2010)
Web-enabled Landsat Data band 2	X	71	Roy and others (2010)
Web-enabled Landsat Data band 3	X	95	Roy and others (2010)
Web-enabled Landsat Data band 4	X	91	Roy and others (2010)
Web-enabled Landsat Data band 5	X	?	Roy and others (2010)
Web-enabled Landsat Data band 6	X	49	Roy and others (2010)
Web-enabled Landsat Data band 7	X	100	Roy and others (2010)
EVI (enhanced vegetation index)	—	—	Ji and others (2014)
gNDVI (green normalized difference vegetation index)	X	68	Ji and others (2014)
NDVI (normalized difference vegetation index)	—	—	Ji and others (2014)
SAVI (soil-adjusted vegetation index)	X	85	Ji and others (2014)
NDII (normalized difference infrared index)	—	—	Ji and others (2011)
NDII7 (normalized difference infrared index using band 7)	X	57	Ji and others (2011)
NDWI (normalized difference water index)	X	47	Ji and others (2011)
NDWI7 (normalized difference water index using band 7)	X	53	Ji and others (2011)
Sum of bands 4, 5, and 6	X	80	NA
Elevation	X	100	Gesch and others (2002)
Slope, in degrees	X	97	NA
Compound terrain index	X	47	Lu (2008)
Radar-based wetlands	X	32	Whitcomb and others (2009)
National Land Cover Database	X	87	Homer and others (2004)
China 2000	X	47	Liao and others (2014)
Soil texture	X	71	Jorgenson, Yoshikawa, and others (2008a)

Table 7.4. Accuracy assessments for the mapping model used to estimate bog and fen distribution compared with Alaska National Wetlands Inventory (NWI) reference classes for fens and bogs based on an independent test of 1,030 randomly selected pixels from the Alaska wetland distribution map developed for this assessment.

[NA, not applicable]

NWI reference	Mapping model				
	Bog	Fen	Other	Sum	Percent agreement
Bog	52	3	64	119	44
Fen	7	188	124	319	59
Other	42	18	532	592	90
Sum	101	209	720	1,030	NA
Percent	52	90	74	NA	75

Table 7.5. Accuracy assessments for the mapping model used to estimate bog and fen distribution compared with Alaska National Wetlands Inventory (NWI) reference classes for fens and bogs based on cross-validation of the pixels from the Alaska wetland distribution map developed for this assessment, not including those withheld for the independent test.

[NA, not applicable]

NWI reference	Mapping model				
	Bog	Fen	Other	Sum	Percent agreement
Bog	1,385	60	1,807	3,252	43
Fen	118	2,077	1,705	3,900	53
Other	985	956	7,901	9,842	80
Sum	2,488	3,093	11,413	16,994	NA
Percent	56	67	69	NA	67

7.4.3. Net Ecosystem Carbon Balance and Ecosystem Carbon Source/Sink Potential

Vegetation carbon stock estimates consisted of the sum of the aboveground and belowground living biomass. Soil carbon stocks consisted of the sum of carbon stored in the dead woody debris fallen to the ground, moss and litter, organic soil layers, and mineral soil layers. Historical changes in soil and vegetation carbon stocks were evaluated by quantifying annual differences of decadal averages between the first decade (1950–1959) and the last decade (2000–2009) of the historical period. Projected changes in soil and vegetation carbon stocks were evaluated by quantifying annual differences of decadal averages between the last decade of the historical period (2000–2009) and the last decade of the projection period (2090–2099).

The net ecosystem carbon balance (NECB) is the difference between total carbon inputs and total carbon outputs to the ecosystem (Chapin and others, 2006). NECB is the sum of all carbon fluxes coming in and out of the ecosystems, through gaseous and nongaseous, dissolved and nondissolved exchanges with the atmosphere and the hydrologic network. In terrestrial wetland ecosystems, NECB is the result of net primary productivity (NPP, net CO_2 uptake by the vegetation) minus heterotrophic respiration (HR), biogenic methane exchange ($BioCH_4$), and fire emissions (Fire). No export of carbon from forest harvest activities (Harvest) was expected in wetlands. No methane consumption was expected in wetlands for the anaerobic conditions are not favorable to methanotrophs activities. Furthermore, logging activities do not take place in lowlands because of limited accessibility and low productivity of forested lowland ecosystems.

$$NECB = NPP - HR - Fire - Harvest - BioCH_4 \quad (7.1)$$

NPP results from carbon assimilation from vegetation photosynthesis minus the respiration of the primary producers (autotrophic respiration). $BioCH_4$ results from the activity of methanogens and methanotrophs under anaerobic conditions. HR results from the decomposition of unfrozen soil organic carbon. Fire emissions encompass CO_2, CH_4, and carbon monoxide (CO) emissions. For the analysis of the inter-annual variations in sections 7.5.1.2 and 7.5.2.1, carbon fluxes were expressed in grams of carbon per square meter per year ($gC/m^2/yr$). For the regional assessments in sections 7.5.1.4 and 7.5.2.3, carbon fluxes were summed across the regions and expressed in teragrams of carbon per year (TgC/yr). Positive NECB indicates a gain of carbon to the ecosystem from the atmosphere, and negative NECB indicates a loss of carbon from the ecosystem to the atmosphere.

The uncertainty of carbon dynamics projected through the 21st century associated with climate forcing was estimated spatially by computing the range of change in NECB among the six climate simulations. For every 1-km grid cell and every climate simulation, the annual change in NECB was computed as the difference in the mean decadal NECB centered on 2095 and 2005 divided by the length of this period:

$$\Delta NECB = \frac{(NECB_{[2090-2099]} - NECB_{[2000-2009]})}{90} \quad (7.2)$$

The uncertainty was computed as the difference between the maximum and minimum ΔNECB among the six climate simulations.

Global warming potential (GWP) across time and the landscape was estimated taking into account that CH_4 has 25 times the GWP of CO_2 over a 100-year timeframe (Forster and others, 2007). GWP was reported in CO_2 equivalent by multiplying C-CH_4 fluxes by 33.33 (see chapter 6, section 6.3.5.2 for details). All C-CO_2 fluxes were converted to CO_2 equivalent by multiplying them by 3.66. CH_4 production from fire emissions ($Fire_{(CH4)}$) was considered in addition to biogenic CH_4 emissions by applying emission factors to CO_2, CH_4, and CO on DOS-TEM simulations of fire emissions (French and others, 2002). The carbon in CO was considered CO_2 because it converts to CO_2 in the atmosphere within a year (Weinstock, 1969).

$$GWP = -44/12 \times (NPP - HR - Harvest - Fire_{(CO2+CO)}) + 25 \times 16/12 \times (Fire_{(CH4)} + BioCH_4) \quad (7.3)$$

Positive GWP indicates a net loss of CO_2 from the ecosystem to the atmosphere, and negative GWP indicates a net gain of CO_2 to the ecosystem from the atmosphere.

Analysis of the time series was conducted using linear regression and the Fisher test for test of significance on the time series. For the analysis of the inter-annual variations in sections 7.5.1.2 and 7.5.2.1, carbon fluxes were expressed in $gC/m^2/yr$ with associated standard deviation (s.d.). For the regional assessments in sections 7.5.1.4 and 7.5.2.3., carbon fluxes were summed across the regions and expressed in TgC/yr. The assumptions of normality and homoscedasticity were verified by examining residual plots. The relative effects of temperature, precipitation, total area burned, and atmospheric CO_2 concentration on the carbon fluxes were tested using multiple regression analysis. The effects were considered significant when the p-value is lower than 0.05.

7.5. Results and Discussion

7.5.1. Historical Assessment of Carbon Dynamics (1950–2009)

7.5.1.1. Model Validation and Verification

For the historical period of the simulations (1950–2009), soil and vegetation carbon stocks were validated when possible by comparing modeled and observed estimates at sites independent from the sites used for model parameterization. When independent data (that is, data collected outside of the sites used for model parameterization) were not available, a verification of modeled versus observed stocks was conducted on the same sites used for model parameterization.

Globally, no significant differences were observed between modeled and observed contemporary vegetation carbon stocks (table 7.6; $p=0.340$) and soil carbon stocks (table 7.7; $p=0.182$). In general, DOS-TEM simulations successfully reproduced differences between land-cover types. Graminoid and wet-sedge tundra and maritime fen presented the lowest vegetation carbon stocks (table 7.3). Boreal lowland forests (that is, deciduous, white spruce, and black spruce lowland forests) had intermediate vegetation carbon stocks, and maritime wetland forest presented the largest vegetation carbon stocks, with 13.6 kilograms of carbon per square meter (kgC/m^2) observed.

In contrast, arctic and alpine tundra wetlands and maritime wetlands contained larger soil carbon stocks than boreal forest ecosystems (table 7.7).

Table 7.6. Comparison of observed and modeled vegetation carbon stocks for the main wetland land-cover types in Alaska.

[kgC/m^2, kilogram of carbon per square meter; NA, not applicable]

Wetland land-cover type	Number of sites used for model testing	Vegetation carbon stocks (kgC/m^2)			
		Mean		Standard deviation	
		Observed	Modeled	Observed	Modeled
Black spruce forest	45	2.47	1.99	0.85	0.38
White spruce forest	20	4.40	4.29	0.74	0.32
Deciduous forest	24	6.85	6.56	0.46	0.85
Graminoid tundra	3	0.56	0.44	0.26	0.21
Wet-sedge tundra	2	0.46	0.83	0.17	0.32
Maritime wetland forest[1]	3	13.62	13.11	1.16	3.26
Maritime fen[1]	1	0.96	1.67	NA	NA

[1]Comparisons between observed and modeled vegetation carbon stocks have been conducted for parameterization (that is, verification).

Table 7.7. Comparison of observed and modeled soil carbon stocks for the main wetland land-cover types in Alaska.

[kgC/m^2, kilogram of carbon per square meter; NA, not applicable]

Wetland land-cover type	Number of sites	Soil carbon stocks (kgC/m^2)			
		Mean		Standard deviation	
		Observed	Modeled	Observed	Modeled
Black spruce forest	22	29.85	46.84	11.15	55.64
White spruce forest	14	23.05	25.18	9.61	54.08
Deciduous forest	8	23.87	22.10	12.96	29.83
Tussock tundra	11	62.53	65.44	20.83	49.59
Wet-sedge tundra	23	42.01	50.73	30.49	31.46
Maritime wetland forest[1]	1	40.71	32.83	NA	NA
Maritime fen[1]	1	61.78	75.87	NA	NA

[1]Comparisons between observed and modeled vegetation carbon stocks have been conducted for parameterization (that is, verification).

7.5.1.2. Time Series Biogenic Methane Emissions, Net Ecosystem Carbon Balance, and Global Warming Potential for Wetland Alaska

For the wetland distribution map, the MDM-TEM simulation estimated net biogenic CH_4 emissions of wetlands in Alaska over the historical period (1950–2009) to be 157 grams of carbon dioxide equivalent per square meter per year (gCO_2-eq/m^2/yr) (s.d. of about 33 gCO_2-eq/m^2/yr), ranging from 97 to 267 gCO_2-eq/m^2/yr (fig. 7.3*A*). Biogenic CH_4 emissions increased significantly during the historical period, at a rate of about 0.977 gCO_2-eq/m^2/yr (Fisher value, $F=20.56$, $p<0.01$). Pyrogenic CH_4 emissions were estimated to be 1.50 gCO_2-eq/m^2/yr, which represented about 1 percent of the biogenic emissions. Pyrogenic CH_4 emissions significantly increased over the historical period ($F=2.13$, $p=0.0383$) at a rate of 0.037 gCO_2-eq/m^2/yr. NECB was estimated at –12.6 gC/m^2/yr (s.d. 7.2 gC/m^2/yr), ranging from –313.3 to 50.5 gC/m^2/yr. NECB did not change significantly over the historical period ($F=0.22$, $p=0.63$, fig. 7.3*B*). The GWP over the historical period indicated that wetlands were a significant source of greenhouse gas forcing of 187.7 gCO_2-eq/m^2/yr (s.d. 112.4 gCO_2-eq/m^2/yr), ranging from 57.4 to 1,399 gCO_2-eq/m^2/yr. GWP did not change significantly over the historical period ($F=0.87$, $p=0.35$, fig. 7.3*C*) and was significantly different from zero ($t=-6.00$; $p<0.01$).

7.5.1.3. Environmental Drivers of the Historical Temporal Variability of Biogenic Methane Emissions, Net Ecosystem Carbon Balance, and Global Warming Potential of Wetland Alaska

Total CH_4 emissions (biogenic and pyrogenic) during the historical period were positively correlated with the annual area of wetlands burned associated with peaks of pyrogenic methane emissions. CH_4 emissions increased with increasing atmospheric CO_2 concentration (table 7.8). The positive relationship between atmospheric CO_2 concentration and CH_4 emissions is likely related to the effect of increasing atmospheric CO_2 on NPP (see chapter 6, section 6.4.2.2). The negative effect of annual area burned on NECB is related to the effect of wildfire on CO_2 emissions from combustion of soil and vegetation carbon. Although GWP is positively correlated with annual area burned, the relationship likely depends on the correlation of GWP and CH_4 emissions.

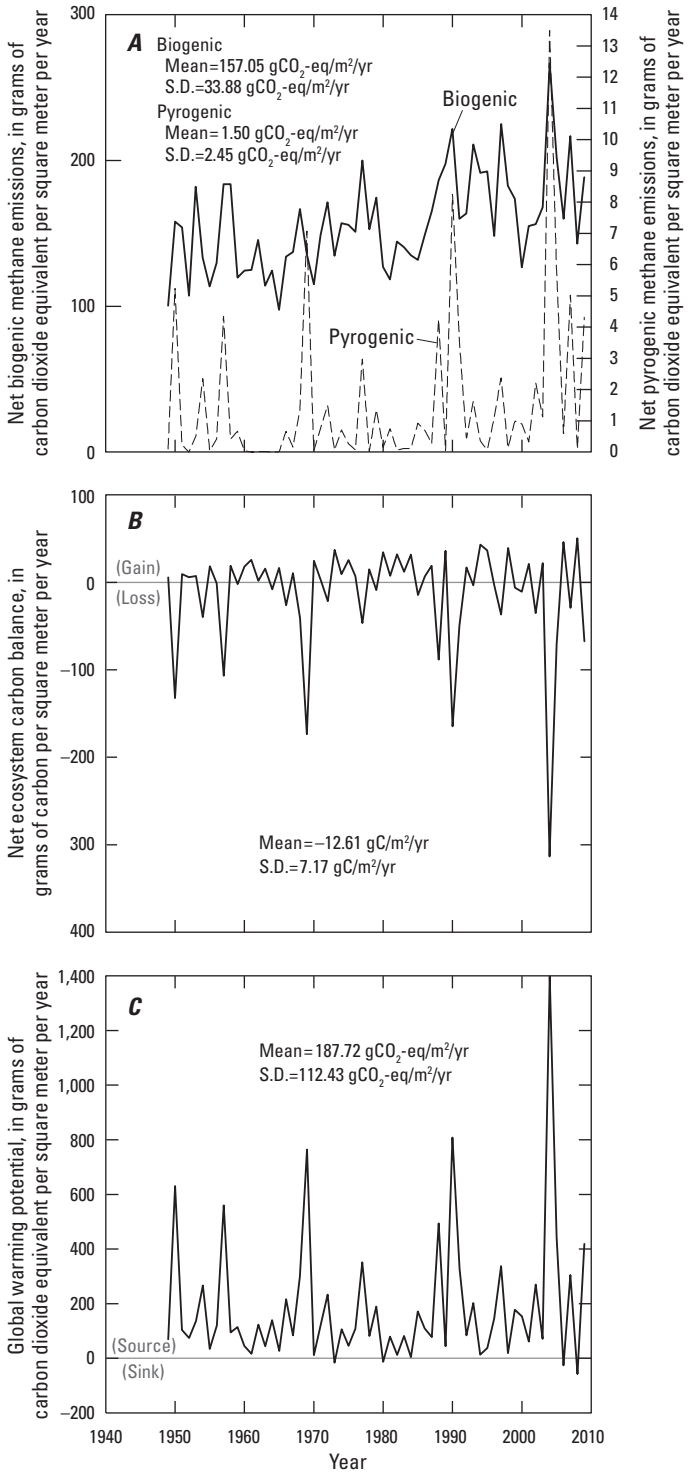

Figure 7.3. Time series of annual *A*, net biogenic and pyrogenic methane emissions; *B*, net ecosystem carbon balance; and *C*, global warming potential during the historical period (1950–2009) for wetland ecosystems of Alaska defined by the wetland distribution map. The mean and standard deviation for the study area are indicated in each panel.

7.5.1.4. Spatial Distribution of Carbon Stocks, Biogenic Methane Emissions, Net Ecosystem Carbon Balance, and Global Warming Potential Across Wetland Alaska

The largest carbon stocks of wetlands in Alaska were located in the Northwest Boreal LCC North (table 7.9), with storage of 427 teragrams of carbon (TgC) in the vegetation and 1,965 TgC in the soil. The Northwest Boreal LCC North also contains the largest proportion of wetlands in Alaska and is the only LCC region in which carbon stocks in the vegetation and the soil decreased during the historical period. The largest increase of carbon stocks in the vegetation and the soil was observed in the Arctic LCC, with a gain of 0.12 TgC/yr and 0.49 TgC/yr in the vegetation and the soil, respectively.

During the first decade of the 21st century (2000–2009), the largest biogenic CH_4 emissions were observed in the Northwest Boreal LCC North (table 7.10, fig. 7.4*A*). The largest NPP also was observed in the Northwest Boreal LCC North but the carbon gain from vegetation growth was offset by carbon loss from heterotrophic respiration and fire emissions, resulting in the wetlands in the region being a net carbon source of –2.21 TgC/yr during the historical period (fig. 7.4*B*), equivalent to 27 teragrams of carbon dioxide equivalent per year ($TgCO_2$-eq/yr) (fig. 7.4*C*). The other LCC regions were carbon sinks during the historical period: the largest sink was located in the Arctic LCC with storage of 0.62 TgC/yr. However, these smaller sinks were not large enough to compensate for the carbon loss from the Northwest Boreal LCC North. Statewide, wetland ecosystems in Alaska were a carbon source during the historical period, losing about 1.34 TgC/yr. The carbon losses were about equally distributed among soil and vegetation (table 7.9). Although total CH_4 emissions represented only 2.6 percent of NPP, the trend of GWP is dominated by CH_4 emissions. As a result, mean annual GWP between 2000 and 2009 was 33 $TgCO_2$-eq/yr in wetlands of Alaska.

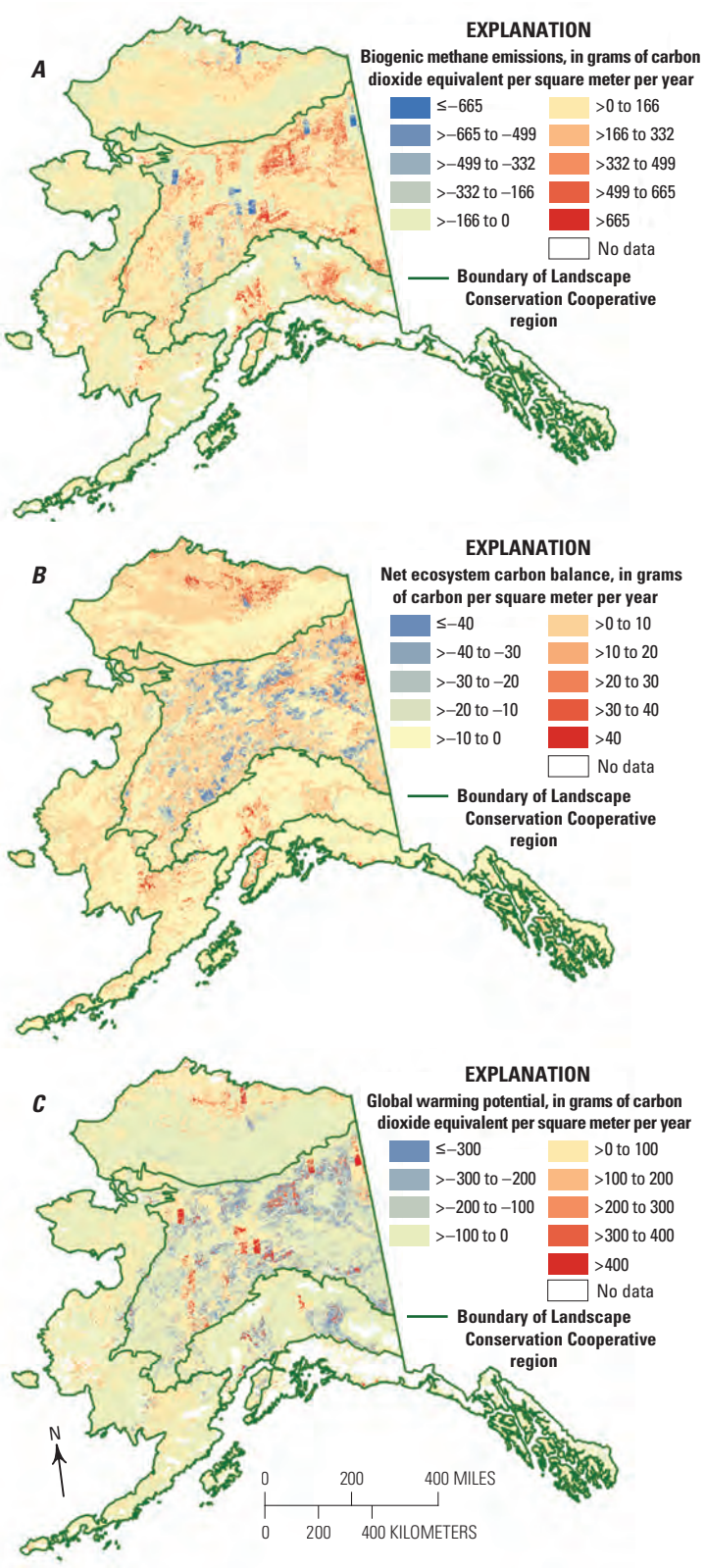

Figure 7.4. Spatial distribution of mean annual *A*, biogenic methane emissions; *B*, net ecosystem carbon balance; and *C*, global warming potential for the historical period (1950–2009) for wetland ecosystems of Alaska.

Table 7.8. Results of multiple linear regressions testing the main drivers of carbon dioxide and total methane (biogenic and pyrogenic) fluxes in wetland ecosystems among total annual precipitation, mean annual temperature, annual area burned, and mean annual atmospheric carbon dioxide concentration during the historical period (1950–2009).

[F, Fisher value; P, probability value. Trend: +, positive; –, negative; n.s., trend not significant. Units: mm, milllimeter; °C, degree Celsius; km^2, square kilometer; ppm, part per million. CO_2, carbon dioxide]

Drivers of carbon dioxide and methane fluxes	Total methane emissions			Net ecosystem carbon balance			Global warming potential		
	F	P	Trend	F	P	Trend	F	P	Trend
Total annual precipitation (mm)	0.01	0.92	n.s.	0.55	0.46	n.s.	0.41	0.52	n.s.
Mean annual temperature (°C)	1.75	0.19	n.s.	0.44	0.51	n.s.	0.02	0.88	n.s.
Annual area burned (km^2)	29.3	<0.01	+	217.77	<0.01	–	221.36	<0.01	+
Mean annual atmospheric CO_2 concentration (ppm)	5.13	<0.01	+	1.07	0.31	n.s.	0.55	0.46	n.s.

Table 7.9. Average vegetation and soil carbon stocks for the last decade of the historical period (2000–2009) and mean annual change in vegetation and soil carbon stocks between the first (1950–1959) and last (2000–2009) decades of the historical period in each Landscape Conservation Cooperative region for wetland ecosystems of Alaska defined by the vegetation distribution map developed for this assessment.

[Data may not add to totals shown because of independent rounding. km^2, square kilometer; TgC, teragram of carbon]

Landscape Conservation Cooperative (LCC) region	Wetland total area (km^2)	Wetland cover (percent)	Vegetation carbon stocks (TgC)		Soil carbon stocks (TgC)	
			Average	Mean annual change	Average	Mean annual change
Arctic LCC	29,818	9.8	44	0.12	1,281	0.49
Western Alaska LCC	14,582	3.9	57	0.04	788	0.06
Northwest Boreal LCC North	112,077	24.5	427	–0.87	1,965	–1.33
Northwest Boreal LCC South	18,627	10.0	83	0.05	865	0.03
North Pacific LCC	1,965	1.3	19	0.00	107	0.06
Total	**177,069**	**12.0**	**630**	**–0.65**	**5,006**	**–0.68**

Table 7.10. Average vegetation and soil carbon fluxes in wetland ecosystems per Landscape Conservation Cooperative region from 2000 through 2009.

[Data may not add to totals or compute to net ecosystem carbon balance shown because of independent rounding. CO_2, carbon dioxide; CO, carbon monoxide; CH_4, methane; TgC/yr, teragram of carbon per year; $TgCO_2$-eq/yr, teragram of carbon dioxide equivalent per year]

Landscape Conservation Cooperative (LCC) region	Pyrogenic CO_2 + CO emissions (TgC/yr)	Pyrogenic CH_4 emissions ($TgCO_2$-eq/yr)	Net primary productivity (TgC/yr)	Biogenic CH_4 emissions ($TgCO_2$-eq/yr)	Heterotrophic respiration (TgC/yr)	Net ecosystem carbon balance (TgC/yr)	Global warming potential ($TgCO_2$-eq/yr)
Arctic LCC	1.08	0.112	4.68	2.49	2.91	0.62	0.06
Western Alaska LCC	0.08	0.008	2.99	1.67	2.76	0.10	1.12
Northwest Boreal LCC North	8.23	0.740	24.95	20.45	18.29	–2.21	27.01
Northwest Boreal LCC South	1.00	0.105	4.11	5.74	2.85	0.08	4.90
North Pacific LCC	0.01	0.001	0.56	0.50	0.47	0.07	0.20
Total	**10.40**	**0.966**	**37.28**	**30.85**	**27.27**	**–1.34**	**33.30**

7.5.2. Future Assessment of Carbon Dynamics (2010–2099)

7.5.2.1. Times Series for Wetland Alaska

Estimates of future biogenic CH_4 emissions exhibited substantial inter-annual variability and substantial differences between climate models for a given emissions scenario and among different emissions scenarios for a given climate model. The greatest mean annual biogenic CH_4 emissions among climate models and emissions scenarios would be about 229 gCO_2-eq/m^2/yr under scenario A1B with ECHAM5. The lowest mean annual biogenic CH_4 emissions were projected under scenario B1 with both climate models (159 gCO_2-eq/m^2/yr and 176 gCO_2-eq/m^2/yr with CGCM3.1 and ECHAM5, respectively; fig. 7.5*A*). Biogenic CH_4 emissions would increase significantly during the 21st century under scenarios B1, A1B, and A2 at a rate of 0.680 gCO_2-eq/m^2/yr, 1.406 gCO_2-eq/m^2/yr, and 3.073 gCO_2-eq/m^2/yr, respectively, with CGCM3.1 and 0.923 gCO_2-eq/m^2/yr, 1.003 gCO_2-eq/m^2/yr, and 2.183 gCO_2-eq/m^2/yr, respectively, with ECHAM5.

Projected mean annual pyrogenic CH_4 emissions were larger for the climate simulations from the ECHAM5 climate model than from the CGCM3.1 climate model (fig. 7.5*B*). Among all climate simulations, mean annual pyrogenic CH_4 emissions would range from 0.967 gCO_2-eq/m^2/yr (s.d. 1.3 gCO_2-eq/m^2/yr) under scenario A1B with CGCM3.1 to 1.467 gCO_2-eq/m^2/yr (s.d. 2.7 gCO_2-eq/m^2/yr) under scenario A2 with ECHAM5. Pyrogenic CH_4 emissions are not projected to significantly increase over time, except for the climate simulations with the largest warming and increase in atmospheric CO_2 concentration (that is, scenario A2 with CGCM3.1 and ECHAM5), for which pyrogenic CH_4 emissions would increase at a rate of 0.00243 gCO_2-eq/m^2/yr and 0.0193 gCO_2-eq/m^2/yr, respectively. Combining historical simulation results, CH_4 emissions significantly increased from 1950 through 2009 by 0.967 gCO_2-eq/m^2/yr.

For each climate model, projected mean annual NECB was the lowest for the lowest CO_2-emissions scenario B1 (13.8 gC/m^2/yr and 23.5 gC/m^2/yr with CGCM3.1 and ECHAM5, respectively) and the highest for the highest CO_2-emissions scenario A2 (33.6 gC/m^2/yr and 31.7 gC/m^2/yr with CGCM3.1 and ECHAM5, respectively). In contrast with CH_4 emissions, NECB would not change significantly over time (fig. 7.5*C*). As a result, GWP was projected to increase during the second half of the 21st century (fig. 7.5*D*). This increase was significant for CGCM3.1 climate simulations under A2 and B1 emissions scenarios (rate of 2.59 gCO_2-eq/m^2/yr and 1.09 gCO_2-eq/m^2/yr, respectively) and the ECHAM5 climate simulation under the A1B scenario (rate of 2.15 gCO_2-eq/m^2/yr).

7.5.2.2. Environmental Drivers of the Future Temporal Variability of Net Ecosystem Carbon Balance and Global Warming Potential in Wetland Alaska

Over the projection period, increasing annual area burned and rising atmospheric CO_2 concentrations were projected to be associated with an increase in CH_4 emissions in wetlands during the 21st century for all six climate simulations. Increasing air temperature also would have a significant positive effect on CH_4 emissions under scenarios A1B and A2 with CGCM3.1 (table 7.11). Increasing annual area burned would have a negative effect on NECB for all climate simulations. Increasing air temperature and atmospheric CO_2 concentration also would have a positive effect on NECB for scenarios B1 and A1B, respectively, with ECHAM5. Increases in GWP would be associated with increases in annual area burned owing to climate warming (see chapter 2, section 2.4.5.2.). For all simulations, fire regime would therefore be the main driver of the carbon balance in wetlands during the 21st century. However, the present assessment does not take into account the effect environmental changes associated with thermokarst formation have on the carbon balance. Permafrost in wetlands of Alaska is often ice rich (Jorgenson, Shur, and others, 2008). With increasing temperature and permafrost thaw, the soil of ice-rich wetlands can collapse as a result of ice melting to water and draining out of the ecosystem (Jorgenson, Yoshikawa, and others, 2008b). These collapses are associated with drastic changes in hydrology—transitioning from moist permafrost plateau to saturated drainage conditions—and important changes in the vegetation composition (from permafrost plateau forest to bog or fen, for instance) (Jorgenson and Osterkamp, 2005). Thermokarsts can be triggered by climate and fire (Myers-Smith and others, 2008). The transition from moist to saturated conditions may considerably affect the local carbon balance, increasing not only CH_4 production (Turetsky and others, 2008) but also soil carbon storage (O'Donnell and others, 2012). However, the extent of thermokarst across Alaska is still unknown. Therefore, it is difficult to assess the effect of thermokarst disturbance on the regional carbon balance of Alaska.

Table 7.11. Results of multiple linear regressions testing the main drivers of carbon dioxide and methane fluxes in wetland ecosystems among total annual precipitation, mean annual temperature, annual area burned, and mean annual atmospheric carbon dioxide concentration for each future climate simulation for the projection period (2010–2099).

[The six future climate simulations are combinations of two general circulation models, version 3.1-T47 of the Coupled Global Climate Model (CGCM3.1) developed by the Canadian Centre for Climate Modelling and Analysis and version 5 of the European Centre Hamburg Model (ECHAM5) developed by the Max Planck Institute, and three climate scenarios of the Intergovernmental Panel on Climate Change's Special Report on Emissions Scenarios (Nakićenović and Swart, 2000), B1, A1B, and A2, in order of low to high projected CO_2 emissions. F, Fisher value; P, probability value. Trend: +, positive; –, negative; n.s., trend not significant. Units: mm, milllimeter; °C, degree Celsius; km^2, square kilometer; ppm, part per million. CO_2, carbon dioxide]

Climate scenario	Parameter	Total methane emissions			Net ecosystem carbon balance			Global warming potential		
		F	P	Trend	F	P	Trend	F	P	Trend
CGCM3.1										
A1B	Total annual precipitation (mm)	0.01	0.92	n.s.	0.1	0.75	n.s.	0.1	0.75	n.s.
	Mean annual temperature (°C)	5.79	0.02	+	3	0.09	n.s.	0.21	0.65	n.s.
	Annual area burned (km^2)	7.04	0.01	+	78.6	<0.01	–	79.63	<0.01	+
	Mean annual atmospheric CO_2 concentration (ppm)	4.42	0.04	+	0.03	0.87	n.s.	0.61	0.44	n.s.
A2	Total annual precipitation (mm)	0.01	0.92	n.s.	0.1	0.75	n.s.	0.1	0.75	n.s.
	Mean annual temperature (°C)	5.79	0.02	+	3	0.09	n.s.	0.21	0.65	n.s.
	Annual area burned (km^2)	7.04	0.01	+	78.6	<0.01	–	79.63	<0.01	+
	Mean annual atmospheric CO_2 concentration (ppm)	4.42	0.04	+	0.03	0.87	n.s.	0.61	0.44	n.s.
B1	Total annual precipitation (mm)	0	0.98	n.s.	0.58	0.45	n.s.	0.46	0.50	n.s.
	Mean annual temperature (°C)	1.49	0.23	n.s.	0.52	0.47	n.s.	0.05	0.82	n.s.
	Annual area burned (km^2)	17.87	<0.01	+	109.52	<0.01	–	119.76	<0.01	+
	Mean annual atmospheric CO_2 concentration (ppm)	4.89	0.03	+	0.17	0.68	n.s.	0.15	0.70	n.s.
ECHAM5										
A1B	Total annual precipitation (mm)	1.78	0.19	n.s.	2.2	0.14	n.s.	3.48	0.07	n.s.
	Mean annual temperature (°C)	0.14	0.71	n.s.	1.64	0.20	n.s.	1.04	0.31	n.s.
	Annual area burned (km^2)	19.61	<0.01	+	169.32	<0.01	–	117.55	<0.01	+
	Mean annual atmospheric CO_2 concentration (ppm)	11.67	<0.01	+	5.86	0.02	+	1.45	0.23	n.s.
A2	Total annual precipitation (mm)	0.47	0.49	n.s.	2.48	0.12	n.s.	2.16	0.15	n.s.
	Mean annual temperature (°C)	9.27	<0.01	+	0.07	0.80	n.s.	2.39	0.13	n.s.
	Annual area burned (km^2)	14.22	<0.01	+	136.49	<0.01	–	106.3	<0.01	+
	Mean annual atmospheric CO_2 concentration (ppm)	0.53	0.47	n.s.	1.27	0.26	n.s.	0.26	0.61	n.s.
B1	Total annual precipitation (mm)	0.97	0.33	n.s.	0.05	0.83	n.s.	0.61	0.44	n.s.
	Mean annual temperature (°C)	0.88	0.35	n.s.	5.03	0.03	+	1.76	0.19	n.s.
	Annual area burned (km^2)	19.03	<0.01	+	150.02	<0.01	–	168.94	<0.01	+
	Mean annual atmospheric CO_2 concentration (ppm)	4.33	0.04	+	0.52	0.47	n.s.	3.49	0.07	n.s.

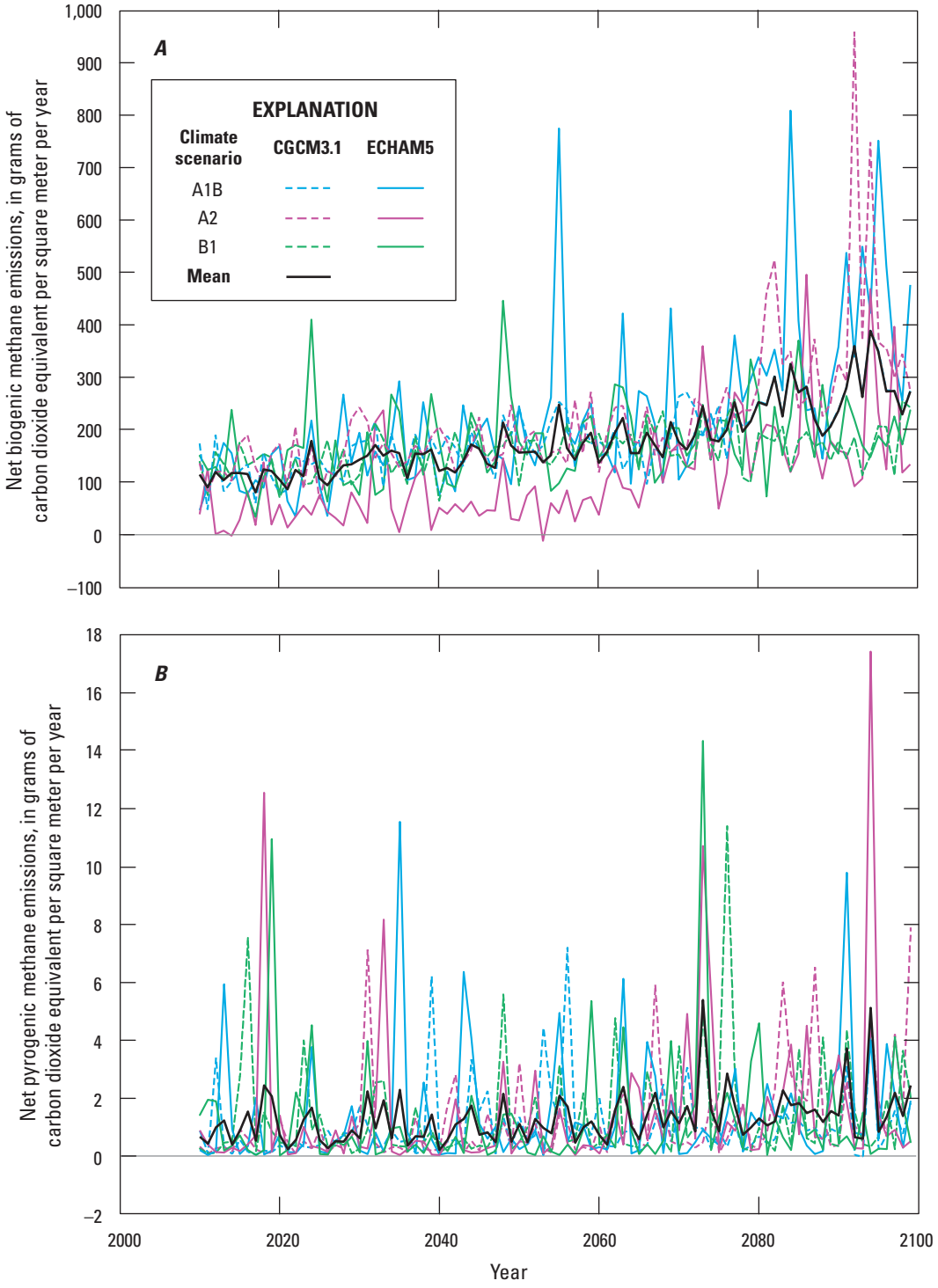

Figure 7.5. (pages 148 and 149). Time series of projected annual *A*, net biogenic methane emissions; *B*, net pyrogenic methane emissions; *C*, net ecosystem carbon balance; and *D*, global warming potential for the projection period (2010–2099) for wetland ecosystems of Alaska defined by the wetland distribution map for the two general circulation models, version 3.1-T47 of the Coupled Global Climate Model (CGCM3.1) developed by the Canadian Centre for Climate Modelling and Analysis and version 5 of the European Centre Hamburg Model (ECHAM5) developed by the Max Planck Institute, under three climate scenarios of the Intergovernmental Panel on Climate Change's Special Report on Emissions Scenarios (Nakićenović and Swart, 2000), B1, A1B, and A2, in order of low to high projected CO_2 emissions.

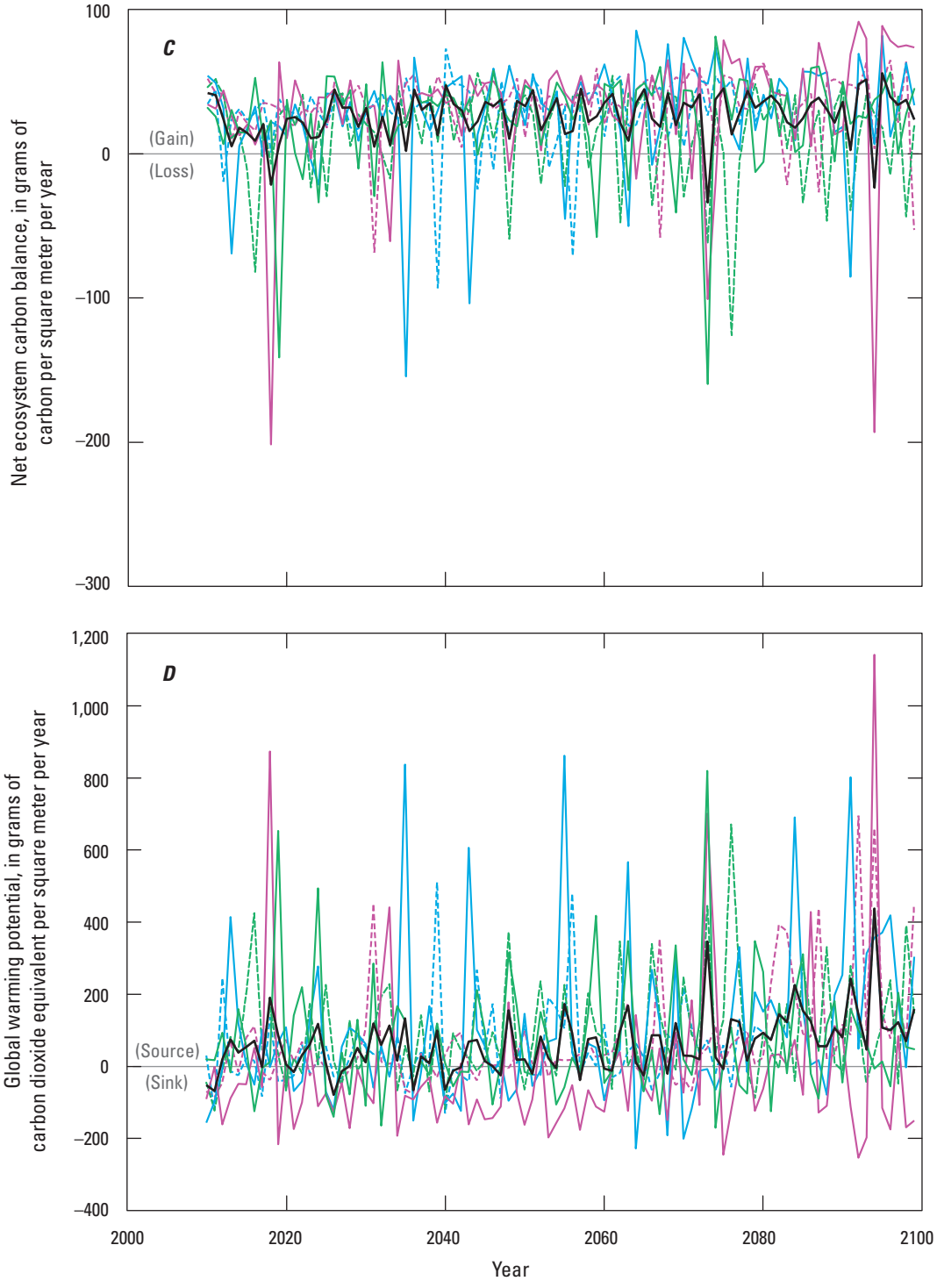

Figure 7.5.—Continued

7.5.2.3. Spatial Distribution of Changes in Carbon Stocks, Biogenic Methane Emissions, Net Ecosystem Carbon Balance, and Global Warming Potential Across Wetland Alaska

For each LCC region, the climate scenario associated with the largest increase in atmospheric CO_2 (that is, emissions scenario A2; table 7.12) induced the largest increase in vegetation and soil carbon stocks by 2099. Vegetation carbon stocks for the ECHAM5 climate simulations were generally projected to be higher than the vegetation carbon stocks for the CGCM3.1 climate simulations. In contrast, soil carbon stocks for the ECHAM5 climate simulations were generally projected to be lower than for the CGCM3.1 climate simulations. These differences were related to the fact that the ECHAM5 simulations presented larger warming trends and larger fire activity than the climate simulations from CGCM3.1 (see chapter 2 for detailed comparison). Warmer temperatures from the ECHAM5 climate simulations induced larger vegetation productivity and biomass compared with the results from the CGCM3.1 simulations. However, the larger litterfall associated with larger vegetation productivity was offset by carbon loss from the higher heterotrophic respiration and larger carbon emissions from wildfire, leading to lower soil carbon stocks projected for the ECHAM5 climate simulations compared with the CGCM3.1 climate simulations. Vegetation and soil carbon stocks were projected to increase from 2010 to 2099 for all regions and all simulations, except for the B1 scenario with CGCM3.1 in the Northwest Boreal LCC South (vegetation carbon stocks only) and the Western Alaska LCC.

Vegetation productivity was generally projected to be higher for the ECHAM5 climate simulations than for the CGCM3.1 climate simulations, except for the North Pacific LCC (table 7.13). Similarly, NPP was projected to increase in response to the scenarios projecting a greater increase in atmospheric CO_2 (scenarios A1B and A2 versus scenario B1). Statewide, mean annual NPP was projected to range from 41.0 to 46.7 TgC/yr between 2090 and 2099.

Among all time periods, the North Pacific LCC remained the minimal contributor to CH_4 emissions owing to the small wetland fraction in that region. Similar to the regional total CH_4 emission, the inter-scenario difference in emission magnitude is generally greater than that between the two GCMs within a scenario (table 7.13), indicating the dominating effects of climate controls on regional CH_4 dynamics. By the end of the 21st century, biogenic and pyrogenic CH_4 emissions were projected to range from 36 to 90 $TgCO_2$-eq/yr with biogenic CH_4 emissions representing 98 to 99 percent of the total emissions.

Projected fire emissions tended to increase in response to warming in the LCC regions. These projected increases were often accompanied by lower projected heterotrophic respiration (compared with simulations with lower warming trends). For instance, in the Northwest Boreal LCC North, whereas fire emissions were projected to increase by 95 percent on average in the A2 simulations compared with the B1 simulations, heterotrophic respiration was projected to decrease by 5 percent (table 7.13). This decrease in heterotrophic respiration is likely caused by the loss of organic horizon carbon from wildfire.

Carbon stocks in wetland ecosystems of all LCC regions were projected to increase within all six future climate simulations. The projected increase in carbon storage for Alaska ranged from 3.01 to 5.28 TgC/yr between the CGCM3.1 climate simulations under scenarios B1 and A2, respectively. NECB was generally projected to be highest for the A2 climate simulations, which had the greatest projected increases in atmospheric CO_2 and warming. Because the projected fire activity for 2090–2099 was lower than during 2000–2009, the NECB of the LCC regions was generally projected to be higher compared with 2000–2009 (table 7.10), except for the Western Alaska LCC under the B1 scenario. However, GWP estimates for the future climates indicate that all LCC regions would become sources of greenhouse gas radiative forcing by the end of the 21st century, except for CGCM3.1 simulations under scenarios A1B and B1 for the Arctic and North Pacific LCCs and the ECHAM5 simulation under scenario A2 for the Arctic LCC.

The spatial distribution of changes in biogenic CH_4 emissions indicated that there are large areas of projected increases in CH_4 emissions across Alaska from 2000–2009 to 2090–2099 (fig. 7.6), especially in central Alaska (Northwest Boreal LCC). Projected increases in central Alaska ranged from 6.7 gCO_2-eq/m^2/yr for the B1 climates to 16.7 gCO_2-eq/m^2/yr for the A2 climates, primarily owing to relatively large vegetation biomass, leaf area index, and productivity, associated with higher CH_4 production.

The average projected increase of NECB from 2000–2009 to 2090–2099 was largest in the Northwest Boreal LCC North (fig. 7.7*A*). The largest variation across climate simulations in changes of the projected NECB was in the Western Alaska LCC and the Northwest Boreal LCC South (fig. 7.7*B*). These regions could therefore be major sources of uncertainty as to how NECB responds to future climate and disturbance regimes.

Table 7.12. Average vegetation and soil carbon stocks for the last decade of the projection period (2090–2099) and mean annual change in vegetation and soil carbon stocks between the last decades of the historical period (2000–2009) and the projection period (2090–2099) per Landscape Conservation Cooperative region for each of the six climate simulations.

[The six climate simulations are combinations of two general circulation models, version 3.1-T47 of the Coupled Global Climate Model (CGCM3.1) developed by the Canadian Centre for Climate Modelling and Analysis and version 5 of the European Centre Hamburg Model (ECHAM5) developed by the Max Planck Institute, and three climate scenarios of the Intergovernmental Panel on Climate Change's Special Report on Emissions Scenarios (Nakićenović and Swart, 2000), B1, A1B, and A2, in order of low to high projected CO_2 emissions. Data may not add to totals shown because of independent rounding. TgC, teragram of carbon]

Climate scenario	Landscape Conservation Cooperative (LCC) region	Vegetation carbon stocks (TgC)		Soil carbon stocks (TgC)	
		Average	Mean annual change	Average	Mean annual change
		CGCM3.1			
A1B	Arctic LCC	59	0.16	1,395	1.23
	Western Alaska LCC	61	0.04	861	0.28
	Northwest Boreal LCC North	546	1.32	2,039	0.70
	Northwest Boreal LCC South	83	0.00	823	0.33
	North Pacific LCC	23	0.04	129	0.09
Total		**771**	**1.57**	**5,248**	**2.64**
A2	Arctic LCC	58	0.15	1,365	0.94
	Western Alaska LCC	63	0.07	816	0.30
	Northwest Boreal LCC North	551	1.38	2,121	1.73
	Northwest Boreal LCC South	87	0.04	912	0.52
	North Pacific LCC	24	0.05	114	0.08
Total		**783**	**1.70**	**5,328**	**3.58**
B1	Arctic LCC	55	0.14	1,323	1.25
	Western Alaska LCC	56	–0.00	836	–0.16
	Northwest Boreal LCC North	512	0.95	2,003	0.46
	Northwest Boreal LCC South	83	–0.01	888	0.24
	North Pacific LCC	23	0.03	116	0.10
Total		**728**	**1.11**	**5,165**	**1.90**
		ECHAM5			
A1B	Arctic LCC	62	0.19	1,354	0.80
	Western Alaska LCC	66	0.10	787	0.03
	Northwest Boreal LCC North	578	1.69	2,074	1.18
	Northwest Boreal LCC South	86	0.04	807	0.27
	North Pacific LCC	24	0.05	124	0.04
Total		**815**	**2.07**	**5,146**	**2.32**
A2	Arctic LCC	62	0.20	1,359	0.90
	Western Alaska LCC	66	0.10	817	0.10
	Northwest Boreal LCC North	579	1.69	2,093	1.38
	Northwest Boreal LCC South	92	0.09	847	0.17
	North Pacific LCC	23	0.04	111	0.04
Total		**822**	**2.13**	**5,226**	**2.58**
B1	Arctic LCC	56	0.13	1,357	0.86
	Western Alaska LCC	64	0.08	796	–0.02
	Northwest Boreal LCC North	563	1.49	2,049	0.71
	Northwest Boreal LCC South	85	0.01	878	0.13
	North Pacific LCC	23	0.04	114	0.07
Total		**791**	**1.75**	**5,193**	**1.75**

Table 7.13. Average annual vegetation and soil carbon fluxes for the last decade of the projection period (2090–2099) per Landscape Conservation Cooperative region for each of the six future climate simulations.

[The six climate simulations are combinations of two general circulation models, version 3.1-T47 of the Coupled Global Climate Model (CGCM3.1) developed by the Canadian Centre for Climate Modelling and Analysis and version 5 of the European Centre Hamburg Model (ECHAM5) developed by the Max Planck Institute, and three climate scenarios of the Intergovernmental Panel on Climate Change's Special Report on Emissions Scenarios (Nakićenović and Swart, 2000), B1, A1B, and A2, in order of low to high projected CO_2 emissions. Data may not add to totals or compute to net ecosystem carbon balance shown because of independent rounding. CO_2, carbon dioxide; CO, carbon monoxide; CH_4, methane; TgC/yr, teragram of carbon per year; $TgCO_2$-eq/yr, teragram of carbon dioxide equivalent per year]

Climate scenario	Landscape Conservation Cooperative (LCC) region	Pyrogenic CO_2 + CO emissions (TgC/yr)	Pyrogenic CH_4 emissions ($TgCO_2$-eq/yr)	Net primary productivity (TgC/yr)	Biogenic CH_4 emissions ($TgCO_2$-eq/yr)	Heterotrophic respiration (TgC/yr)	Net ecosystem carbon balance (TgC/yr)	Global warming potential ($TgCO_2$-eq/yr)
				CGCM3.1				
A1B	Arctic LCC	0.00	0.00	6.16	2.63	4.68	1.40	–2.77
	Western Alaska LCC	0.50	0.05	3.48	1.98	2.59	0.32	0.63
	Northwest Boreal LCC North	2.65	0.24	28.20	24.36	22.79	2.02	14.55
	Northwest Boreal LCC South	0.45	0.04	4.36	6.66	3.38	0.33	4.76
	North Pacific LCC	0.01	0.00	0.68	0.49	0.52	0.13	–0.04
	Total	**3.61**	**0.34**	**42.87**	**36.13**	**33.96**	**4.20**	**17.13**
A2	Arctic LCC	2.86	0.30	6.86	4.29	2.77	1.09	0.10
	Western Alaska LCC	2.38	0.24	3.68	3.07	0.82	0.38	1.57
	Northwest Boreal LCC North	3.70	0.35	28.35	44.94	20.17	3.12	28.98
	Northwest Boreal LCC South	1.57	0.16	4.61	11.45	2.12	0.57	8.27
	North Pacific LCC	0.17	0.02	0.79	0.69	0.47	0.13	0.17
	Total	**10.68**	**1.06**	**44.29**	**64.44**	**26.36**	**5.28**	**39.09**
B1	Arctic LCC	0.00	0.00	6.18	2.57	4.71	1.39	–2.82
	Western Alaska LCC	1.33	0.13	3.30	1.85	2.07	–0.16	2.36
	Northwest Boreal LCC North	2.58	0.24	26.64	24.97	21.89	1.40	17.34
	Northwest Boreal LCC South	0.96	0.10	4.21	7.15	2.80	0.24	5.59
	North Pacific LCC	0.00	0.00	0.66	0.52	0.51	0.13	–0.01
	Total	**4.87**	**0.47**	**40.99**	**37.06**	**31.98**	**3.01**	**22.46**
				ECHAM5				
A1B	Arctic LCC	3.54	0.37	7.50	6.23	2.77	0.99	2.25
	Western Alaska LCC	2.16	0.22	3.82	3.95	1.40	0.13	3.23
	Northwest Boreal LCC North	3.81	0.35	29.02	61.48	20.49	2.87	44.65
	Northwest Boreal LCC South	1.84	0.18	4.68	15.72	2.05	0.31	13.05
	North Pacific LCC	0.20	0.02	0.78	1.28	0.44	0.09	0.83
	Total	**11.55**	**1.15**	**45.80**	**88.66**	**27.15**	**4.39**	**64.02**
A2	Arctic LCC	3.59	0.37	7.51	3.32	2.72	1.10	–0.72
	Western Alaska LCC	2.20	0.22	3.92	3.84	1.40	0.20	2.91
	Northwest Boreal LCC North	3.56	0.33	29.57	35.24	21.87	3.07	20.48
	Northwest Boreal LCC South	1.76	0.18	4.99	10.82	2.63	0.27	8.82
	North Pacific LCC	0.10	0.01	0.74	0.86	0.53	0.08	0.49
	Total	**11.22**	**1.11**	**46.73**	**54.09**	**29.15**	**4.71**	**31.99**
B1	Arctic LCC	1.22	0.13	6.30	4.19	3.96	0.99	0.21
	Western Alaska LCC	0.78	0.08	3.28	2.64	2.36	0.06	2.22
	Northwest Boreal LCC North	1.44	0.13	26.98	28.40	22.49	2.20	17.41
	Northwest Boreal LCC South	0.76	0.08	4.12	7.56	2.99	0.14	6.28
	North Pacific LCC	0.09	0.01	0.69	0.55	0.47	0.10	0.11
	Total	**4.29**	**0.42**	**41.36**	**43.34**	**32.26**	**3.49**	**26.23**

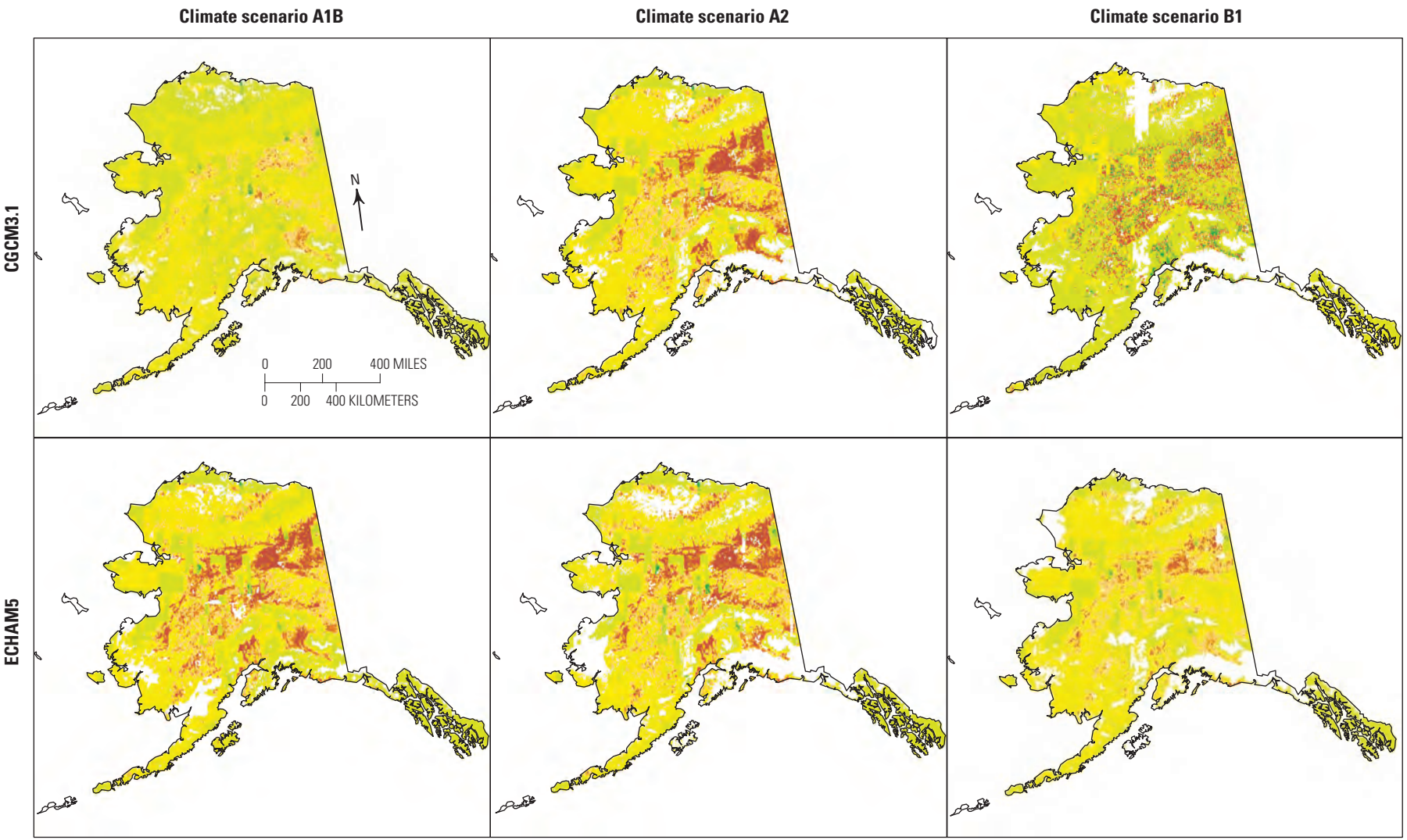

Figure 7.6. Spatial distribution of annual change in net methane emissions between the last decades of the historical period (2000–2009) and the projection period (2090–2099) for wetland ecosystems of Alaska for the two general circulation models, version 3.1-T47 of the Coupled Global Climate Model (CGCM3.1) developed by the Canadian Centre for Climate Modelling and Analysis and version 5 of the European Centre Hamburg Model (ECHAM5) developed by the Max Planck Institute, under three climate scenarios of the Intergovernmental Panel on Climate Change's Special Report on Emissions Scenarios (Nakićenović and Swart, 2000), B1, A1B, and A2, in order of low to high projected CO_2 emissions.

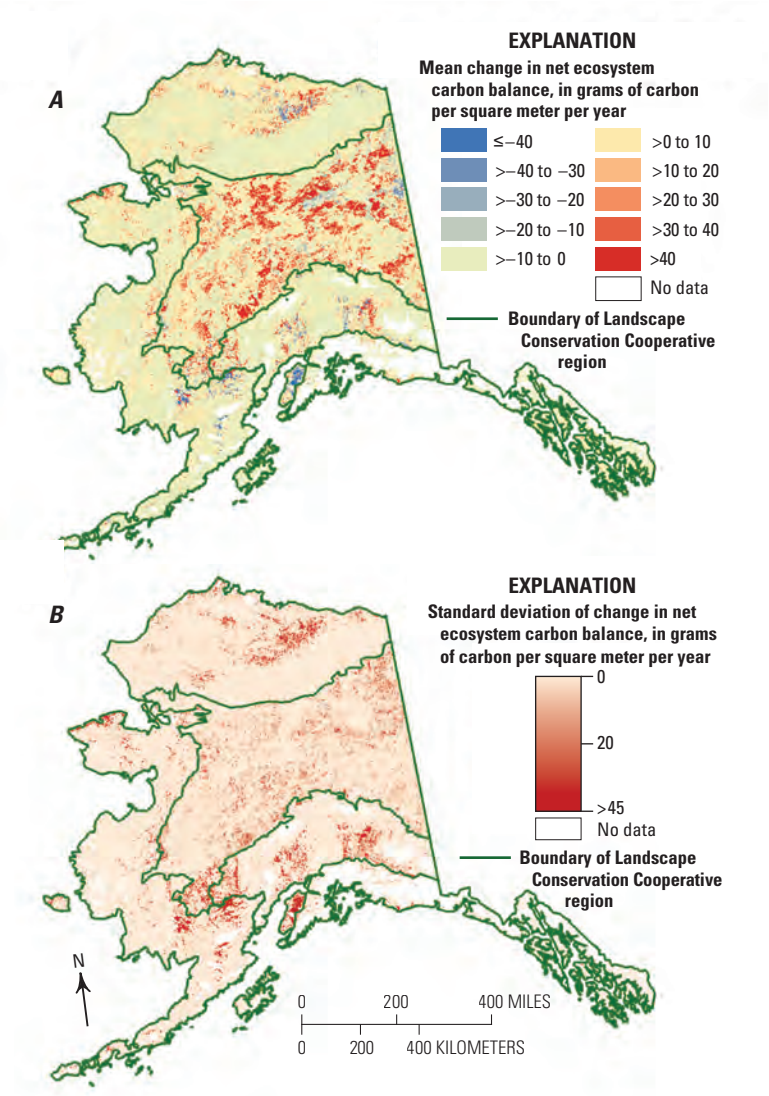

Figure 7.7. Spatial distribution of *A*, mean change in net ecosystem carbon balance between the last decades of the historical period (2000–2009) and the projection period (2090–2099) among the six climate simulations and *B*, corresponding standard deviation. The six climate simulations used in this report are combinations of two general circulation models, version 3.1-T47 of the Coupled Global Climate Model (CGCM3.1) developed by the Canadian Centre for Climate Modelling and Analysis and version 5 of the European Centre Hamburg Model (ECHAM5) developed by the Max Planck Institute, under three climate scenarios of the Intergovernmental Panel on Climate Change's Special Report on Emissions Scenarios (Nakićenović and Swart, 2000), B1, A1B, and A2, in order of low to high projected CO_2 emissions.

7.6. Conclusions

Alaska's wetland ecosystems were estimated to have produced net CH_4 emissions averaging 1 TgC/yr from 1950 through 2009. Biogenic CH_4 accounted for most (>90 percent) of the total emissions. Estimates of NECB during the historical period indicated that all LCC regions in Alaska were net carbon sinks except the Northwest Boreal LCC North. Carbon loss in the Northwest Boreal LCC North offset carbon gain from the other regions. As a result, 1.3 TgC/yr was lost during the historical period statewide—in addition to the 1 TgC/yr lost as CH_4, 0.3 TgC/yr was lost because of changes in NPP and wildfire emission—and the carbon loss was about equally distributed in the soil and the vegetation. The GWP of wetlands over the historical period indicated that wetlands were a significant source of greenhouse gas forcing at 33 $TgCO_2$-eq/yr.

The projected total CH_4 emissions across three anthropogenic CO_2 emissions scenarios and two GCMs were estimated to range from 36 to 90 $TgCO_2$-eq/yr by the 2090s, which represented an increase of 15 to 182 percent from the historical period. Comparatively, projected NPP ranged from 41.0 to 46.7 TgC/yr, which represented an increase of 10 to 25 percent from the historical period. Projected HR ranged from 26.4 to 34.0 TgC/yr, which represented a change of –3 to 25 percent from the historical period. Overall, by the end of the 21st century, carbon stocks in wetland ecosystems of all LCC regions of Alaska were projected to continue or start to grow. On average, wetland ecosystems would store 4.2 TgC/yr in 2090–2099, ranging from 3.0 to 5.3 TgC/yr statewide depending on climate simulation. Despite the uncertainty around the absolute value of projected NECB related to climate forcing, the trend of NECB is consistent among all six climate simulations, predicting that wetlands in Alaska will be a net carbon sink by 2099.

However, mainly because of the relatively large increase in CH_4 emissions during the projected period, GWP is projected to remain positive by the 2090s, ranging from 17.1 to 64.0 $TgCO_2$-eq/yr, which represented a change of –49 to 92 percent compared with the historical period. Atmospheric CO_2 concentration and mean annual temperature were identified to be the primary environmental controls of the projected increase in biogenic CH_4 emissions. The increase in vegetation productivity and subsequent increase in substrate for CH_4 production was the likely cause of the projected increased CH_4 production in response to climate change. This projected increase was enough to offset projected carbon storage in wetlands of Alaska during the 21st century. Furthermore, little is known about the environmental controls of thermokarst disturbance and its effect on local and regional carbon balance. For this reason, thermokarst disturbance was not included in the present assessment. However, field evidence suggests that changes in drainage conditions associated with thermokarst formation may increase CH_4 production and potentially increase the release of greenhouse gas in wetlands of Alaska.

7.7. References Cited

Chapin, F.S., III, Woodwell, G.M., Randerson, J.T., Rastetter, E.B., Lovett, G.M., Baldocchi, D.D., Clark, D.A., Harmon, M.E., Schimel, D.S., Valentini, R., Wirth, C., Aber, J.D., Cole, J.J., Goulden, M.L., Harden, J.W., Heimann, M., Howarth, R.W., Matson, P.A., McGuire, A.D., Melillo, J.M., Mooney, H.A., Neff, J.C., Houghton, R.A., Pace, M.L., Ryan, M.G., Running, S.W., Sala, O.E., Schlesinger, W.H., and Schulze, E.-D., 2006, Reconciling carbon-cycle concepts, terminology, and methods: Ecosystems, v. 9, no. 7, p. 1041–1050, http://dx.doi.org/10.1007/s10021-005-0105-7.

Clein, J.S., McGuire, A.D., Zhang, X., Kicklighter, D.W., Melillo, J.M., Wofsy, S.C., Jarvis, P.G., and Massheder, J.M., 2002, Historical and projected carbon balance of mature black spruce ecosystems across North America; The role of carbon-nitrogen interactions: Plant and Soil, v. 242, no. 1, p. 15–32, http://dx.doi.org/10.1023/a:1019673420225.

Euskirchen, E.S., Bret-Harte, M.S., Scott, G.J., Edgar, C., Shaver, G.R., 2012, Seasonal patterns of carbon dioxide and water fluxes in three representative tundra ecosystems in northern Alaska: Ecosphere, v. 3, no. 1, article 4, 19 p., http://dx.doi.org/10.1890/ES11-00202.1.

Fisher, J.B., Sikka, M., Oechel, W.C., Huntzinger, D.N., Melton, J.R., Koven, C.D., Ahlström, A., Arain, M.A., Baker, I., Chen, J.M., Ciais, P., Davidson, C., Dietze, M., El-Masri, B., Hayes, D., Huntingford, C., Jain, A.K., Levy, P.E., Lomas, M.R., Poulter, B., Price, D., Sahoo, A.K., Schaefer, K., Tian, H., Tomelleri, E., Verbeeck, H., Viovy, N., Wania, R., Zeng, N., and Miller, C.E., 2014, Carbon cycle uncertainty in the Alaskan Arctic: Biogeosciences, v. 11, p. 4271–4288, http://dx.doi.org/10.5194/bg-11-4271-2014.

Forster, Piers, Ramaswamy, Venkatachalam, Artaxo, Paulo, Berntsen, Terje, Betts, Richard, Fahey, D.W., Haywood, James, Lean, Judith, Lowe, D.C., Myhre, Gunnar, Nganga, John, Prinn, Ronald, Raga, Graciela, Schulz, Michael, and Van Dorland, Robert, 2007, Changes in atmospheric constituents and in radiative forcing, chap. 2 *of* Solomon, Susan, Qin, Dahe, Manning, Martin, Chen, Zhenlin, Marquis, Melinda, Averyt, Kristen, Tignor, M.M.B., and Miller, H.L., Jr., eds., Climate change 2007—The physical science basis; Contribution of Working Group I to the Fourth Assessment Report of the Intergovernmental Panel on Climate Change: Cambridge, United Kingdom, and New York, Cambridge University Press, p. 129–234. [Also available at http://www.ipcc.ch/publications_and_data/publications_ipcc_fourth_assessment_report_wg1_report_the_physical_science_basis.htm.]

French, N.H.F., Kasischke, E.S., and Williams, D.G., 2002, Variability in the emission of carbon-based trace gases from wildfire in the Alaskan boreal forest, Journal of Geophysical Research, v. 107, no. D1, p. FFR 7–1 to FFR 7–11, http://dx.doi.org/10.1029/2001JD000480.

Frolking, Steve, and Roulet, N.T., 2007, Holocene radiative forcing impact of northern peatland carbon accumulation and methane emissions: Global Change Biology, v. 13, no. 5, p. 1079–1088, http://dx.doi.org/10.1111/j.1365-2486.2007.01339.x.

Genet, H., McGuire, A.D., Barrett, K., Breen, A., Euskirchen, E.S., Johnstone, J.F., Kasischke, E.S., Melvin, A.M., Bennett, A., Mack, M.C., Rupp, T.S., Schuur, E.A.G., Turetsky, M.R., and Yuan, F., 2013, Modeling the effects of fire severity and climate warming on active layer thickness and soil carbon storage of black spruce forests across the landscape in interior Alaska: Environmental Research Letters, v. 8, no. 4, letter 045016, 13 p., http://dx.doi.org/10.1088/1748-9326/8/4/045016.

Gesch, D., Oimoen, M., Greenlee, S., Nelson, C., Steuck, M., and Tyler, D., 2002, The national elevation dataset: Photogrammetric Engineering and Remote Sensing, v. 68, no. 1, p. 5–11.

Gough, Laura, Moore, J.C., Shaver, G.R., Simpson, R.T., and Johnson, D.R., 2012, Above- and belowground responses of arctic tundra ecosystems to altered soil nutrients and mammalian herbivory: Ecology, v. 93, no. 7, p. 1683–1694, http://dx.doi.org/10.1890/11-1631.1.

Grand, J.B., Flint, P.L., and Heglund, P.J., 1997, Habitat use by nesting and brood rearing northern pintails on the Yukon-Kuskokwim Delta, Alaska: The Journal of Wildlife Management, v. 61, no. 4, p. 1199–1207, http://dx.doi.org/10.2307/3802117.

Harris, I., Jones, P.D., Osborn, T.J., and Lister, D.H., 2014, Updated high-resolution grids of monthly climatic observations—the CRU TS3.10 dataset: International Journal of Climatology, v. 34, no. 3, p. 623–642, http://dx.doi.org/10.1002/joc.3711.

He, Yujie, Jones, M.C., Zhuang, Qianlai, Bochicchio, Christopher, Felzer, B.S., Mason, Erik, and Yu, Zicheng, 2014, Evaluating CO_2 and CH_4 dynamics of Alaskan ecosystems during the Holocene Thermal Maximum: Quaternary Science Reviews, v. 86, p. 63–77, http://dx.doi.org/10.1016/j.quascirev.2013.12.019.

Homer, Collin, Huang, Chengquan, Yang, Limin, Wylie, Bruce, and Coan, Michael, 2004, Development of a 2001 National Land-Cover Database for the United States: Photogrammetric Engineering and Remote Sensing, v. 70, no. 7, p. 829–840, http://dx.doi.org/10.14358/PERS.70.7.829.

Ji, Lei, Zhang, Li, Rover, Jennifer, Wylie, B.K., and Chen, Xuexia, 2014, Geostatistical estimation of signal-to-noise ratios for spectral vegetation indices: ISPRS Journal of Photogrammetry and Remote Sensing, v. 96, p. 20–27, http://dx.doi.org/10.1016/j.isprsjprs.2014.06.013.

Ji, Lei, Zhang, Li, Wylie, B.K., and Rover, Jennifer, 2011, On the terminology of the spectral vegetation index (NIR–SWIR)/(NIR+SWIR): International Journal of Remote Sensing, v. 32, no.21, p. 6901–6909, http://dx.doi.org/10.1080/01431161.2010.510811.

Johnson, K.D., Harden, Jennifer, McGuire, A.D., Bliss, N.B., Bockheim, J.G., Clark, Mark, Nettleton-Hollingsworth, Teresa, Jorgenson, M.T, Kane, E.S., Mack, Michelle, O'Donnell, Jonathan, Ping, C.-L., Schuur, E.A.G., Turetsky, M.R., and Valentine, D.W., 2011, Soil carbon distribution in Alaska in relation to soil-forming factors: Geoderma, v. 167–168, p. 71–84, http://dx.doi.org/10.1016/j.geoderma.2011.10.006.

Jorgenson, M.T., and Osterkamp, T.E., 2005, Response of boreal ecosystems to varying modes of permafrost degradation: Canadian Journal of Forest Research, v. 35, no. 9, p. 2100–2111, http://dx.doi.org/10.1139/x05-153.

Jorgenson, M.T., Shur, Y.L., and Osterkamp, T.E., 2008, Thermokarst in Alaska, *in* Kane, D.L., and Hinkel, K.M., eds., Proceedings of the Ninth International Conference on Permafrost, Fairbanks, Alaska, June 29 to July 3, 2008: Institute of Northern Engineering, University of Alaska-Fairbanks, p. 869–876.

Jorgenson, Torre, Yoshikawa, Kenji, Kanevskiy, Mikhail, Shur, Yuri, Romanovsky, Vladimir, Marchenko, Sergei, Grosse, Guido, Brown, Jerry, and Jones, Ben, 2008a, Permafrost characteristics of Alaska, *in* Kane, D.L., and Hinkel, K.M., eds., Proceedings of the Ninth International Conference on Permafrost, Fairbanks, Alaska, June 29 to July 3, 2008: Institute of Northern Engineering, University of Alaska-Fairbanks, p. 121–122.

Jorgenson, Torre, Yoshikawa, Kenji, Kanevskiy, Mikhail, Shur, Yuri, Romanovsky, Vladimir, Marchenko, Sergei, Grosse, Guido, Brown, Jerry, and Jones, Ben, 2008b, Permafrost characteristics of Alaska (December 2008 update to July 2008 Ninth International Conference on Permafrost [NICOP] map): Fairbanks, Alaska, University of Alaska-Fairbanks, Institute of Northern Engineering, scale 1:7,200,000, http://permafrost.gi.alaska.edu/sites/default/files/AlaskaPermafrostMap_Front_Dec2008_Jorgenson_etal_2008.pdf.

Kasischke, E.S., and Turetsky, M.R., 2006, Recent changes in the fire regime across the North American boreal region—Spatial and temporal patterns of burning across Canada and Alaska: Geophysical Research Letters, v. 33, no. 9, letter L09703, 5 p., http://dx.doi.org/10.1029/2006GL025677.

Kivinen, J., Warmuth, M.K., and Auer, P., 1997, The Perceptron algorithm versus Winnow; Linear versus logarithmic mistake bounds when few input variables are relevant: Artificial Intelligence, v. 97, nos. 1–2, p. 325–343, http://dx.doi.org/10.1016/S0004-3702(97)00039-8.

Koven, C.D., Ringeval, Bruno, Friedlingstein, Pierre, Ciais, Philippe, Cadule, Patricia, Khvorostyanov, Dmitry, Krinner, Gerhard, and Tarnocai, Charles, 2011, Permafrost carbon-climate feedbacks accelerate global warming: National Academy of Sciences Proceedings, v. 108, no. 36, p. 14769–14774, http://dx.doi.org/10.1073/pnas.1103910108.

Lehner, Bernhard, and Döll, Petra, 2004, Development and validation of a global database of lakes, reservoirs and wetlands: Journal of Hydrology, v. 296, nos. 1–4, p. 1–22, http://dx.doi.org/10.1016/j.jhydrol.2004.03.028.

Liao, AnPing, Chen, LiJun, Chen, Jun, He, ChaoYing, Cao, Xin, Chen, Jin, Peng, Shu, Sun, FangDi, and Gong, Peng, 2014, High-resolution remote sensing mapping of global land water: Science China Earth Sciences, v. 57, no. 10, p. 2305–2316, http://dx.doi.org/10.1007/s11430-014-4918-0.

Lu, Huaxing, 2008, Modelling terrain complexity, *in* Zhou, Qiming, Lees, Brian, and Tang, Guo-an, eds., Advances in digital terrain analysis: Lecture Notes in Geoinformation and Cartography, p. 159–176, http://dx.doi.org/10.1007/978-3-540-77800-4_9.

Malone, Thomas, Liang, Jingjing, and Packee, E.C., 2009, Cooperative Alaska Forest Inventory: U.S. Department of Agriculture, Forest Service, Pacific Northwest Research Station, General Technical Report PNW–GTR–785, 42 p. [Also available at http://www.fs.fed.us/pnw/pubs/pnw_gtr785.pdf.]

Martin, P.D., Jenkins, J.L., Adams, F.J., Jorgenson, M.T., Matz, A.C., Payer, D.C., Reynolds, P.E., Tidwell, A.C., and Zelenak, J.R., 2009, Wildlife response to environmental Arctic change—Predicting future habitats of Arctic Alaska; Report of the Wildlife Response to Environmental Arctic Change (WildREACH) Predicting the Future Habitats of Arctic Alaska Workshop, Fairbanks, Alaska, November, 17–18, 2008: U.S. Fish and Wildlife Service, 138 p. [Also available at http://arcticlcc.org/assets/resources/WildREACH_Workshop_Report_Final.pdf.]

McFarlane, N.A., Boer, G.J., Blanchet, J.-P., and Lazare, M., 1992, The Canadian Climate Centre second-generation general circulation model and its equilibrium climate: Journal of Climate, v. 5, no. 10, p. 1013–1044, http://dx.doi.org/10.1175/1520-0442(1992)005<1013:TCCCSG>2.0.CO;2.

Myers-Smith, I.H., Harden, J.W., Wilmking, M., Fuller, C.C., McGuire, A.D., and Chapin, F.S., III, 2008, Wetland succession in a permafrost collapse; Interactions between fire and thermokarst: Biogeosciences, v. 5, no. 5, p. 1273–1286, http://dx.doi.org/10.5194/bg-5-1273-2008.

Nakićenović, Nebojša, and Swart, Robert, eds., 2000, Special report on emissions scenarios—A special report of Working Group III of the Intergovernmental Panel on Climate Change: Cambridge, United Kingdom, Cambridge University Press, 599 p. [Also available at http://www.ipcc.ch/ipccreports/sres/emission/index.php?idp=0.]

O'Donnell, J.A., Jorgenson, M.T., Harden, J.W., McGuire, A.D., Kanevskiy, M.Z., and Wickland, K.P., 2012, The effects of permafrost thaw on soil hydrologic, thermal, and carbon dynamics in an Alaskan peatland: Ecosystems, v. 15, no. 2, p. 213–229, http://dx.doi.org/10.1007/s10021-011-9504-0.

Rastetter, E.B., King, A.W., Cosby, B.J., Hornberger, G.M., O'Neill, R.V., and Hobbie, J.E., 1992, Aggregating fine-scale ecological knowledge to model coarser-scale attributes of ecosystems: Ecological Applications, v. 2, no. 1, p. 55–70, http://dx.doi.org/10.2307/1941889.

Roeckner, E., Bäuml, G., Bonaventura, L., Brokopf, R., Esch, M., Giorgetta, M., Hagemann, S., Kirchner, I., Kornblueh, L., Manzini, E., Rhodin, A., Schlese, U., Schulzweida, U., and Tompkins, A., 2003, The atmospheric general circulation model ECHAM5, part I—Model description: Max-Planck-Institut für Meteorologie Report, no. 349, 127 p. [Also available at https://www.mpimet.mpg.de/fileadmin/publikationen/Reports/max_scirep_349.pdf.]

Roeckner, E., Brokopf, R., Esch, M., Giorgetta, M., Hagemann, S., Kornblueh, L., Manzini, E., Schlese, U., and Schulzweida, U., 2004, The atmospheric general circulation model ECHAM5, part II—Sensitivity of simulated climate to horizontal and vertical resolution: Max-Planck-Institut für Meteorologie Report No. 354, 56 p. [Also available at http://pubman.mpdl.mpg.de/pubman/item/escidoc:995221:8/component/escidoc:995220/MPI_Report354.pdf.]

Roy, D.P., Ju, Junchang, Kline, Kristi, Scaramuzza, P.L., Kovalskyy, Valeriy, Hansen, Matthew, Loveland, T.R., Vermote, Eric, and Zhang, Chunsun, 2010, Web-enabled Landsat Data (WELD); Landsat ETM+ composited mosaics of the conterminous United States: Remote Sensing of Environment, v. 114, no. 1, p. 35–49, http://dx.doi.org/10.1016/j.rse.2009.08.011.

Rupp, T.S., Chen, Xi, Olson, Mark, and McGuire, A.D., 2007, Sensitivity of simulated boreal fire dynamics to uncertainties in climate drivers: Earth Interactions, v. 11, no. 3, p. 1–21, http://dx.doi.org/10.1175/EI189.1.

Rupp, T.S., Starfield, A.M., and Chapin, F.S., III, 2000, A frame-based spatially explicit model of subarctic vegetation response to climatic change; Comparison with a point model: Landscape Ecology, v. 15, no. 4, p. 383–400, http://dx.doi.org/10.1023/A:1008168418778.

Rupp, T.S., Starfield, A.M., Chapin, F.S., III, and Duffy, P., 2002, Modeling the impact of black spruce on the fire regime of Alaskan boreal forest: Climatic Change, v. 55, no. 1–2, p. 213–233, http://dx.doi.org/10.1023/A:1020247405652.

Schaefer, Kevin, Zhang, Tingjun, Bruhwiler, Lori, and Barrett, A.P., 2011, Amount and timing of permafrost carbon release in response to climate warming: Tellus; Series B, Chemical and Physical Meteorology, v. 63B, no. 2, p. 165–180, http://dx.doi.org/10.1111/j.1600-0889.2011.00527.x.

Schuur, E.A.G., Bockheim, James, Canadell, J.G., Euskirchen, Eugenie, Field, C.B., Goryachkin, S.V., Hagemann, Stefan, Kuhry, Peter, Lafleur, P.M., Lee, Hanna, Mazhitova, Galina, Nelson, F.E., Rinke, Annette, Romanovsky, V.E., Shiklomanov, Nikolay, Tarnocai, Charles, Venevsky, Sergey, Vogel, J.G., and Zimov, S.A., 2008, Vulnerability of permafrost carbon to climate change; Implications for the global carbon cycle: BioScience, v. 58, no. 8, p. 701–714, http://dx.doi.org/10.1641/b580807.

Shaver, G.R., and Chapin, F.S., III, 1986, Effect of fertilizer on production and biomass of tussock tundra, Alaska, U.S.A.: Arctic and Alpine Research, v. 18, no. 3, p. 261–268. [Also available at http://dx.doi.org/10.2307/1550883.]

Shaver, G.R., and Chapin, F.S., III, 1991, Production; Biomass relationships and element cycling in contrasting arctic vegetation types: Ecological Monographs, v. 61, no. 1, p. 1–31, http://dx.doi.org/10.2307/1942997.

Sistla, S.A., Moore, J.C., Simpson, R.T., Gough, Laura, Shaver, G.R., and Schimel, J.P., 2013, Long-term warming restructures Arctic tundra without changing net soil carbon storage: Nature, v. 497, no. 7451, p. 615–618, http://dx.doi.org/10.1038/nature12129.

Stocker, T.F., Qin, Dahe, Plattner, G.-K., Tignor, M.M.B., Allen, S.K., Boschung, Judith, Nauels, Alexander, Xia, Yu, Bex, Vincent, and Midgley, P.M., eds., 2013, Summary for policymakers, *in* Climate change 2013—The physical science basis, Contribution of Working Group I to the Fifth Assessment Report of the Intergovernmental Panel on Climate Change: Cambridge, United Kingdom, Cambridge University Press, p. 3–29. [Also available at http://www.ipcc.ch/report/ar5/wg1/.]

Sullivan, P.F., Sommerkorn, Martin, Rueth, H.M., Nadelhoffer, K.J., Shaver, G.R., and Welker, J.M., 2007, Climate and species affect fine root production with long-term fertilization in acidic tussock tundra near Toolik Lake, Alaska: Oecologia, v. 153, no. 3, p. 643–652, http://dx.doi.org/10.1007/s00442-007-0753-8.

Sutton, C.D., 2005, Classification and regression trees, bagging, and boosting: Handbook of Statistics, v. 24, p. 303–329, http://dx.doi.org/10.1016/S0169-7161(04)24011-1.

Turetsky, M.R., Kane, E.S., Harden, J.W., Ottmar, R.D., Manies, K.L., Hoy, Elizabeth, and Kasischke, E.S., 2011, Recent acceleration of biomass burning and carbon losses in Alaskan forests and peatlands: Nature Geoscience, v. 4, no. 1, p. 27–31, http://dx.doi.org/10.1038/ngeo1027.

Turetsky, M.R., Treat, C.C., Waldrop, M.P., Waddington, J.M., Harden, J.W., and McGuire, A.D., 2008, Short-term response of methane fluxes and methanogen activity to water table and soil warming manipulations in an Alaskan peatland: Journal of Geophysical Research; Biogeosciences, v. 113, no. G3, article G00A10, 15 p., http://dx.doi.org/10.1029/2007JG000496.

Van Wijk, M.T., Williams, M., Gough, L., Hobbie, S.E., and Shaver, G.R., 2003, Luxury consumption of soil nutrients; A possible competitive strategy in above-ground and below-ground biomass allocation and root morphology for slow-growing arctic vegetation?: Journal of Ecology, v. 91, no. 4, p. 664–676, http://dx.doi.org/10.1046/j.1365-2745.2003.00788.x.

Whitcomb, Jane, Moghaddam, Mahta, McDonald, Kyle, Kellndorfer, Josef, and Podest, Erika, 2009, Mapping vegetated wetlands of Alaska using L-band radar satellite imagery: Canadian Journal of Remote Sensing, v. 35, no. 1, p. 54–72, http://dx.doi.org/10.5589/m08-080.

Yi, Shuhua, Manies, Kristen, Harden, Jennifer, and McGuire, A.D., 2009, Characteristics of organic soil in black spruce forests; Implications for the application of land surface and ecosystem models in cold regions: Geophysical Research Letters, v. 36, no. 5, letter L05501, 5 p., http://dx.doi.org/10.1029/2008GL037014.

Yi, Shuhua, McGuire, A.D., Harden, Jennifer, Kasischke, Eric, Manies, Kristen, Hinzman, Larry, Liljedahl, Anna, Randerson, Jim, Liu, Heping, Romanovsky, Vladimir, Marchenko, Sergei, and Kim, Yongwon, 2009, Interactions between soil thermal and hydrological dynamics in the response of Alaska ecosystems to fire disturbance: Journal of Geophysical Research; Biogeosciences, v. 114, no. G2, article G02015, 20 p., http://dx.doi.org/10.1029/2008JG000841.

Yi, Shuhua, McGuire, A.D., Kasischke, Eric, Harden, Jennifer, Manies, Kristen, Mack, Michelle, and Turetsky, Merritt, 2010, A dynamic organic soil biogeochemical model for simulating the effects of wildfire on soil environmental conditions and carbon dynamics of black spruce forests: Journal of Geophysical Research; Biogeosciences, v. 115, no. G4, article G04015, 15 p., http://dx.doi.org/10.1029/2010JG001302.

Yuan, F.-M., Yi, S.-H., McGuire, A.D., Johnson, K.D., Liang, J., Harden, J.W., Kasischke, E.S., and Kurz, W.A., 2012, Assessment of boreal forest historical C dynamics in the Yukon River Basin; Relative roles of warming and fire regime change: Ecological Applications, v. 22, no. 8, p. 2091–2109, http://dx.doi.org/10.1890/11-1957.1.

Zhuang, Q., McGuire, A.D., Melillo, J.M., Clein, J.S., Dargaville, R.J., Kicklighter, D.W., Myneni, R.B., Dong, J., Romanovsky, V.E., Harden, J., and Hobbie, J.E., 2003, Carbon cycling in extratropical terrestrial ecosystems of the Northern Hemisphere during the 20th century; A modeling analysis of the influences of soil thermal dynamics: Tellus; Series B, Chemical and Physical Meteorology, v. 55B, no. 3, p. 751–776, http://dx.doi.org/10.1034/j.1600-0889.2003.00060.x.

Zhuang, Q., McGuire, A.D., O'Neill, K.P., Harden, J.W., Romanovsky, V.E., and Yarie, J., 2002, Modeling soil thermal and carbon dynamics of a fire chronosequence in interior Alaska: Journal of Geophysical Research; Atmospheres, v. 107, no. D1, p. FFR 3–1 to FFR 3–26, http://dx.doi.org/10.1029/2001jd001244.

Zhuang, Q., Melillo, J.M., Kicklighter, D.W., Prinn, R.G., McGuire, A.D., Steudler, P.A., Felzer, B.S., and Hu, S., 2004, Methane fluxes between terrestrial ecosystems and the atmosphere at northern high latitudes during the past century; A retrospective analysis with a process-based biogeochemistry model: Global Biogeochemical Cycles, v. 18, no. 3, article GB3010, 23 p., http://dx.doi.org/10.1029/2004GB002239.

Zhuang, Q., Romanovsky, V.E., and McGuire, A.D., 2001, Incorporation of a permafrost model into a large-scale ecosystem model; Evaluation of temporal and spatial scaling issues in simulating soil thermal dynamics: Journal of Geophysical Research; Atmospheres, v. 106, no. D24, p. 33649–33670, http://dx.doi.org/10.1029/2001jd900151.

Chapter 8. Carbon Burial, Transport, and Emission from Inland Aquatic Ecosystems in Alaska

By Sarah Stackpoole,[1] David Butman,[1,2] David Clow,[1] Kris Verdin,[1] Ben Gaglioti,[1,3] and Robert Striegl[1]

8.1. Highlights

- The total estimated surface area of inland waters in Alaska was approximately 60,000 square kilometers (km^2), which represents nearly 3.5 percent of the total land surface area.
- The total net estimated carbon flux (coastal export plus carbon dioxide [CO_2] emissions from rivers and lakes minus burial in lake sediments) from inland waters of Alaska was 41.2 teragrams of carbon per year (TgC/yr) (5th and 95th percentiles of 30.4 TgC/yr and 59.7 TgC/yr). Total carbon yield based on total land surface area was 27.5 grams of carbon per square meter per year ($gC/m^2/yr$) (5th and 95th percentiles of 20.1 $gC/m^2/yr$ and 39.5 $gC/m^2/yr$).
- Riverine systems of Alaska functioned as carbon sources to coastal ecosystems and the atmosphere. Dissolved inorganic carbon and total organic carbon exports to coastal areas were 12.2 $gC/m^2/yr$ (5th and 95th percentiles of 10.8 $gC/m^2/yr$ and 16.6 $gC/m^2/yr$) and CO_2 emissions to the atmosphere were 11.0 $gC/m^2/yr$ (5th and 95th percentiles of 6.0 $gC/m^2/yr$ and 17.4 $gC/m^2/yr$).
- Lacustrine systems acted as both sources and sinks of carbon with 5.5 $gC/m^2/yr$ (5th and 95th percentiles of 4.0 $gC/m^2/yr$ and 7.4 $gC/m^2/yr$) emitted as CO_2 to the atmosphere and –1.2 $gC/m^2/yr$ (5th and 95th percentiles of –0.7 $gC/m^2/yr$ and –1.9 $gC/m^2/yr$) of organic carbon buried in lake sediments. Negative values represent sequestration.
- There was considerable variability in the estimated carbon fluxes of inland waters among the six hydrologic regions in Alaska. This was due to the differences in the size and abundance of water bodies, topography, climate, land cover, permafrost, and glacier extent associated with each region.

8.2. Introduction

Section 712 of the Energy Independence and Security Act (EISA) of 2007 required an assessment of carbon fluxes related to freshwater aquatic ecosystems, including rivers and lakes, which collectively are categorized as inland waters. Carbon fluxes associated with aquatic ecosystems (this chapter) are assessed separately from those of the terrestrial ecosystems (chapters 6 and 7) in this report because of limited empirical aquatic data and a lack of a large-scale, spatially explicit carbon model that integrates terrestrial and aquatic fluxes.

Inland aquatic ecosystems are critical components of the carbon cycle. Rivers and lakes serve as sites for biogeochemical carbon reactions that result in an exchange of carbon dioxide (CO_2) among aquatic and terrestrial environments and the atmosphere, and rivers act as conduits that deliver carbon to the coast (Kling and others, 1992; Striegl and others, 2012; Tank, Raymond, and others, 2012; Crawford and others, 2013; McClelland and others, 2014; Sepulveda-Jauregui and others, 2014). Carbon sequestration in lake sediments may offset fluxes to oceans and the atmosphere (Naidu and others, 1999; Walter Anthony and others, 2014). Collectively, the amount of carbon moving through, into, and out of aquatic ecosystems makes them a significant component of carbon budgets at local, regional, and global scales (Cole and others, 2007;

[1]U.S. Geological Survey, Denver, Colo.

[2]University of Washington, Seattle, Wash.

[3]University of Alaska-Fairbanks, Fairbanks, Alaska.

Tranvik and others, 2009; Aufdenkampe and others, 2011; Butman and Raymond, 2011; Crawford and others, 2013; Raymond and others, 2013).

The objective of this chapter is to provide baseline estimates of aquatic carbon fluxes from inland waters for the six main hydrologic regions of Alaska: the Arctic Slope (called North Slope in this report), Northwest, Yukon, Southwest, South-Central, and Southeast (Seaber and others, 1987) (fig. 8.1).

These regions were chosen as the reporting units because, unlike the Alaska Landscape Conservation Cooperatives used in previous chapters of this report, the boundaries of the hydrologic regions coincide with natural drainage areas for rivers within the State. By leveraging existing hydrologic and carbon chemistry datasets, we estimated the following aquatic carbon fluxes: (1) lateral transport of dissolved inorganic carbon (DIC) and total organic carbon (TOC, composed of dissolved and particulate phases) from riverine systems to the coast, (2) gaseous carbon emissions of CO_2 from riverine systems, (3) gaseous carbon emissions of CO_2 from lacustrine systems, and (4) carbon burial in sediments of lakes. Aquatic flux values presented in this chapter were normalized to total land surface area to produce yield estimates, and comparisons of regional variability among yields are presented. Given the vulnerability of carbon stored in the soils and permafrost of Alaska to a warming climate and the strong linkages between terrestrial and aquatic ecosystems, it is important to provide accurate estimates of current carbon fluxes in aquatic environments, so that future climate change effects can be determined.

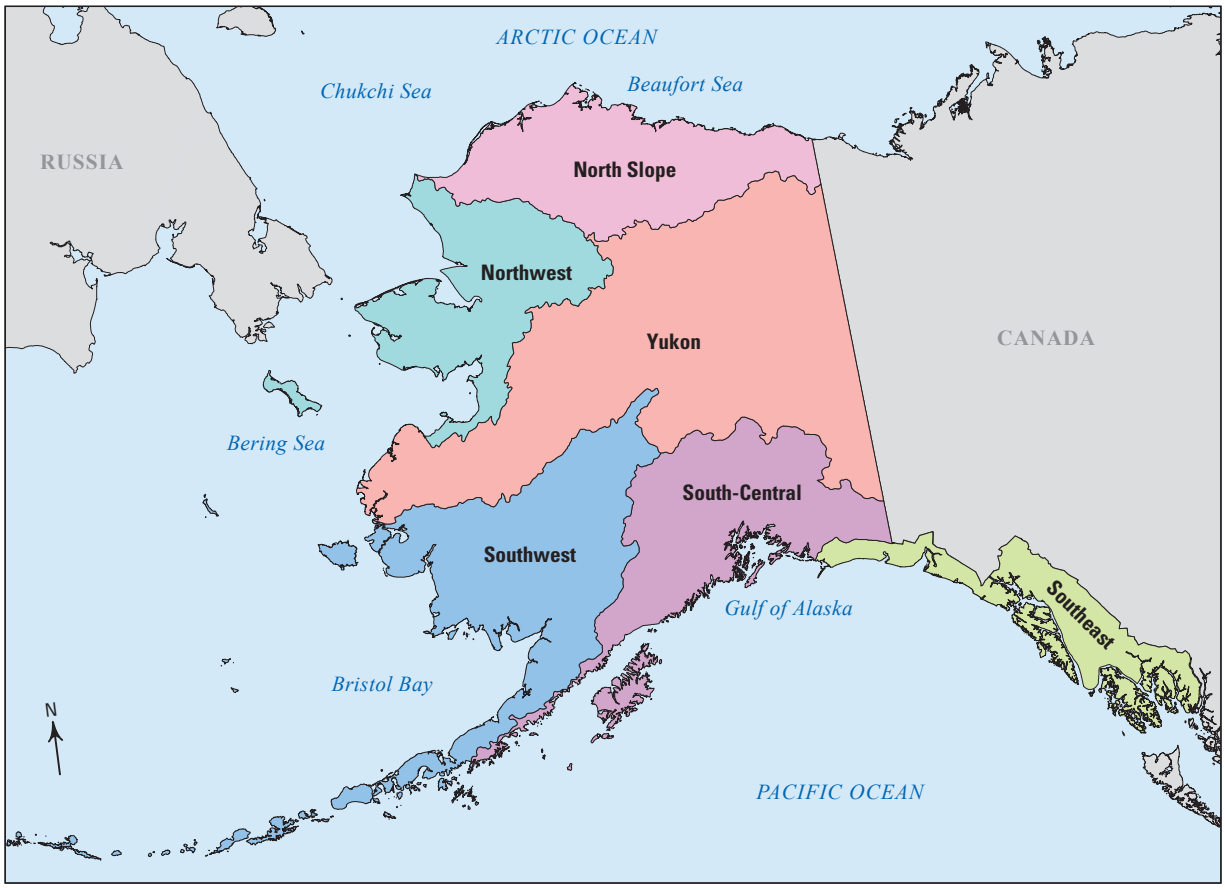

Figure 8.1. The six major hydrologic regions of Alaska: the Arctic Slope, called North Slope in this report, Northwest, Yukon, Southwest, South-Central, and Southeast from Seaber and others (1987).

8.3. Methods and Data

8.3.1. Physiography of Alaska Related to Inland Waters

The regional hydrology of Alaska is influenced by the State's varied physiography. The North Slope hydrologic region is characterized largely by an arctic coastal plain, which is poorly drained and dominated by dune-trough (Jorgenson and Shur, 2007) and thermokarst (Frohn and others, 2005) lakes. This region is underlain mostly by continuous permafrost (Jorgenson and others, 2008; Schuur and others, 2008). The Colville, Kuparuk, and Sagavanirktok Rivers, the largest rivers in the region, drain from the northern slope of the Brooks Range into the Beaufort Sea (fig. 8.2). The mountains in the Northwest hydrologic region have small pockets of glaciers and lakes at higher elevations (Wahrhaftig, 1965). Scattered lakes occur in lower elevation areas embedded in multiple sequences representing the late-Pleistocene (Hamilton, 1982) and Holocene glacial advances (Ellis and Calkin, 1984). The Kobuk and Noatak Rivers, the major rivers of the Northwest region, drain into the Chukchi Sea.

The intermontane plateau, commonly known as interior Alaska, occurs between the Brooks Range and the coastal mountain ranges of the Gulf of Alaska, and constitutes the Yukon hydrologic region. This region is underlain by discontinuous permafrost (Jorgenson and others, 2008; Schuur and

Figure 8.2. Coastal receiving waters and mountain ranges in the State of Alaska. Letters indicate major rivers: A, Unuk; B, Stikine; C, Taku; D, Alsek; E, Copper; F, Susitna; G, Nushagak; H, Kuskokwim; I, Yukon; J, Kobuk; K, Noatak; L, Colville; M, Kuparuk; and N, Sagavanirktok.

others, 2008) and, outside of the Brooks and Alaska Ranges, most of this region has never been glaciated. The Yukon River (3,340-kilometer [km] long) flows through this region to the Bering Sea and is the largest free-flowing river in the world. In the lowland areas near the Yukon River, there are areas with high density of lake coverage (Williams, 1962; Patton and Miller, 1970; Patton, 1973). The southwestern part of the intermontane plateau (the Southwest hydrologic region), is underlain by discontinuous, sporadic, and isolated permafrost (Jorgenson and others, 2008). Lowland areas contain many morainal lakes. Many large lakes occur in this region, and Lake Iliamna is the largest of these with a surface area of 2,600 square kilometers (km^2). The major rivers are the Nushagak River, which drains into Bristol Bay, and the Kuskokwim River, which drains to Kuskokwim Bay on the Bering Sea.

In the South-Central hydrologic region, the coastal mountain ranges contribute meltwater that is the dominant flow to the Susitna and Copper Rivers, which empty into the Cook Inlet and the Gulf of Alaska, respectively. The area is underlain by discontinuous and sporadic permafrost, and the mountainous areas contain glaciated regions, where many lakes are found in the ice-carved bedrock basins (Wahrhaftig, 1965). In the Southeast hydrologic region, short meltwater streams contribute a large volume of flow to the Gulf of Alaska. Larger transboundary rivers, including the Stikine, Taku, and Unuk Rivers, originate in the coastal mountain forests of Canada and contribute to the large volumes of flow in this region. The high-elevation mountains in this region have few lakes, but at lower elevations, rock-basin, cirque, and proglacial fjord lakes are abundant.

8.3.2. Estimating River Discharge, Watershed Area, and Lake Area

Estimates of mean annual discharge for the entire State of Alaska were made by applying previously developed regional regression equations (Parks and Madison, 1985), whereas the underlying framework, which provided the stream network and connectivity, was developed using the Elevation Derivatives for National Applications (EDNA) database (Verdin, 2000; Kost and others, 2002). The regional regression equations take the form of equation 8.1:

$$Q=(10a)\times(DAb)\times(Pc) \quad (8.1)$$

where

Q is the mean annual streamflow, in cubic meters per second (m^3/s),

DA is the drainage area, in km^2,

P is the precipitation, in meters (m), and

a, b, and c are regression parameters that vary by hydrologic regions.

Equation 8.1 was evaluated in a raster environment for every location (pixel) within the State of Alaska. Inputs to equation 8.1 for mean annual streamflow were derived from two main data sources: (1) Drainage area was derived from the EDNA layers, with necessary adjustments to account for drainage from Canada. The area was represented in the flow accumulation values associated with each pixel, converted to square kilometers. (2) The precipitation data used to evaluate equation 8.1 were historical monthly precipitation data that were obtained from the Scenarios Network for Alaska and Arctic Planning (SNAP, 2014). The original climate data were derived from the University of East Anglia Climatic Research Unit gridded high-resolution (0.5°×0.5°) global climate dataset (1901 to 2009) (CRU TS v. 3.10.01; New and others, 1999, 2000; Harris and others, 2014). The SNAP team extracted data for the State of Alaska and western Canada from the global dataset, and these files were bias corrected and downscaled via the delta method using the 1961–1990 Parameter-elevation Relationships on Independent Slopes Model (PRISM; PRISM Climate Group, 2004). These data were averaged and processed into pixel-specific basin averages using the continuous parameterization technique of Verdin and Worstell (2008). The discharge estimates were developed for the entire Alaska land mass and transferred onto the EDNA-derived stream network.

Alaska is not a self-contained drainage system, as portions of some watersheds lie within Canada. The EDNA database does not extend into Canada; therefore, the Canadian portion of the drainage basin and the associated flow estimates were developed using the National Aeronautics and Space Administration Shuttle Radar Topographic Mission data (NASA-SRTM; Jarvis and others, 2008). Discharge derived from these basins was calculated and propagated into the Canadian flow network through the EDNA-derived drainage network in Alaska. This report accounts for the discharge coming from Canada for basins with a greater-than-10-km^2 drainage threshold.

The National Hydrography Dataset (NHD, at a scale of 1:63,360; U.S. Geological Survey, 2014a) was used to estimate the number and area of lakes in Alaska. The NHD data were compiled to meet the National Map Accuracy Standards. Within the NHD water body geodatabase attributes, vectors classified as reservoirs, lakes, or ponds were extracted to represent surface water extents in each of the study areas.

Discharge, watershed area, and lake area were summarized by 4-digit hydrologic regions using the U.S. Geological Survey (USGS) Hydrologic Unit Codes (HUCs; Seaber and others, 1987). There are six 4-digit hydrologic regions covering the State of Alaska (fig. 8.1).

8.3.3. Coastal Export of Carbon From Riverine Systems

Alkalinity, temperature, and pH measurements for rivers in Alaska were obtained from the USGS's National Water Information Service (NWIS; U.S. Geological Survey, 2014b),

the U.S. Environmental Protection Agency's Storage and Retrieval System (STORET; U.S. Environmental Protection Agency, 2014), and the Pebble Partnership's baseline water-quality datasets for the Bristol Bay and Cook Inlet drainages (Pebble Partnership, 2011a,b). We converted the various alkalinity measurements (alkalinity, bicarbonate, carbonate, and acid neutralizing capacity) to "alkalinity as calcium carbonate." Organic acids are a major contributor to noncarbonate alkalinity at low pH levels (Driscoll and others, 1989). We did not have enough organic carbon data to pair with our alkalinity data to directly estimate organic acid contribution to alkalinity, but we did remove alkalinity values that had an associated pH of less than 5.6 (Driscoll and others, 1989). Only sites with paired daily alkalinity, temperature, and pH data for 1970 to 2013 were used in this assessment. These 7,563 data points were representative of 1,301 individual sites on rivers throughout Alaska (fig. 8.3*A*).

Estimated dissolved DIC, composed of CO_2, bicarbonate, and carbonate, was computed using the speciation model of PHREEQC (Parkhurst and Appelo, 1999; Charlton and others, 2014). Required input variables were water temperature, pH, and alkalinity concentrations. We removed any DIC estimates that fell outside of the interval (Q1–IQR, Q3+IQR), where IQR is the interquartile range and Q1 and Q3 are the first and third quartiles, respectively. This resulted in the removal of 18 data points, so that our final DIC concentration dataset had 7,545 data points from 1,296 sites.

Dissolved organic carbon (DOC) and total organic carbon (TOC) values for rivers in Alaska were obtained from NWIS (U.S. Geological Survey, 2014b), the Pebble Partnership (2011a,b), and from various existing datasets in the Southwest (Daniel E. Schindler and Gordon Holtgrieve, University of Washington, unpub. data, October 23, 2013), Northwest (Larouche and others, 2012), and North Slope regions (Josh Koch, USGS, Anchorage, Alaska, unpub. data, November 5, 2013). We compiled a total of 1,679 DOC samples and 623 TOC samples. To use the more extensive DOC concentration dataset in our TOC flux estimates, we built a simple-linear-regression (SLR) model between paired TOC and DOC collected at the same site on the same day. We used the results of the SLR ($R^2 = 0.88$, $y = 0.25 + 1.00481x$, where R^2 is the coefficient of determination, x is the DOC concentration, and y is the TOC concentration) to predict TOC from the extensive DOC dataset. This process resulted in a TOC dataset with 2,574 samples from 519 sites. We removed any samples that fell outside of the interquartile range as described above. This resulted in the removal of 14 data points, so that our final TOC concentration dataset had 2,560 data points from 515 sites.

Carbon fluxes for coastal watersheds in Alaska were estimated in three different ways, depending on the amount of data available for each particular watershed. For coastal watersheds that contained USGS gaging stations with robust DIC and TOC concentration datasets and 3 years or more of daily discharge, carbon fluxes were estimated using the USGS Load Estimator program (LOADEST; Runkel and others, 2004). LOADEST is a multiple-regression adjusted maximum likelihood estimation model that uses measured DIC or TOC concentration values to calibrate a regression between constituent load, streamflow, seasonality, and time. The model requires at least 13 paired concentration and daily discharge values. Daily streamflow values were downloaded from NWIS. The LOADEST model uses the Akaike (1981) Information Criterion (AIC) to select the best combination of coefficients at each streamgage station from the full model, which is based on the equation:

$$\ln Flux = a_0 + a_1 \ln Q + a_2 \ln Q^2 + a_3 \sin(2\pi dtime) + a_4 \cos(2\pi dtime) + a_5 dtime + a_6 dtime^2 + \varepsilon \quad (8.2)$$

where

$\ln Flux$ is the natural log of the constituent flux, in kilograms per day (kg/d),

Q is the discharge, in m^3/s,

$dtime$ is time, in decimal years,

$a_0, a_1, \ldots a_6$ are regression coefficients, and

ε is an independent and normally distributed error.

The input data were log-transformed to avoid bias and centered to avoid multicollinearity. The model produces a flux estimate (in kg/d) with standard error values, which were used to create a distribution of LOADEST modeled fluxes for these watersheds.

For coastal watersheds that had 3 years or more of daily discharge but did not have sufficient concentration records for use in the LOADEST model, we multiplied carbon concentration by discharge to obtain a flux using the following equation:

$$Flux = C \times Q \quad (8.3)$$

where

$Flux$ is the constituent flux, in kg/d,

C is carbon concentration of surface water at the site, in milligrams per liter (mg/L), and

Q is discharge, in m^3/s.

A specified range of discharge and concentration values were used in equation 8.3 for each watershed. The distribution of empirical streamflow for each watershed was based on the standard deviation (s.d.) of recorded flows for that site. The distribution of carbon concentrations was based on all available carbon concentrations within that regional HUC. If the coastal watershed lay within the boundaries of the Southeast region, then the concentration distribution for that watershed was drawn from all concentration values within that region. In the Southeast region, 226 DIC values and 45 TOC measurements were used to create the concentration distributions.

A. **Riverine lateral carbon fluxes to coastal waters**

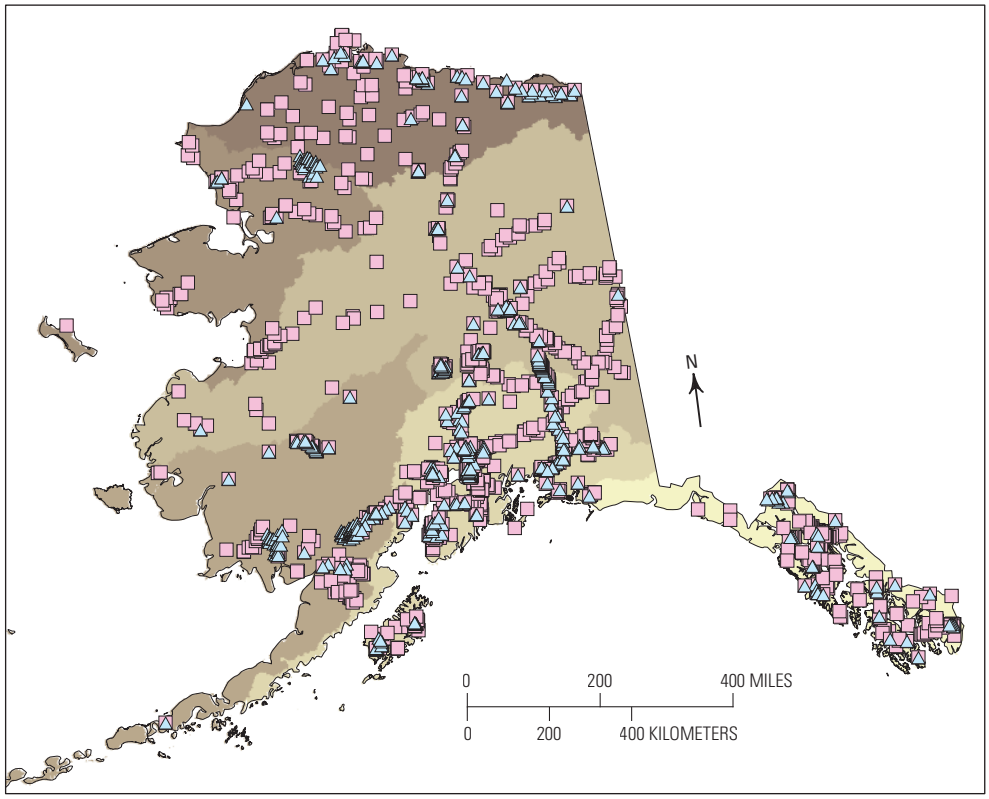

EXPLANATION

Carbon yield, in grams of carbon per square meter per year

- 0 to 4
- >4 to 8.7
- >8.7 to 9.0
- >9.0 to 10.5
- >10.5 to 16.9
- >16.9 to 36.7

Carbon sample used for analysis

- △ Total organic carbon
- □ Dissolved inorganic carbon

B. **Riverine carbon dioxide emissions**

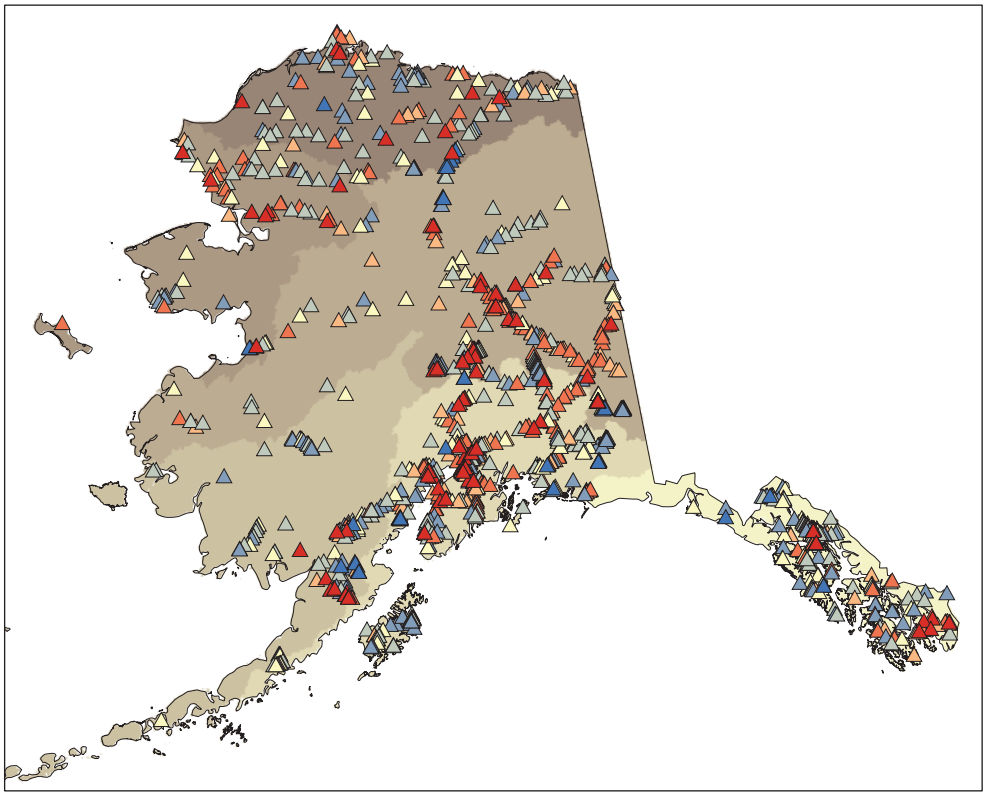

Carbon yield, in grams of carbon per square meter per year

- 0 to 4
- >4 to 5.2
- >5.2 to 8.0
- >8.0 to 11.2
- >11.2 to 21.2
- >21.2 to 36.0

Partial pressure of carbon dioxide, in microatmospheres

- 0 to 400
- >400 to 1,000
- >1,000 to 2,000
- >2,000 to 3,000
- >3,000 to 4,000
- >4000 to 10,000
- >10,000

Figure 8.3. Estimated relative magnitude of carbon yields. *A*, Coastal carbon transport by rivers. *B*, Carbon dioxide (CO_2) emissions from rivers. *C*, CO_2 emissions from lakes. *D*, Carbon burial rates in lakes. *B* and *C* also indicate the estimated relative magnitude of the partial pressure of CO_2 (pCO_2) concentrations at the sampling locations.

C. **Lacustrine carbon dioxide emissions**

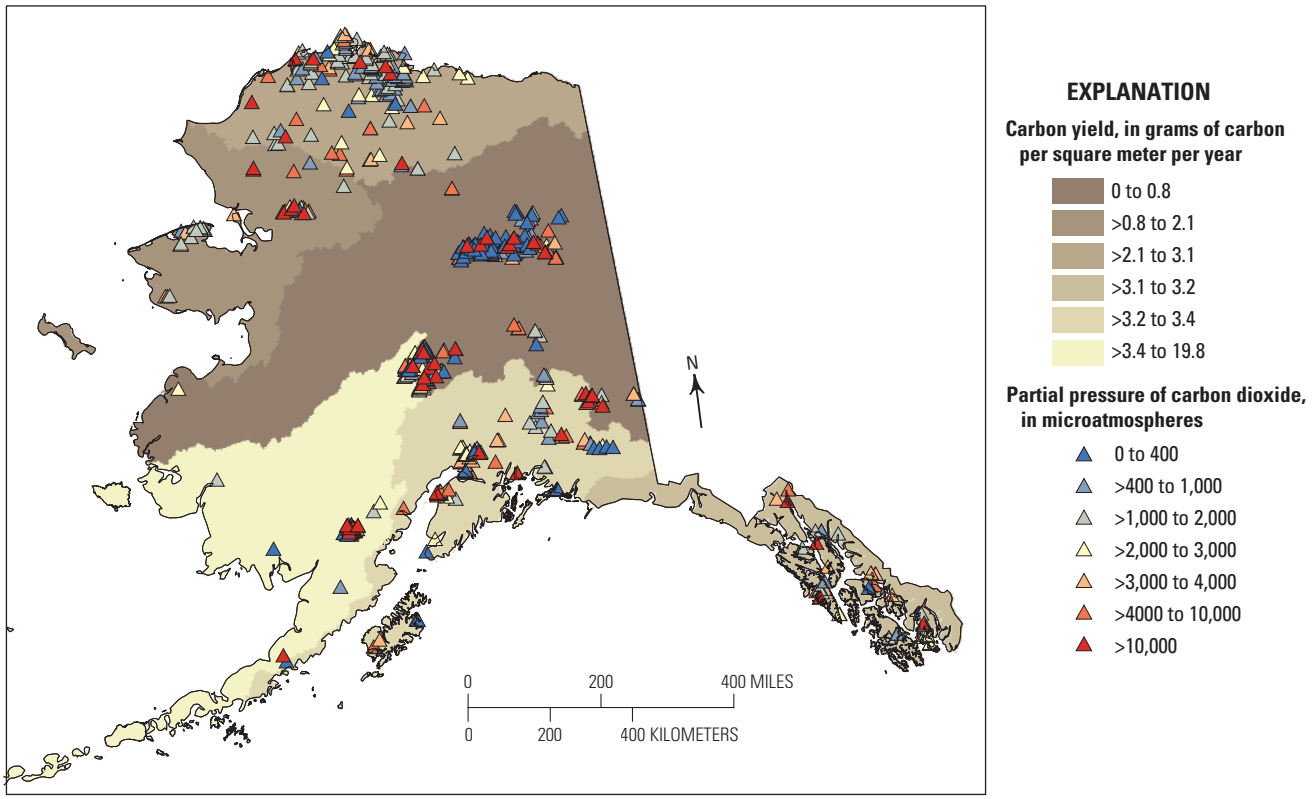

D. **Lacustrine organic carbon burial**

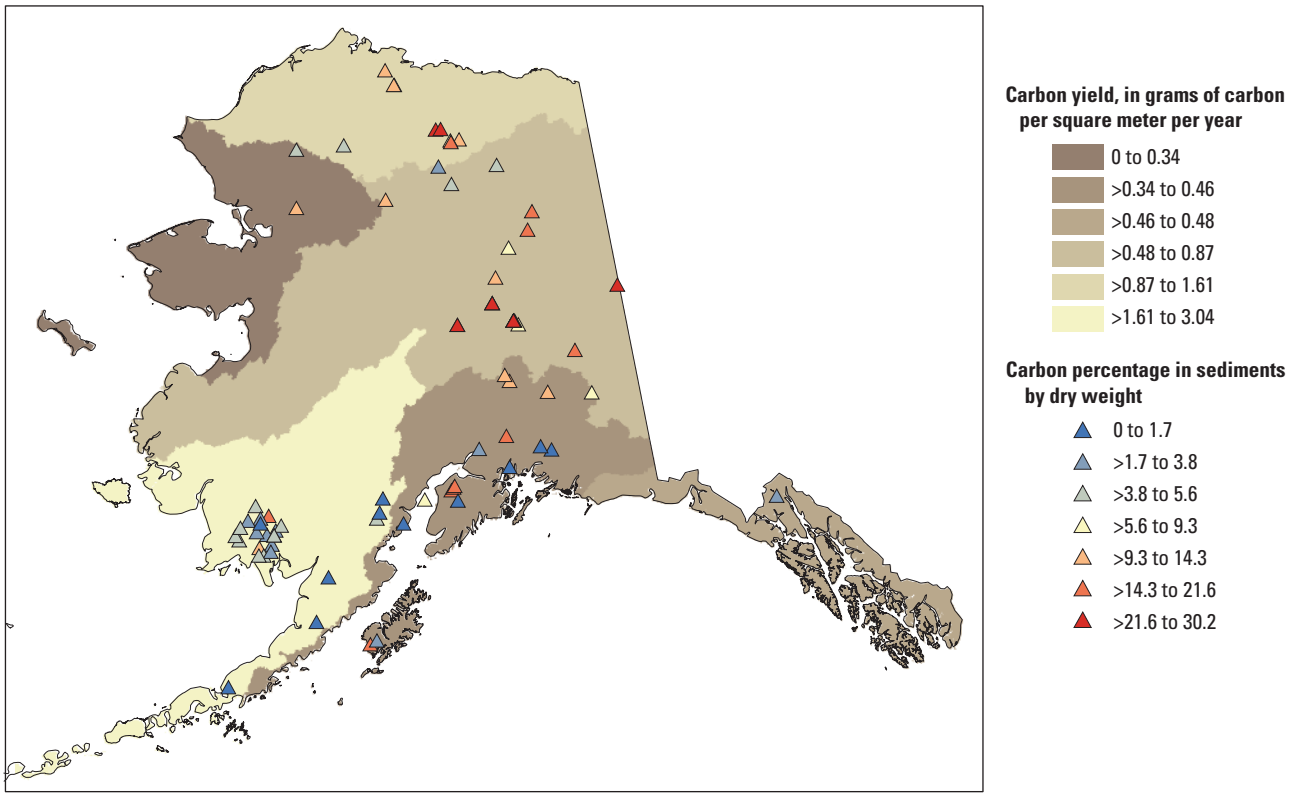

Figure 8.3. Estimated relative magnitude of carbon yields. *A*, Coastal carbon transport by rivers. *B*, Carbon dioxide (CO_2) emissions from rivers. *C*, CO_2 emissions from lakes. *D*, Carbon burial rates in lakes. *B* and *C* also indicate the estimated relative magnitude of the partial pressure of CO_2 (pCO_2) concentrations at the sampling locations.—Continued

If empirical carbon concentration and streamflow data were not available for a watershed, the distribution of carbon concentrations was established as described in the previous paragraph. To generate a distribution of discharge values for each watershed, we developed prediction intervals of discharge estimated using EDNA (see section 8.3.2) using the predict function in R (R Development Core Team, 2008). The predict function was based on the output from a simple linear model that describes estimated EDNA discharge values by empirical NWIS discharge values.

We used the distribution of LOADEST fluxes, concentrations, and discharge values as described in the previous three paragraphs in a Monte Carlo approach with 10,000 iterations to estimate total flux estimates for the approximately 6,000 coastal watersheds draining Alaska. The DIC and TOC fluxes were summed for each watershed, and the fluxes from all the watersheds within a region were summed, so that each of the six regions had 10,000 possible total carbon flux estimates. The median flux with 5th and 95th percentiles from that range of values are presented in table 8.1. Yields were calculated by dividing the total carbon flux by HUC area. The percent of the total area of the State of Alaska that was represented by LOADEST modeled fluxes (equation 8.2) was 75 percent for DIC and 65 percent for TOC, and the carbon fluxes for the remainder of the land surface area were estimated using equation 8.3.

The contribution of the Canadian drainage area to the total Alaskan coastal carbon flux estimates is also presented in table 8.1. The Yukon River, along with several smaller rivers in the Southeast and South-Central regions that drain into the Gulf of Alaska, has headwaters in Canada. We used equation 8.2 to estimate Yukon River carbon sourced in Canada with discharge and DIC and TOC concentration data (1990–2005) from a streamgage just inside the border of Alaska, the Yukon River at Eagle (NWIS station ID=15356000). We used equation 8.3 to estimate carbon fluxes from Canada for rivers in the Southeast and South-Central regions, including the Alsek, Stikine, and Taku Rivers, with EDNA-derived discharge values and carbon concentration values from Environment and Climate Change Canada (2014).

Table 8.1. Estimated coastal carbon exports and yields from riverine systems in Alaska.

[Sites are locations for which dissolved inorganic carbon (DIC) or total organic carbon (TOC) concentration data were available. Values are estimates of the median with 5th and 95th percentile estimates in parentheses. Total exports and total yields were calculated by summing dissolved inorganic carbon (DIC) and total organic carbon (TOC). km^2, square kilometer; DIC, dissolved inorganic carbon; TOC, total organic carbon; km^3/yr, cubic kilometer per year; TgC/yr, teragram of carbon per year; $gC/m^2/yr$, gram of carbon per square meter per year]

Hydrologic region	Area of hydrologic region (km^2)	Number of sites with concentration data		Estimated total discharge (km^3/yr)	Estimated total carbon export (TgC/yr)	Estimated total carbon yield ($gC/m^2/yr$)	Estimated carbon export as DIC (percent)
		DIC	TOC				
Southeast	104,000	226	45	356 (297, 569)	3.8 (3.4, 5.3)[a]	36.7 (32.4, 50.7)	67.2
South-Central	207,000	454	185	220 (156, 514)	3.5 (3.1, 5.0)[b]	17.0 (15.1, 24.0)	73.5
Southwest	291,000	169	130	174 (142, 260)	2.7 (2.2, 3.4)	9.2 (7.7, 11.6)	78.4
Yukon	526,000	264	73	144 (35, 685)	5.5 (5.4, 5.7)[c]	10.5 (10.2, 10.8)	67.1
Northwest	178,000	76	31	69 (52, 176)	1.5 (1.3, 3.4)	8.7 (7.2, 19.0)	76.7
North Slope	204,000	107	51	53 (44, 132)	1.3 (0.9, 2.3)	6.1 (4.3, 11.5)	62.3
Total or mean	**1,510,000**	**1,296**	**515**	**1,015 (725, 2,237)**	**18.3 (16.3, 25.0)**	**12.2 (10.8, 16.6)**	**69.8**

[a]Includes estimated sum lateral flux from transboundary Canadian rivers into the Southeast region of 0.13 (0.1, 0.17) TgC/yr.

[b]Includes estimated sum lateral flux from transboundary Canadian rivers into the South-Central region of 2.7 (2.1, 3.4) TgC/yr.

[c]Includes estimated sum lateral flux from transboundary Canadian rivers into the Yukon region of 1.7 (1.6, 1.8) TgC/yr.

8.3.4. Carbon Dioxide Flux From Riverine Systems

Three variables were required to estimate the CO_2 gas fluxes from aquatic systems: (1) the concentration of dissolved CO_2, (2) the gas transfer velocity, and (3) the surface area of the water body. The CO_2 emission from rivers (and lakes, see section 8.3.5) across Alaska was modeled according to established methods (Butman and Raymond, 2011; Zhu and Reed, 2012, 2014) and as outlined in equation 8.4:

$$CO_2\ flux = (CO_{2\text{-}water} - CO_{2\text{-}air}) \times kCO_2 \times SA \qquad (8.4)$$

where

$CO_2\ flux$ is the total net emission of CO_2 from rivers of Alaska, in teragrams of carbon per year (TgC/yr),

$CO_{2\text{-}water}$ is the CO_2 concentration of the water, in moles per liter (mol/L),

$CO_{2\text{-}air}$ is the CO_2 concentration in the atmosphere, in mol/L,

kCO_2 is the river or lake gas transfer velocity of CO_2 across the air-water interface, in meters per day (m/d), and

SA is the river or lake surface area, in square meters (m^2).

The total flux was estimated by summing all of the mean annual fluxes for a stream order (Strahler, 1952) within a hydrologic region.

The median dissolved CO_2 concentrations ($CO_{2\text{-}water}$) were estimated from stream and river alkalinity data available from the same three data sources listed in section 8.3.3. All alkalinity measurements were converted to dissolved CO_2 using the CO2SYS program (Van Heuven and others, 2011). Daily measurements of pH paired with temperature and alkalinity measurements from the late 1960s through 2013 were used to estimate dissolved CO_2. Similar to the methods described in section 8.3.3, alkalinity data with an associated pH of less than 5.6 were removed to reduce the effect of organic acids on alkalinity (Driscoll and others, 1989). A total of 9,466 daily chemical measurements from 1,469 sampling locations was used (fig. 8.3*B*). For equation 8.4, current atmospheric partial pressure of carbon dioxide (pCO_2) was assumed to be 390 microatmospheres (µatm) for all of the hydrologic regions across Alaska.

The gas transfer velocity (kCO_2) was modeled based on a meta-analysis of measurements of gas exchange and the gas transfer velocity made by direct tracer injections across small- to mid-sized river systems in the United States (Melching and Flores, 1999; Raymond and others, 2012). The variation in gas transfer velocities within rivers was a function of turbulence at the air-water interface (Zappa and others, 2007). Physical parameters of stream slope and water velocity were used to predict gas transfer velocity:

$$kCO_{2\text{–}river} = S \times V \times 2{,}841.6 + 2.03 \qquad (8.5)$$

where

$kCO_{2\text{–}river}$ is the gas transfer velocity of CO_2 (in m/d) normalized to the Schmidt number (a dimensionless ratio that approximates the relationship between the viscosity and gas diffusivity across a boundary layer) for CO_2 at ambient water temperature and standard atmospheric pressure (Wanninkhof, 1992; Raymond and others, 2012),

S is the average slope of a stream reach, and

V is the average velocity of water, in m/d.

A total of 563 independent gas tracer injection measurements was included in the development of this equation.

A total of 32,672 discharge measurements was used to derive hydraulic geometry coefficients specific to each hydrologic region. Hydraulic geometry of stream reaches showed remarkable consistency to approximate channel width within and across watersheds (Leopold and Maddock, 1953; Park, 1977). All scaling relationships to estimate width derived by the calculation of hydraulic geometry coefficients were statistically significant (p-value$<$0.001) with coefficients ranging from 0.46 in the Southeast region to 0.57 in the Southwest region. R^2 values for the nonlinear regression between width and stream discharge ranged from 0.90 to 0.96. Modeled average annual discharge (see section 8.3.2) was used to estimate average channel width and velocity using the hydraulic geometry coefficients specific to each hydrologic region. Both stream velocity and slope estimates were normalized by total length and aggregated to hydrologic regions by stream order. Average slope and velocity were then calculated by stream order to estimate the gas transfer velocity of CO_2 according to equation 8.5.

River surface area (SA) was calculated based on the same hydraulic geometry coefficients discussed above for width within each hydrologic region. Average discharge was used to then calculate an average width for each stream order within a hydrologic region. The total stream length was then calculated for each stream order within a hydrologic region. Stream and river surface area was then calculated as the product of the average width and total length of streams by stream order.

Error propagation and uncertainty analyses were performed for each component of equation 8.4. To estimate error, we utilized a bootstrapping technique as outlined in Efron and Tibshirani (1994) and Butman and Raymond (2011). Bootstrap with replacement was run for 1,000 iterations to calculate 95 percent confidence intervals for the pCO_2 values for each stream order within a hydrologic region. Similarly, bootstrap with replacement was used to estimate confidence intervals associated with the hydraulic geometry coefficients derived from the measurements of stream width and velocity, which were subsequently used to estimate both the river surface area and gas transfer velocity. Overall bias associated with estimates of pCO_2 remained low and had a negligible effect on the error associated with the use of the median value for each stream order. Similarly, the effect of bootstrapping the hydraulic geometry coefficients produced minimal bias.

A Monte Carlo simulation was performed for each stream order estimate of the total flux (in TgC/yr) from river surfaces (equation 8.4). The confidences derived from the bootstrapping procedure were used to bound the Monte Carlo simulation for each parameter of equation 8.4. The total flux calculation was replicated 1,000 times. Gas transfer velocities were not permitted to exceed 30 m/d. This selection criterion only affected first through third stream orders in the Southeast and South-Central regions. This constraint was placed because of the lack of measurements above that value presented in Raymond and others (2012), and there is a lack of evidence in the literature that small streams can exceed this threshold.

All estimates for the total carbon flux within each hydrologic unit were presented with the 5th and 95th percentiles derived from the Monte Carlo simulation. This approach is considered conservative as it allowed for the same probability for all combinations of each parameter in the total flux equation to be selected for each stream order and may have overestimated the error associated with the river CO_2 emission. In general, this conservative approach biased the range of estimates high owing to a slight skew in the distribution of pCO_2 values within a stream order and hydrologic region. But by using median values and bootstrapped 5th and 95th percentiles, this skew is minimized. All estimates derived from the Monte Carlo simulation were adjusted to account for monthly temperatures below freezing under the assumption that river CO_2 emission did not occur when monthly temperatures averaged below 0 degrees Celsius (°C). Average monthly temperatures were derived from the WorldClim 1-km monthly averages spanning from 1950 to 2000 (Hijmans and others, 2004). Each stream segment was attributed with a proportion of the year as frozen. This adjustment reduced the efflux for the Southeast region by 32 percent, South-Central region by 50 percent, Southwest region by 54 percent, Yukon region by 59 percent, Northwest region by 62 percent, and North Slope region by 69 percent.

8.3.5. Carbon Dioxide Flux From Lacustrine Systems

Water-chemistry data used to estimate lake CO_2 emissions from Alaska were obtained from NWIS (U.S. Geological Survey, 2014b), STORET (U.S. Environmental Protection Agency, 2014), the Pebble Partnership (2011a,b), the U.S. National Park Service Shallow Lake Monitoring Program (Larsen and Kristenson, 2012), and the dataset from studies of lakes at Yukon Flats, Alaska (Halm and Guldager, 2013; Halm and Griffith, 2014). A total of 891 locations and 1,329 measurements with daily lake chemistry data suitable for CO_2 emission estimates collected between 1949 and 2011 (fig. 8.3*C*) were used in this study.

The estimated CO_2 emission from lakes was also calculated using the general equation 8.4. Dissolved CO_2 values were also calculated using the CO2SYS program (Van Heuven and others, 2011). We did not have enough organic carbon data to pair with our alkalinity data to directly measure organic acid contribution to alkalinity. In general, noncarbonate alkalinity will introduce a bias resulting in higher alkalinity generating a higher calculated pCO_2; however, a recent estimate of bias for the evasion of CO_2 from lakes in the conterminous United States suggests that this will alter flux measurements by no more than 2 to 5 percent (McDonald and others, 2013).

All lakes within the high-resolution NHD were attributed with average summer wind speed (U_{10}), median pCO_2, and the annual ice-free fraction needed to calculate the vertical efflux of carbon. This method differs from those of McDonald and others (2013) in that, for Alaska, a single flux is calculated for each specific lake and then aggregated into regional estimates. McDonald others (2013) summed lake area only by region, then used average ecoregional wind speed and carbon concentrations to calculate fluxes.

The gas transfer velocity for lakes (kCO_{2-lake}) was calculated as a function of wind speed (Cole and Caraco, 1998; Cole and others, 2007):

$$kCO_{2-lake} = 2.07 + 0.215 \times U_{10}^{1.7} \quad (8.6)$$

where

kCO_{2-lake} is a gas transfer coefficient normalized to ambient water temperature and atmospheric pressure (STP), in m/d, and

U_{10} is the surface wind speed above the lake surface, in m/d.

The estimated mean summer (June to September) wind speeds for each hydrologic region were determined from the National Aeronautics and Space Administration (NASA; 2014) surface meteorology and solar energy data. Each lake within the NHD was assigned a CO_2-specific transfer coefficient for lake surface efflux.

Many of the parameters involved in these calculations violated normality assumptions; therefore, nonparametric

confidence intervals (95 percent) were determined on 10,000 ordinary bootstrap replicates. Bootstrapped nonparametric confidence intervals for median pCO_2 values were calculated in R using the bias corrected and accelerated methods of Efron and Tibshirani (1994) in each distribution of values by hydrologic region. Median values were chosen owing to the highly skewed distributions of concentration data. Bootstrapped confidence intervals for water temperature were similarly calculated. In general, water temperature was normally distributed about the mean value allowing normal confidence intervals to be used. Each lake within a region was assumed to have a range of potential dissolved CO_2 within the calculated nonparametric confidence intervals. The total flux by region was calculated holding the average wind speed for a lake constant. In the case of the total flux from Alaska, the 5th and 95th percentiles were assumed to be additive (uncertainty was not propagated) because potential errors in the regional estimates were likely to be systematic. Similar to the methods for river CO_2 emission, each lake within a region was attributed with a scalar representing the proportion of the year below freezing, when flux was assumed to equal zero. This scalar was applied to each lake and had the same reducing effect as for river CO_2 emission. This approach was conservative because CO_2 produced and stored under ice is commonly released rapidly when the ice melts (Anderson and others, 1999). Final estimates represent total fluxes for each hydrologic region, with 5th and 95th percentiles.

8.3.6. Carbon Burial in Lacustrine Systems

Carbon burial in lakes, which is a function of sedimentation rates, bulk density of the sediment, sediment carbon concentrations, and lake area (Mulholland and Elwood, 1982; Dean and Gorham, 1998), was estimated as:

$$C_{burial} = SA_{WB} \times SedRt \times C_{conc} \times 10^{-12} \quad (8.7)$$

where

C_{burial} is the carbon burial rate, in TgC/yr,

SA_{WB} is the surface area of the water body, in m^2,

$SedRt$ is the sedimentation rate, in grams of carbon per square meter per year ($gC/m^2/yr$),

C_{conc} is the concentration of carbon in sediments (percent carbon by dry weight of sediment divided by 100), and

10^{-12} is a conversion factor to convert from grams to teragrams.

Water body surface areas were derived from the high-resolution NHD and included lakes, ponds, and reservoirs. We did not differentiate between lakes and reservoirs in this report. Data on sedimentation rates and lake sediment carbon concentrations were derived from previously collected and dated sediment cores from 70 Alaskan lakes; these data were obtained from published and unpublished sources (table 8.2; fig. 8.3*D*). The cores were dated using ^{210}Pb and ^{137}Cs isotope techniques, as well as ^{14}C dating of terrestrial plants deposited in near-surface layers. Sedimentation results pertain to the most recent 100 years of sediment accumulation, which typically corresponds to the top 5 to 15 centimeters (cm) of sediment, depending on sedimentation rates. For ^{14}C-dated cores, sedimentation rates were interpolated based on linear sedimentation rates from the most recent ^{14}C date to the top of the core, which we assumed represents the year of collection.

Data from the cores were used to build geostatistical models for sedimentation rates and sediment carbon concentrations using stepwise multiple linear regression (MLR); these predictive equations were applied statewide. Potential explanatory variables included lake area and lake elevation from the NHD, mean annual precipitation and temperature from SNAP, vegetation characteristics from the National Land Cover Database (NLCD) 2006 (Fry and others, 2011), permafrost and bog extent from chapters 3 and 7 of this report, and soil organic carbon in the top 152 cm of soil from the state soil geographic database (STATSGO; U.S. Department of Agriculture, Natural Resource Conservation Service, 2014). Each of these parameters was calculated for the 12-digit HUC that intersected each water body. In the MLR, the independent variable that explained the most variance in the dependent variable entered the model first. The variances explained by the remaining independent variables were recalculated, and the variable that explained the next greatest amount of variance entered the model next. This iterative process was repeated until the minimum AIC was obtained (Akaike, 1981). Multicollinearity among explanatory variables was evaluated using the variance inflation factor ($1/(1–R^2)$; Hair and others, 2006) with a threshold for exclusion of 2.0. Uncertainty in model predications was evaluated by using a Monte Carlo approach in which the coefficients for model parameters were allowed to vary randomly within their 5th and 95th percentiles; this procedure was repeated for 1,000 iterations, yielding 1,000 estimates of sedimentation rate and sediment carbon concentration for each water body in the Alaska NHD. Results are summarized for each of the six hydrologic regions in Alaska.

8.3.7. Limitations and Uncertainties

Methods used to calculate river dissolved carbon fluxes to the coast had some limitations. For 25 to 35 percent of the land surface area, carbon flux was calculated simply as flow multiplied by concentration (equation 8.3), which does not allow for variability in seasonal discharge of carbon concentrations (Runkel and others, 2004). Additionally, the concentration data used in the coastal flux estimates had relatively good spatial coverage, and watersheds with DIC or TOC concentrations represented over 50 percent of the

Table 8.2. Site information and data sources used to develop multiple-linear-regression models for estimation of carbon burial in Alaskan water bodies.

[Data included sediment carbon concentrations, sediment accumulation rates, and dry bulk density. Coordinates are in decimal degrees, NAD 83; HUC; hydrologic unit code; 1901, Southeast hydrologic region; 1902; South-Central hydrologic region; 1903, Southwest hydrologic region; 1904, Yukon hydrologic region; 1905, Northwest hydrologic region; 1906, North Slope hydrologic region]

4-digit HUC	Site name	Latitude	Longitude	References and data sources
1901	Chilkat Lake	59.33	–135.90	Barto (2004)
1902	Long Lake	62.55	–143.40	N. Bigelow, University of Alaska-Fairbanks, unpub. data (2014)
1902	Hickerson Lake	59.93	–152.92	Cohn (2009)
1902	Frazer Lake	57.26	–154.14	B. Finney, Idaho State University, unpub. data (2014)
1902	Coghill Lake	61.09	–147.82	B. Finney, Idaho State University, unpub. data (2014)
1902	Phalarope Lake	57.18	–154.41	Jones, Peteet, and others (2009)
1902	Rock Lake	60.65	–150.64	Lynch and others (2002)
1902	Arrow Lake	60.75	–150.49	Lynch and others (2002)
1902	Portage Lake	60.72	–150.53	Lynch and others (2002); Hinzman and others (2005)
1902	Greyling Lake	61.38	–145.74	McKay and Kaufman (2009)
1902	Hallet Lake	61.49	–146.24	McKay and Kaufman (2009)
1902	Skilak Lake	60.42	–150.37	Naidu and others (1999)
1902	Packer Lake	60.47	–151.92	Rogers and others (2013)
1902	Swampbuggy Lake	63.05	–147.42	Rohr (2001)
1902	Nutella Lake	63.20	–147.63	Rohr (2001)
1902	Canyon Lake	62.70	–145.57	Shimer (2009)
1902	Kepler Lake	61.55	–149.21	Yu and others (2008)
1902	Hundred Mile Lake	61.81	–147.85	Yu and others (2008)
1903	Little Swift Lake	60.22	–159.77	Axford and Kaufman (2004)
1903	Ongoke Lake	59.27	–159.43	Chipman and others (2009)
1903	Kontrashabuna Lake	60.19	–154.03	Cohn (2009)
1903	Portage Lake	60.50	–153.86	Cohn (2009)
1903	Lower Ugashik Lake	57.66	–156.73	B. Finney, Idaho State University, unpub. data (2014)
1903	Lone Spruce Pond	60.01	–159.15	Kaufman and others (2012)
1903	Aleknagik Lake	59.36	–158.89	Rogers and others (2013)
1903	Amanka Lake	59.10	–159.22	Rogers and others (2013)
1903	Bear Lake	56.02	–160.25	Rogers and others (2013)
1903	Beverly Lake	59.68	–158.77	Rogers and others (2013)
1903	Gechiak Lake	59.39	–160.37	Rogers and others (2013)
1903	Goodnews Lake	59.49	–160.56	Rogers and others (2013)
1903	Grant Lake	59.81	–158.53	Rogers and others (2013)
1903	High Lake	59.94	–159.50	Rogers and others (2013)
1903	Kagati Lake	59.87	–160.06	Rogers and others (2013)
1903	Little Togiak Lake	59.58	–159.15	Rogers and others (2013)
1903	Nagugun Lake	59.69	–160.39	Rogers and others (2013)
1903	Naknek Lake	58.69	–156.28	Rogers and others (2013)
1903	Nerka Lake	59.58	–158.83	Rogers and others (2013)
1903	Nunavaugaluk Lake	59.20	–158.91	Rogers and others (2013)
1903	Tazmina Lake	60.05	–154.15	Rogers and others (2013)
1903	Togiak Lake	59.61	–159.62	Rogers and others (2013)
1903	Ualik Lake	59.09	–159.44	Rogers and others (2013)
1903	Upper Togiak Lake	59.83	–159.48	Rogers and others (2013)

Table 8.2. Site information and data sources used to develop multiple-linear-regression models for estimation of carbon burial in Alaskan water bodies.—Continued

[Data included sediment carbon concentrations, sediment accumulation rates, and dry bulk density. Coordinates are in decimal degrees, NAD 83; HUC; hydrologic unit code; 1901, Southeast hydrologic region; 1902; South-Central hydrologic region; 1903, Southwest hydrologic region; 1904, Yukon hydrologic region; 1905, Northwest hydrologic region; 1906, North Slope hydrologic region]

4-digit HUC	Site name	Latitude	Longitude	References and data sources
1904	Birch Lake	64.31	–146.66	Abbott and others (2000)
1904	Tangled Up Lake	67.67	–149.72	Anderson and others (2001)
1904	Track Lake	66.86	–145.17	D. Anderson, U.S. Geological Survey, unpub. data (2014)
1904	Greenpepper Lake	66.09	–146.73	D. Anderson, U.S. Geological Survey, unpub. data (2014)
1904	Twelve-Mile Lake	66.45	–145.55	D. Anderson, U.S. Geological Survey, unpub. data (2014)
1904	Six Mile Lake	64.87	–141.12	N. Bigelow, University of Alaska-Fairbanks, unpub. data (2014)
1904	Little Harding Lake	64.41	–146.90	Brady (2013)
1904	Jan Lake	63.56	–143.92	Carlson and Finney (2004)
1904	Keche Lake	68.02	–146.93	Chipman and others (2012)
1904	Takahula Lake	67.35	–153.67	Clegg and Hu (2010)
1904	Harding Lake	64.42	–146.85	Finkenbinder and others (2014)
1904	Dune Lake	64.42	–149.90	Finney and others (2012)
1904	Oops Lake	65.44	–147.63	Finney, University of Idaho, unpub. data (2014)
1904	Ace Lake	64.86	–147.94	B. Gaglioti, University of Alaska-Fairbanks, unpub. data (2014)
1904	Deuce Lake	64.86	–147.94	Lynch and others (2002)
1905	Burial Lake	68.43	–159.17	Abbott and others (2010)
1905	Lake Wolverine	67.09	–158.92	Mann and others (2002)
1906	Meli Lake	68.68	–149.08	Anderson and others (2001)
1906	Blue Lake	68.09	–150.47	Bird and others (2009)
1906	Lake Helen	70.36	–153.68	B. Gaglioti, University of Alaska-Fairbanks, unpub. data (2014)
1906	Nikivlik Lake	68.59	–156.25	B. Gaglioti, University of Alaska-Fairbanks, unpub. data (2014)
1906	Dimple Lake	68.94	–150.50	Johnson and others (2011)
1906	NE-14	68.67	–149.63	Johnson and others (2011)
1906	Perch Lake	68.95	–150.20	Johnson and others (2011)
1906	Toolik Lake	68.63	–149.61	Johnson and others (2011)

total regional area. There were some gaps, however, and the watersheds that contained DIC concentration data only represented 16 percent of the total area of the Southeast region, and the watersheds that contained TOC concentration data only represented 8 percent of total area of the Southeast region and 35 percent of the Southwest region.

Summertime concentrations were better represented in the concentration datasets than those collected in the winter. The Southeast, South-Central, Southwest, and Yukon regions had DIC concentrations collected through the year. However, nearly 80 percent of the DIC values and 65 percent of TOC values for the North Slope region were collected in June through August, with no TOC values for January, February, or March. Nearly 60 percent of DIC and TOC samples in the Northwest region were collected from June through August, which may have biased distributions of concentrations to represent more carbon transport via surface-water rather than groundwater flow.

In this assessment, the gas transfer velocity for CO_2 efflux calculation for rivers was not permitted to exceed 30 m/d based on equation 8.5. It is important to note that the model to estimate gas transfer velocity of CO_2 outlined in Raymond and others (2012) and used for this assessment was developed from a dataset that did not include any measurements from steep-slope or high-altitude locations and, as such, the results of this model in highly diverse landscapes should be interpreted with appropriate caution. Validation data to support evasion rates of this magnitude do not currently exist; however, recent research measuring oxygen transfer rates suggests that gas transfer velocities in the upper reaches of the Colorado River can range from 9 m/d in the large main channels up to 338 m/d in rapids (Hall and others, 2012).

The estimates of stream and river surface area for each hydrologic region ranged from 0.3 to 0.8 percent of the total area and are consistent with other published values (Aufdenkampe and others, 2011; Downing and others, 2012); however, remote sensing techniques could be used to further constrain the hydraulic geometry coefficients that are appropriate at the basin scale (Striegl and others, 2012). Specifically, there is a need to constrain the surface areas of first-order stream systems in headwater areas that may be poorly characterized within the EDNA dataset. The underlying 30-m digital elevation model used to define stream reaches is coarse, did not capture strong seasonal variation in flow, and had some inaccurate streamflow lines, particularly in low-elevation areas (Holmes and others, 2000).

The locations of USGS streamgages, which were used to calculate the hydraulic geometry coefficients, introduced a bias because they were placed in a location that was best suited for accurate discharge measurements (Leopold and Maddock, 1953; Park, 1977). Therefore, the locations most likely do not represent the entire range of variability in the relationships among stream depth, width, and velocity that exists for river channels across the State of Alaska. A wider range of variability of these stream geomorphology factors likely exists in Alaska because of the low levels of human development and lack of stream channelization or other flow restrictions.

Using the available data, we were not able to accurately model the effect of seasonality on estimated mean CO_2 emission from lacustrine or riverine systems (Rouse and others, 1997). In dimictic lakes (lakes that experience ice cover and mix completely in the spring and fall), CO_2 concentrations build up under ice cover and in the hypolimnetic bottom waters as a result of heterotrophic respiration and are degassed rapidly during mixing following ice melt (Michmerhuizen and others, 1996; Riera and others, 1999). In addition, boreal and arctic lakes are commonly shallow, resulting in a higher susceptibility to climate and seasonal shifts in temperature, reducing ice cover and increasing levels of light penetration to sediments, which could, in turn, influence the seasonality of dissolved CO_2 through biological metabolism and thermal stratification (Rouse and others, 1997; Smol and others, 2005). These aspects of the seasonal pCO_2 dynamics were not included in the estimates.

Changes in permafrost are likely to have effects on regional-scale hydrology (Osterkamp and others, 2000; Walvoord and others, 2012), particularly related to lake surface area. Lake surface area was a key component in the modeling of CO_2 emissions and carbon burial in lakes in this assessment. Some studies in regions with degrading permafrost have reported significant decreases in lake surface area extent (Riordan and others, 2006; Roach and others, 2013), whereas others report no substantial change in lake surface area for most lakes in a study region (Jones, Arp, and others, 2009; Rover and others, 2012). Regardless of the study, it is clear that accurate assessment of changes in lake surface area relies on proper treatment of both inter- and intra-annual time scales (Rover and others, 2012; Chen and others, 2013). However, a remote sensing data archive that can address both inter- and intra-annual variability in lake surface areas in continuous and discontinuous permafrost regions for the entire State of Alaska is currently not available. Given that the aquatic carbon flux results in this chapter represent long-term annual averages and that roughly half of the lake surface area lies in nonpermafrost regions of Alaska, the effect of changes in lake surface area on these regional results is expected to be minimal.

There were several important sources of uncertainty in the carbon burial estimates including (1) loss of sediment carbon to postdepositional mineralization at 100 years, (2) effects of within-basin variability of sedimentation rates, and (3) extrapolation of sedimentation rate and sediment carbon concentration data from a relatively small sample ($n=70$) of lakes to the larger population of lakes in Alaska (approximately 1 million). Loss of carbon in sediments because of mineralization occurs primarily in the top layers of sediments, where oxygen concentrations are highest (Sobek and others, 2009). This loss of carbon was partly compensated for by using an average carbon concentration for the sediment deposited during the previous 100 years, which typically was the top 5 to 15 cm of sediments. Additional research is needed to better account for variations in carbon burial efficiency in Alaskan lakes. Sediment focusing refers to the propensity for fine-grained sediment to accumulate preferentially in the deepest part of the lake (Davis and Ford, 1982). Alternatively, in calm-water lakes, where sediment redistribution is rare, littoral areas can have higher sedimentation rates because of highly productive macrophyte beds, high allochthonous subsidies nearshore, and (or) thermokarsting lake margins. The sediment focusing factor (the ratio of sedimentation at a specific location in a lake to average sedimentation in the lake) for lakes in Alaska varies widely and appears to be at least partly a function of lake morphometry, with steep-sided lakes having high sediment focusing factors. Focusing factors also can change over time, as young, steep-sided lakes fill in (Blais and Kalff, 1995). A study of eight high-elevation lakes in the Rocky Mountain and Glacier National Parks indicated that sediment focusing factors averaged 1.6 ± 0.5 (mean $\pm$ s.d.; 1 anomalous sample excluded) (Mast and others, 2010). Most of these lakes are in glacial cirques with high relief and have steeply sloping lake bottoms; thus, they may represent the upper end of the range of sediment focusing effects. If postdepositional sediment carbon mineralization and sediment focusing are important in Alaskan lakes, the estimated carbon burial rates are likely overestimated. Error in regression model predictions represents another source of uncertainty in carbon burial calculations. Although the MLR models for sedimentation rates and sediment carbon concentrations (key parameters in the carbon burial calculations) explained 70 to 75 percent of the variance in observed values, at least 25 to 30 percent of the variance remains unexplained. An additional concern is that the suite of lakes that was used to derive the MLR models was not selected randomly from the entire lake population, potentially biasing the model regressions; this deficiency could be at least partly addressed through additional sampling.

8.4. Results

8.4.1. Coastal Carbon Export From Riverine Systems

The total coastal carbon export for the State of Alaska was 18.3 TgC/yr (5th and 95th percentiles of 16.3 TgC/yr and 25.0 TgC/yr; table 8.1) with 70 percent of the export as inorganic carbon. The highest total carbon export was from the Yukon region, at 5.5 TgC/yr. Most of the flux is from the Yukon River, which had the single highest flux for any river in the State. The coastal flux from the Yukon River flows north through the Bering Strait to the Arctic Ocean.

The Southeast and South-Central regions exported similar magnitudes of carbon to the coast, 3.8 TgC/yr (5th and 95th percentiles of 3.4 TgC/yr and 5.3 TgC/yr), and 3.5 TgC/yr (5th and 95th percentiles of 3.1 TgC/yr and 5.0 TgC/yr), respectively (table 8.1). The Southwest region had a lower flux of 2.7 TgC/yr (5th and 95th percentiles of 2.2 TgC/yr and 3.4 TgC/yr). The Northwest and North Slope regions had the lowest annual carbon fluxes of 1.5 TgC/yr (5th and 95th percentiles of 1.3 TgC/yr and 3.4 TgC/yr) and 1.3 TgC/yr (5th and 95th percentiles of 0.9 TgC/yr and 2.3 TgC/yr), respectively.

To illustrate the connectivity between the aquatic fluxes and contributing terrestrial drainage area, we divided carbon fluxes by watershed area to produce a carbon yield. The estimated total carbon yields were by far the highest in the Southeast region at 36.7 $gC/m^2/yr$ (5th and 95th percentiles of 32.4 $gC/m^2/yr$ and 50.7 $gC/m^2/yr$; table 8.1). The second highest yields were in the South-Central region at 17.0 $gC/m^2/yr$ (5th and 95th percentiles of 15.1 $gC/m^2/yr$ and 24.0 $gC/m^2/yr$). The lowest carbon yields were in the North Slope region with 6.1 $gC/m^2/yr$ (5th and 95th percentiles of 4.3 $gC/m^2/yr$ and 11.5 $gC/m^2/yr$).

There was substantial variability in the mean runoff among the regions, with the greatest total runoff in the Southeast region at 3.4 meters per year (m/yr) (5th and 95th percentiles of 2.9 m/yr and 5.5 m/yr) and the smallest total runoff in the North Slope region at 0.3 m/yr (5th and 95th percentiles of 0.2 m/yr and 0.6 m/yr). The mean DIC concentration in the Yukon region of 18.7 mg/L (s.d. of 9.9 mg/L) was nearly three times higher than the estimated mean DIC concentration in the Southeast region, which was 6.6 mg/L (s.d. of 5.2 mg/L). The range of TOC concentrations were narrower, with the highest estimated mean concentration in the North Slope region at 8.5 mg/L (s.d. of 6.1 mg/L) and the lowest in the Southwest region at 2.4 mg/L (s.d. of 1.9 mg/L).

8.4.2. Carbon Dioxide Flux From Riverine Systems

Overall, median pCO^2 values ranged from 1,000 to 5,900 µatm across all stream orders and hydrologic regions, representing a gradient spanning 3 to 15 times the mean atmospheric CO_2 concentration. This suggests that streams and rivers in the State remain continuously supersaturated compared with atmospheric CO_2 concentrations. The highest median pCO_2 value by region was in the Northwest region at 3,100 µatm, whereas the lowest median pCO_2 value of 1,700 µatm was in the Southeast region. Measurements of dissolved CO_2 are defined by the pH, alkalinity, and temperature at the time of measurement, and the small sample size within the Northwest region affected these concentration distributions. Average median pCO_2 for the State of Alaska was 2,200 µatm, or 5.6 times the approximate atmospheric CO_2 concentration of 390 µatm.

Estimated stream and river surface area was 8,000 km^2 (5th and 95th percentiles of 7,600 km^2 and 8,300 km^2), representing about 0.5 percent of the total area of Alaska (table 8.3). The highest total stream surface area of 4,200 km^2 (5th and 95th percentiles of 4,100 km^2 and 4,400 km^2) was in the Yukon region, whereas the smallest total stream surface area

Table 8.3. Estimated river and stream surface area and vertical fluxes and yields of carbon dioxide from riverine systems in Alaska.

[Sites are those used in the calculation of estimated partial pressure of carbon dioxide (pCO_2). Values are estimates of the total median river and stream surface areas, fluxes, and yields (fluxes normalized to watershed areas), and those presented in parentheses represent associated errors at the 5th and 95th percentiles. Total yields were calculated by dividing the estimated total flux by the regional area. Units: km^2, square kilometer; TgC/yr, teragram of carbon per year; $gC/m^2/yr$, gram of carbon per square meter per year]

Hydrologic region	Number of sites	River and stream surface area (km^2)	Estimated total carbon flux (TgC/yr)	Estimated total carbon yield ($gC/m^2/yr$)
Southeast	242	486 (461, 512)	3.9 (2.2, 5.8)	37.3 (21.2, 55.6)
South-Central	511	1,003 (947, 1,061)	4.5 (2.5, 6.8)	21.7 (12, 32.9)
Southwest	166	1,235 (1,164, 1,307)	3.1 (1.6, 5.0)	10.5 (5.6, 17.3)
Yukon	333	4,217 (4,063, 4,379)	3.7 (2.0, 6.3)	7.1 (3.7, 12)
Northwest	81	507 (481, 533)	0.8 (0.4, 1.3)	4.2 (2.2, 7.1)
North Slope	136	524 (496, 553)	0.6 (0.3, 1.1)	3.1 (1.7, 5.3)
Total or mean	**1,469**	**7,972 (7,612, 8,345)**	**16.6 (9.0, 26.3)**	**11.0 (6.0, 17.4)**

was in the Southeast region at 490 km^2 (5th and 95th percentiles of 460 km^2 and 510 km^2). Stream and river surface area as a percentage of the landscape was largest in the Yukon region at 0.80 percent (5th and 95th percentiles of 0.77 percent and 0.83 percent), but only 0.26 percent (5th and 95th percentiles of 0.24 percent and 0.27 percent) across the North Slope region.

Total efflux of CO_2 from rivers in Alaska was 16.6 TgC/yr (5th and 95th percentiles of 9.0 TgC/yr and 26.3 TgC/yr) with the highest fluxes from the Yukon and South-Central regions at 3.7 TgC/yr (5th and 95th percentiles of 2.0 TgC/yr and 6.3 TgC/yr) and 4.5 TgC/yr (5th and 95th percentiles of 2.5 TgC/yr and 6.8 TgC/yr), respectively (table 8.3). The smallest efflux was estimated for the North Slope region at 0.6 TgC/yr (5th and 95th percentiles of 0.3 TgC/yr and 1.1 TgC/yr). Normalizing greenhouse-gas emissions to CO_2 equivalent using global warming potentials produced a total river efflux of 58.7 teragrams of carbon dioxide equivalent per year ($TgCO_2$-eq/yr) for the State of Alaska.

Carbon yield for the State of Alaska was 11.0 gC/m^2/yr (5th and 95th percentiles of 6.0 gC/m^2/yr and 17.4 gC/m^2/yr). The distribution of yield estimates across regions differed from the distribution of total flux estimates. Highest yield was estimated for the Southeast region at 37.3 gC/m^2/yr (5th and 95th percentiles of 21.2 gC/m^2/yr and 55.6 gC/m^2/yr), whereas the smallest yield was estimated for the North Slope region at 3.1 gC/m^2/yr (5th and 95th percentiles of 1.7 gC/m^2/yr and 5.3 gC/m^2/yr). In general, the range of yield estimates among the six regions of Alaska decreased with increasing latitude, where colder regions tended to have smaller yields primarily because of a larger proportion of defined ice cover throughout the year.

8.4.3. Carbon Dioxide Flux from Lacustrine Systems

Across the State, median lake pCO_2 concentrations ranged from 973 µatm, or 2 times atmospheric concentration, across the Yukon region to a high of 4,189 µatm, or nearly 10 times atmospheric concentration, in the Southwest region. These numbers represent high estimates for the dissolved CO_2 concentrations; however, limited measurements (n=1,329) may be contributing a bias to these calculations.

Overall, 1,019,224 individual lakes and reservoirs derived from the NHD dataset were used for this study, totaling 52,300 km^2 representing 4 percent of the State of Alaska (table 8.4). The proportion of lake area varied across each of the six hydrologic regions from a low of 2 percent in the Southeast region up to 7 percent in the Southwest region. This very high value of 7 percent is the result of a few very large lakes found within the Southwest region and is dominated by Lake Iliamna, which has a surface area of approximately 2,600 km^2.

Gas transfer velocities (kCO_{2-lake}) calculated using equation 8.6 averaged across regions did not vary significantly because of similarity in average wind speeds (U_{10}). Lowest kCO_{2-lake} values were estimated for the Southeast region at 0.6 m/d, (s.d. of 0.04 m/d) ranging to a high of 0.8 m/d (s.d. of 0.1 m/d) for the Northwest region.

Total lake CO_2 emission was estimated to be 8.2 TgC/yr (5th and 95th percentiles of 6.1 TgC/yr and 11.2 TgC/yr; table 8.4). The highest lake efflux was estimated for the Southwest region at 5.8 TgC/yr (5th and 95th percentiles of 4.3 TgC/yr and 7.6 TgC/yr). The flux from this region was an order of magnitude larger than the remaining regions

Table 8.4. Estimated lake surface area and vertical fluxes and yields of carbon dioxide from lacustrine systems in Alaska.

[Sites are those used in the calculation of the partial pressure of carbon dioxide (pCO_2). Values are estimates of the total median lake surface areas, fluxes, and yields (fluxes normalized to watershed areas), and those presented in parentheses represent associated errors at the 5th and 95th percentiles. Total yields were calculated by dividing the estimated total flux by the regional area. Units: km^2, square kilometer; TgC/yr, teragram of carbon per year; gC/m^2/yr, gram of carbon per square meter per year]

Hydrologic region	Number of sites	Lake surface area (km^2)	Estimated total carbon flux (TgC/yr)	Estimated total carbon yield (gC/m^2/yr)
Southeast	44	1,587	0.3 (0.2, 0.4)	3.2 (2.2, 3.8)
South-Central	148	3,841	0.7 (0.6, 0.9)	3.4 (2.8, 4.4)
Southwest	214	20,946	5.8 (4.3, 7.6)	19.8 (14.9, 26.1)
Yukon	305	10,947	0.4 (0.2, 0.6)	0.8 (0.4, 1.2)
Northwest	46	4,069	0.4 (0.3, 0.8)	2.1 (1.5, 4.3)
North Slope	133	10,886	0.6 (0.5, 0.9)	3.1 (2.2, 4.5)
Total or mean	**890**	**52,276**	**8.2 (6.1, 11.2)**	**5.5 (4.0, 7.4)**

across Alaska. Lowest lake fluxes were estimated for the Southeast region at 0.3 TgC/yr (5th and 95th percentiles of 0.2 TgC/yr and 0.4 TgC/yr). Excluding the estimated flux for the Southwest, lake emission ranged from 0.3 to 0.7 TgC/yr across all other hydrologic regions. Normalizing greenhouse-gas emissions to CO_2 equivalent produced a total lake CO_2 emission of 30.1 $TgCO_2$-eq/yr (5th and 95th percentiles of 22.4 $TgCO_2$-eq/yr and 41.1 $TgCO_2$-eq/yr).

Average lake yield for the State of Alaska was 5.5 $gC/m^2/yr$ (5th and 95th percentiles of 4.0 $gC/m^2/yr$ and 7.4 $gC/m^2/yr$). Highest yield was estimated for the Southwest region at 19.8 $gC/m^2/yr$ (5th and 95th percentiles of 14.9 $gC/m^2/yr$ and 26.1 $gC/m^2/yr$), whereas the smallest yield was estimated for the Yukon region at 0.8 $gC/m^2/yr$ (5th and 95th percentiles of 0.4 $gC/m^2/yr$ and 1.2 $gC/m^2/yr$). Overall, the variation in both the total efflux and yield estimates among the regions was driven primarily by regional differences in the median lake CO_2 concentrations and total lake area.

8.4.4. Carbon Burial in Lacustrine Systems

Observed water body sedimentation rates at the cored lakes ranged from 0.1 to 5.3 millimeters per year (mm/yr) and had an exponential or log-normal distribution. The estimated median sedimentation rate for lakes of Alaska was 1.5 mm/yr, with the lowest rates in the Northwest and South-Central regions (0.4 mm/yr and 0.6 mm/yr); intermediate rates in the North Slope, Yukon, and Southeast regions (1.2 to 1.8 mm/yr); and highest rates in the Southwest region (2.3 mm/yr).

Observed sediment carbon concentrations at the cored lakes ranged from 0.6 to 30.7 percent (by dry weight) and were exponentially or log-normally distributed. The estimated median sediment carbon concentration in lakes of Alaska was 18.2 percent and were lowest in the Southeast, Southwest, and North Slope regions (16.6 to 17.7 percent); intermediate in the Northwest and South-Central regions (18.0 percent and 18.1 percent); and highest in the Yukon region (19.1 percent).

The median estimated total flux of carbon owing to burial in lakes of Alaska was –1.88 TgC/yr (5th and 95th percentiles of –1.03 TgC/yr and –2.82 TgC/yr), and values varied substantially among hydrologic regions (table 8.5). Estimated flux from carbon burial was smallest in the Southeast, Northwest, and South-Central regions (–0.05 to –0.10 TgC/yr); intermediate in the North Slope and Yukon regions (–0.33 TgC/yr and –0.46 TgC/yr, respectively); and greatest in the Southwest region (–0.88 TgC/yr). When normalized to the area of each hydrologic region (yield), the median estimated flux from carbon burial in lakes was –1.2 $gC/m^2/yr$ (5th and 95th percentile estimates of –0.7 $gC/m^2/yr$ and –1.9 $gC/m^2/yr$). Carbon burial yields were lowest in the Northwest, Southeast, and South-Central regions (–0.3 to –0.5 $gC/m^2/yr$); intermediate in the Yukon region (–0.9 $gC/m^2/yr$); and highest in the North Slope and Southwest regions (–1.6 $gC/m^2/yr$ and –3.0 $gC/m^2/yr$, respectively).

The estimated carbon burial rate normalized to water body area was –31 $gC/m^2/yr$ for Alaska, but the rates varied substantially among hydrologic regions. The Northwest and South-Central regions had the lowest estimated carbon burial rates (–8 $gC/m^2/yr$ and –11 $gC/m^2/yr$); the North Slope and Yukon regions had intermediate rates (–23 $gC/m^2/yr$ and –30 $gC/m^2/yr$); and the Southeast and Southwest regions had the highest rates (–36 $gC/m^2/yr$ and –44 $gC/m^2/yr$; table 8.5).

Table 8.5. Estimated carbon burial in lacustrine sediments in Alaska.

[Sites are those where carbon burial was calculated from sediment cores. Values are estimates of the total median fluxes, yields (fluxes normalized to watershed areas), and burial rates, and those presented in parentheses represent associated errors at the 5th and 95th percentiles. Carbon yields were calculated by dividing the estimated total flux divided by the hydrologic region area. Negative values represent sequestration. Units: TgC/yr, teragram of carbon per year; $gC/m^2/yr$, gram of carbon per square meter per year]

Hydrologic region	Number of sites	Estimated total carbon flux (TgC/yr)	Estimated total carbon yield normalized to watershed area ($gC/m^2/yr$)	Estimated carbon burial rate normalized to water body area ($gC/m^2/yr$)
Southeast	1	–0.05 (–0.03, –0.07)	–0.5 (–0.3, –0.6)	–36 (–22, –50)
South-Central	17	–0.10 (–0.07, –0.13)	–0.5 (–0.3, –0.6)	–11 (–2, –22)
Southwest	24	–0.88 (–0.54, –1.24)	–3.0 (–1.9, –4.3)	–44 (–27, –63)
Yukon	15	–0.46 (–0.26, –0.64)	–0.9 (–0.5, –1.2)	–30 (–16, –44)
Northwest	2	–0.06 (–0.02, –0.12)	–0.3 (–0.1, –0.7)	–8 (–2, –23)
North Slope	9	–0.33 (–0.10, –0.62)	–1.6 (–0.5, –3.0)	–23 (–2, –47)
Total or mean	**68**	**–1.88 (–1.03, –2.82)**	**–1.2 (–0.7, –1.9)**	**–31 (–16, –49)**

8.5. Discussion

The magnitude of carbon transported laterally, emitted, and stored in inland waters is controlled largely by variability in climate, hydrology, and exchanges of both inorganic and organic carbon among the terrestrial landscape, aquatic environments, and the atmosphere. The source of aquatic carbon is the combination of instream production and delivery of terrestrially derived carbon via surface-water or groundwater flow paths. Rising temperatures have already affected the large pools of carbon stored in the soils and permafrost (Striegl and others, 2007; Schuur and others, 2008; Frey and McClelland, 2009; Tarnocai and others, 2009) and have reduced the size of glaciers in Alaska (Arendt and others, 2002; Berthier and others, 2010). Therefore, it is important to provide accurate estimates of current carbon fluxes in aquatic environments, so that future effects of climate change can be determined.

8.5.1. Coastal Export and Carbon Dioxide Flux From Riverine Systems

The coastal carbon export from the Southeast and South-Central regions of Alaska accounted for approximately 40 percent of the State's total lateral flux at 7.3 TgC/yr. The lateral carbon yields from the Southeast region were the highest in the State at 36.7 $gC/m^2/yr$. The South-Central region had total carbon export nearly equivalent to that of the Southeast region; however, given its larger total area, the yields were lower (17.0 $gC/m^2/yr$). The mean annual precipitation for these regions, particularly along the coast, can be between 2 and 3 m, and in mountainous headwaters mean annual precipitation can be a great as 8 m (Powell and Molnia, 1989). Heavy precipitation produces an abundance of small, swift-moving streams. For the Southeast region, the estimated magnitude of total discharge was 356 cubic kilometers per year (km^3/yr), which translates to a runoff of 3.4 m/yr. Total discharge for the South-Central region was 220 km^3/yr, which translates to a water yield of 1.1 m/yr (5th and 95th percentiles of 0.8 m/yr and 2.5 m/yr).

Forested and wetland soils in the Southeast and South-Central regions of Alaska deliver organic carbon to streams draining to the coast (Fellman and others, 2008; D'Amore and others, 2010), and mean organic carbon concentrations for these regions were between 3 and 4 mg/L. The organic carbon fluxes estimated within this report are comparable with other estimates for this region (D'Amore and others, 2015). With substantial ice cover in these two regions, glacial runoff is a significant source of organic carbon (Hood and others, 2009; Schroth and others, 2011) and inorganic carbon, as considerable rock weathering occurs under ice sheets (Ludwig and others, 1999). Mean inorganic carbon concentrations for rivers and streams were 6.6 mg/L and 11 mg/L for the Southeast and South-Central regions, respectively.

Estimated riverine CO_2 efflux from the Southeast and South-Central regions was over 50 percent of the total vertical CO_2 emission for the State of Alaska at 8.4 TgC/yr, yet these regions only account for 19 percent of the total water area. These two regions had very high yield estimates—from 21.7 $gC/m^2/yr$ for the South-Central region to 37.3 $gC/m^2/yr$ for the Southeast region. Average gas transfer velocities in this region were the highest in the State at approximately 24 m/d. Although this is within published estimates of stream kCO_2 (Hall and others, 2012; Huotari and others, 2013), it remains unclear if riverine CO_2 emissions can be maintained with transfer rates this high. To date, there are no comparable vertical CO_2 emissions from riverine systems for these two regions.

The coastal carbon export combined with CO_2 emissions produced a river carbon flux of 5.8 TgC/yr from the Southwest region. This region had a high percent of total carbon flux as DIC (78.4 percent). This is likely due to the sedimentary rocks rich in carbonates that underlie this region (Dürr and others, 2005), and the Kuskwokwim River has significantly affected the carbonate saturation indices of the Bering Sea (Mathis and others, 2011). Currently, there are no other studies that can be used as a comparison for the estimates from this region.

Carbon cycling and storage at high latitudes have been key issues in carbon cycle science. Therefore, estimates of aquatic carbon fluxes exist for major watersheds draining to the Arctic Ocean, including the Yukon River and several of the main rivers draining the North Slope of Alaska (Colville, Kuparuk, and Sagavanirktok Rivers). The results presented in this chapter support many of these existing flux estimates.

The highest lateral carbon fluxes for Alaska, estimated at 5.5 TgC/yr, were in the Yukon River Basin, likely owing to high discharge (125 km^3/yr), DIC concentration (18.6 mg/L, s.d. of 10.0 mg/L), and TOC concentration (4.8 mg/L, s.d. of 10.0 mg/L). This estimate is about 35 percent lower than previous Yukon River carbon flux estimates of 7.2 TgC/yr (Striegl and others, 2007), in part because of the difference in the period of record between the two studies. This report used data from 1975 to 2013 to calculate fluxes for the Yukon River at Pilot Station (NWIS station ID=15565447), but Striegl and others (2007) only used data between 2001 and 2005. The water chemistry data for these two different studies were comparable. The median alkalinity as calcium carbonate for the Yukon River at Pilot Station was 76.2 mg/L in this assessment compared with 74.5 mg/L of Striegl and others (2007). The median alkalinity as DOC was 5.6 mg/L in this assessment compared with 5.5 mg/L of Striegl and others (2007). However the median discharge of 125 km^3/yr in this report was much lower than 146 km^3/yr for the time period used in Striegl and others (2007). The 17-percent difference in discharge is likely the main cause for different flux estimates between the two studies.

In this assessment, riverine CO_2 emission from the Yukon region was estimated to be 3.7 TgC/yr (5th and 95th percentiles of 2.0 TgC/yr and 6.3 TgC/yr), which is lower compared

with 7.7 TgC/yr (5th and 95th percentiles of 6.7 TgC/yr and 9.2 TgC/yr) of Striegl and others (2012; herein called Striegl and others). In this report, the yield estimate for the Yukon region was 7.1 gC/m^2/yr (5th and 95th percentiles of 3.7 gC/m^2/yr and 12.0 gC/m^2/yr), which is lower than 10.5 g/C/m^2/yr (5th and 95th percentiles of 9.0 gC/m^2/yr and 13.0 gC/m^2/yr) of Striegl and others, although their value falls within our error estimate.

Multiple factors contributed to the difference in total river evasion estimates between the two studies. Striegl and others included the total efflux for the Canadian proportion of the Yukon River Basin, whereas this study presents fluxes only for the portion of the basin within the Alaskan State boundary. The area of the Yukon River Basin within the State of Alaska estimated in this report was approximately 530,000 km^2, which represents 60 percent of the total Yukon River Basin. Additionally, Striegl and others used high-resolution remote sensing methods to determine stream and river surface area for all but the smaller tributaries and estimated a total river surface area of 10,000 km^2, which is 1.2 percent of the total land area in the Yukon River Basin. In this report, the water surface area was lower, about 0.8 percent of the land area, because EDNA did not adequately represent low-order streams.

Another methodological difference between the two studies was that this report used modeled estimates for $kCO_{2-river}$ that ranged from 2.5 to 28.0 m/d from first through tenth stream orders for the Yukon River according to methods outlined in Zhu and Reed (2014), but the maximum $kCO_{2-river}$ used by Striegl and others approached 6.9 m/d with a minimum of 0.3 m/d along the main stem of the upper Yukon River Basin. In addition, Striegl and others estimated a total of 200 days, or 54 percent of the year, where no efflux occurred based on ice cover conditions; this was applied uniformly across the basin to the total flux estimate. In this report, ice cover was estimated spatially using mean monthly temperature to produce a range of 145 to 152 days that are ice free depending upon topographic location. Thus, this report presents higher flux rates for shorter periods of time and for less surface area compared with Striegl and others. Because of the difference in methods between the two studies, identification of CO_2 emission hotspots also diverged. The methods used to derive the CO_2 emission estimates from rivers presented in this report indicated that the dominant fluxes occurred either in the smaller tributaries or the highest order main stem of the river network determined by $kCO_{2-river}$ or by area, respectively. In contrast, Striegl and others suggest that the majority of the efflux occurs within the tributaries only. Despite these methodological differences, if we increase our flux by the increased proportion of surface area suggested by Striegl and others, we obtain a yield of 9.6 gC/m^2/yr, which is very similar to their 10.5 gC/m^2/yr.

Despite relatively high DIC (14.7 mg/L) and TOC concentrations (8.5 mg/L), the North Slope region had a low coastal carbon export rate of 1.3 TgC/yr, likely owing to relatively low discharge of 53 km^3/yr. This region had the highest TOC concentrations and the highest regional value of total carbon flux as TOC (38 percent). The summed organic carbon flux estimate for the Sagavanirktok, Kuparuk, and Colville Rivers in the North Slope region presented in this report was 0.41 TgC/yr (5th and 95th percentiles of 0.05 TgC/yr and 0.8 TgC/yr), which encompassed the McClelland and others (2014) estimate of 0.30 TgC/yr (s.d. of 0.03 TgC/yr) for the same rivers. Overall, the Northwest region is one of the most data-poor regions in the State, and this report presents the first estimates for river coastal carbon flux from this region of 1.5 TgC/yr.

The riverine CO_2 effluxes for the North Slope and Northwest regions were estimated to be 0.6 TgC/yr and 0.8 TgC/yr with yields of 3.1 gC/m^2/yr and 4.2 gC/m^2/yr, respectively. These regions represent only 10 percent of the total statewide riverine efflux, and the flux was driven primarily by a short ice-free period, averaging a total of 113 to 138 days, and by small surface areas of streams and rivers, representing only 0.26 percent of the land surface area in the North Slope region and 0.29 percent in the Northwest region. These yield estimates are larger than those derived from within the Kuparuk River watershed as part of the Toolik Lake LTER (Kling and others, 1992, 2000). At 3.8 gC/m^2/yr, this report's value is double the estimate for the Kuparuk River network of 1.7 gC/m^2/yr derived for 1994 through 1996 (Hobbie and Kling, 2014) and significantly higher than a more recent estimate for the same watershed of 0.02 gC/m^2/yr (Cory and others, 2014). Cory and others (2014) estimated the proportion of the landscape as stream and river surface to be about 0.23 percent, which is similar to this report's estimate, although it remains unclear how they estimated lateral inputs of DIC contributing to pCO_2 in their study, possibly biasing their total flux to be low.

8.5.2. Carbon Dioxide Flux From and Carbon Burial in Lacustrine Systems

The Southeast and South-Central regions showed nearly identical lake vertical flux estimates at 3.2 gC/m^2/yr and 3.4 gC/m^2/yr, respectively. To our knowledge, these are the first estimates for lake efflux in coastal regions that include temperate rainforest ecosystems. The calculated pCO_2 values were nearly identical across both the Southeast and South-Central regions at about 2,600 µatm. Input of organic carbon from forested and wetland systems may affect lake pCO_2 estimates, as median alkalinity estimates for the Southeast region were very low at around 2 mg/L, whereas median pH was 6.7 (David D'Amore, U.S. Department of Agriculture, Forest Service, written commun., November 3, 2014). A complication for modeling the efflux of CO_2 from lake ecosystems within these regions is the lack of data from central lake locations. Nearly all identified sites in the Southeast region of Alaska are from samples taken at either inlet or

outlet of a lake. These concentrations are likely to be different than the carbon concentrations at central points within the lake, where the greatest turbulence and greatest gas emission rates likely occur.

A very high lake CO_2 emission of 5.8 TgC/yr was calculated for the Southwest region. This value is larger than all other regions in Alaska combined. The median estimated pCO_2 value for this region was 4,200 µatm, with values ranging between 19 and 71,000 µatm. There are currently no published estimates of direct measurements of lake CO_2 concentrations within this region for comparison. Direct measurements refer to in situ monitoring of CO_2 with a type of infrared sensor, as opposed to the indirect measurement used in this report by estimating CO_2 concentrations from alkalinity, pH, and temperature measurements. Unpublished direct dissolved CO_2 measurements for small lakes near Lake Iliamna had a maximum pCO_2 of 2,800 µatm and were undersaturated (<390 µatm) for half of the period that the lake was covered with ice (G. Holtgrieve, University of Washington-Seattle, written commun.). In addition to the high concentration of dissolved CO_2 identified within the Southwest region, this region also has significantly higher lake surface area at 21,000 km^2, nearly double the estimates for the Yukon and North Slope regions. Obtaining direct dissolved CO_2 concentration measurements from multiple points on large lakes is critical to reducing the uncertainty for the high estimated lake carbon emissions in this region.

Current research on boreal and arctic lakes consistently show annual dissolved CO_2 concentrations to be in excess of atmospheric CO_2 (Huttunen and others, 2003; Sobek and others, 2005; Jonsson and others, 2008). In lakes across the boreal and arctic regions of Alaska, including the North Slope, Northwest, and Yukon regions, median pCO_2 values ranged from about 970 µatm in the Yukon to about 1,900 µatm in the Northwest. Much of the CO_2 supersaturation is hypothesized to originate from the mineralization of both allochthonous and autochthonous carbon sources (Roehm and others, 2009; Solomon and others, 2013). However, although DOC correlates with dissolved CO_2 values, significant regional variation exists so that a model that can be applied across the circumboreal region is still not available (Roehm and others, 2009).

For this study, the North Slope lake efflux was estimated to be 0.6 TgC/yr (5th and 95th percentiles of 0.5 TgC/yr and 0.9 TgC/yr), resulting in a flux of 3.1 $gC/m^2/yr$ (5th and 95th percentiles of 2.2 $gC/m^2/yr$ and 4.5 $gC/m^2/yr$). Previous lake studies at the Toolik Lake LTER estimated fluxes of 1.1 $gC/m^2/yr$ (Hobbie and Kling, 2014) and 0.4 $gC/m^2/yr$ (Cory and others, 2014). These flux measurements, made at a single site, were estimated with data from two different time periods—1994 through 1996 for the Hobbie and Kling study and 2001 through 2013 for the Cory and others study. These differences indicate that there is significant temporal variation in carbon fluxes within the Arctic. The lake CO_2 emissions estimated for the North Slope region in this study may be high owing to high initial DIC concentrations derived from the calculation of pCO_2 from ancillary data and because the timing of samples taken for this analysis may not be representative of the influence that seasonal hydrology and in situ primary production impart on carbon concentrations (Huttunen and others, 2003).

For lakes in the Yukon Flats area, the lake CO_2 emissions were estimated with direct dissolved CO_2 concentrations (Halm and Guldager, 2013; Halm and Griffith, 2014). The Yukon region's average pCO_2 values were the lowest across all regions, and the median value of 970 µatm was considerably lower than the next closest median pCO_2 value of 1,400 µatm, which was calculated for the North Slope region. The Yukon Flats data represent only single measurements, usually made during the summer, and significant seasonal fluctuations in these values are likely. Additional direct seasonal measurements of CO_2 concentrations for lakes throughout Alaska are necessary to determine if (1) low pCO_2 values are representative of lakes in other regions and (2) low concentrations persist even under seasonal fluctuations of in-lake biological processes, including photosynthesis and respiration.

The average sedimentation rate observed in Alaskan lakes (1.5 mm/yr) was similar to those from a study of lakes in eastern North America, which reported that historical sedimentation rates had a log-normal distribution, with a median of 2.2 mm/yr (Webb and Webb, 1988). A few studies have reported sedimentation rates for Alaskan lakes: Cornwell (1985) reported a sediment accumulation rate of 0.16 mm/yr for Toolik Lake, in the foothills of the North Slope region, and noted that low rainfall, a short runoff period, and stabilization of soils by thick organic matter layers and nearly continuous tundra vegetation contribute to low sedimentation rates in the lake. Higher sedimentation rates (2.5 mm/yr) were reported for Black Lake, on the Alaskan Peninsula, which receives more precipitation and is covered in dense forest, rather than tundra vegetation (Post, 2011).

Sediment carbon concentrations for Alaskan lakes were similar to those documented for 3 oligotrophic, humic-rich lakes in Sweden (21 to 31 percent; Sobek and others, 2009, 2014), 16 lakes in western Ontario (20 percent, s.d. of 7 percent), and 23 lakes in Wisconsin (20 percent, s.d. of 10 percent) (Brunskill and others, 1971). In contrast, sediment carbon concentrations were much lower in seven lakes in western Greenland (1.8 to 8.9 percent); the study area was cold and dry, with a mean annual temperature of –6 °C and mean annual precipitation of 150 mm/yr (Sobek and others, 2014); sparse vegetation and poorly developed soils may have limited contributions of organic matter to the lakes from the surrounding terrestrial environment.

Variations in carbon burial rate in Alaska reflect differences in sedimentation rate, sediment carbon concentration, and the extent of water bodies (see equation 8.7). Based on results from the stepwise MLR modeling, sedimentation rates were strongly related to land-cover type, with shrubland,

mixed forest, and herbaceous wetland exerting a positive influence and permafrost exerting a negative influence (table 8.6). The positive influence of shrubland on sedimentation rates may reflect the susceptibility of this land-cover type to erosion, whereas the positive influence of mixed forest and herbaceous wetlands may be related to high productivity of vegetation in these areas. In addition, shrub distribution in tundra terrain is often confined to recently eroded gullies and water-track habitats, which may indicate recent erosion (Tape and others, 2011). The negative influence of permafrost on sedimentation rates probably is due to low erosion rates of frozen soil, except in areas with thermokarst where erosion can be important (Osterkamp and others, 2000). Differences in estimated sedimentation rates among regions reflect the relative abundance of land-cover types and permafrost. Low estimated sedimentation rates in the Northwest region, for example, may be attributed to the importance of permafrost, which underlies over 70 percent of the landscape in this region (chapter 3 of this report; Pastick, Jorgenson, and others, 2014). Relatively high sedimentation rates were estimated for the Southwest region, which has abundant shrubland and herbaceous wetlands and relatively little permafrost.

The stepwise MLR modeling indicated that sediment carbon concentrations were strongly related to log water body surface area, mean basin elevation, and percent of basin covered by bogs (table 8.6). Sediment carbon concentrations were inversely related to water body surface area, reflecting relatively high productivity rates in the littoral zone of lakes compared to deeper water zones; small lakes typically are shallower than large lakes, and littoral zones constitute a greater percentage of total lake area (Wetzel, 2001). Mean basin elevation also was a negative influence on sediment carbon concentration, probably because of decreases in primary productivity and associated soil organic carbon with elevation (Jobbágy and Jackson, 2000; Ping and others, 2008). Bogs were a positive influence on sediment carbon, as expected given the high organic carbon content of bog soils that have the potential for providing carbon subsidies to nearby lakes (Jobbágy and Jackson, 2000; Pastick, Rigge, and others, 2014).

The carbon burial rate estimated for Alaskan lakes in this study normalized to lake area (–31 $gC/m^2/yr$) is higher than long-term (Holocene) rates for boreal lakes in northern Quebec (–3.8 $gC/m^2/yr$; Ferland and others, 2012) and Finland (–0.2 to –8.5 $gC/m^2/yr$; Kortelainen and others, 2004); however, our estimates pertain only to the past 100 years. The carbon burial rates estimated herein for Alaska approach those in thermokarst lakes in Siberia (–47±10 $gC/m^2/yr$), which are relatively high because of thermokarst erosion, which contributes organic matter and nutrients to lakes, and cold temperatures, which limit decomposition (Walter Anthony and others, 2014). At the global scale, Dean and Gorham (1998) noted an inverse relation between carbon burial rates and lake area and estimated an average carbon accumulation rate of –5 $gC/m^2/yr$ for large lakes and –72 $gC/m^2/yr$ for small lakes; an inverse relation between carbon burial rates and lake size was observed in the present study as well.

Variations in estimated total carbon burial fluxes (in TgC/yr) among hydrologic regions primarily reflect differences in sedimentation rates and the areal extent of water bodies; these parameters showed much more variability among regions than sediment carbon concentrations, as indicated by the coefficient of variation (CV) for each parameter. The CV for sedimentation rates and water body area were 0.51 and 0.14, whereas the CV for sediment carbon concentrations was only 0.04. The Southwest region had the highest carbon burial rates among the regions of Alaska (table 8.5); this region also had greatest water body surface area (table 8.4) and the highest sedimentation rates. In contrast, carbon burial in lakes of the South-Central and Northwest regions was much smaller (table 8.5), reflecting lower water body surface areas (table 8.4) and sedimentation rates.

Table 8.6. Estimates, standard error of estimates, and p-values for independent variables used in multiple-linear-regression models for sedimentation rates and sediment carbon concentrations in Alaskan water bodies.

[km^2, square kilometer; m, meter]

Independent variable	Sedimentation rate model					Sediment carbon concentration model			
	Intercept	Mixed forest (percent)	Shrubland (percent)	Herbaceous wetland (percent)	Permafrost (percent)	Intercept	Log lake area (km^2)	Mean elevation (m)	Bogs (percent)
Estimate	–0.0117	0.0161	0.0017	0.0126	–0.0013	10.838	–3.2805	–0.0093	0.3781
Standard error of estimate	–0.0117	0.0161	0.0017	0.0126	–0.0013	1.0039	0.5014	0.0016	0.0518
p-value	0.63	<0.0001	<0.0001	<0.0001	0.0008	<0.0001	<0.0001	<0.0001	<0.0001

8.6. Summary and Conclusions

The total statewide carbon flux from inland waters (coastal export plus CO_2 emissions from rivers and lakes minus burial in sediments) was 41.2 TgC/yr, and total carbon yields were 27.5 gC/m^2/yr. The greenhouse-gas-emission estimates reported in this chapter may be low because methane (CH_4) fluxes were not included owing to a lack of lacustrine and riverine CH_4 concentration data across Alaska. Recent studies have documented that both CO_2 and CH_4 may represent a consistent carbon loss pathway from aquatic ecosystems to the atmosphere (Walter and others, 2007; Crawford and others, 2013; Sepulveda-Jauregui and others, 2014). Using the lake CH_4 estimates for northern latitudes (Wik and others, 2016) and applying them to the lake surface area of Alaska indicates that lake CH_4 emissions may equal 0.5 TgC/yr. Current modeling efforts strive to integrate CH_4 concentration samples from a variety of lake types, including deep glacial lakes as well as thermokarst water bodies in Alaska, as well as low- and high-order streams and rivers in order to provide an accurate estimate of current lake and river CH_4 emissions in Alaska.

There was considerable variability in the estimated inland waters' carbon fluxes among the six hydrologic regions in Alaska. The Southeast region, with high precipitation rates and an abundance of short, steep streams, had the highest total yield (flux divided by hydrologic area) in the State at 76.7 gC/m^2/yr. The South-Central region had the second highest total yield of 41.6 gC/m^2/yr. The Southwest region had the highest lake surface area (nearly 21,000 km^2) and the highest lake CO_2 emission rates (5.8 TgC/yr), which contributed to the relatively high overall yield of 36.5 gC/m^2/yr. The Yukon region had a total yield of 17.5 gC/m^2/yr. Both the Northwest and the North Slope regions, with the lowest temperatures and precipitation among the six regions, had the smallest overall combined yields of 14.7 gC/m^2/yr and 10.7 gC/m^2/yr, respectively.

This chapter focused on presenting results of current carbon fluxes from inland aquatic systems, but projected climate changes are likely to influence the magnitude of aquatic carbon fluxes in future decades. Predicted changes to the hydrologic cycle include increased streamflow in high-latitude regions (Hinzman and others, 2005; Brabets and Walvoord, 2009) and increased runoff owing to increased rates of glacier melt (Arendt and others, 2002). The influence of groundwater on regional hydrology is also likely to change because of permafrost thaw (Walvoord and others, 2012). Increased forest fires (Kasischke and others, 2010), permafrost thaw (Walvoord and Striegl, 2007; Tank, Frey, and others, 2012), and changes in vegetation composition (Chapin and others, 1995) are all likely to affect the amount and composition of carbon delivered to aquatic systems. Coupling both hydrologic and biogeochemical reactions over space and time will be key to accurately predicting changes in the magnitude of aquatic carbon fluxes in the future.

The results presented in this chapter indicate that the magnitude of inland waters' aquatic carbon fluxes is significant at 41.2 TgC/yr. Since the models that produced the soil CO_2 flux estimates in the assessment were not coupled with the models that produced the riverine inorganic carbon flux or the vertical CO_2 emissions, the appropriate amount of CO_2 that is emitted from the aquatic ecosystems was not subtracted from the heterotrophic respiration term, which may lead to double counting. Additionally, if the DOC leaching from soil organic matter pools was not adequately represented within the terrestrial modeling environment, the modeled soil pools could be amassing organic carbon that has actually been transported, processed, or stored in aquatic ecosystems. Development of a model framework that couples the terrestrial and aquatic carbon processing and transport is key to understanding whether terrestrial landscapes represent a dominant source of carbon to freshwater systems. Chapter 9 of this report will present a complete picture of terrestrial and aquatic ecosystems and will illustrate a comparison that indicates that the linkage between these two environments is important to understand fully the role they play in greenhouse-gas storage and cycling.

8.7. References Cited

Abbott, M.B., Edwards, M.E., and Finney, B.P., 2010, A 40,000-yr record of environmental change from Burial Lake in northwest Alaska: Quaternary Research, v. 74, no. 1, p. 156–165, http://dx.doi.org/10.1016/j.yqres.2010.03.007.

Abbott, M.B., Finney, B.P., Edwards, M.E., and Kelts, K.R., 2000, Lake-level reconstructions and paleohydrology of Birch Lake, central Alaska, based on seismic reflection profiles and core transects: Quaternary Research, v. 53, no. 2, p. 154–166, http://dx.doi.org/10.1006/qres.1999.2112.

Akaike, Hirotugu, 1981, Likelihood of a model and information criteria: Journal of Econometrics, v. 16, no. 1, p. 3–14, http://dx.doi.org/10.1016/0304-4076(81)90071-3.

Anderson, D.E., Striegl, R.G., Stannard, D.I., Michmerhuizen, C.M., McConnaughey, T.A., and LaBaugh, J.W., 1999, Estimating lake-atmosphere CO_2 exchange: Limnology and Oceanography, v. 44, no. 4, p. 988–1001, http://dx.doi.org/10.4319/lo.1999.44.4.0988.

Anderson, Lesleigh, Abbott, M.B., and Finney, B.P., 2001, Holocene climate inferred from oxygen isotope ratios in lake sediments, central Brooks Range, Alaska: Quaternary Research, v. 55, no. 3, p. 313–321, http://dx.doi.org/10.1006/qres.2001.2219.

Arendt, A.A., Echelmeyer, K.A., Harrison, W.D., Lingle, C.S., and Valentine, V.B., 2002, Rapid wastage of Alaska glaciers and their contribution to rising sea level: Science, v. 297, no. 5580, p. 382–386, http://dx.doi.org/10.1126/science.1072497.

Aufdenkampe, A.K., Mayorga, Emilio, Raymond, P.A., Melack, J.M., Doney, S.C., Alin, S.R., Aalto, R.E., and Yoo, Kyungsoo, 2011, Riverine coupling of biogeochemical cycles between land, oceans, and atmosphere: Frontiers in Ecology and the Environment, v. 9, no. 1, p. 53–60, http://dx.doi.org/10.1890/100014.

Axford, Yarrow, and Kaufman, D.S., 2004, Late glacial and Holocene glacier and vegetation fluctuations at Little Swift Lake, southwestern Alaska, U.S.A.: Arctic, Antarctic, and Alpine Research, v. 36, no. 2, p. 139–146, http://dx.doi.org/10.1657/1523-0430(2004)036[0139:LGAHGA]2.0.CO;2.

Barto, David, 2004, Assessing the production of sockeye salmon (*Oncorhynchus nerka*) at Chilkat Lake, southeast Alaska, using current trophic conditions and the paleolimnologic sediment record: Fairbanks, Alaska, University of Alaska, M.S. thesis, 111 p.

Berthier, E., Schiefer, E., Clarke, G.K.C., Menounos, B., and Rémy, F., 2010, Contribution of Alaskan glaciers to sea-level rise derived from satellite imagery: Nature Geoscience, v. 3, no. 2, p. 92–95, http://dx.doi.org/10.1038/ngeo737.

Bird, B.W., Abbott, M.B., Finney, B.P., and Kutchko, Barbara, 2009, A 2000 year varve-based climate record from the central Brooks Range, Alaska: Journal of Paleolimnology, v. 41, no. 1, p. 25–41, http://dx.doi.org/10.1007/s10933-008-9262-y.

Blais, J.M., and Kalff, Jacob, 1995, The influence of lake morphometry on sediment focusing: Limnology and Oceanography, v. 40, no. 3, p. 582–588, http://dx.doi.org/10.4319/lo.1995.40.3.0582.

Brabets, T.P., and Walvoord, M.A., 2009, Trends in streamflow in the Yukon River Basin from 1944 to 2005 and the influence of the Pacific Decadal Oscillation: Journal of Hydrology, v. 371, nos. 1–4, p. 108–119, http://dx.doi.org/10.1016/j.jhydrol.2009.03.018.

Brady, S.M., 2013, A multi-proxy approach to late quaternary environmental change at Little Harding Lake, interior Alaska: Pocatello, Idaho, Idaho State University, M.S. thesis, 157 p.

Brunskill, G.J., Povoledo, D., Graham, B.W., and Stainton, M.P., 1971, Chemistry of surface sediments of sixteen lakes in the Experimental Lakes Area, northwestern Ontario: Journal of the Fisheries Research Board of Canada, v. 28, no. 2, p. 277–294, http://dx.doi.org/10.1139/f71-038.

Butman, David, and Raymond, P.A., 2011, Significant efflux of carbon dioxide from streams and rivers in the United States: Nature Geoscience, v. 4, no. 12, p. 839–842, http://dx.doi.org/10.1038/ngeo1294.

Carlson, L.J., and Finney, B.P., 2004, A 13,000-year history of vegetation and environmental change at Jan Lake, east-central Alaska: The Holocene, v. 14, no. 6, p. 818–827, http://dx.doi.org/10.1191/0959683604hl762rp.

Chapin, F.S., III, Shaver, G.R., Giblin, A.E., Nadelhoffer, K.J., and Laundre, J.A., 1995, Responses of arctic tundra to experimental and observed changes in climate: Ecology, v. 76, no. 3, p. 694–711, http://dx.doi.org/10.2307/1939337.

Charlton, S.R., Parkhurst, D.L., and Appelo, C.A.J., 2014, Phreeqc—R interface to geochemical modeling software (ver. 3): U.S. Geological Survey, accessed July 1, 2014, at http://cran.r-project.org/web/packages/phreeqc/index.html.

Chen, Min, Rowland, J.C., Wilson, C.J., Altmann, G.L., and Brumby, S.P., 2013, The importance of natural variability in lake areas on the detection of permafrost degradation; A case study in the Yukon Flats, Alaska: Permafrost and Periglacial Processes, v. 24, no. 3, p. 224–240, http://dx.doi.org/10.1002/ppp.1783.

Chipman, M.L., Clarke, G.H., Clegg, B.F., Gregory-Eaves, Irene, and Hu, F.S., 2009, A 2000 year record of climatic change at Ongoke Lake, southwest Alaska: Journal of Paleolimnology, v. 41, no. 1, p. 57–75, http://dx.doi.org/10.1007/s10933-008-9257-8.

Chipman, M.L., Clegg, B.F., and Hu, F.S., 2012, Variation in the moisture regime of northeastern interior Alaska and possible linkages to the Aleutian Low; Inferences from a late-Holocene $\delta^{18}O$ record: Journal of Paleolimnology, v. 48, no. 1, p. 69–81, http://dx.doi.org/10.1007/s10933-012-9599-0.

Clegg, B.F., and Hu, F.S., 2010, An oxygen-isotope record of Holocene climate change in the south-central Brooks Range, Alaska: Quaternary Science Reviews, v. 29, nos. 7–8, p. 928–939, http://dx.doi.org/10.1016/j.quascirev.2009.12.009.

Cohn, B.R., 2009, Recent paleoenvironmental changes recorded in three non-anadromous lakes in southwest Alaska; Effects of climatic and vegetation dynamics on lake productivity: Fairbanks, Alaska, University of Alaska, M.S. thesis, 121 p.

Cole, J.J., and Caraco, N.F., 1998, Atmospheric exchange of carbon dioxide in a low-wind oligotrophic lake measured by the addition of SF_6: Limnology and Oceanography, v. 43, no. 4, p. 647–656, http://dx.doi.org/10.4319/lo.1998.43.4.0647.

Cole, J.J., Prairie, Y.T., Caraco, N.F., McDowell, W.H., Tranvik, L.J., Striegl, R.G., Duarte, C.M., Kortelainen, P., Downing, J.A., Middelburg, J.J., and Melack, J., 2007, Plumbing the global carbon cycle; Integrating inland waters into the terrestrial carbon budget: Ecosystems, v. 10, no. 1, p. 171–185, http://dx.doi.org/10.1007/s10021-006-9013-8.

Cornwell, J.C., 1985, Sediment accumulation rates in an Alaskan arctic lake using a modified ^{210}Pb technique: Canadian Journal of Fisheries and Aquatic Sciences, v. 42, no. 4, p. 809–814, http://dx.doi.org/10.1139/f85-103.

Cory, R.M., Ward, C.P., Crump, B.C., and Kling, G.W., 2014, Sunlight controls water column processing of carbon in arctic fresh waters: Science, v. 345, no. 6199, p. 925–928, http://dx.doi.org/10.1126/science.1253119.

Crawford, J.T., Striegl, R.G., Wickland, K.P., Dornblaser, M.M., and Stanley, E.H., 2013, Emissions of carbon dioxide and methane from a headwater stream network of interior Alaska: Journal of Geophysical Research; Biogeosciences, v. 118, no. 2, p. 482–494, http://dx.doi.org/10.1002/jgrg.20034.

D'Amore, D.V., Edwards, R.T., Herendeen, P.A., Hood, Eran, and Fellman, J.B., 2015, Dissolved organic carbon fluxes from hydropedologic units in Alaskan coastal temperate rainforest watersheds: Soil Science Society of America Journal, v. 79, no. 2, p. 378–388, http://dx.doi.org/10.2136/sssaj2014.09.0380.

D'Amore, D.V., Fellman, J.B., Edwards, R.T., and Hood, Eran, 2010, Controls on dissolved organic matter concentrations in soils and streams from a forested wetland and sloping bog in southeast Alaska: Ecohydrology, v. 3, no. 3, p. 249–261, http://dx.doi.org/10.1002/eco.101.

Davis, M.B., and Ford, M.S., 1982, Sediment focusing in Mirror Lake, New Hampshire: Limnology and Oceanography, v. 27, no. 1, p. 137–150, http://dx.doi.org/10.4319/lo.1982.27.1.0137.

Dean, W.E., and Gorham, Eville, 1998, Magnitude and significance of carbon burial in lakes, reservoirs, and peatlands: Geology, v. 26, no. 6, p. 535–538, http://dx.doi.org/10.1130/0091-7613(1998)026<0535:MASOCB>2.3.CO;2.

Driscoll, C.T., Fuller, R.D., and Schecher, W.D., 1989, The role of organic acids in the acidification of surface waters in the Eastern U.S.: Water, Air, and Soil Pollution, v. 43, no. 1–2, p. 21–40, http://dx.doi.org/10.1007/BF00175580.

Dürr, H.H., Meybeck, Michel, and Dürr, S.H., 2005, Lithologic composition of the Earth's continental surfaces derived from a new digital map emphasizing riverine material transfer: Global Biogeochemical Cycles, v. 19, no. 4, article GB4S10, 22 p., http://dx.doi.org/10.1029/2005GB002515.

Efron, Bradley, and Tibshirani, R.J., 1994, An introduction to the bootstrap: Boca Raton, Fla., Chapman & Hall/CRC, Monographs on Statistics and Applied Probability, v. 57, 456 p.

Ellis, J.M., and Calkin, P.E., 1984, Chronology of Holocene glaciation, central Brooks Range, Alaska: Geological Society of America Bulletin, v. 95, no. 8, p. 897–912, http://dx.doi.org/10.1130/0016-7606(1984)95<897:COHGCB>2.0.CO;2.

Environment and Climate Change Canada, 2014, Fresh Water Quality Monitoring—Online data: Environment and Climate Change Canada, accessed October 27, 2014, at https://www.ec.gc.ca/eaudouce-freshwater/default.asp?lang=En&n=EFDA57C6-1.

Fellman, J.B., D'Amore, D.V., Hood, Eran, and Boone, R.D., 2008, Fluorescence characteristics and biodegradability of dissolved organic matter in forest and wetland soils from coastal temperate watersheds in southeast Alaska: Biogeochemistry, v. 88, no. 2, p. 169–184, http://dx.doi.org/10.1007/s10533-008-9203-x.

Ferland, M.-E., del Giorgio, P.A., Teodoru, C.R., and Prairie, Y.T., 2012, Long-term C accumulation and total C stocks in boreal lakes in northern Québec: Global Biogeochemical Cycles, v. 26, no. 4, article GB0E04, 10 p., http://dx.doi.org/10.1029/2011GB004241.

Finkenbinder, M.S., Abbott, M.B., Edwards, M.E., Langdon, C.T., Steinman, B.A., and Finney, B.P., 2014, A 31,000 year record of paleoenvironmental and lake-level change from Harding Lake, Alaska, USA: Quaternary Science Reviews, v. 87, p. 98–113, http://dx.doi.org/10.1016/j.quascirev.2014.01.005.

Finney, B.P., Bigelow, N.H., Barber, V.A., and Edwards, M.E., 2012, Holocene climate change and carbon cycling in a groundwater-fed, boreal forest lake; Dune Lake, Alaska: Journal of Paleolimnology, v. 48, no. 1, p. 43–54, http://dx.doi.org/10.1007/s10933-012-9617-2.

Frey, K.E., and McClelland, J.W., 2009, Impacts of permafrost degradation on arctic river biogeochemistry: Hydrological Processes, v. 23, no. 1, p. 169–182, http://dx.doi.org/10.1002/hyp.7196.

Frohn, R.C., Hinkel, K.M., and Eisner, W.R., 2005, Satellite remote sensing classification of thaw lakes and drained thaw lake basins on the North Slope of Alaska: Remote Sensing of Environment, v. 97, no. 1, p. 116–126, http://dx.doi.org/10.1016/j.rse.2005.04.022.

Fry, J.A., Xian, George, Jin, Suming, Dewitz, J.A., Homer, C.G., Yang, Limin, Barnes, C.A., Herold, N.D., and Wickham, J.D., 2011, Completion of the 2006 National Land Cover Database for the conterminous United States: Photogrammetric Engineering & Remote Sensing, v. 77, no. 9, p. 858–864. [Also available at http://www.mrlc.gov/nlcd2006.php.]

Hair, J.F., Black, Bill, Babin, Barry, Anderson, R.E., and Tatham, R.L., 2006, Multivariate data analysis (6th ed.): Upper Saddle River, N.J., Pearson Prentice Hall, 899 p.

Hall, R.O., Jr., Kennedy, T.A., and Rosi-Marshall, E.J., 2012, Air–water oxygen exchange in a large whitewater river: Limnology and Oceanography; Fluids and Environments, v. 2, no. 1, p. 1–11, http://dx.doi.org/10.1215/21573689-1572535.

Halm, D.R., and Griffith, Brad, 2014, Water-quality data from lakes in the Yukon Flats, Alaska, 2010–2011: U.S. Geological Survey Open-File Report 2014–1181, 6 p., http://dx.doi.org/10.3133/ofr20141181.

Halm, D.R., and Guldager, Nikki, 2013, Water-quality data of lakes and wetlands in the Yukon Flats, Alaska, 2007–2009: U.S. Geological Survey Open-File Report 2012–1208, 13 p., http://pubs.usgs.gov/of/2012/1208/.

Hamilton, T.D., 1982, A late Pleistocene glacial chronology for the southern Brooks Range; Stratigraphic record and regional significance: Geological Society of America Bulletin, v. 93, no. 8, p. 700–716, http://dx.doi.org/10.1130/0016-7606(1982)93<700:ALPGCF>2.0.CO;2.

Harris, I., Jones, P.D., Osborn, T.J., and Lister, D.H., 2014, Updated high-resolution grids of monthly climatic observations—the CRU TS3.10 dataset: International Journal of Climatology, v. 34, no. 3, p. 623–642, http://dx.doi.org/10.1002/joc.3711.

Hijmans, Robert, Cameron, Susan, Parra, Juan, Jones, Peter, and Jarvis, Andrew, 2004, The WorldClim interpolated global terrestrial climate surfaces (ver. 1.3): WorldClim dataset, accessed March 24, 2014, at http://www.worldclim.org/current.

Hinzman, L.D., Bettez, N.D., Bolton, W.R., Chapin, F.S., Dyurgerov, M.B., Fastie, C.L., Griffith, Brad, Hollister, R.D., Hope, Allen, Huntington, H.P., Jensen, A.M., Jia, G.J., Jorgenson, Torre, Kane, D.L., Klein, D.R., Kofinas, Gary, Lynch, A.H., Lloyd, A.H., McGuire, A.D., Nelson, F.E., Oechel, W.C., Osterkamp, T.E., Racine, C.H., Romanovsky, V.E., Stone, R.S., Stow, D.A., Sturm, Matthew, Tweedie, C.E., Vourlitis, G.L., Walker, M.D., Walker, D.A., Webber, P.J., Welker, J.M., Winker, K.S., and Yoshikawa, Kenji, 2005, Evidence and implications of recent climate change in northern Alaska and other Arctic regions: Climatic Change, v. 72, no. 3, p. 251–298, http://dx.doi.org/10.1007/s10584-005-5352-2.

Hobbie, J.E., and Kling, G.W., eds., 2014, Alaska's changing Arctic; Ecological consequences for tundra, streams, and lakes: New York, Oxford University Press, 321 p.

Holmes, K.W., Chadwick, O.A., and Kyriakidis, P.C., 2000, Error in a USGS 30-meter digital elevation model and its impact on terrain modeling: Journal of Hydrology, v. 233, nos. 1–4, p. 154–173, http://dx.doi.org/10.1016/S0022-1694(00)00229-8.

Hood, Eran, Fellman, Jason, Spencer, R.G.M., Hernes, P.J., Edwards, Rick, D'Amore, David, and Scott, Durelle, 2009, Glaciers as a source of ancient and labile organic matter to the marine environment: Nature, v. 462, no. 7276, p. 1044–1047, http://dx.doi.org/10.1038/nature08580.

Huotari, Jussi, Haapanala, Sami, Pumpanen, Jukka, Vesala, Timo, and Ojala, Anne, 2013, Efficient gas exchange between a boreal river and the atmosphere: Geophysical Research Letters, v. 40, no. 21, p. 5683–5686, http://dx.doi.org/10.1002/2013GL057705.

Huttunen, J.T., Alm, Jukka, Liikanen, Anu, Juutinen, Sari, Larmola, Tuula, Hammar, Taina, Silvola, Jouko, and Martikainen, P.J., 2003, Fluxes of methane, carbon dioxide and nitrous oxide in boreal lakes and potential anthropogenic effects on the aquatic greenhouse gas emissions: Chemosphere, v. 52, no. 3, p. 609–621, http://dx.doi.org/10.1016/S0045-6535(03)00243-1.

Jarvis, A., Reuter, H.I., Nelson, A., and Guevara, E., 2008, Hole-filled SRTM for the globe (ver. 4): Consortium for Spatial Information (CGIAR-CSI) SRTM 90-m database, http://srtm.csi.cgiar.org.

Jobbágy, E.G., and Jackson, R.B., 2000, The vertical distribution of soil organic carbon and its relation to climate and vegetation: Ecological Applications, v. 10, no. 2, p. 423–436, http://dx.doi.org/10.1890/1051-0761(2000)010[0423:TVDOSO]2.0.CO;2.

Johnson, Cody, Kling, George, and Giblin, Anne, 2011, Sedimentation rate, concentration of macronutrients and flux for NE14, Toolik, Dimple, Perched during summer 2009: Long Term Ecological Research Network, http://dx.doi.org/10.6073/pasta/e2db8161be27bdbdcd398b0290f63f39.

Jones, B.M., Arp, C.D., Hinkel, K.M., Beck, R.A., Schmutz, J.A., and Winston, Barry, 2009, Arctic lake physical processes and regimes with implications for winter water availability and management in the National Petroleum Reserve Alaska: Environmental Management, v. 43, no. 6, p. 1071–1084, http://dx.doi.org/10.1007/s00267-008-9241-0.

Jones, M.C., Peteet, D.M., Kurdyla, Dorothy, and Guilderson, Thomas, 2009, Climate and vegetation history from a 14,000-year peatland record, Kenai Peninsula, Alaska: Quaternary Research, v. 72, no. 2, p. 207–217, http://dx.doi.org/10.1016/j.yqres.2009.04.002.

Jonsson, A., Åberg, J., Lindroth, A., and Jansson, M., 2008, Gas transfer rate and CO_2 flux between an unproductive lake and the atmosphere in northern Sweden: Journal of Geophysical Research; Biogeosciences, v. 113, no. G4, article G04006, 13 p., http://dx.doi.org/10.1029/2008JG000688.

Jorgenson, M.T., and Shur, Yuri, 2007, Evolution of lakes and basins in northern Alaska and discussion of the thaw lake cycle: Journal of Geophysical Research; Earth Surface, v. 112, no. F2, article F02S17, 12 p., http://dx.doi.org/10.1029/2006JF000531.

Jorgenson, Torre, Yoshikawa, Kenji, Kanevskiy, Mikhail, Shur, Yuri, Romanovsky, Vladimir, Marchenko, Sergei, Grosse, Guido, Brown, Jerry, and Jones, Ben, 2008, Permafrost characteristics of Alaska (December 2008 update to July 2008 Ninth International Conference on Permafrost [NICOP] map): Fairbanks, Alaska, University of Alaska-Fairbanks, Institute of Northern Engineering, scale 1:7,200,000, accessed August, 1, 2014, http://permafrost.gi.alaska.edu/sites/default/files/AlaskaPermafrostMap_Front_Dec2008_Jorgenson_etal_2008.pdf.

Kasischke, E.S., Verbyla, D.L., Rupp, T.S., McGuire, A.D., Murphy, K.A., Jandt, Randi, Barnes, J.L., Hoy, E.E., Duffy, P.A., Calef, Monika, and Turetsky, M.R., 2010, Alaska's changing fire regime—Implications for the vulnerability of its boreal forests: Canadian Journal of Forest Research, v. 40, no. 7, p. 1313–1324, http://dx.doi.org/10.1139/X10-098.

Kaufman, D.S., Axford, Yarrow, Anderson, R.S., Lamoureux, S.F., Schindler, D.E., Walker, I.R., and Werner, Al, 2012, A multi-proxy record of the Last Glacial Maximum and last 14,500 years of paleoenvironmental change at Lone Spruce Pond, southwestern Alaska: Journal of Paleolimnology, v. 48, no. 1, p. 9–26, http://dx.doi.org/10.1007/s10933-012-9607-4.

Kling, G.W., Kipphut, G.W., and Miller, M.C., 1992, The flux of CO_2 and CH_4 from lakes and rivers in arctic Alaska: Hydrobiologia, v. 240, no. 1–3, p. 23–36, http://dx.doi.org/10.1007/BF00013449.

Kling, G.W., Kipphut, G.W., Miller, M.M., and O'Brien, W.J., 2000, Integration of lakes and streams in a landscape perspective; The importance of material processing on spatial patterns and temporal coherence: Freshwater Biology, v. 43, no. 3, p. 477–497, http://dx.doi.org/10.1046/j.1365-2427.2000.00515.x.

Kortelainen, Pirkko, Pajunen, Hannu, Rantakari, Miitta, and Saarnisto, Matti, 2004, A large carbon pool and small sink in boreal Holocene lake sediments: Global Change Biology, v. 10, no. 10, p. 1648–1653, http://dx.doi.org/10.1111/j.1365-2486.2004.00848.x.

Kost, J.R., Verdin, K.L., Worstell, B.B., and Kelly, G.G., 2002, Methods and tools for the development of hydrologically conditioned elevation data and derivatives for national applications, *in* 2nd Annual Conference on Watershed Modeling, Las Vegas, Nev., 2002: 12 p.

Larouche, J.R., Bowden, W.B., Giordano, Rosanna, Flinn, M.B., and Crump, B.C., 2012, Microbial biogeography of arctic streams; Exploring influences of lithology and habitat: Frontiers in Microbiology, v. 3, article 309, 9 p., http://dx.doi.org/10.3389/fmicb.2012.00309.

Larsen, A.S., and Kristenson, Heidi, 2012, Alaska Shallow Lake Monitoring Program—Limnology of Denali National Park and Preserve: Fort Collins, Colo., National Park Service, Natural Resource Data Series NPS/CAKN/NRDS–2012/410, 37 p.

Leopold, L.B., and Maddock, Thomas, Jr., 1953, The hydraulic geometry of stream channels and some physiographic implications: U.S. Geological Survey Professional Paper 252, 57 p. [Also available at http://pubs.er.usgs.gov/publication/pp252.]

Ludwig, Wolfgang, Amiotte-Suchet, Philippe, and Probst, J.-L., 1999, Enhanced chemical weathering of rocks during the last glacial maximum; A sink for atmospheric CO_2?: Chemical Geology, v. 159, nos. 1–4, p. 147–161, http://dx.doi.org/10.1016/S0009-2541(99)00038-8.

Lynch, J.A., Clark, J.S., Bigelow, N.H., Edwards, M.E., and Finney, B.P., 2002, Geographic and temporal variations in fire history in boreal ecosystems of Alaska: Journal of Geophysical Research; Atmospheres, v. 107, no. D1, p. FFR 8–1 to FFR 8–17, http://dx.doi.org/10.1029/2001JD000332.

Mann, D.H., Heiser, P.A., and Finney, B.P., 2002, Holocene history of the Great Kobuk Sand Dunes, northwestern Alaska: Quaternary Science Reviews, v. 21, nos. 4–6, p. 709–731, http://dx.doi.org/10.1016/S0277-3791(01)00120-2.

Mast, M.A., Manthorne, D.J., and Roth, D.A., 2010, Historical deposition of mercury and selected trace elements to high-elevation National Parks in the Western U.S. inferred from lake-sediment cores: Atmospheric Environment, v. 44, nos. 21–22, p. 2577–2586, http://dx.doi.org/10.1016/j.atmosenv.2010.04.024.

Mathis, J.T., Cross, J.N., and Bates, N.R., 2011, Coupling primary production and terrestrial runoff to ocean acidification and carbonate mineral suppression in the eastern Bering Sea: Journal of Geophysical Research; Oceans, v. 116, no. C2, article C02030, 24 p., http://dx.doi.org/10.1029/2010JC006453.

McClelland, J.W., Townsend-Small, A., Holmes, R.M., Pan, Feifei, Stieglitz, M., Khosh, M., and Peterson, B.J., 2014, River export of nutrients and organic matter from the North Slope of Alaska to the Beaufort Sea: Water Resources Research, v. 50, no. 2, p. 1823–1839, http://dx.doi.org/10.1002/2013WR014722.

McDonald, C.P., Stets, E.G., Striegl, R.G., and Butman, David, 2013, Inorganic carbon loading as a primary driver of dissolved carbon dioxide concentrations in the lakes and reservoirs of the contiguous United States: Global Biogeochemical Cycles, v. 27, no. 2, p. 285–295, http://dx.doi.org/10.1002/gbc.20032.

McKay, N.P., and Kaufman, D.S., 2009, Holocene climate and glacier variability at Hallet and Greyling Lakes, Chugach Mountains, south-central Alaska: Journal of Paleolimnology, v. 41, no. 1, p. 143–159, http://dx.doi.org/10.1007/s10933-008-9260-0.

Melching, C.S., and Flores, H.E., 1999, Reaeration equations derived from U.S. Geological Survey database: Journal of Environmental Engineering, v. 125, no. 5, p. 407–414, http://dx.doi.org/10.1061/(ASCE)0733-9372(1999)125:5(407).

Michmerhuizen, C.M., Striegl, R.G., and McDonald, M.E., 1996, Potential methane emission from north-temperate lakes following ice melt: Limnology and Oceanography, v. 41, no. 5, p. 985–991, http://dx.doi.org/10.4319/lo.1996.41.5.0985.

Mulholland, P.J., and Elwood, J.W., 1982, The role of lake and reservoir sediments as sinks in the perturbed global carbon cycle: Tellus, v. 34, no. 5, p. 490–499, http://dx.doi.org/10.1111/j.2153-3490.1982.tb01837.x.

Naidu, A.S., Finney, B.P., and Baskaran, M., 1999, ^{210}Pb- and ^{137}Cs-based sediment accumulation rates in inner shelves and coastal lakes of subarctic and arctic Alaska; A synthesis, *in* Bruns, P., and Hass, H.C., eds., On the determination of sediment accumulation rates: GeoResearch Forum, v. 5, p. 185–196.

National Aeronautics and Space Administration (NASA), 2014, Surface meteorology and solar energy: National Aeronautics and Space Administration, accessed June 12, 2014, at https://eosweb.larc.nasa.gov/sse/.

New, Mark, Hulme, Mike, and Jones, Phil, 1999, Representing twentieth-century space–time climate variability, part I; Development of a 1961–90 mean monthly terrestrial climatology: Journal of Climate, v. 12, no. 3, p. 829–856, http://dx.doi.org/10.1175/1520-0442(1999)012<0829:RTCSTC>2.0.CO;2.

New, Mark, Hulme, Mike, and Jones, Phil, 2000, Representing twentieth-century space–time climate variability, part II; Development of 1901–96 monthly grids of terrestrial surface climate: Journal of Climate, v. 13, no. 13, p. 2217–2238, http://dx.doi.org/10.1175/1520-0442(2000)013<2217:RTCSTC>2.0.CO;2.

Osterkamp, T.E., Viereck, L., Shur, Y., Jorgenson, M.T., Racine, C., Doyle, A., and Boone, R.D., 2000, Observations of thermokarst and its impact on boreal forests in Alaska, U.S.A.: Arctic, Antarctic, and Alpine Research, v. 32, no. 3, p. 303–315, http://dx.doi.org/10.2307/1552529.

Park, C.C., 1977, World-wide variations in hydraulic geometry exponents of stream channels; An analysis and some observations: Journal of Hydrology, v. 33, nos. 1–2, p. 133–146, http://dx.doi.org/10.1016/0022-1694(77)90103-2.

Parks, Bruce, and Madison, R.J., 1985, Estimation of selected flow and water-quality characteristics of Alaskan streams: U.S. Geological Survey Water-Resources Investigations Report 84–4247, 64 p., https://pubs.er.usgs.gov/publication/wri844247.

Parkhurst, D.L., and Appelo, C.A.J., 1999, User's guide to PHREEQC (ver. 2)—A computer program for speciation, batch-reaction, one-dimensional transport, and inverse geochemical calculations: U.S. Geological Survey Water-Resources Investigations Report 99–4259, 312 p. [Also available at http://pubs.er.usgs.gov/publication/wri994259.]

Pastick, N.J., Jorgenson, M.T., Wylie, B.K., Rose, J.R., Rigge, Matthew, and Walvoord, M.A., 2014, Spatial variability and landscape controls of near-surface permafrost within the Alaskan Yukon River Basin: Journal of Geophysical Research; Biogeosciences, v. 119, no. 6, p. 1244–1265, http://dx.doi.org/10.1002/2013JG002594.

Pastick, N.J., Rigge, Matthew, Wylie, B.K., Jorgenson, M.T., Rose, J.R., Johnson, K.D., and Ji, Lei, 2014, Distribution and landscape controls of organic layer thickness and carbon within the Alaskan Yukon River Basin: Geoderma, v. 230–231, p. 79–94, http://dx.doi.org/10.1016/j.geoderma.2014.04.008.

Patton, W.W., Jr., 1973, Reconnaissance geology of the northern Yukon-Koyukuk Province, Alaska: U.S. Geological Survey Professional Paper 774–A, 17 p. [Also available at http://pubs.er.usgs.gov/publication/pp774A.]

Patton, W.W., Jr., and Miller, T.P., 1970, Preliminary geologic investigations in the Kanuti River region, Alaska: U.S. Geological Survey Bulletin 1312–J, 10 p. [Also available at http://pubs.er.usgs.gov/publication/b1312J.]

Pebble Partnership, 2011a, Water quality—Bristol Bay drainages, chap. 9 *of* Pebble Project Environmental Baseline Document 2004 through 2008: Pebble Partnership, variously paged, http://pebbleresearch.com/download/.

Pebble Partnership, 2011b, Surface water quality—Cook Inlet drainages, chap. 33 *of* Pebble Project Environmental Baseline Document 2004 through 2008: Pebble Partnership, variously paged, http://pebbleresearch.com/download/.

Ping, C.-L., Michaelson, G.J., Jorgenson, M.T., Kimble, J.M., Epstein, Howard, Romanovsky, V.E., and Walker, D.A., 2008, High stocks of soil organic carbon in the North American Arctic region: Nature Geoscience, v. 1, no. 9, p. 615–619, http://dx.doi.org/10.1038/ngeo284.

Post, R.A., 2011, Determining lake sedimentation rates using radionuclide tracers: Iowa City, Iowa, University of Iowa, M.S. thesis, 67 p.

Powell, R.D., and Molnia, B.F., 1989, Glacimarine sedimentary processes, facies and morphology of the south-southeast Alaska shelf and fjords: Marine Geology, v. 85, nos. 2–4, p. 359–390, http://dx.doi.org/10.1016/0025-3227(89)90160-6.

PRISM Climate Group, 2004, Parameter-elevation Relationships on Independent Slopes Model (PRISM): Oregon State University, accessed June 24, 2014, at http://prism.oregonstate.edu.

R Development Core Team, 2008, R—A language and environment for statistical computing: Vienna, Austria, R Foundation for Statistical Computing, http://www.R-project.org.

Raymond, P.A., Hartmann, Jens, Lauerwald, Ronny, Sobek, Sebastian, McDonald, Cory, Hoover, Mark, Butman, David, Striegl, Robert, Mayorga, Emilio, Humborg, Christoph, Kortelainen, Pirkko, Dürr, Hans, Meybeck, Michel, Ciais, Philippe, and Guth, Peter, 2013, Global carbon dioxide emissions from inland waters: Nature, v. 503, no. 7476, p. 355–359, http://dx.doi.org/10.1038/nature12760.

Raymond, P.A., Zappa, C.J., Butman, David, Bott, T.L., Potter, Jody, Mulholland, Patrick, Laursen, A.E., McDowell, W.H., and Newbold, Denis, 2012, Scaling the gas transfer velocity and hydraulic geometry in streams and small rivers: Limnology and Oceanography; Fluids and Environments, v. 2, no. 1, p. 41–53, http://dx.doi.org/10.1215/21573689-1597669.

Riera, J.L., Schindler, J.E., and Kratz, T.K., 1999, Seasonal dynamics of carbon dioxide and methane in two clear-water lakes and two bog lakes in northern Wisconsin, U.S.A.: Canadian Journal of Fisheries and Aquatic Sciences, v. 56, no. 2, p. 265–274, http://dx.doi.org/10.1139/f98-182.

Riordan, Brian, Verbyla, David, and McGuire, A.D., 2006, Shrinking ponds in subarctic Alaska based on 1950–2002 remotely sensed images: Journal of Geophysical Research; Biogeosciences, v. 111, no. G4, article G04002, 11 p., http://dx.doi.org/10.1029/2005JG000150.

Roach, J.K., Griffith, Brad, and Verbyla, David, 2013, Landscape influences on climate-related lake shrinkage at high latitudes: Global Change Biology, v. 19, no. 7, p. 2276–2284, http://dx.doi.org/10.1111/gcb.12196.

Roehm, C.L., Prairie, Y.T., and del Giorgio, P.A., 2009, The pCO_2 dynamics in lakes in the boreal region of northern Québec, Canada: Global Biogeochemical Cycles, v. 23, no. 3, article GB3013, 9 p., http://dx.doi.org/10.1029/2008GB003297.

Rogers, L.A., Schindler, D.E., Lisi, P.J., Holtgrieve, G.W., Leavitt, P.R., Bunting, Lynda, Finney, B.P., Selbie, D.T., Chen, Guangjie, and Gregory-Eaves, Irene, 2013, Centennial-scale fluctuations and regional complexity characterize Pacific salmon population dynamics over the past five centuries: National Academy of Sciences Proceedings, v. 110, no. 5, p. 1750–1755, http://dx.doi.org/10.1073/pnas.1212858110.

Rohr, Melanie, 2001, Paleoenvironmental changes at treeline in central Alaska; A 6,500 year long pollen and stable isotope record: Fairbanks, Alaska, University of Alaska, M.S. thesis, 186 p.

Rouse, W.R., Douglas, M.S.V., Hecky, R.E., Hershey, A.E., Kling, G.W., Lesack, Lance, Marsh, Philip, McDonald, Michael, Nicholson, B.J., Roulet, N.T., and Smol, J.P., 1997, Effects of climate change on the freshwaters of arctic and subarctic North America: Hydrological Processes, v. 11, no. 8, p. 873–902, http://dx.doi.org/10.1002/(SICI)1099-1085(19970630)11:8<873::AID-HYP510>3.0.CO;2-6.

Rover, Jennifer, Ji, Lei, Wylie, B.K., and Tieszen, L.L., 2012, Establishing water body areal extent trends in interior Alaska from multi-temporal Landsat data: Remote Sensing Letters, v. 3, no. 7, p. 595–604, http://dx.doi.org/10.1080/01431161.2011.643507.

Runkel, R.L., Crawford, C.G., and Cohn, T.A., 2004, Load estimator (LOADEST); a FORTRAN program for estimating constituent loads in streams and rivers: U.S. Geological Survey Techniques and Methods Book 4, Chapter A5, 69 p.

Scenarios Network for Alaska and Arctic Planning (SNAP), 2014, Historical monthly temperature and precipitation and historical derived temperature products: Scenarios Network for Alaska and Arctic Planning, accessed November 28, 2014, at http://www.snap.uaf.edu/data.php.

Schroth, A.W., Crusius, John, Chever, Fanny, Bostick, B.C., and Rouxel, O.J., 2011, Glacial influence on the geochemistry of riverine iron fluxes to the Gulf of Alaska and effects of deglaciation: Geophysical Research Letters, v. 38, no. 16, letter L16605, 6 p., http://dx.doi.org/10.1029/2011GL048367.

Schuur, E.A.G., Bockheim, James, Canadell, J.G., Euskirchen, Eugenie, Field, C.B., Goryachkin, S.V., Hagemann, Stefan, Kuhry, Peter, Lafleur, P.M., Lee, Hanna, Mazhitova, Galina, Nelson, F.E., Rinke, Annette, Romanovsky, V.E., Shiklomanov, Nikolay, Tarnocai, Charles, Venevsky, Sergey, Vogel, J.G., and Zimov, S.A., 2008, Vulnerability of permafrost carbon to climate change; Implications for the global carbon cycle: BioScience, v. 58, no. 8, p. 701–714, http://dx.doi.org/10.1641/B580807.

Seaber, P.R., Kapinos, F.P., and Knapp, G.L., 1987, Hydrologic unit maps: U.S. Geological Survey Water-Supply Paper 2294, 63 p., 1 pl., scale 1:7,500,000. [Also available at http://pubs.usgs.gov/wsp/wsp2294/.]

Sepulveda-Jauregui, A., Walter Anthony, K.M., Martinez-Cruz, K., Greene, S., and Thalasso, F., 2014, Methane and carbon dioxide emissions from 40 lakes along a north–south latitudinal transect in Alaska: Biogeosciences; Discussions, v. 11, no. 9, p. 13251–13307, http://dx.doi.org/10.5194/bgd-11-13251-2014.

Shimer, Grant, 2009, Holocene vegetation and climate change at Canyon Lake, Copper River Basin, Alaska: Fairbanks, Alaska, University of Alaska, M.S. thesis, 89 p.

Smol, J.P., Wolfe, A.P., Birks, H.J.B., Douglas, M.S.V., Jones, V.J., Korhola, Atte, Pienitz, Reinhard, Rühland, Kathleen, Sorvari, Sanna, Antoniades, Dermot, Brooks, S.J., Fallu, M.-A., Hughes, Mike, Keatley, B.E., Laing, T.E., Michelutti, Neal, Nazarova, Larisa, Nyman, Marjut, Paterson, A.M., Perren, Bianca, Quinlan, Roberto, Rautio, Milla, Saulnier-Talbot, Émilie, Siitonen, Susanna, Solovieva, Nadia, and Weckström, Jan, 2005, Climate-driven regime shifts in the biological communities of arctic lakes: National Academy of Sciences Proceedings, v. 102, no. 12, p. 4397–4402, http://dx.doi.org/10.1073/pnas.0500245102.

Sobek, S., Anderson, N.J., Bernasconi, S.M., and Del Sontro, T., 2014, Low organic carbon burial efficiency in arctic lake sediments: Journal of Geophysical Research; Biogeosciences, v. 119, no. 6, p. 1231–1243, http://dx.doi.org/10.1002/2014JG002612.

Sobek, Sebastian, Durisch-Kaiser, Edith, Zurbrügg, Roland, Wongfun, Nuttakan, Wessels, Martin, Pasche, Natacha, and Wehrli, Bernhard, 2009, Organic carbon burial efficiency in lake sediments controlled by oxygen exposure time and sediment source: Limnology and Oceanography, v. 54, no. 6, p. 2243–2254, http://dx.doi.org/10.4319/lo.2009.54.6.2243.

Sobek, Sebastian, Tranvik, L.J., and Cole, J.J., 2005, Temperature independence of carbon dioxide supersaturation in global lakes: Global Biogeochemical Cycles, v. 19, no. 2, article GB2003, 10 p., http://dx.doi.org/10.1029/2004GB002264.

Solomon, C.T., Bruesewitz, D.A., Richardson, D.C., Rose, K.C., Van de Bogert, M.C., Hanson, P.C., Kratz, T.K., Larget, Bret, Adrian, Rita, Babin, B.L., Chiu, C.-Y., Hamilton, D.P., Gaiser, E.E., Hendricks, Susan, Istvánovics, Vera, Laas, Alo, O'Donnell, D.M., Pace, M.L., Ryder, Elizabeth, Staehr, P.A., Torgersen, Thomas, Vanni, M.J., Weathers, K.C., and Zhu, Guangwei, 2013, Ecosystem respiration; Drivers of daily variability and background respiration in lakes around the globe: Limnology and Oceanography, v. 58, no. 3, p. 849–866, http://dx.doi.org/10.4319/lo.2013.58.3.0849.

Strahler, A.N., 1952, Dynamic basis of geomorphology: Geological Society of America Bulletin, v. 63, no. 9, p. 923–938, http://dx.doi.org/10.1130/0016-7606(1952)63[923:DBOG]2.0.CO;2.

Striegl, R.G., Dornblaser, M.M., Aiken, G.R., Wickland, K.P., and Raymond, P.A., 2007, Carbon export and cycling by the Yukon, Tanana, and Porcupine Rivers, Alaska, 2001–2005: Water Resources Research, v. 43, no. 2, article W02411, http://dx.doi.org/10.1029/2006WR005201.

Striegl, R.G., Dornblaser, M.M., McDonald, C.P., Rover, J.R., and Stets, E.G., 2012, Carbon dioxide and methane emissions from the Yukon River system: Global Biogeochemical Cycles, v. 26, no. 4, article GB0E05, 11 p., http://dx.doi.org/10.1029/2012GB004306.

Tank, S.E., Frey, K.E., Striegl, R.G., Raymond, P.A., Holmes, R.M., McClelland, J.W., and Peterson, B.J., 2012, Landscape-level controls on dissolved carbon flux from diverse catchments of the circumboreal: Global Biogeochemical Cycles, v. 26, no. 4, article BG0E02, 15 p., http://dx.doi.org/10.1029/2012GB004299.

Tank, S.E., Raymond, P.A., Striegl, R.G., McClelland, J.W., Holmes, R.M., Fiske, G.J., and Peterson, B.J., 2012, A land-to-ocean perspective on the magnitude, source and implication of DIC flux from major Arctic rivers to the Arctic Ocean: Global Biogeochemical Cycles, v. 26, no. 4, 15 p., http://dx.doi.org/10.1029/2011GB004192.

Tape, K.D., Verbyla, David, and Welker, J.M., 2011, Twentieth century erosion in Arctic Alaska foothills; The influence of shrubs, runoff, and permafrost: Journal of Geophysical Research; Biogeosciences, v. 116, no. G4, article G04024, 11 p., http://dx.doi.org/10.1029/2011JG001795.

Tarnocai, C., Canadell, J.G., Schuur, E.A.G., Kuhry, P., Mazhitova, G., and Zimov, S., 2009, Soil organic carbon pools in the northern circumpolar permafrost region: Global Biogeochemical Cycles, v. 23, no. 2, article GB2023, 11 p., http://dx.doi.org/10.1029/2008GB003327.

Tranvik, L.J., Downing, J.A., Cotner, J.B., Loiselle, S.A., Striegl, R.G., Ballatore, T.J., Dillon, Peter, Finlay, Kerri, Fortino, Kenneth, Knoll, L.B., Kortelainen, P.L., Kutser, Tiit, Larsen, Soren, Laurion, Isabelle, Leech, D.M., McCallister, S.L., McKnight, D.M., Melack, J.M., Overholt, Erin, Porter, J.A., Prairie, Yves, Renwick, W.H., Roland, Fabio, Sherman, B.S., Schindler, D.W., Sobek, Sebastian, Tremblay, Alain, Vanni, M.J., Verschoor, A.M., von Wachenfeldt, Eddie, and Weyhenmeyer, G.A., 2009, Lakes and reservoirs as regulators of carbon cycling and climate: Limnology and Oceanography, v. 54, no. 6, part 2, p. 2298–2314, http://dx.doi.org/10.4319/lo.2009.54.6_part_2.2298.

U.S. Department of Agriculture, Natural Resource Conservation Service, 2014, U.S. general soil map (STATSGO): U.S. Department of Agriculture, Natural Resource Conservation Service, accessed October 5, 2014, at http://sdmdataaccess.nrcs.usda.gov/.

U.S. Environmental Protection Agency, 2014, STORET data warehouse: U.S. Environmental Protection Agency, accessed July 21, 2014, at http://www.epa.gov/storet/dbtop.html.

U.S. Geological Survey, 2014a, National hydrography dataset: U.S. Geological Survey database, accessed April 7, 2014, at http://nhd.usgs.gov.

U.S. Geological Survey, 2014b, National water information service: U.S. Geological Survey Web site, accessed July 7, 2014, at http://waterdata.usgs.gov/nwis.

Van Heuven, S., Pierrot, D., Rae, J.W.B., Lewis, E., and Wallace, D.W.R., 2011, MATLAB program developed for CO_2 system calculations; ORNL/CDIAC-105b (ver. 1.1): U.S. Department of Energy, Oak Ridge National Laboratory, Carbon Dioxide Information Analysis Center, http://dx.doi.org/10.3334/CDIAC/otg.CO2SYS_MATLAB_v1.1.

Verdin, K.L., 2000, Development of the National Elevation Dataset Hydrologic Derivatives (NED-H): Proceedings of the 20th Annual ESRI International User Conference, San Diego, Calif., July 2000, accessed January 1, 2014, at http://training.esri.com/bibliography/index.cfm?event=general.recordDetail&ID=9086.

Verdin, K.L., and Worstell, Bruce, 2008, A fully distributed implementation of mean annual streamflow regional regression equations: JAWRA Journal of the American Water Resources Association, v. 44, no. 6, p. 1537–1547, http://dx.doi.org/10.1111/j.1752-1688.2008.00258.x.

Wahrhaftig, Clyde, 1965, Physiographic divisions of Alaska: U.S. Geological Survey Professional Paper 482, 52 p. [Also available at http://pubs.er.usgs.gov/publication/pp482.]

Walter, K.M., Edwards, M.E., Grosse, G., Zimov, S.A., and Chapin, F.S., III, 2007, Thermokarst lakes as a source of atmospheric CH_4 during the last deglaciation: Science, v. 318, no. 5850, p. 633–636, http://dx.doi.org/10.1126/science.1142924.

Walter Anthony, K.M., Zimov, S.A., Grosse, G., Jones, M.C., Anthony, P.M., Chapin, F.S., III, Finlay, J.C., Mack, M.C., Davydov, S., Frenzel, P., and Frolking, S., 2014, A shift of thermokarst lakes from carbon sources to sinks during the Holocene epoch: Nature, v. 511, no. 7510, p. 452–456, http://dx.doi.org/10.1038/nature13560.

Walvoord, M.A., and Striegl, R.G., 2007, Increased groundwater to stream discharge from permafrost thawing in the Yukon River Basin; Potential impacts on lateral export of carbon and nitrogen: Geophysical Research Letters, v. 34, no. 12, letter L12402, 6 p., http://dx.doi.org/10.1029/2007GL030216.

Walvoord, M.A., Voss, C.I., and Wellman, T.P., 2012, Influence of permafrost distribution on groundwater flow in the context of climate-driven permafrost thaw; Example from Yukon Flats Basin, Alaska, United States: Water Resources Research, v. 48, no. 7, article W07524, 17 p., http://dx.doi.org/10.1029/2011WR011595.

Wanninkhof, Rik, 1992, Relationship between wind speed and gas exchange over the ocean: Journal of Geophysical Research; Oceans, v. 97, no. C5, p. 7373–7382, http://dx.doi.org/10.1029/92JC00188.

Webb, R.S., and Webb, Thompson, III, 1988, Rates of sediment accumulation in pollen cores from small lakes and mires of eastern North America: Quaternary Research, v. 30, no. 3, p. 284–297, http://dx.doi.org/10.1016/0033-5894(88)90004-X.

Wetzel, R.G., 2001, Limnology—Lake and river ecosystems (3d ed.): San Diego, Calif., Academic Press, 1006 p.

Wik, Martin, Varner, R.K., Walter Anthony, Katey, MacIntyre, Sally, and Bastviken, David, 2016, Climate-sensitive northern lakes and ponds are critical components of methane release: Nature Geoscience, v. 9, no. 2, p. 99–106, http://dx.doi.org/10.1038/ngeo2578.

Williams, J.R., 1962, Geologic reconnaissance of the Yukon Flats district, Alaska: U.S. Geological Survey Bulletin 1111–H, p. 289–331. [Also available at http://pubs.er.usgs.gov/publication/b1111H.]

Yu, Zicheng, Walker, K.N., Evenson, E.B., and Hajdas, Irka, 2008, Lateglacial and early Holocene climate oscillations in the Matanuska Valley, south-central Alaska: Quaternary Science Reviews, v. 27, nos. 1–2, p. 148–161, http://dx.doi.org/10.1016/j.quascirev.2007.02.020.

Zappa, C.J., McGillis, W.R., Raymond, P.A., Edson, J.B., Hintsa, E.J., Zemmelink, H.J., Dacey, J.W.H., and Ho, D.T., 2007, Environmental turbulent mixing controls on air-water gas exchange in marine and aquatic systems: Geophysical Research Letters, v. 34, no. 10, letter L10601, 6 p., http://dx.doi.org/10.1029/2006GL028790.

Zhu, Zhiliang, and Reed, B.C., eds., 2012, Baseline and projected future carbon storage and greenhouse-gas fluxes in ecosystems of the Western United States: U.S. Geological Survey Professional Paper 1797, 192 p. [Also available at http://pubs.usgs.gov/pp/1797/.]

Zhu, Zhiliang, and Reed, B.C., eds., 2014, Baseline and projected future carbon storage and greenhouse-gas fluxes in ecosystems of the Eastern United States: U.S. Geological Survey Professional Paper 1804, 204 p. [Also available at http://dx.doi.org/10.3133/pp1804.]

Chapter 9. Alaska Carbon Balance

By A. David McGuire,[1] Hélène Genet,[2] Yujie He,[3] Sarah Stackpoole,[4] David D'Amore,[5] T. Scott Rupp,[2] Bruce K. Wylie,[6] Xiaoping Zhou,[7] and Zhiliang Zhu[8]

9.1. Highlights

- Ecosystem carbon balance of the Alaska assessment domain (as outlined in chapter 1) was estimated for two time periods, a historical period (1950–2009) and a projection period (2010–2099) by synthesizing results for upland (chapter 6), wetland (chapter 7), and inland aquatic (chapter 8) ecosystems.
- The total area of Alaska considered in this assessment was 1,475,089 square kilometers (km^2) (97.9 percent of the State), which is composed of 84 percent uplands, 12 percent wetlands, and 4 percent inland waters.
- Between 1950 and 2009, the upland and wetland ecosystems of the State were estimated to have sequestered an average of 3.7 teragrams of carbon per year (TgC/yr) (–141.4 to 72.0 TgC/yr inter-annual variability), which was 1.5 percent of net primary productivity (NPP) in upland and wetland ecosystems. However, this sequestration is spatially variable with the Northwest Boreal Landscape Conservation Cooperative (LCC) North losing carbon because of fire disturbance and other regions gaining carbon.
- The combined carbon loss through various pathways of the inland aquatic ecosystems of Alaska was estimated to be 41.2 TgC/yr (5th and 95th percentiles of 30.4 TgC/yr and 59.7 TgC/yr), or about 17 percent of upland and wetland NPP.
- The greenhouse gas forcing potential of upland and wetland ecosystems of Alaska was estimated to be 17.3 teragrams of carbon dioxide equivalent per year during the historical period, and for the State as a whole was likely substantially larger because of methane (CH_4) emissions from lake ecosystems.
- During the projection period (2010–2099), carbon sequestration of upland and wetland ecosystems of Alaska were projected to increase substantially (18.2 to 34.4 TgC/yr) primarily because of an increase in NPP of 12 to 30 percent associated with responses to rising atmospheric carbon dioxide (CO_2), increased nitrogen cycling, and longer growing seasons. Although carbon emissions to the atmosphere from wildfire were projected to increase substantially for all of the projected climates, the increases in NPP would more than compensate for those losses.
- Upland and wetland ecosystems were projected to be sinks for greenhouse gases (GHGs) for all but one of the simulations during the projection period. However, as in the case of the analysis of the historical period, there was an uncertainty as to whether the State would be a net source for GHGs if emissions of CH_4 from lakes in Alaska were considered.

[1]U.S. Geological Survey, Fairbanks, Alaska.

[2]University of Alaska-Fairbanks, Fairbanks, Alaska.

[3]Purdue University, West Lafayette, Ind.

[4]U.S. Geological Survey, Denver, Colo.

[5]U.S. Department of Agriculture Forest Service, Juneau, Alaska.

[6]U.S. Geological Survey, Sioux Falls, S. Dak.

[7]U.S. Department of Agriculture Forest Service, Portland, Oreg.

[8]U.S. Geological Survey, Reston, Va.

9.2. Introduction

Alaska occupies an area that is approximately one-fifth that of the conterminous United States. Ongoing warming in Alaska has the potential to substantially alter the exchange of carbon dioxide (CO_2) and methane (CH_4) between ecosystems and the atmosphere and the overall ecosystem carbon balance of the State (Striegl and others, 2007; Zhuang and others, 2007; Wolken and others, 2011; Yuan and others, 2012). Thus, the response of carbon balance to changes in climate and CO_2 concentrations in Alaska has implications for policies concerning the management of carbon in the United States. However, much of Alaska has not previously been included in any major national carbon and greenhouse-gas inventory reports. Thus, the historical baseline carbon balance is poorly understood at a statewide level, and the potential for climate change to affect carbon dynamics in Alaska has not been formally assessed.

The main outcomes of this assessment for Alaska include (1) estimates of the amount of carbon stored in ecosystems (such as forests and wetlands), (2) estimates of the capacity of ecosystems to sequester carbon, (3) estimates of the rate of greenhouse-gas (GHG) fluxes in and out of the ecosystems, and (4) evaluation of the effects of processes or driving forces that control ecosystem carbon balance and GHG fluxes. To support the outcomes of the assessment for the entire State of Alaska, the assessors sought to address questions within regions of Alaska. These questions include (1) what are the magnitudes of carbon pools and fluxes of soil, biomass, and surface waters for different regions of Alaska?; (2) how are changes in fire regime, vegetation distribution, permafrost dynamics, and forest management influencing carbon balance in different regions of Alaska?; and (3) how might estimated sources and sinks of CO_2 and CH_4 of arctic, boreal, and maritime ecosystems change in response to projected changes in climate, fire regime, permafrost dynamics, and forest management? Chapters 2 through 8 of this report addressed various aspects of these questions. This chapter focuses on synthesizing results across uplands, wetlands, and inland aquatic ecosystems to summarize information from this assessment at the statewide level on changes in carbon stocks, carbon fluxes, and greenhouse gas forcing for (1) historical/baseline (1950–2009) and (2) projection (2010–2099) periods.

9.3. Methods

9.3.1. Synthesis Estimates of Changes in Carbon Stocks

Changes in carbon stocks were estimated for upland and wetland ecosystems, but were not estimated for inland aquatic ecosystems because of a lack of data on carbon stocks in inland aquatic ecosystems. For the historical period, mean annual changes in vegetation and soil carbon stocks were calculated separately for uplands and wetlands by subtracting the area-weighted mean, in grams of carbon per square meter (gC/m^2), at the end of December 1949 from the area-weighted mean at the end of December 2009 and then dividing by 60 years. The area-weighted means were obtained from the simulations conducted by the Dynamic Organic Soil version of the Terrestrial Ecosystem Model (DOS-TEM; Genet and others, 2013) for uplands (chapter 6) and wetlands (chapter 7). To convert to units of teragrams of carbon per year (TgC/yr), the mean change in carbon stocks for uplands and wetlands was multiplied by the area in square meters (m^2) occupied by uplands (1.237774×10^{12} m^2) and wetlands (0.177069×10^{12} m^2). A similar procedure was followed for the projection period, except that the area-weighted mean for December 2009 was subtracted from the area-weighted mean for December 2099 and then divided by 90 years.

9.3.2. Synthesis Estimates of Carbon Fluxes

For uplands and wetlands, we report synthesis estimates of net primary productivity (NPP), heterotrophic respiration (HR), fire emissions (Fire), biogenic methane exchange ($BioCH_4$), and forest harvest (Harvest). Biogenic methane exchange was dominated by uptake of CH_4 from the atmosphere in uplands and by emissions of CH_4 to the atmosphere in wetlands. For the historical period, each mean annual carbon flux was separately calculated for uplands and wetlands by averaging the area-weighted mean flux in grams of carbon per square meter per year ($gC/m^2/yr$) from 1950 through 2009. The area-weighted means were obtained from the simulations conducted by DOS-TEM for uplands (chapter 6) and wetlands (chapter 7). The mean flux was then multiplied by the respective area of uplands and wetlands (see above) to convert to units of TgC/yr. A similar procedure was followed for the projection period, except that the area-weighted mean flux was averaged from 2010 through 2099. We calculated net ecosystem carbon balance (NECB; see Chapin and others, 2006) for upland and wetland ecosystems as follows:

$$NECB = NPP - HR - Fire - Harvest - BioCH_4 \quad (9.1)$$

for which the acronyms for the fluxes are defined as above.

For inland aquatic ecosystems, we report synthesis estimates of the export of carbon from rivers to the coastal ocean, the emission of CO_2 from rivers, the emission of CO_2 from lakes, and the burial of carbon in lakes. Estimates were obtained from chapter 8 in TgC/yr for the historical period.

9.3.3. Synthesis Estimates of Greenhouse Gas Forcing

We used the global warming potential (GWP) concept to estimate the greenhouse gas forcing potential across terrestrial upland and wetland ecosystems of Alaska. In our calculations of GWP, we assumed that CH_4 has 25 times the GWP of

CO_2 over a 100-year timeframe (Forster and others, 2007). GWP was reported in CO_2 equivalent: (1) C-CH_4 fluxes were converted to CH_4 equivalent by multiplying the fluxes by 16/12, the ratio of the molecular weight of CH_4 to the weight of carbon in CH_4, and the CH_4 equivalent fluxes were then converted to CO_2 equivalent multiplying them by 25, and (2) all C-CO_2 fluxes were converted to CO_2 equivalent by multiplying them by 44/12, the ratio of the molecular weight of CO_2 to the weight of carbon in CO_2. Positive GWP indicates net CO_2 emissions from the ecosystem to the atmosphere, and negative GWP indicates net removal of greenhouse gases by ecosystems.

9.4. Results and Discussion

9.4.1. Synthesis of Carbon Dynamics in the Historical Period (1950–2009)

Average soil carbon storage in Alaskan terrestrial ecosystems for the last decade of the historical period (2000–2009) was estimated to be 52.1 petagrams of carbon (PgC), with 47.1 PgC stored in upland ecosystems. Vegetation carbon storage in Alaskan terrestrial ecosystems over the same period was estimated to be 5.0 PgC with 4.3 PgC stored in upland ecosystems. The storage in upland ecosystems is greater because they occupy about 84 percent of the area (1.24 million square kilometers [km^2]) in Alaska compared with wetland coverage of 12 percent (0.18 million km^2); inland aquatic ecosystems occupy 4 percent (0.06 million km^2) of Alaska.

Between 1950 and 2009, upland and wetland terrestrial ecosystems of Alaska were estimated to have sequestered 3.7 TgC/yr (–141.4 to 72.0 TgC/yr inter-annual variability), which is 1.5 percent of annual NPP (table 9.1, fig. 9.1). This was largely because soil carbon sequestration (4.6 TgC/yr) more than offset losses of vegetation carbon (–0.9 TgC/yr). Upland ecosystems of Alaska were primarily responsible for the gain in soil carbon (5.3 TgC/yr) as wetland ecosystems were estimated to have lost soil carbon (–0.7 TgC/yr). Vegetation carbon was estimated to have decreased in upland ecosystems at –0.3 TgC/yr and in wetland ecosystems at –0.7 TgC/yr. The magnitude of NPP and HR in uplands was approximately six times greater than that in wetlands, and the loss of carbon in wildfire was three times greater in uplands than in wetlands. Modeled forest harvest was entirely concentrated in uplands, and modeled biogenic methane emissions were entirely concentrated in wetlands. Fire was the primary reason for the loss of vegetation carbon in the historical period, and most of the loss occurred in recent decades and in the Northwest Boreal Landscape Conservation Cooperative (LCC) North (chapters 6 and 7). Although the Northwest Boreal LCC North lost soil carbon because of fire, upland ecosystems of other LCC regions gained soil carbon during the historical period.

Terrestrial upland and wetland ecosystems of Alaska were estimated to have been a carbon source of 17.3 teragrams of carbon dioxide equivalent per year ($TgCO_2$-eq/yr) with respect to greenhouse gas forcing of the climate system during the historical period as net CO_2 uptake from uplands (NPP – HR – Fire = –16.0 $TgCO_2$-eq/yr as a sink) was lower in magnitude than the global warming potential of wetlands (33.3 $TgCO_2$-eq/yr), which is dominated by biogenic methane emissions. It is important to note that harvested carbon was transferred from live vegetation to an inert carbon pool, and it did not contribute to our estimate of HR. If we had considered the decomposition of harvested carbon in our analysis, it would have resulted in terrestrial uplands and wetlands of Alaska being a larger net source of greenhouse gases between 1950 and 2009 than we have estimated.

Inland aquatic ecosystems were estimated to have lost 41.2 TgC/yr (5th and 95th percentiles of 30.4 TgC/yr and 59.7 TgC/yr) through export to the coast and CO_2 emissions from rivers and lakes, minus burial in lake sediments (table 9.2; fig. 9.1, chapter 8), which is about 17 percent of NPP in terrestrial ecosystems. This report does not include estimates of stock changes in aquatic ecosystems and, because terrestrial and aquatic models were not integrated, terrestrial loading of carbon to aquatic ecosystems was not quantified. However, the sum of lateral export of carbon to Alaska coasts and carbon emissions across water surfaces is significant, and

Table 9.1. Sixty-year carbon balance of upland and wetland ecosystems in Alaska during the historical period (1950–2009).

[Soil carbon includes carbon in fibric, humic, and mineral soil horizons as well as carbon in coarse woody debris. Net ecosystem carbon balance is calculated as either change in vegetation carbon plus change in soil carbon or as net primary productivity minus heterotrophic respiration minus fire emissions minus biogenic methane emissions minus forest harvest. Positive values of net ecosystem carbon balance indicate increases in pools or fluxes of carbon into the ecosystem. Data may not add to totals or compute to net ecosystem carbon balance shown because of independent rounding. TgC/yr, teragram of carbon per year; $TgCO_2$-eq/yr, teragram of carbon dioxide equivalent per year]

Terrestrial component	Change in vegetation carbon	Change in soil carbon	Net primary productivity	Heterotrophic respiration	Fire emissions	Biogenic methane emissions	Forest harvest	Net ecosystem carbon balance	Global warming potential ($TgCO_2$-eq/yr)
	(TgC/yr)								
Upland	–0.3	5.3	212.0	175.0	29.0	0.0	2.9	5.0	–16.0
Wetland	–0.7	–0.7	37.3	27.3	10.4	0.9	0.0	–1.3	33.3
Total	**–0.9**	**4.6**	**249.2**	**202.3**	**39.4**	**0.9**	**2.9**	**3.7**	**17.3**

these results suggest that, when the processing and removal of carbon through inland waters is properly taken into account, the calculated capacity of soil and vegetation to store carbon and the heterotrophic respiration estimates for uplands and wetlands (table 9.1) may be reduced.

The methodology applied in this assessment does not allow us to combine the estimated carbon balance of upland and wetland ecosystems with the estimated carbon balance of inland aquatic ecosystems over the historical period. Thus, it is not clear whether Alaskan ecosystems have acted to sequester carbon in the historical period or whether they have lost carbon. The key methodological uncertainties concern both the heterotrophic respiration flux and the flux of carbon from terrestrial to inland aquatic ecosystems. The heterotrophic respiration estimate (205.2 TgC/yr, table 9.1) is likely an overestimate because the DOS-TEM model does not represent losses to inland aquatic ecosystems. If the estimated heterotrophic respiration flux were reduced by an amount to

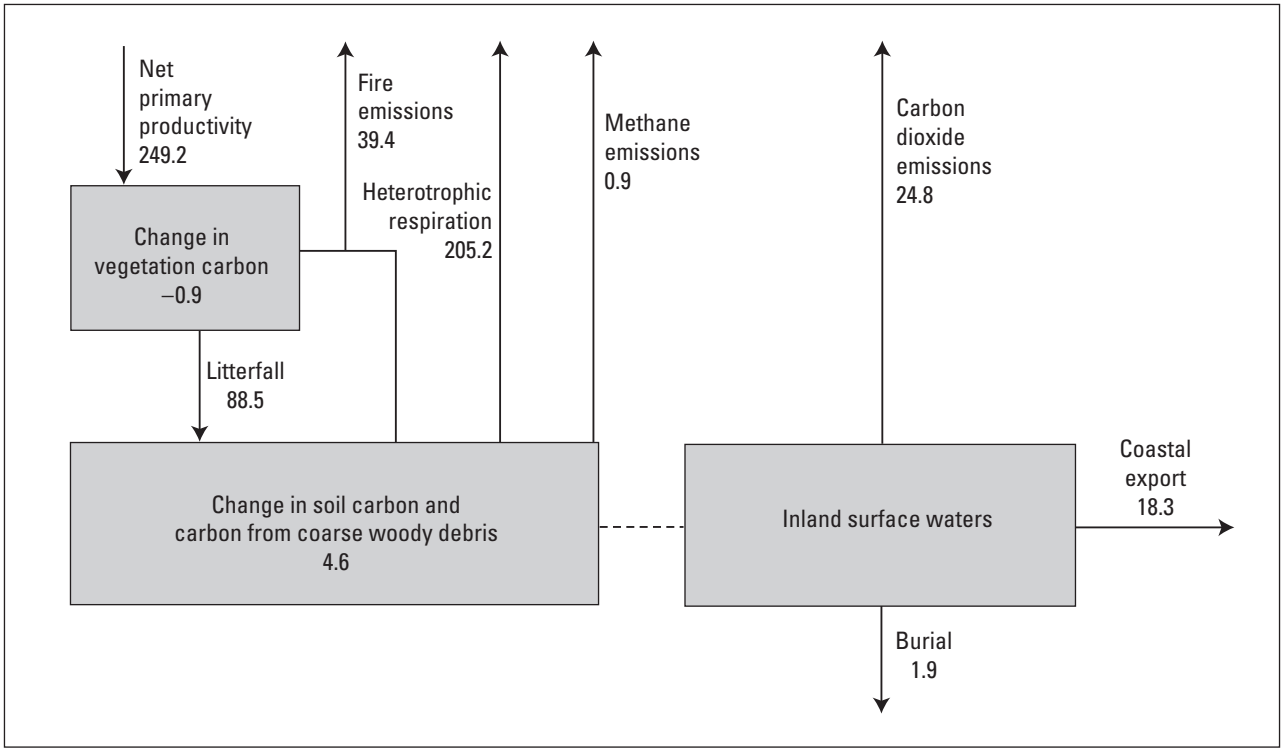

Figure 9.1. The carbon balance of the historical period (1950–2009) of this assessment estimated for the terrestrial (upland and wetland) component (left) and the inland aquatic component (right), in teragrams of carbon per year (TgC/yr). The arrows indicate the direction of carbon flows between the pools (including the atmosphere [not shown]) considered in this assessment. The litterfall flux of carbon from terrestrial vegetation to soil (88.5 TgC/yr) is provided in this figure to provide information relevant to the mass balance of terrestrial soil carbon. The linkage between fluxes of terrestrial vegetation and soil and that of the inland aquatic environment, as indicated by the dashed line, was not investigated in this assessment.

Table 9.2. Sixty-year carbon balance of inland aquatic ecosystems in Alaska during the historical period (1950–2009).

[Net ecosystem carbon balance for inland aquatic ecosystems is calculated as coastal carbon export from riverine systems plus carbon dioxide emissions from riverine systems plus carbon dioxide emissions from lacustrine systems plus methane emissions from lacustrine systems minus carbon burial in lacustrine systems. Because methane emissions from lacustrine systems were not estimated in this assessment, net ecosystem carbon balance was also not estimated. Net ecosystem carbon balance for aquatic systems can also be measured as change in carbon storage of inland aquatic ecosystems plus input of carbon into inland aquatic ecosystems from terrestrial (upland and wetland ecosystems), but neither of these was estimated in this assessment. TgC/yr, teragram of carbon per year; NE, not estimated]

Coastal carbon export from riverine systems (TgC/yr)	Carbon dioxide emissions from riverine systems (TgC/yr)	Carbon dioxide emissions from lacustrine systems (TgC/yr)	Methane emissions from lacustrine systems (TgC/yr)	Carbon burial in lacustrine systems (TgC/yr)	Net ecosystem carbon balance (TgC/yr)
18.3	16.6	8.2	NE	1.9	NE

balance the carbon budget of inland aquatic ecosystems, then the carbon balance for Alaska during the historical period would be equivalent to the total NECB of terrestrial uplands and wetlands (carbon sequestration of 3.7 TgC/yr, table 9.1). Clearly, it is important to treat the carbon dynamics of upland, wetland, and aquatic ecosystems as an integrated system to better estimate the net carbon balance of Alaska. The State as a whole was likely a much stronger source for greenhouse gas forcing to the climate system than estimated from uplands and wetlands alone because of CH_4 emissions from lake ecosystems, which we did not estimate in this assessment.

The estimates of soil and vegetation carbon storage by DOS-TEM were validated with data independent from those used in model development (chapters 6 and 7). The evaluation of the soil carbon estimates of DOS-TEM generally indicated good agreement with other available products for Alaska (chapter 3). There were no available products of vegetation carbon storage at the statewide level with which to evaluate the vegetation carbon estimates of DOS-TEM.

The large-scale flux estimates of the historical period are difficult to evaluate with independent analyses, because these analyses are restricted in spatial and temporal scope. For example, the synthesis of eddy covariance data in Alaska by Ueyama and others (2013) found that all five of the boreal and seven of the eight arctic tundra ecosystems analyzed acted as CO_2 sinks during the growing season. Our results for the historical period of mature undisturbed ecosystems of Alaska are certainly consistent with this result, but the study of Ueyama and others (2013) doesn't provide a quantitative means of evaluating the DOS-TEM simulations at the State scale and across the 60 years of the historical period. Our estimate of CH_4 emissions from wetlands for the historical period of 0.9 TgC/yr (1.2 teragrams of methane per year [$TgCH_4$/yr]) is substantially less than the estimate of 1.6 TgC/yr (2.1 $TgCH_4$/yr) for Alaska from May to September 2012 based on data from an aircraft sampling campaign (Chang and others, 2014). The difference in magnitude between the two estimates may, in part, be from CH_4 emissions of lakes, which we did not estimate in this assessment (table 9.2). Although the observational data on carbon dynamics in Alaska do not yet provide enough information for fully evaluating the exchange of greenhouse gases estimated by process-based models, the observational information is useful for some first-order evaluation of the magnitude and seasonality simulated by process-based models.

9.4.2. Assessment of Future Potential Carbon Dynamics (2010–2099)

Our assessment of future estimated carbon dynamics of Alaska (2010–2099) focused primarily on terrestrial upland and wetland ecosystems. The simulations indicated that carbon storage in terrestrial ecosystems would substantially increase across all six climate simulations—combinations of three climate scenarios (B1, A1B, and A2, in order of low to high projected CO_2 emissions) of the Intergovernmental Panel on Climate Change's Special Report on Emissions Scenarios (Nakićenović and Swart, 2000) used to force two general circulation models, version 3.1-T47 of the Canadian Centre for Climate Modelling and Analysis' Coupled Global Climate Model (CGCM3.1) and version 5 of the Max Planck Institute's European Centre Hamburg Model (ECHAM5). The range of carbon storage values, from 18.2 TgC/yr under scenario B1 with ECHAM5 to 34.4 TgC/yr under scenario A1B with CGCM3.1 (NECB in table 9.3), represents an approximate fivefold to ninefold increase over NECB for the historical period (3.7 TgC/yr, table 9.1). It should be noted that our simulations with DOS-TEM reported here did not model future forest harvest in southeast Alaska. The business-as-usual forest harvest we considered in chapter 5 for southeast Alaska would likely translate to an approximately 3-TgC/yr decrease in NECB (see chapter 6), and therefore would have little effect on the projected estimates of NECB we report here. The projected increase in carbon storage is primarily driven by increases in NPP of between 12 and 30 percent associated with increases in atmospheric CO_2 concentration, increases in nitrogen cycling, and longer growing seasons. Projected fire emissions across the climate simulations varied from a 36-percent decrease to a 212-percent increase. Projected HR across the climate simulations varied from an 18-percent decrease to a 13-percent increase primarily because increased fire in the Northwest Boreal LCC North would cause a substantial decrease in HR in that region associated with the substantial loss of soil carbon in fire. In other LCC regions, HR would increase in the future because of warmer soils, which would lead to higher rates of nitrogen cycling that increase NPP and lead to greater soil carbon stocks.

Our simulations indicated that terrestrial uplands and wetlands would act as sinks for greenhouse gases from 2010 through 2099 with GWP ranging from –24.5 to –91.6 $TgCO_2$-eq/yr, except for one simulation (11.6 $TgCO_2$-eq/yr, under scenario A1B with ECHAM5) for which biogenic CH_4 emissions and fire emissions were greater than for other simulations (table 9.3). Although we project that biogenic CH_4 emissions from wetlands will increase between 17 and 187 percent depending on the climate simulation, the increases do not offset the net increase in CO_2 uptake by upland and wetland ecosystems of Alaska for five of the six climate simulations in this assessment. This contrasts with our analysis for the historical period, which indicated that uplands and wetlands of Alaska were sources of greenhouse gas forcing. Because we did not assess the future dynamics of CH_4 emissions from lakes, we do not know if Alaska would be a net sink or source for greenhouse gases in the future.

Table 9.3. Projected carbon balance and global warming potential of terrestrial upland and wetland ecosystems in Alaska for the projection period (2010–2099).

[The six climate simulations are combinations of two general circulation models, version 3.1-T47 of the Coupled Global Climate Model (CGCM3.1) developed by the Canadian Centre for Climate Modelling and Analysis and version 5 of the European Centre Hamburg Model (ECHAM5) developed by the Max Planck Institute, and three climate scenarios of the Intergovernmental Panel on Climate Change's Special Report on Emissions Scenarios (Nakićenović and Swart, 2000), B1, A1B, and A2, in order of low to high projected CO_2 emissions. Soil carbon includes carbon in fibric, humic, and mineral soil horizons as well as carbon in coarse woody debris. Net ecosystem carbon balance is calculated as either change in vegetation carbon plus change in soil carbon or as net primary productivity minus heterotrophic respiration minus fire emissions minus biogenic methane emissions. Positive net ecosystem carbon balance indicates an increases in pools or fluxes of carbon into the ecosystem. Positive global warming potential indicates a net flux of greenhouse gas from the ecosystem to the atmosphere. Data may not compute to net ecosystem carbon balance shown because of independent rounding. TgC/yr, teragram of carbon per year; $TgCO_2$-eq/yr, teragram of carbon dioxide equivalent per year]

Climate scenario	Change in vegetation carbon (TgC/yr)	Change in soil carbon (TgC/yr)	Net primary productivity (TgC/yr)	Heterotrophic respiration (TgC/yr)	Fire emissions (TgC/yr)	Biogenic methane emissions ($TgCO_2$-eq/yr)	Net ecosystem carbon balance (TgC/yr)	Global warming potential ($TgCO_2$-eq/yr)
CGCM3.1								
A1B	8.8	25.6	292.6	232.0	25.1	36.1	34.4	–91.6
A2	10.2	21.9	306.6	168.7	103.4	64.4	32.2	–51.0
B1	6.2	20.5	278.2	219.9	30.4	37.1	26.8	–62.4
ECHAM5								
A1B	12.6	8.9	324.1	176.9	122.7	88.7	21.4	11.6
A2	12.5	11.7	323.3	190.5	106.4	54.1	24.3	–31.2
B1	9.8	8.5	282.3	222.4	40.3	43.3	18.2	–24.5

9.5. Conclusions

Our synthesis of carbon dynamics in Alaska indicates that between 1950 and 2009 the upland and wetland ecosystems of the State have sequestered 3.7 TgC/yr, which is almost 2 percent of upland and wetland NPP. However, this sequestration was spatially variable, with the Northwest Boreal LCC North losing carbon because of fire disturbance and other regions gaining carbon. We estimate that inland aquatic ecosystems of Alaska lost 41.2 TgC/yr, or about 17 percent of upland and wetland NPP, through various pathways. We estimate that the greenhouse gas forcing potential of upland and wetland ecosystems of Alaska was a source during the historical period, and we infer that the State as a whole was likely an even greater source for greenhouse gas forcing to the climate system because of CH_4 emissions from lake ecosystems, which we did not estimate in this assessment.

In contrast to the historical period, our synthesis of carbon dynamics in the projection period (2010–2099) indicates that carbon sequestration of upland and wetland ecosystems of Alaska would increase substantially (18.2 to 34.4 TgC/yr) primarily because of an increase in NPP of 12 to 30 percent associated with responses to rising atmospheric CO_2, increased nitrogen cycling, and longer growing seasons. Although carbon emissions to the atmosphere from wildfire were projected to increase substantially for all climate simulations, the increases in NPP would more than compensate for those losses. Our analysis indicates that upland and wetland ecosystems would be sinks for greenhouse gases for all scenarios during the projection period. Because we did not assess the future dynamics of CH_4 emissions from lakes, we do not know if Alaska would be a net sink or source for greenhouse gases in the future.

The results of our synthesis have implications for carbon management strategies that might be implemented as part of national policies aimed at controlling the rate and overall magnitude of climate change. These results suggest that Alaska could be a sink for greenhouse gases under some climate scenarios, but under others it could be a source, depending on the response of CH_4 emissions of lakes. However, it is important to recognize that CH_4 emissions from lakes have not been considered in this assessment, and it is likely that Alaska would be a source of greenhouse gases under all climate simulations if these emissions were considered in the assessment. Models have recently been developed for simulating CH_4 emissions of arctic lakes (Tan and others, 2015), and these models may be useful for estimating regional CH_4 emissions of lakes in Alaska in future assessments to more fully inform policy decisions concerning the mitigation of greenhouse-gas emissions in the United States.

It is important to recognize that there are many uncertainties in the results reported here. At the top of the list is the fact that the analyses of inland aquatic ecosystems were not integrated with those of upland and wetland ecosystems, which likely compromises the estimates of heterotrophic respiration because losses of carbon to aquatic ecosystems are not taken into account. Also, CH_4 emissions of lakes were not quantified in either the historical or projection time periods, and whether or not Alaska is a sink or source of greenhouse gases depends substantially on the magnitude of CH_4 emissions from lakes. The effects of insect disturbance were not considered in this study because of a lack of information on the effects of insects on carbon dynamics, the lack of a regional dataset on historical insect disturbance, and the lack of a model capable of making estimates of future insect disturbance. Our analyses in this study also did not consider the effect of thermokarst disturbance associated with the thawing of ice-rich permafrost, which often results in the subsidence and the development of wetlands. Finally, the process-based models used in this study, although extensively evaluated in this assessment and in previous studies, also have substantial conceptual and parameterization uncertainties. These uncertainties have been discussed in chapters 6, 7, and 8. Reduction in these uncertainties will require enhancements in observation systems, research on landscape dynamics, process-based research, and modeling research. Key enhancements in observation systems would include forest inventory measurements in interior Alaska, CO_2 concentration measurements in large lakes, and measurements of CH_4 emissions from lakes and wetlands. Key enhancements in research on landscape dynamics include improved regional datasets on vegetation dynamics, lake dynamics, and insect and thermokarst disturbance. Key enhancements in process-based research would include improved understanding of the transfer of carbon between terrestrial and inland aquatic ecosystems, of CH_4 dynamics of inland aquatic ecosystems, and of controls over insect and thermokarst disturbance. Finally, key enhancements in modeling research would include the development of models that can treat terrestrial-aquatic carbon linkages as an integrated system, improved modeling of wetland and lake CO_2 and CH_4 dynamics, and the prognostic modeling of insect and thermokarst disturbance and their effects on carbon dynamics. Although there are substantial uncertainties in our analyses, the analyses themselves represent state-of-the-art science, and this assessment provides information for priorities in reducing uncertainties that should improve future assessments.

9.6. References Cited

Chang, R.Y.-W., Miller, C.E., Dinardo, S.J., Karion, Anna, Sweeney, Colm, Daube, B.C., Henderson, J.M., Mountain, M.E., Eluszkiewicz, Janusz, Miller, J.B., Bruhwiler, L.M.P., and Wofsy, S.C., 2014, Methane emissions from Alaska in 2012 from CARVE airborne observations: National Academy of Science Proceedings, v. 111, no. 47, p. 16694–16699, http://dx.doi.org/10.1073/pnas.1412953111.

Chapin, F.S., III, Woodwell, G.M., Randerson, J.T., Rastetter, E.B., Lovett, G.M., Baldocchi, D.D., Clark, D.A., Harmon, M.E., Schimel, D.S., Valentini, R., Wirth, C., Aber, J.D., Cole, J.J., Goulden, M.L., Harden, J.W., Heimann, M., Howarth, R.W., Matson, P.A., McGuire, A.D., Melillo, J.M., Mooney, H.A., Neff, J.C., Houghton, R.A., Pace, M.L., Ryan, M.G., Running, S.W., Sala, O.E., Schlesinger, W.H., and Schulze, E.-D., 2006, Reconciling carbon-cycle concepts, terminology, and methods: Ecosystems, v. 9, no. 7, p. 1041–1050, http://dx.doi.org/10.1007/s10021-005-0105-7.

Forster, Piers, Ramaswamy, Venkatachalam, Artaxo, Paulo, Berntsen, Terje, Betts, Richard, Fahey, D.W., Haywood, James, Lean, Judith, Lowe, D.C., Myhre, Gunnar, Nganga, John, Prinn, Ronald, Raga, Graciela, Schulz, Michael, and Van Dorland, Robert, 2007, Changes in atmospheric constituents and in radiative forcing, chap. 2 *of* Solomon, Susan, Qin, Dahe, Manning, Martin, Chen, Zhenlin, Marquis, Melinda, Averyt, Kristen, Tignor, M.M.B., and Miller, H.L., Jr., eds., Climate Change 2007—The physical science basis, Contribution of Working Group I to the Fourth Assessment Report of the Intergovernmental Panel on Climate Change: Cambridge, United Kingdom, Cambridge University Press, p. 129–234. [Also available at http://www.ipcc.ch/publications_and_data/publications_ipcc_fourth_assessment_report_wg1_report_the_physical_science_basis.htm.]

Genet, H., McGuire, A.D., Barrett, K., Breen, A., Euskirchen, E.S., Johnstone, J.F., Kasischke, E.S., Melvin, A.M., Bennett, A., Mack, M.C., Rupp, T.S., Schuur, E.A.G., Turetsky, M.R., and Yuan, F., 2013, Modeling the effects of fire severity and climate warming on active layer thickness and soil carbon storage of black spruce forests across the landscape in interior Alaska: Environmental Research Letters, v. 8, no. 4, letter 045016, 13 p., http://dx.doi.org/10.1088/1748-9326/8/4/045016.

Nakićenović, Nebojša, and Swart, Robert, eds., 2000, Special report on emissions scenarios—A special report of Working Group III of the Intergovernmental Panel on Climate Change: Cambridge, United Kingdom, Cambridge University Press, 599 p. [Also available at http://www.ipcc.ch/ipccreports/sres/emission/index.php?idp=0.]

Striegl, R.G., Dornblaser, M.M., Aiken, G.R., Wickland, K.P., and Raymond, P.A., 2007, Carbon export and cycling by the Yukon, Tanana, and Porcupine Rivers, Alaska, 2001–2005: Water Resources Research, v. 43, no. 2, article W02411, http://dx.doi.org/10.1029/2006WR005201.

Tan, Zeli, Zhuang, Qianlai, and Walter Anthony, Katey, 2015, Modeling methane emissions from arctic lakes; Model development and site-level study: Journal of Advances in Modeling Earth Systems, v. 7, no. 2, p. 459–483, http://dx.doi.org/10.1002/2014MS000344.

Ueyama, Masahito, Iwata, Hiroki, Harazono, Yoshinobu, Euskirchen, E.S., Oechel, W.C., and Zona, Donatella, 2013, Growing season and spatial variations of carbon fluxes of Arctic and boreal ecosystems in Alaska (USA): Ecological Applications, v. 23, no. 8, p. 1798–1816, http://dx.doi.org/10.1890/11-0875.1.

Wolken, J.M., Hollingsworth, T.N., Rupp, T.S., Chapin, F.S., III, Trainor, S.F., Barrett, T.M., Sullivan, P.F., McGuire, A.D., Euskirchen, E.S., Hennon, P.E., Beever, E.A., Conn, J.S., Crone, L.K., D'Amore, D.V., Fresco, Nancy, Hanley, T.A., Kielland, Knut, Kruse, J.J., Patterson, Trista, Schuur, E.A.G., Verbyla, D.L., and Yarie, John, 2011, Evidence and implications of recent and projected climate change in Alaska's forest ecosystems: Ecosphere, v. 2, no. 11, article 124, 35 p., http://dx.doi.org/10.1890/ES11-00288.1.

Yuan, F.-M, Yi, S.-H., McGuire, A.D., Johnson, K.D., Liang, J., Harden, J.W., Kasischke, E.S., and Kurz, W.A., 2012, Assessment of boreal forest historical C dynamics in the Yukon River Basin; Relative roles of warming and fire regime change: Ecological Applications, v. 22, no. 8, p. 2091–2109, http://dx.doi.org/10.1890/11-1957.1.

Zhuang, Q., Melillo, J.M., McGuire, A.D., Kicklighter, D.W., Prinn, R.G., Steudler, P.A., Felzer, B.S., and Hu, S., 2007, Net emissions of CH_4 and CO_2 in Alaska; Implications for the region's greenhouse gas budget: Ecological Applications, v. 17, no. 1, p. 203–212, http://dx.doi.org/10.1890/1051-0761(2007)017[0203:NEOCAC]2.0.CO;2.

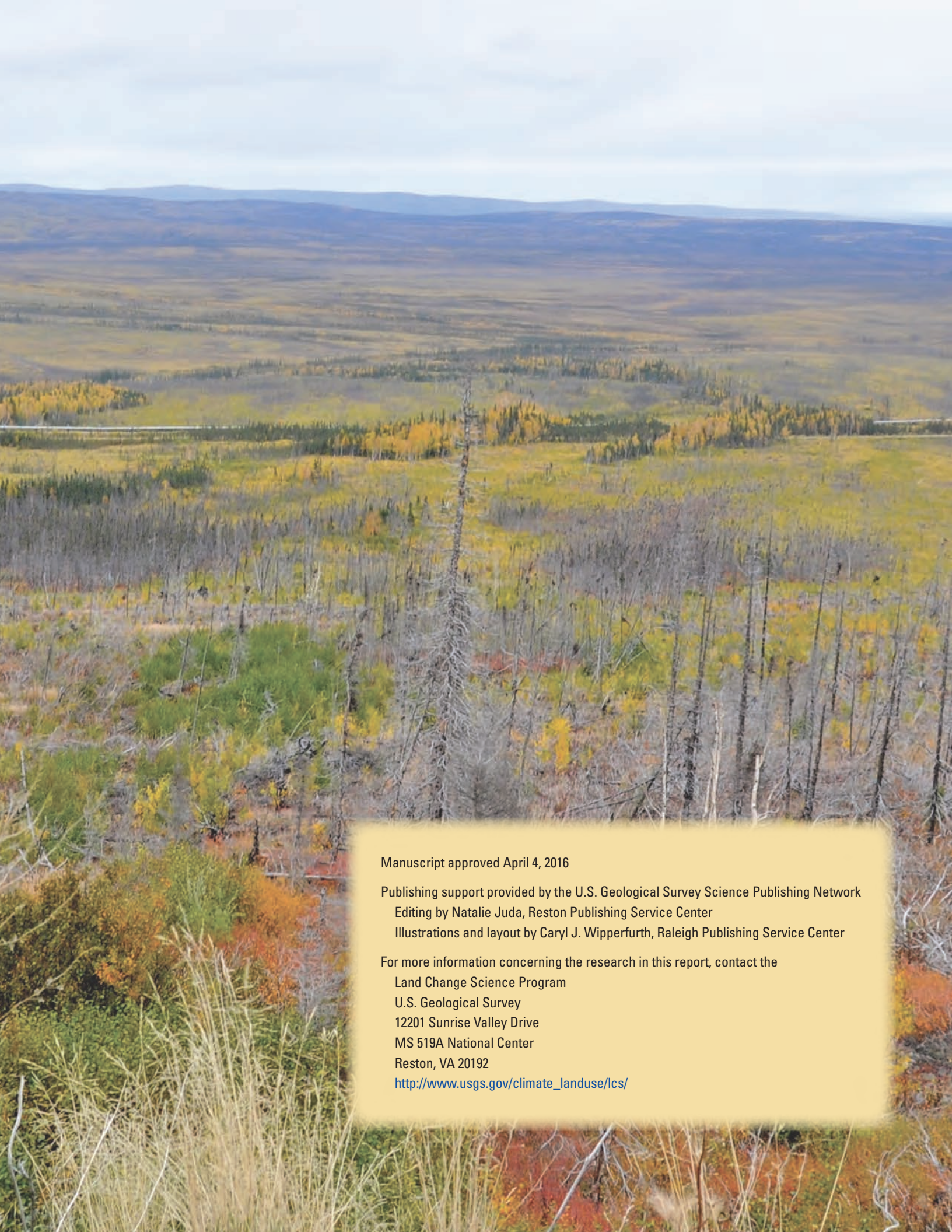

Manuscript approved April 4, 2016

Publishing support provided by the U.S. Geological Survey Science Publishing Network
Editing by Natalie Juda, Reston Publishing Service Center
Illustrations and layout by Caryl J. Wipperfurth, Raleigh Publishing Service Center

For more information concerning the research in this report, contact the
Land Change Science Program
U.S. Geological Survey
12201 Sunrise Valley Drive
MS 519A National Center
Reston, VA 20192
http://www.usgs.gov/climate_landuse/lcs/

ISBN 978-1-4113-4038-1

ISSN 1044-9612 (print)
ISSN 2330-7102 (online)
http://dx.doi.org/10.3133/pp1826

Printed on recycled paper

Zhu and McGuire, eds.—**Baseline and Projected Future Carbon Storage and Greenhouse-Gas Fluxes in Ecosystems of Alaska**—Professional Paper 1826